THE UNIVERSITY
of EDINBURGH

Controlling the Thermal and Photochemical Reactivity of the Uranyl Ion

Jamie M. Purkis

The University of Edinburgh

Submitted for the degree of Doctor of Philosophy

November 2019

Declaration

The work described in this thesis is my own, except where I have given reference to a published source or acknowledged help from a named person. This thesis has not been submitted, in whole or in part, for any degree at this or any other university. This work was carried out under the supervision of Professors Polly L. Arnold FRS OBE FRSC FRSE and Jason B. Love FRSC, from September 2015 to July 2019.

Signature:

Date: 20th July 2019 (*with corrections 15th November 2019*)

Abstract

Chapter one of this thesis introduces the chemistry of the element uranium, and its environmentally ubiquitous ion, the urany(VI) ion, $U^{VI}O_2^{2+}$. Fundamental chemical properties of this oxycation are discussed, alongside its behaviour in the aqueous environment. Particular attention is paid to its photophysical properties, which are discussed in detail.

Chapter two discusses the complexation of simple organic ligands to the uranyl(VI) ion. The synthesis and characterisation of a number of novel complexes of the uranyl(VI) ion with simple organic ligands that are solution- and photo-stable reported, with attention given to the electronic properties of these complexes, investigated by electronic absorption and fluorescence spectroscopies. The solution-phase and coordination chemistry of the neptunyl(VI) ion with simple *N*-heterocycle ligands in CH_3CN solvent is reported for the first time, and investigated by electronic and vibrational spectroscopy. A particular focus for this chapter is the novel uranyl(VI)-phenanthroline complex $[UO_2(NO_3)_2(Ph_2phen)]$ (**U^{Ph2phen}**). Efforts to develop suitable uranyl(VI)-based complexes to investigate the anaerobic photoreactivity of the $U^{VI}O_2^{2+}$ ion are also discussed.

Chapter three discusses the photochemical reactivity of the uranyl(VI) ion with a wide range of simple, organic substrates, to determine the functional group compatibility of uranyl-based photocatalysts. This includes the first comprehensive substrate scope involving the uranyl(VI) ion, using $[UO_2(NO_3)_2(OH_2)_2]\cdot 4H_2O$ (**U^{NO3}**). The products of photocatalytic reactions are analysed by ^{1}H NMR spectroscopy and GC-MS. The products of uranyl-mediated photocatalysis of a lignin mimic compound, 1-phenoxy-2-phenylethanol, are discussed. Also investigated are simple mechanistic differences between the archetypal uranyl(VI) catalyst, **U^{NO3}**, and **U^{Ph2phen}**, in the photocatalytic C-H bond activation reactions of these complexes with simple substrates containing a benzylic C-H bond.

In chapter four, investigations of the reductive oxo-functionalisation of the uranyl(VI) ion are expanded from previous literature. These include efforts to obtain a convenient synthesis route into the extremely rare $U^V_2O_4$ 'butterfly' motif, by the thermal reduction of the uranyl(VI) ion, and the photochemical reduction and oxo-functionalisation of the uranyl(VI) ion, constrained in a tetrapyrrolic Schiff-base 'Pacman' macrocyclic framework. Preliminary investigations into the anaerobic photochemical reactivity of the uranyl(VI) ion are also discussed.

Chapter five outlines the experimental and all relevant characterisation data for this thesis.

Lay Summary

Nuclear power, which is used to generate about 10% of the world's electricity, uses the element uranium as a fuel source. However, only a small fraction of the uranium that is mined for this purpose is suitable for use in nuclear reactors. This creates a lot of waste, and an estimated one-and-a-half million tonnes of waste uranium that is not suitable for use in nuclear power exists globally, making dealing with nuclear waste an expensive, and therefore politically sensitive, problem to deal with.

Despite nuclear waste being very tightly regulated, uranium enters the environment in a number of ways, including large-scale accidents (for example, Chernobyl), or smaller scale events, both of which are very hard to control. When uranium leaks into the environment, it reacts with water to create the "uranyl" ion, UO_2^{2+}, in which one uranium atom reacts with two oxygen atoms from water. This ion is very common and accounts for approximately one-half of all known uranium-containing compounds. The study of this ion is therefore very important to understanding how uranium behaves in the environment, and to reduce the large costs of nuclear waste remediation (which cost billions of pounds annually in the UK alone).

When sunlight interacts with the uranyl ion, it becomes capable of performing reactions called oxidations, in which oxygen, normally from the air, reacts with a wide number of chemicals to transform them, for example, turning alkanes into alcohols. Many examples of these reactions are known but the products of these reactions are often poorly understood and complicated to investigate. This can make dealing with these expensive nuclear wastes more difficult.

This thesis studies these oxidation reactions in more detail. This helps us understand how light affects the clean-up of nuclear wastes, as well as study how uranium might be useful in industrially-important chemical reactions. This thesis describes the synthesis of a number of new uranyl-containing molecules, which help us study how the uranyl ion interacts with light. By comparing differences in oxidation reactions involving these new uranyl-containing molecules with uranyl-containing molecules present in nuclear waste, this thesis outlines how the photochemical behaviour of the uranyl ion might be controlled, and therefore improve our ability to clean up nuclear wastes.

Acknowledgements

First and foremost, I owe thanks to Professor Polly L. Arnold, for her supervision, brilliant chemical and scientific insight, and above all, superb guidance and support, pastoral and otherwise, throughout the last few years. In all probability I wouldn't still be here if it wasn't for you and so, from the finish line of this most enjoyable of marathons, I say thank you very much indeed. Best of luck in LBNL and in all future endeavours.

Second, I wish to thank my secondary academic supervisor, Professor Jason B. Love, and industrial supervisor, Dr Jonathan Austin, for many fruitful discussions, chemical, pastoral and otherwise, and for helping keep me focussed on the important parts of chemistry during the undertaking of this project. Thanks also to the National Nuclear Laboratory, the NNL, and the Nuclear Decommissioning Authority, the NDA, for making this thesis possible, and for the continual support and training schemes and opportunities made possible throughout this project.

Particular thanks are owed to Drs. Nicola Bell and Euan Doidge and Mr. Simon Cummings, who are, in a word, outstanding. Our many discussions, political, cultural, philosophical, or just downright embarassing(!), were certainly a high point when not worrying about the chemistry presented in this thesis. I have no doubt that you'll go on to achieve many great things in your academic and personal lives. Thank you very much indeed.

To the project and visiting students I have had the distinct pleasure of working with over the last three and a bit years, I also owe you my thanks and sincere appreciation. Particularly to Alberto Botti and Ryte Rutkauskaite, to large sections of chapter two, and to Dr. Daniel Kovacs, whose steadfast, outstanding experimentation is responsible for large parts of chapter three. To Ryte and Alberto I wish the best of luck with your doctorate studies (I'll be watching the literature for your upcoming publications!), and to Daniel, all the best in Oxford.

I also wish to thank Brian Shaw, Lotte van Rees, Paul Ewing, Liam Donnelly, Connor Halliday, Steven Gray, Francis Lam, Lars Thode, Dr. Ryan Kerr, (now-Dr.!) Megan Seymour, Dr. Max McMullon, Dr. Max Curcio, Dr. Kai Wang, Dr. Tatsumi Ochiai, Dr. Laura Puig Urrea, and all other full, visiting and honorary members of the Love and Arnold groups, past and present, including those I've missed here. I have enjoyed the time I have spent with each and every one of you, and I wish you all the very best in your future endeavours, wherever they may take you. I will particularly miss Brian and Lotte, and the many varied conversations we had, which are too innumerate and varied to be listed here; thanks for putting up with my many inane ramblings and assorted whiteboard scribbles. I also wish to thank Drs. Amy

Price, Brad Cowie and Rory Kelly for the proof-reading of this thesis, and for the excellent supervision that you have all provided over the last few years.

Thanks also to the various technical staff at Edinburgh and beyond, including (but certainly not limited to) Mr. Juraj Bella for NMR spectroscopy, Drs. Alan Taylor, Faye Cruickshank and C. Logan McKay for mass spectrometry assistance, to Dr. Gylen Odling for many hours of UV-vis spectroscopy, to Dr. Louise Natrajan and Prof. Anita Jones and groups for discussions on fluorescence spectroscopy, and to Dr. Mark Sarsfield and the radiochemistry team at the NNL, for the neptunyl work described in this thesis. Thanks too to the members of the Arnold and Love group responsible for the data acquisition of many of the crystal structures outlined in this thesis.

Naturally, I wish to thank my family and friends, and Sean, in Southampton, here in Edinburgh, and abroad, for making the last few years very enjoyable, and thoroughly memorable indeed. It has certainly not been easy at times, but I've grown more than I thought possible just a few years ago, and it is through your support, love and kindness that I've been able to complete this most enjoyable project. I am eternally indebted to each and every one of you.

Lastly, I wish to dedicate this thesis to my granddad. I will always look back with great fondness on our many caravan trips and walks we spent together, talking about all manner of things scientific and otherwise. It is your philosophy of never taking anything for granted, always questioning and enquiring, and always wanting to make a positive contribution and difference that has, in large part, motivated all that I have achieved in the last few years. Simply put, this thesis is a practical manifestation of that axiom; using the skills that I've acquired from my A levels and through to my MChem degree to make a positive contribution to the world around me. That philosophy will be with me until I'm not around anymore, and it is one I will treasure for a lifetime. Thanks, grandad.

"Nothing in life is to be feared, it is only to be understood. Now is the time to understand more, so that we may fear less."

-- Marie Curie

Abbreviations

General	
2P-1P-E	2-Phenoxy-1-PhenylEthanol
18-c-6	18-crown-6
OAc	Acetate, $-CH_3CO_2$
An	Actinide
Ar	Aryl
APPI	Atmospheric Pressure PhotoIonisation
ATR	Attenuated Total Reflectance
(a)sym.	(a)Symmetric
Avg.	Average
bipy	2,2'-Bipyridine
ΔE_{diss}	Bond dissociation energy
Bu	Butyl
b.v. or b.w.	By Volume or Weight
CHON	Carbon, Hydrogen, Oxygen, Nitrogen
cat.	Catalyst
cat	catecholato, 1,2-diphenoxylate
CCIs	Cation-Cation Interactions
ca.	*circa* (approximately)
cf.	*conferatur* (compare)
Cp	C_5H_5
Cp*	C_5Me_5
Da	Dalton
DFT	Density Functional Theory
DHA	9,10-DiHydroAnthracene
DMSO	DiMethylSulfOxide
ESI	ElectroSpray Ionisation
E	Element
equiv(s).	Equivalent(s)
etc.	*Et cetera* (and other things)
Et	Ethyl
ES	Excited State

e.g.	*Exempli Gratia* (for example)
FT	Fourier Transform
GC	Gas Chromatography
GS	Ground State
HOMO	Highest Occupied Molecular Orbital
HAA	Hydrogen Atom Abstraction
ITU	Institute for TransUranium elements
ICR	Ion Cyclotron Resonance
ipht/Hipht	Isophthalate/Isophthalic acid
K_{eq}	(equilibrium) dissociation constant
Ln	Lanthanide
LHS	Left-Hand Side
LMCT	Ligand-Metal Charge Transfer
LUMO	Lowest Unoccupied Molecular Orbital
Me	Methyl
m/z	Mass over charge
NNL	National Nuclear Laboratory
NFSI	*N*-FluorobenzeneSulfonImide
n/a	Not Applicable
n.d.	Not Detected
n.r.	Not Reported
NDA	Nuclear Decommissioning Authority
N''	$-N(SiMe_3)_2$
ppm/ppb	Parts Per Million/Billion (*etc*.)
phen	1,10-Phenanthroline
Ph	Phenyl
pht/Hpht	Phthalate/Phthalic acid
pin	pinacolato, 2,3-dimethyl-2,3-butanediolate
PUREX	Plutonium Uranium Redox EXtraction
Pr	Propyl
py	Pyridine
pK_a	logarithm of the acid dissociation constant, K_a
RhB	Rhodamine B

RHS	Right Hand Side
r.t.	Room Temperature
Sol./Solv.	Solvent
s.u.s	Standard UncertaintieS
T	Temperature
terpy	2,2';6',2"-terpyridine
TPP	Tetra-2-PyridinylPyrazine
THF	TetraHydroFuran
TODGA	N,N,N',N'-TetraOctaDiGlycolAmide
t	time
TM	Transition Metal
TBP	TriButyl Phosphate
OTf	Triflate, $-OSO_2CF_3$
TFA	TriFluoroAcetic acid
U.K.	United Kingdom
vs.	*Versus*
WRT	With Respect To

Symbols and Units	
∠	Angle
Å	Angstrom, 10^{-10} m
cal	Calorie(s)
δ	Chemical shift
d	Day(s)
°	Degrees
ε (ε_{max}; ε_x)	Molar extinction coefficient (maxima; at wavelength x)
ν	Frequency
g	Gram(s)
Hz	Hertz
h	hour(s)
J	Joule(s) or Coupling constant
K	Kelvin
L	Litre

m	Metre(s) or Minute(s)
mol	Mole(s)
M	mol.dm^{-3}, Moles per cubic decimetre
h	Planck's constant, 6.63 x 10^{-34} J.s
s	Second(s)
V	Volt(s)
W	Watt(s)
λ (λ_{max})	Wavelength (wavelength maxima)

Spectroscopy	
EPR	Electron Paramagnetic Resonance
EXAFS	Extended X-ray Absorption Fine Structure
IR	InfraRed
KF	Karl-Fischer
MS	Mass Spectrometry
NMR	Nuclear Magnetic Resonance
(SC)XRD	(Single-Crystal) X-Ray Diffraction
UV	UltraViolet
UV-vis-NIR	UltraViolet-visible-Near InfraRed
s	Singlet
d	Doublet
t	Triplet
q	Quarter
dd	Doublet of doublets
dt	Doublet of triplets
dq	Doublet of quartets
tt	Triplet of triplets
w	Weak
m	Medium
s	Strong
vs	Very strong
br	Broad
sh	Shoulder

Complexes

U^{NO3}	$[UO_2(NO_3)_2(OH_2)_2]\cdot 4H_2O$
$U^{Ph2phen}$	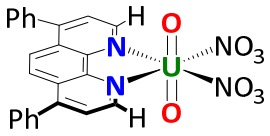
U^{phen}	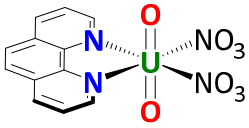
U^{mal} U^{malPh2} U^{malPh4} $U^{mali Pr4}$	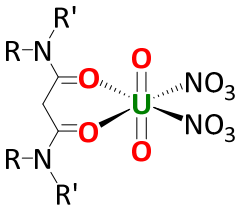 U^{mal} (R = R' = H) U^{malPh2} (R = H, R' = Ph) U^{malPh4} (R = R' = Ph) $U^{mali Pr4}$ ($R = R' = {}^{i}Pr$)
$U^{benzNH2}$ $U^{benzNHPh}$ $U^{benzNPh2}$ $U^{piv iPr2}$	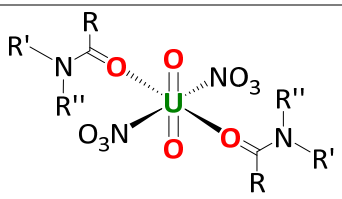 $U^{benzNH2}$ (R = Ph, R' = R'' = H) $U^{benzNHPh}$ (R = R' = Ph, R'' = H) $U^{benzNHPh2}$ (R = R' = R'' = Ph) $U^{piv iPr2}$ ($R = {}^{t}Bu$, R' = R'' = ^{i}Pr)
U^{tetNO3}	$[{}^{n}Bu_4N]_2[UO_2(NO_3)_4]$
U^{SO4}	$[UO_2(SO_4)]$
U^{OAc}	$[UO_2(OAc)_2]\cdot 2H_2O$
4.L.THF	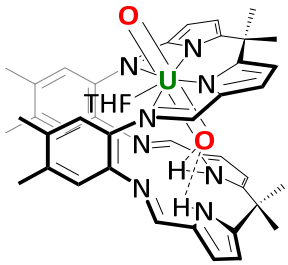

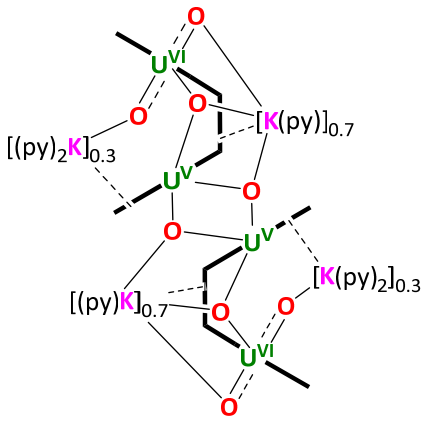

4.1

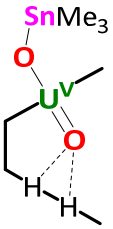

4.2

Publications resulting from this thesis

P. L. Arnold*, J. M. Purkis, R. Rutkauskaite, D. Kovacs, J. B. Love*, J. Austin, **Controlled photocatalytic hydrocarbon oxidation by uranyl complexes**, *ChemCatChem.,* 2019, 11, 3786. (Special Issue; "Women of Catalysis"), https://doi.org/10.1002/cctc.201900037,

B. E. Cowie, J. M. Purkis, P. L. Arnold*, J. B. Love*, J. Austin, **Thermal and photochemical reduction chemistry of the uranyl dication**, *Chem. Rev.*, 2019, 18, 10595, https://pubs.acs.org/doi/10.1021/acs.chemrev.9b00048

P. L. Arnold*, M. Zegke, G. Schreckenbach, J. M. Purkis, *et al.*, **Competition for U(V) uranyl oxo-group bonding between the uranium and metal cations from groups 1, 2, 4, and 12; a computational and synthetic study**, *Chem. Sci.*, 2019, *Manuscript in press,* https://pubs.rsc.org/en/content/articlelanding/2019/sc/c8sc05717f

Table of Contents

Chapter 1: Introduction

Elemental uranium is among the heaviest naturally occurring elements in the Earth's lithosphere (*ca.* 2.6 ppm) and oceans (*ca*. 4.5 billion tonnes),[1] with the five major radioisotopes, $^{233\text{-}236}$U and ^{238}U, dominated by ^{238}U and ^{235}U at 99.2% at 0.72% abundance, respectively.[2] Uranium was first used by Enrico Fermi and co-workers in 1942 to assemble the world's first self-sustaining nuclear pile in New York,[3] and subsequently in nuclear power where, alongside plutonium and thorium, it is a major component of current generation III+ and future generation IV+ nuclear reactors.[4-6] Owing to safety[7] and proliferation[8] concerns, the use of uranium is also heavily regulated. However as ^{238}U is not fissile, it is predominantly a by-product of the uranium enrichment process, from which it is primarily discarded. Consequently, global stocks of depleted uranium total an estimated 1.7 million tonnes and increase by approximately 50,000 tonnes per annum.[9] This has an economic cost, and in the UK the total cost of remediating all nuclear legacy sites, including processing uranium wastes, is estimated to be £234 billion over the next 120 years (as of 2017-2018).[10] There are therefore both environmental and economic drivers for further study of uranium compounds, particularly in catalysis, in which uranium has been proposed as an alternative to other rarer transition metals.[11]

1.1 The Uranyl(VI) Ion, $U^{VI}O_2^{2+}$

The predominant form of uranium, both in the environment and of most relevance to nuclear fuel reprocessing, is the dioxidouranium(VI) cation, the uranyl(VI) ion, $U^{VI}O_2^{2+}$. The structure of this oxycation is shown in Figure 1.1. Note that here, the terms uranyl, uranyl(VI), UO_2^{2+}, and $U^{VI}O_2^{2+}$ are used interchangeably.

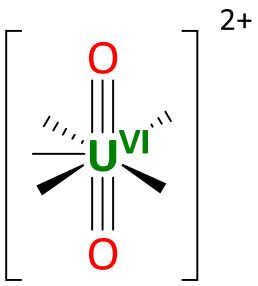

Figure 1.1 – The uranyl(VI) cation, $U^{VI}O_2^{2+}$.

The uranyl(VI) ion contains a formal triple bond, denoted formally as 'U≡O', but by convention as U=O; the latter is used herein. The three bonds arise from overlap of oxygen 2*p* orbitals and a hybrid state of the 5*f* and 6*d* orbitals on uranium, resulting in one σ– and two π-bonds (Figure 1.2, below).[12]

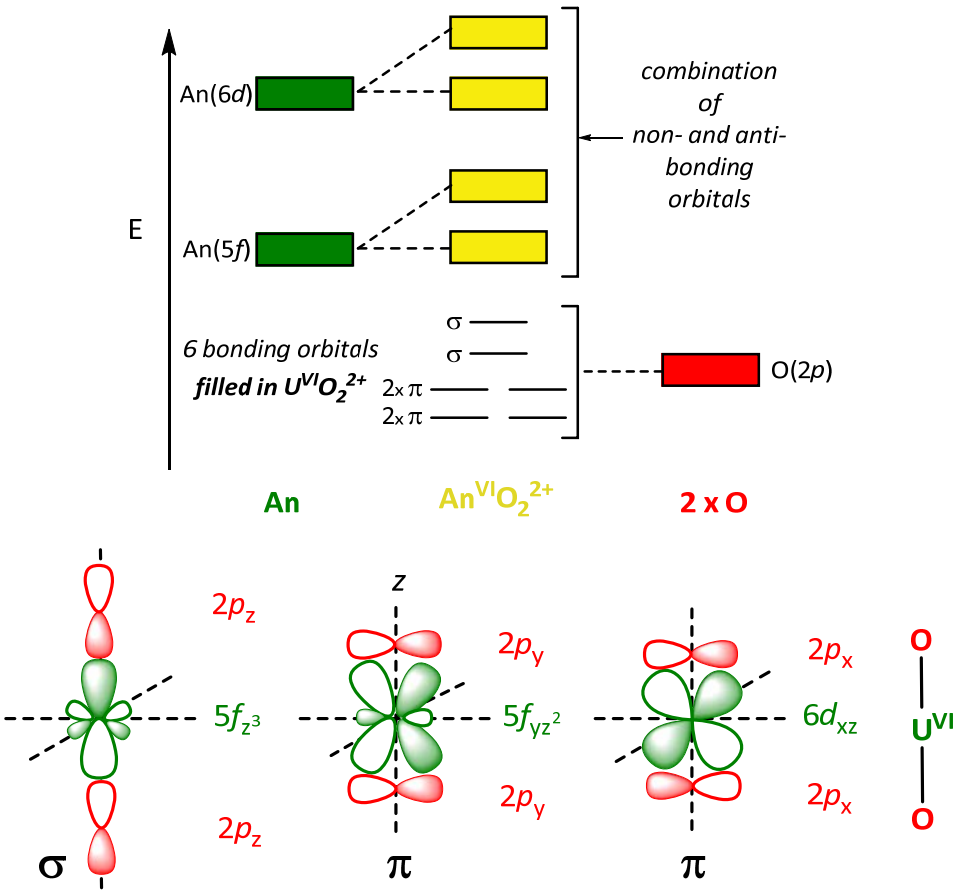

Figure 1.2 – Top, simplified molecular orbital energy level diagram for bonding in the actinyl(VI) ion (An = U–Am); bottom, selected examples of possible orbital overlap between O 2*p* and U 5*f* and 6*d* orbitals in $U^{VI}O_2^{2+}$. *p*-orbitals (that is, $2p_x$ and $2p_y$) on O are used interchangeably (*e.g.* $2p_x/6d_{xz}$ is degenerate with $2p_y/6d_{yz}$ overlap). Figures are adapted from Kaltsoyannis and Scott[13] and G. M. Jones' Ph.D. thesis.[14] The involvement of U 6*p* orbitals, not outlined here, is in part responsible for the unusual energy ordering of π- and σ-bonding orbitals ('pushing from below').[13]

This *trans*-uranyl motif, $[O=U=O]^{2+}$, is rigidly linear and chemically stable, resulting in most chemistry occurring in the plane perpendicular to the OUO internuclear axis. The actinyl ion, AnO_2^{n+}, is also known to occur for elements to americium (*e.g.* Z = 92–95),[15] but with decreasing stabilities. This results from addition of electrons to higher energy non- and anti-bonding molecular orbitals moving from $U^{VI}O_2^{2+}$ to $Np^{VI}O_2^{2+}$, $Pu^{VI}O_2^{2+}$ and finally $Am^{VI}O_2^{2+}$, highlighted in Figure 1.2. The stabilities of $An^{VI}O_2^{2+}$ ions are therefore An = U > Np > Pu > Am, with electron configurations $[Rn]5f^n$, n = 0–3, respectively. Coordination geometries of up to eight are common, with seven-coordinate geometries (*e.g.* actinyl, plus five equatorial ligands) the most commonly observed configuration for monodentate σ-bonding ligands, such as aquo (H_2O) ligands (*e.g.* $[UO_2(OH_2)_5]^{2+}$).

1.2 The Uranyl Ion in the Aqueous Environment

There are a number of routes through which uranium can enter the terrestrial environment, including acute point-source pollution (*e.g.* the Fukushima-Daiichi meltdown),[16] chronic seepage and corrosion of solid wastes (*e.g.* legacy magnox storage ponds at Sellafield),[17] geological instability with deep

geological facilities,[18] and mining waste runoff.[19] Along with other actinyl(VI) ions, $An^{VI}O_2^{2+}$ (An = Np, Pu and Am), the $U^{VI}O_2^{2+}$ ion is soluble in water, making it highly mobile in aqueous environments.

However, the reduction of uranyl(VI)-containing species is readily achieved in the environment, with the uranyl(V) ion, $U^{V}O_2^{+}$, as the main product. Unstable in water outside a narrow pH (2–2.5)[20] range, the $U^{V}O_2^{+}$ ion readily disproportionates to regenerate the uranyl(VI) ion, and precipitate U^{IV}-containing solids (*e.g.*, UO_2); Scheme 1.1, below. The formation of U^{IV}-containing solids, which are insoluble in water, helps to immobilise uranium products, reducing the environmental impact of uranium-containing wastes in the aqueous environment.

$$2\,U^{VI}O_2^{2+} \xrightarrow{\text{i}} 2\,U^{V}O_2^{+} + 4\,H^{+} \xrightarrow{\text{ii}} U^{VI}O_2^{2+} + U^{IV} + 2\,H_2O$$

Scheme 1.1 – Reduction of $U^{VI}O_2^{2+}$ and subsequent disproportionation of $U^{V}O_2^{+}$, resulting in insoluble U^{IV} precipitates. Reaction i is the reduction of $U^{VI}O_2^{2+}$ to $U^{V}O_2^{+}$, and reaction ii is the disproportionation of water-unstable $U^{V}O_2^{+}$ ion back to $U^{VI}O_2^{2+}$ and U^{IV}. Reaction ii is discussed further in chapter 4.

The environmental reduction of $U^{VI}O_2^{2+}$ to $U^{V}O_2^{+}$ is typically mediated biologically, or heterogeneously. The anaerobic microbial reduction of uranyl(VI) with sulfate-reducing micro-organisms[21, 22] has been extensively investigated as a bio-remedial technique for the decontamination of affected sites, for example, in groundwater at the Oak Ridge National Laboratories in the USA where, after 50 days of bio-remedial treatment with a *Geobacter* strain, Anderson *et al*. were able to show a reduced concentration of $U^{VI}O_2^{2+}$ from harmful to negligible levels in contaminated soils.[23] Heterogeneously, the reduction of the $U^{VI}O_2^{2+}$ ion is known to occur at the surface of many iron-containing minerals (*e.g.*, goethite,[24] magnetite,[25] *etc.*), and zero-valent iron.[26] In these systems the $U^{VI}O_2^{2+}$ ions interact with iron nanoparticles, undergoing reduction to U^{IV}; these precipitates are strongly bound, and therefore immobilised, on the surfaces of hydrated iron oxide particulates (rusts).

The predominant uranyl complex in water at pH values of < 3 is the pentaaquouranyl(VI) ion, $[U^{VI}O_2(OH_2)_5]^{2+}$.[27, 28] At pH 3–5, hydroxido complexes start to form, including $[(UO_2)_2(OH)_2(OH_2)_6]^{2+}$, $[UO_2(OH)]^{+}$ and $[(UO_2)_3(O)(OH)_3(OH_2)_6]^{+}$.[29, 30] Successively higher pH values (> 5) increase the complexity and number of uranyl-hydroxido complexes that form, including $[UO_2(OH)_3]^{-}$, $[UO_2(OH)_4]^{2-}$, $[(UO_2)_3(OH)_7]^{-}$, $[(UO_2)_4(OH)_7]^{+}$, $[(UO_2)_3(OH)_4]^{2+}$, and $[(UO_2)_2(OH)]^{3+}$, *etc*. and polynuclear clusters are common.[31, 32] Figure 1.3 illustrates the complex and pH-dependent aqueous speciation of the $U^{VI}O_2^{2+}$ ion.

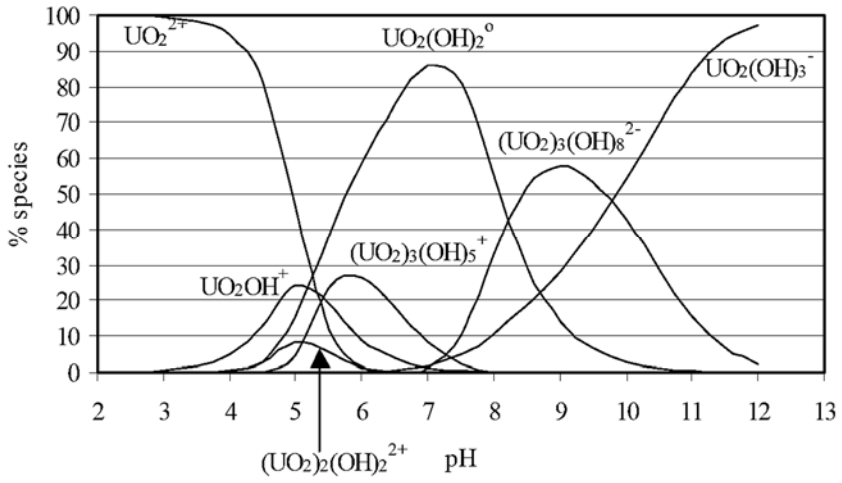

Figure 1.3 – Speciation diagram for the $U^{VI}O_2^{2+}$ ion in water, $[U^{VI}O_2^{2+}] = 0.01$ M, adapted from Krestou and Panias.[33]

The aqueous speciation of the uranyl(VI) ion is similarly intricate in the presence of environmentally ubiquitous ions,[32] and uranyl complexes of the form $[U^{VI}O_2(X)_n]^{m-}$ (n = 1, m = 0; n = 2, m = 2; n = 3, m = 4) are known for X = CO_3^{2-} or SO_4^{2-} ions.[34, 35] These myriad complexes can make controlling the reactivity of the uranyl ion in aqueous solution problematic.

1.3 Photophysics of the Uranyl(VI) Ion

With the advent of atomic weaponry and nuclear power arising from the Manhattan Project, the properties of uranium were intensively studied in the 1950s and 60s. However, despite historical knowledge that uranium compounds are photoactive (Adolph Gehlen noted in 1804 that UCl_4 degrades upon exposure to light)[36] it was not until the seminal investigations of Eisenstein and Pryce[37] and Bell and Biggers[38, 39] that a detailed description of the photochemical behaviour of the $U^{VI}O_2^{2+}$ ion was produced. Figure 1.4, below, shows a detailed energy level diagram for the uranyl(VI) ion, adapted from Bell and Biggers.[38, 39]

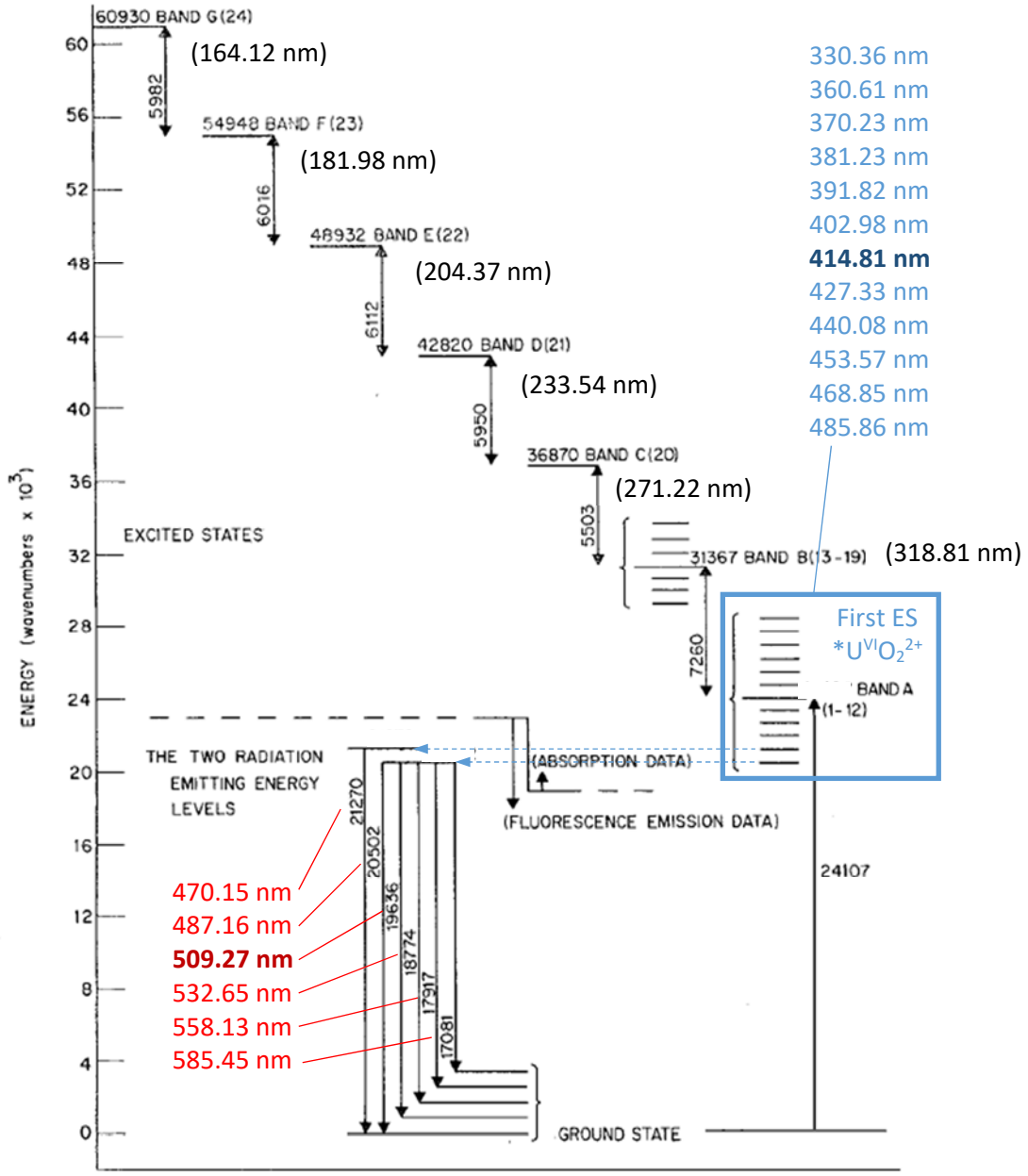

Figure 1.4 – Energy level diagram for the absorption (**BLUE**; Figure 1.5) and emission (**RED**; Figure 1.6) processes of the uranyl(VI) ion. Numbers are the wavelengths corresponding to the wavenumber values (cm^{-1}) from the original figure, with emboldened values representing λ_{max} for the absorption or emission processes, respectively. ES is excited state, and the figure is adapted from Bell and Biggers.[38, 39]

The electronic structure of the $U^{VI}O_2^{2+}$ ion results in a symmetric absorption spectrum that extends into the visible region (*ca*. 500 nm). There are 12 distinct bands, corresponding to vibronic fine structure (*e.g*. the symmetric uranyl stretch, $\nu_{sym}(U{=}O_{yl})$ at *ca*. 800 cm^{-1}), outlined below (Figure 1.5) in the absorption spectrum of the $U^{VI}O_2^{2+}$ ion in aqueous perchlorate media.[40]

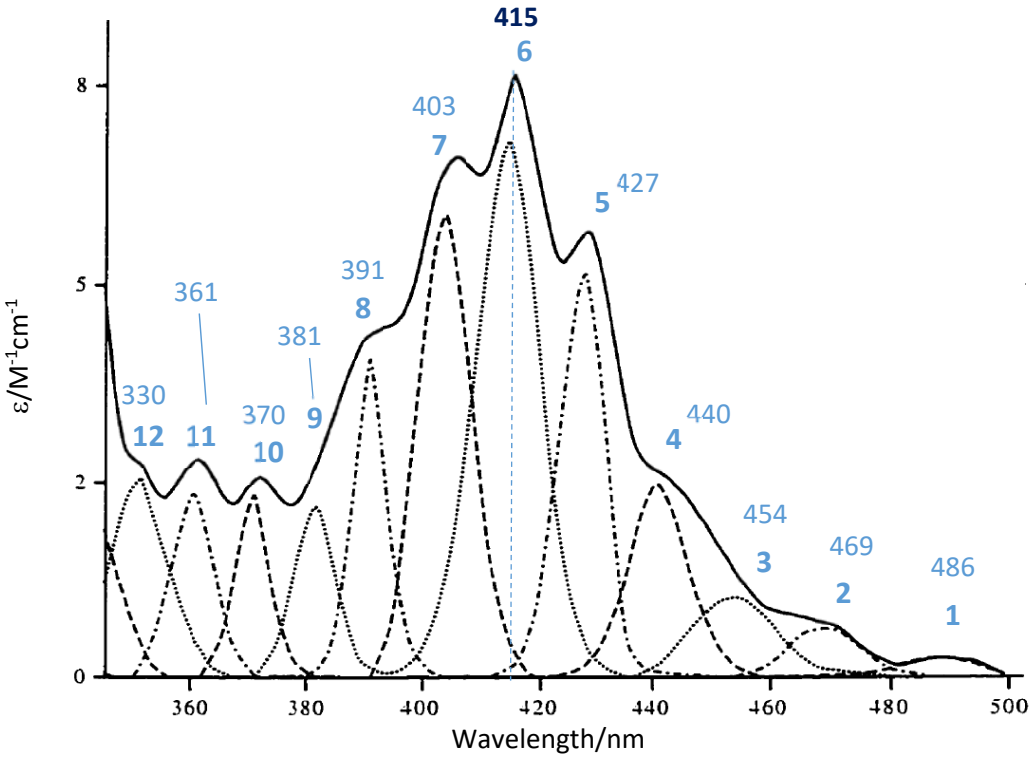

Figure 1.5 – Electronic absorption spectrum of the $U^{VI}O_2^{2+}$ ion ($[U^{VI}O_2^{2+}]$ = 9.15 mM) in $HClO_4$ ($[ClO_4^-]$ = 1.4 mM), highlighting the 12 distinct bands associated with the first ES of the $U^{VI}O_2^{2+}$ ion, with associated wavelength values. Adapted from Burrows and Kemp.[41]

When exposed to near-ultraviolet (UV) or UV light sources (*ca.* < 480 nm, *cf.* blue or purple light), the (singlet)[32] ground electronic state, closed-shell $5f^0$ $U^{VI}O_2^{2+}$ ion undergoes an excitation to the first electronically excited state, $*U^{VI}O_2^{2+}$, which possesses an open-shell, $5f^1$ configuration. The λ_{max} for this transition is *ca.* 415–420 nm. This triplet[32, 42] state is long-lived (≤ μs), and is explained simply as the ligand-to-metal charge transfer (LMCT) of an electron from a fully occupied $2p_\sigma$ or $2p_\pi$ orbital of primarily oxygen-character to a non-bonding $5f_\delta$ or $5f_\varphi$ orbital of primarily uranium-character (*e.g.* $\sigma_u \rightarrow 5f_{\delta/\varphi}$). This corresponds to a reduction in the bond order of the U^{VI}=O bond from 3 to 2.5 as an electron is excited from a bonding to a non-bonding orbital, resulting in π-bond U-O homolysis to give a *pseudo*-U^V metal centre, and highly reactive oxyl radical (O•) in the $[^\bullet O\text{-}U^V{=}O]^{2+}$ ion, scheme 1.2. The $*U^{VI}O_2^{2+}$ ion is highly oxidizing with an oxidation potential of *ca.* +2.6 V, similar to elemental fluorine.

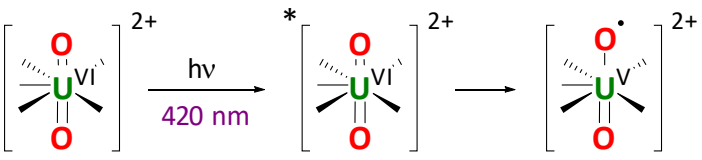

Scheme 1.2 – Exposure of the $U^{VI}O_2^{2+}$ ion to hν (420 nm) leads first to excitation, giving the $*U^{VI}O_2^{2+}$ ion, then bond cleavage, resulting in the highly-oxidising $[^\bullet O\text{-}U^V{=}O]^{2+}$ ion. The reactivity of the $[^\bullet O\text{-}U^V{=}O]^{2+}$ ion is discussed in chapter 3.

Therefore the uranium centre in the $U^{VI}O_2^{2+}$ ion can easily be excited to a highly oxidizing, reactive species by simple irradiation of uranyl-containing compounds with blue or purple visible, or UV, light.

This makes photochemical reactions with the uranyl(VI) ion convenient to access. With the global oversupply of (depleted) uranium, these factors also make uranyl-mediated photocatalysis a tempting target for the degradation of volatile organic compounds, VOCs. Indeed, several systems, including the uranyl-mediated photocatalytic methanol oxidation[43] and the destruction of linear alkanes,[44] have been reported in the chemical literature.

Another characteristic feature of the uranyl(VI) ion is the distinctively emissive nature of its compounds. Arising from radiative relaxation of the $*U^{VI}O_2^{2+}$ ion to the GS $U^{VI}O_2^{2+}$ ion, the emission profile of the uranyl(VI) ion contains six bands, which become discrete and well-defined at 77 K.[45] The bands typically lie within a range of *ca*. 470–600 nm, and a representative electronic emission spectrum of the $U^{VI}O_2^{2+}$ ion in aqueous perchlorate solution is given in Figure 1.6, below.

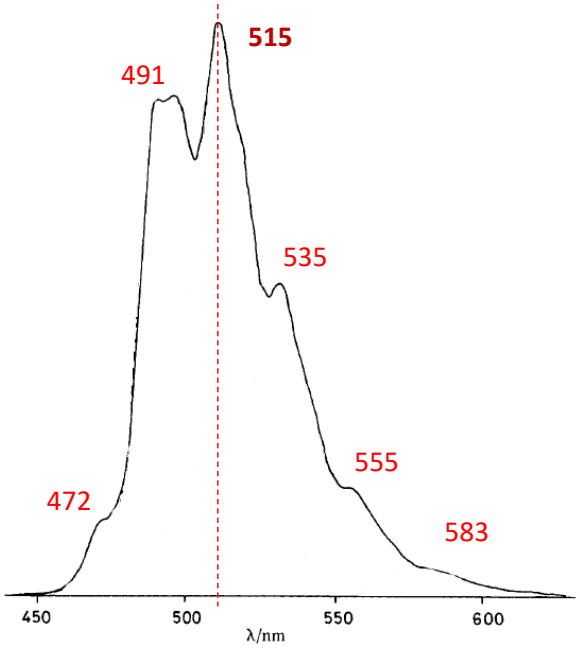

Figure 1.6 – Electronic emission spectrum of $U^{VI}O_2^{2+}$ ($[U^{VI}O_2^{2+}]$ = 50 mM, pH 3.1 ($HClO_4$)). Adapted from Formosinho *et al.*[46] Numbers are wavelength values in nm.

The peak emission wavelength for a complex is invariably longer than that of an absorption, due to non-radiative losses between the various vibrational states of electronically excited states. According to Kasha's rule,[47] this occurs from the lowest-lying excited state, and thus the values outlined in Figure 1.4 correspond approximately to the values for absorption and emission in Figures 1.5 and 1.6. The difference in λ_{max} for absorption and emission, the Stokes shift, is also an important value in fluorescence spectroscopy as large values (*ca*. 7000–10000 cm^{-1}) correspond to excited-state reactions, and therefore the nature of reactivity of a complex upon irradiation. Smaller values (3000–5000 cm^{-1}) are typical of solvent-only processes, that is, reorganisation of the solvent cage upon transitioning between the ground to the electronically excited state(s) of a molecule.[48]

1.4 Aims of this Thesis

The aims of this thesis are discussed in more detail in the specific chapter introductions. Generally, however, this thesis describes efforts to develop new uranyl(VI)-based photocatalysts to explore the photochemical reactivity of this ion, with complementary investigations into its thermal reactivity.

In order to exploit the beneficial photochemical properties of the $U^{VI}O_2^{2+}$ ion outlined in Section 1.3, a range of novel uranyl(VI)-based complexes with ligand-modified electronic properties will be targeted, to enhance the photochemical reactivity of the uranyl ion. The effects that ligands have on the electronic and solution-phase properties of uranyl(VI)-based complexes will be investigated.

With uranyl(VI)-based complexes that possess unique photochemical properties in hand, the photocatalytic reactivity of these complexes will be investigated, with a range of organic substrates. Any reactivity differences of these complexes will be correlated with photochemical properties, with particular effort towards enhancing the use of uranyl(VI)-complexes in controlled C-H bond activation.

Lastly, the thermal and photochemical reactivity of the uranyl(VI) ion in a carefully controlled 'Pacman' macrocyclic framework is targeted. This 'Pacman' framework has been used previously to isolate and characterise novel uranyl(V) and (VI)-based complexes, and efforts towards developing the reductive oxo-functionalisation chemistry of the uranyl(VI) ion in this framework are also targeted.

1.5 References

1. N. Seko, A. Katakai, S. Hasegawa, M. Tamada, N. Kasai, H. Takeda, T. Sugo and K. Saito, *Nucl. Technol.*, 2003, **144**, 274.
2. D. R. Lide, *CRC Handbook of Chemistry and Physics*, 85th edn., CRC Press, Boca Raton, Florida, 2004.
3. Y. I. Chang and C. E. Till, *Plentiful Energy: The Story of the Integral Fast Reactor*, CreateSpace Independent Publishing, 2011.
4. R. C. Ewing, W. J. Weber and J. Lian, *J. Appl. Phys.*, 2004, **95**, 5949.
5. R. C. Ewing, *Proc. Natl. Acad. Sci. USA*, 1999, **96**, 3432.
6. R. K. Sinha and A. Kakodar, *Nucl. Eng. Des.*, 2006, **236**, 683.
7. E. S. Craft, A. W. Abu-Qare, M. M. Flaherty, M. C. Garofolo, H. L. Rincavage and M. B. Abou-Donia, *J. Toxicol. Environ. Health B Crit. Rev.*, 2004, **7**, 297.
8. V. A. Apse, V. B. Glebov, E. F. Kryuchkov, M. S. Kushnarev and A. N. Shmelev, *Prog. Nucl. Energ.*, 2008, **50**, 643.
9. OECD Nuclear Energy Agency and IAEA, *Management of depleted uranium: a joint report*, Paris, 2001.
10. Nuclear Decommissioning Authority, *Annual Report and Accounts 2017 to 2018*, 2018.
11. S. T. Liddle, *Angew. Chem. Int. Ed.*, 2015, **54**, 8604.
12. R. G. Denning, *J. Phys. Chem. A*, 2007, **111**, 4125.
13. N. Kaltsoyannis and P. Scott, *Oxford Chemistry Primers: the f-elements*, Oxford University Press, Oxford, UK, 1999.
14. G. M. Jones, *PhD Thesis: Reduction and functionalisation of binuclear uranium-oxo complexes*, University of Edinburgh, 2013.

15. N. Kaltsoyannis, *Chem. Eur. J.*, 2018, **24**, 2815.
16. P. G. Martin, I. Griffiths, C. P. Jones, C. A. Stitt, M. Davies-Milner, J. F. W. Mosselmans, Y. Yamashiki, D. A. Richards and T. B. Scott, *Spectrochim. Acta B: Atom. Spectrosc.*, 2016, **117**, 1.
17. N. L. Newsome, K. Morris, D. Trivedi, N. Atherton and J. R. Lloyd, *Appl. Geochem.*, 2014, **51**, 55.
18. M. Amme, T. Wis, H. Thiele, P. Boulet and H. Lang, *J. Nucl. Mater.*, 2005, **341**, 209.
19. J. L. de Lemos, B. C. Bostick, A. N. Quicksall, J. D. Landis, C. C. George, N. L. Slagowski, T. Rock, D. Brugge, J. Lewis and J. L. Durant, *Environ. Sci. Technol.*, 2008, **42**, 3951.
20. F. Weigl, in *The Chemistry of the Actinide Elements*, eds. J. J. Katz, L. R. Morss and G. T. Seaborg, Chapman and Hill, London, UK, 1986.
21. J. C. Renshaw, L. J. C. Butchins, F. R. Livens, I. May, J. M. Charnock and J. R. Lloyd, *Environ. Sci. Technol.*, 2005, **39**, 5657.
22. D. L. Cologgi, A. M. Speers, B. A. Bullard, S. D. Kelly and G. Reguera, *Appl. Environ. Microbiol.*, 2014, **80**, 6638.
23. R. T. Anderson, H. A. Vrionis, I. Ortiz-Bernad, C. T. Resch, P. E. Long, R. Dayvault, K. Karp, S. Marutzky, D. R. Metzler, A. Peacock, D. C. White, M. Lowe and D. R. Lovley, *Appl. Environ. Microbiol.*, 2003, **69**, 5884.
24. T. Cheng, M. O. Barnett, E. E. Roden and J. Zhuang, *Environ. Sci. Technol.*, 2004, **38**, 6059.
25. C. J. Dodge, A. J. Francis, J. B. Gillow, G. P. Halada and C. R. Clayton, *Environ. Sci. Technol.*, 2002, **36**, 3504.
26. J. N. Fiedor, W. D. Bostick, R. J. Jarabek and J. Farrell, *Environ. Sci. Technol.*, 1998, **32**, 1466.
27. I. Farkas, I. Bányai, Z. Szabó, U. Wahlgren and I. Grenthe, *Inorg. Chem.*, 2000, **39**, 799.
28. V. Vallet, U. Wahlgren, B. Schimmelpfennig, Z. Szabó and I. Grenthe, *J. Am. Chem. Soc.*, 2001, **123**, 11999.
29. Z. Szabó and I. Grenthe, *Inorg. Chem.*, 2007, **46**, 9372.
30. F. Réal, V. Vallet, U. Wahlgren and I. Grenthe, *J. Am. Chem. Soc.*, 2008, **130**, 11742.
31. G. Meinrath, *Freiberg On-line Geosci.*, 1998, **1**, 1.
32. L. S. Natrajan, *Coordin. Chem. Rev.*, 2012, **256**, 1583.
33. A. Krestou and D. Panias, *Eur. J. Miner. Process. Environ. Protect.*, 2004, **4**, 113.
34. L. Ciavatta, D. Ferri, I. Grenthe and F. Salvatore, *Inorg. Chem.*, 1981, **20**, 463.
35. T. Vercouter, P. Vitorge, B. Amekraz and C. Moulin, *Inorg. Chem.*, 2008, **47**, 2180.
36. W. J. Harrison, *A History of Photography*, Scovill Manufacturing Company, New York, 1887.
37. J. C. Eisenstein and M. H. L. Pryce, *Proc. R. Soc. Lond. A*, 1955, **229**, 20.
38. J. T. Bell and R. E. Biggers, *J. Mol. Spectrosc.*, 1965, **18**, 247.
39. J. T. Bell and R. E. Biggers, *J. Mol. Spectrosc.*, 1968, **25**, 312.
40. R. G. Denning, *Struc. Bond.*, 1992, **79**, 215.
41. H. D. Burrows and T. J. Kemp, *Chem. Soc. Rev.*, 1974, **3**, 139.
42. R. Ghosh, J. A. Mondal, H. N. Ghosh and D. K. Palit, *J. Phys. Chem. A*, 2010, **114**, 5263.
43. K. Vidya, V. S. Kamble, P. Selvam and N. M. Gupta, *Appl. Catal. B: Environ.*, 2004, **54**, 145.
44. V. Krishna, V. S. Kamble, N. M. Gupta and P. Selvam, *J. Phys. Chem. C*, 2008, **112**, 15832.
45. A. F. Leung, L. Hayashibara and J. Spadaro, *J. Phys. Chem. Solids*, 1999, **60**, 299.
46. S. J. Formosinho, M. G. M. Miguel and H. D. Burrows, *J. Chem. Soc., Faraday Trans. 1*, 1984, **80**, 1717.
47. A. D. McNaught and A. Wilkinson, *IUPAC Compendium of Chemical Terminology (the "Gold Book")*, 2nd edn., IUPAC and Blackwell Scientific Publications, Oxford, 1997.
48. J. R. Lakowicz, *Principles of Fluorescence Spectroscopy*, 3rd edn., Springer, Heidelberg, 2006.

Chapter 2: Synthesis and Characterisation of New Photoactive Uranyl(VI) and Neptunyl(VI) Complexes

---

2.1 Introduction

In order to synthesise effective uranyl(VI)-based photocatalysts, there are several properties that are *essential* to a ligand for it to be useful for the purposes of this investigation (the 'design principles'):

1. resistant to photolysis (*e.g.* be suitable for use as a photocatalyst),
2. solution stable upon complexation to $U^{VI}O_2^{2+}$ (*e.g.* ideally with known speciation in solution, making the computational and theoretical modelling of the target compound easier),
3. soluble in organic solvents (*e.g.* CH_3CN, optically transparent at 420 nm, $\lambda_{max}(U^{VI}O_2^{2+})$, and oxidatively inert).

Additionally, *advantageous* properties for any candidate ligands are that they should be:

4. simple to synthesise (or, better, commercially available, and therefore convenient to obtain),
5. in fulfilment of the CHON principle (*e.g.* contain only C, H, O and N, being cleanly incinerable and resistant to α-radiolysis),[1]
6. resistant to protonation (reducing competing pathway to complexation of UO_2^{2+}),
7. already known as ligands for UO_2^{2+} in chemical industry,
8. easily characterisable (by ^{1}H NMR or IR spectroscopy, *etc*.),
9. known to modify the luminescent properties of metal centres.

Some potential ligands that meet criterion 7 (*e.g.* are already used widely in industrial processes involving the uranyl(VI) ion) such as TBP (tri-*n*-butyl-phosphate, $(^n BuO)_3PO$), which is used in the solvent separation of spent nuclear fuels (Section 2.1.3), could be very easily applied if found to impart unique photochemical reactivity on the uranyl ion.

Many different ligand classes have been complexed to the uranyl(VI) ion, including ketone[2] and ketonate,[3] oxime,[4] semicarbazone,[5] thiosemicarbazone,[6] crown ether,[7] aza-crown,[8] hydrazide,[9] hydrazone,[10] salen- (*N*,*N*'-ethylenebis(salicylimine)) and derivatives,[11, 12] *N*-heterocycle,[13, 14] phthalate,[15, 16] phospha-oxo,[17, 18] and monodentate,[19] bidentate,[20] or multidentate[21] amide ligands. It is clearly impossible to review all of the relevant literature here, and readers are instead referred to other texts for a more authoritative treatment on this subject.[22]

However, one class of ligands that matches nearly all of these criteria are simple *N*-heterocycle ligands, namely, 1,10-phenanthroline (phen), 2,2′-bipyridine (bipy) and 2,6-bis(2-pyridyl)pyridine (terpy). These ligands are soluble in a variety of organic solvents, resist photolysis, are solution stable (owing to formation of pentahedral chelate rings on coordination to a metal ion; the chelate effect), are commercially available, fulfil the CHON principle, and are easily characterisable (*e.g.* ^{1}H NMR spectroscopy). Additionally, although phen, terpy or bipy ligands are not themselves currently used in actinide reprocessing, structural analogues of these ligands, bis-triazinyl bipyridine ligands, BTBs, are proposed as alternatives to ubiquitous TBP ligands, particularly in the processing of uranyl-containing wastes.[14] These ligands are known to not be susceptible to radiolysis, unlike TBP, which slowly degrades from α-radiolysis. One disadvantage of using *N*-heterocycles is their susceptibility to protonation, however (phen, bipy and terpy are all effective as both Lewis and Brønsted bases), and this is discussed further in Section 2.2.4.

2.1.1 *f*-Element Complexes with Simple *N*-Heterocycle Ligands and Redox Non-innocence

While there are no studies examining the potential redox non-innocence of phen, terpy or bipy ligands with uranyl(VI), there have been several examples with other *f*-block complexes in lower oxidation states. These include [$(Cp^*)_2Yb^{II}$(phen)] (**2.A**),[23] [$(Cp^*)_2U^{III}$(bipy)] (**2.B**),[24] [$(Tp^*)_2U^{III}$(bipy)] (**2.C**, Tp* = hydrotris(3,5-dimethylpyrazolyl)borate),[25] [$(Cp^*)(C_8H_8)U^{III}(Me_2bipy)$] (**2.D**),[26] [$(Ar(R)N)_2U^{III}(bipy)_2$] (**2.E**, Ar = 3,5-$C_6H_3Me_2$; R = ^{t}Bu or Ad, where Ad = 1-adamantyl),[27] and $[Na(THF)_6][U(bipy)_4]$ (**2.F**).[28] In these examples of U^{III}-bipy complexes, researchers are primarily concerned with probing the unique redox properties imparted by ligand redox non-innocence on the uranium centre rather than exploring unique chemical and photochemical reactivity.

In [$(Cp^*)_2Yb^{II}$(phen)] (**2.A**), however, the phen ligands are present as the radical anion, phen$^{\bullet-}$, and were observed to undergo reversible C-C bond formation and cleavage (Scheme 2.1), highlighting the potential that phen ligands have to participate in unusual chemistry with *f*-elements.[23]

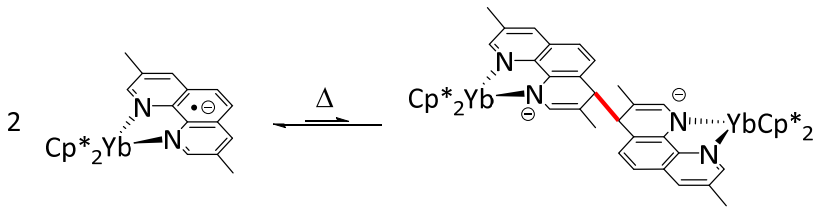

Scheme 2.1 – Reversible dimerization of [$(Cp^*)_2Yb^{II}$(phen)] (**2.A**) involving formation of a new C-C bond on the phen ligand. The dimeric and monomeric forms are interchanged at high temperature, with dimeric form thermolysing at > 180 °C.

Additionally to the *N*-heterocyclic complexes of uranium described in above, a number of non-*N*-heterocyclic ligand complexes of the uranyl(VI) ion are known, particularly ones incorporating redox non-innocent ligands. These include $[U^{x+}O_2(gha)(DMSO)]^{n-}$ (**2.G**, gha = glyoxal bis(2-hydroxanil)ate),

present as [gha]$^{\bullet 3-}$; x = 5, n = 1; x = 6, n = 0),[29] [$U^{VI}O_2$(phen-BIAN)]$_2$ (**2.H**, phen-BIAN = *N*,*N*′-bis-(iminophenol)acenaphthene),[30] [(Cp*)$U^{VI}O_2$(^{t}Bu-^{Mes}PDI^{Me})] (**2.I**, ^{t}Bu-^{Mes}PDI^{Me} = 2,6-((Mes)-N=CMe)$_2$-*p*-C(CH$_3$)$_3$C$_5$H$_2$N; Mes = 2,4,6-trimethylphenyl),[31] [$U^{VI}O_2$Cl(L)] (**2.J**, L = an acyclic diimino-dipyrrin radical anion, see Figure 2.1),[32] [$U^{VI}O_2$(salophen)(OH$_2$)] (**2.K**, salophen = *N*,*N*′-bis(3-tert-butyl-(5*R*)-salicylidene)-1,2-phenylenediamine),[33] [Et$_4$N]$_3$[$U^{VI}O_2$(NCSe)$_5$] (**2.L**) where the radical is delocalised across all five isoselenocyanato ligands,[34] or [$U^{VI}O_2$(^{dipp}isq)$_2$] (**2.M**, ^{dipp}isq = di-*iso*propylphenyliminosemiquinone, a monoanionic ligand).[35] These are summarised in Figure 2.1, below. Considering the redox non-innocence of uranyl(VI)-bound ligands becomes important when the possibility of ligand-centred radicals are generated, as discussed in Section 2.2.2 (and Figure 2.16).

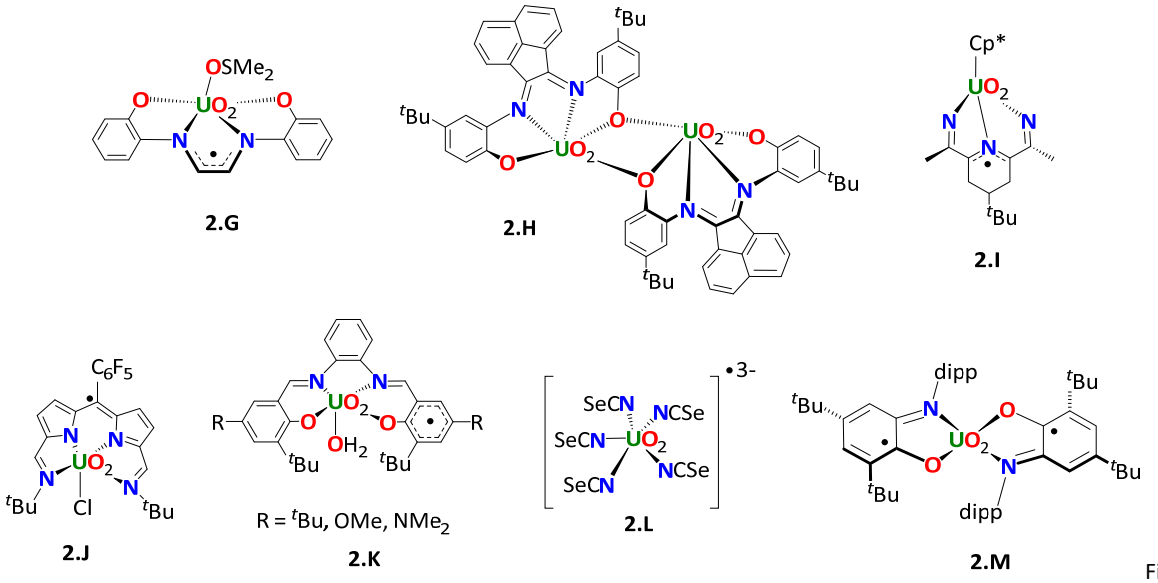

Figure 2.1 – Examples of uranyl complexes reported to have redox non-innocent ligands. Structures in which authors have highlighted localisation of electron density are shown as the radical. Cp* is C$_5$Me$_5$; dipp is 2,6-di-*iso*-propylphenyl.

This point is further evidenced by the synthesis and photochemical characterisation of a series of solid-state uranyl coordination polymers incorporating either terpy[36, 37] or bipy[38] functionalities. In these reports the effect of the ligand on the luminescence properties of the uranyl ion are often poorly rationalised, with other properties of the materials, such as halogen bonding or supramolecular behaviour[37] overshadowing considerations of the uranyl luminescence.

Therefore, in order to investigate the effect of simple *N*-heterocycles on the luminescence properties of uranyl, phen, terpy and bipy ligand complexes of uranyl will be synthesised, and their chemical and photochemical behaviours investigated. These reactions are outlined in Section 2.2.

2.1.2 *N*-Heterocycle Complexes of the Neptunyl(VI) Ion

While the photochemistry of the uranyl(VI) ion is well-established, the photochemistry of the transuranic actinyl ions, in particular $Np^{V}O_2^{+}$, $Np^{VI}O_2^{2+}$ and $Pu^{VI}O_2^{2+}$, is comparatively much less well-

developed, with many fewer reports examining the photochemistry of these species in solution.[39] These studies tend to focus on the practical utility of photochemical redox processes in aiding the remediation of transuranic effluent streams; Section 3.1.5.

To the best knowledge of the author, there are no studies that examine the use of Np^{VI} for other photochemical transformations, including photocatalytic reactions. These may be important as photochemical reactions of Np^{IV}, Np^{V} and Np^{VI} carbonate solutions (which are often present in Np-contaminated water) are known to influence the neptunium speciation (*e.g.* at $[CO_3^{2-}]_{(aq)}$ and $[HCO_3^-]_{(aq)}$ > 1M, $[Np^{VI}O_2(CO_3)_2]^{2-}$, $[Np^{VI}O_2(CO_3)_4]^{2-}$, $[Np^{VI}O_2(OH)_2(CO_3)]^{2-}$, *etc.*, dominate) and therefore environmental mobility on exposure to sunlight (*e.g.* decreasing $[CO_3^{2-}]$ or $[HCO_3^-]$ (*cf.* decreasing pH or increasing $[H^+]$) increases rate of $Np^{VI}O_2^{2+}$ photoreduction in water).[40] The inherent redox instability of the neptunyl(VI) ion in solution compared to neptunyl(V)[41] makes investigating the photochemical properties of this ion (Np^{VI}) considerably harder than the analogous uranyl(VI) ion. For example, the neptunyl(VI) chloride-THF solvate $[Np^{VI}O_2Cl_2(THF)]_n$ (**2.N**) undergoes partial or complete reduction to the corresponding Np^{V} salt in THF or methanol solvent (*e.g.* $[(Np^{VI}O_2Cl_2)(Np^{V}O_2Cl(THF)_3)_2]$, **2.O**)[42] and addition of 18-crown-6 to a solution of $Np^{VI}O_2^{2+}$ in perchloric or triflic acid results in the isolation of the corresponding $Np^{V}O_2^+$ crown ether complex $[Np^{V}O_2(18\text{-crown-6})][A]$ (where A = ClO_4 (**2.P.1**) or OTf (**2.P.2**)), which persists even in the presence of ozone as an oxidant.[43] Nevertheless, several redox-stable $Np^{VI}O_2^{2+}$ complexes have been reported, including $[Np^{VI}O_2(salen)(MeOH)]$ (**2.Q**),[44] $[Np^{VI}O_2(TPIP)_2(OPPh_3)]$ (**2.R**, TPIP = tetraphenylimidodiphosphinato),[41] $[Np^{VI}O_2(DPPMO_2)_2Cl]_2[Np^{VI}O_2Cl_4]$ (**2.S**) and $[Ph_3PNH_2]_2[Np^{VI}O_2Cl_4]$ (**2.T**) ($DPPMO_2$ = bis(diphenylphosphino)methanedioxido),[45] and $Np^{VI}O_2^{2+}$ acetates, $[Np^{VI}O_2(OAc)_x]^n$ (**2.U.1**, x = 1, n = 1+; **2.U.2**, x = 2, n = 0; **2.U.3**, x = 3, n = 1-).[46] These are shown in Figure 2.2, and **2.AC**, in Figure 2.3.

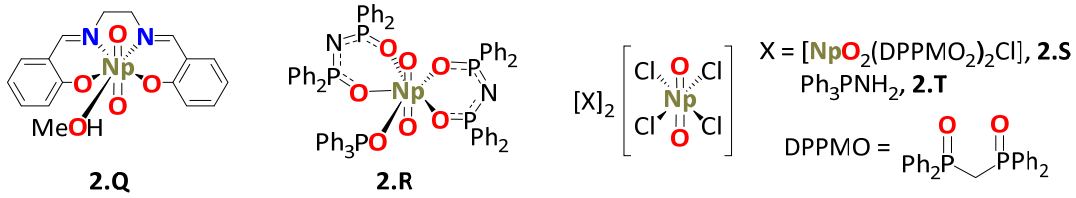

Figure 2.2 – Examples of structurally-characterised, redox-stable neptunyl complexes. The Np oxidation state in all of these complexes is VI; *e.g.*, $Np^{VI}O_2^{2+}$.

Similarly to uranyl(VI) complexes with phen, terpy or bipy and related *N*-heterocycles, it was envisaged that the coordination of these ligands may result in enhanced photochemical stability of the neptunyl(VI) ion (*e.g.* by increasing the longevity of $*Np^{VI}O_2^{2+}$). Several reports of the coordination chemistry of $Np^{V}O_2^+$ or $Np^{VI}O_2^{2+}$ with phen, terpy or bipy ligands are known (see Figure 2.3), including the neptunyl(V) complexes $[Np^{V}O_2(phen)(AcOPh)]$ (**2.V**),[47] $[Np^{VI}O_2(phen)(\mu\text{-}F)(F)]_2$ (**2.W**),[48]

$[Np^{V}O_2(Re^{VII}O_4)(phen)(OH_2)_2]$ (**2.X**),[49] $[Np^{V}O_2(N_3)(phen)(OH_2)]_2{\cdot}3H_2O$ (**2.Y**),[50] $[Np^{V}O_2(NO_3)(terpy)(OH_2)]$ (**2.Z**),[51] $[Np^{V}O_2(CH_3SO_3)(terpy)(OH_2)]{\cdot}2H_2O$ (**2.AA**),[52] and the neptunyl(VI) complexes $[Np^{VI}O_2(bipy)(AcOPh)_2]$ (**2.AB**),[53] and $[Np^{VI}O_2(bipy)(NO_3)_2]$ (**2.AC**).[54, 55]

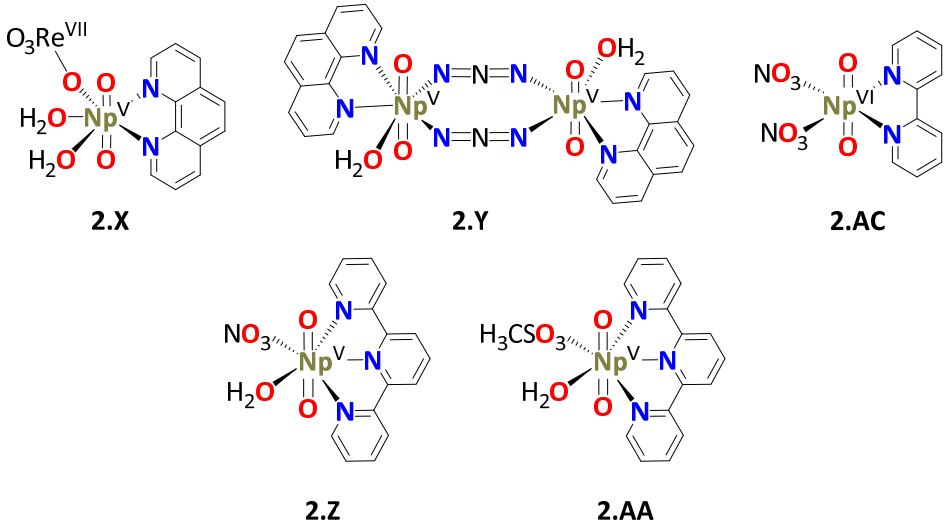

Figure 2.3 – Examples of structurally-characterised, *N*-heterocycle complexes of the $Np^{V}O_2^{+}$ or $Np^{VI}O_2^{2+}$ ion.

In the majority of these reports only the solid-phase properties are reported, with little information on solution-phase behaviour being presented; this is therefore a focus of this thesis.

2.1.3 Amide Complexes of the Uranyl Ion

Uranium (and plutonium) are extracted from spent nuclear fuel *via* the PUREX process (plutonium-uranium redox extraction). This process, summarised in Figure 2.4, relies on selective extraction of uranyl- and plutonium-nitrates from a nitric acid/kerosene mixture, using TBP as the extractant.[56]

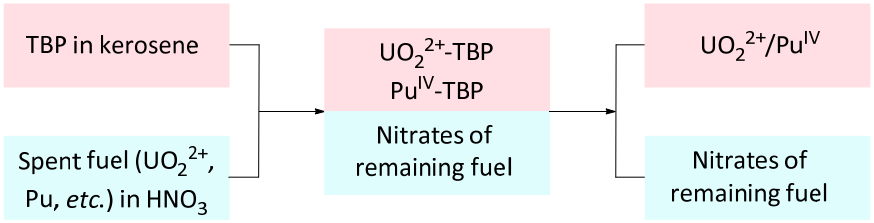

Figure 2.4 – Summary of key stages in the PUREX process. U^{VI} and Pu^{IV} are selectively extracted into an organic solution and, following further treatment steps after solvent separation, as the oxides, $U^{IV}O_2$ and $Pu^{IV}O_2$.

Mono-amide ligands were first postulated as alternatives to TBP for actinide solvent extraction during the 1950s[57] and 1960s[58] owing to their advantages over organo-phosphorus analogues[59] (*e.g.* TBP) for enhanced radiolytic and hydrolytic stability and cleaner disposal pathways (incineration).[60] Consequently, there are many examples of organic amide ligands complexed to the uranyl(VI) ion, including monodentate amides ($R\text{-}CONR_2$), bidentate amides ($R_2NCO\text{-}(CH_2)_n\text{-}CONR_2$) or tridentate di-

amide (R_2NCO-$(CH_2)_m$-X-$(CH_2)_n$-$CONR_2$), where R = H, an alkyl or aryl group, X is a donor atom O or N, and m and n are integer values. Examples of these classes of ligands are shown below in Figure 2.5.

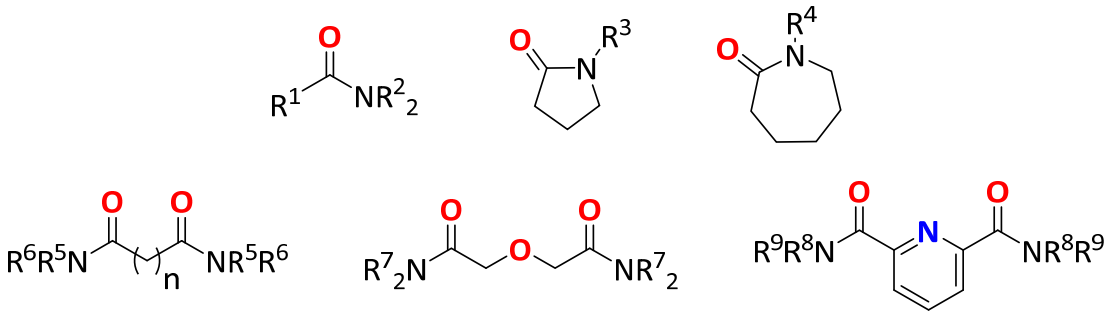

Figure 2.5 – Representative examples of mono- and di-amide ligands used to complex uranyl. R^1 = ^{i}Pr, R^2 = ^{i}Pr, ^{i}Bu or ^{s}Bu;[61] R^1 = R^2 = ^{i}Pr;[62] R^1 = C_5H_{11} (neopentyl), R^2 = ^{n}Bu;[63] R^1 = $C_{11}H_{23}$, R^2 = ^{n}Bu;[64] R^3 = H, ^{n}Pr, ^{i}Pr, ^{s}Bu, ^{t}Bu, *etc.*;[65] R^3 = C_5H_9;[66] R^4 = H;[67] R^4 = Et;[68] R^5 = R^6 = C_6H_{13}, n = 1;[20] R^5 = R^6 = Et, n = 1–6;[69] R^5 = R^6 = Me, n = 1;[70] R^5 = Ph, R^6 = Me, n = 1;[71] R^7 = Me;[21] R^7 = ^{i}Pr;[72] R^8 = R^9 = ^{i}Pr, ^{t}Bu or ^{s}Bu;[73] R^8 = Et, R^9 = ^{p}tolyl.[74]

Two main classes of mono-amide ligands are typically employed in solvent extraction studies of the uranyl ion, *N,N*-alkylated mono-amides,[61-64] and cyclams, including *N*-alkylated pyrrolidone,[65, 75, 76] and caprolactams.[67, 68] For diamides, this is expanded to give uranyl(VI) complexes of bidentate diamides, R_2NCO-$(CH_2)_n$-$CONR_2$ where n = 1[20, 70, 71, 77] and 2–6,[69] and tridentate diamides, including diglycolamides[21, 72, 78] and picolinamides.[73, 74, 79]

Amide ligands are employed in this study as these are widely soluble in organic solvents (criterion 3), simple to synthesise (*e.g.* acid chloride/amine condensation, or are commercially available, criterion 4), in agreement with the CHON principle (criterion 5), are able to resist protonation (extractions are often performed in concentrated acid, criterion 6), and are easily characterisable (*e.g.* ^{1}H NMR spectroscopy, ν(C=O) in IR spectroscopy, criterion 8).

2.1.4 Oxime Complexes of the Uranyl Ion

Motivated by the damaging effects of uranium mining, the extraction of uranium from alternative sources remains an important target for chemists. Here, although the concentration of uranium in seawater is very low ($\sim$ 3 ppb), the total estimated resources of uranium are *ca*. 4.5 billion tonnes,[80] enough to meet current and projected demand virtually indefinitely. Among the most effective methods to extract this uranium is the adsorption of aqueous uranyl ions to polymer nets onto which oxime and aldoxime materials are grafted.[81] The efficacy of this approach was highlighted by Japanese researchers in a series of extraction trials in the Pacific Ocean, where between 1999 and 2002 approximately 1 kg of uranium oxides (U_3O_8, UO_2, UO_3) were isolated from polythene fibres grafted with aldoxime ligands.[82]

In light of these and other studies examining the binding of oxime ligands with the uranyl ion, including ethanediamidoxime,[83] salicylaldoxime,[84] glutardiamidoxime,[85] amidoximes,[86] and pyridyl-oximes,[4] (Figure 2.6) it was decided that the third class of ligands examined for the synthesis of new photoactive uranyl complexes would be oximes. The chemistry of these complexes is discussed in Section 2.6. The use of oxime ligands fulfils many of the criteria outlined in Section 2.1, being soluble in a number of organic solvents, commercially available, in agreement with the CHON principle, and easily characterisable (*e.g.* ^{1}H NMR spectroscopy, ν(C=N) and ν(O-H) by IR spectroscopy). Oximes are also becoming industrially relevant, with several projects established by the United States' Department of Energy Office of Nuclear Energy Fuel Resources Program (*e.g.* ORNL/TM-2013/295) examining the feasibility of using oximes for commercial uranium extraction from seawater.

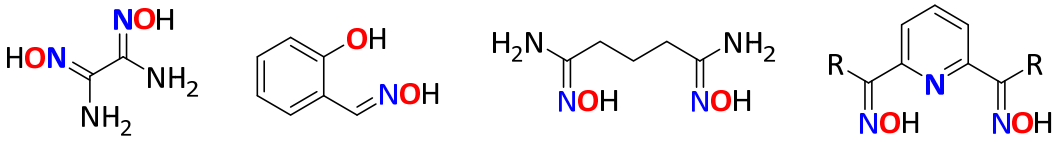

ethane-diamidoxime | salicylaldoxime | glutardiamidoxime | pyridyl-oximes *R = H, Me, Ph, CN*

Figure 2.6 – Examples of ligands previously employed to study the behaviour of oxime ligands with the uranyl(VI) ion.

Indeed, a very recent report has highlighted the effect that pyridyl-oxime ligands can have on the emissive properties of $U^{VI}O_2^{2+}$. For example, fluorescence emission in $[U^{VI}O_2Cl(dapdoH)]_2$ (**2.AD**, see Figure 2.7, $dapdoH_2$ = diacetylpyridine dioxime), centred at 499 nm, is blue-shifted compared to the parent uranyl acetate, $[U^{VI}O_2(OAc)_2]$ (**U^{OAc}**).[87]

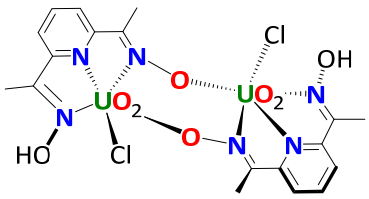

2.AD

Figure 2.7 – Structure of the dimeric complex $[U^{VI}O_2Cl(dapdoH)]_2$ (**2.AD**).[87]

Although this was poorly explained by the authors, this suggests that oxime ligands may, with further investigation, be useful in tuning the photochemical properties of the uranyl ion in future.

2.1.5 Anaerobic Uranyl Complexes

The literature contains many examples of the aerobic photochemical reactivity of the uranyl ion, as outlined in Section 3.1. However, there is a comparative paucity of literature examining the anaerobic photoreactivity of the uranyl(VI) ion. The exclusion of dioxygen from photocatalytic reactions involving

the $*U^{VI}O_2^{2+}$ ion can lead to non-oxygenated products being formed. This provides the opportunity to access new substrate reactivity, for example, C-H bond fluorination,[88] and is discussed more fully Sections 3.6 and 4.3.

2.2 Complexes of the Uranyl Ion with *N*-heterocycles

2.2.1 Synthesis and Characterisation of $[UO_2(NO_3)_2(Ph_2phen)]$, $\mathbf{U^{Ph2phen}}$

It is known that 4,7- and 2,9-disubstituted phenanthroline ligands with aromatic appendages possess enhanced fluorescent properties compared to phen,[89] as the gap between the π and π* molecular orbitals (*e.g.* upon excitation, the π-π* state) in phen ligands, which are normally far apart in energy, is reduced by extending conjugation. For phen ligands the π-π* state is emissive, leading to a low quantum yield with poor fluorescence efficiency when the energy gap between π and π* molecular orbitals is large. Extending the conjugation, for example by attaching aromatic groups to the phen framework, reduces this energy gap, increasing the population of this emissive π-π* state and thus the quantum yield; phen in CH_2Cl_2 at r.t. is 0.0087, compared to 0.16 for the symmetrically substituted 2,9-diphenyl-1,10-phenanthroline, under analogous conditions.[90]

However, as a 2,9-substitution pattern on the phen ligand was shown to prevent complexation to the uranyl ion (**2.1.Me$_2$phen** and **2.1.Me$_2$Ph$_2$phen**, Scheme 2.3, Section 2.2.4), the 4,7-disubstituted phenanthroline, 4,7-diphenyl-1,10-phenanthroline, Ph_2phen, was used instead, where it was complexed to uranyl nitrate hexahydrate, $[UO_2(NO_3)_2(OH_2)_2]\cdot 4H_2O$, $\mathbf{U^{NO3}}$, in CH_3CN solvent. The resulting complex, $[UO_2(NO_3)_2(Ph_2phen)]$, $\mathbf{U^{Ph2phen}}$, is isolated as a dark yellow powdery solid in 94% yield, as depicted in Scheme 2.2, below.

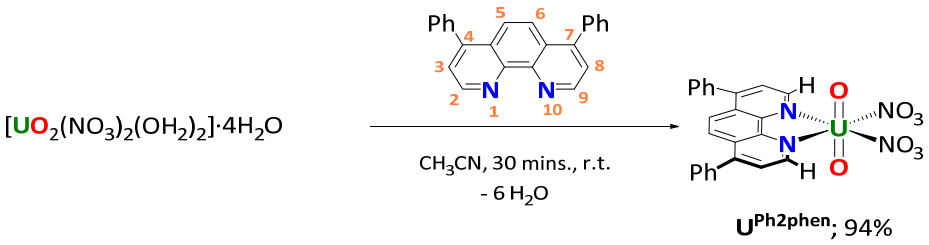

Scheme 2.2 – Synthesis of $\mathbf{U^{Ph2phen}}$. A numbering scheme for the phen ligand is given in orange.

All characterisation data are consistent with the formulation of $\mathbf{U^{Ph2phen}}$, and are distinct from those of free Ph_2phen, protonated Ph_2phen ($[Ph_2phen\text{-}H][CF_3CO_2]$) and $\mathbf{U^{NO3}}$. The solution-phase ^1H NMR spectrum of $\mathbf{U^{Ph2phen}}$ has resonances at 10.56, 8.36, 8.31, 7.70 and 7.64 ppm, shifted to higher frequencies from those of free (9.17, 7.86, 7.64 and 7.57 ppm) or protonated (9.25, 8.19, 8.13 and 6.56 ppm) Ph_2phen. Most notable is the large (1.4 ppm) shift (to higher frequencies) of the protons at the 2- and 9-positions between $\mathbf{U^{Ph2phen}}$ and uncomplexed Ph_2phen. These are the closest (spatially

and through-bond) protons to the U^{VI} centre, and thus experience the greatest deshielding effect upon complexation (but, to clarify, this does not indicate U-H interactions, only that these are closest to the Lewis acidic U^{VI} centre). **$U^{Ph2phen}$** is also air- and moisture-stable for > 12 months, with no degradation observed by ^{1}H NMR spectroscopy on this timescale. Indeed, addition of successive equiv. of water to an NMR sample of **$U^{Ph2phen}$** in CD_3CN showed that an approximately thirty-fold excess of water is required to observe signal broadening in the ^{1}H NMR spectra of this mixture, Figure 2.8, below. This probably results from dynamic exchange of the Ph_2phen ligand with the increasing amounts of water.

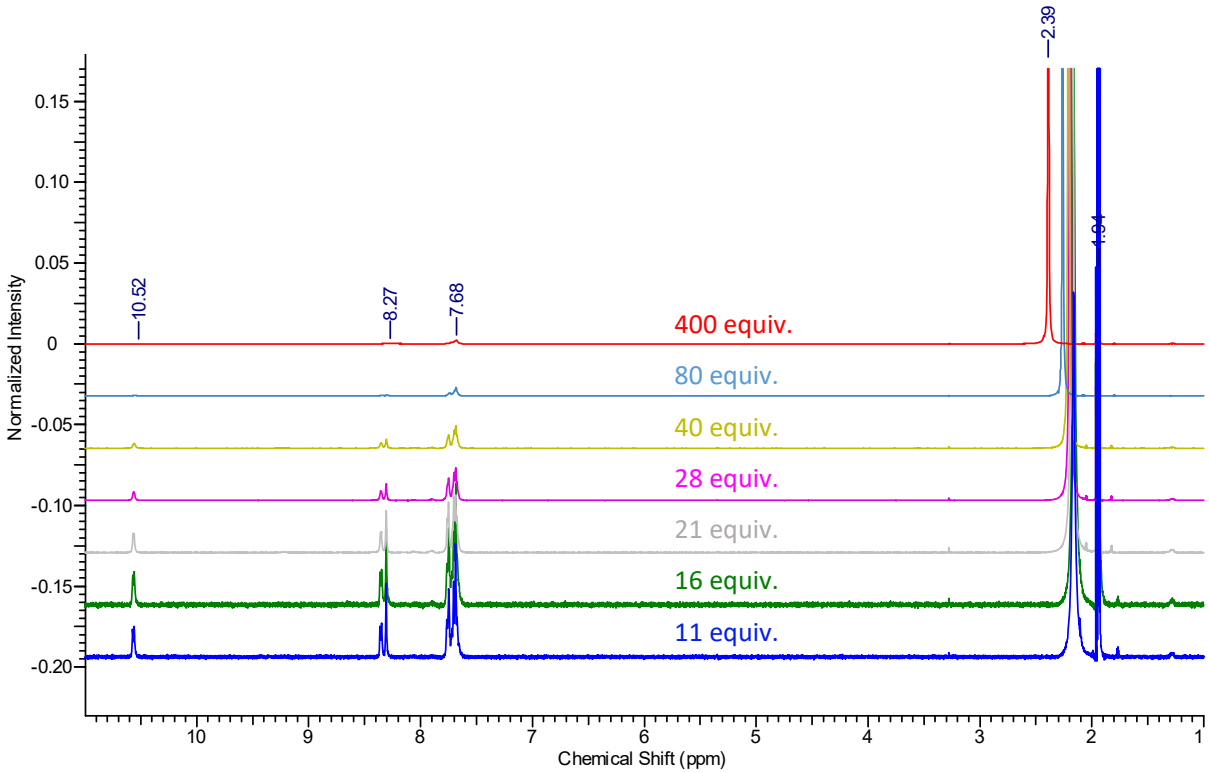

Figure 2.8 – ^{1}H NMR spectra of **$U^{Ph2phen}$** with increasing equivalents of water in wet (ca. 11.5 equiv. of water) CH_3CN.

Compared to **U^{NO3}**, which is a hexahydrate, the IR spectrum of **$U^{Ph2phen}$** exhibits no broad O-H stretching band at *ca*. 3400 cm^{-1}, indicating that **$U^{Ph2phen}$** is anhydrous. Although $\nu(NO_3)$ shifts by *ca*. 40 cm^{-1} from **U^{NO3}** (1301, 1332 cm^{-1}) to **$U^{Ph2phen}$** (1253, 1270 cm^{-1}), the retention of the bidentate binding mode of nitrato ligands is indicated. The ν_{asym}(U=O) at 936 cm^{-1} (IR) or ν_{sym}(U=O) at 867 cm^{-1} (Raman) are the same between **U^{NO3}** and **$U^{Ph2phen}$**, suggesting the strength of the U^{VI}=O_{yl} bonds are minimally affected by phenanthroline coordination. These values are comparable to the phenanthroline complex $[UO_2(NO_3)_2(phen)]$, **U^{phen}**, which has a bidentate nitrato stretch (ν_4) centred at 1286 cm^{-1} and ν_{asym}(U=O) at 942 cm^{-1}.[91]

The solid-state structure of **$U^{Ph2phen}$** (Figure 2.9, Table 2.1) is unremarkable in terms of U^{VI}=O_{yl} parameters, with the central UO_2(phen) motif analogous to the parent **U^{phen}** complex.[92]

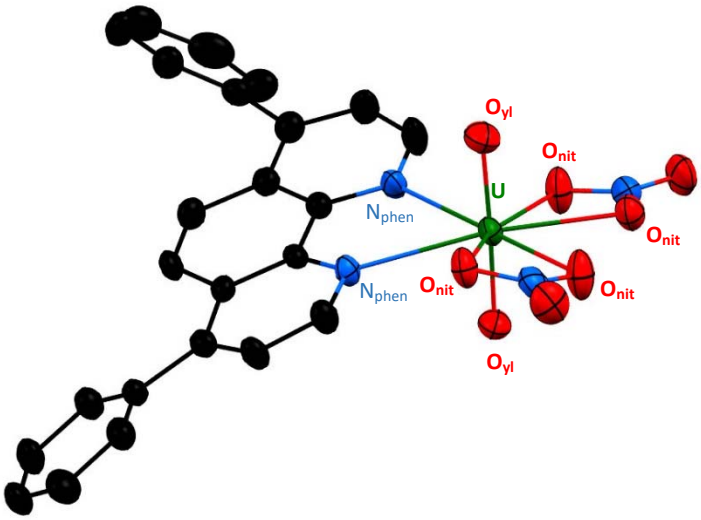

Figure 2.9 – Thermal ellipsoid plot of **U^{Ph2phen}**. Ellipsoids drawn at 50% probability, and H-atoms are omitted for clarity. Key: uranium, oxygen, nitrogen, carbon.

Parameter	U^{Ph2phen}	U^{phen}, [UO$_2$(NO$_3$)$_2$(phen)] [92]
U=O$_{yl}$ distance, d(U=O$_{yl}$)	1.747(3), 1.756(3)	1.735(10)
U-O$_{nitrate}$ distance, d(U-O$_{nit}$)	2.473(3)–2.501(3)	2.491(12)
U-N$_{phen}$ distance, d(U-N$_{phen}$)	2.589(3), 2.625(4)	2.556(22)
O-U-O angle, ∠(OUO)	177.28(14)	178.7(7)

Table 2.1 – Key parameters (bond lengths/Å, and angles/°) for the solid-state structures of **U^{Ph2phen}** compared **U^{phen}**, with uncertainties in parentheses.

The unit cell contains two crystallographically-independent molecules, with distorted hexagonal bipyramidal (8-coordinate) uranium centres. There is distortion of the ligand away from the essentially idealised perpendicular plane of the nitrate ligands by 21.9° (Figure 2.10a), comparable to analogous *N*-heterocycle complexes of the uranyl(VI) ion with bipy (25.3°)[54] and phen (20.4° for **U^{phen}**).[92] The phenyl rings on the Ph$_2$phen backbone are also twisted from planarity, which is the structure adopted in the free ligand (uncomplexed Ph$_2$phen is flat). The twisting of the phenyl rings and structural distortion of the ligand in the **U^{Ph2phen}** complex likely arises from extended packing in the crystal structure, in which (sandwich-type) π-π stacking (Figure 2.10b) between two **U^{Ph2phen}** molecules occurs at an approximate distance of 3.8 Å with the planar portions of the Ph$_2$phen ligands aligning.

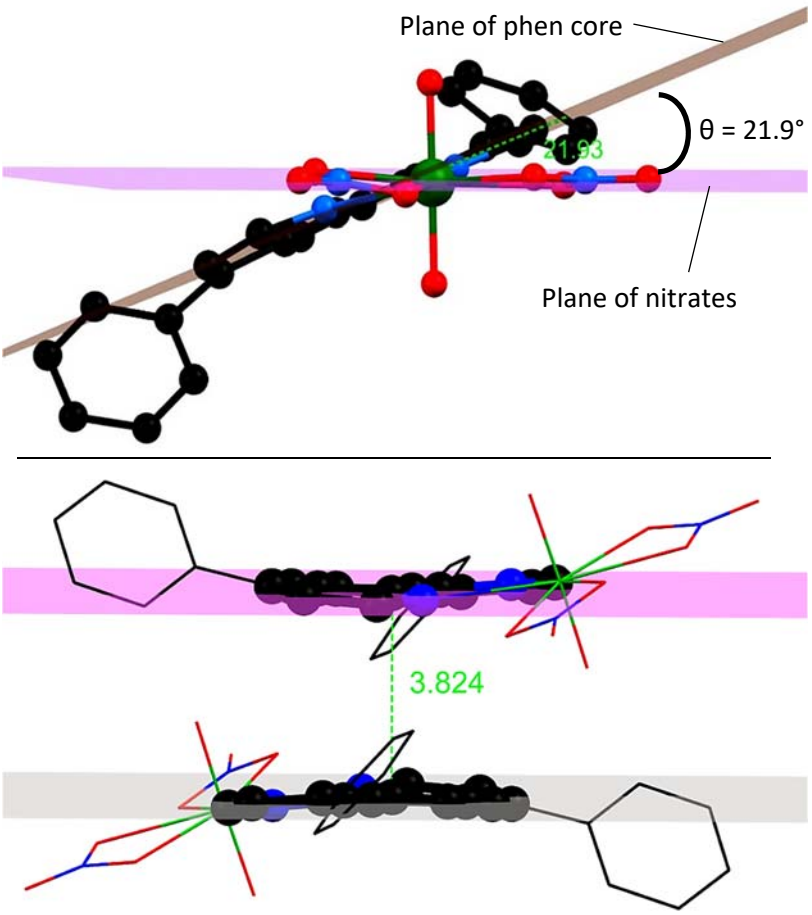

Figure 2.10a (top) – Ball-and-stick representation of one molecule of $\mathbf{U^{Ph2phen}}$, showing the plane of ligand twisted away from the plane of the nitrate groups; Figure 2.10b (bottom) – Two molecules of $\mathbf{U^{Ph2phen}}$ showing the distance between two bisecting planes through the planar fragment of the Ph_2phen ligand. Key: uranium, oxygen, nitrogen, carbon. Selected portions of the $\mathbf{U^{Ph2phen}}$ molecules in the bottom picture are depicted as a 'wireframe' for clarity.

Complexation of Ph_2phen to $\mathbf{U^{NO3}}$ is also indicated by gas-phase characterisation, with high-resolution electrospray ionisation-mass spectrometry, ESI-MS, showing signals consistent with $[UO_2(NO_3)(Ph_2phen)\text{-}H]^+$, $[UO_2(NO_3)(Ph_2phen)\text{-}Na]^+$ and $[UO_2(NO_3)(Ph_2phen)_2]^+$ at 665.268, 687.250 and 996.282 Da, respectively. These data are given in full in section 5.2.1.

2.2.2 Photo- and Redox-stability, and Electronic Spectroscopy of $\mathbf{U^{Ph2phen}}$

With $\mathbf{U^{Ph2phen}}$ in hand, the photolytic and redox stability of $\mathbf{U^{Ph2phen}}$ was then examined. If $\mathbf{U^{Ph2phen}}$ was found stable to photo-degradation, then the complex would serve as an expedient route into modifying the photochemistry of the uranyl(VI) ion, particularly given the use of phenanthrolines as important ligands in uranium and neptunium chemistry (Sections 2.1.1 and 2.1.2).

Although the complex is sparingly soluble in CH_3CN (*ca*. 3 mg mL^{-1}), CH_3CN was selected as the solvent of choice as it is oxidatively inert, optically transparent to λ_{max} for the uranyl(VI) ion (*ca*. 420 nm), and has been previously employed in photocatalytic studies involving uranyl(VI) complexes.[88] To test its photostability, a saturated solution of $\mathbf{U^{Ph2phen}}$ in CH_3CN was irradiated overnight (16 hours), and ^1H

NMR spectra before and after irradiation were compared. No discernible changes were observed by ^{1}H NMR spectroscopy and therefore the photochemical properties of $\mathbf{U^{Ph2phen}}$ were further analysed by electronic absorption spectroscopy in CH_3CN, Figures 2.11 and 2.12.

The redox stability of $\mathbf{U^{Ph2phen}}$ was also tested by addition of *ca*. one equiv. of KC_8 or $[Co^{II}(C_5Me_5)_2]$ to saturated solutions of $\mathbf{U^{Ph2phen}}$ in CH_3CN under inert atmosphere. In both cases, ^{1}H NMR spectroscopy showed resonances consistent with free ligand, suggesting the complex is unstable in the presence of strong reducing agents; attempts to gain further insight into these process by electrochemical, spectroelectrochemical or Raman spectroscopies (*e.g.* to determine the presence of Ph_2phen radicals generated *in-situ* at a specified potential)[93, 94] were unsuccessful.

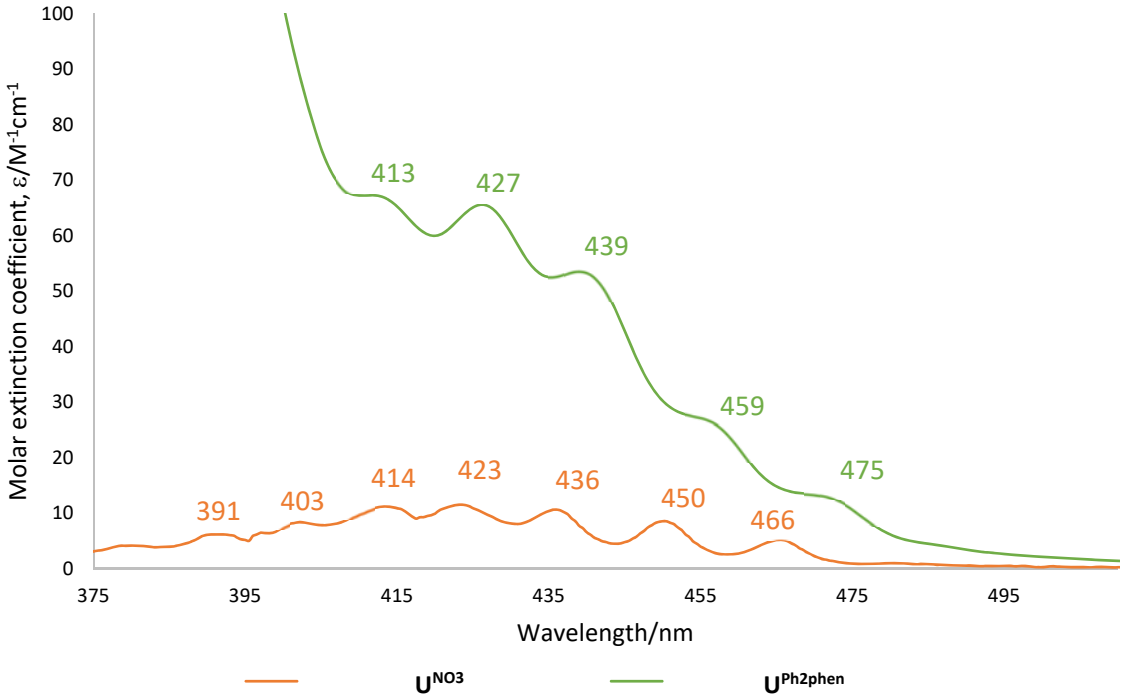

Figure 2.11 – Electronic absorption spectra of $\mathbf{U^{NO3}}$ (ORANGE) and $\mathbf{U^{Ph2phen}}$ (GREEN) in CH_3CN; $[\mathbf{U^{NO3}}] = 1.13 \times 10^{-3}$ M, $[\mathbf{U^{Ph2phen}}] = 2.43 \times 10^{-3}$ M. Numbers are wavelengths in nm.

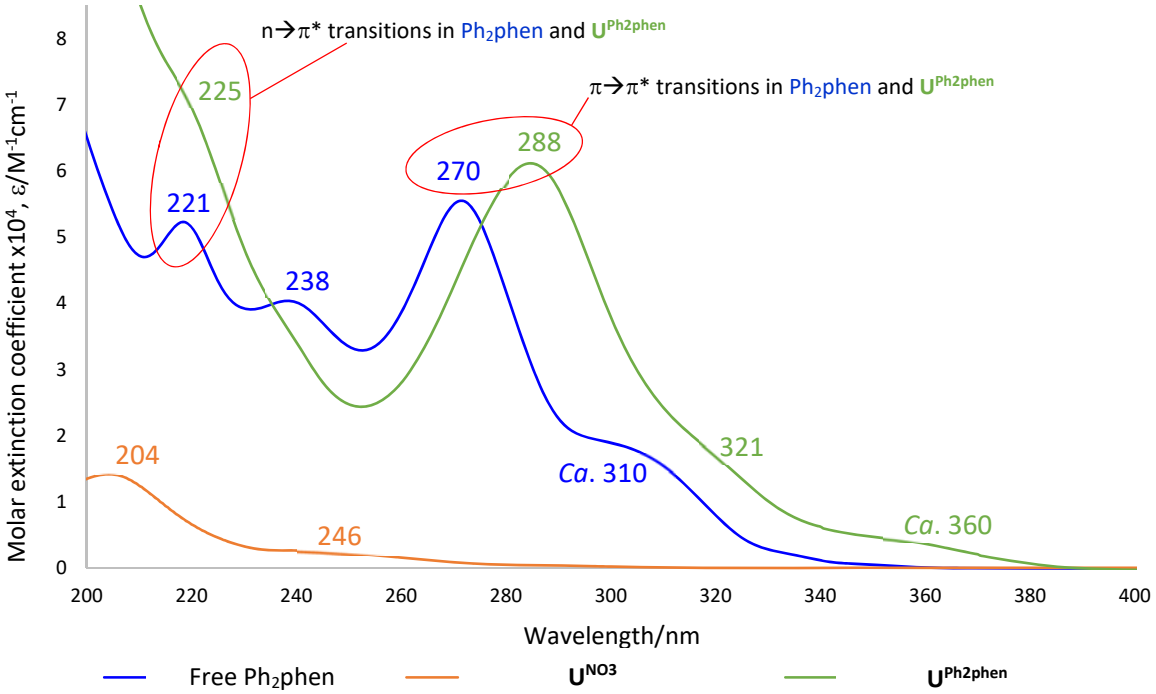

Figure 2.12 – Electronic absorption spectra of uncomplexed Ph_2phen (BLUE), $\mathbf{U^{NO3}}$ (ORANGE), $\mathbf{U^{Ph2phen}}$ (GREEN) in CH_3CN; $[Ph_2phen] = 1.203 \times 10^{-5}$ M, $[\mathbf{U^{NO3}}] = 3.76 \times 10^{-5}$ M, $[\mathbf{U^{Ph2phen}}] = 1.22 \times 10^{-5}$ M. Numbers are wavelengths in nm. Bands corresponding to the n→π* and π→π* absorptions are highlighted.

Whereas $\mathbf{U^{NO3}}$ is a pale (ε_{425} = 11 $M^{-1}cm^{-1}$) yellow solid, $\mathbf{U^{Ph2phen}}$ is a much more intensely coloured yellow solid (ε_{427} = 65 $M^{-1}cm^{-1}$), Figure 2.11. This multiband absorption at *ca.* 420nm is consistent with other uranyl(VI) complexes, corresponding to the U(5*f*)←O(2*p*) LMCT band (Section 1.3). The UV-energy (< 400 nm) absorptions for $\mathbf{U^{Ph2phen}}$ are also red-shifted (*e.g.* towards the visible)**;** the π→π* (HOMO-LUMO) ligand transition[89, 95] centred at 270 nm in Ph_2phen, shifts to 288 nm in $\mathbf{U^{Ph2phen}}$, corresponding to a reduction in the HOMO-LUMO gap for the Ph_2phen ligand of 1949 cm^{-1}, or 23.3 $kJmol^{-1}$, upon complexation. A much smaller red-shift is observed for the n→π* transition in the Ph_2phen ligand, which shifts from 221 nm to 225 nm upon complexation, and a new broad, featureless band is also observed at *ca*. 360 nm in $\mathbf{U^{Ph2phen}}$.

To interrogate the effects of complexation on the electronic structure of both the uranyl and the Ph_2phen groups, excitation and emission spectra of $\mathbf{U^{NO3}}$ and $\mathbf{U^{Ph2phen}}$ were collected in CH_3CN. These spectra are shown in Figures 2.13, 2.14 and 2.15, below.

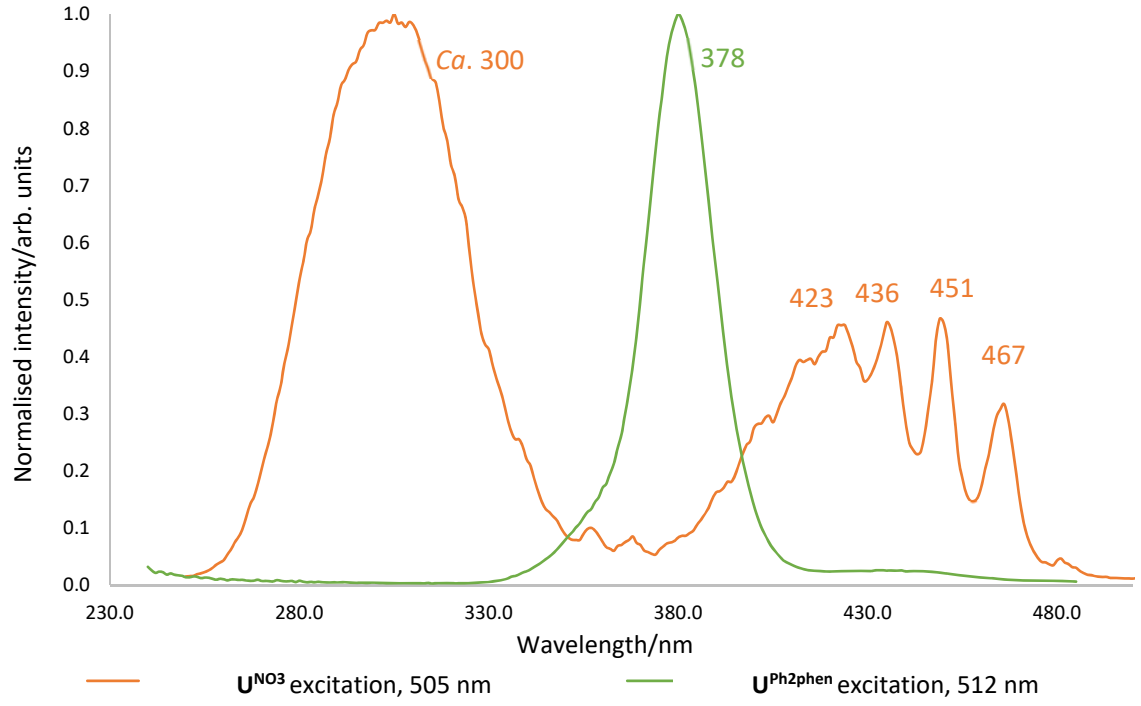

Figure 2.13 – Excitation spectra of $\mathbf{U}^{\mathbf{NO3}}$ (ORANGE) and $\mathbf{U}^{\mathbf{Ph2phen}}$ (GREEN) in CH_3CN; $[\mathbf{U}^{\mathbf{NO3}}] = 7.50 \times 10^{-3}$ M, $[\mathbf{U}^{\mathbf{Ph2phen}}] = 2.40 \times 10^{-3}$ M. Numbers are wavelengths in nm.

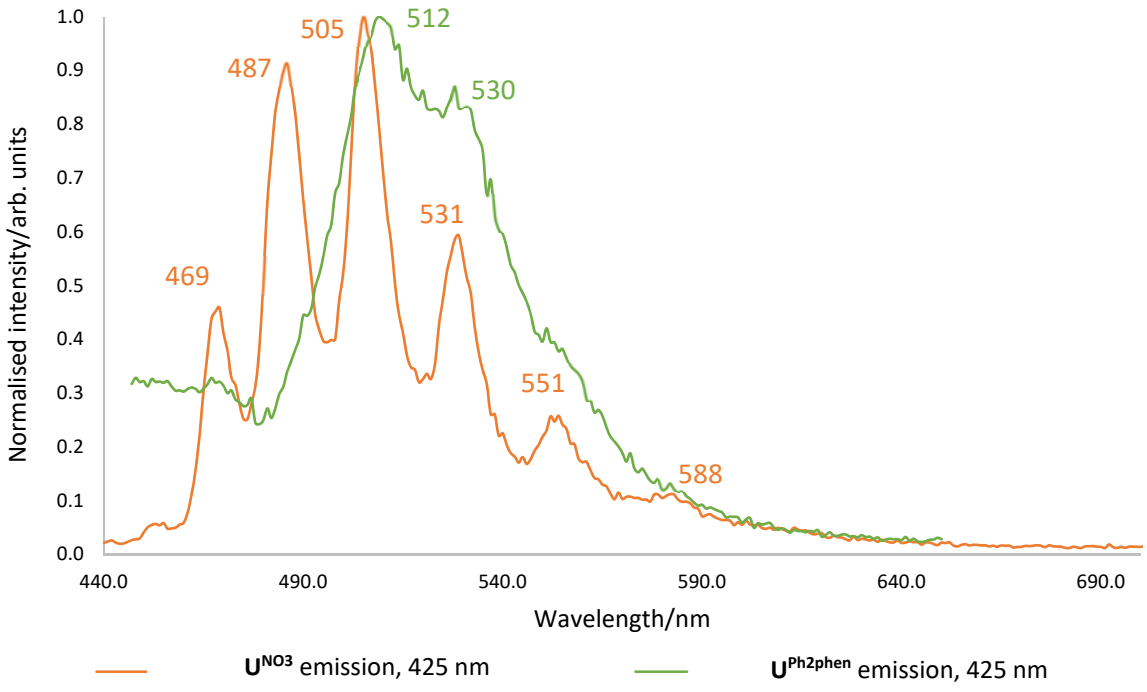

Figure 2.14 – Emission spectra of $\mathbf{U}^{\mathbf{NO3}}$ (ORANGE) and $\mathbf{U}^{\mathbf{Ph2phen}}$ (GREEN) in CH_3CN; $[\mathbf{U}^{\mathbf{NO3}}] = 7.50 \times 10^{-3}$ M, $[\mathbf{U}^{\mathbf{Ph2phen}}] = 2.40 \times 10^{-3}$ M. Numbers are wavelengths in nm.

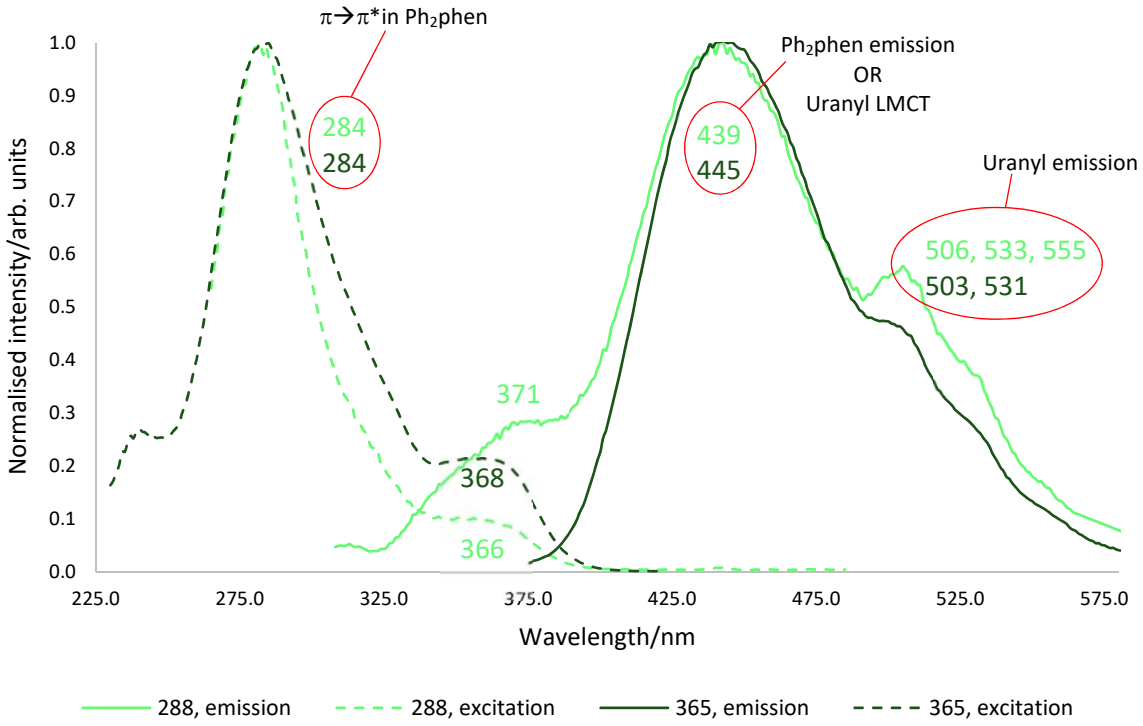

Figure 2.15 – Comparative excitation and emission spectra of $\mathbf{U^{Ph2phen}}$ (288 and 365 nm), in CH_3CN. $[\mathbf{U^{Ph2phen}}]_{288}$ = 1.46 x10^{-6} M, $[\mathbf{U^{Ph2phen}}]_{365}$ = 1.38 x10^{-5} M. Numbers are wavelengths in nm.

The emission band of $\mathbf{U^{NO3}}$ at *ca*. 505 nm broadens substantially and loses fine structure upon the complexation of Ph_2phen (*e.g.* in $\mathbf{U^{Ph2phen}}$), which is attributed primarily to a loss of symmetry at the uranium centre ($\mathbf{U^{NO3}}$ possesses D_{2h} symmetry, whereas $\mathbf{U^{Ph2phen}}$ is C_1-symmetric), though collisional quenching with solvent cannot be ruled out entirely.

The reduction in symmetry may also effect the Stokes shift of $\mathbf{U^{Ph2phen}}$ (4645 cm^{-1}) compared to $\mathbf{U^{NO3}}$ (3820 cm^{-1}) which is consistent with greater structural reorganisation of the solvent cage upon excitation.[96] The effects of the solvent cage on excited states tend only to lead to minor (< 3000 cm^{-1}) changes in Stokes shift, however, suggesting this increase in Stokes shift between $\mathbf{U^{NO3}}$ and $\mathbf{U^{Ph2phen}}$ (825 cm^{-1}) is likely ligand-mediated,[97] arising from differences between $\mathbf{U^{NO3}}$ and $\mathbf{U^{Ph2phen}}$ that remain poorly understood. These values are typical of uranyl(VI) complexes, and compare well to the values reported by Meinrath *et al*. in emission spectra of $[UO_2(OH_2)_5]^{2+}$, $[(UO_2)_2(OH)_2(OH_2)_6]^{2+}$ and $[(UO_2)_3(O)(OH)_3(OH_2)_6]^{+}$ ($[U^{VI}O_2^{2+}]$ = 0.2–6 mM, pH = 2.4–4.8), where Stokes shifts of 4520, 4440, and 4548 cm^{-1}, respectively, were observed (Table 3.1).[98] The differences in Stokes shift between $\mathbf{U^{NO3}}$ and those reported by Meinrath *et al*. are probably the result of differing solvents, with CH_3CN used here and water used by Meinrath *et al*.

While the excitation spectrum (of the band) at 505 nm in $\mathbf{U^{NO3}}$ (Figure 2.13) shows the expected fine structure of the multi-band absorption at *ca*. 420 nm (*e.g.* the emission band of $\mathbf{U^{NO3}}$ at *ca*. 505 nm is largely due to the U(5*f*)←O(2*p*) LMCT processes), the excitation spectrum of the band at 520 nm in

U^{Ph2phen} is dominated by a broad band at 378 nm, along with the expected, albeit broadened, LMCT band at 420–450 nm. This correlates well with the tailing edge of the new band in the absorption spectrum of **U^{Ph2phen}** (Figure 2.12), which only appears on coordination to the uranyl(VI) ion, at *ca*. 370 nm. Further, the emission spectra generated from excitation of the bands at 288 nm and 365 nm for **U^{Ph2phen}** (Figure 2.15) also results in the broad, featureless band at 520 nm, as observed for the emission spectrum of LMCT band for **U^{Ph2phen}** at *ca*. 420 nm; that is, absorption bands in the electronic absorption spectrum of **U^{Ph2phen}** at 288, 365 and 420 nm all show the same broad featureless emission band at *ca.* 520 nm in their emission spectra for **U^{Ph2phen}**. Given the 288 nm absorption band in the electronic absorption spectrum of **U^{Ph2phen}** (Figure 2.12) has been identified as a $\pi \rightarrow \pi^*$ transition in the Ph_2phen ligand, and the 420 nm band is ascribed to a uranyl-based transition, this suggests that coordination of the Ph_2phen ligand to the uranyl ion results in a ligand-modified excited state to which both ligand- and metal-centred transitions contribute. The emission spectra of both the bands at 288 and 365 nm also illustrates that these ligand centred absorptions both emit at *ca*. 440 nm, which overlaps well with the U(5*f*)←O(2*p*) LMCT band at *ca*. 420 nm. It is therefore speculated that (a) ligand-modified electronic state(s) of $*U^{VI}O_2^{2+}$ and ligand emission may combine to modify the photochemistry of the uranyl(VI) ion in **U^{Ph2phen}**, in a way that remains to be fully understood.

Elucidating excited-state photochemical processes is computationally non-trivial, particularly for heavier, open-shell intermediates such as the $5f^1$ $U^VO_2^+$ ion, as is the case here.[99] Excited-state processes involving the uranyl(VI) ion, $*U^{VI}O_2^{2+}$, are also known to be markedly different to those of the ground-state $U^{VI}O_2^{2+}$ ion.[100] To probe these uranyl-Ph_2phen interactions, and the effect that Ph_2phen complexation has on the $*U^{VI}O_2^{2+}$ ion, computational collaborations with Prof. Georg Schreckenbach (University of Manitoba, Canada) are ongoing. Preliminary results as to whether or not the Ph_2phen ligand, analogously to bipy, terpy and phen ligand radical complexes discussed in Section 2.1.1, is able to act as a reservoir for electron density from the *pseudo*-U^V centre (*cf*. product of homolytic cleavage of one $*U^{VI}{=}O_{yl}$ bond) are ongoing. The computed spin densities of the triplet excited state of ***U^{Ph2phen}** are given in Figure 2.16, below, along with a simplified graphic to highlight the likely structure.

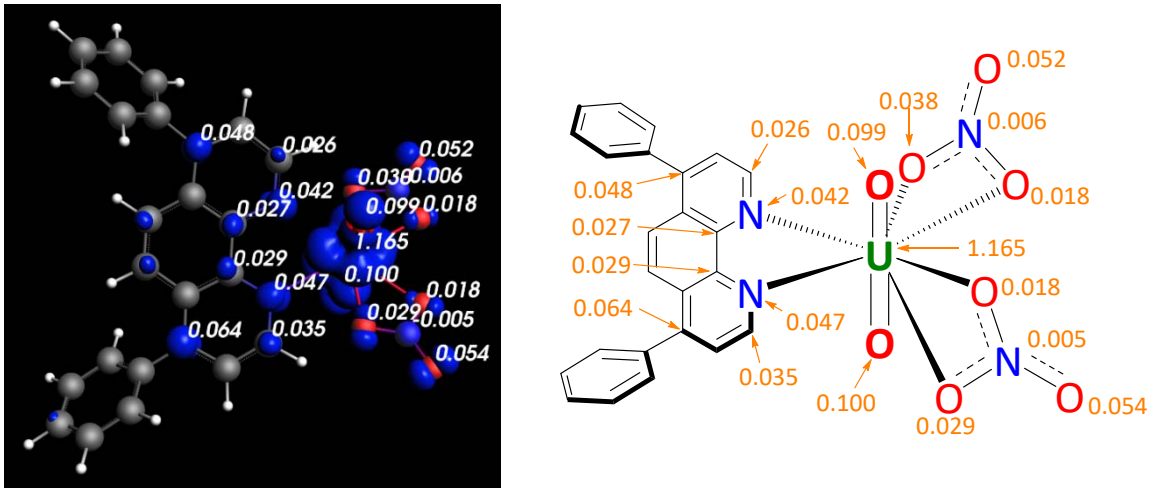

Figure 2.16 – (L) Spin density diagram for *$\mathbf{U}^{\mathbf{Ph2phen}}$, and (R) estimated structure of excited state, with spin densities highlighted in orange. Calculations were performed and optimised by Payal Grover and Prof. Georg Schrekenbach, University of Manitoba, Canada, using the PBE-D3/TZP-SmallCore/scalar-ZORA level and ADF program, and are ongoing. The numbers represent the spin densities of each atom; larger numbers correspond to greater spin density.

Given the majority of calculated density resides on the uranium centre (1.165) with only a slight delocalisation onto the Ph_2phen ligand, it is speculated at this stage that the ligand *does not* act to stabilise the intermediate *pseudo*-U^{V} radical generated from *$\mathbf{U}^{\mathbf{Ph2phen}}$; *e.g.,* it is a metal-centred radical. While DFT calculations have highlighted the strong σ-donor, π-acceptor nature of phen ligands,[101] further work remains to identify possible interactions between π* orbitals on the Ph_2phen ligand and orbitals of appropriate symmetry on the $U^{VI}O_2^{2+}$ unit.

2.2.3 Electronic Spectroscopy of $\mathbf{U}^{\mathbf{phen}}$

The synthesis and characterisation of various 1,10-phenanthroline-containing uranyl complexes is discussed elsewhere in the literature and will not be discussed here in detail; examples include ($[UO_2(NO_3)_2(phen)]$ (**$\mathbf{U}^{\mathbf{phen}}$**),[92, 102] $[UO_2(phen)_2][NO_3]_2$ (**2.AE**),[103] $[UO_2Cl_2(phen)_2]$ (**2.AF**),[104] $[UO_2(phen)_3][OTf]_2$ (**2.AG**),[105] *etc*. Instead, a very brief comparison of the electronic spectral properties of **$\mathbf{U}^{\mathbf{phen}}$** *vs*. **$\mathbf{U}^{\mathbf{Ph2phen}}$** is presented. It is also worth noting that despite having been previously synthesised, the only reference to the electronic spectral properties of **$\mathbf{U}^{\mathbf{phen}}$** that the author can find is a Soviet-era report (1971) that places the λ_{max} of **$\mathbf{U}^{\mathbf{phen}}$** at 485 nm.[106] This is well outside the normal range for the LMCT transition in the $U^{VI}O_2^{2+}$ ion (*ca*. 420 nm), and is questionable given the age and source of the article.

The electronic spectra of **$\mathbf{U}^{\mathbf{phen}}$** (synthesised in methanol) and **$\mathbf{U}^{\mathbf{Ph2phen}}$** are very similar, and are not discussed here for brevity. The only noteworthy difference is the ease of spectral acquisition; while **$\mathbf{U}^{\mathbf{Ph2phen}}$** is sparingly soluble in CH_3CN, **$\mathbf{U}^{\mathbf{phen}}$** is practically insoluble in CH_3CN. This prevented an accurate determination of extinction coefficients for **$\mathbf{U}^{\mathbf{phen}}$**, though differences in peak intensities are likely negligible between the two compounds. The λ_{max} for the LMCT band in **$\mathbf{U}^{\mathbf{phen}}$** is 429 nm, which is

comparable to the λ_{max} of 427 nm for **U^{Ph2phen}**, Figure 2.11. The $\pi \rightarrow \pi^*$ transition for the phen ligand in **U^{phen}** appears at 272.5 nm (uncomplexed phen has a $\pi \rightarrow \pi^*$ transition centred at 265 nm in dry cyclopentane).[95] This is comparable to the $\pi \rightarrow \pi^*$ transition for Ph_2phen (270 nm), which shifts to 285 nm in **U^{Ph2phen}**, Figure 2.12. Excitation and emission spectra of the peak arising from the U(5*f*)←O(2p) LMCT band at *ca*. 420 nm also show little difference between the two complexes, with peaks centred at $\lambda_{emis,max}$ of 470, 505 and 532 nm for **U^{phen}**, which compare well to $\lambda_{emis,max}$ values of 512 and 530 nm for **U^{Ph2phen}**. The Stokes shift is also very similar between the two complexes (4823 cm^{-1} for **U^{phen}**, *vs*. 4645 cm^{-1} for **U^{Ph2phen}**). As expected these data indicate that the photochemical properties between **U^{phen}** and **U^{Ph2phen}** are very similar, with **U^{Ph2phen}** only being preferred owing to its increased solubility in CH_3CN. The effects on the photochemical reactivity of $*U^{VI}O_2^{2+}$ upon complexation of either phen or Ph_2phen should therefore be very similar.

2.2.4 Other Uranyl-phenanthroline Complexes

However, reactions aiming to replicate the synthesis of **U^{Ph2phen}** with other substituted phenanthroline ligands were unsuccessful, as phen ligands that direct steric bulk towards the equatorial plane of the uranyl unit do not complex effectively. Schemes depicting the reactions of **U^{NO3}** with 2,9-dimethyl-1,10-phenanthroline, Me_2phen, and 2,9-dimethyl-4,7-diphenyl-1,10-phenanthroline, Me_2Ph_2phen, along with the desired and obtained products, are given below in Scheme 2.3.

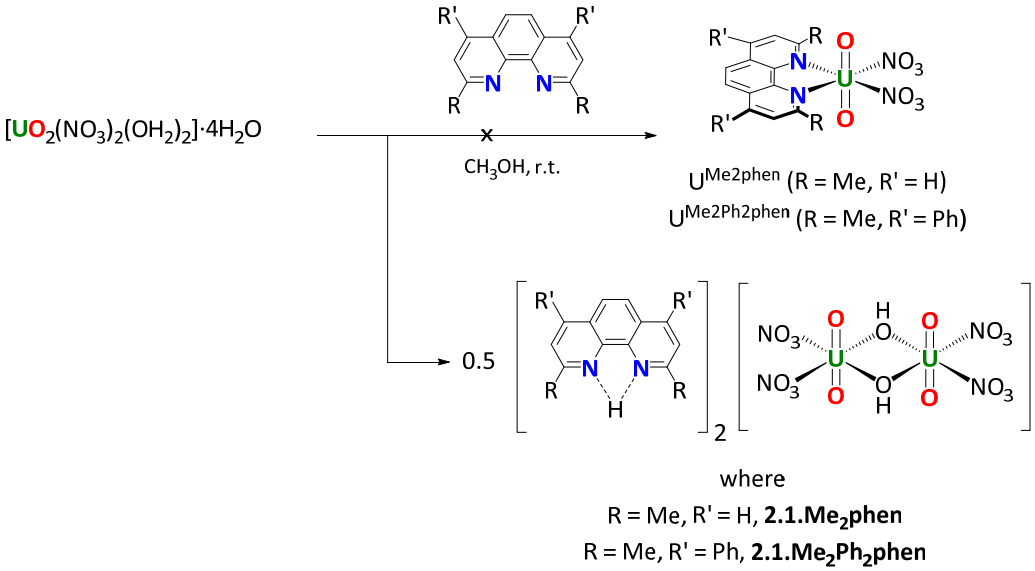

Scheme 2.3 – Unsuccessful syntheses of **U^{Me2phen}** (R = Me, R′ = H), and **U^{Me2Ph2phen}** (R = Me, R′ = Ph), showing instead the synthesis of compounds **2.1**, the products of protonation of the phen ligands rather than complexation.

The ^{1}H NMR spectra (CD_3OD) for both reactions (performed in CH_3OH) showed that instead of complexation, the Me_2phen and Me_2Ph_2phen ligands had protonated, forming the respective phenanthrolinium salts with an anionic uranyl counteranion, $[(UO_2(\mu\text{-}OH)(NO_3)_2)_2]^{2-}$. Taking Me_2phen

as an example, the likely product is $[Me_2phen\text{-}H]_2[(UO_2(\mu\text{-}OH)(NO_3)_2)_2]$ (**2.1.Me$_2$phen**), not **U^{Me2phen}** (*cf.* $[UO_2(NO_3)_2(Me_2phen)]$, on account of the ^{1}H NMR spectra. The resonances (CD_3OD) for $[Me_2phen\text{-}H]_2[(UO_2(\mu\text{-}OH)(NO_3)_2)_2]$ (**2.1.Me$_2$phen**, 8.69, 8.09, 7.92 ppm and 3.02 ppm) are consistent with deliberately protonated Me_2phen ligand (trifluoroacetic acid and Me_2phen, $[Me_2phen\text{-}H][CF_3CO_2]$; 8.74, 8.11, 7.94 and 3.03 ppm, CD_3OD), and are distinct from uncomplexed Me_2phen (8.29, 7.81, 7.61 and 2.87 ppm, CD_3OD). The ^{1}H NMR spectra of $[Me_2Ph_2phen\text{-}H][CF_3CO_2]$ and $[Me_2Ph_2phen\text{-}H]_2[(UO_2(\mu\text{-}OH)(NO_3)_2)_2]$ (**2.1.Me$_2$Ph$_2$phen**) are also similar.

Protonation, not complexation, of the Me_2phen and Me_2Ph_2phen ligands is probably the result of the steric bulk of these ligands, which both have methyl groups aligned in the direction of complexation to the uranyl ion. Given the structural inflexibility of the Me_2phen and Me_2Ph_2phen ligands, the distortion of methyl groups required to accommodate the uranyl unit in the ligand cavity is probably too large, and so protonation, which requires very little structural distortion, results. The proton source is likely to be U-bound water (or methanol), forming U-bonded hydroxides; water molecules covalently bonded to metals are known to be better Brønsted acids.[107] This is known to occur with other *N*-heterocycle complexes of uranyl, *e.g.* in $[UO_2(\mu\text{-}OH)(terpy)]_2[ClO_4]_2$ (**2.AH**).[108] The solid-state structure of the reaction product between **U^{NO3}** and Me_2Ph_2phen (Figure 2.17) also supports this assignment; the connectivity-only structure clearly shows charged separated uranyl and ligand units, and is assigned as $[Me_2Ph_2phen\text{-}H]_2[(UO_2(\mu\text{-}OH)(NO_3)_2)_2]$ (**2.1.Me$_2$Ph$_2$phen**).

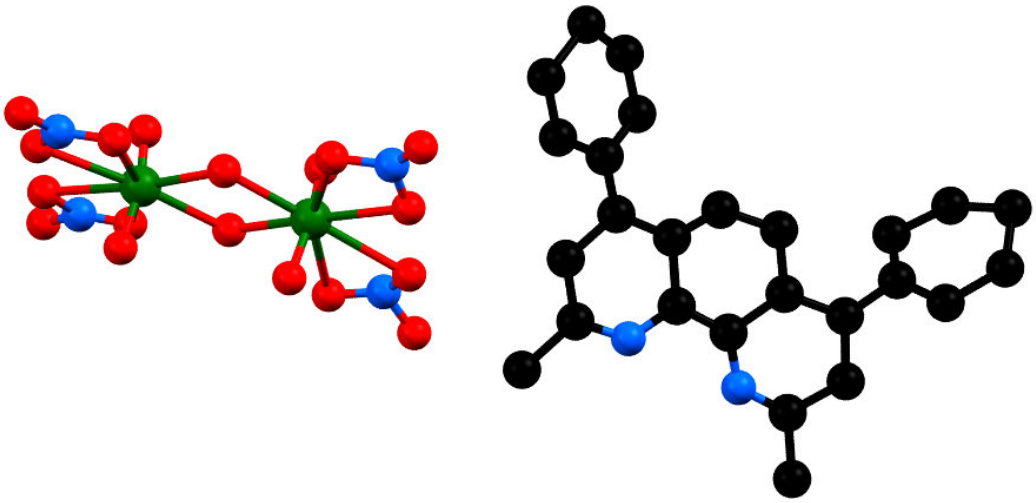

Figure 2.17 – Connectivity-only, solid-state structure of $[Me_2Ph_2phen\text{-}H]_2[(UO_2(\mu\text{-}OH)(NO_3)_2)_2]$ (**2.1.Me$_2$Ph$_2$phen**). Only one $[Me_2Ph_2phen\text{-}H]^+$ unit is depicted as the second $[Me_2Ph_2phen\text{-}H]^+$ unit, though clearly visible in the expanded structure, comprises disjoined fragments and so is omitted for clarity. Key: uranium, oxygen, nitrogen, carbon.

This formulation, $[L\text{-}H]_2[(UO_2(\mu\text{-}OH)(NO_3)_2)_2]$ (**2.1**), is additionally supported by IR spectra of both solids (*e.g.* L = Me_2phen and Me_2Ph_2phen), where $\nu_{asym}(U{=}O)$ is 926 cm^{-1}, suggesting the same uranyl(VI)-containing structure is formed in both cases (likely $[(UO_2(\mu\text{-}OH)(NO_3)_2)_2]^{2-}$). Uranyl-bound

nitrates are also retained (1305 and 1283 cm^{-1}, and 1286 cm^{-1} for L = Me_2phen and Me_2Ph_2phen, respectively).

2.2.5 Complexation of Uranyl with Terpyridine, terpy

The synthesis and solid-state structure of $[UO_2(NO_3)_2(terpy)]$ (**2.AI**) has been previously described elsewhere (from the reaction between equimolar amounts of terpy and $\mathbf{U^{NO3}}$ in acetone, Scheme 2.4).[109] Here, this synthesis was repeated, and the yellow products isolated characterised by ^{1}H NMR and IR spectroscopy. A solid-state structure of $[UO_2(MeOH)(MeO)(terpy)]_2[UO_2(NO_3)_4]$ (**2.2**) was also obtained for the reaction with two equiv. of terpy, Scheme 2.4 and Figure 2.18.

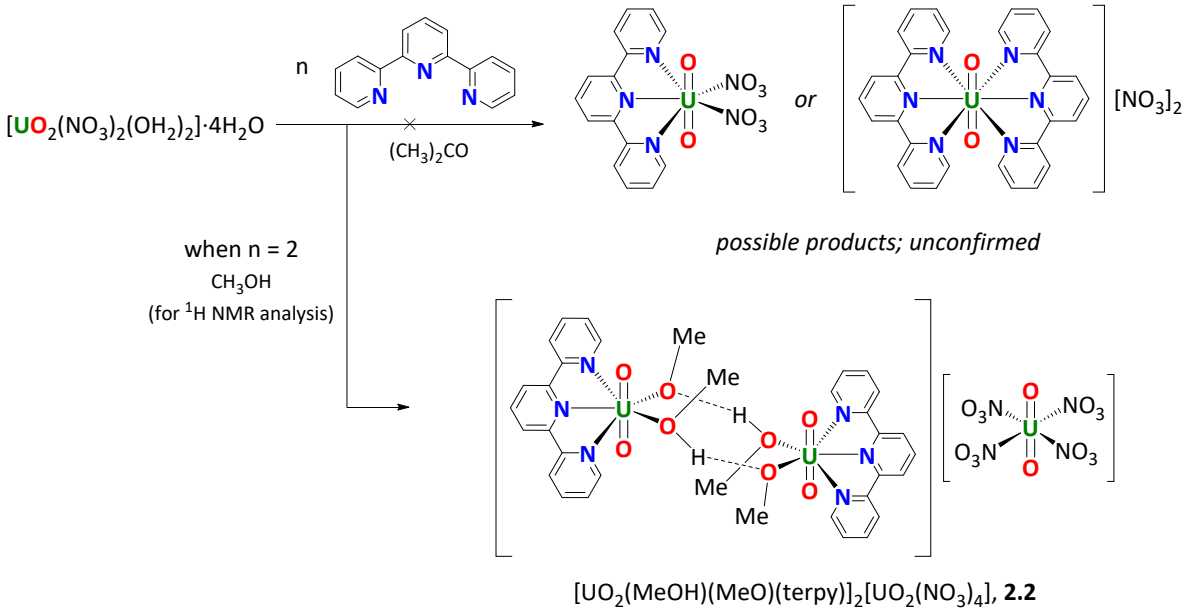

Scheme 2.4 – The reaction of terpy with $\mathbf{U^{NO3}}$ in acetone, n = 1 or 2. From the n = 2 reaction, when CH_3OH was added, product **2.2**, $[UO_2(MeOH)(MeO)(terpy)]_2[UO_2(NO_3)_4]$, crystallised. Given the uncertain nature of these reactions and the products formed, the stoichiometries of terpy are left deliberately unbalanced.

The ^{1}H NMR spectra of both solutions (from one or two equiv. of added terpy) in CD_3OD solution have resonances that are distinct from both protonated ($[terpy\text{-}H]^+$) and uncoordinated ligand, suggesting an interaction with the uranyl ion in solution. However, the ^{1}H NMR spectra for both reactions are different; for the product of addition of one equiv. of terpy, there are two sets of signals (two sets of six distinct 2:2:2:2:2:1 environments), in an approximately 3:1 ratio. For the product of addition of two equiv. of terpy, there are 10 signals between *ca*. 7 and 9 ppm making it likely that there is signal convolution with some larger resonances masking smaller ones. Attempts to deconvolute the ^{1}H NMR spectrum by ^{1}H-^{1}H COSY were unsuccessful. This is perhaps unsurprising, as dynamic exchange of the multidentate *N*-heterocycle rbtp ligand (Rbtp = 2,6-bis(5,6-dimethyl-1,2,4-triazin-3-yl)pyridine) in $[UO_2(NO_3)_2(rbtp)]$ (**2.AJ**) is known to occur even at -20°C in CD_3CN.[14] One possibility is simply that methanol, a common donor solvent, competes with terpy and nitrate for coordination to uranyl, forming an unidentified adduct(s). Conductivity measurements of $\mathbf{U^{NO3}}$ in CH_3OH have previously

demonstrated CH_3OH competes with nitrate for coordination to uranyl,[110] and ESI-MS analysis on the product of addition of two equiv. of terpy examined here also shows masses corresponding to a variety of methanol, nitrate and terpy adducts of uranyl.

Indeed, when the product of two equiv. of terpy with $\mathbf{U^{NO3}}$ is crystallised by slow evaporation from CH_3OH solution, small yellow crystals consistent with the formula $[UO_2(MeOH)(MeO)(terpy)]_2[UO_2(NO_3)_4]$ (**2.2**) were obtained (Figure 2.18, Table 2.2).

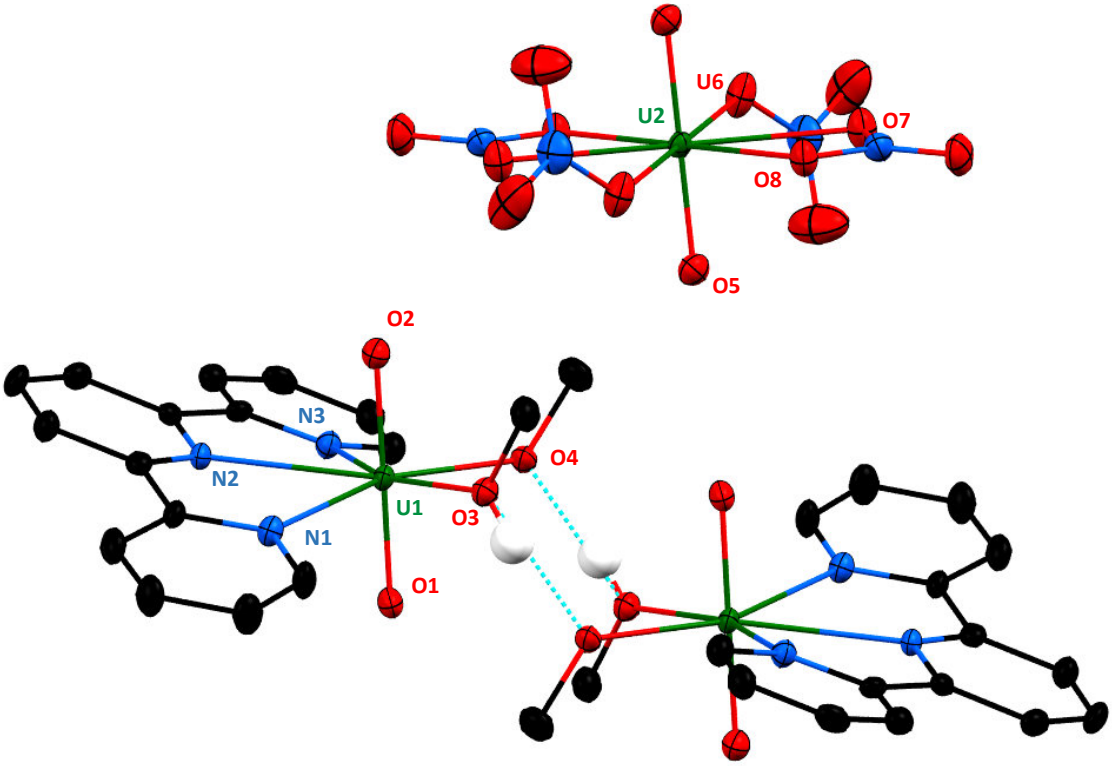

Figure 2.18 – Thermal ellipsoid plot of $[UO_2(MeOH)(MeO)(terpy)]_2[UO_2(NO_3)_4]$ (**2.2**) with ellipsoids drawn at 50% probability. All non H-bonding H-atoms are omitted for clarity. Key: uranium, oxygen, nitrogen, carbon.

Parameter	$[UO_2(NO_3)_4]^{2-}$ unit	$[UO_2(MeOH)(MeO)(terpy)]^{+}$ unit
d(U=O_{yl})	1.765(3) Å	1.773(3) (O1), 1.768(3) (O2) Å
d(U-O_{nit})	2.406(3) Å (O6; κ^1-NO_3) 2.491(3) (O8), 2.542(3) (O7) Å (κ^2-NO_3)	n/a
d(U-O_{MeO})	n/a	2.328(3) (O3), 2.235(3) (O4) Å
d(U-N_{terpy})	n/a	2.573(4) (N1), 2.588(3) (N2), 2.567(4) (N3) Å
∠(OUO)	180 °	178.77(15) °

Table 2.2 – Key parameters (bond lengths/Å, and angles/°) for the solid-state structure of $[UO_2(MeOH)(MeO)(terpy)]_2[UO_2(NO_3)_4]$ (**2.2**), with uncertainties in parentheses.

Structurally, both uranium centres (*e.g.* $[UO_2(NO_3)_4]^{2-}$ and $[UO_2(MeOH)(MeO)(terpy)]^+$) have parameters consistent with the uranyl(VI) ion,[111] with $U{=}O_{yl}$ bond lengths of between 1.765(3) Å and 1.773(3) Å, and essentially linear O=U=O angles. Some slight desymmetrisation of $U^{VI}{=}O_{yl}$ bond lengths is observed but this is not uncommon in uranyl(VI) complexes with sterically bulky ligands. The uranium centre in the $[UO_2(NO_3)_4]^{2-}$ unit has a distorted 8-coordinate geometry. In the $[UO_2(MeOH)(MeO)(terpy)]^+$ unit, the uranium is distorted 7-coordinate (pentagonal bipyramidal), with the distortion probably arising from the rigidity of the N_3-donor terpy ligand. The structure also shows a slight distortion from idealised planarity of the terpy ligand, with N1 being distorted away from the equatorial plane of the uranyl (atoms N2, N3, U1, O3, O4) by 22.1°. This distortion may also partly be caused by hydrogen bonding between the methanol ligand of one and methoxide ligand of another $[UO_2(MeOH)(MeO)(terpy)]^+$ unit, which align to create a H-bonded dimer, Figure 2.18. Although the initial stoichiometry of U:terpy was 1:2, the U:terpy ratio in $[UO_2(MeOH)(MeO)(terpy)]_2[UO_2(NO_3)_4]$ (**2.2**) is 3:2, meaning that this formula does not account for all the equivs. of terpy present.

The IR spectra of products from both reactions are nearly identical, containing only a single $\nu_{asym}(U{=}O)$ at 933 cm^{-1}, respectively (with nitrate stretches at 1293 and 1277 cm^{-1} for the product of two equiv. of added terpy, and 1293 and 1275 cm^{-1} for the product of one equiv. of added terpy). It is known that salts containing the $[UO_2(NO_3)_3]^-$ (*cf.* $[UO_2(NO_3)_4]^{2-}$) unit have $\nu_{asym}(U{=}O) > 950$ cm^{-1},[112] however, suggesting that the solid-state structure isolated (Figure 2.18) may not be representative of the bulk.

2.2.6 Complexation of Uranyl with Other Poly(pyridyl) Ligands

With the aim of synthesising solution stable uranyl dimers, other poly(pyridyl) ligands were then complexed with the uranyl(VI) ion. A general procedure for the targeted complexation with $\mathbf{U^{NO3}}$ with selected ligands, 2,3-bis(2-pyridyl)pyrazine (reaction **2.3.A**), tetra-2-pyridinylpyrazine (reaction **2.3.B**), and 2,2′-biquinoline (reaction **2.3.C**) is shown in Scheme 2.4, below. None of these reactions yielded the desired product.

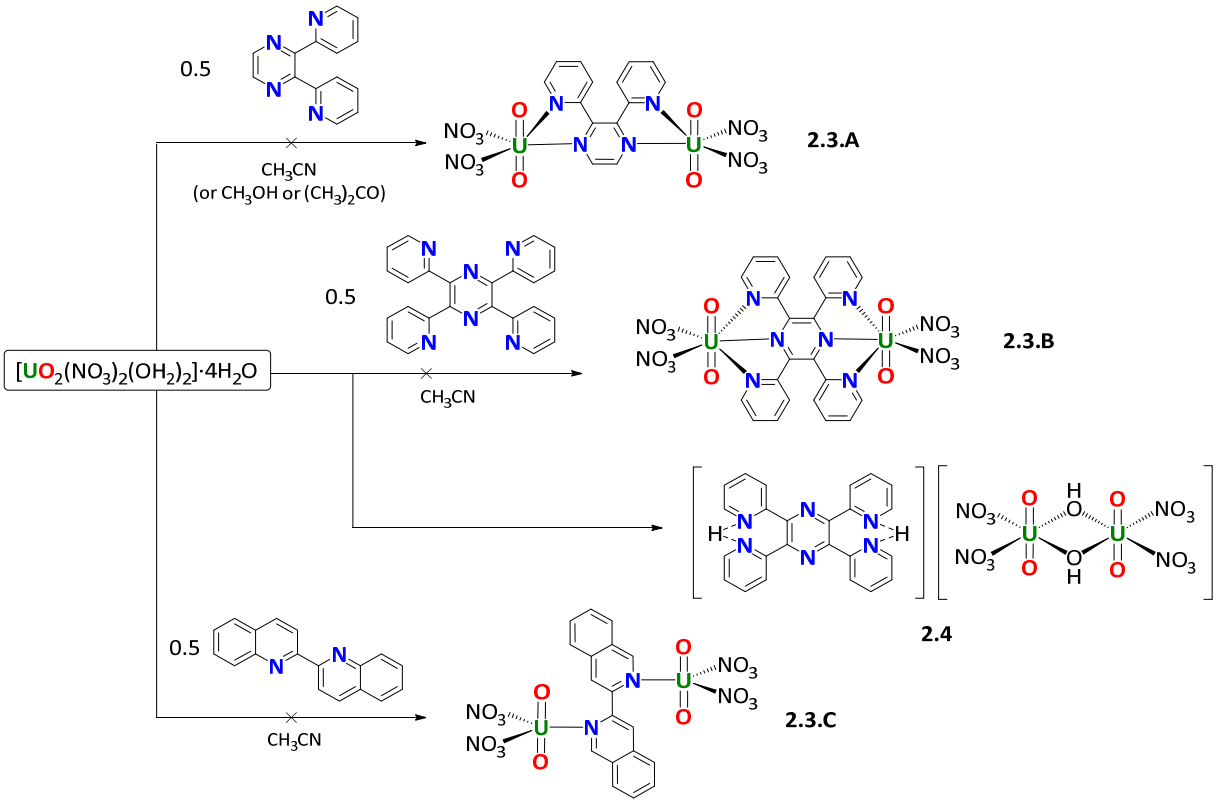

Scheme 2.1 – Unsuccessful complexation of $\mathbf{U^{NO3}}$ with 2,3-bis(2-pyridyl)pyrazine, tetra-2-pyridinylpyrazine (TPP) and 2,2'-biquinoline, reactions **2.3.A**, **2.3.B**, and **2.3.C**, respectively. Product **2.4**, which was obtained instead of the targeted complex **2.3.B**, is discussed in further detail below and in Figure 2.19.

Firstly, solution-phase characterisation of the product of addition of 2,3-bis(2-pyridyl)pyrazine to $\mathbf{U^{NO3}}$ (reaction **2.3.A**, Scheme 2.4) was hindered by its insolubility in CH_3CN, CH_3OH and acetone. Attempts to use more polar solvents, such as water, produced a white solid and yellow supernatant, consistent with decomplexation and precipitation of uncomplexed or protonated 2,3-bis(2-pyridyl)pyrazine, which are both white. IR spectroscopy of yellow solids from the reaction performed in CH_3CN clearly showed a weakening of the $\nu_{asym}(U{=}O)$ band at 915 cm^{-1} (*cf.* $\mathbf{U^{NO3}}$, 936 cm^{-1}), with water (broad peak at *ca.* 3100 cm^{-1}) and complexed nitrate (1285 cm^{-1}) also present. However, given the insolubility of the product, this reaction was not pursued further.

Secondly, and unlike 2,3-bis(2-pyridyl)pyrazine (*e.g.* reaction **2.3.A**), the product of addition of tetra-2-pyridinylpyrazine (TPP) to $\mathbf{U^{NO3}}$ (reaction **2.3.B**, Scheme 2.4) is soluble in CD_3CN, and was therefore analysed by ^1H NMR spectroscopy. The ^1H NMR spectrum shows resonances that are distinct from protonated TPP ($[TPP\text{-}H_2]^{2+}$) or free ligand (TPP), but show several sets of resonances, consistent with a mixture, as seen for the uranyl-terpy systems (Section 2.25). This is in contrast to the solid-state behaviour TPP with the $U^{VI}O_2^{2+}$ ion, in which a structure containing a protonated TPP unit, $[TPP\text{-}2H]^{2+}$, is observed. The structure of $[TPP\text{-}2H][(UO_2(\mu\text{-}OH)(NO_3)_2)_2]$ **2.4** is given in Figure 2.19 and Table 2.3.

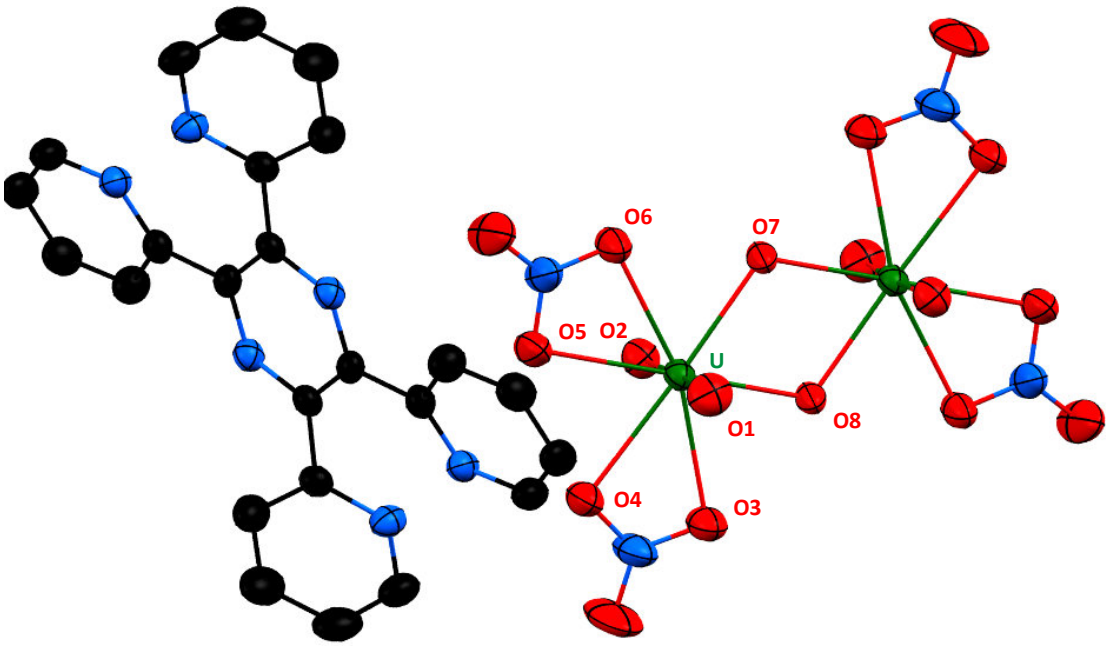

Figure 2.19 – Thermal ellipsoid plot of [TPP-2H][(UO_2(μ-OH)(NO_3)$_2$)$_2$] (**2.4**), with ellipsoids drawn at 50% probability. All H-atoms are omitted for clarity. Key: uranium, oxygen, nitrogen, carbon.

Parameter	Values
d(U=O_{yl})	1.759(3) (O1), 1.763(4) (O2) Å
d(U-O_{nit})	2.548(3) (O3), 2.544(3) (O4), 2.551(3) (O5), 2.524(3) (O6) Å
d(U-O_{OH})	2.341(3) (O7), 2.323(3) (O8) Å
∠(OUO)	174.9(1) °

Table 2.3 – Key parameters (bond lengths/Å, and angles/°) for the solid-state structure of [TPP-2H][(UO_2(μ-OH)(NO_3)$_2$)$_2$] (**2.4**) with uncertainties in parentheses.

All parameters for the uranyl unit in **2.4** are consistent with the uranyl(VI) ion reported in [H_2APTSC]$_2$[(UO_2(μ-OH)(NO_3)$_2$)$_2$] (**2.AK**, APTSC = acetylpyridine thiosemicarbazone, Figure 2.20).[6]

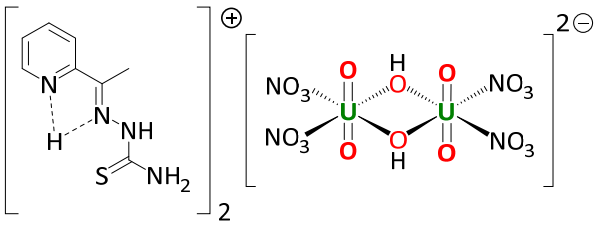

Figure 2.20 – Structure of [H_2APTSC]$_2$[(UO_2(μ-OH)(NO_3)$_2$)$_2$] (**2.AK**).[6]

By charge balance, this results in a dicationic, doubly protonated ligand, $[TPP\text{-}2H]^{2+}$, consistent with a $[(UO_2(\mu\text{-}OH)(NO_3)_2)_2]^{2-}$ dianion, in a 1:1 ratio in the unit cell of **2.4**. The bond lengths of the U-O_{OH} bonds, U-O7 and U-O8, are 2.341(3) Å and 2.323(3) Å, respectively, consistent with U-O_{OH} bond lengths of 2.317(4) Å reported in the $[(UO_2(\mu\text{-}OH)(NO_3)_2)_2]^{2-}$ unit of complex **2.AK**.[6] The U-O_{OH} bond lengths in [TPP-2H][(UO_2(μ-OH)(NO_3)$_2$)$_2$] **2.4** are slightly shorter than the U-O_{OH2} bond lengths reported for

bridging water ligands in $[(UO_2(\mu\text{-}OH_2)(NO_3)_2)_2]$ **2.AL**, which are 2.368(8) Å,[113] and are unlikely to be bridging water ligands as the charge would not balance. IR spectroscopic analysis of $[TPP\text{-}2H][(UO_2(\mu\text{-}OH)(NO_3)_2)_2]$ **2.4** also shows two uranyl peaks, $\nu_{asym}(U{=}O)$, 936 and 923 cm^{-1}, along with water (*ca.* 3400 cm^{-1}) and nitrate (1261 cm^{-1}) peaks, though the broad nature of all these peaks makes confirming the presence of $[TPP\text{-}2H]^{2+}$ in the bulk solid difficult.

Thirdly, the product mixture of reaction of $\mathbf{U^{NO3}}$ with 2,2′-biquinoline (reaction **2.3.C**, Scheme 2.4) is also soluble in CD_3CN, with the ^1H NMR spectrum for this yellow solution also having resonances distinct from both free and protonated 2,2′-biquinoline. There is a shift in the $\nu_{asym}(U{=}O)$ from 936 cm^{-1} in $\mathbf{U^{NO3}}$ to 909 cm^{-1} in the solid-state IR spectrum, suggesting a product in which the $U^{VI}{=}O_{yl}$ bonds are significantly weakened, which is distinct from 943 cm^{-1} in the analogous bipy complex, $[UO_2(NO_3)_2(bipy)]$, **2.AM**.[114] The product also retains bidentate, uranyl-bound nitrates (1277 and 1293 cm^{-1}), and is a hydrate (peak at *ca*. 3500 cm^{-1}).

2.3 Complexes of the Neptunyl(VI) Ion with *N*-heterocycles

All data collected for the neptunyl complexes described were collected in collaboration with Dr. Mark Sarsfield and Mr. Joshua Holt, of the National Nuclear Laboratory, NNL, UK; Dr. Sarsfield and Mr. Holt acquired the spectra under supervision from the author, who drew, interpreted and analysed the data. Np(VI) is prepared electrochemically from the oxidation of the stock of Np(V) stored by the NNL. This process involved treatment with HNO_3, nitric acid, so all analysis occurred in the presence of NO_3^- ions.

2.3.1 Stability of $Np^{VI}O_2^{2+}$ in CH_3CN Solvent

Many studies of the neptunyl(VI) ion, $Np^{VI}O_2^{2+}$, in organic solvents are limited by the inherent instability of Np(VI) relative to its neptunyl(V) congener, $Np^{V}O_2^{+}$, which is far more common in organic solvent (Section 2.1.2). However, to the best knowledge of the author, no studies of the solution speciation of neptunium exist in CH_3CN, though in the solid-state CH_3CN has been reported as a solvent of crystallisation in the structure of the dimeric neptunyl(V) acetate $[(Np^{V}O_2)_2(OAc)_2(OH_2)_2]\cdot CH_3CN$ (**2.AN**).[115] Therefore in order to determine the stability of $Np^{VI}O_2^{2+}$ in CH_3CN solution, a sample of neptunyl(VI) nitrate was dissolved in CH_3CN and the acquired electronic spectrum compared to that of a known sample of $Np^{VI}O_2^{2+}$ in 0.5 M HNO_3. These spectra are shown in Figures 2.21a and b, and 2.22.

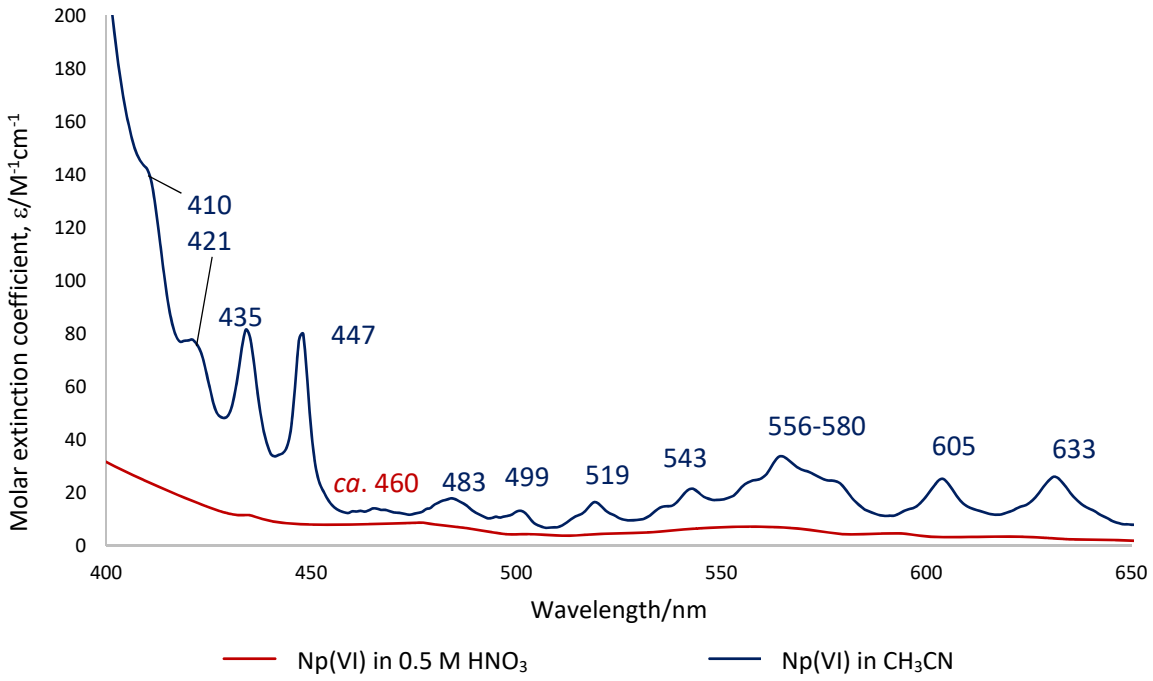

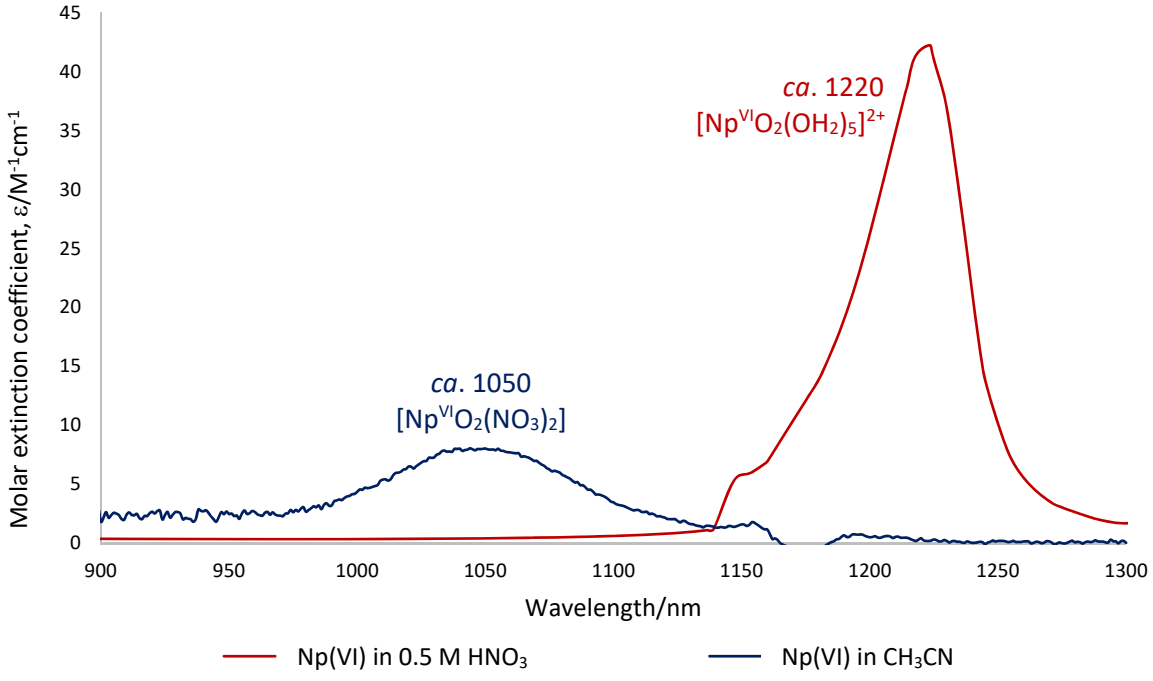

Figures 2.21a and b – Electronic absorption spectra of $Np^{VI}O_2^{2+}$ in 0.5 M HNO_3 (RED) or CH_3CN (BLUE) ([Np^{VI}] = 1.6 x 10^{-3} M). Top, 400–650 nm, bottom, 900–1300 nm. Numbers are wavelengths in nm.

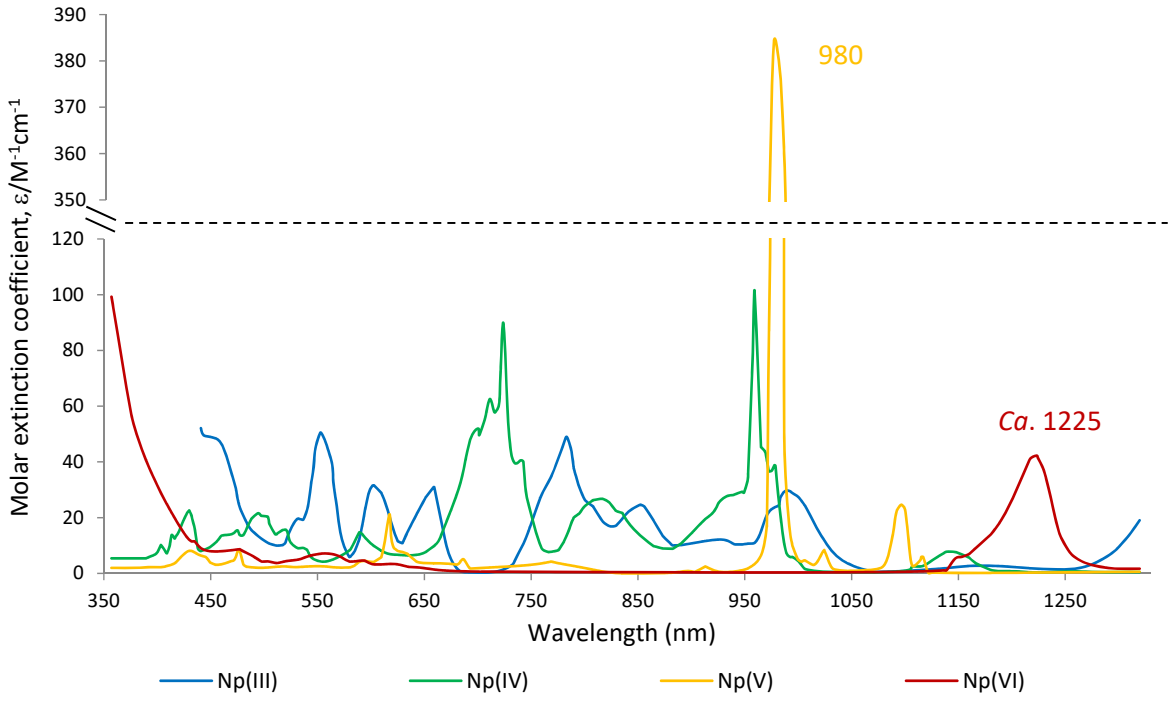

Figure 2.22 – Electronic absorption spectra of Np oxidation states +3 to +6 in 0.5 M HNO_3; // is an axis break. The data were collected by Dr. Mark Sarsfield of the NNL and used with permission. Numbers are wavelengths in nm.

Given the absence of the relatively strong *f-f* transition ($\varepsilon \sim 385$ $M^{-1}cm^{-1}$) at *ca*. 980 nm, Figure 2.21b, it is likely that the $Np^{VI}O_2^{2+}$ ion is redox-stable in CH_3CN; no disproportionation or reduction (*etc*.) to $Np^{V}O_2^{+}$ (or Np^{III} or Np^{IV}) is observed under these conditions. The electronic absorption spectrum of $Np^{VI}O_2^{2+}$ in CH_3CN after 3 days is identical to that in Figures 2.21a and b.

The *f-f* transition of $Np^{VI}O_2^{2+}$ at *ca*. 1220 nm in 0.5 M HNO_3 is excitation of the $5f^1$ electron from the ground state to the second excited state of $Np^{VI}O_2^{2+}$.[116] This transition is known to occur below *ca*. 4 M (*e.g.* pH > -0.6) $HClO_4$[117, 118] or HNO_3,[119] where $[Np^{VI}O_2(OH_2)_5]^{2+}$ (**2.AO**) predominates, and results in $\varepsilon_{1222} = 40–50$ $M^{-1}cm^{-1}$ in either $HClO_4$[118] or HNO_3.[120] Between 4–7 M of nitric acid (pH -0.6 to -0.85) the predominant $Np^{VI}O_2^{2+}$ species in solution is $[Np^{VI}O_2(NO_3)(OH_2)_x]^{+}$ (**2.AP**; x = an integer value), which has very similar λ_{max} and ε_{max} properties to $[Np^{VI}O_2(OH_2)_5]^{2+}$ (**2.AO**). However, at > 7 M HNO_3 (pH < -0.85), '$[Np^{VI}O_2(NO_3)_2]$' (**2.AQ**) is the predominant species; note, that while Lindqvist-Reis *et al*.[120] represent $Np^{VI}O_2^{2+}$-nitrates as unsolvated, *e.g.* as $[Np^{VI}O_2(NO_3)_2]$, it is possible that the complex is solvated in CH_3CN. Conflicting reports exist on whether solvent is coordinated directly to the Np^{VI} centre in $Np^{VI}O_2^{2+}$; in aqueous solution, DFT calculations suggest a formulation of $[Np^{VI}O_2(NO_3)_2(OH_2)_2]$ to be correct,[121] whereas molar conductivity measurements on the analogous $U^{VI}O_2^{2+}$ ion in CH_3CN solution have previously suggested a formulation of $[U^{VI}O_2(NO_3)_2]\cdot 2(CH_3CN)$.[122] In light of this ambiguity, the $Np^{VI}O_2^{2+}$ ion in the presence of nitrate ions in CH_3CN solvent is tentatively represented as '$[Np^{VI}O_2(NO_3)_2]$' (**2.AQ**) as the coordination of CH_3CN molecules to the $Np^{VI}O_2^{2+}$ ion in wet

(*ca*. 100–1000 ppm) CH_3CN could not be confirmed satisfactorily within the experimental limitations of the NNL radiochemical laboratories. A summary of these data are given in Table 2.4, below.

Source:	**Literature**			**This work**
$[HNO_3]$/M	**0–4**	**4–7**	**> 7**	$Np^{VI}O_2^{2+}$ derived
pH	7 to -0.6	-0.6 to -0.85	< -0.85	from Np^{V} in CH_3CN
Complex	$[Np^{VI}O_2(OH_2)_5]^{2+}$	$[Np^{VI}O_2(NO_3)(OH_2)_x]^{+}$	$[Np^{VI}O_2(NO_3)_2]$	(+ trace HNO_3),
(name)	(**2.AO**)	(**2.AP**)	(**2.AQ**)	electrochemically
λ_{max}/nm	1220	1228	1120 (+ 1080 sh)	*ca*. 1050 (Figure 2.21b)
$\varepsilon_{max}/M^{-1}cm^{-1}$	*ca*. 50	*ca*. 50	< 10	< 10

Table 2.4 – Electronic spectral parameters for $Np^{VI}O_2^{2+}$ complexes in varying concentrations of HNO_3 from the literature, compared to this work (CH_3CN). sh is shoulder.

The characteristic *f-f* band of $Np^{VI}O_2^{2+}$ in CH_3CN for this work occurs at 1050 nm (ε_{1050} < 10 $M^{-1}cm^{-1}$), suggesting the $Np^{VI}O_2^{2+}$ ion under these conditions is $[Np^{VI}O_2(NO_3)_2]$. This is based on the data in Table 2.4. It is not likely to be $[Np^{VI}O_2(OH_2)_5]^{2+}$ or $[Np^{VI}O_2(NO_3)(OH_2)_x]^{+}$ as the λ_{max} and ε_{max} are dissimilar to that observed in this work.

To determine the sensitivity of this complex, $[Np^{VI}O_2(NO_3)_2]$ (**2.AQ**) to hydrolysis, gradually increasing amounts of water were pipetted into a solution containing 0.016 M $Np^{VI}O_2^{2+}$ in CH_3CN, and the results solutions analysed by UV-vis-NIR spectroscopy, Figure 2.23.

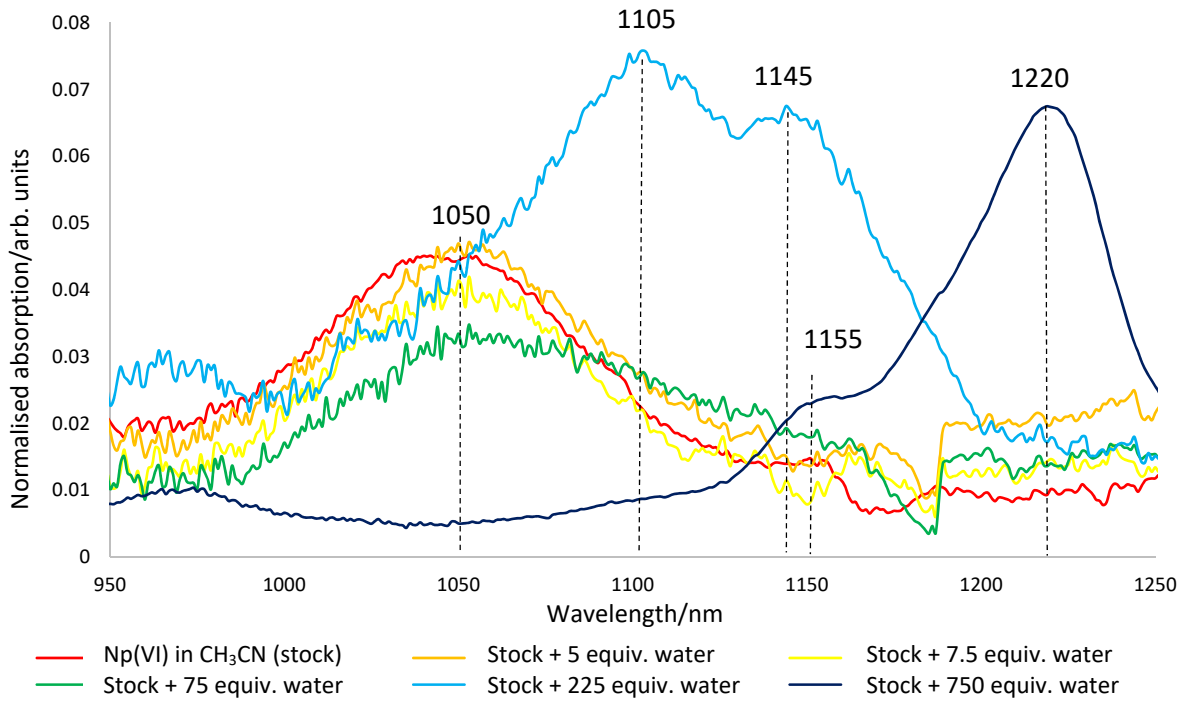

Figure 2.23 – Electronic absorption spectra of $Np^{VI}O_2^{2+}$ in CH_3CN with increasing amounts of water. Stock solution $[Np^{VI}O_2^{2+}]$ = 0.016 M.

Approximately 75 equiv. of water added to the stock CH_3CN solution (*cf*. $[Np^{VI}O_2(NO_3)_2]$) is required to observe a change in the speciation of $Np^{VI}O_2^{2+}$, judging from the disappearance of the band at *ca*. 1050 nm. Additional water (225, then 750 equiv.) results in several different species that are spectrally distinct from $[Np^{VI}O_2(NO_3)_2]$ (**2.AQ**). The UV-vis-NIR spectrum of $Np^{VI}O_2^{2+}$ in the presence of 750 equiv. of water has a band with $\lambda_{max} \sim 1220$ nm, suggesting water at this concentration becomes sufficient to displace coordinated nitrates and form $[Np^{VI}O_2(OH_2)_5]^{2+}$ (**2.AO**). There were no changes in the positions of bands < 750 nm in all solutions with added water.

2.3.2 Complexes of $Np^{VI}O_2^{2+}$ in CH_3CN Solvent with terpy and phen

To identify speciation of the products of addition of L to solutions of $Np^{VI}O_2^{2+}$ (L = phen or terpy, or Ph_2phen), solutions of L were titrated against the stock $Np^{VI}O_2^{2+}$ solution in CH_3CN, Scheme 2.5.

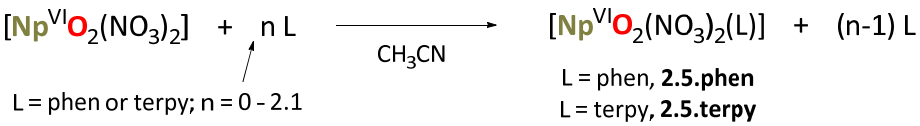

Scheme 2.5 – General procedure for the addition of variable amounts of phen or terpy ligand to the $Np^{VI}O_2^{2+}$ stock solution in CH_3CN, identified as $[Np^{VI}O_2(NO_3)_2]$ (**2.AQ**) in Section 2.3.1 based on UV-vis spectra. The likely formulation of the product, $[Np^{VI}O_2(NO_3)_2(L)]$ (L = phen, **2.5.phen**; L = terpy, **2.5.terpy**), is derived from UV-vis-NIR spectral data and is discussed further, below.

The UV-vis-NIR spectra were then recorded after each addition of L, which are shown in Figures 2.24 and 2.25, for L = phen or terpy, respectively. A UV-vis-NIR absorption spectrum was also recorded for one equiv. of phen with excess (one-hundred equiv.) of water, to determine hydrolytic stability of **2.5.phen**.

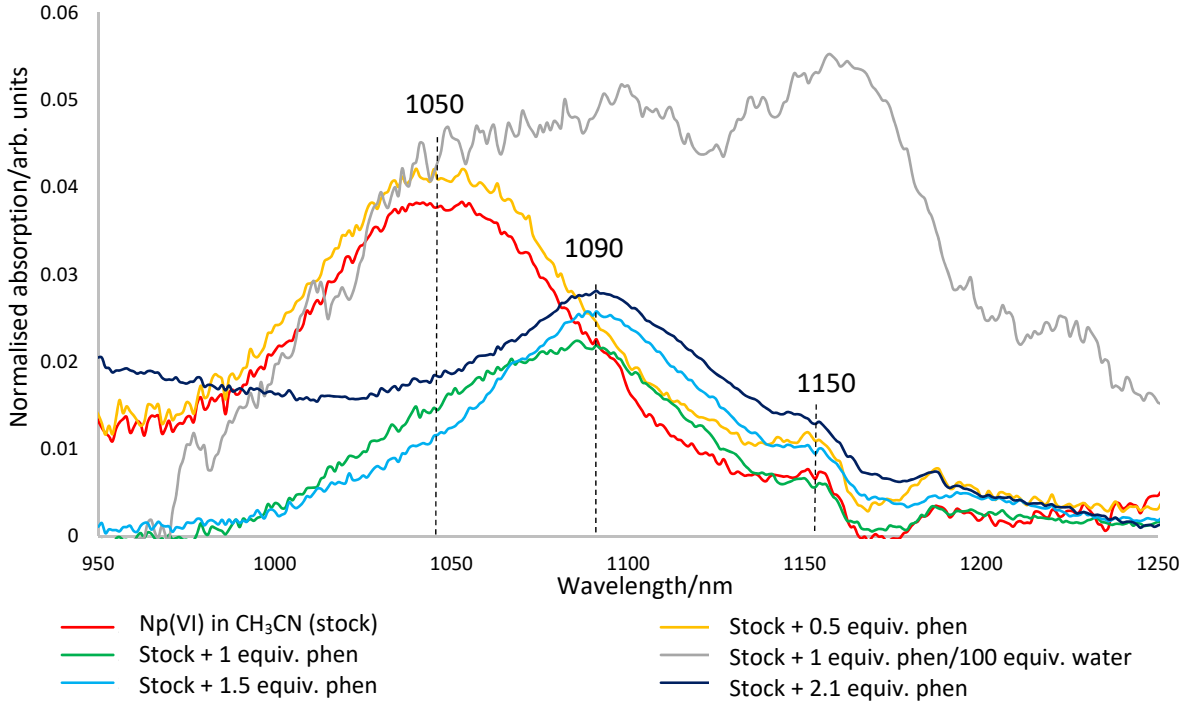

Figure 2.24 – Electronic absorption spectra of $Np^{VI}O_2^{2+}$ in CH_3CN with increasing amounts of phen, **2.5.phen**. $[Np^{VI}O_2^{2+}]$ = 0.016 M. Numbers are wavelengths in nm.

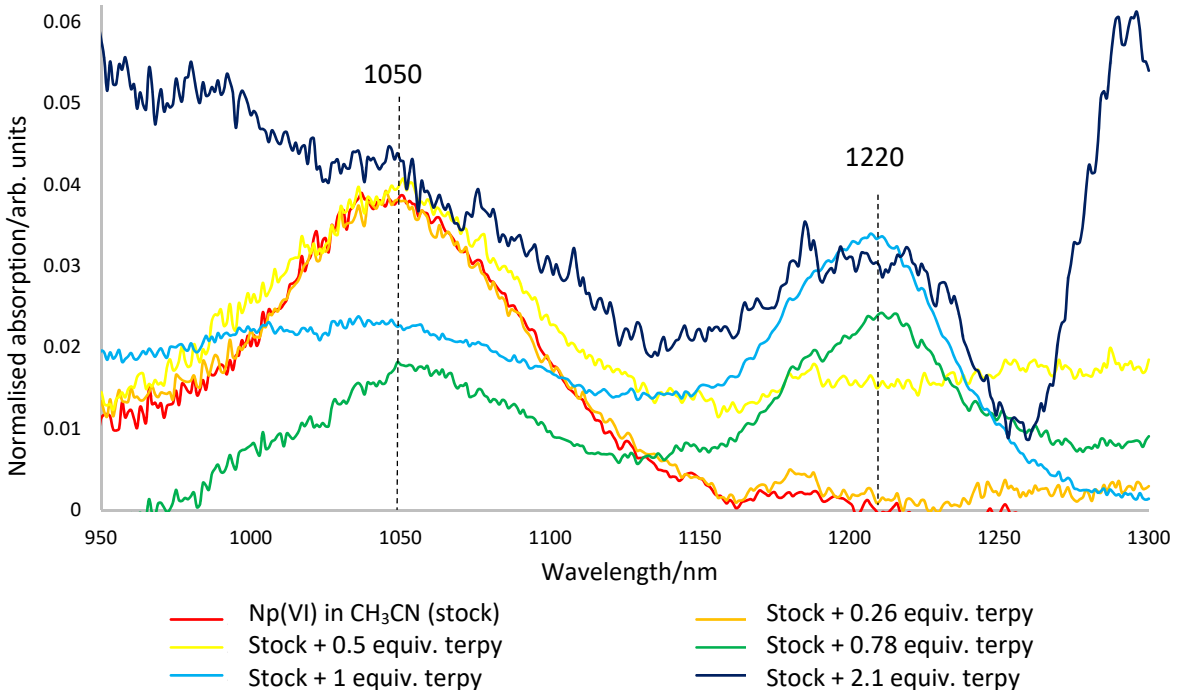

Figure 2.25 – Electronic absorption spectra of $Np^{VI}O_2^{2+}$ in CH_3CN with increasing amounts of terpy, **2.5.terpy**. [$Np^{VI}O_2^{2+}$] = 0.016 M. Numbers are wavelengths in nm.

For L = phen or terpy it is apparent that addition of one equiv. of L causes a red-shift in the *f-f* transition energy, shifting from *ca*. 1050 nm with no added L to 1090 nm for L = phen, and to 1210 nm for L = terpy. Spectral changes only occur upon addition of stoichiometric amounts of either phen or terpy, suggesting that 1:1 $Np^{VI}O_2^{2+}$:L complexes are formed preferentially. No further changes are observed when one extra equiv. of ligand is added (for both L = phen and L = terpy), suggesting that the $Np^{VI}O_2^{2+}$ complex $[Np^{VI}O_2(NO_3)_2(L)]$ (**2.5**), is stable in CH_3CN as the 1:1 complex, retaining its stoichiometry in the presence of excess ligand. A new band at *ca*. 1290 nm also appears for **2.5.terpy** where 2 equiv. of terpy are added, Figure 2.25. The identity of the species responsible for this band is unclear.

As there are immediate colour and spectral changes upon addition of either phen or terpy to $Np^{VI}O_2^{2+}$ in CH_3CN, it is speculated that the $[Np^{VI}O_2(NO_3)_2(L)]$ (**2.5**) complexes form very quickly, and that analogously to $U^{VI}O_2^{2+}$ complexes with phen derivatives, these complexes possess large K_{eq} values (*e.g.* log(K_1) for $U^{VI}O_2^{2+}$ + PDA^{2-} ⇆ $[U^{VI}O_2(PDA)]$ is 16.5(1) (PDA = 1,10-phenanthroline-2,9-dicarboxylic acid)).[123] UV-vis-NIR spectra recorded after three days on both $Np^{VI}O_2^{2+}$-phen or -terpy solutions (**2.5.phen** and **2.5.terpy**) in CH_3CN were identical to those recorded in Figures 2.24 and 2.25, suggesting the complexes formed are stable to decomposition in air for at least three days. Due to precipitation of yellow solids (Figure 2.26), it was not possible to calculate an exact concentration of Np^{VI} in solution, and so data

are presented as normalised absorbances rather than ε. Complexes with Ph_2phen could not be detected spectroscopically due to the low relative solubility of Ph_2phen in CH_3CN compared to phen or terpy.

As discussed above, addition of CH_3CN solutions of terpy or phen to the solution of $Np^{VI}O_2^{2+}$, **2.5.phen** and **2.5.terpy,** causes colour changes from pale to dark yellow, with concomitant precipitation of dark yellow solids. With terpy, these solids appear crystalline under light microscopy (Figure 2.26), and may therefore be suitable for X-ray diffraction for structural determination (a series of $[Me_4N]_2[((An^{VI}O_2)(\mu\text{-}OH)(NO_3))_2]$, where An = U^{VI}, Np^{VI}, and Pu^{VI} complexes have very recently been reported by structural characterisation).[124] Discussions are underway to replicate this chemistry at the Institute for Transuranium Elements (ITU) in Karlsruhe, Germany, but this work will unfortunately not be complete by the submission of this thesis.

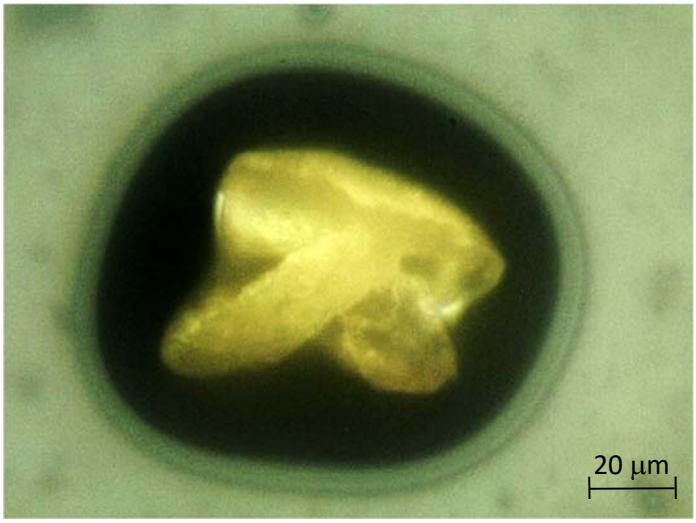

Figure 2.26 – Light microscope picture of crystalline solids obtained after addition of 2 equiv. of terpy to a stock solution of $Np^{VI}O_2^{2+}$ in CH_3CN ([Np^{VI}] = 0.016 M), likely **2.5.terpy**, $[Np^{VI}O_2(NO_3)_2(terpy)]$.

In certain cases it was also possible to acquire Raman spectra, namely, on solutions of $Np^{VI}O_2^{2+}$ in CH_3CN, $Np^{VI}O_2^{2+}$ in CH_3CN with 75 equiv. of water, and $Np^{VI}O_2^{2+}$ with one equiv. of added terpy. It was also possible to acquire a Raman spectrum of the solids represented in Figure 2.26 ($Np^{VI}O_2^{2+}$ + two equiv. terpy). These spectra are overlaid and shown in Figures 2.27a and b, below.

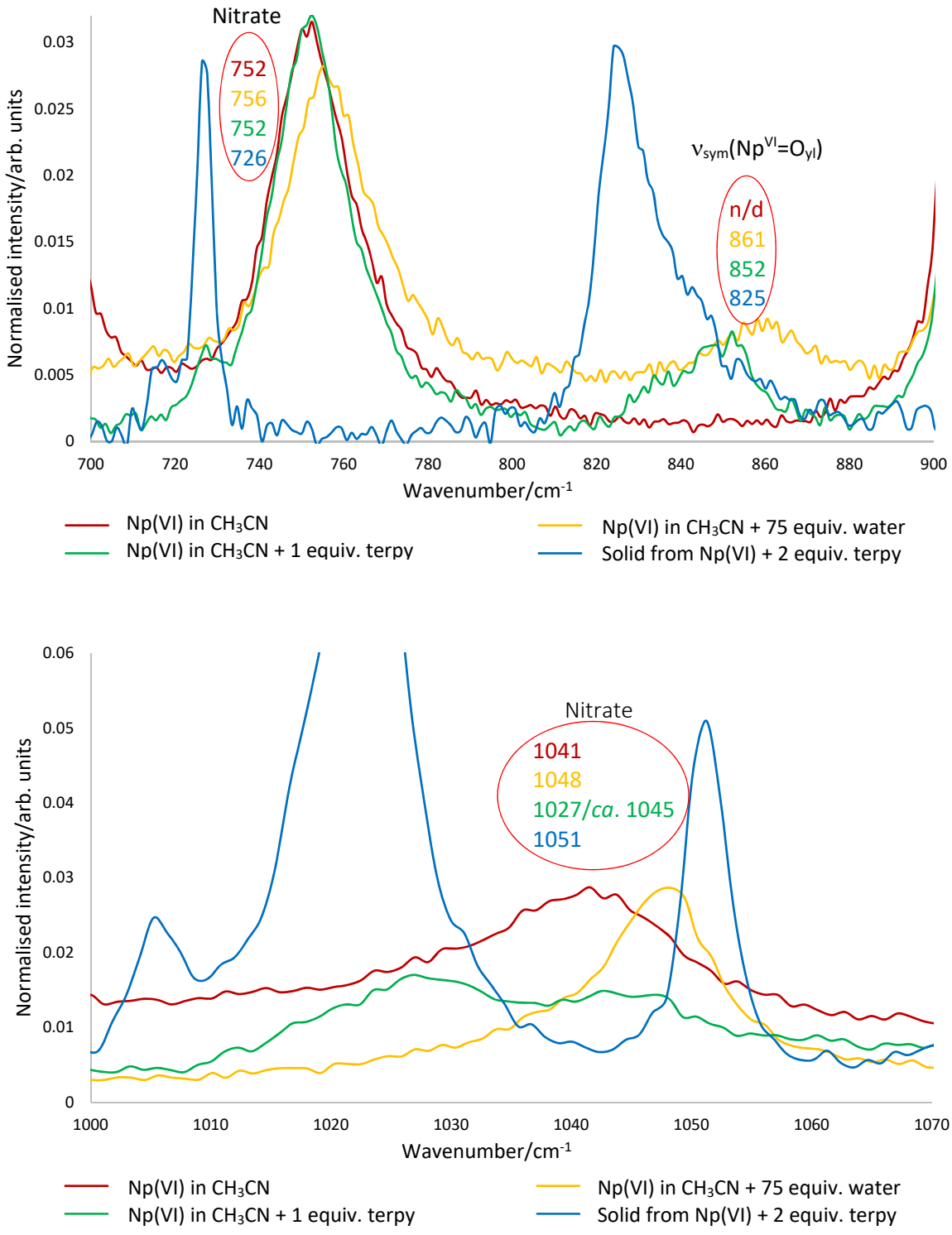

Figures 2.27a and b – Raman spectra of $Np^{VI}O_2^{2+}$ in CH_3CN between 700–900 cm^{-1} (top) and 1000–1070 cm^{-1} (bottom), with added water or terpy, and solids resulting from one equiv. of terpy. [$Np^{VI}O_2^{2+}$] = 0.016 M. n/d is not detected. Numbers are wavelengths in nm.

These Raman spectra support the assignment of $Np^{VI}O_2^{2+}$ with bound nitrates; peaks at *ca*. 760 cm^{-1} and 1040–1050 cm^{-1} are Raman active modes of the NO_3^- ion. No evidence of $Np^{V}O_2^{+}$ (Raman stretches of 760–820 cm^{-1}) is observed.[125] When in 14 M HNO_3[120] or 1 M HNO_3/$Ca(NO_3)_2$[126] the Raman spectra

of $Np^{VI}O_2^{2+}$ (*cf*. $[Np^{VI}O_2(NO_3)_2]$ (**2.AQ**)) show bands at 750 and 1040 cm^{-1}, and 740 cm^{-1}, respectively. The Raman spectra of hydrated, complexed nitrate has bands at 720 cm^{-1} in HNO_3,[126] suggesting that no free nitrate groups are present for $Np^{VI}O_2^{2+}$ in CH_3CN. For comparison, nitrate groups in $\mathbf{U^{NO3}}$ have absorptions at 754 and 1030 cm^{-1} in CH_3CN solution (this work).

For $Np^{VI}O_2^{2+}$ with added water, or with added terpy, the peaks at *ca*. 850–860 cm^{-1} (for those recorded in solution) agree well with the values of 853–863 cm^{-1} recorded for the $\nu_{sym}(Np^{VI}=O)$ of $Np^{VI}O_2^{2+}$ in acidic media (*e.g.* 853 cm^{-1} in 14 M HNO_3,[120] 854 cm^{-1} or 856 cm^{-1} in 1 M HNO_3[127] or $HClO_4$,[128] or for the $\nu_{sym}(U^{VI}=O)$ of $\mathbf{U^{NO3}}$ recorded in CH_3CN (869 cm^{-1}; this work), further supporting the assignment of $Np^{VI}O_2^{2+}$. Though there are some differences between the solid and the solution spectra resulting from addition of terpy (*e.g.* solution, $\nu(Np^{VI}=O)$ = 852 cm^{-1}, solid, $\nu(Np=O)$ = 825 cm^{-1}), no evidence of $Np^{V}O_2^{+}$ ($\nu_{sym}(Np^{V}=O)$ *ca.* 760–780 cm^{-1})[125, 127] is observed.

2.3.3 Concluding Remarks and Further Work

Overall, neptunium, present as $Np^{VI}O_2^{2+}$, appears both soluble and stable in CH_3CN for at least three days in the presence of air and water, forming $[Np^{VI}O_2(NO_3)_2]$ (**2.AQ**), as indicated by UV-vis-NIR and Raman spectroscopies. This complex (**2.AQ**) appears stable to a large excess (< 100 equiv.) of water, and spectral changes consistent with formation of a 1:1 $Np^{VI}O_2^{2+}$/L complex ($[Np^{VI}O_2(NO_3)_2(L)]$) observed when L = phen (**2.5.phen**) or terpy (**2.5.terpy**) were added to a solution of $Np^{VI}O_2^{2+}$ in CH_3CN. These complexes likely form quickly upon addition of L, are tolerant of at least one additional equiv. of ligand, and are stable to decomposition for at least three days by UV-vis-NIR spectroscopy. Crystalline solids that may be suitable for X-ray crystallography have been observed when L = terpy (**2.5.terpy**), with discussions underway at suitable facilities to analyse this product further.

Due to experimental time constraints, there was not enough time to investigate the photochemistry of solutions of $[Np^{VI}O_2(NO_3)_2(L)]$ (**2.5**) in CH_3CN on model substrates, DHA and xanthene, and monitor the production of either anthracene or xanthone (analogously to uranyl; Sections 3.3 and 3.4) spectroscopically (*e.g.* by Raman spectroscopy), with the objective being a proof-of-concept (*e.g.* as with $*U^{VI}O_2^{2+}$, to test the hypothesis the photochemical reactivity of $*Np^{VI}O_2^{2+}$ could be enhanced by addition of *N*-heterocycles). As there are no examples of Np of any oxidation state being exploited photocatalytically this would represent the first example of a transuranium actinyl ion being utilised in such a way, offering insights into new (photo-)chemistry of the other actinyl (neptunyl or plutonyl) ions. Unlike the monochromatic or high-energy light source required to access $*U^{VI}O_2^{2+}$, the large number of absorptions in the visible region (400–750 nm) for $Np^{VI}O_2^{2+}$ in CH_3CN suggests that a broad spectrum white light should be suitable to access $*Np^{VI}O_2^{2+}$.

2.4 Complexes of the Uranyl Ion with Multidentate Amides

In order to develop a more complete picture of suitable ligands to use with the uranyl(VI) ion (Section 2.13), amide ligands were used to synthesise uranyl complexes with modified photochemical properties. Three types of amide ligands were used: malonamides; diglycolamides, and other tridentate amides; and other monodentate amides.

2.4.1 Synthesis and Characterisation of $\mathbf{U^{mal}}$, $\mathbf{U^{malPh2}}$, $\mathbf{U^{malPh4}}$ and $\mathbf{U^{mal\textit{i}Pr4}}$

Given its commercial availability, low cost and endogenous non-toxicity, the reactions of malonamide and easily synthesised *N,N*′-aryl or -isopropyl substituted derivatives with $\mathbf{U^{NO3}}$ were among the first reactions studied (Scheme 2.6), giving $[UO_2(NO_3)_2(L)]$, in all cases. Where L = malonamide (mal), the product is $[UO_2(NO_3)_2(mal)]$, $\mathbf{U^{mal}}$; where L = *N,N*′-diphenylmalonamide ($malPh_2$), the product is $[UO_2(NO_3)_2(malPh_2)]$, $\mathbf{U^{malPh2}}$; where L = *N,N,N*′,*N*′-tetraphenylmalonamide ($malPh_4$), the product is $[UO_2(NO_3)_2(malPh_4)]$, $\mathbf{U^{malPh4}}$; where L = *N,N,N*′,*N*′-tetraisopropylmalonamide (mal^iPr4), the product is $[UO_2(NO_3)_2(mal^iPr_4)]$ $\mathbf{U^{mal\textit{i}Pr4}}$. The suitability of the parent $\mathbf{U^{mal}}$ complex for i) solution-phase and ii) photolytic stability was then examined by ^{1}H NMR, (ATR-)IR and electronic absorption and fluorescence spectroscopies, and SCXRD. All four complexes, $\mathbf{U^{mal}}$, $\mathbf{U^{malPh2}}$, $\mathbf{U^{malPh4}}$ and $\mathbf{U^{mal\textit{i}Pr4}}$, are isolated in high yields (> 90%) as yellow or dark yellow powders upon removal of volatiles *in vacuo*.

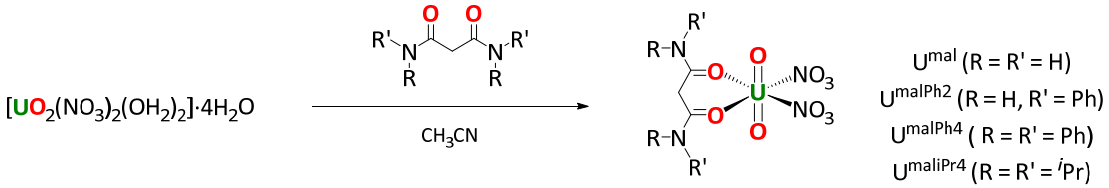

Scheme 2.6 – Complexation of malonamide ligands with uranyl, $\mathbf{U^{NO3}}$, in CH_3CN, giving $\mathbf{U^{mal}}$ (with mal, R = R′ = H), $\mathbf{U^{malPh2}}$ (with $malPh_2$, R = H, R′ = Ph), $\mathbf{U^{malPh4}}$ (with $malPh_4$, R = R′ = Ph), or $\mathbf{U^{maliPr4}}$ (with mal^iPr4, R = R′ = ^{i}Pr).

^{1}H NMR spectra of $\mathbf{U^{mal}}$, $\mathbf{U^{malPh2}}$, $\mathbf{U^{malPh4}}$ and $\mathbf{U^{mal\textit{i}Pr4}}$ in CD_3CN solution all show resonances that are distinct from uncomplexed mal, $malPh_2$, $malPh_4$ or mal^iPr_4, respectively, with N-H environments, where present, being particularly informative. For example, in $\mathbf{U^{mal}}$ N-H signals are inequivalent broad singlets in CD_3CN solution at 8.07 and 7.89 ppm, appearing at a higher frequency than mal, which has N-H signals at 6.74 and 5.81 ppm, respectively.

Resonances consistent with uncomplexed water are also observed at *ca*. 2.1–2.4 ppm for each of the four complexes. For example, with $\mathbf{U^{mal}}$, the resonance of water is found to be *ca*. 2.1 ppm, consistent with uncomplexed water in CD_3CN.[129] This is clearly distinct from the very broad singlet at *ca*. 4–6 ppm that normally predominates in the ^{1}H NMR spectrum of $\mathbf{U^{NO3}}$ in CD_3CN (this work), where water is suggested to undergo rapid dynamic exchange in solution.[130] This suggests the interaction of water with the uranium centre is limited where bidentate amide ligands are employed.

Experiments were then performed to determine the longer term stability of these complexes in solution. The stability of $\mathbf{U}^{\mathbf{mal}}$, $\mathbf{U}^{\mathbf{malPh2}}$ and $\mathbf{U}^{\mathbf{malPh4}}$ was tested in wet solvent, by reflux, or irradiation. For standing in wet solvent, saturated solutions of $\mathbf{U}^{\mathbf{mal}}$, $\mathbf{U}^{\mathbf{malPh2}}$ and $\mathbf{U}^{\mathbf{malPh4}}$ in CD_3CN were analysed by ^1H NMR spectroscopy after 16 hours of standing in the dark, and compared to ^1H NMR spectra taken at t = 0. This was repeated on fresh, saturated solutions of $\mathbf{U}^{\mathbf{mal}}$, $\mathbf{U}^{\mathbf{malPh2}}$ and $\mathbf{U}^{\mathbf{malPh4}}$ in CD_3CN, which were either refluxed or irradiated for 16 hours (420 nm), as required.

After 16 hours, the ^1H NMR spectra of $\mathbf{U}^{\mathbf{mal}}$ in CD_3CN (standing in CD_3CN, reflux or irradiation) showed a 1:1:1 triplet, centred at 6.00 ppm, consistent with production of NH_4^+. This was additionally confirmed by ^1H-^{15}N HSQC NMR spectroscopy, showing a correlation between the 1:1:1 triplet at *ca.* 6.00 ppm and a peak at 23.63 ppm, consistent with NH_4^+ in CD_3CN.[131] Similar signals were observed in the ^1H NMR spectra of $\mathbf{U}^{\mathbf{malPh2}}$ and $\mathbf{U}^{\mathbf{malPh4}}$ in CD_3CN (*e.g.*, NH_3Ph^+ or $NH_2Ph_2^+$, respectively).

In order to discount photolytic production of NH_4^+, a sample of $\mathbf{U}^{\mathbf{mal}}$ was then dissolved in CD_3CN and stored in the dark for one week, and analysed by ^1H NMR spectroscopy. Peaks consistent with production of NH_4^+ were once again observed, suggesting that production of NH_4^+ in $\mathbf{U}^{\mathbf{mal}}$ (and by extension $\mathbf{U}^{\mathbf{malPh2}}$ and $\mathbf{U}^{\mathbf{malPh4}}$) occurs *via* a pathway that is not light induced. Given the Lewis acidity of U^{VI} in $U^{VI}O_2^{2+}$, it is likely that the amide functionalities in $\mathbf{U}^{\mathbf{mal}}$, $\mathbf{U}^{\mathbf{malPh2}}$ and $\mathbf{U}^{\mathbf{malPh4}}$ are hydrolytically sensitive, according to Scheme 2.7. Attempts to characterise the hypothesised intermediate amide-carboxylate uranyl(VI) complex by ^1H NMR or IR spectroscopy were unsuccessful.

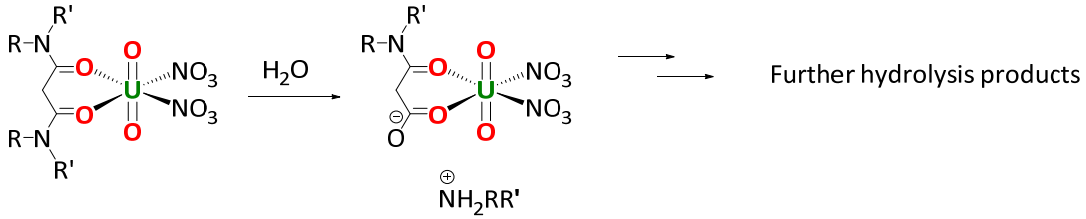

Scheme 2.7 – Proposed mechanism for the hydrolysis of $\mathbf{U}^{\mathbf{mal}}$ (R = R′ = H), $\mathbf{U}^{\mathbf{malPh2}}$ (R = H, R′ = Ph) and $\mathbf{U}^{\mathbf{malPh4}}$ (R = R′ = Ph).

Successive *N*-aryl substitution appears to increase the hydrolytic sensitivity of the amide groups, as no signals consistent with $\mathbf{U}^{\mathbf{malPh4}}$ were observed by ^1H NMR spectroscopy after one week in CH_3CN, compared with approximately 55% of $\mathbf{U}^{\mathbf{malPh2}}$ and 80% of $\mathbf{U}^{\mathbf{mal}}$ remaining (*e.g.*, hydrolytic stability of $\mathbf{U}^{\mathbf{malPh4}} < \mathbf{U}^{\mathbf{malPh2}} < \mathbf{U}^{\mathbf{mal}}$). No decomposition of a saturated CH_3CN solution of $\mathbf{U}^{\mathbf{mal}i\mathbf{Pr4}}$ (stored in the dark) was observed by ^1H NMR spectroscopy after one week.

To further investigate the solution-phase lability of $\mathbf{U}^{\mathbf{mal}}$ (*cf.* monodentate amides were found to have solution-phase equilibria, Section 2.5), variable temperature ^1H NMR spectroscopy experiments $\mathbf{U}^{\mathbf{mal}}$

in CD_3CN were undertaken. Figure 2.28, below, shows the stacked ^1H NMR spectra of $\mathbf{U}^{mal}$ at 233 K (-40°C), 298 K (25°C) and 340 K (67°C) in CD_3CN.

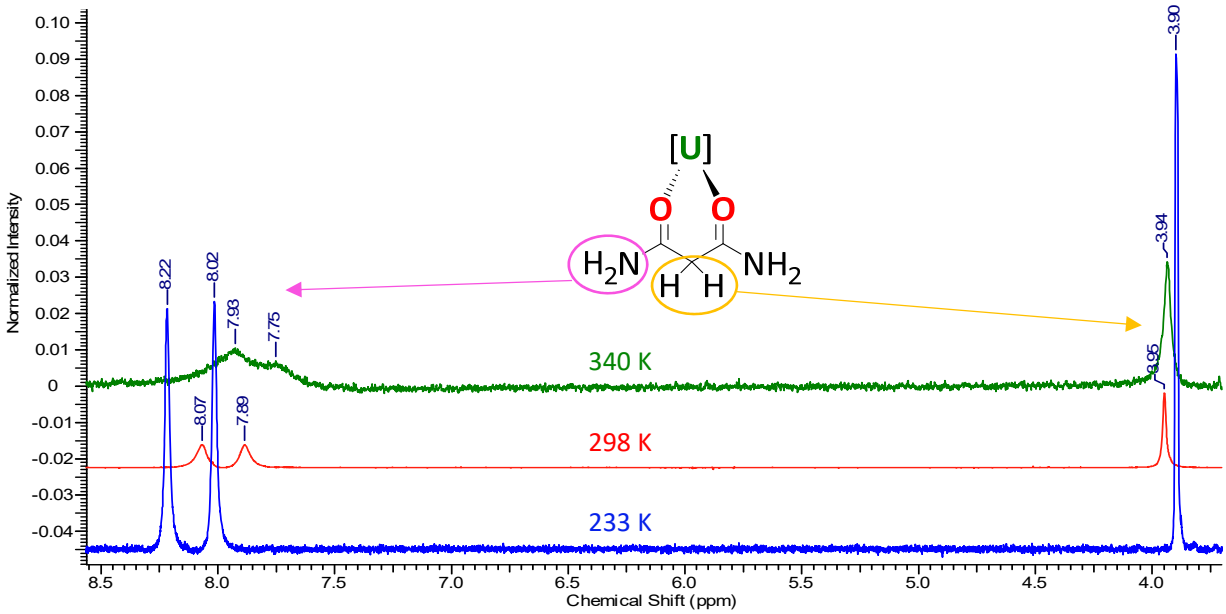

Figure 2.28 – Stacked ^1H NMR spectra of $\mathbf{U}^{mal}$ in CD_3CN at 233 K, 298 K and 340 K, along with highlighted protons on the malonamide ligand backbone of $\mathbf{U}^{mal}$. The remainder of the $\mathbf{U}^{mal}$ complex is abbreviated to [U] for clarity.

The ^1H NMR spectrum of $\mathbf{U}^{mal}$ at 233 K shows only two N-H proton environments, consistent with one species in solution, with slight broadening of these resonances at 298 K. This suggests that $\mathbf{U}^{mal}$ is stable in solution at r.t. This is in contrast to the ^1H NMR spectra for monodentate amide complexes of the uranyl(VI) ion where low-temperature ^1H NMR studies showed the presence of multiple N-H environments, interpreted as multiple uranyl complexes, in CD_3CN solution; Section 2.5.

To further investigate the solution-phase behaviour of $\mathbf{U}^{mal}$, and any differences that arise from the use of bidentate rather than monodentate amides, a saturated solution of $\mathbf{U}^{mal}$ in CD_3CN was prepared, and known quantities of acetamide (1 or 2 equiv.) added. This is depicted in Scheme 2.8, below. The solutions were then analysed by ^1H NMR spectroscopy.

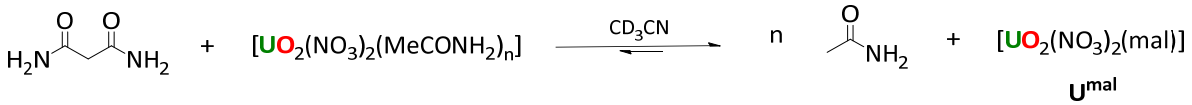

Scheme 2.8 – Addition of n (= 1 or 2) equiv. of acetamide to $\mathbf{U}^{mal}$.

The ^1H NMR spectra of these solutions were then compared to the ^1H NMR spectrum of $\mathbf{U}^{mal}$ in CD_3CN with two equiv. of malonamide, along with the ^1H NMR spectra of uncomplexed acetamide and malonamide in CD_3CN. These stacked ^1H NMR spectra are shown in Figure 2.29, below.

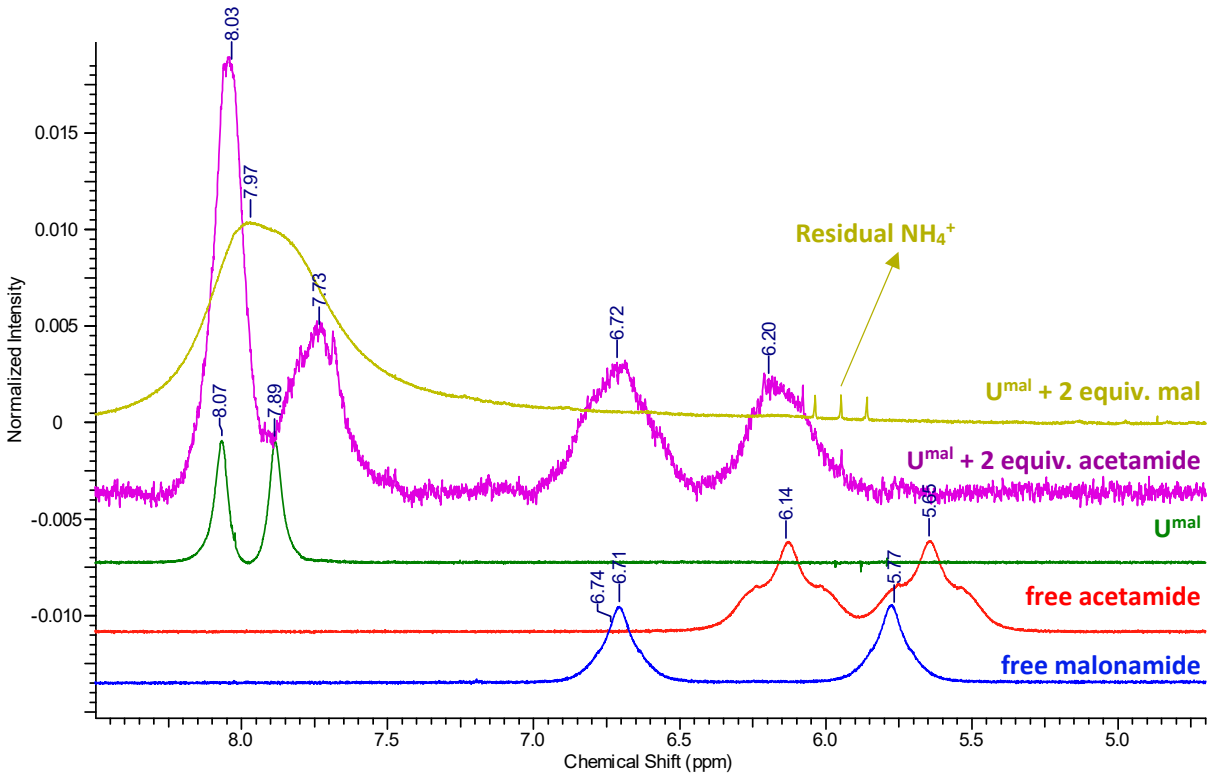

Figure 2.29 – Stacked ^{1}H NMR spectra (CD_3CN) showing the N-H resonances of i) uncomplexed malonamide, ii) uncomplexed acetamide, iii) **U^{mal}**, iv) **U^{mal}** + 2 equiv. of uncomplexed acetamide, and v) **U^{mal}** + 2 equiv. of uncomplexed malonamide. Resonances corresponding to NH_4^+ in the ^{1}H NMR spectrum of **U^{mal}** are also highlighted.

The stacked spectra suggest that an excess (two equiv.) of the monodentate acetamide makes little difference in the resonances of the N-H protons in **U^{mal}**, shifting from 8.07 and 7.89, to 8.03 and 7.73 ppm, respectively. Addition of an excess of malonamide to a solution of **U^{mal}** in CD_3CN, however, causes an averaging of peaks consistent with the amide N-H protons (7.97 ppm), with significant broadening, resulting from fast exchange on the NMR timescale. This suggests that malonamide outcompetes monodentate amides for coordination to $U^{VI}O_2^{2+}$ ions in CD_3CN solution (presumably by forming a 6-membered chelating ring), but that there is exchange between uncoordinated and coordinated malonamide ligands when an excess of malonamide ligand is present in a solution of **U^{mal}**.

The UV-vis spectra of **U^{mal}**, **U^{malPh2}** and **U^{malPh4}** in CH_3CN are all very similar, possessing features similar to **U^{NO3}**; for example, the ε_{max} and λ_{max} values for the LMCT band are < 20 $M^{-1}cm^{-1}$ and *ca*. 420 nm in all cases, respectively. These results agree with electronic absorption spectrum recorded for $[UO_2(NO_3)_2(DMDBMA)]$ (**2.AR**, DMDBMA = *N,N′*-dimethyl-*N,N′*-dibutylmalonamide) in which no discernible spectral changes were observed on complexation for the LMCT band at *ca*. 420 nm for $[UO_2(NO_3)_2(DMDBMA)]$ (**2.AR**) compared to **U^{NO3}** in CH_3CN at 292 K (19°C).[132]

The excitation and emission spectra for **U^{mal}** are also unremarkable, with both relative intensities and peak positions being nearly identical to those recorded in the electronic spectra of **U^{NO3}**, Figure. 2.30.

This suggests that excitation of both catalysts, $\mathbf{U}^{\mathbf{NO3}}$ or $\mathbf{U}^{\mathbf{mal}}$, with 420 nm light produces $*U^{VI}O_2^{2+}$ ions with very similar photochemical properties.

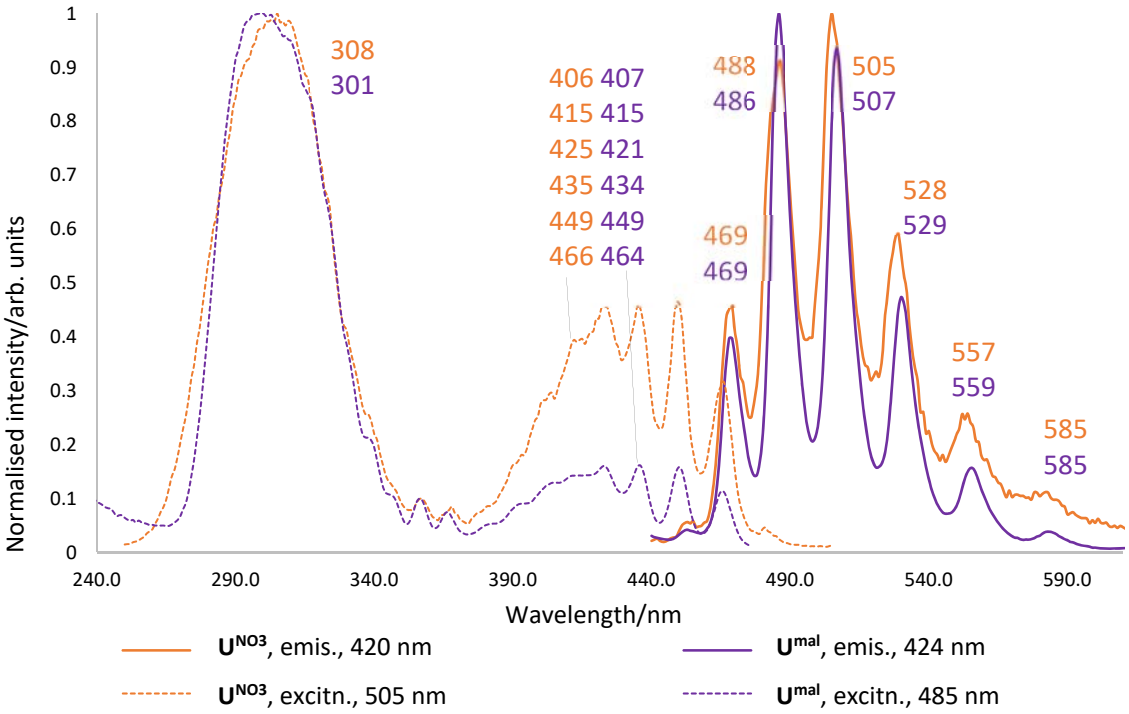

Figure 2.30 – Combined excitation and emission spectra of $\mathbf{U}^{\mathbf{NO3}}$ (ORANGE) and $\mathbf{U}^{\mathbf{mal}}$ (PURPLE) in CH_3CN; [$\mathbf{U}^{\mathbf{NO3}}$] = 7.50 x 10^{-3} M, [$\mathbf{U}^{\mathbf{mal}}$] = 2.99 x 10^{-3} M. Numbers are wavelengths in nm.

The Stokes shifts for $\mathbf{U}^{\mathbf{NO3}}$ (3820 cm^{-1}) and $\mathbf{U}^{\mathbf{mal}}$ (3008 cm^{-1}) are also reasonably similar, with the value for $\mathbf{U}^{\mathbf{mal}}$ suggesting there is a smaller solvent cage reorganisation upon excitation than that present in $\mathbf{U}^{\mathbf{NO3}}$. This difference is small, however, and further highlights that complexation of malonamide only minimally influences the electronic structure of the uranyl(VI) ion.

The solid-state structures of $\mathbf{U}^{\mathbf{mal}}$, $\mathbf{U}^{\mathbf{malPh2}}$, $\mathbf{U}^{\mathbf{malPh4}}$ and $\mathbf{U}^{\mathbf{mali\mathrm{Pr}4}}$ are also very similar. The crystal structures of $\mathbf{U}^{\mathbf{mal}}$, $\mathbf{U}^{\mathbf{malPh2}}$, $\mathbf{U}^{\mathbf{malPh4}}$ and $\mathbf{U}^{\mathbf{mali\mathrm{Pr}4}}$ are given below in Figures 2.31A-F and Table 2.5.

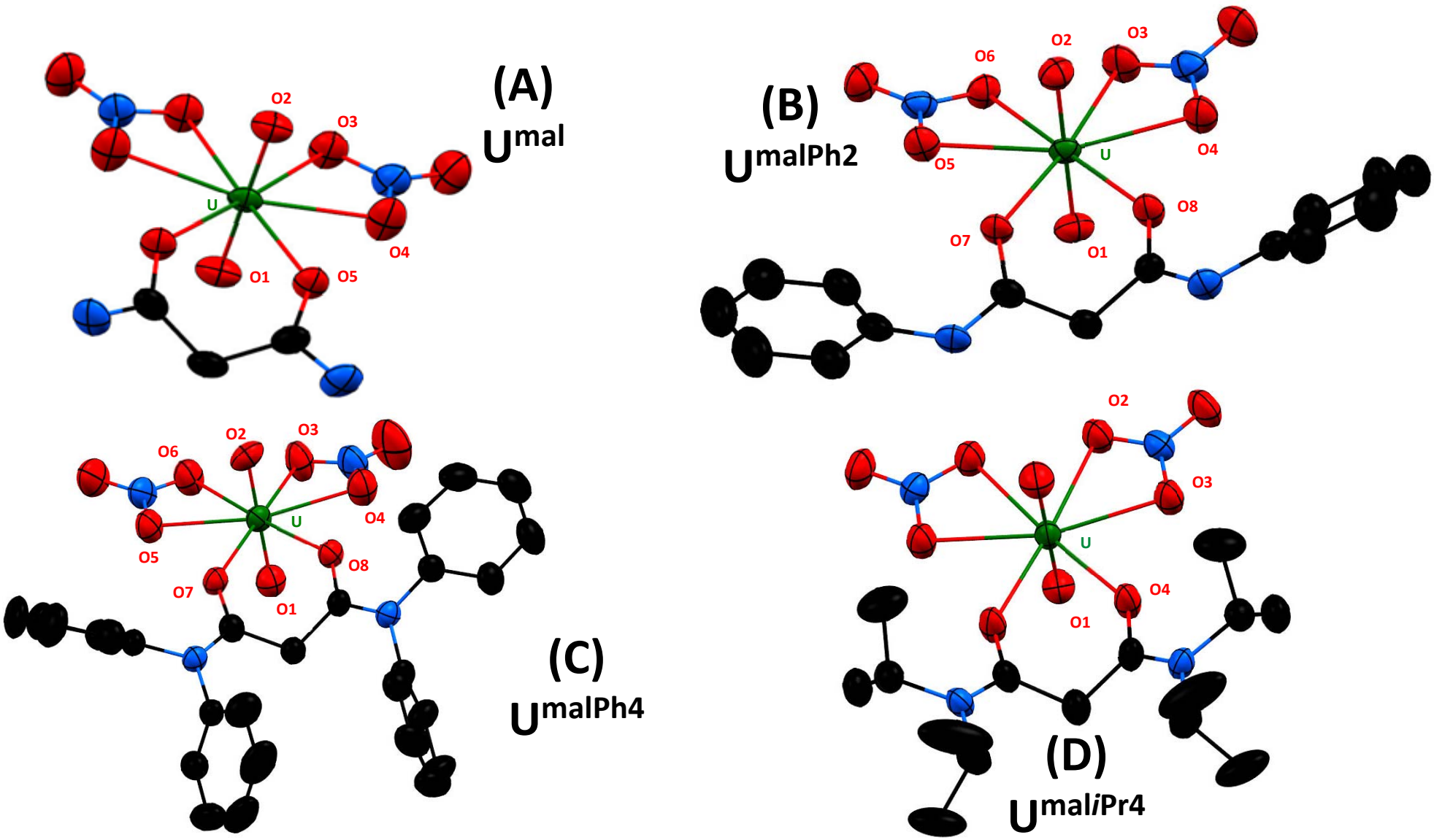

Figure 2.31**A**–**D** – Thermal ellipsoid plots (50% probability) of $\mathbf{U^{mal}}$ **(A)**, $\mathbf{U^{malPh2}}$ **(B)**, $\mathbf{U^{malPh4}}$ **(C)** and $\mathbf{U^{mal\textit{i}Pr4}}$ **(D)**. One uncoordinated mal ligand in $\mathbf{U^{mal}}$, and one CH_3CN molecule in $\mathbf{U^{malPh4}}$ are omitted for clarity. Key: uranium, oxygen, nitrogen, carbon. H atoms are omitted for clarity.

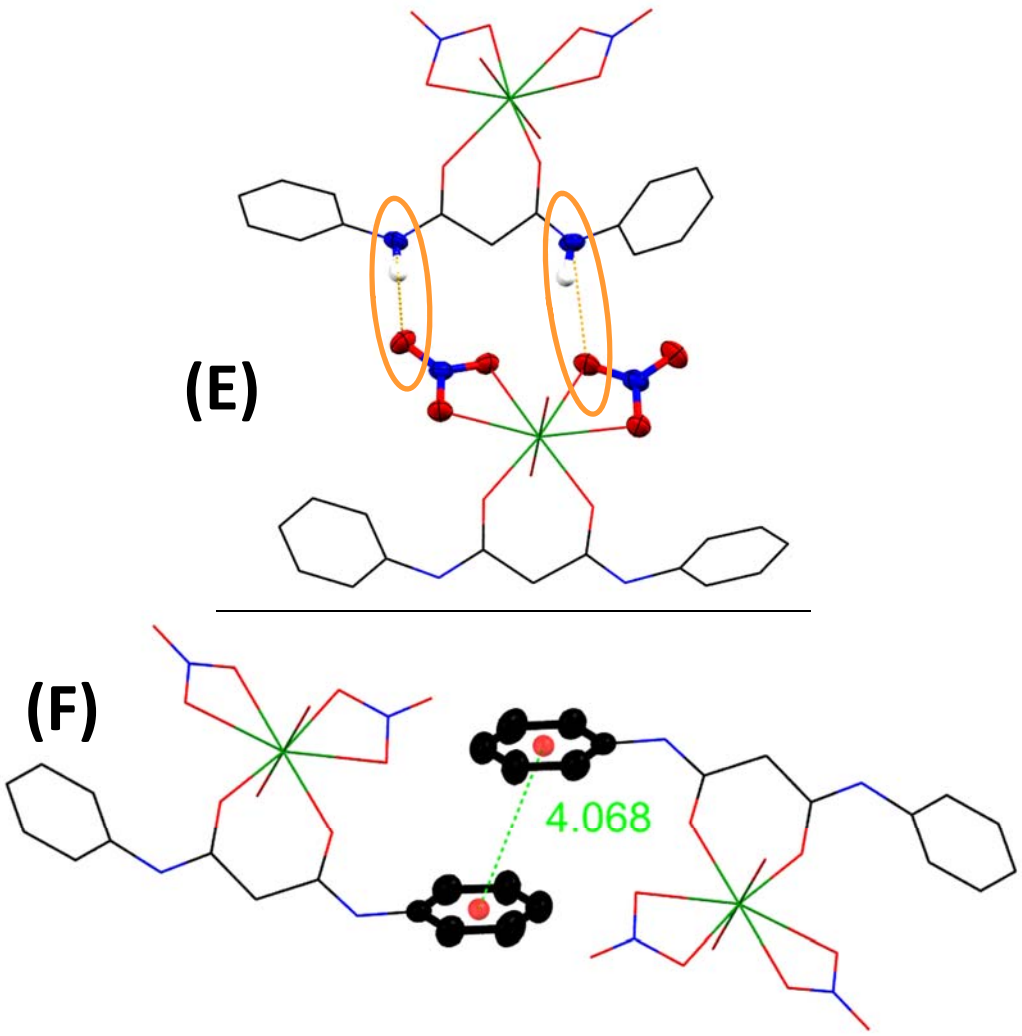

Figures 2.31**E** – Extended non-covalent interactions present in, for example, $\mathbf{U^{malPh2}}$, highlighting amide N-H groups interacting *via* H-bonding (orange ovals) with nitrate groups of a neighbouring molecule; and **F** – interactions of π-π stacking between two phenyl rings in neighbouring $\mathbf{U^{malPh2}}$ molecules. The distance between two ring centroids, represented as red circles, is *ca*. 4.07 Å. For both figures, relevant parts of the molecule are shown as ellipsoids at 50% probability with the remainder drawn as a 'wireframe'. Key: uranium, oxygen, nitrogen, carbon.

Parameter	$\mathbf{U^{mal}}$	$\mathbf{U^{malPh2}}$	$\mathbf{U^{malPh4}}$	$\mathbf{U^{mali Pr4}}$
d(U=O_{yl})/ Å	1.751(3) (O1) 1.754(3) (O2)	1.755(3) (O1, O2)	1.723(5) (O1) 1.737(5) (O2)	1.753(5) (O1)
d(U-O_{nit})/ Å	2.540(3) (O3) 2.495(4) (O4)	2.488(4) (O3) 2.509(4) (O4) 2.543(4) (O5) 2.520(4) (O6)	2.491(5) (O3) 2.493(6) (O4) 2.494(4) (O5) 2.502(5) (O6)	2.525(7) (O2) 2.508(8) (O3)
d(U-O_{amide})/ Å	2.402(4) (O5)	2.385(4) (O7) 2.377(4) (O8)	2.397(4) (O7) 2.404(4) (O8)	2.380(2) (O4)
∠(OUO)/ °	179.28(4)	179.7(2)	179.6(2)	177.3(3)

Table 2.5 – Key parameters (bond lengths/Å, angles/°) for the solid-state structures of $\mathbf{U^{mal}}$, $\mathbf{U^{malPh2}}$, $\mathbf{U^{malPh4}}$ and $\mathbf{U^{mali Pr4}}$.

In each structure the uranium centre is eight-coordinate, with all O=U=O angles being essentially linear, consistent with U^{VI} in all cases (*cf*. $U^{VI}O_2^{2+}$).[111] All U^{VI}=O_{yl}, U-O_{nit} and U-O_{mal} bonds are also very similar (*ca*. 1.72-1.75, 2.5, and 2.4 Å, respectively), with any structural changes (such as H-bonding and π-π stacking, Figures 2.31E and F) likely driven by changes in crystal packing (*e.g.* 0x, 2x, or 4x Ph, and 4x ^{i}Pr groups), rather than electronic effects from the malonamide ligands. These distances and angles are similar to analogous *N,N*′-dialkylmalonamides reported, including $[UO_2(NO_3)_2(DMMA)]$[133] (**2.AS**, DMMA = *N,N*′-dimethylmalonamide; ∠(OUO) = 178.5(13)°, U^{VI}=O_{yl} = 1.775(5) Å, U-O_{nit} = 2.51(2), 2.513(8) Å, and U-O_{mal} = 2.41(2) Å), and $[UO_2(NO_3)_2(DEMA)]$[69] (**2.AT**, DEMA = *N,N*′-diethylmalonamide; ∠(OUO) = 177.57(13)°, U^{VI}=O_{yl} = 1.763(3), 1.770(3) Å, U-O_{nit} = 2.523(3), 2.526(2) Å, and U-O_{mal} = 2.340(2) Å), further suggesting malonamide complexation has little effect on the solid-state structures of the $U^{VI}O_2^{2+}$ ion. This is also reflected in the solid-phase IR spectral data for **U^{mal}**, **U^{malPh2}**, **U^{malPh4}**, and **U$^{mal\mathit{i}Pr4}$** with carbonyl, nitrate, and uranyl stretches appearing at *ca*. 1640, 1290, and 940 cm^{-1}, respectively, in all cases. An exact assignment of carbonyl or nitrate bands at *ca*. 1630–1650 or 1250–1300 cm^{-1} is complicated by the large number of bands within these ranges for each complex.

Though **U^{mal}** possesses no luminescent features distinct from **U^{NO3}**, use of malonamide ligands may, when combined with other groups, *e.g.* pyridyl functionalities, be useful in modifying the electronic properties of uranyl to induce unusual or novel reactivity. This hypothesis forms the basis for the use of the tridentate diamides, discussed in below in Section 2.4.2.

2.4.2 Reactions of U^{NO3} with Tridentate Diamides

The spectroscopic data collected for **U^{mal}** (Section 2.4.1, Figure 2.30) suggest that uranyl-diamide complexes are solution-stable. As the fluorescence spectroscopic data collected for the *N*-heterocycle-uranyl complexes (Sections 2.2.2 and 2.2.3) suggested that pyridyl functionalities may modify the electronic properties of the excited-state uranyl ion, $*U^{VI}O_2^{2+}$, a ligand where amide and pyridyl groups combine was desired. The ligand selected, 2,6-pyridinedicarboxamide, has a rigid pyridyl linking group. Therefore the direct reaction of 2,6-pyridinedicarboxamide, $py(CONH_2)_2$ with **U^{NO3}** in an equimolar ratio in CH_3CN was undertaken, Scheme 2.9.

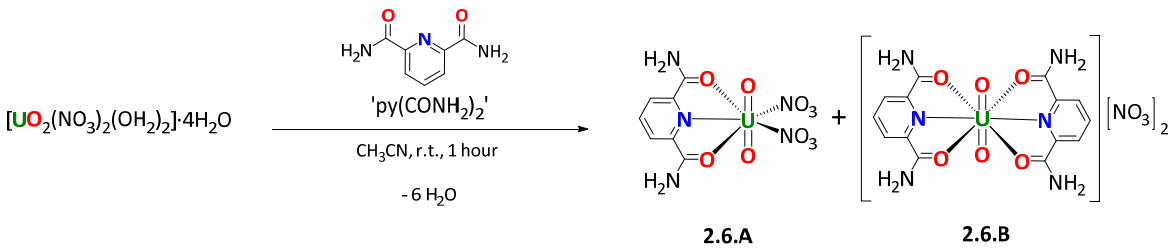

Scheme 2.9 – Complexation of $\mathbf{U^{NO3}}$ with 2,6-pyridinedicarboxamide, py(CONH$_2$)$_2$. ^{1}H NMR spectral analysis of the product mixture, referred to as **2.6**, was consistent with two products, A and B, above, in an approximate 5:4 ratio. As it was not possible to adequately resolve signals for **2.6.A** or **2.6.B** separately, '**2.6**' refers to the whole product mixture, rather than individual components.

^{1}H NMR spectroscopy of the product solution (**2.6**) indicated resonances consistent with complexation, distinct from uncomplexed or protonated py(CONH$_2$)$_2$. For example, the ^{1}H NMR spectrum of product mixture **2.6** shows two groups of broad singlets centred at 8.80 ppm and 8.15 ppm, in an approximate 5:4 ratio. ^{1}H NMR spectra of uncomplexed, and protonated, py(CONH$_2$)$_2$ both show one resonance centred at 8.20–8.30 ppm, which are not present in the ^{1}H NMR spectrum of product mixture **2.6**. Given the broad and overlapping nature of all the peaks observed in the ^{1}H NMR spectrum of product mixture **2.6**, it was not possible to satisfactorily assign individual resonances to a particular product, **2.6.A** or **2.6.B**.

It is speculated that these two sets of resonances in the ^{1}H NMR spectrum of product mixture **2.6** are two complexes, probably [UO$_2$(NO$_3$)$_2$(py(CONH$_2$)$_2$)] (**2.6.A**) and [UO$_2$(py(CONH$_2$)$_2$)$_2$][NO$_3$]$_2$ (**2.6.B**), that undergo exchange on the NMR timescale. This suggests that the tridentate py(CONH$_2$)$_2$ donor is sufficiently powerful enough to displace the nitrate ligands from the uranyl(VI) ion in solution, probably driven by formation of the five-membered chelate rings formed upon complexation. This gives both the 1:1 and 2:1 ligand:uranyl complexes in CD$_3$CN, complexes **2.6.A** and **2.6.B**, respectively, and has precedent in the chemical literature where solvent polarity has been shown sufficient to favour either the 1:1 or 2:1 ligand:uranyl (L/U) complex for an analogous *N,N'*-di-*p*-tolyl-*N,N'*-diethyl-2,6-pyridinedicarboxamide, py(CON^{p}tolEt)$_2$-uranyl complex. The predominant product of the reaction between py(CON^{p}tolEt)$_2$ and $\mathbf{U^{NO3}}$ in molecular solvent (CH$_2$Cl$_2$[134] or phenyltrifluoromethyl sulfone[135]) is the 1:1 L/U complex, [UO$_2$(NO$_3$)$_2$(py(CON^{p}tolEt)$_2$)] (**2.AU.1**), which is different to that reported for the same reaction performed in the ionic liquid [C$_4$mim][NTf$_2$] ([C$_4$mim] is 1-butyl-3-methylimidazolium and NTf$_2$, bis(trifluoromethanesulfonyl)imide), where the 2:1 L/U complex, [UO$_2$(py(CON^{p}tolEt)$_2$)$_2$][NTf$_2$]$_2$ (**2.AU.2**), was observed, Scheme 2.10.[74]

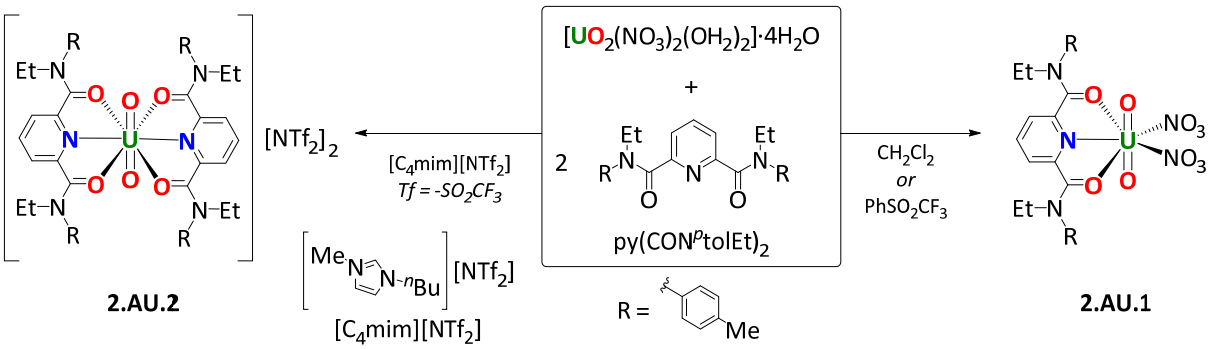

Scheme 2.10 – Synthesis of complex **2.AU.1** or **2.AU.2**, using py(CON^{p}tolEt)$_2$ ligand in either molecular solvents (CH_2Cl_2 or phenyltrifluoromethyl sulfone) or ionic liquid, [C_4mim][NTf_2], to give the 1:1 or 2:1 L/U complexes, respectively.

Here, in CD_3CN resonances consistent with both $[UO_2(NO_3)_2(py(CONH_2)_2)]$ (**2.6.A**) and $[UO_2(py(CONH_2)_2)_2][NO_3]_2$ (**2.6.B**) are speculated to be observed in solution by ^{1}H NMR spectroscopy. Given the importance of having only one uranyl(VI)-containing complex in CH_3CN, this renders photocatalytically-active uranyl(VI) complexes derived from $py(CONH_2)_2$ ligands impractical. The product mixture (**2.6**) is also unstable to photolysis (420 nm, 16 hours, r.t.), with many new resonances appearing after photolysis that were not present in the ^{1}H NMR spectrum of the product mixture **2.6**.

However, solid-phase IR spectroscopy of the product mixture (**2.6**) after the removal of volatiles shows the retention of nitrate ligands, judging from the band (ν_{asym}(N-O)) at 1270 cm^{-1} in the solid state, which is distinct from **U^{NO3}** (1333 and 1302 cm^{-1}), but similar to **U^{mal}**, **U^{malPh2}**, **U^{malPh4}** and **U$^{mali Pr4}$** (*ca*. 1290 cm^{-1}) described in Section 2.4.1. The $U^{VI}O_2^{2+}$ ion is indicated by the strong absorption (ν_{asym}(U=O)) at 938 cm^{-1}, similar to that of **U^{NO3}**, 935 cm^{-1}. There is negligible observed change in the carbonyl stretches in the mixture (**2.6**) and uncomplexed $py(CONH)_2$, 1666 and 1664 cm^{-1}, respectively.

Although attempts to clarify the composition of the product mixture (**2.6**) by crystallography were unsuccessful, it was possible to isolate a solid-state structure of $[UO_2(py(CONHMe)_2)_2][NO_3]_2$ (**2.7**) by using an *N*-methylated version of $py(CONH_2)_2$. This new ligand, *N*,*N*'-dimethyl-2,6-pyridinedicarboxamide, $py(CONHMe)_2$, was reacted with **U^{NO3}** in a 2:1 CH_3CN/H_2O co-solvent mixture, to give product **2.7**, outlined in Scheme 2.11. The solid-state structure and key parameters of the product (**2.7**) are given in Figure 2.32 and Table 2.6. Attempts to analyse the product (**2.7**) by ^{1}H NMR spectroscopy were not successful as the product was, surprisingly, insoluble in CD_3CN or CD_3OD.

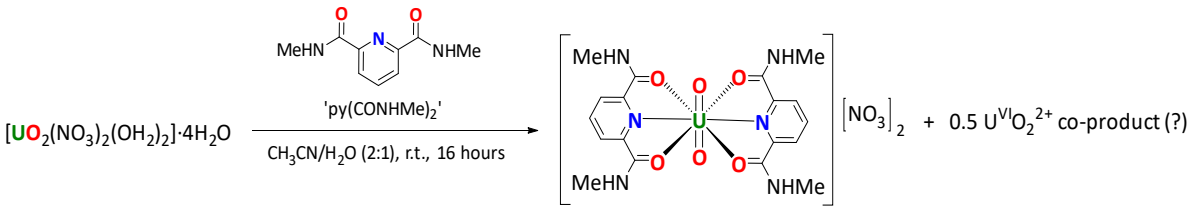

2.7

Scheme 2.11 – Complexation of $\mathbf{U^{NO3}}$ with *N*,*N*′-dimethyl-2,6-pyridinedicarboxamide, py(CONHMe)$_2$. As the stoichiometry does not balance in the product, [UO$_2$(py(CONHMe)$_2$)$_2$][NO$_3$]$_2$ (**2.7**), 0.5 equiv. of another $U^{VI}O_2^{2+}$ co-product, or unreacted $\mathbf{U^{NO3}}$, is required to balance the stoichiometry of the reaction. The identity of this possible co-product is not clear.

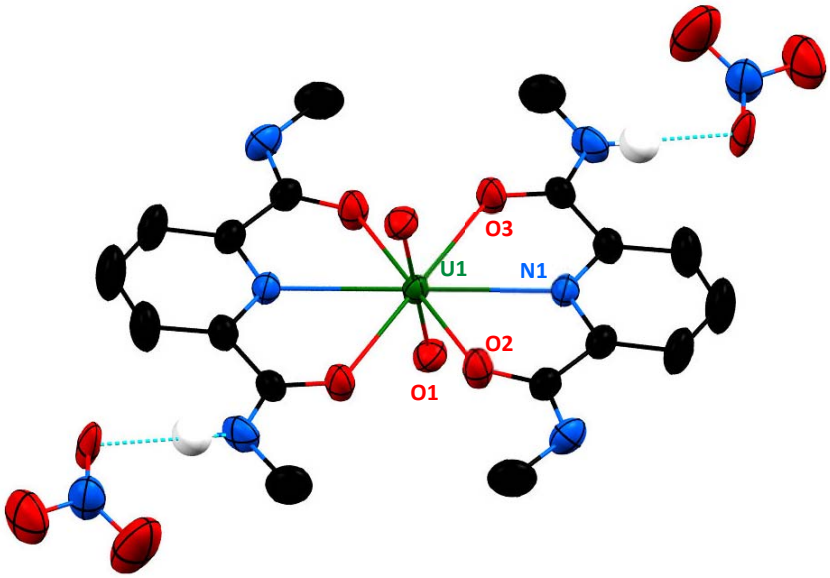

Figure 2.32 – Thermal ellipsoid plot of [UO$_2$(py(CONHMe)$_2$)$_2$][NO$_3$]$_2$ (**2.7**). The nitrate counteranions are positionally disordered over two sites in shared 0.45/0.55 occupancy, with those of 0.55 occupancy, along with H-bonding H-atoms, displayed for clarity. Ellipsoids are drawn at 50% probability. Key: uranium, oxygen, nitrogen, carbon.

Parameter	Complex 2.7	$[UO_2(NO_3)_2(py(CON^{p}tolEt_2))]$ (**2.AU.1**)[134]	$[UO_2Cl_2(py(CON^{i}Pr_2))]$ (**2.AV**)[73]	$[UO_2(py(CON^{p}tolEt)_2)_2][NTf_2]_2$ (**2.AU.2**)[74]
d(U=O_{yl})	1.757(5) (O1) Å	1.761(3), 1.765(3) Å	1.760(2), 1.763(2) Å	1.751(3) Å
d(U-O_{amide})	2.428(5) (O2), 2.428(4) (O3) Å	2.394(3), 2.460(3) Å	2.378(2), 2.404(2) Å	2.413(3), 2.440(4) Å
d(U-N_{py})	2.663(5) (N1) Å	2.661(3) Å	2.663(2) Å	2.716(2) Å
∠(OUO)	180°	171.10(1)°	174.9(1)°	180°
∠($O_{amide}UO_{amide}$)	117.6(3)° (O2-U-O3)	120.34(9)°	123.27(1)°	117.6(5)°

Table 2.6 – Key parameters (bond lengths/Å, angles/°) for the solid-state structure of $[UO_2(py(CONHMe)_2)_2][NO_3]_2$ (**2.7**), compared to analogous literature complexes.

All parameters for $[UO_2(py(CONHMe)_2)_2][NO_3]_2$ (**2.7**) are consistent with the uranyl(VI) ion,[111] and compare well to those reported for the analogous 2:1 L/U $[UO_2(py(CON^{p}tolEt)_2)_2][NTf_2]_2$ complex (**2.AU.2,** Table 2.6).[74] The O_{amide}-U-O_{amide} and O_{yl}=U=O_{yl} bond angles are also similar to those reported for the 1:1 L/U complexes $[UO_2(NO_3)_2(py(CON^{p}tolEt_2))]$[134] (**2.AU.1**) and $[UO_2Cl_2(py(CON^{i}Pr_2))]$ (**2.AV**).[73] The deciding factor in speciation of uranyl(VI) complexes with $py(CONR)_2$ ligands in the solid-state is currently unclear, though the choice of solvent is posited to be an important factor; the related molecular compounds, $[UO_2(NO_3)_2(py(CON^{p}tolEt_2))]$[134] (**2.AU.1**) and $[UO_2Cl_2(py(CON^{i}Pr_2))]$[73] (**2.AV**) were isolated from non-polar molecular solvents, CH_2Cl_2 (Scheme 2.10) or $C_6H_5NO_2$, respectively, whereas the ion-pair complex $[UO_2(py(CON^{p}tolEt)_2)_2][NTf_2]_2$ (**2.AU.2**) was crystallised from $[C_4mim][NTf_2]$ ionic liquid (Scheme 2.10).[74]

To investigate the binding mode of the tridentate, di-amides to the uranyl ion, a series of complexes of $\mathbf{U^{NO3}}$ with diglycolamides, $R_2NC(O)CH_2OCH_2C(O)NR_2$, were synthesised. As discussed in Section 2.1.3, diglycolamide ligands are also commonly employed in the solvent extraction of the actinides, especially uranyl, which is advantageous as there is pre-existing knowledge of uranyl speciation in the presence of diglycolamide ligands.[78] Two ligands, diglycolamide (digly) and TODGA (*N,N,N′,N′*-tetraoctadiglycolamide), were selected for their simplicity, and previous use in solvent extraction studies of uranyl (for TODGA, in nitric acid).[136, 137] Scheme 2.12 shows the unsuccessful complexation reactions of $\mathbf{U^{NO3}}$ with equimolar amounts diglycolamide or TODGA in CH_3CN.

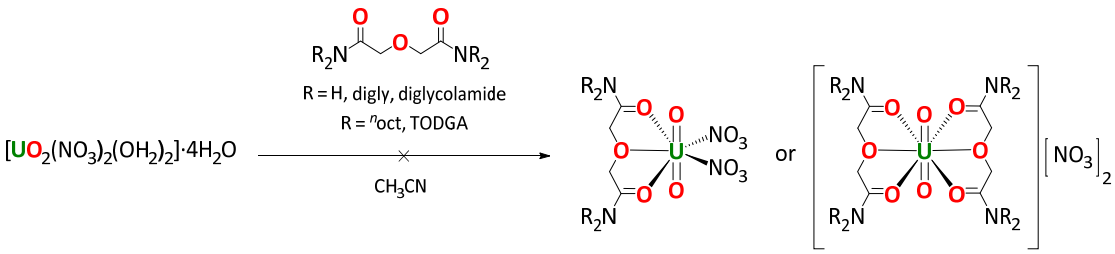

Scheme 2.12 – Unsuccessful syntheses of $[UO_2(NO_3)_2(digly)]$ or $[UO_2(digly)_2][NO_3]_2$ (reaction **2.8**, where R = H, diglycolamide, digly), or $[UO_2(NO_3)_2(TODGA)]$ or $[UO_2(TODGA)_2][NO_3]_2$ (reaction **2.9**, where R = C_8H_{17}, TODGA).

The product solution resulting from addition of diglycolamide to $\mathbf{U^{NO3}}$, reaction **2.8**, contained significant quantities of NH_4^+, clearly visible by the appearance of the characteristic 1:1:1 triplet centred at 6 ppm in the ^{1}H NMR spectrum of product mixture **2.8**. These data contradict the previously reported isolation of $[UO_2Cl_2(O(CH_2CONR_2)_2)]$ (R = ^{i}Pr, **2.AW.^{i}Pr**; or ^{i}Bu, **2.AW.^{i}Bu**), which are stable by ^{1}H NMR spectroscopy in CD_3OD.[72] It is currently unclear why this occurs, particularly as $–NH_2$ malonamides are more stable to hydrolysis than their $–N(aryl)_2$ analogues when complexed with $\mathbf{U^{NO3}}$ (Section 2.4.1) Given the appearance of NH_4^+ in the ^{1}H NMR spectrum of product mixture **2.8**, the complexation of digly to uranyl(VI) was not pursued further.

Unlike reaction **2.8**, the ^{1}H NMR spectrum of product mixture **2.9** (**U^{NO3}** + TODGA) shows no resonances consistent with NH_4^+. Resonances distinct from uncomplexed TODGA are observed, with shifts to a higher frequency of 0.26 (3.15 → 3.41 ppm) and 0.63 ppm (3.22 → 3.85 ppm), and 1.3 ppm (4.14 → 5.45 ppm), for the diagnostic O-C$\underline{H}_2$- and N-C$\underline{H}_2$-(C_7H_{15}) environments, respectively, and may be indicative of complexation to the uranyl(VI) ion. Solution-phase IR spectroscopy performed on the product mixture (**2.9**) in CH_3CN shows bands that also do not correspond to uncomplexed TODGA, with ν(C=O) shifting from 1654 cm^{-1} in uncomplexed TODGA in CH_3CN to 1624 cm^{-1} upon addition of **U^{NO3}**, suggesting coordination, which occurs *via* the amide oxygen groups in solution. The ν_{asym}(U=O) and ν_{sym}(N-O) absorptions are shifted compared to **U^{NO3}**, from 936 to 945 cm^{-1}, and *ca*. 1300 to 1276 cm^{-1}, respectively. Attempts to crystallise the product were unsuccessful. Photolysis of the product mixture (**2.9**) for 16 hours using 420 nm produced a ^{1}H NMR spectrum with many new, small resonances, consistent with degradation of the components in the product mixture. As a result, the product(s) of complexation of uranyl(VI) with TODGA was not investigated further.

2.4.3 Reactions of U^{NO3} with Other Diamides

Simple and commercially-available, cheap ligands, such as *N,N′*-dimethyloxamide and adipamide, were firstly employed as it is known that the length of the carbon chain connecting the two amide groups affects coordination of the amides to the uranyl(VI) ion in **U^{NO3}** (*e.g.* $R_2NC(O)$-$(CH_2)_n$-$C(O)NR_2$). Where n < 3, such as for *N,N′*-dimethyloxamide (R = Me, n = 0), monomeric complexes of the form $[UO_2(NO_3)(L)]$ (L = a diamide) are obtained in the solid-state, but for n ≥ 3, such as for adipamide (R = H, n = 4), complexes of the form $[UO_2(NO_3)(L)]_2$ are obtained.[69] Large carbon chains connecting the two amide groups in the diamide create a highly flexible ligand which is too flexible to coordinate a second amide group intra-molecularly after coordination of the first amide group (to the uranyl). Inter-molecular coordination is therefore favoured, with long (n ≥ 3) bidentate amide ligands complexing two uranyl units monodentate, rather than one uranyl unit bidentate.

Other ligands previously employed towards enhancing the photochemical properties of 4*f*-element luminescent probes, such as phthalamide,[138] isophthalamide[139] and terephthalamide derivatives,[140] were also targeted. The desired complexation products of complexation of **U^{NO3}** with *N,N′*-dimethyloxamide (reaction **2.10**), adipamide (reaction **2.11**), phthalamide (reaction **2.12**), isophthalamide (reaction **2.13**), or *N,N′*-diphenylterephthalamide (reaction **2.14**) are summarised in Scheme 2.13, below.

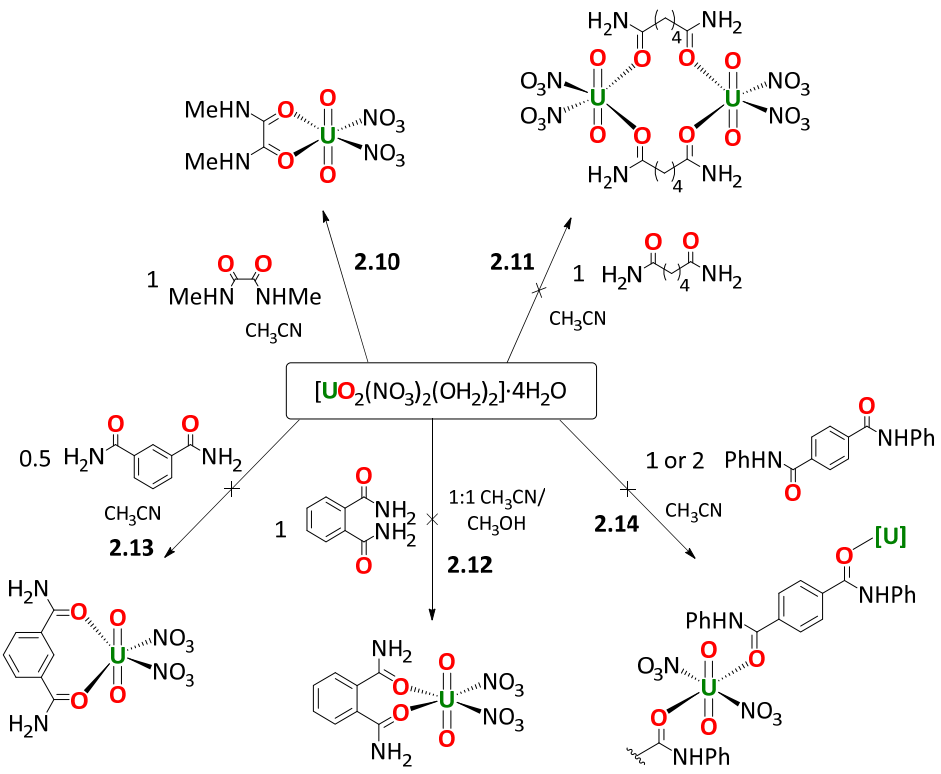

Scheme 2.13 – Unsuccessful complexation reactions of various diamide ligands with the uranyl(VI) ion. The target products, not those isolated or characterised, are depicted, given the ambiguous nature of the products of reactions **2.10**–**2.14**.

Only reaction **2.10** resulted in a soluble product, with reactions **2.11**–**2.14** resulting in precipitates that were not soluble in CH_3CN. These reactions were not pursued further.

The product of reaction **2.10** is also photolytically unstable; ^{1}H NMR spectroscopic analysis of reaction **2.10** after 16 hours of photolysis at 254 nm showed resonances consistent with multiple, unidentified products, alongside the characteristic 1:1:1 triplet centred at *ca*. 6 ppm, indicating the formation of NH_4^+. Although resonances distinct from that of free *N,N*′-dimethyloxamide (therefore likely indicating complex formation) were observed, the formation of NH_4^+ suggests that the product is unstable in solution (either to photolysis or, more likely, hydrolysis; Section 2.4.1 and Scheme 2.7), rendering it unsuitable for further study as a ligand for uranyl complexation.

2.5 Complexes of the Uranyl Ion with Monodentate Amides

2.5.1 Synthesis and Characterisation of $U^{benzNH2}$, $U^{benzNHPh}$, $U^{benzNPh2}$ and $U^{piv/Pr2}$

As outlined in Section 2.1.3, both *N*-aryl and *N*-alkyl monoamides are alternatives to the ubiquitous U^{VI} extractant TBP in the solvent extraction and remediation of spent nuclear fuels. Consequently, there is widespread literature examining their solution-phase behaviour, making them a logical starting point from which to isolate solution-stable uranyl complexes, and then to probe their photocatalytic behaviour. Scheme 2.14, below, outlines the syntheses of the complexes $\mathbf{U^{benzNH2}}$,

$\mathbf{U^{benzNHPh}}$, $\mathbf{U^{benzNPh2}}$ and $\mathbf{U^{piv^iPr2}}$, where $benzNH_2$ is benzamide, benzNHPh is benzanilide (*N*-phenylbenzamide), $benzNPh_2$ is *N,N*-diphenylbenzamide, and piv^iPr_2 is *N,N*-diisopropylpivalamide. All complexes are yellow solids isolated in high (> 90%) yields.

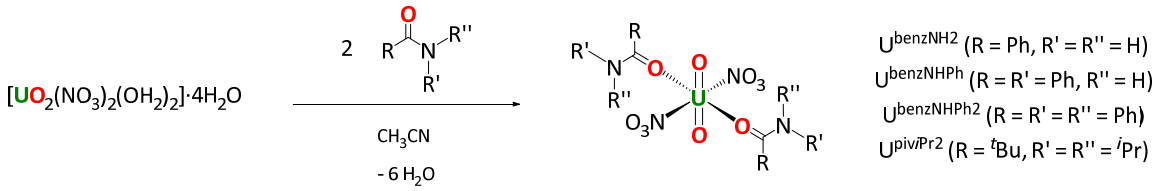

Scheme 2.14 – Complexation of monoamides with $\mathbf{U^{NO3}}$ in CH_3CN; $\mathbf{U^{benzNH2}}$ (with $benzNH_2$, R = Ph, R′ = R″ = H), $\mathbf{U^{benzNHPh}}$ (with benzNHPh, R = R′ = Ph, R″ = H), $\mathbf{U^{benzNPh2}}$ (with $benzNPh_2$, R = R′ = R″ = Ph) and $\mathbf{U^{piviPr2}}$ (with piv^iPr_2, R = ^{t}Bu, R′ = R″ = ^{i}Pr).

Analogously to $\mathbf{U^{mal}}$ and $\mathbf{U^{malPh2}}$, amide NH resonances are particularly diagnostic in the ^{1}H NMR spectra of $\mathbf{U^{benzNH2}}$ and $\mathbf{U^{benzNHPh}}$, which both display clearly shifted resonances compared to uncomplexed $benzNH_2$ or benzNHPh ligand (7.90 and 7.11 ppm, and 9.16 ppm, for $\mathbf{U^{benzNH2}}$ and $\mathbf{U^{benzNHPh}}$, respectively, compared to 6.77 and 6.06 ppm, and 8.73 ppm, for $benzNH_2$ or benzNHPh, respectively). However, this only suggests that there is an interaction of $benzNH_2$ or benzNHPh with the uranyl(VI) ion in CD_3CN, not that the resultant complexes are solution stable. To further analyse this, the resonance of water in solution was again particularly informative; as discussed in Section 2.4.1, a broad singlet at resonances significantly (*ca*. > 0.2 ppm) different from *ca*. 2.1 ppm (water in CD_3CN)[129] may indicate rapid between water and ligands for coordination to uranium.

The ^{1}H NMR spectra of $\mathbf{U^{benzNH2}}$, $\mathbf{U^{benzNHPh}}$ and $\mathbf{U^{benzNPh2}}$ all show a broad singlet significantly shifted from *ca*. 2.1 ppm. This suggests rapid exchange between the uranyl-bound monoamide ligands and water on the NMR timescales of these spectra; 2.80, 3.76 and 2.85 ppm for $\mathbf{U^{benzNH2}}$, $\mathbf{U^{benzNHPh}}$ and $\mathbf{U^{benzNPh2}}$, respectively, which are distinct from the resonances of water in the ^{1}H NMR spectra of uncomplexed $benzNH_2$ or benzNHPh, 2.16, and 2.14 ppm, respectively. The resonance of water was not reported for free $benzNPh_2$,[141] and was not visible in the ^{1}H NMR spectra of $\mathbf{U^{piv^iPr2}}$ or piv^iPr_2.

The presence of multiple species in solution is supported by solution-phase IR data acquired on $\mathbf{U^{benzNH2}}$ and $\mathbf{U^{benzNHPh}}$, which both show multiple bands for ν_{asym}(U=O) at *ca*. 940 cm^{-1}. Low temperature (233 K) ^{1}H NMR spectroscopy of $\mathbf{U^{benzNHPh}}$ in CD_3CN also shows deconvolution of the broad NH peak at 9.16 ppm into at least four broad singlets (unlike $\mathbf{U^{mal}}$ at variable temperatures, Section 2.4.1 and Figure 2.28), at 10.35, 10.24, 10.06 and 8.93 ppm, further consistent with variable speciation in CD_3CN solution. This peak (at 9.16 ppm) broadens substantially on addition of an excess (two equiv.) of uncomplexed benzNHPh ligand. Previous solvent extraction studies on UO_2^{2+} in HNO_3 with monoamides with long-chain *N*-alkyl groups have shown that multiple inner- and outer-sphere uranyl-monoamide complexes exist (*e.g.* $[UO_2(NO_3)_2(DOTA)_2]\cdot(DOTA)$ (**2.AX**, where DOTA =

(^{t}BuCH(Et)CH$_2$)$_2$NCOCH$_2$-^{t}Bu).[142] These data suggest monoamide ligands are insufficiently complexing to outcompete water for coordination of uranyl in CH_3CN solution, and are therefore not suitable for the purposes of this project (*e.g.* are not stable in CH_3CN solution).

The solid-state structures of UO_2^{2+} ions with two equiv. of monoamide ligands are well-established in the chemical literature, where amides with linear- (Me,[143] ^{n}Bu,[60, 62] or ^{i}Pr, ^{i}Bu and ^{s}Bu[61]) or cyclic-[144] *N*-alkyl groups have been reported, in addition to pyrrolidinyl groups.[65, 76] By far the most common motif isolated is $[UO_2(NO_3)_2(L)_2]$, with *trans*-NO_3 and –L groups, where L is a monodentate amide (which are mutually *trans* to minimise unfavourable steric clash). Here, crystals of the yellow **U$^{piv iPr2}$** were isolated (Figure 2.33, Table 2.7) and while it was not possible to isolate crystals of **U^{benzNH2}**, **U^{benzNHPh}** or **U^{benzNPh2}** that were suitable for X-ray diffraction, it is expected that this general form, *trans*-$[UO_2(NO_3)_2(L)_2]$, also represents the likely solid-phase structures of **U^{benzNH2}**, **U^{benzNHPh}** or **U^{benzNPh2}**.

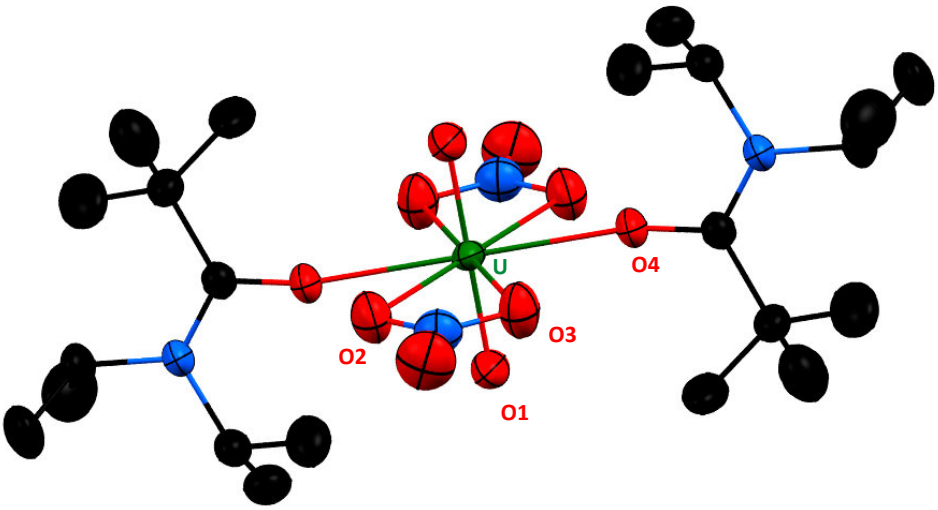

Figure 2.33 – Thermal ellipsoid plot of **U$^{piv iPr2}$**. Ellipsoids drawn at 50% probability with H-atoms omitted for clarity. Key: uranium, oxygen, nitrogen, carbon.

Parameter	U$^{piv iPr2}$	[UO$_2$(NO$_3$)$_2$(^{i}PrCON(^{i}Bu)$_2$)$_2$] (**2.AY**)[62]
d(U=O$_{yl}$)	1.758(8) (O1) Å	1.756(6) Å
d(U-O$_{nit}$)	2.508(9) (O2), 2.514(10) (O3) Å	2.527(7), 2.535(8) Å
d(U-O$_{amide}$)	2.406(7) (O4) Å	2.349(6) Å
∠(OUO)	180°	180°

Table 2.7 – Key parameters (bond lengths/Å, angles/°) for the solid-state structure of **U$^{piv iPr2}$** with uncertainties in parentheses.

All key bond lengths are very similar to those reported for **U$^{mal iPr4}$** (Table 2.6) and for $[UO_2(NO_3)_2(^i$PrCON(^{i}Bu)$_2)_2]$ (**2.AY**, Table 2.7).[62] Additional evidence for the formation of **U^{benzNH2}**, **U^{benzNHPh}** and **U$^{piv iPr2}$** in the solid-state is observed in the ATR-IR spectra of these compounds, where all

$\nu(NO_3)$ and $\nu_{asym}(U{=}O)$ appeared in the expected wavenumber range for $U^{VI}O_2^{2+}$-nitrates; that is, *ca.* 1280 and 940 cm^{-1}, respectively. Despite the consistent formulae (*e.g.* $[UO_2(NO_3)(L)_2]$) of these complexes, the solution-phase lability precluded their use here, and they were not pursued further.

2.6 Complexes of the Uranyl Ion with Oximes

The coordination chemistry of a range of simple oxime ligands with the uranyl(VI) ion was then investigated, following on from Section 2.1.4 (extraction of uranium from alternative sources and numerous binding studies of oximes with the uranyl ion). Here, one to five equiv. of selected oxime ligands were treated with $\mathbf{U^{NO3}}$ in CH_3CN, and the products investigated by ^1H NMR spectroscopy. Scheme 2.15, below, shows a summary of the oxime ligands used, where benzophenone oxime, Ph_2-oxime (reaction **2.15**), and 9-fluorenone oxime, fl-oxime (reaction **2.16**), possess only aromatic C-H bonds, and cyclohexanone oxime, cy-oxime (reaction **2.17**) and indan-1-one oxime, ind-oxime (reaction **2.18**), both possess aliphatic C-H groups.

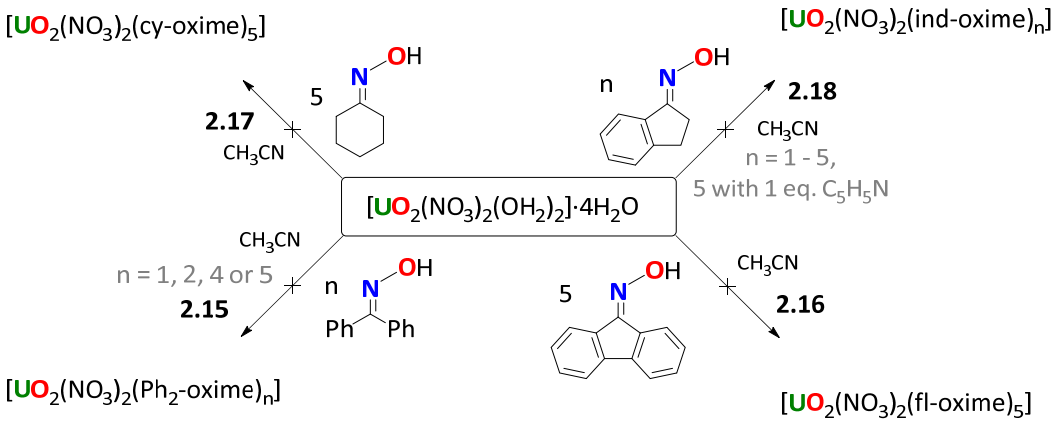

Scheme 2.15 – Unsuccessful complexation of oxime ligands with uranyl, $\mathbf{U^{NO3}}$, in CH_3CN. cy-oxime is cyclohexanone oxime, ind-oxime is indan-1-one oxime, Ph_2-oxime is benzophenone oxime, and fl-oxime is 9-fluorenone oxime.

The ^1H NMR spectra of these product solutions, **2.15**–**2.18**, all show numerous, broad singlets, suggesting rapid exchange between multiple products in CD_3CN solution. There is also little difference in the ^1H NMR spectra for solutions containing n equiv. of either ind-oxime or Ph_2-oxime (reactions **2.15** and **2.18**, n = 1–5, or 1, 2, 4 or 5, respectively), suggesting addition of even stoichiometric amounts ind-oxime or Ph_2-oxime to $\mathbf{U^{NO3}}$ still results in dynamic exchange or variable binding modes of the oxime in CH_3CN solution.

However, a brief comment on solid-phase structural information is warranted as two reactions, the addition of i) two equiv. of ind-oxime (reaction **2.18** where n = 2; Figure 2.34, Table 2.8), and of ii) five equiv. of fl-oxime (reaction 2.16 where n = 5; Figure 2.35, Table 2.9), to $\mathbf{U^{NO3}}$ yielded solid-state structures that provide useful insights into possible fate of the oximes upon addition to $\mathbf{U^{NO3}}$ in CH_3CN.

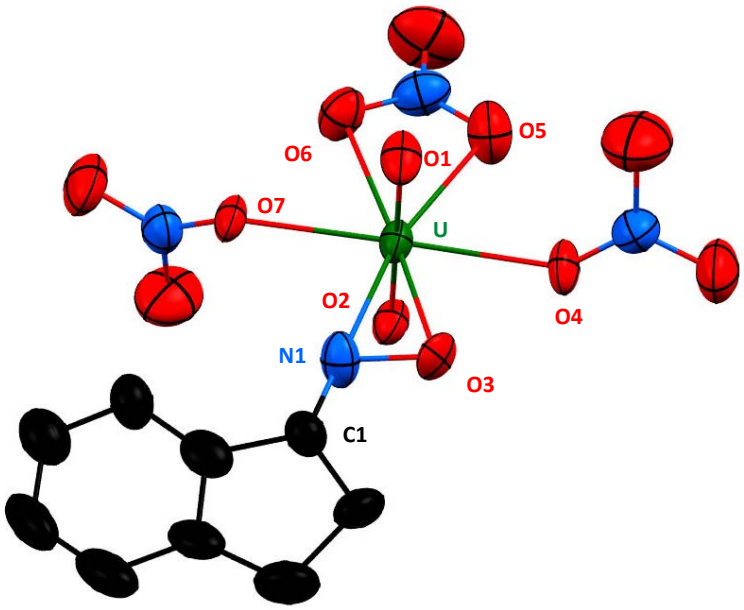

Figure 2.34 – Thermal ellipsoid plot of the structure tentatively assigned as $[UO_2(NO_3)_3$(ind-oxime-H)] (**2.19**), from reaction **2.18** (n = 2). Ellipsoids drawn at 50% probability and H-atoms omitted for clarity. Key: uranium, oxygen, nitrogen, carbon.

Parameter	Values
d(U=O_{yl})	1.754(13) (O1), 1.771(14) (O2) Å
d(U-O_{nit})	2.443(14) (O4), 2.562(13) (O5), 2.581(13) (O6), 2.404(13) (O7) Å
d(U-X_{ox})	2.418(13) (N1) Å
X = O, N	2.267(11) (O3) Å
d(ind-oxime)	1.38(2) (N1-O3)
	1.31(2) (C1-N1)
∠(OUO)	177.8(9)°
∠($N_{ox}UO_{ox}$)	34.1(5) (N1-U-O3)°

Table 2.8 – Key parameters (bond lengths/Å, angles/°) for the solid-state structure tentatively assigned as $[UO_2(NO_3)_3$(ind-oxime-H)] (**2.19**), with uncertainties in parentheses. ox is oxime.

Although it appears '$[UO_2(NO_3)_3$(ind-oxime-H)]' (**2.19**) possesses unusually asymmetric U^{VI}=O_{yl} bonds (of 1.754(13) and 1.771(14) Å, the large standard uncertainties (s.u.) of the bonds give a weighed standard deviation (*cf.* $((s.u._1)^2+(s.u._2)^2)^{0.5}$) of 0.057 Å. This is greater than the difference between the two lengths (0.017 Å), meaning these bonds are not statistically different. Similarly, all other major parameters have large s.u.s, and thus are not compared to analogous structures (*e.g.* $[UO_2$(ph-pao)$_2$(MeOH)$_2]$[4] (**2.AZ**, Ph-paoH is pyridyl-2-phenyl ketoxime) or $[UO_2(OH_2)_2$(napth-ox)$_2]$[145] (**2.BA**, napth-ox is 1,2-naphthoquinone-2-oximate)).

Although a number of uranyl-oxime complexes are known (Section 2.1.4), here, the hydrolytic sensitivity of oxime ligands is highlighted in crystals isolated from the reaction between five equiv. of

fl-oxime and **U^{NO3}** (reaction **2.16,** where n = 5; Figure 2.35, Table 2.9), where the fl-oxime appears to have hydrolysed to the constituent ketone, 9-fluorenone, which is insufficiently complexing to displace either the water or nitrate ligands in **U^{NO3}**. Instead, the ketone forms H-bonds with the uranyl-coordinated water ligands, forming a secondary coordination sphere around the **U^{NO3}** molecule.

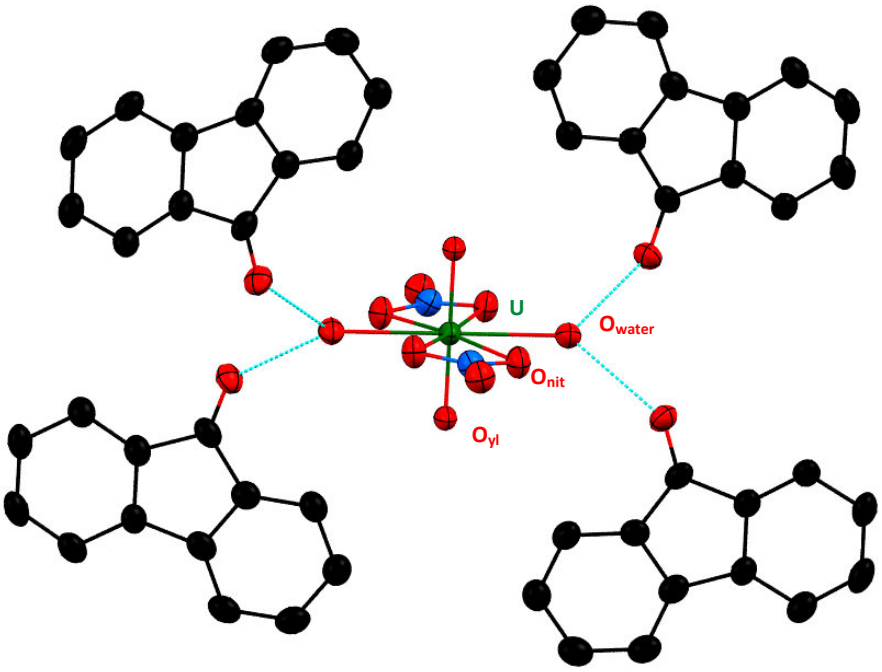

Figure 2.35 – Thermal ellipsoid plot of $[UO_2(NO_3)_2(OH_2)_2]\cdot(\text{fl-one})_4$ (**2.20**) where fl-one is 9-fluorenone, isolated from reaction **2.16** (n = 5). Ellipsoids drawn at 50% probability. H-atoms on water could not be adequately modelled due to rotational disorder and are thus omitted for clarity. Calculated H-bonds are shown as blue dashed lines. Key: uranium, oxygen, nitrogen, carbon.

Parameter	Values	**U^{NO3}** (by neutron diffraction) [146]
d(U=O$_{yl}$)	1.765(6) Å	1.749(7), 1.770 (7) Å
d(U-O$_{nit}$)	2.516(5) Å	2.504(5), 2.547(6) Å
d(U-O$_{water}$)	2.432(6) Å	2.397(3) Å
∠(OUO)	180°	179.1(5)°

Table 2.9 – Key parameters (lengths/Å, angles/°) for $[UO_2(NO_3)_2(OH_2)_2]\cdot(\text{fl-one})_4$ (**2.20**), with uncertainties in parentheses.

The structure of $[UO_2(NO_3)_2(OH_2)_2]\cdot(\text{fl-one})_4$ (**2.20**) is analogous to **U^{NO3}** reported by neutron diffraction,[146] with only slight variations in bond lengths, attributable to crystal packing or differences in H-bonding strength between outer-sphere coordinated water (in **U^{NO3}**) or fl-one (in $[UO_2(NO_3)_2(OH_2)_2]\cdot(\text{fl-one})_4$ (**2.20**). As with $[UO_2(NO_3)_3(\text{ind-oxime-H})]$ (**2.19**; Figure 2.34, Table 2.8) the stoichiometry reported for $[UO_2(NO_3)_2(OH_2)_2]\cdot(\text{fl-one})_4$ (**2.20**) does not fully account for the initial stoichiometry of U:fl-oxime used (1:5).

Overall, the ambiguous speciation (resulting from the proposed solution-phase dynamic exchange of oximes with nitrates, water, *etc*.) renders them unsuitable ligands for the criteria as discussed in Section 2.1. Oximes may be combined with other ligand functionalities, particularly given emerging literature regarding uranyl(VI)-oxime complexes with modified photochemical properties (Section 2.1.4, Figure 2.7),[87] but for the purposes of this study this hypothesis was not pursued further.

2.7 Complexes of the Uranyl Ion with Other *O*-donors

Having studied a range of uranyl-amide and -oxime complexes, a brief series of reactions of **U^{NO3}** with other simple *O*-donor ligands was undertaken, so as to provide insights into the possible utility of urea ligands or carboxylic acids as ligands for uranyl complexation, Section 2.1.1.

2.7.1 Complexation with ^{t}Bu$_2$-urea, U^{tBu2urea}

As a ligand, urea has been postulated to complex to the uranyl(VI) ion in a 1:2 U:urea stoichiometry, when measured spectrophotometrically in ethanol.[147] With *N,N*′-alkyl groups, urea ligands have also recently been explored as an alternatives to TBP for the selective separation of uranyl(VI) ions from Th(IV), Pu(IV) and Ln(III) (Ln = La, Sm, Eu) in a nitric acid medium.[148] Therefore, 1,3-di-*tert*-butylurea, ^{t}Bu$_2$-urea, was reacted with **U^{NO3}** in CH_3CN (Scheme 2.16), and the solution-phase behaviour investigated by ^{1}H NMR spectroscopy. All data are consistent with formation of [$UO_2(NO_3)_2$(^{t}Bu$_2$-urea)$_2$], **U^{tBu2urea}**, as the only product (a dark yellow powdery solid), formed in 92% yield.

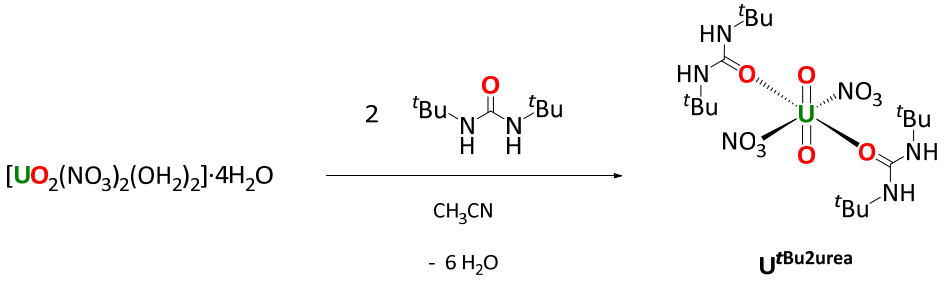

Scheme 2.16 – Complexation of **U^{NO3}** with 1,3-di-*tert*-butylurea, ^{t}Bu$_2$-urea, in CH_3CN, resulting in **U^{tBu2urea}**.

Similarly to the ^{1}H NMR spectra of the uranyl-monoamide complexes **U^{benzNH2}**, **U^{benzPh2}**, **U^{benzNPh2}** and **U^{piviPr2}** described in Section 2.4.1, the resonances corresponding to the NH protons are shifted and broadened WRT uncomplexed ^{t}Bu$_2$-urea in CD_3CN, suggesting dynamic exchange between complexed and uncomplexed ^{t}Bu$_2$-urea, and water. This is consistent with ^{1}H NMR spectra of the uranyl-monoamide complexes discussed in Section 2.5.1. No evidence for the formation of NH_4^+ (*e.g.* 1:1:1 triplet at *ca*. 6 ppm) was observed.

The IR spectrum of **U^{tBu2urea}** has bands consistent with retention of uranyl-bound NO_3 (1276 cm^{-1}), and a weakening of the C=O bond in **U^{tBu2urea}** (ν(C=O) = 1596 cm^{-1}) when compared to ^{t}Bu$_2$-urea (ν(C=O) =

1637 cm^{-1}). This is consistent with coordination of $^{t}Bu_2$-urea *via* the carbonyl oxygen of the urea group, something observed in the solid-state structure of **U^{tBu2urea}**, Figure 2.36 and Table 2.10.

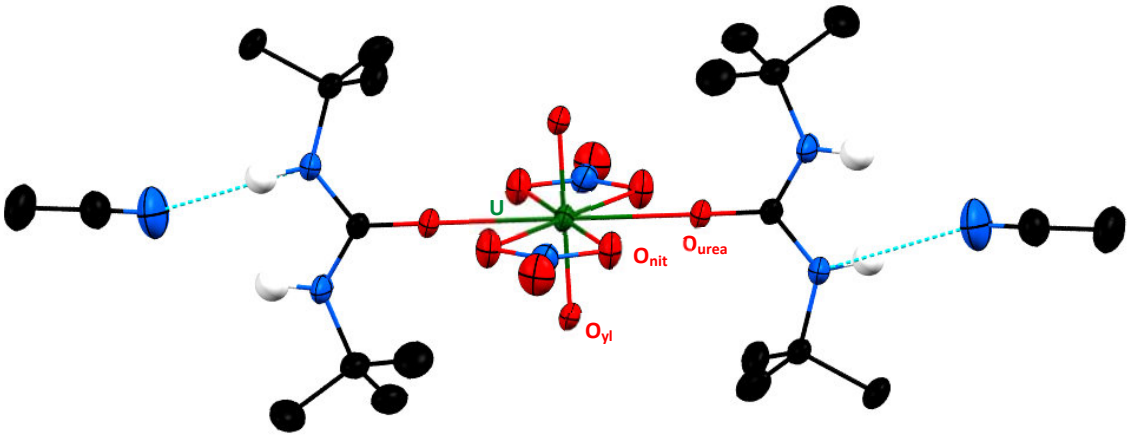

Figure 2.36 – Thermal ellipsoid plot of $[UO_2(NO_3)_2(^{t}Bu_2\text{-urea})_2]]\cdot 2(CH_3CN)$, **U^{tBu2urea}** (with two CH_3CN solvents of crystallisation). Ellipsoids drawn at 50% probability. H-atoms apart from N-H protons are omitted for clarity. Calculated H-bonds are shown as light blue dashed lines. Key: uranium, oxygen, nitrogen, carbon.

Parameter	U^{tBu2urea}·2(CH$_3$CN)	[UO$_2$(NO$_3$)$_2$(^{i}Bu$_2$Et$_2$urea)$_2$] (**2.BB**)[148]
d(U=O$_{yl}$)	1.756(2) Å	1.746(6), 1.742(10) Å
d(U-O$_{nit}$)	2.521(2) Å	2.532(12), 2.534(14), 2.541(14), 2.545(14) Å
d(U-O$_{urea}$)	2.3865(18) Å	2.327(14), 2.350(14) Å
∠(OUO)	180°	179.6(5)°

Table 2.10 – Key parameters (bond lengths/Å, angles/°) for **U^{tBu2urea}**·2(CH_3CN) and $[UO_2(NO_3)_2(^{i}Bu_2Et_2urea)_2]$ (**2.BB**) with uncertainties in parentheses. $^{i}Bu_2Et_2$urea is *N,N*-di-*iso*-butyl-*N'*,*N'*-diethylurea.

All the key structural parameters of **U^{tBu2urea}** are consistent with uranyl(VI) ions,[111] and an analogous uranyl(VI)-urea complex, $[UO_2(NO_3)_2(^{i}Bu_2Et_2urea)_2]$ (**2.BB**).[148] The *trans*-NO_3, *trans*-$^{t}Bu_2$-urea arrangement of ligands is also consistent with the solid-state structure of **U$^{piv/Pr2}$** (Figure 2.33), further suggesting similarities between uranyl(VI)-bound mono-amide and mono-urea complexes.

Urea groups may, therefore, when combined with other organic groups, present a potential avenue from which to construct a solution-stable uranyl(VI) complex. With judicious choice of co-ligand (for example, poly-pyridyl groups, see Section 2.4.2) it may then be possible to influence the electronic structure of the uranyl(VI) to affect interesting or novel photochemical behaviour, but for the purposes of this thesis, this hypothesis was not pursued further.

2.7.2 Unsuccessful Complexation with Phthalic Acids

As it is known that phthalates[149] and carboxylates[150] are capable of modifying the luminescent properties of uranyl-coordination polymers, it was envisaged that if a soluble, solution-stable uranyl-phthalate or -isophthalate complex could be synthesised, this may possess interesting photochemical properties. Accordingly, Scheme 2.17 shows the unsuccessful complexation of **U^{NO3}** with phthalic (Hpht) or isophthalic acid (Hipht). Note that phthalate is denoted here as pht, and isophthalate, ipht.

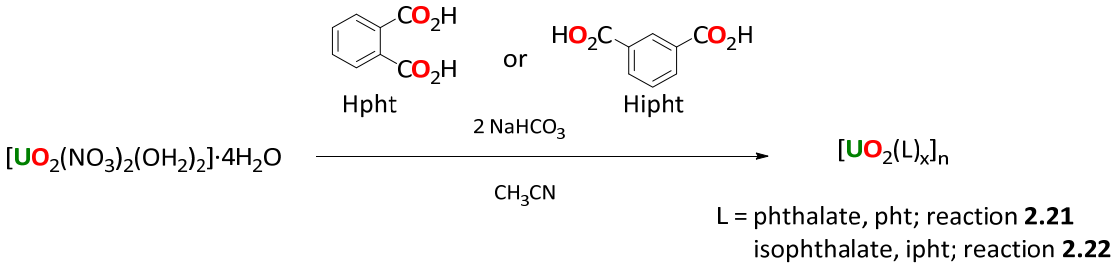

Scheme 2.17 – Reactions of **U^{NO3}** with phthalic acid, Hpht, or isophthalic acid, Hipht, in reactions **2.21** and **2.22**, respectively. Given the likely polymeric nature of the product(s), x is likely 1 or 2, and n is > 1. The fate of water and Na^+- and HCO_3^--containing product(s) remains unclear.

Both the products of reactions **2.21** (Hpht and **U^{NO3}**) and **2.22** (Hipth and **U^{NO3}**) resulted in insoluble (CH_3CN, CH_3OH or acetone) yellow powders, which could not be analysed by ^{1}H NMR spectroscopy.

To investigate the solid-state structures further, IR spectra acquired of the product(s) of reactions **2.21** and **2.22**. No peaks consistent with nitrate were observed (for $U^{VI}O_2^{2+}$-bound nitrate groups, normally *ca*. 1280 cm^{-1}), suggesting substitution of the nitrate groups in **U^{NO3}** with the phthalate or isophthalate, respectively; *e.g.* $[UO_2(L)_x]_n$, where L = pht or ipht, and x = 1 or 2, and n is > 1. Coordination polymers with the formulae $[UO_2(L)]_n$ (L = 1,4-benzenedicarboxylate (**2.BC.1**), 4,4′-biphenyldicarboxylate (**2.BC.2**), 4,4′-azobenzenedicarboxylate (**2.BC.3**) or 1,3-benzenedicarboxylate (**2.BC.4**), where n > 1)[151] or $[UO_2(pht)(H_2O)]\cdot H_2O$ (**2.BD**) and $[(UO_2)_2(ipht)_4(H_2O)_2]$ (**2.BE**) are known (*via* hydrothermal synthesis),[152] suggesting that ligands possessing only carboxylic acid groups may not be suitable for the synthesis of photochemically-modified uranyl(VI) complexes that are soluble in organic solvent. Heterogeneous uranyl(VI)-pht or -ipht complexes have been studied in the degradation of model organic pollutants[152] and, while outside the remit of this thesis, may present a potential use of these complexes in the future.

2.8 Preparation of Anaerobic Uranyl Photocatalysts

As discussed in Section 2.1.5 and Section 3.6, the anaerobic photoreactivity of the uranyl(VI) ion is chronically underdeveloped. Examining the complexation and photochemistry of anaerobic uranyl complexes may therefore provide avenues into developing new photochemical reactions involving the uranyl(VI) ion.[153]

To this end, samples of $\mathbf{U^{Ph2phen}}$ and $\mathbf{U^{mal}}$, the two most promising complexes for either modifying the electronic properties of this ion, or controlling the solution-phase behaviour, respectively, were dried, in order to remove water. For $\mathbf{U^{Ph2phen,}}$ this was accomplished by drying for two hours on a rotary evaporator (< 100 mbar, water bath at 40°C), but for $\mathbf{U^{mal}}$, this required drying *in vacuo* (< 10^{-2} mbar) on a Schlenk line for at least two days, resulting in a sample of $\mathbf{U^{mal}}$ containing *ca*. 20–30 ppm (0.002–0.003%) water, by Karl-Fischer titrimetry. In this method an alcohol is converted to an alkyl sulfite in the presence of a base, which is further oxidised to an alkyl sulfate with iodine. This second reaction consumes equimolar amounts of iodine and water, and thus the amount of iodine consumed is measured and correlated to the amount of water in a given sample.

Both $\mathbf{U^{Ph2phen}}$ and $\mathbf{U^{mal}}$ are, however, poorly soluble in CD_3CN or CH_3CN, limiting their usefulness in performing small-scale anaerobic photochemical testing reactions, which often require stoichiometric amounts of uranyl(VI) and substrate (*e.g.* no oxygen for catalyst turnover). This increases the amount of "catalyst" needed for each reaction from the single-digit to the tens of mg, meaning larger quantities of dry CH_3CN and uranyl complex would be required. As this is synthetically laborious, a highly organic-soluble, simple uranyl complex was desired, ideally one that has literature precedent which does not incorporate a ligand where there are C-H groups proximal to the $*UO_2^{2+}$ ion (*e.g.* reducing likelihood of unwanted photochemical degradation).

Uranyl(VI) complexes of the form $[X][UO_2(NO_3)_3]$ (**2.BF**, X = Cs^+ ions[154] (**2.BF.1**) or R_4N^+ where R = H (**2.BF.2**),[155] ^{n}Pr (**2.BF.3**) or ^{n}Bu (**2.BF.4**),[156] or Me (**2.BF.5**))[157] and $[X]_2[UO_2(NO_3)_4]$ (**2.BG**, X = NH_4^+ (**2.BG.1**))[158] are known to be straightforward to synthesize and characterise in organic solvents, and it was thus decided that an ion-pair uranyl(VI) complex was most suitable for this investigation. Further, given that metal cations are known to physically quench the photo-excited state of the uranyl(VI) cation (Section 3.1.1), it was decided $[X][UO_2(NO_3)_3]$ (**2.BF**) or $[X]_2[UO_2(NO_3)_4]$ (**2.BG**) where X is an organic ammonium cation ($^nPr_4N^+$, $^nBu_4N^+$ or Me_4N^+) would be most suitable of the uranyl(VI) ion-pair complexes. Of these, X = $^nBu_4N^+$ was synthesised, according to the procedure outlined in Scheme 2.18.

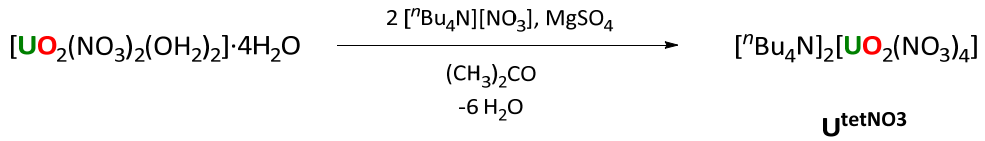

Scheme 2.18 – Synthesis of $\mathbf{U^{tetNO3}}$.

Though the solid-phase structures of both the $[UO_2(NO_3)_3]^-$ anion[159] and $[UO_2(NO_3)_4]^{2-}$ dianion[158] are known, the solution-phase behaviour of the uranyl tri- or tetra-nitrate (di-)anion is less well-established. Recent reports investigating the speciation of $[Me_4N][UO_2(NO_3)_3]$ (**2.BF.5**) in CH_3CN show clearly that addition of one equiv. of $[Me_4N][NO_3]$ (as source of NO_3^-) results in a product to which

addition of an additional equiv. of $[Me_4N][NO_3]$ results in no spectral change; *e.g.* consistent with a formulation of $[Me_4N][UO_2(NO_3)_3]$ (**2.BF.5**) in CH_3CN solution.[157] However, ^{1}H NMR spectroscopy with an internal standard (mesitylene) performed on a sample of $[^nBu_4N]_2[UO_2(NO_3)_4]$ for this work in CD_3CN shows that two equiv. of $[^nBu_4N]^+$ are retained after work-up, consistent with $[^nBu_4N]_2[UO_2(NO_3)_4]$. Further, elemental (combustion) analysis (C, 37.59%, H, 8.86%, N, 8.05%) is consistent with a formula of $[^nBu_4N]_2[UO_2(NO_3)_4]$ (C, 38.3%, H, 7.24%, N, 8.38%) rather than $[^nBu_4N][UO_2(NO_3)_3]$ (C, 27.51%, H, 5.2%, N, 8.02%). Solution-phase Raman spectroscopy indicates the presence of uranyl-bound nitrate (*ca*. 1040 cm^{-1}),[160] and a solid-state structure consistent with $[^nBu_4N]_2[UO_2(NO_3)_4]$ was also characterised, though for brevity is not discussed (key structural parameters are only marginally different to those reported elsewhere).[158] Therefore, though the presence of $[^nBu_4N][UO_2(NO_3)_3]$ cannot be conclusively ruled out, attempts to isolate it here were unsuccessful, with data instead suggesting a formulation of $[^nBu_4N]_2[UO_2(NO_3)_4]$ (**U^{tetNO3}**) to be correct under these conditions.

To further probe the suitability of **U^{tetNO3}** as a photocatalyst, the emission and excitation spectra were recorded in dry CH_3CN, and compared to those of **U^{NO3}**; these spectra are shown in Figures 2.37 and 2.38, below. The photostability of **U^{tetNO3}** was also tested, with very little degradation observed after 16 hours of photolysis (420 nm) by ^{1}H NMR spectroscopy (< 1% by integration).

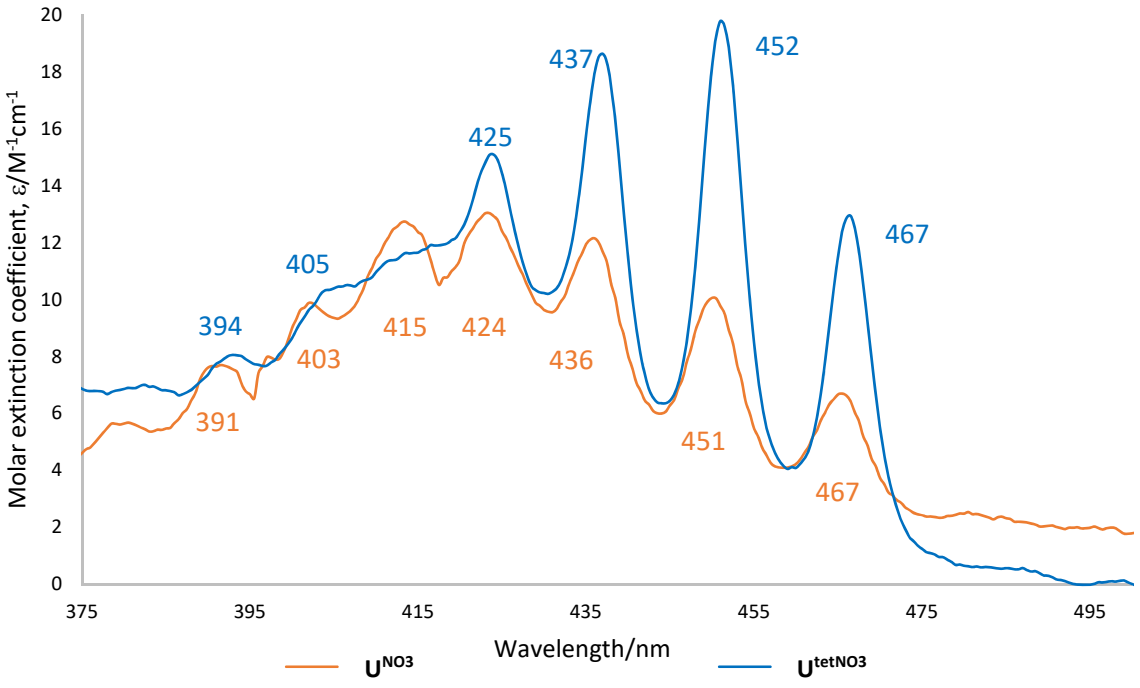

Figure 2.37 – Electronic absorption spectra of **U^{NO3}** (ORANGE) and **U^{tetNO3}** (BLUE) in CH_3CN; [**U^{NO3}**] = 1.13 x 10^{-3} M, [**U^{tetNO3}**] = 0.79 x 10^{-3} M. Numbers are wavelengths in nm.

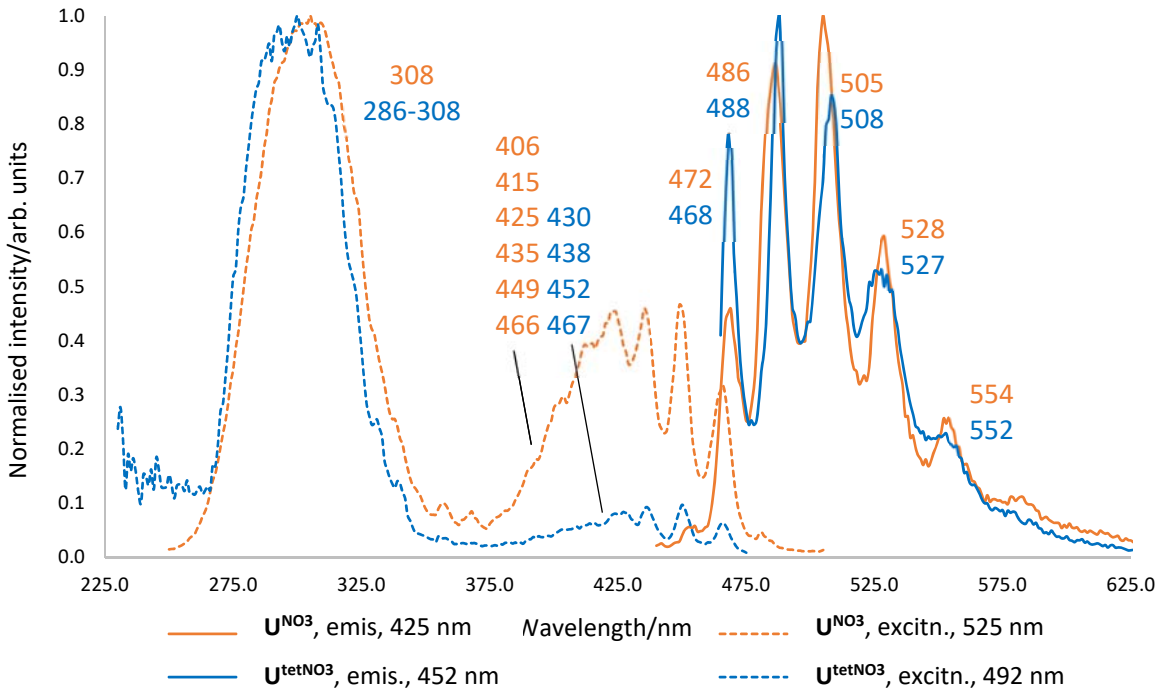

Figure 2.38 – Excitation and emission spectra of $\mathbf{U^{NO3}}$ (ORANGE) and $\mathbf{U^{tetNO3}}$ (BLUE) in CH_3CN; [$\mathbf{U^{NO3}}$] = 1.13 x 10^{-3} M, [$\mathbf{U^{tetNO3}}$] = 0.19 x 10^{-3} M. Numbers are wavelengths in nm.

There is little difference in the electronic absorption spectra of $\mathbf{U^{tetNO3}}$ and $\mathbf{U^{NO3}}$ (Figure 2.37), with ε_{max} values of < 20 $M^{-1}cm^{-1}$ in both cases. The biggest difference between $\mathbf{U^{tetNO3}}$ and $\mathbf{U^{NO3}}$ is the λ_{max}, which red-shifts from *ca*. 425 nm in $\mathbf{U^{NO3}}$ to 452 nm in $\mathbf{U^{tetNO3}}$, consistent with the similar trinitrato uranyl complex, $[Me_4N][UO_2(NO_3)_3]$ (**2.BF.5**) in CH_3CN.[157] The emission and excitation spectra of $\mathbf{U^{tetNO3}}$ (Figure 2.38) exhibit only minor differences to those of $\mathbf{U^{NO3}}$, and as the absorption, emission and excitation spectra of $\mathbf{U^{tetNO3}}$ were acquired in anhydrous CH_3CN, it is not possible to rationalise changes in the Stokes shift between $\mathbf{U^{NO3}}$ (which used 'bench' CH_3CN, < 0.1% water; 3820 cm^{-1}) and $\mathbf{U^{tetNO3}}$ (1632 cm^{-1}). The synthetic utility of $\mathbf{U^{tetNO3}}$ therefore appears primarily to be a source of the anhydrous $U^{VI}O_2^{2+}$ ion, which was confirmed upon drying a sample of $\mathbf{U^{tetNO3}}$ *in vacuo* for 48 hours (< 10^{-2} mbar); a water content of 11–13 ppm (0.0011–0.0013%) was determined by Karl-Fischer titrimetry. As $\mathbf{U^{tetNO3}}$ contains less water than $\mathbf{U^{mal}}$ and is more soluble than $\mathbf{U^{mal}}$ and $\mathbf{U^{Ph2phen}}$ in CH_3CN, it is the primary source of the anhydrous $U^{VI}O_2^{2+}$ ion described in this thesis. Together, these properties are vital for the novel uranyl(VI)-based anhydrous, photochemical reactions discussed in Section 3.6.

2.9 Summary and Outlook

Several ligand classes have been found suitable for the synthesis of novel photoactive uranyl complexes, using the criteria set out at the beginning of this chapter.

With *N*-heterocycles, the ligands are stable to photolysis, stable in CH_3CN solution, and for Ph_2phen, sparingly soluble in CH_3CN solvent. **U^{Ph2phen}** is easy to characterise (Section 2.2.1), appears resistant to protonation (unlike other 2,9-disubstituted phenanthrolines), and, pertinently, appears to modify the luminescent properties of the $*U^{VI}O_2^{2+}$ ion, probably *via* a ligand-modified excited state, overlap of ligand emission with uranyl(VI) absorption, or both. Though it was not possible to study the photo-excited uranyl(VI) complexes by spin trapping (*e.g.* of intermediate radicals)[161] or by fluorescence lifetime studies, these should provide more evidence about the nature of the interaction of Ph_2phen with UO_2^{2+} in **U^{Ph2phen}**; indeed, EPR spin-trapping has been previously employed to examine ligand radicals of uranyl in organic solution.[162] Additionally, if a method of preventing protonation could be identified, then other *N*-heterocycles including terpy and quinolines should also be feasible ligands for modifying the chemical behaviour of the $*UO_2^{2+}$ ion. This is particularly important as protonation of terpy is known to modify its luminescent properties.[163] Discussions are currently underway with the EPSRC National Service for EPR spectroscopy, and Dr. Louise Natrajan, at the University of Manchester, UK, to characterise **U^{Ph2phen}** further, but will unfortunately not be complete by submission of this thesis.

Complexes of bipy are also not discussed here, though as outlined in Section 2.2.1, possess a rich redox chemistry when complexed to uranium(III) and uranium(IV). These may make for excellent ligands with which to modify the photochemical properties of uranyl(VI), and efforts to isolate and photochemically characterise bipy complexes of $U^{VI}O_2^{2+}$ are particularly encouraged.

Complexes of (L =) phen and terpy with $Np^{VI}O_2^{2+}$ are solution- and redox-stable in CH_3CN, with UV-vis-NIR suggesting complexes of the form $[Np^{VI}O_2(NO_3)_2(L)]$ (**2.5.phen** and **2.5.terpy**) are produced, Section 2.3.2. Although it was not possible to investigate the photochemical and photocatalytic properties of these complexes, studies investigating the behaviour of $*Np^{VI}O_2^{2+}$ ions in CH_3CN using these complexes are eagerly anticipated. Further work with the NNL to investigate this is planned. The photochemical properties of the $Np^{VI}O_2^{2+}$ ion are discussed in further in Section 3.1.5.

Uranyl-amide and -oxime complexes are mostly unstable in solution, being susceptible to dynamic exchange between free and complexed ligand. This may be ameliorated through using multidentate ligands, *e.g.* malonamide, where judicious choice of *N*-alkyl or –aryl groups is required with $–NH_2$ groups shown to be the most resistant to either hydrolysis or photolytic degradation. Combination with other ligand functionalities is advised, with the combination of $-CONH_2$ amides with *N*-heterocycle groups being especially encouraged. Of particular interest is a series of macrocyclic ligands employed by Sessler *et al.*, which are known to have unique photochemical and electronic properties.[164-166] Although these complexes are outside the remit of this thesis, such complexes may provide unique routes into ligand-modified electronically excited states of the uranyl(VI) ion in the

future, either by modifying the electronic properties of $*U^{VI}O_2^{2+}$, or by lengthening its excited state lifetime. This latter point forms the basis for several new uranyl complexes appearing in the literature and is discussed further in chapter 3.

2.10 References

1. G. Modolo, A. Geist and M. Miguirditchian, in *Reprocessing and Recycling of Spent Nuclear Fuel*, ed. R. Taylor, Woodhead Publishing, Cambridge, 2015.
2. K. Takao and Y. Ikeda, *Acta Cryst. Sect. E*, 2008, **64**, 219.
3. R. Tamilarasan, T. Ramakrishan and J. F. Endicot, *Inorg. Chim. Acta*, 1988, **142**, 321.
4. S. T. Tsantis, E. Zagoraiou, A. Savvidou, C. P. Raptopoulou, V. Psycharis, L. Szyrwiel, M. Hołyńska and S. P. Perlepes, *Dalton Trans.*, 2016, **45**, 9307.
5. C. C. Gatto, E. S. Lang, A. Jagst and U. Abram, *Inorg. Chim. Acta*, 2004, **357**, 4405.
6. U. Abram, E. S. Lang and E. Bonfada, *Z. Anorg. Allg. Chem.*, 2002, **628**, 1873.
7. K. Servaes, S. D. Houwer, C. Görller-Walrand and K. Binnemans, *Phys. Chem. Chem. Phys.*, 2004, **6**, 2946.
8. M. Nierlich, J.-M. Sabattie, N. Keller, M. Lance and J.-D. Vigner, *Acta Cryst. Sect. C*, 1994, **50**, 52.
9. J. Ferry, J. Gallagher, D. Cunningham and P. McArdle, *Polyhedron*, 1989, **8**, 1733.
10. R. A. Lal, S. Das and R. K. Thapa, *Inorg. Chim. Acta*, 1987, **132**, 129.
11. X. Zhao, D. Zhang, R. Yu, S. Chen and D. Zhao, *Eur. J. Inorg. Chem.*, 2018, 1185.
12. L. Leoni, R. Puttreddy, O. Jurček, A. Mele, I. Giannicchi, F. Y. Mihan, K. Rissanen and A. D. Cort, *Chem. Eur. J.*, 2016, **22**, 18714.
13. J. L. Sessler, P. J. Melfi and G. D. Pantos, *Coordin. Chem. Rev.*, 2006, **250**, 816.
14. J.-C. Berthet, P. Thuéry, J.-P. Dognon, D. Guillaneux and M. Ephritikhine, *Inorg. Chem.*, 2008, **47**, 6850.
15. G. J. Vazquez, C. J. Dodge and A. J. Francis, *Inorg. Chem.*, 2008, **47**, 10739.
16. N. G. Palaskar, D. V. Jahagirdar and D. D. Khanolkar, *J. Inorg. Nucl. Chem.*, 1976, **38**, 1673.
17. A. R. de Aquinom, G. Bombieri, P. C. Isolani, G. Vicentini and J. Zukerman-Schpector, *Inorg. Chim. Acta*, 2000, **306**, 101.
18. X. Ye, S. Cui, V. F. de Almeida, B. P. Hay and B. Khomami, *Phys. Chem. Chem. Phys.*, 2010, **12**, 15406.
19. A. Prestianni, L. Joubert, A. Chagnes, G. Cote, M.-N. Ohnet, C. Rabbe, M.-C. Charbonnel and C. Adamo, *J. Phys. Chem. A*, 2010, **114**, 10878.
20. G. J. Lumetta, B. K. McNamara, B. M. Rapko and J. E. Hutchison, *Inorg. Chim. Acta*, 1999, **293**, 195.
21. G. Tian, L. Rao and S. J. Teat, *Chem. Eur. J.*, 2009, **15**, 4172.
22. F. Weigl, in *The Chemistry of the Actinide Elements*, eds. J. J. Katz, L. R. Morss and G. T. Seaborg, Chapman and Hill, London, UK, 1986.
23. G. Nocton, W. W. Lukens, C. H. Booth, S. S. Rozenel, S. A. Medling, L. Maron and R. A. Anderson, *J. Am. Chem. Soc.*, 2014, **136**, 8626.
24. G. Zi, L. Jia, E. L. Werkema, M. D. Walter, J. P. Gottfriedsen and R. A. Andersen, *Organometallics*, 2005, **24**, 4251.
25. S. J. Kraft, P. E. Fanwick and S. C. Bart, *Inorg. Chem.*, 2010, **49**, 1103.
26. M. K. Takase, M. Fang, J. W. Ziller, F. Furche and W. J. Evans, *Inorg. Chim. Acta*, 2010, **364**, 167.
27. P. L. Diaconescu and C. C. Cummins, *Dalton Trans.*, 2015, **44**, 2676.
28. S. Fortier, J. Veleta, A. Pialat, J. Le Roy, K. B. Ghiassi, M. M. Olmstead, A. Metta-Magaña, M. Murugesu and D. Villagrán, *Chem. Eur. J.*, 2016, **22**, 1931.
29. K. Takao, S. Tsushima, T. Ogura, T. Tsubomura and Y. Ikeda, *Inorg. Chem.*, 2014, **53**, 5772.
30. J. E. Niklas, B. H. Farnum, J. D. Gorden and A. E. V. Gorden, *Organometallics*, 2017, **36**, 4626.

31. J. J. Kiernicki, D. P. Cladis, P. E. Fanwick, M. Zeller and S. C. Bart, *J. Am. Chem. Soc.*, 2015, **137**, 11115.
32. N. L. Bell, M. Zegke, L. N. Platts, C. A. Lamfsus, L. Maron, L. S. Natrajan, S. Sproules, P. L. Arnold and J. B. Love, *Chem. Sci.*, 2017, **8**, 108.
33. K. Herasymchuk, L. Chiang, C. E. Hayes, M. L. Brown, J. S. Ovens, B. O. Patrick, D. B. Leznoff and T. Storr, *Dalton Trans.*, 2016, **45**, 12576.
34. S. Nuzzo, M. P. Browne, B. Twamley, M. E. G. Lyons and R. J. Baker, *Inorganics*, 2016, **4**, 4.
35. E. J. Coughlin, Y. Qiao, E. Lapsheva, M. Zeller, E. J. Schelter and S. C. Bart, *J. Am. Chem. Soc.*, 2019, **141**, 1016.
36. S. G. Thangvelu, S. J. A. Pope and C. L. Cahill, *CrystEngComm*, 2015, **17**, 6236.
37. K. P. Carter, M. Kalaj and C. L. Cahill, *Eur. J. Inorg. Chem.*, 2016, 126.
38. P. O. Adelani and P. C. Burns, *Inorg. Chem.*, 2012, **51**, 11177.
39. L. S. Natrajan, *Coordin. Chem. Rev.*, 2012, **256**, 1583.
40. V. P. Shilov and A. B. Yusov, *Radiochem.*, 2001, **43**, 371.
41. S. D. Woodall, A. N. Swinburne, N. L. Banik, A. Kerridge, P. D. Pietro, C. Adam, P. Kaden and L. S. Natrajan, *Chem. Commun.*, 2015, **51**, 5402.
42. S. M. Cornet, L. J. L. Haller, M. J. Sarsfield, D. Collison, M. Helliwell, I. May and N. Kaltsoyannis, *Chem. Commun.*, 2009, 917.
43. D. L. Clark, D. W. Keogh, P. D. Palmer, B. L. Scott and C. D. Tait, *Angew. Chem., Int. Ed.*, 1998, **37**, 164.
44. D. G. Chuguryan, V. I. Dzyubenko, M. S. Grigorev, A. I. Yanovskii and Y. T. Struchkov, *Radiokhim.*, 1988, **30**, 39.
45. S. M. Cornet, M. P. Redmond, D. Collison, C. A. Sharrad, M. Helliwell and J. Warren, *C. R. Chim.*, 2010, **13**, 832.
46. K. Takao, S. Takao, A. C. Scheinost, G. Bernhard and C. Hennig, *Inorg. Chem.*, 2018, **48**, 8803.
47. A. A. Bessonov, N. N. Krot, M. S. Grigorev and V. I. Makarenkov, *Radiochem.*, 2009, **51**, 231.
48. Q.-J. Pan, Y.-M. Wang, R.-X. Wang, H.-Y. Wu, W. Yang, Z.-M. Sun and H.-X. Zhang, *RSC Adv.*, 2013, **3**, 1572.
49. N. A. Budantseva, G. B. Andreev, A. M. Fedoseev and M. Y. Antipin, *Russ. J. Coordin. Chem.*, 2003, **29**, 322.
50. N. A. Budantseva, G. B. Andreev, A. M. Fedoseev and M. Y. Antipin, *Russ. J. Coordin. Chem.*, 2003, **29**, 265.
51. N. A. Budantseva, G. B. Andreev, A. M. Fedoseev, M. Y. Antipin and J.-C. Krupa, *Crystallogr. Rep.*, 2003, **48**, 56.
52. G. B. Andreev, N. A. Budantseva, I. G. Tananaev and B. F. Myasoedov, *Radiochem.*, 2009, **51**, 225.
53. M. N. Sokolova, A. A. Bessonov and A. M. Fedoseev, *Radiochem.*, 2012, **54**, 341.
54. N. W. Alcock, D. J. Flanders and D. Brown, *J. Chem. Soc., Dalton Trans.*, 1985, 1001.
55. N. W. Alcock, D. J. Flanders and D. Brown, *Inorg. Chim. Acta*, 1984, **94**, 279.
56. R. S. Herbst, P. Baron and M. Nilsson, *Standard and advanced separation: PUREX processes for nuclear fuel reprocessing*, Woodhead Publishing, Cambridge, UK, 2011.
57. H. M. Feder, *Report ANL-4675*, Argonne National Laboratory, Chicago, 1951.
58. T. H. Siddall III, *J. Phys. Chem.*, 1960, **64**, 1863.
59. C. Boxall, G. Le Gurun, R. J. Taylor and S. Xiao, in *Environmental Photochemistry Part II*, eds. P. Boule, D. W. Bahnemann and P. K. J. Robertson, Springer, Heidelberg, 2005.
60. E. Acher, Y. H. Cherkaski, T. Dumas, C. Tamain, D. Guillaumont, N. Boubals, G. Javierre, C. Hennig, P. L. Solaris and M.-C. Charbonnel, *Inorg. Chem.*, 2016, **55**, 5558.
61. S. Kannan, C. L. Barnes and P. B. Duval, *Chem. Commun.*, 2005, 5997.
62. S. Kannan, S. B. Deb, J. S. Gamare and M. G. B. Drew, *Polyhedron*, 2008, **27**, 2557.
63. P. Charpin, M. Lance, M. Nierlich, D. Vigner and C. Musikas, *Acta Cryst. Sect. C*, 1987, **43**, 231.

64. P. Charpin, M. Lance, M. Nierlich, D. Vigner, N. Descouls and C. Musikas, *Acta Cryst. Sect. C*, 1986, **42**, 560.
65. K. Takao, K. Noda, Y. Morita, K. Nishimura and Y. Ikeda, *Cryst. Growth Des.*, 2008, **8**, 2364.
66. T. R. Varga, A. C. Bényei, Z. Fazekas, H. Tomiyasu and Y. Ikeda, *Inorg. Chim. Acta*, 2003, **342**, 291.
67. Z. Cao, H. Wang, J. Gu, L. Zhu and K. Yu, *Acta Cryst. Sect. C*, 1993, **49**, 1942.
68. H. Z. Wang and Z. B. Cao, *Chin. Chem. Lett.*, 1993, **3**, 211.
69. S. Wahu, J.-C. Berthet, P. Thuéry, D. Guillaumont, M. Ephritikhine, R. Guillot, G. Cote and C. Bresson, *Eur. J. Inorg. Chem.*, 2012, 3747.
70. M. Buhl, H. Kabrede, R. Diss and G. Wipff, *J. Am. Chem. Soc.*, 2006, **128**, 6357.
71. Z.-B. Xie, H.-T. Kang, Z.-S. Chen, S.-H. Zhang and Z.-G. Le, *J. Radioanal. Nucl. Chem.*, 2016, **308**, 573.
72. S. Kannan, M. A. Moody, C. L. Barnes and P. B. Duval, *Inorg. Chem.*, 2008, **47**, 4691.
73. P. B. Duval, S. Kannan and C. L. Barnes, *Inorg. Chem. Commun.*, 2006, **9**, 426.
74. L.-Y. Yuan, M. Sun, L. Mei, L. Wang, L.-R. Zheng, Z.-Q. Gao, J. Zhang, Y.-L. Zhao, Z.-F. Chai and W.-Q. Shi, *Inorg. Chem.*, 2015, **54**, 1992.
75. H. Kazama, S. Tsushima, Y. Ikeda and K. Takao, *Inorg. Chem.*, 2017, **56**, 13530.
76. N. Koshino, M. Harada, M. Nogami, Y. Morita, T. Kikuchi and Y. Ikeda, *Inorg. Chim. Acta*, 2005, **358**, 1857.
77. L. Nigond, C. Musikas and C. Cuillerdier, *Solv. Extr. Ion Exch.*, 1993, **12**, 297.
78. S. A. Ansari, P. Pathak, P. K. Mohapatra and V. K. Manchanda, *Chem. Rev.*, 2012, **112**, 1751.
79. Y. Zhang, M. Bhadbhade, J. Gao, I. Karatchevtseva, J. R. Price and G. R. Lumpkin, *Inorg. Chem. Commun.*, 2013, **37**, 219.
80. R. V. Davies, J. Kennedy, R. W. McIlroy, R. Spence and K. M. Hill, *Nature*, 1964, **203**, 1110.
81. C. W. Abney, R. T. Mayes, T. Saito and S. Dai, *Chem. Rev.*, 2017, **117**, 13935.
82. M. Tanada, in *International Seminar on Nuclear War and Planetary Emergencies (The Science and Culture Series - Nuclear Strategy and Peace Technology)*, ed. R. Ragaini, World Scientific Publishing, Hackensack, NJ, USA, 2010.
83. R. Jara, J. M. Estela and V. Cerdá, *Thermochim. Acta*, 1991, **177**, 229.
84. N. Mehio, A. S. Ivanov, N. J. Williams, R. T. Mayes, V. S. Bryantsev, R. D. Hancock and S. Dai, *Dalton Trans.*, 2016, **45**, 9051.
85. G. Tian, S. J. Teat and L. Rao, *Dalton Trans.*, 2013, **42**, 5690.
86. C. W. Abney, S. Liu and W. Lin, *J. Phys. Chem. A*, 2013, **117**, 11558.
87. D. I. Alexandropoulos, E. C. Mazarakioti, S. A. Corrales, J. T. Bryant, L. V. Gasparov, C. Lampropoulos and T. C. Stamatatos, *Inorg. Chem. Commun.*, 2017, **78**, 13.
88. J. G. West, T. A. Bedell and E. J. Sorensen, *Angew. Chem. Int. Ed.*, 2016, **55**, 8923.
89. G. Accorsi, A. Listorti, K. Yoosafa and N. Armaroli, *Chem. Soc. Rev.*, 2009, **38**, 1690.
90. N. Armaroli, L. D. Cola, V. Balzani, J.-P. Sauvage, C. O. Dietrich-Buchecker and J.-M. Kern, *J. Chem. Soc., Faraday Trans.*, 1992, **88**, 553.
91. I. S. Ahuja and R. Singh, *J. Inorg. Nucl. Chem.*, 1973, **35**, 2075.
92. N. W. Alcock, D. J. Flanders and M. Pennington, *Acta Cryst. Sect. C*, 1988, **44**, 247.
93. C. Turró, Y. C. Chung, N. Leventis, M. E. Kuchenmeister, P. J. Wagner and G. E. Leroi, *Inorg. Chem.*, 1996, **35**, 5104.
94. T. Koizumi, Y. Yokoyama and K. Morihashi, *Bull. Chem. Soc. Jpn.*, 1992, **65**, 2839.
95. M. S. Henry and M. Z. Hoffman, *J. Phys. Chem.*, 1979, **83**, 618.
96. T.-B. Ren, W. Xu, W. Zhang, X.-X. Zhang, Z.-Y. Wang, Z. Xiang, L. Yuan and X.-B. Zhang, *J. Am. Chem. Soc.*, 2018, **140**, 7716.
97. H. D. Burrows and T. J. Kemp, *Chem. Soc. Rev.*, 1974, **3**, 139.
98. G. Meinrath, Y. Kato, T. Kimura and Z. Yoshida, *Radiochim. Acta*, 1998, **82**, 115.
99. N. Kaltsoyannis, *Chem. Eur. J.*, 2018, **24**, 2815.

100. C. K. Jørgensen and R. Reisfeld, *Uranyl Photophysics: Topics in Inorganic and Physical Chemistry, Structure and Bonding*, Springer, Heidelberg, 1982.
101. S. R. Maqsood, N. Islam, S. Bashir, B. Khan and A. H. Pandith, *J. Coordin. Chem.*, 2013, **66**, 2308.
102. I. S. Ahuja, *Synth. React. Inorg. Met.-Org. Chem.*, 1985, **15**, 93.
103. S. P. McGlynn, J. K. Smith and W. C. Neely, *J. Chem. Phys.*, 1961, **35**, 105.
104. S. Schöne, T. Radoske, J. März, T. Stumpf, M. Patzschke and A. Ikeda-Ohno, *Chem. Eur. J.*, 2017, **23**, 13574.
105. J.-C. Berthet, M. Nierlich and M. Ephritikhine, *Dalton Trans.*, 2004, 2814.
106. Z. M. Alikhanova, V. F. Zolin, S. I. Rozman, P. S. Fisher and V. G. Ellert, *Optik. Spektrosk.*, 1971, **31**, 325.
107. K. Salazar-Salinas, P. A. Baldera-Aguayo, J. J. Encomendero-Risco, M. Orihuela, P. Sheen, J. M. Seminario and a. M. Zimic, *J. Phys. Chem. B*, 2014, **118**, 10065.
108. K. Lyczko and L. Steczek, *J. Struct. Chem.*, 2017, **58**, 102.
109. I. A. Charushnikova and C. D. Auwer, *Russ. J. Coordin. Chem.*, 2004, **30**, 511.
110. J. Jeżowska-Trzebiatowska and S. Ernst, *J. Inorg. Nucl. Chem.*, 1964, **26**, 837.
111. B. E. Cowie, J. M. Purkis, P. L. Arnold, J. B. Love and J. Austin, *Chem. Rev.*, 2019, **119**, 10595.
112. J. I. Bullock, *J. Inorg. Nucl. Chem.*, 1967, **29**, 2257.
113. R. Hämäläinen, U. Turpeinen and I. Mutikainen, *Acta Cryst. Sect. C*, 1996, **52**, 16.
114. P. V. Balakrishnan, S. K. Patil, H. D. Sharma and H. V. Venkatasetty, *Can. J. Chem.*, 1965, **43**, 2052.
115. I. A. Charushikova, V. P. Perminov and S. B. Katser, *Radiokhim.*, 1995, **37**, 493.
116. R. G. Denning, J. O. W. Norris and D. Brown, *Mol. Phys.*, 1982, **46**, 287.
117. H. A. Friedman, L. M. Toth and M. M. Osborne, *J. Inorg. Nucl. Chem.*, 1979, **41**, 1339.
118. P. G. Hagan and J. M. Cleveland, *J. Inorg. Nucl. Chem.*, 1966, **28**, 2905.
119. L. M. Toth and H. A. Friedman, *Radiochim. Acta*, 1980, **27**, 173.
120. P. Lindqvist-Reis, C. Apostolidis, O. Walter, R. Marsac, N. L. Banik, M. Y. Skripkin, J. Rothe and A. Morgenstern, *Dalton Trans.*, 2013, **42**, 15275.
121. Y.-P. Yin, C.-Z. Dong and X.-B. Ding, *Chem. Phys. Lett.*, 2015, **635**, 134.
122. B. Jezowska-Trzebiatowska and M. Chmielowska, *J. Inorg. Nucl. Chem.*, 1961, **20**, 106.
123. M. A. Lashley, A. S. Ivanov, V. S. Bryantsev, S. Dai and R. D. Hancock, *Inorg. Chem.*, 2016, **55**, 10818.
124. M. Autillo and R. E. Wilson, *Inorg. Chem.*, 2019, **58**, 3203.
125. G. B. Jin, S. Skanthakumar and L. Soderholm, *Inorg. Chem.*, 2012, **51**, 3220.
126. T. Fujii, G. Okude, A. Uehara and H. Yamana, *IOP Conf. Ser.: Mater. Sci. Eng.*, 2010, **9**, 012061.
127. L. J. Basile, J. C. Sullivan, J. R. Ferraro and P. LaBonville, *Appl. Spectrosc.*, 1974, **28**, 142.
128. C. Madic, G. M. Begun, D. E. Hobart and R. L. Hahn, *Inorg. Chem.*, 1984, **23**, 1914.
129. G. R. Fulmer, A. J. M. Miller, N. H. Sherden, H. E. Gottlieb, A. Nudelman, B. M. Stoltz, J. E. Bercaw and K. I. Goldberg, *Organometallics*, 2010, **29**, 2176.
130. M. Bühl and H. Kabrede, *Inorg. Chem.*, 2006, **45**, 3834.
131. P. R. Srinivasan and R. L. Lichter, *J. Magn. Reson.*, 1969, **28**, 227.
132. T. Nakamura and C. Miyake, *J. Alloy. Compd.*, 1996, **233**, 1.
133. G. J. Lumetta, B. K. McNamara, B. M. Rapko, R. L. Sell, R. D. Rogers, G. Broker and J. E. Hutchinson, *Inorg. Chim. Acta*, 2000, **309**, 103.
134. J. L. Lapka, A. Paulenova, L. N. Zakharov, M. Y. Alyapyshev and V. A. Babain, *IOP Conf. Ser.: Mater. Sci. Eng.*, 2010, **9**, 012029.
135. J. L. Lapka, A. Paulenova, M. Y. Alyapyshev, V. A. Babain, R. S. Herbst and J. D. Law, *Radiochim. Acta*, 2009, **67**, 291.
136. M. Boltoeva, C. Gaillard, S. Georg, V. K.Karandashev and A. N.Turanov, *Sep. Purif. Technol.*, 2018, **203**, 11.
137. X. Liu, G. Sun, X. Cai, X. Yang, Y. Li, Z. Sun and Y. Cui, *J. Radioanal. Nucl. Chem.*, 2015, **306**, 549.
138. S. Petoud, S. M. Cohen, J.-C. G. Bünzli and K. N. Raymond, *J. Am. Chem. Soc.*, 2003, **125**, 13324.

139. K. L. Peterson, M. J. Margherio, P. Doan, K. T. Wilke and V. C. Pierre, *Inorg. Chem.*, 2013, **52**, 9390.
140. E. J. Werner, J. Kozhukh, M. Botta, E. G. Moore, S. Avedano, S. Aime and K. N. Raymond, *Inorg. Chem.*, 2009, **48**, 277.
141. G. Pandey, S. Koley, R. Talukdar and P. K. Sahani, *Org. Lett.*, 2018, **20**, 5861.
142. C. Musikas, *Inorg. Chim. Acta*, 1987, **140**, 197.
143. J. Martin-Gil, F. J. Martin-Gil, A. Perales, J. Fayos and M. Martínez-Ripoll, *Acta Cryst. Sect. C*, 1983, **39**, 44.
144. G. Honan, D. Kepert, S. Lincoln, J. Patrick and A. White, *Aust. J. Chem.*, 1980, **33**, 69.
145. R. Graziani, U. Casellato, P. A. Vigato, S. Tamburini and M. Vidali, *J. Chem. Soc., Dalton Trans.*, 1983, 697.
146. J. C. Taylor and M. H. Mueller, *Acta Cryst.*, 1965, **19**, 536.
147. P. S. Gentile and L. H. Talley, *J. Am. Chem. Soc.*, 1957, **79**, 4296.
148. B. G. Vats, D. Das, B. Sadhu, S. Kannan, I. C. Pius, D. M. Noronha, M. Sundararajan and M. Kumar, *Dalton Trans.*, 2016, **45**, 10319.
149. W. Yang, W.-G. Tian, X.-X. Liu, L. Wang and Z.-M. Sun, *Cryst. Growth Des.*, 2014, **14**, 5904.
150. Z.-L. Liao, G.-D. Li, M.-H. Bi and J.-S. Chen, *Inorg. Chem.*, 2008, **47**, 4844.
151. I. Mihalcea, N. Henry, T. Bousquet, C. Volkringer and T. Loiseau, *Cryst. Growth Des.*, 2012, **12**, 4641.
152. X. Gao, C. Wang, Z.-F. Shi, J. Song, F.-Y. Bai, J.-X. Wang and Y.-H. Xing, *Dalton Trans.*, 2015, **44**, 11562.
153. S. T. Liddle, *Angew. Chem. Int. Ed.*, 2015, **54**, 8604.
154. R. G. Denning, D. N. P. Foster, T. R. Snellgrove and D. R. Woddwark, *Mol. Phys.*, 1979, **37**, 1089.
155. V. I. Belomestnykh, L. B. Sveshnikova, Y. N. Mikhailov and A. S. Kanishcheva, *Russ. J. Inorg. Chem.*, 2011, **56**, 1894.
156. M. Gál, P. L. Goggin and J. Mink, *Spectrochim. Acta A: Mol. Spectrosc.*, 1992, **48**, 121.
157. S. Kumar, S. Maji, K. Sundararajan and K. Sankaran, *Luminescence*, 2018, **33**, 611.
158. V. I. Belomestnykh, L. B. Sveshnikova, A. V. Churakov, A. S. Kanishcheva and Y. N. Mikhailov, *Russ. J. Inorg. Chem.*, 2011, **56**, 1899.
159. K. M. Ok, M. B. Doran and D. O'Hare, *J. Mater. Chem.*, 2006, **16**.
160. M. H. Brooker, C.-B. Huang and J. Sylwestrowicz, *J. Inorg. Nucl. Chem.*, 1980, **42**, 1431.
161. A. Ledwith, P. J. Russell and L. H. Sutcliffe, *J. Chem. Soc. D: Chem. Commun.*, 1971, 964.
162. D. Rehorek, *Radiochem. Radioanal. Lett.*, 1978, **36**, 85.
163. D. W. Fink and W. E. Ohnesorge, *J. Phys. Chem.*, 1970, **74**, 72.
164. G. Anguera, J. T. Brewster, M. D. Moore, J. Lee, G. I. Vargas-Zúñiga, H. Zafar, V. M. Lynch and J. L. Sessler, *Inorg. Chem.*, 2017, **56**, 9409.
165. I.-T. Ho, Z. Zhang, M. Ishida, V. M. Lynch, W.-Y. Cha, Y. M. Sung, D. Kim and J. L. Sessler, *J. Am. Chem. Soc.*, 2014, **136**, 4281.
166. C. M. Davis, K. Ohkubo, I.-T. Ho, Z. Zhang, M. Ishida, Y. Fang, V. M. Lynch, K. M. Kadish, J. L. Sessler and S. Fukuzumi, *Chem. Commun.*, 2015, **51**, 6757.

Chapter 3: Substrate Reactivity of the Uranyl(VI) Ion

3.1 Introduction

Although photochemical reactions can often lead to products not accessible by thermal means, there are a number of pathways by which electronically excited molecules can become quenched in solution; here, quenching is taken to mean the deactivation of an electronically excited state molecule.[1] For the electronically excited state of the uranyl(VI) ion, $*U^{VI}O_2^{2+}$, this involves physical or chemical quenching.[2] Physical quenching pathways where the substrate is not chemically changed, including fluorescence, collisional deactivation, *etc*. of the uranyl(VI) ion are comparatively more widely studied, and are normally discussed in terms of the effect of the substrate on the luminescence properties of $*U^{VI}O_2^{2+}$. The chemical quenching of the uranyl(VI) ion, where a chemical reaction occurs with an external substrate, commonly occurs *via* one of two pathways, hydrogen-atom abstraction (HAA) or electron transfer (Sections 3.1.2 and 3.13). Both chemical quenching pathways occur *via* U^V intermediates, which have been detected by EPR[3] and electronic spectroscopy.[4] A summary of key quenching mechanisms for the uranyl(VI) ion is given in Scheme 3.1, below.

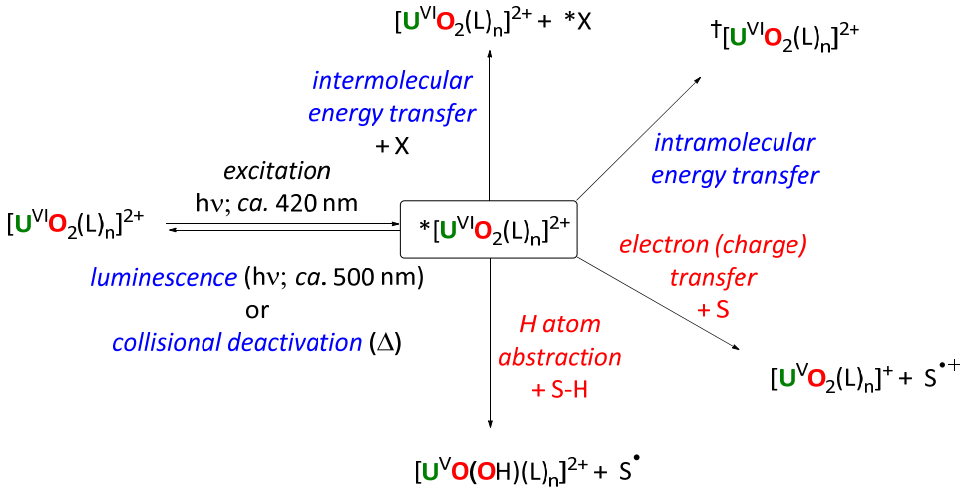

Scheme 3.1 – General quenching mechanisms for the uranyl ion, and excitation. L is a neutral ligand, making n an integer value; X and S are substrates, and † indicates another electronically-excited state. Physical quenching pathways are shown in blue and chemical quenching pathways in red. Other quenching pathways exist, such oxo-atom dissociation, but these pathways are slow ($k < 10^{-8}$ s^{-1})[5, 6] under non-acidic conditions and are thus not included.

Thermal reactions are governed by temperature, solvent effects, reagent concentrations, *etc*. In addition to these parameters, photochemical reactions must also consider light intensity and wavelength, the relative concentrations and rate of formation and consumption of ground *and* excited states, *etc*.[7] For example, on the quenching of $*U^{VI}O_2^{2+}$ with alcohols, Sakuraba and Matsushima proposed[8-12] that the photoreactivity of $\mathbf{U^{NO3}}$ with simple aliphatic alcohols is dependent upon light

intensity, temperature, pH, alcohol concentration, and that quenching of $*U^{VI}O_2^{2+}$ predominantly involves only one excited state. However, by modifying the temperature and solution pH, Mercantonatos[13, 14] (and later Burrows and Formosinho, *et al*.)[15-17] demonstrated that $U^{VI}O_2^{2+}$ quenching with the same alcohols can occur from multiple excited states. The fact that subtle changes in reaction conditions can change reaction mechanisms can make photochemical reactions challenging to understand.

3.1.1 Physical Quenching of the $U^{VI}O_2^{2+}$ ion

With the completion of the Manhattan Project in the 1940s and the move to civilian nuclear research, the post-war years (*ca.* 1945–1980) saw rapid development in the research of uranyl ion reactivity with substrates, particularly with photoirradiation. Accordingly, there are many examples of the substrate-promoted physical quenching of $*U^{VI}O_2^{2+}$. These include alcohols,[18-21] aldehydes,[22] carboxylic acids,[18, 23, 24] ethers,[18, 20] alkenes,[25, 26] haloalkanes,[27] *N*-heterocycle compounds,[28] amines such as hydrazine[29] and trimethylamine,[30] halogens,[31, 32] sulfur-containing substrates including thioethers[33-35] and sulfoxides,[31] metals including Dy(III),[36] cations from groups 1 and 2,[37] Fe(II),[38] Cu(II),[39] Ln(III) (Ln = Pr, Nd, Sm–Yb),[40] Ce(IV),[41] Tl(I),[42] $U^{V}O_2^{+}$,[43] (and others, including Ag(I), Pb(II), Mn(II), Ce(III), Ni(III), Co(III) and Cm(III))[44] and heavier heteroatom-containing substrates from groups 14 (Si–Pb)[27] and 15 (As–Bi).[45-49] In light of the role that TBP plays in uranium waste remediation, the quenching of $*U^{VI}O_2^{2+}$ with phosphorus-containing substrates, including phosphites,[50, 51] phosphates[52-55] (and under anhydrous conditions),[56] and phosphines,[57, 58] has also been examined. Given the large number of examples readers are referred to other, more detailed accounts[7, 44, 59] of the physical quenching of the $*U^{VI}O_2^{2+}$ ion.

3.1.2 Chemical Quenching of $*U^{VI}O_2^{2+}$ by Electron Transfer

The chemical quenching of $*U^{VI}O_2^{2+}$ *via* electron transfer occurs with substrates that possess unsaturation, such as alkenes and aromatics. It is known that the quenching of $*U^{VI}O_2^{2+}$ readily occurs by collisional quenching of aromatic substrates *via* formation of exciplex (excited duplex) complexes, an example of which is outlined in Scheme 3.2, below (here, exciplex refers to an interaction between one molecule in an electronically excited state with another, not necessarily different, molecule in its electronic ground state).[1] The interactions of aromatic systems with $*U^{VI}O_2^{2+}$ have only been computationally investigated[60] very recently, in which significant charge transfer was calculated to occur between hybrid orbitals of σ symmetry in $*U^{VI}O_2^{2+}$ and π^* orbitals of the anisole substrate.

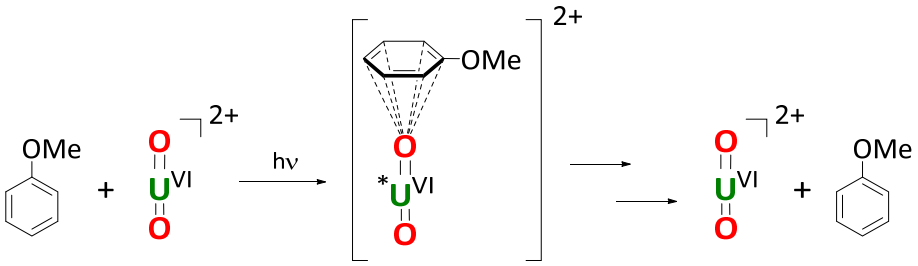

Scheme 3.2 – An example of a physical quenching pathway for $*U^{VI}O_2^{2+}$ in the presence of aromatic substrates, here, exemplified with anisole. There is no net chemical change in the substrate and calculations were performed using complete active space self-consistent field (CASSCF) methods, with geometry optimisation by DFT at the B3LYP/6-31g* level.[61]

While physical quenching of $*U^{VI}O_2^{2+}$ with aromatic (and carbonylic)[61] substrates normally leads to no reaction (*e.g.* benzene; Section 3.2.5, Table 3.4) there are two exceptions to this rule; aromatic substrates that possess exocyclic aliphatic groups (*e.g.* toluene), and polycyclic aromatic or phenolic substrates. For the former HAA normally dominates, with low product yields commonly observed due to significant collisional quenching. For example, the oxidation of toluene with $U^{VI}O_2^{2+}$ in $HClO_4$ or H_3PO_4 occurs with less than 1% conversion, with benzaldehyde as the major product.[62] Significant physical quenching of $*U^{VI}O_2^{2+}$ is also observed in the photoirradiation of di- and tri-phenylmethane.[63]

For polycyclic aromatic or phenolic substrates, however, electron transfer mechanisms involving $*U^{VI}O_2^{2+}$ are considerably more nuanced, and often produce unique product mixtures, Scheme 3.3, reactions i) – iii). For example, after having reasoned that polycyclic aromatics have lower ionisation potentials than benzene, Bakac and Mao demonstrated that electron transfer involving $*U^{VI}O_2^{2+}$ and naphthalene led to a number of oxygenated products, including cinnamaldehyde and naphthols.[64] However, the photoirradiation of azulene and $*U^{VI}O_2^{2+}$ was speculated to lead to the selective formation of poly(azulene).[65] Phenols and chlorophenols are known to chemically quench $*U^{VI}O_2^{2+}$ by dimerising, resulting from formation of an oxyl radical *via* HAA.[66, 67]

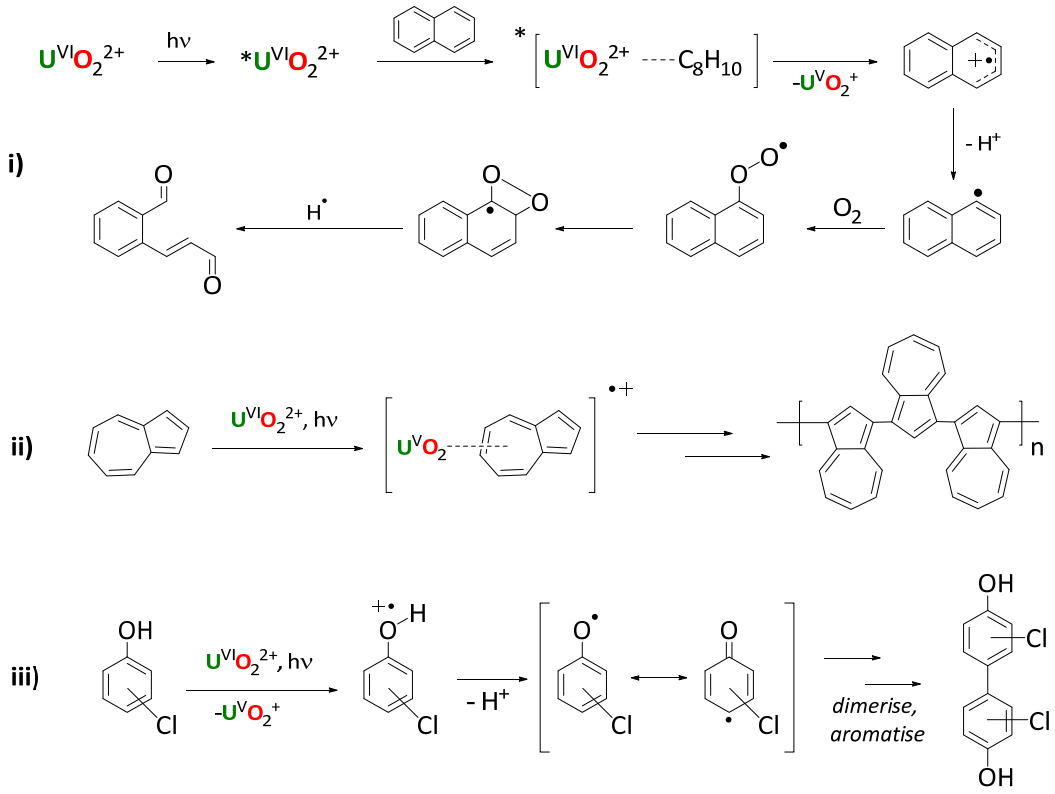

Scheme 3.3 – Electron transfer reactions of aromatic substrates with $*U^{VI}O_2^{2+}$ for the i) oxidation of naphthalene to 2-formyl-*trans*-cinnamaldehyde, ii) polymerisation of azulene and iii) dimerization of chlorophenols. For reaction iii) only the product of *o*- and *m*-substituted chlorophenols is shown; *p*-substitution is known to result in differently substituted dimers.

The $*U^{VI}O_2^{2+}$ ion is also reported to possess complex chemical quenching mechanisms in the presence of alkene substrates, such as cyclohexene.[68] For example, while collisional quenching of $*U^{VI}O_2^{2+}$ by cyclohexene has been reported (leading to recovery of reactants),[69] other reports have suggested β-hydroxycyclohexyl peroxides as likely intermediates,[70, 71] which involve the eventual production of ketones and alcohols. The ambiguity surrounding the likely quenching mechanisms of $*U^{VI}O_2^{2+}$ by alkenes was eventually addressed by McCleskey *et al.*,[72] in which a clear correlation between the quenching rate constant of $*U^{VI}O_2^{2+}$ and alkene ionisation potential (*cf.* ease of ionisation) was observed; that is, alkenes react with $*U^{VI}O_2^{2+}$ *via* electron transfer. Limited details of product formation exist in these studies, but it is known chemical quenching of $*U^{VI}O_2^{2+}$ with 1-hexene (in acetone)[72] or cyclohexene[68] produces nonan-2-one or 2-cyclohexen-1-one, respectively. No details of the selectivity of these substrate reactions were given. It is also known that the $*U^{VI}O_2^{2+}$ ion can act as a photoinitiator for the polymerisation of acrylamides. The proposed mechanism involves electron transfer from U^{VI} to the acrylamide, binding of resulting acrylamide radical to the uranyl ion and termination by radical coupling (that is, polymerisation).[73]

3.1.3 Chemical Quenching of $*U^{VI}O_2^{2+}$ by HAA

The major alternative mechanism of chemical quenching of the $*U^{VI}O_2^{2+}$ ion with substrates is HAA, which normally occurs in saturated substrates, such as alkanes and alcohols.

For alkanes, only the photoreactivity of a handful of simple alkanes with $*U^{VI}O_2^{2+}$ has been reported, including the oxidative quenching of isobutane (2-methylpropane)[74, 75] and cyclopentane,[68] or the fluorination of simple cyclic and linear alkanes.[61] In all three cases $*U^{VI}O_2^{2+}$ is known to quench by the formation of $U^{V}O(OH)^{2+}$, along with the formation of a substrate radical, according to the HAA pathway outlined in Scheme 3.1. This is further exemplified below in Scheme 3.4 (reaction i) in the photo-oxidation of cyclopentane mediated by $*U^{VI}O_2^{2+}$.

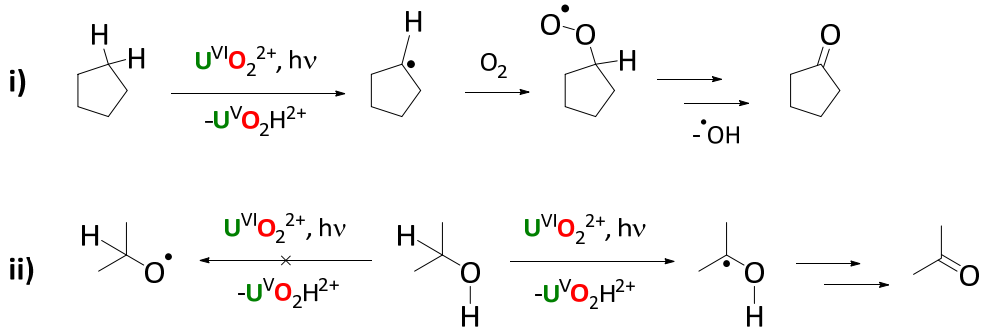

Scheme 3.4 – i) Aerobic photo-oxidation of cyclopentane to cyclopentanone, mediated by $*U^{VI}O_2^{2+}$, *via* the intermediate cyclopentyl peroxide radical, and ii) regioselectivity of the oxidation of a secondary alcohol, isopropanol.

Here, the precise nature of the decomposition of the intermediate peroxide (cyclopentyl peroxide) was unclear, speculated to occur either by autodegradation (to the ketone) with accompanying loss of hydroxyl radicals (*cf*. ½ equiv. of H_2O_2), or by formation of a uranyl-substrate complex (*e.g.* $[U^{VI}\text{-}C_5H_9O_2]^{\bullet}$ or $[U^{V}O_2(C_5H_9O_2)]^{+}$). No alcohol (cyclopentanol) was detected, with the only product observed the ketone, cyclopentanone.

For alkane substrates where there are multiple and different C-H bonds that can undergo HAA, the regioselectivity is governed by C-H bond strength. For example, in the oxidation of isobutane Waltz *et al*. observed that the major product (85±5%) was *t*-butanol, not isobutanol (2-methylpropan-1-ol) or isobutene (2-methylprop-1-ene); Scheme 3.5.[75]

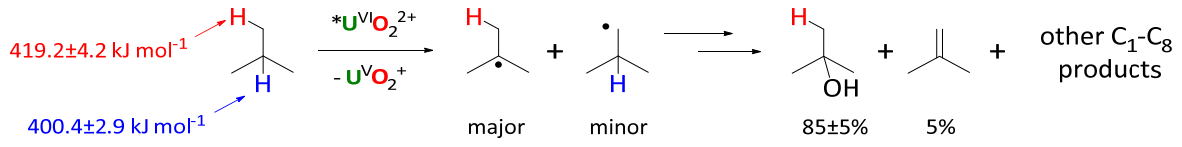

Scheme 3.5 – Bond strengths of C-H bonds in isobutane, which produces *t*-butanol and isobutene upon oxidation in the presence of $*U^{VI}O_2^{2+}$. While the source of the oxygen was not specified by the authors, it is likely to be either atmosphere oxygen, or water, rather than the uranyl-oxo atoms as such processes (oxo-abstraction) is typically slow ($k < 10^{-8}$ s^{-1})[5, 6].

This trend is also known for alcohols, where the oxidation of isopropanol by $\mathbf{U^{NO3}}$ or $\mathbf{U^{OAc}}$ (uranyl acetate) is known to occur only at the secondary carbon, leading to the formation of acetone (Scheme 3.4).[76] The formation of carbon-centred radicals is supported by extensive EPR spectroscopy measurements on methanol, ethanol, propan-1-ol and butanol in the presence of $*U^{VI}O_2^{2+}$ ions,[77] and by TD-DFT calculations on the interactions of methanol with $[UO_2(OH_2)_5]^{2+}$ (**3.A**), where mechanisms involving the formation of weak H-bonds from the uranyl-oxo atoms to either the C-H or O-H groups in methanol have been proposed.[78] Although comparatively little work has been performed on aldehydes, there is evidence to suggest that aldehydes, such as ethanal, react with $*U^{VI}O_2^{2+}$ by HAA, forming a carbonyl carbon-centred radical that quenches with O_2 to give the peroxy acid, and finally the carboxylic acid, ethanoic acid.[68]

Perhaps the most significant report on $*U^{VI}O_2^{2+}$ quenching by HAA in recent years was reported by Sorensen *et al.*,[61] that the $*U^{VI}O_2^{2+}$ ion is capable of fluorinating simple (cyclic or linear) sp^3 alkanes, by visible light irradiation in high yields, outlined in Scheme 3.6.

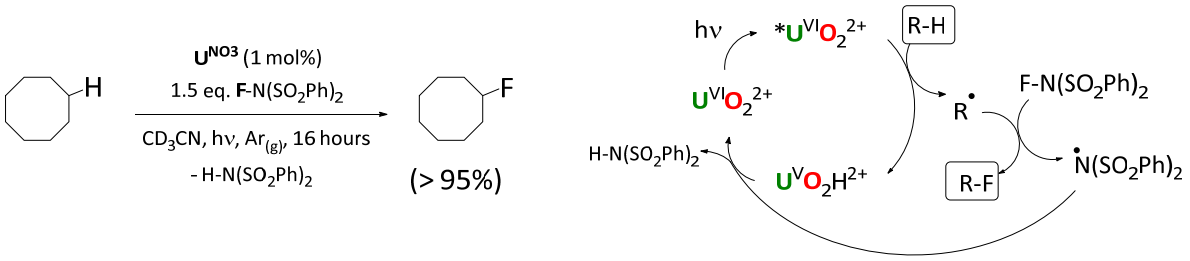

Scheme 3.6 – (L) Photocatalytic fluorination of unactivated sp^3 C-H bonds, here, represented in the mono-fluorination of cyclooctane; (R) general catalytic cycle for the fluorination of alkanes.

This report highlighted for the first time that the photocatalytic reactions involving $*U^{VI}O_2^{2+}$ can be applied to key industrial reactions, such as alkane fluorination, which is of great importance to the agrochemical and pharmaceutical sectors. This report was also among the first to highlight that oxygen is not necessary for $*U^{VI}O_2^{2+}$ regeneration, suggesting a wider array of reactions may be possible upon the exclusion of oxygen from reactions involving the $*U^{VI}O_2^{2+}$ ion (Section 3.6 and 4.3). The precise mechanism of the cyclooctane fluorination was only very recently explored by DFT by Dolg *et al*,[60] where the importance of the uranyl-oxo groups was highlighted in keeping substrates proximal to the $U^{VI}O_2^{2+}$ unit, analogously to the computed mechanism for alcohols reported previously.[78] Here, the cyclooctane C-H has a weak, non-covalent interaction with the uranyl-oxo groups which, together with the predominantly electrostatic interactions of the NO_3^- groups in $\mathbf{U^{NO3}}$ with the sulfone groups in $FN(SO_2Ph)_2$, is thought to ensure that all components are proximal (*e.g.* '[*c*-C_8H_{16}---$U^{VI}O_2^{2+}$---$(SO_2Ph)_2NF$]') and thus able to promote an effective and facile chemical reaction.

This report by Sorensen *et al*. is also, to the best knowledge of the author, the first report investigating the photoreactivity of $*U^{VI}O_2^{2+}$ in a solvent (CD_3CN) that is known to not chemically quench $*U^{VI}O_2^{2+}$. Although other reactions involving $*U^{VI}O_2^{2+}$ in organic solvent are known, these are generally reactions in which the solvent reacts with $*U^{VI}O_2^{2+}$; examples include methanol,[65, 79, 80] and aqueous acetone.[72] Although many investigations of the photocatalytic reactivity of $*U^{VI}O_2^{2+}$ take place in aqueous solution, multiple $U^{VI}O_2^{2+}$ species are present in water (Section 1.2). This is problematic, as the common forms of the hydrated and hydrolysed uranyl ions, $[UO_2(OH_2)_5]^{2+}$ (**3.A**), $[(UO_2)_2(OH)_2(OH_2)_6]^{2+}$ (**3.B**) and $[(UO_2)_3(O)(OH)_3(OH_2)_6]^{+}$ (**3.C**) possess unique photophysical properties that influence their photochemical behaviour; the key photophysical parameters for these complexes and $[UO_2(CO_3)(OH_2)_3]$ (**3.D**) are highlighted in Table 3.1.[81]

Complex	**Absorption**		**Emission**	
	λ_{max}/nm	ε_{max}/$M^{-1}cm^{-1}$	Emission peaks/nm	Excited state lifetime/μs
$[UO_2(OH_2)_5]^{2+}$ (3.A)	414	9.7 ± 0.2	473, 488, **509**, 534, 560, 588	0.9 ± 0.3
$[(UO_2)_2(OH)_2(OH_2)_6]^{2+}$ (3.B)	422	101 ± 2	499, **519**, 542, 556	2.9 ± 0.4
$[(UO_2)_3(O)(OH)_3(OH_2)_6]^{+}$ (3.C)	429	474 ± 7	516, **533**, 554	7 ± 1
$[UO_2(CO_3)(OH_2)_3]$ (3.D)	400	36 ± 3	464, 481, 504, 532	35 ± 5

Table 3.1 – Selected photophysical parameters for $[UO_2(OH_2)_5]^{2+}$ (**3.A**), $[(UO_2)_2(OH)_2(OH_2)_6]^{2+}$ (**3.B**), $[(UO_2)_3(O)(OH)_3(OH_2)_6]^{+}$ (**3.C**), and $[UO_2(CO_3)(OH_2)_3]$ (**3.D**). Values in bold represent the emission maxima, $\lambda_{max,emis}$, where reported. All data from Meinrath *et al*.[81]

Unlike many of the reports described previously, in which little attention is paid to the nature of the uranyl complex (typically nitrate, acetate, perchlorate or phosphate complexes of uranyl of varying concentrations in water), a small number of reports have recently emerged where the coordination of the uranyl ion is controlled.

3.1.4 Controlled Uranyl Ion Photoreactivity

By controlling the equatorial coordination of the uranyl ion, the presence of multiple uranyl species with different photochemical properties can be avoided (Section 3.13, Table 3.1), enabling selected uranyl complexes to be used and their photochemical reactivities investigated under more controlled conditions. For example, Azam *et al*. recently reported the synthesis and photocatalytic reactivity of a

novel uranyl(VI) salen complex, [$U^{VI}O_2$(HOEt)($L^{salenCy}$)] (**3.E**, $L^{salenCy}$ = 2,2'-((1E,1'E)-((1R,2R)-cyclohexane-1,2-diylbis(azanylylidene))bis-(methanylylidene))-diphenol).[82] This complex, depicted below in Scheme 3.7, was shown to be considerably more effective than $\mathbf{U^{OAc}}$ in the cyanation of anilines where, after 8 hours of irradiation at 420 nm, conversion of *N,N*-dimethylaniline was 97% using [$U^{VI}O_2$(HOEt)($L^{salenCy}$)] (**3.E**), compared to trace, with $\mathbf{U^{OAc}}$.

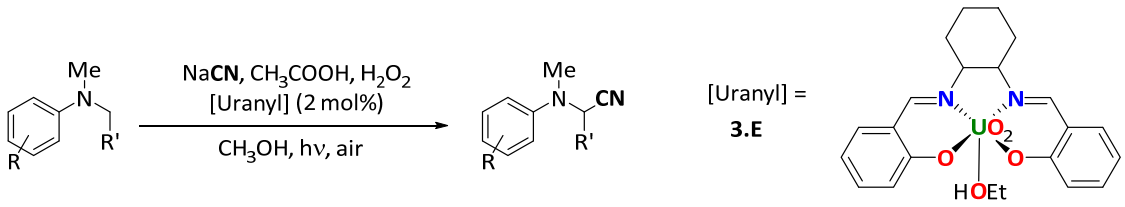

Scheme 3.7 – α-Cyanation of anilines with [$U^{VI}O_2$(HOEt)($L^{salenCy}$)] (**3.E**). R = H, CH_3, OCH_3, Cl, Br; R' = H, CH_3.

Although a tentative mechanism was proposed (hydrogen abstraction followed by nucleophilic cyanide attack), the authors did not speculate on why conversion for [$U^{VI}O_2$(HOEt)($L^{salenCy}$)] (**3.E**) was superior to $\mathbf{U^{OAc}}$. Dolg *et al.*[60] have suggested that restricting the equatorial binding sites of $U^{VI}O_2^{2+}$ with a single, multidentate ligand (such as a salen ligand in [$U^{VI}O_2$(HOEt)($L^{salenCy}$)], **3.E**) may help reduce the non-radiative decay of $*U^{VI}O_2^{2+}$ by collisional quenching or dynamic exchange with solvent molecules, thus increasing its excited state lifetime and quantum yield.

A common method to measure the efficiency of uranyl photocatalysts is to monitor the degradation of rhodamine B, RhB, a common organic dye over time. RhB is convenient to monitor by electronic spectroscopy as it has a diagnostic absorption at 554 nm, and is known to degrade by an electron transfer mechanism.[83] Using this substrate, a small number of photoactive uranyl complexes have recently been reported. These include [UO_2($L^{salenPr}$)(S)][84] (**3.F**; $L^{salenPr}$ = *N,N*'-bis(2-hydroxybenzylidene)-2,2-dimethyl-1,3-propanediamine, S = solvent, either THF, **3.F.THF**, or EtOH, **3.F.EtOH**) and [UO_2(dhpb)$_2$][85] (**3.G**; dhbp = 2,3-dihydroxy-*N*-phenylbenzamide) for the degradation of RhB. The structures of these complexes, along with RhB, are summarised in Figure 3.1.

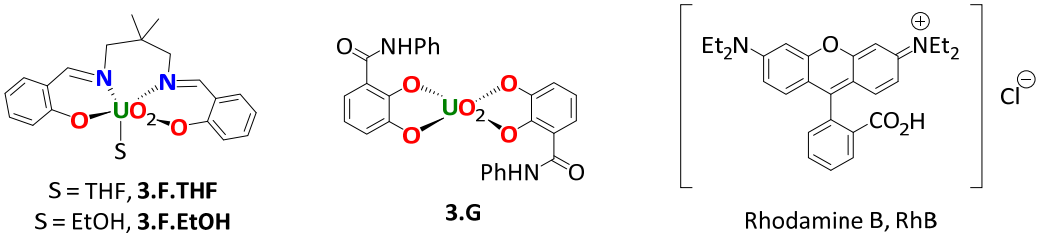

S = THF, **3.F.THF**
S = EtOH, **3.F.EtOH**

3.G

Rhodamine B, RhB

Figure 3.1 – Examples of recent uranyl photocatalysts employed in the degradation of RhB organic dye. S = THF or EtOH.

Both photocatalysts, [UO_2($L^{salenPr}$)(S)] (**3.F**) and [UO_2(dhpb)$_2$] (**3.G**), were found to be effective for the degradation of RhB, with conversions of 90% (S = THF; **3.F.THF**) and 70% (S = EtOH, **3.F.EtOH**) in water,

> 400 nm, 3 hours), and *ca*. 70% for $[UO_2(dhpb)_2]$ (**3.G**; 3 hours, water, 254 nm). The proposed mechanisms for RhB degradation (electron transfer) are consistent with the interaction of aromatic ligands with $*U^{VI}O_2^{2+}$, with further oxidative degradation by oxygen or water-derived radicals or radical ions. Crucially, both complexes were also stable in water, with no observable ligand decomplexation detected by NMR or UV-vis spectroscopies. As $\mathbf{U^{NO3}}$ is known to be a poor catalyst for the photodegradation of RhB in water,[86] the complexation of specific ligands is probably necessary for the unique photoreactivity observed in these systems, but further work remains to confirm this hypothesis, particularly for these homogeneous systems.

3.1.5 Photochemical Properties of $An^{VI}O_2^{2+}$ (An = Np, Pu)

Unlike the long-lived triplet state in $*U^{VI}O_2^{2+}$, $Np^{VI}O_2^{2+}$ and $Pu^{VI}O_2^{2+}$ ions do not possess long-lived excited states[87] as transitions with these open-shell actinyl ions occur within *f*-orbitals, unlike the $2p_\sigma \rightarrow 5f_{\delta/\varphi}$ transition in the uranyl ion. Not only does this reduce the quantum yield of $*Np^{VI}O_2^{2+}$ and $*Pu^{VI}O_2^{2+}$, it also renders supplementary excitation and emission spectroscopy impractical to perform, with current equipment unable to adequately detect the excited state lifetimes of these species. Examples include estimated excited state lifetimes of < 10 ns for $*[Np^{VI}O_2(OH_2)_5]^{2+}$ (**3.H**) in D_2O,[88] < 10 ns in plutonyl(VI)-doped $[Cs]_2[U^{VI}_x(Pu^{VI})_{1-x}O_2Cl_4]$ (**3.I**),[89] and approximately 1.5 ns for $[Np^{VI}O_2(TPIP)_2(OPPh_3)]$ (**3.J**; TPIP = tetraphenylimidodiphosphinato).[90] This suggests that the non-radiative (physical) quenching pathways of $*Np^{VI}O_2^{2+}$ in D_2O (*cf.* water) and of $Pu^{VI}O_2^{2+}$ in the solid state are extremely efficient, which for the former probably results from very fast dynamic ligand exchange and O-H bond vibrations.[91] The incorporation of bulky groups such as the heteropolyanionic tungstate $[PW_9O_{34}]^{9-}$ has been shown to increase the excited state lifetime of $*Np^{VI}O_2^{2+}$ (*e.g.* $[Na_2(*Np^{VI}O_2)_2(PW_9O_{34})_2]^{12-}$, **3.K**, to at least 62 ns in D_2O, compared to < 10 ns for $[*Np^{VI}O_2(OH_2)_5]^{2+}$, **3.H**). By extension, the ligation of other bulky, multidentate ligands (*e.g.* phen, salen *etc.*) to $Np^{VI}O_2^{2+}$ may mimic this effect, by excluding solvent molecules such as water from the primary coordination sphere of Np.[59] Although the dense number of orbitals in the open-shell $An^{VI}O_2^{2+}$ (An = Np, Pu) ions leads to a high number of electronic states (and, consequently, difficulty computing accurate energies for these states),[92] chloride ligands (*e.g.* in $[Np^{VI}O_2Cl_4]^{2-}$) are known to significantly change the experimentally-measured transition energies when compared to the free ion, $Np^{VI}O_2^{2+}$.[93] This raises the possibility that, with careful choice of ligands, the electronic properties of the $Np^{VI}O_2^{2+}$ ion may be modified in the future to allow feasible neptunyl-based photocatalysts to be synthesised.

However, studies on the photoreactivity of $Np^{VI}O_2^{2+}$ have thus far been limited to the feasibility of reductive stripping of $Np^{VI}O_2^{2+}$ from HNO_3 solutions and its possible application to nuclear fuel remediation.[94-96] Under irradiation (254 nm) the nitrate ion, NO_3^-, is reduced to the nitrite ion, NO_2^-,

which reacts with $Np^{VI}O_2^{2+}$ in a series of photoreactions to produce $Np^{V}O_2^{+}$ and Np^{IV}, which are shown in reactions i) and ii)-iv) in Scheme 3.8, respectively. No reaction of $Np^{VI}O_2^{2+}$ occurs with visible light, suggesting nitrate photoreduction (*cf*. UV light) is necessary for Np^{VI} reduction to occur.

i) $NO_3^- + 2H^+ \xrightarrow[254\ nm]{h\nu} NO_2^- + H_2O$

ii) $2\mathbf{Np^{VI}}O_2^{2+} + NO_2^- + H_2O \overset{h\nu}{\rightleftharpoons} 2\mathbf{Np^{V}}O_2^{+} + NO_3^- + 2H^+$

iii) $2\mathbf{Np^{V}}O_2^{+} + NO_2^- + 6H^+ \overset{h\nu}{\rightleftharpoons} 2\mathbf{Np^{IV}} + NO_3^- + 3H_2O$

iv) $2\mathbf{Np^{V}}O_2^{+} + 4H^+ \overset{h\nu}{\rightleftharpoons} \mathbf{Np^{IV}} + \mathbf{Np^{VI}}O_2^{2+} + 2H_2O$

Scheme 3.8 – Reactions for the photoirradiation of NO_3^-, nitrate, to give the nitrite ion, NO_2^- (i) which can then photochemically convert $Np^{VI}O_2^{2+}$ ion into $Np^{V}O_2^{+}$ ions (ii), then Np^{IV} (iii). The disproportionation of $Np^{V}O_2^{+}$ is reaction (iv).

Although the photochemical reactivities of $Pu^{VI}O_2^{2+}$ and $Np^{VI}O_2^{2+}$ are very similar, Bell and Friedman have previously reported the photoreduction of $Pu^{VI}O_2^{2+}$ in the presence of an organic substrate, ethanol,[97] something which has not been recorded for $Np^{VI}O_2^{2+}$. Using aqueous $Pu^{VI}O_2^{2+}$ in $HClO_4$ and 254 nm irradiation, the authors proposed that ethanal was the main product of the photoreduction of $*Pu^{VI}O_2^{2+}$ by ethanol (Scheme 3.9), as had been observed for the analogous reaction of $*U^{VI}O_2^{2+}$ under photochemical conditions.[21]

$$Pu^{VI}O_2^{2+} + \text{CH}_3\text{CH}_2\text{OH} \xrightarrow[HClO_4]{h\nu\ (254nm)} Pu^{V}O_2^{+} + \text{CH}_3\text{CH}\dot{\text{O}} + H^+$$

Scheme 3.9 – The proposed photo-oxidation of ethanol to ethanal using $*Pu^{VI}O_2^{2+}$. The radical produced, recorded as $C_2H_5O^{\bullet}$, presumably decomposes to ethanal by quenching with oxygen, as for the analogous uranyl(VI) reaction.

The quantum yield for this $Pu^{VI}O_2^{2+}$/ethanol reaction, 0.02, is considerably lower than values reported for the analogous $U^{VI}O_2^{2+}$/ethanol photoreaction, which in acidic media is approximately 0.6.[21]

Other oxidation states of Np and Pu undergo photochemical reactions in acidic or basic media. However, these reactions are highly complex and often dependent on the addition of reductants, to which $An^{VI}O_2^{2+}$ (An = Np, Pu) are unstable. Readers are referred elsewhere for detailed accounts of these reactions.[2, 98]

3.1.6 Objectives for Chapter 3

Given the large number of photochemical reactions involving the $U^{VI}O_2^{2+}$ ion in which the products are poorly or not characterised, and the importance of uranium in the environment (Section 1.2), the aims of this chapter are to:

1. Characterise the products of the photoreactivity of a number of substrates with the photo-excited $U^{VI}O_2^{2+}$ ion, and test the functional group tolerances,
2. Investigate and rationalise potential differences in reactivity between $\mathbf{U^{NO3}}$, taken here as an archetypal $U^{VI}O_2^{2+}$-containing compound, with $\mathbf{U^{Ph2phen}}$, given the spectroscopic features of $\mathbf{U^{Ph2phen}}$ outlined in Section 2.2.2,
3. Investigate further the anaerobic reactivity of the $U^{VI}O_2^{2+}$ ion, which remains poorly understood.

3.2 Substrate Photoreactivity of the Uranyl Ion

As discussed in Section 3.1.1 the products of chemical quenching of substrates with the photoexcited uranyl ion, $*U^{VI}O_2^{2+}$, remain poorly characterised. Therefore in order to both develop current knowledge on the interactions of selected substrates with the $*U^{VI}O_2^{2+}$ ion, and to determine appropriate substrates with which to investigate differences in photochemical reactivity using $\mathbf{U^{NO3}}$, a number of substrates, outlined in Figure 3.2, were tested. This range of substrates represents a broad range of chemical functionalities, which were selected to provide a comprehensive study into products of chemical quenching of the $*U^{VI}O_2^{2+}$ ion.

3.2.1 Rationale for Substrate Choices

Many of the hydrocarbon-only and O-containing substrates examined here possess benzylic C-H bonds, which are widely employed in C-H bond activation studies due to the relative weakness of the $PhCR_2$-H bond (R = H, alkyl, *etc*.) relative to other C-H bonds. For example, the C-H bond strength of the exocyclic methyl group in toluene, 375.5 ± 5.0 $kJmol^{-1}$, is *ca*. 10% weaker than the C-H bond in cyclohexane, 416.3 $kJmol^{-1}$.[99] The ubiquity of these substrates in mechanistic studies involving a multitude of transition metal complexes for HAA mechanisms[100, 101] made them natural choices with which to investigate the analogous mechanisms for $*U^{VI}O_2^{2+}$. As the reactivity of these substrates was found to be suitable for further comparative study with $\mathbf{U^{Ph2phen}}$, the outcomes of these reactions are described separately in Section 3.2.3.

The reactivity of several *O*-containing substrates such as benzyl methyl ether, benzyl phenyl ether and 2P1PE (2-phenoxy-1-phenylethanol) with $*U^{VI}O_2^{2+}$ was also investigated, so as to probe possible interactions of uranyl wastes with ligninosic biomatter in the environment, as these are substrates that chemically mimic lignin. Previous studies examining the photochemistry of the uranyl ion with environmentally-relevant molecules, including polycatecholates as mimics of humic acids,[102] phenylalanine[103] and cellulose[104] have suggested the degradation of organic material in solution may occur in uranyl-contaminated wastes or land upon exposure to sunlight. Examples of such sites include

the First Generation Magnox storage pond at the Sellafield industrial complex in the UK, or solid emissions from the Fukushima-Daiichi reactor meltdown (2011), both of which are known to contain uranium wastes in contact with organic matter in sunlight.[105] The reactivity of 2P1PE, a lignin mimic found to be effectively degraded by $*U^{VI}O_2^{2+}$, is described in Section 3.2.4.

Although the physical quenching of the $*U^{VI}O_2^{2+}$ ion with aromatic hydrocarbons is well-documented (Section 3.1.1 and 3.1.2), few reports detail the interactions of the $*U^{VI}O_2^{2+}$ ion with *N*-heterocyclic aromatics. These include mechanisms of physical quenching of $*U^{VI}O_2^{2+}$ with a range of *N*-heterocycles,[28] and the proposed redox non-innocence of pyridine as a solvent in the photo-oxidation of alkenes;[71] no studies on either the feasibility or products of chemical quenching of the $*U^{VI}O_2^{2+}$ ion with *N*-heterocycle substrates exist in the chemical literature. Given the ubiquity of these groups (*e.g.* pyrroles, pyridines, *etc*.) in organic molecules, this was surprising, and justified the use of *N*-containing heterocycles in this investigation.

Other substrates were chosen on account of their unique structures or functional groups. These include cyclohexane, oxidation products of which include cyclohexanol and cyclohexanone, which are important industrial precursors in the manufacture of plastics.[106] The reactivity of ring-strained systems (represented here with tetramethylcyclopropane) has not been explicitly investigated with the uranyl(VI) ion before, however, the photo-dimerisation of benzylidenes with the uranyl(VI) ion is known.[107] Salicylaldehyde derivatives were included because of the ketone and phenolic functionalities, which are known to react with $*U^{VI}O_2^{2+}$ *via* different mechanisms (Sections 3.1.2 and 3.1.3). Given the presence of plastics[108] (*cf*. Teflon, poly(tetrafluoroethylene)) and organic lubricants[109] and contaminants in low-level nuclear waste, a molecular analogue of Teflon (perfluorononane) and several sulfur-containing substrates (methylimidazoles, alkyl sulfides, thiophenes, benzothiophenes) were also tested. These sulfur-containing compounds are known components of kerosene, which is used in the PUREX process.[110]

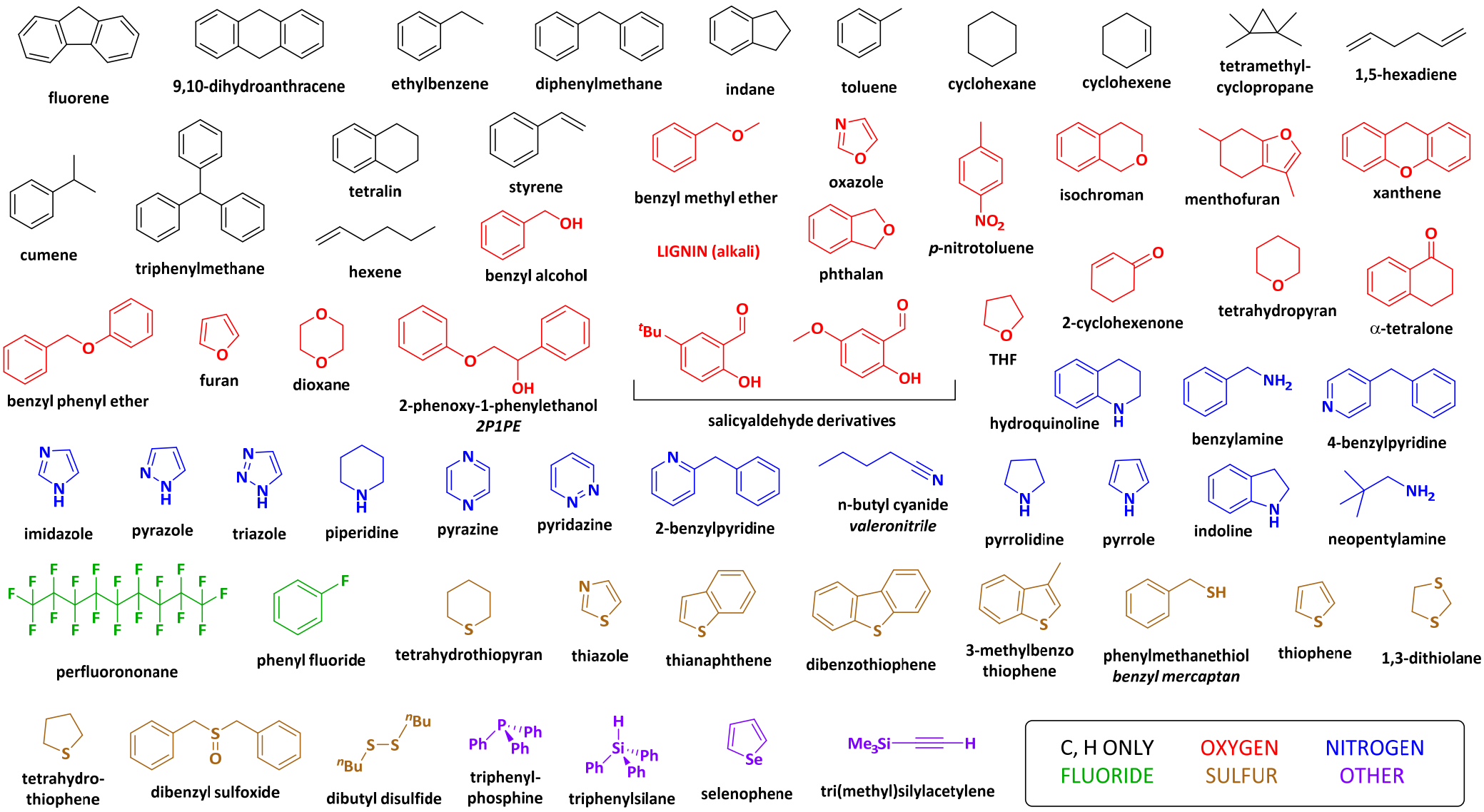

Figure 3.2 – Substrates studied in the substrate scope for the photoreactivity of $\mathbf{U}^{NO3}$. Substrates are colour-coded according to the heaviest atom present.

3.2.2 Products of Substrate Photo-Oxidation with U^{NO3}

The outcomes of the substrate screening reactions are given below in Table 3.2. The substrates were dissolved in 5 mL CH_3CN in air, and 10 mol% $\mathbf{U^{NO3}}$ added. These solutions were then magnetically stirred and irradiated with 420 nm light for 16 hours. The reactions were secured with screw-top lids, and to enable continual airflow into the reaction these lids were perforated with an approximately 2 mm aperture, small enough to prevent significant evaporation of the CH_3CN solvent. A catalyst loading of 10 mol% was selected to ensure collisional quenching of $\mathbf{U^{NO3}}$ by CH_3CN solvent was minimised (*e.g.* not too low), but that enough $\mathbf{U^{NO3}}$ was present in solution to ensure adequate reactivity. Scheme 3.10 and Figure 3.3 outline the general reaction scheme, and reaction set-up for these substrate conversion tests, respectively. In order to avoid unwanted NO_3^- photoreactions (Scheme 3.8), all reactions were carried out in the presence of visible light (420 nm), which is also safer for human operators (UV light is hazardous with prolonged exposure). The lamp was kept at a constant distance from the reaction sample(s), 11 cm, with temperature monitored (digital thermometer) at 22 ± 2°C.

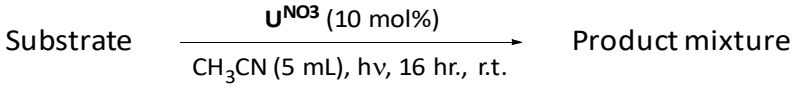

Scheme 3.10 – General scheme for the oxidation of substrates with $\mathbf{U^{NO3}}$.

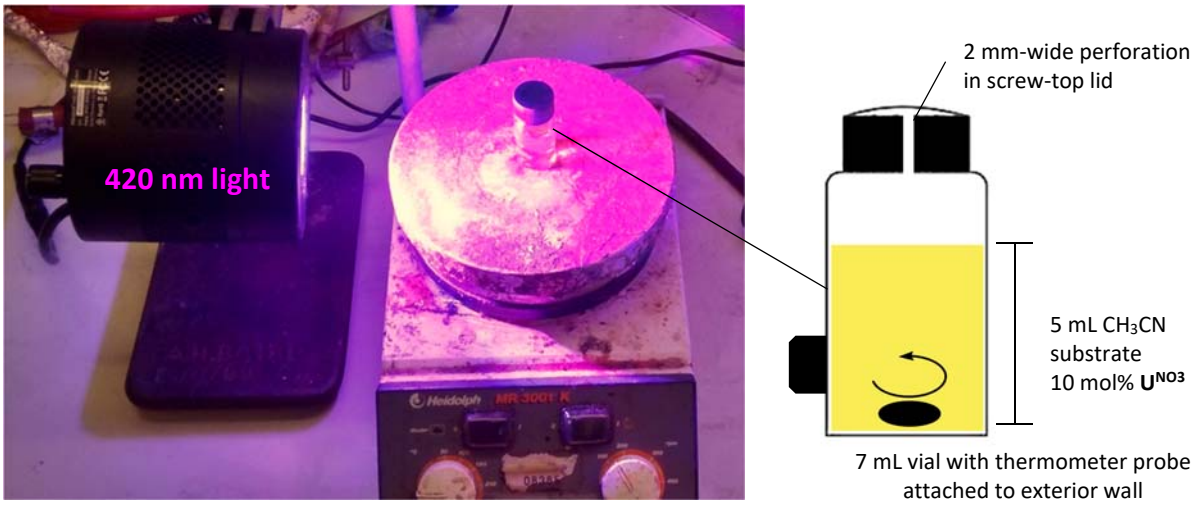

Figure 3.3 – Typical reaction set-up for the substrate scope involving $\mathbf{U^{NO3}}$.

The products of these reactions were then probed spectrometrically, by GC-MS and for cases with greater than 10% substrate conversion, ^{1}H NMR spectroscopy. Control reactions involving the photolysis of only substrates in CH_3CN were also tested; all the substrates listed below in Table 3.2, below, gave no reaction upon photoirradiation at 420 nm for 16 hours in the absence of $\mathbf{U^{NO3}}$.

Entry	Substrate	Structure	Total conversion	Identifiable product(s) *in-situ* yield/%
1	Ethylbenzene	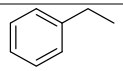	2%	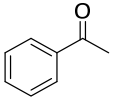 1%
2	Cumene	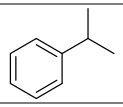		No conversion
3	Tetramethylcyclopropane	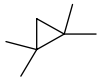		No conversion
4	1-Hexene	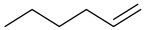	> 99%	Oxidation appears indiscriminate; many unidentifiable products by GC-MS
5	Styrene	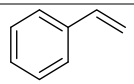	> 99%	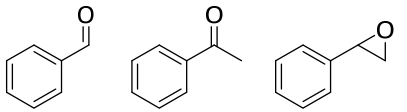 20% 7% 3% *plus unidentified products*
6	Tetralin	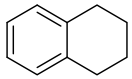		No conversion
7	Lignin	See caption		Insoluble
8	Tetrahydropyran			No conversion
9	Benzyl alcohol	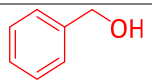	7%	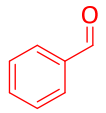 6%
10	Benzyl methyl ether	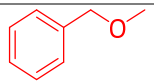	19%	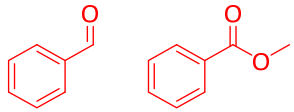 9% 9%

11	Benzyl phenyl ether	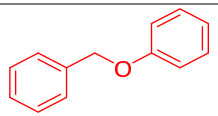	6%	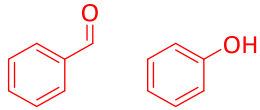 1% 1% *plus unidentified products*
12 ***Section 3.2.6***	Furan *and* THF			Furan: No reaction *and* THF: > 99%, indiscriminate oxidation
13	1,4-Dioxane		84%	Oxidation appears indiscriminate; many unidentifiable products by GC-MS
14	Oxazole			No conversion
15	*p*-Nitrotoluene	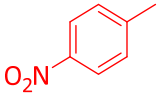		No conversion
16	Menthofuran	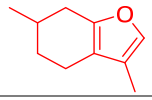		No conversion
17	5-Tert-butyl-2-hydroxybenzaldehyde	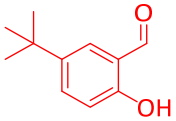		No conversion
18	2-cyclohexeneone	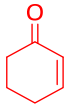		No conversion
19	2-Hydroxy-5-methoxy-benzaldehyde	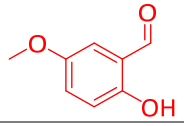		No conversion
20	α-Tetralone	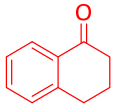		No conversion

21	4-Benzylpyridine	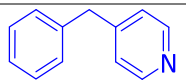	No conversion
22	Benzylamine	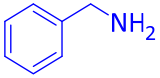	Benzylamine acts as a Brønsted base, rather than reacting photochemically
23	2-Benzylpyridine	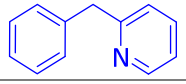	No conversion
24	Indoline	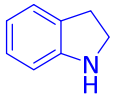	No conversion
25	Tetrahydroisoquinoline	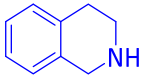	No conversion
26	Pyrrolidine		No conversion
27	Pyrrole		Under the photolysis conditions, pyrrole polymerises
28	Imidazole		No conversion
29	Pyrazole		No conversion
30	1,2,3-Triazole		No conversion
31	Piperidine	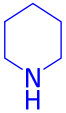	No conversion
32	Pyrazine		No conversion
33	Pyridazine		No conversion

34	Tetrahydrocarbazole	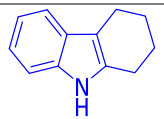		No conversion
35	Neopentylamine	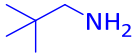	Neopentylamine acts as a Brønsted base, rather than reacting photochemically	
36	Perfluorononane	C_9F_{20}		No conversion
37	Fluorobenzene	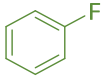		No conversion
38	Thiazole			No conversion
39	Thianaphthene	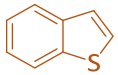		No conversion
40	Dibenzothiophene	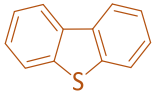		No conversion
41	Tetrahydrothiophene		24%	 24% *only product*
42	1,3-Dithiolane			No conversion
43	Thiophene			No conversion
44	3-Methylbenzothiophene	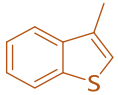		No conversion
45	Benzyl mercaptan	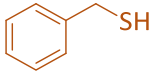		No conversion
46	Dibutyl disulfide	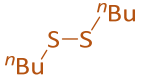	> 99%	Oxidation appears indiscriminate; many unidentifiable products by GC-MS

47	Dibenzyl sulfoxide	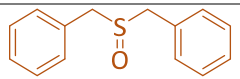		No conversion
48	Tetrahydrothiopyran			No conversion
49	Selenophene			No conversion
50	Triphenylsilane		3%	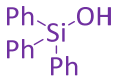 3% *only product*
51	Triphenylphosphine		10%	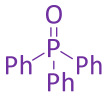 10% *only product*
52	Tri(methyl)silylacetylene		Unstable in GC-MS column (forms poly(cyclosiloxanes))	

Table 3.2 – Substrates tested in the substrate scope with $\mathbf{U^{NO3}}$. Carbon-, oxygen-, nitrogen-, fluorine-, and sulfur-containing substrates, and miscellaneous substrates are colour coded. Alkali lignin was used for the reaction with lignin. Note that for entry 12, furan and THF are presented together in order to highlight the differences between the similar structures; see Section 3.2.6.

As many 'benzylic hydrocarbon substrates' were found to have undergone significant conversion, photoreactions of these substrates with the $*U^{VI}O_2^{2+}$ ion were investigated more fully with the $\mathbf{U^{NO3}}$ and $\mathbf{U^{Ph2phen}}$ photocatalysts. The product mixtures of reactions in the presence of each of these photocatalysts were then compared, and are described separately in Section 3.2.3 and Table 3.3. For brevity these are not included in Table 3.2. Note that 'benzylic hydrocarbon substrates' refers to C- and H-containing substrates that possesses a benzylic C-H bond.

Here, the first observation of note is the susceptibility of $*U^{VI}O_2^{2+}$ to be effectively and physical quenched by a number of substrates or, simply, the non-reactivity of substrates with the uranyl ion. This includes aromatic and oxygen containing substrates (entries 14–20, Table 3.2), many *N*- and *S*-containing substrates (entries 21, 23-26, 28-34, and 38-40, 42-45, 47-48, respectively, Table 3.2), and both *F*-containing substrates (entries 36, 37; Table 3.2), all of which show no conversion by GC-MS.

Several substrates are also unsuitable for substrate reactivity studies, including 1-hexene, 1,4-dioxane, pyrrole, dibutyl disulfide and tri(methyl)silylacetylene (indiscriminate oxidation or unstable in column of GC-MS spectrometer;[111] entries 4, 13, 27, 46 and 52, Table 3.2), and benzylamine and neopentylamine (which deprotonate $\mathbf{U^{NO3}}$ and form intractable solids; entries 22 and 35, Table 3.2) Uranyl speciation in aqueous solutions of pH values of *ca*. 8 or more is known to result in precipitation of mixed oxo- and hydroxo-uranyl compounds[112] (Section 1.2, Figure 1.3), and it is speculated that similar behaviour is observed here in the presence of these amine Brønsted bases in CH_3CN solvent.

For non-benzylic substrates showing conversion > 10%, namely styrene (entry 5, Table 3.2; > 99% conversion), benzyl methyl ether (entry 10, Table 3.2; 19% conversion), tetrahydrothiophene (entry 41, Table 3.2; 24% conversion) and triphenylphosphine (entry 51, Table 3.2; 10% conversion), only two (tetrahydrothiophene and triphenylphosphine) produced product mixtures with fewer than five products. The photochemical conversions of styrene (to form polystyrene, unlike benzaldehyde; entry 5, Table 3.2),[113] benzyl ether derivatives (to form benzaldehyde, benzoic acid, *etc*.),[114] and tetrahydrothiophene (to form tetrahydrothiophene-*S*-oxide and a ring-opened disulfide analogue) have all been reported.[115] Although conversions of these substrates were above 10%, these substrates were not analysed further, due to reactivity not occurring at C-H bonds (*e.g.* tetrahydrothiophene, triphenylphosphine), or where complex product mixtures (*e.g.* styrene) were obtained. Furan and THF, jointly presented as entry 12 in Table 3.2, have markedly different conversions, despite having analogous structures. This is discussed further in Section 3.2.6.

3.2.3 Products of Photo-oxidation of Benzylic Substrates with U^{NO3} and $U^{Ph2phen}$

However, for those benzylic substrates not discussed in Section 3.2.2, analysis of the product mixtures showed effective conversion in most cases, > 10%, with one exception (toluene, with $\mathbf{U^{NO3}}$; entry 2, Table 3.3). In many cases product mixtures were also simple to analyse, with four or fewer products.

These attributes (that is, > 10% conversion and simple product mixtures) made these substrates attractive for a more detailed study, in order to compare the reactivities of $\mathbf{U^{NO3}}$ and $\mathbf{U^{Ph2phen}}$, the catalyst described in Sections 2.2.1 and 2.2.2. Given the increased absorption of $\mathbf{U^{Ph2phen}}$ compared to $\mathbf{U^{NO3}}$ at *ca*. 420 nm (ε_{427}, $\mathbf{U^{Ph2phen}}$ = 65 $M^{-1}cm^{-1}$; ε_{425}, $\mathbf{U^{NO3}}$ = 11 $M^{-1}cm^{-1}$; Figure 2.11) it was envisaged that $\mathbf{U^{Ph2phen}}$ would be a superior photocatalyst to $\mathbf{U^{NO3}}$ in terms of substrate conversion.

In order to compare the effectiveness of $\mathbf{U^{NO3}}$ and $\mathbf{U^{Ph2phen}}$ in the photo-oxidations of these benzylic substrates, a separate series of experiments was undertaken, in which the conversions of these substrates with 10 mol% $\mathbf{U^{NO3}}$ or 5 mol% loading of $\mathbf{U^{Ph2phen}}$ in 5 mL CH_3CN was analysed by ^1H NMR spectroscopy and GC-MS spectrometry, after 16 hours of irradiation at 420 nm in air. The products of oxidation of these benzylic substrates are given in Table 3.3, and Figures 3.4 and 3.5.

Substrate (Entry)	pK_a of indicated proton (in DMSO)	ΔE_{diss}(C-H)/kJ.mol^{-1} (highlighted in red)	Overall conversion[a] U^{NO3}	Overall conversion[a] $U^{Ph2phen}$	Major (and minor) measurable product(s) of oxidation (yield/%) U^{NO3}	Major (and minor) measurable product(s) of oxidation (yield/%) $U^{Ph2phen}$
DHA[d] 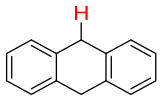 **1** ***See Section 3.3***	30	326	68%[b]	89%[b]	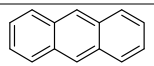 67%[e]	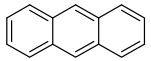 73%[e] 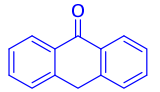 7% 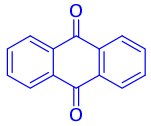 6%
Toluene **$PhCH_3$** **2**	43	375.5 ± 5.0	2%[b]	35%[c]	 2%	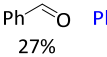 27%  3%
Diphenylmethane **Ph_2CH_2** **3**	32.2	353.5 ± 2.1	21%[c]	33%[b]	 12%  4% 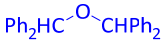 5%	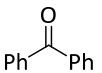 21% 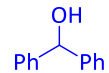 12%
Triphenylmethane **Ph_3CH** **4**	30.6	338.9 ± 8.4	14%[b]	37%[b]	 4%  10%	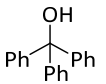 25%
Indane  **5**	n.r	357	47%[b]	87%[b]	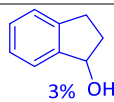 3% 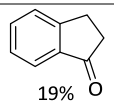 19%	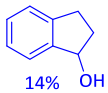 14% 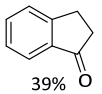 39% 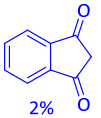 2%
Phthalan 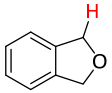 **6**	n.r.	*ca.* 360[g]	99%[b]	99%[c]	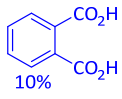 10% 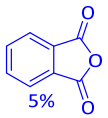 5% 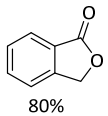 80%	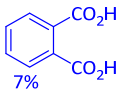 7% 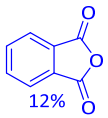 12% 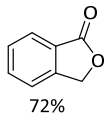 72%

Isochroman 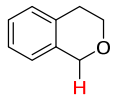 **7**	n.r.	*ca*. 360[g]	35%[b]	80%[c]	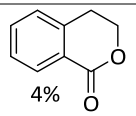 4%	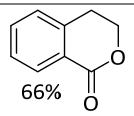 66%
2P1PE[f] 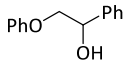 **8**	n/a (C-C, not C-H, bond cleavage)		19%[c]	18%[c]	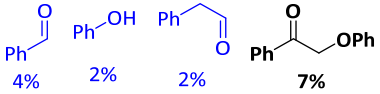 4% 2% 2% **7%**	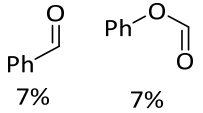 7% 7%
DHA, control[h] **9**	--	--	0%	0%	--	--

Table 3.3 – Comparison of $\mathbf{U^{Ph2phen}}$ and $\mathbf{U^{NO3}}$ as homogeneous photocatalysts for the controlled C-H bond cleavage of a range of benzylic substrates. [a] $\mathbf{U^{NO3}}$ 10 mol% or $\mathbf{U^{Ph2phen}}$ 5 mol%, in CH_3CN (5 mL) for 16 hours at 293 K with hν (420 nm); [b] GC-MS; [c] ^{1}H NMR spectroscopy and GC-MS; [d] DHA is 9,10-dihydroanthracene; [e] inferred (anthracene photo-degrades under these conditions); [f] 2P1PE is 2-phenoxy-1-phenylethanol; [g] approximation based on benzyl methyl ether; [h] same as for condition [a], just without catalyst. n.r. is not reported, n/a is not applicable. Where the sum of conversions of measurable products is less than total substrate conversion, there were unidentified and hence unreported products observed spectroscopically. pK_a values for toluene and DHA are from Bordwell[116] and for di- and tri-phenylmethane, Bordwell *et al*.[117] C-H bond strengths from the *CRC Handbook of Chemical Bond Energies*,[99] and are converted from kcal.mol^{-1} (1 kcal.mol^{-1} = 4.18 kJ.mol^{-1}).

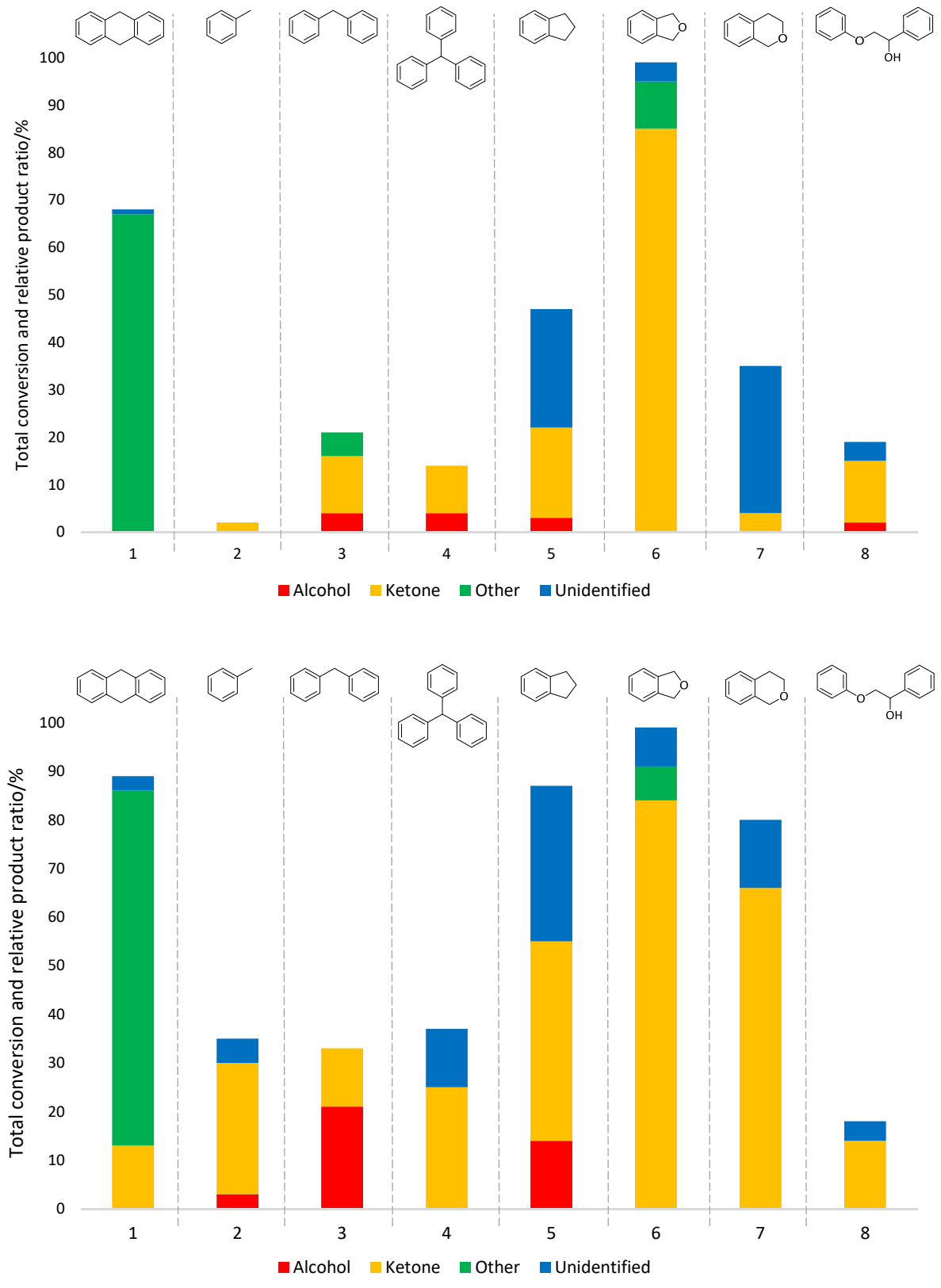

Figures 3.4 and 3.5 – Product profiles (conversions and selectivities) for screening reactions of benzylic substrates with $\mathbf{U}^{NO3}$ (top) and $\mathbf{U}^{Ph2phen}$ (bottom). $\mathbf{U}^{NO3}$ = 10 mol% or $\mathbf{U}^{Ph2phen}$ = 5 mol%, in CH_3CN (5 mL) for 16 hours at r.t., 420 nm.

Firstly, $\mathbf{U}^{Ph2phen}$ gives higher substrate conversion than $\mathbf{U}^{NO3}$ in practically all cases for the given conditions, entries 1–5 and 7, Table 3.3. Toluene (entry 2, Table 3.3; 2% conversion with $\mathbf{U}^{NO3}$, 35%

with $\mathbf{U^{Ph2phen}}$), triphenylmethane (entry 4, Table 3.3; 14% conversion with $\mathbf{U^{NO3}}$, 37% with $\mathbf{U^{Ph2phen}}$), indane (entry 5, Table 3.3; 47% conversion with $\mathbf{U^{NO3}}$, 87% with $\mathbf{U^{Ph2phen}}$) and isochroman (entry 7, Table 3.3; 35% conversion with $\mathbf{U^{NO3}}$, 80% with $\mathbf{U^{Ph2phen}}$) appear particularly affected. With the notable exceptions of DHA and triphenylmethane (entries 1 and 4, Table 3.3), the favoured product in all cases is a ketone, $R_2C{=}O$, rather than an alcohol, $R_3C\text{-}OH$ (R = hydrocarbyl; rest of substrate). Where there are multiple possible sites for C-H bond oxidation (*e.g.* indane, isochroman, entries 5 and 7, Table 3.3, the ketone is selectively formed at the benzylic position of the respective substrates, *e.g.* to form 1-indanone or 1-isochromanone. The largest increase in product selectivity between $\mathbf{U^{NO3}}$ and $\mathbf{U^{Ph2phen}}$ is with isochroman as the substrate (entry 7, Table 3.3), where 1-isochromanone is formed in 4% yield (comprising *ca*. 11% of overall product mixture) using $\mathbf{U^{NO3}}$ as the catalyst, compared to 66% (comprising *ca*. 83% of overall product mixture) using $\mathbf{U^{Ph2phen}}$. Conversions for phthalan (entry 6, Table 3.3) appear quantitative with both $\mathbf{U^{NO3}}$ and $\mathbf{U^{Ph2phen}}$, with little difference in product selectivity. Control irradiations of DHA (hν, 420 nm, 16 hours) in CH_3CN in the absence of $\mathbf{U^{NO3}}$ or $\mathbf{U^{Ph2phen}}$ showed no conversion by ^{1}H NMR spectroscopy (entry 9, Table 3.3). There are also limited differences in product selectivity for $\mathbf{U^{NO3}}$ and $\mathbf{U^{Ph2phen}}$, for example, entries 3 (diphenylmethane; reaction with $\mathbf{U^{Ph2phen}}$ produces more diphenylmethanol), 4 (triphenylmethane; reaction with $\mathbf{U^{Ph2phen}}$ produces no triphenylmethanol) and 7 (isochroman; reaction with $\mathbf{U^{NO3}}$ produces considerably less ketone), Table 3.3. The reasons for these differing product selectivities are not clear but mechanistic investigations with collaborators are underway.

Although substrate conversions are generally lower than analogous non-*f*-block catalysts, product distributions remain reasonably consistent with the established literature. For example, the conversion of toluene is regularly reported for a number of catalysts to be high (> 50%), unlike the 2% and 35% conversion reported here, for $\mathbf{U^{NO3}}$ and $\mathbf{U^{Ph2phen}}$, respectively. Examples include 91% conversion with 100% selectivity for benzaldehyde with UV irradiation of a *trans*-$[Ru^{VI}O_2(L)]^{2+}$ complex (L = a neutral, 14-membered macrocyclic cyclophane ligand) in CH_3CN under N_2,[118] or 70% conversion with 100% selectivity for benzaldehyde using $Cr^{VI}O_3$ in acetic acid.[119] The *trans*-$[Ru^{VI}O_2]^{2+}$-containing complex is a rare example of a UV-active *d*-block *trans*-oxo metal catalyst in which, unlike $U^{VI}O_2^{2+}$, the Ru centre loses both oxo groups (to give *trans*-$[Ru^{II}(L)(NCMe)_2]^{2+}$, which is regenerated to *trans*-$[Ru^{VI}O_2]^{2+}$ by oxygen). It is currently unclear why the conversion of toluene with the *d*-block, metal-oxo photocatalyst is higher (70%, *vs*. max. 35% for $\mathbf{U^{Ph2phen}}$, entry 2 in Table 3.3), the use of UV light over visible light and the oxo-transfer mechanism (compared to $[U^{VI}O_2]^{2+}$, in which oxo-groups are not transferred) are possible reasons. Further investigation is required to understand the differences in reactivity between *d*- and *f*-block metal-oxo catalysts.

Unlike the oxidation of toluene to benzoic acid with [^{n}Bu$_4$N][MnO$_4$] in toluene reported by Mayer *et al.*,[120] no benzoic acid was detected by GC-MS with **U^{NO3}** or **U^{Ph2phen}**, suggesting toluene conversion stops at the aldehyde. Similarly, conversions for di- and tri-phenylmethane oxidations with **U^{NO3}** and **U^{Ph2phen}** are lower than reported for thermal and photochemical reactions with other catalysts. For diphenylmethane these include 71% conversion with 100% selectivity for diphenylmethanol using UV irradiation in wet CH_2Cl_2 with *N*-bromosuccinimide,[121] and 73% conversion with 61% selectivity for benzophenone and 12% selectivity for diphenylmethanol using [Ce^{IV}(OTf)$_4$] in H_2O at r.t. over 24 hours.[122] Reports of triphenylmethane oxidation include 99% conversion with 100% selectivity for triphenylmethanol using Cr$^{VI}O_2Cl_2$ in CCl_4 at 22°C over 30 minutes,[123] and 48% conversion with 100% selectivity for benzophenone using an Fe^{IV}-oxo complex in CH_2Cl_2/CH_3CN at 25°C under N_2.[124]

Conversions for indane, phthalan and isochroman (entries 5–7, Table 3.3) are higher than those for toluene or di- and tri-phenylmethane (entries 2–4, Table 3.3). Conversions of 95% and 76% (with 100% selectivity for 1-indanone) have been reported using thermal ($KMnO_4$/$FeCl_3$ in acetone at -20°C over 16 hours)[125] or photochemical (ozone, 20°C, 8 hours, 254 nm)[126] conditions, respectively. Conversions for phthalan appear to suffer from poor product selectivity in the literature (*e.g.* mono- and di-ketone, alcohol, di-aldehyde and carboxylic acids have all been reported in the oxidation of phthalan with N_2O in CH_3CN at 60°C),[127] though conversions are often high (*e.g.* 94% with Cr$^{VI}O_3$ and HIO_4 in CH_3CN).[128] Conversions are also often high for isochroman, with conversions of 100% (to isochroman-1-one with SeO_2)[129] and 72% (with $CuCl_2$ and O_2)[130] having been reported.

Additionally, there does not appear to be a correlation between C-H bond strength or pK_a and substrate conversion. For example, toluene and di- and tri-phenylmethane all have similar conversions when **U^{Ph2phen}** is the photocatalyst (*ca*. 35%), despite toluene having both less acidic and stronger C-H bonds. Similar trends are observed for diphenylmethane and indane, which have similar bond strengths (*ca*. 355 kJmol^{-1}); the conversion for indane with **U^{NO3}** is more than double that for diphenylmethane (47% and 21% respectively). This suggests that the effectiveness of substrate conversion with the *U$^{VI}O_2^{2+}$ ion is not governed by C-H bond strength but, rather, by the efficiency with which substrates are able to physically quench the *U$^{VI}O_2^{2+}$ ion.

3.2.4 Reactivity with 2P1PE

To further investigate new types of photochemical reactivity that could be undertaken with *U$^{VI}O_2^{2+}$, and to model possible interactions of *U$^{VI}O_2^{2+}$ with lignin motifs present in the environment,[131] a lignin mimic, 2P1PE (2-phenoxy-1-phenylethanol), was reacted photocatalytically with both **U^{NO3}** and **U^{Ph2phen}** (entry 8, Table 3.3), and the products analysed spectroscopically. Lignin model compounds are known to undergo both C-C or C-O bond cleavage,[132] and it was envisaged that similarly to other C-H

bond oxidation catalysts (see below), $*U^{VI}O_2^{2+}$ would be a capable photocatalyst for model lignin decomposition.

This hypothesis was confirmed, with roughly 20% conversion of 2P1PE to other products after 16 hours of irradiation in CH_3CN. These products include benzaldehyde *via* C-O bond cleavage and phenyl formate, formed *via* C-C bond cleavage. Although inferior to a reported 54% conversion of 2P1PE with a vanadyl(V) $[V^VO_2(acac)]$ complex (**3.L**, acac = acetylacetonate) in CH_3CN,[133] these conversions of *ca*. 20% for both $\mathbf{U^{NO3}}$ and $\mathbf{U^{Ph2phen}}$ suggest that uranyl-mediated decomposition reactions may be viable for lignin decomposition with further investigation.

3.2.5 Reactivity with Non-Benzylic Substrates

The photocatalytic oxidations of several non-benzylic substrates were also tested with $\mathbf{U^{NO3}}$ and $\mathbf{U^{Ph2phen}}$, so as to investigate any differences in reactivity between the two catalysts. Table 3.4 below summarises several key photoreactions of $\mathbf{U^{NO3}}$ or $\mathbf{U^{Ph2phen}}$ with cyclohexane and cyclohexene. Valeronitrile, *n*-butyl cyanide, was also reacted with $\mathbf{U^{NO3}}$ or $\mathbf{U^{Ph2phen}}$ under photoirradiation but analysis of product mixtures was often contradictory by GC-MS analysis and so these results are not included. The reaction conditions were identical to those outlined in Figure 3.3 (420 nm, 5 mL CH_3CN, 16 hours). Benzene was also included as a non-benzylic substrate, given the strong C-H bond (472.2 ± 2.2 kJ.mol^{-1})[99] and ubiquity as a functional group in organic substrates.

Substrate	Entry	Overall conversion[a]	
		$\mathbf{U^{NO3}}$	$\mathbf{U^{Ph2phen}}$
Cyclohexane 	1	*See text*	
Cyclohexene 	2	> 99%[d]	> 99%[d]
Benzene 	3	0%[b]	0%[c]

Table 3.4 – Comparison of $\mathbf{U^{Ph2phen}}$ and $\mathbf{U^{NO3}}$ as homogeneous photocatalysts for the controlled bond cleavage of a range of non-benzylic substrates. [a] $\mathbf{U^{NO3}}$ 10 mol% or $\mathbf{U^{Ph2phen}}$ 5 mol%, in CH_3CN (5 mL) for 16 hours at 293 K with hν (420 nm); [b] GC-MS; [c] ^{1}H NMR spectroscopy and GC-MS; [d] ^{1}H NMR spectroscopy only.

Both cyclohexane and cyclohexene (entries 1 and 2, Table 3.4) showed a range of oxidation products after photolysis in the presence of $\mathbf{U^{NO3}}$ or $\mathbf{U^{Ph2phen}}$ catalyst. However, it was not possible to accurately discriminate between these products or their relative ratios in the product mixtures by GC-MS as the products are thermally sensitive, thermolysing in the column of the GC-MS instrument; varying the column or injection temperature resulted in markedly different products and relative ratios. The ^{1}H

NMR spectra of either cyclohexane or cyclohexene photolysis reactions with $\mathbf{U^{NO3}}$ or $\mathbf{U^{Ph2phen}}$ have resonances consistent with alcohols or ketones (*e.g.* -OH singlet at *ca*. 2.6 ppm, -CH_2-C(O)- multiplet at *ca*. 2.4 ppm), but it was not possible to identify individual products, given the large number of similar resonances in all cases. By ^{1}H NMR spectroscopy all cyclohexene had reacted with both photocatalysts, $\mathbf{U^{NO3}}$ and $\mathbf{U^{Ph2phen}}$, illustrated by loss of characteristic alkene resonances at 5.6 ppm in CD_3CN, and thus (quantitative) conversions for cyclohexene are reported in entry 2, Table 3.4. As cyclohexane possesses no chemically distinct proton environments from its oxidation products in its ^{1}H NMR spectrum, it was not possible to accurately determine conversion by either GC-MS or ^{1}H NMR spectroscopy, and is so data for its conversion are omitted from Table 3.4.

To determine the effectiveness of either $\mathbf{U^{NO3}}$ or $\mathbf{U^{Ph2phen}}$ in the photo-oxidation of substrates containing only aromatic C-H bonds, a solution of benzene in CH_3CN was reacted under analogous conditions and the reaction examined spectroscopically (entry 3, Table 3.4). Despite numerous repeat attempts there was no observed reactivity with benzene for either $\mathbf{U^{NO3}}$ or $\mathbf{U^{Ph2phen}}$ in CH_3CN, probably owing to rapid[12] exciplex decay between the $^*U^{VI}O_2^{2+}$ ion and the π-system of the aromatic ring.[62]

3.2.6 Reactivity with Substrate as Solvent

Following the photoreactions of $\mathbf{U^{NO3}}$ and $\mathbf{U^{Ph2phen}}$ with substrates in CH_3CN, the feasibility of using liquid substrates as the reaction solvents themselves was examined. Performing catalysis in which the substrate is the solvent has obvious potential advantages, possibly reducing or removing the need for a separate solvent.

Given its ubiquity as an organic solvent, ability to dissolve both $\mathbf{U^{NO3}}$ and $\mathbf{U^{Ph2phen}}$, and markedly different conversion from its unsaturated congener, furan (jointly, entry 12 in Table 3.2), THF was selected as the substrate and solvent (5 mL) to investigate this hypothesis, according to Scheme 3.11.

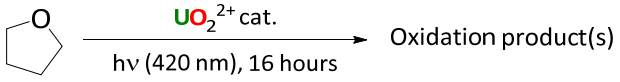

Scheme 3.11 – Photocatalytic reaction of $\mathbf{U^{NO3}}$ or $\mathbf{U^{Ph2phen}}$ (0.1 mol%) with THF as the substrate, and solvent (5 mL).

Analysis by ^{1}H NMR spectroscopy showed that unlike the photocatalytic reaction of THF with $\mathbf{U^{NO3}}$ (10 mol%) in CH_3CN in which THF is completely, but indiscriminately, degraded by $\mathbf{U^{NO3}}$ (conversion > 99%, entry 12, Table 3.2), conversion with $\mathbf{U^{NO3}}$ and $\mathbf{U^{Ph2phen}}$ in THF is markedly reduced, at *ca*. 5% in both cases with 0.1 mol% catalyst. This is a similar result to that reported by Sorensen *et al*. in which there was no reaction (in the unsuccessful fluorination) of the structurally analogous *tert*-butyl methyl ether with 1 mol% $\mathbf{U^{NO3}}$.[61] This suggests that ethers are generally effective quenchers of the $^*U^{VI}O_2^{2+}$ ion,

possibly by physical quenching of $U^{VI}O_2^{2+}$, or by steric crowding of uranyl-coordinated ethers that inhibit substrate approach to the oxyl group in the $U^{V}O_2^{+}$ (*cf*. [$O=U^{V}-O^{\bullet}$]) intermediate.

Compared to furan, the conversion of THF is still more effective, even when present in vast excess (compared to 10 equiv. as outlined in entry 12 in Table 3.2). This suggests that unsaturation (*cf*. the C-C π-bonds) in furan is considerably more efficient at physically quenching the $*U^{VI}O_2^{2+}$ ion than THF, further supporting the observation outlined in Section 3.2.2 that unsaturated substrates, namely aromatics, are very effective quenchers of the $*U^{VI}O_2^{2+}$ ion, and that with minor changes in substrate functionality (*e.g.* THF to furan), large changes in substrate quenching ability may be observed.

3.3 Photoreactivity of 9,10-Dihydroanthracene (DHA) with the Uranyl Ion

In order to further interrogate reactivity differences (*e.g.* effects of catalyst concentration, solvent, water, air, time, *etc*.) between $\mathbf{U^{NO3}}$ and $\mathbf{U^{Ph2phen}}$, a simple, easily characterisable substrate was selected, enabling other reaction conditions (*e.g.* the effect of water, oxygen, *etc*.) to be carefully controlled. 9,10-Dihydroanthracene (DHA) was selected as it has a simple product distribution (anthracene is the major product), alongside a weak, slightly acidic *meso*-C-H bond (ΔE_{diss}(C-H) $\sim$ 326 kJ.mol^{-1}, pK_a 30 in DMSO; entry 1, Table 3.3) that is weaker than the C-H bonds in cyclohexane (*ca*. 410 kJ.mol^{-1}) or benzene (*ca*. 470 kJ.mol^{-1}).[99]

3.3.1 Effect of Catalyst Loading

In order to determine the reaction order in catalyst, the loading of $\mathbf{U^{NO3}}$ or $\mathbf{U^{Ph2phen}}$ (see Tables 3.5 and 3.6) was modified as DHA concentration (50 mM) was maintained in a solution of CH_3CN (or PhCN, Section 3.3.3). The reactions were irradiated at 420 nm over time approximately 11 cm from the reaction solution, which was monitored at 22 ± 2°C by digital thermometer. The conversion of DHA was monitored over time by ^{1}H NMR spectroscopy relative to integral of DHA at t=0. A general reaction summary is given in Scheme 3.12, below.

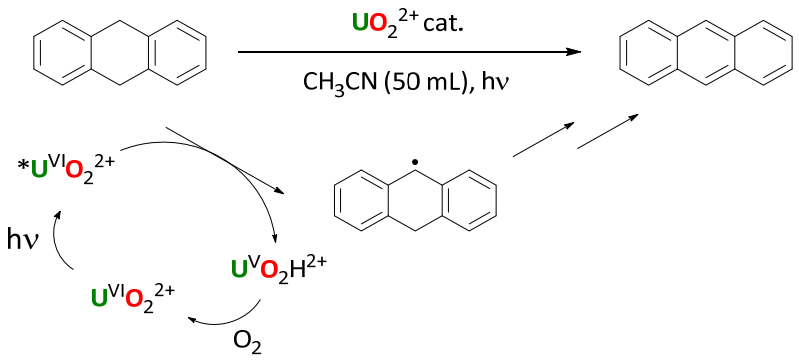

Scheme 3.12 – Aerobic DHA oxidation using variable $\mathbf{U^{NO3}}$ or $\mathbf{U^{Ph2phen}}$ catalyst loadings, and proposed mechanism for formation of anthracene from DHA. The conversion of the proposed intermediate radical to anthracene is deliberately omitted as further work is needed to investigate the role of the uranyl catalyst, oxygen, *etc.* on this step or steps.

With $\mathbf{U^{NO3}}$, DHA oxidation was observed to be effective across a very wide range of catalyst loadings, from 0.001–25 mol%, with conversions consistently between 30 and 40%. There is no discernible change on DHA conversion at higher $\mathbf{U^{NO3}}$ loadings with conversion at 0.001 mol% $\mathbf{U^{NO3}}$ (33%, Table 3.5, entry 1) approximately the same as 25 mol% $\mathbf{U^{NO3}}$ (35%, Table 3.5, entry 15); *e.g.* catalyst concentration does not influence the amount of DHA consumed, inferring that the reaction is zeroth order WRT $\mathbf{U^{NO3}}$ under these conditions. A complete list of conversions (from 0.001–1000 mol% loading, $\mathbf{U^{NO3}}$) is given in Table 3.5, below, along with comparative conversion profiles for the two catalysts ($\mathbf{U^{NO3}}$ and $\mathbf{U^{Ph2phen}}$) in Figures 3.6 to 3.10, below.

Entry	Catalyst loading/%	*In-situ* DHA consumption[f], U^{NO3}/%
1	0.001	33
2	0.01	36
3	0.1	32
4	0.25	38
5	0.5	31
6	0.5[a]	38
7	0.5[b]	21
8	1	37
9	2	39
10	5	36
11	5[c]	11
12	5[d]	37
13	5[e]	32
14	10	34
15	25	35
16	100	49
17	200	53
18	400	66
19	1000	85

Table 3.5 – Conversions of DHA employing **U^{NO3}** as the photocatalyst over 3 hours of irradiation (420 nm) in 50 mL of CH_3CN with stirring in air, unless stated. [a] with 1 equiv. anthracene added at start of reaction; [b] in benzonitrile, PhCN, rather than CH_3CN; [c] anaerobic; [d] with 100 equiv. of water added at start of reaction; [e] with 3 drops of mercury (*ca*. 60 μL) in the reaction; [f] by ^{1}H NMR spectroscopy.

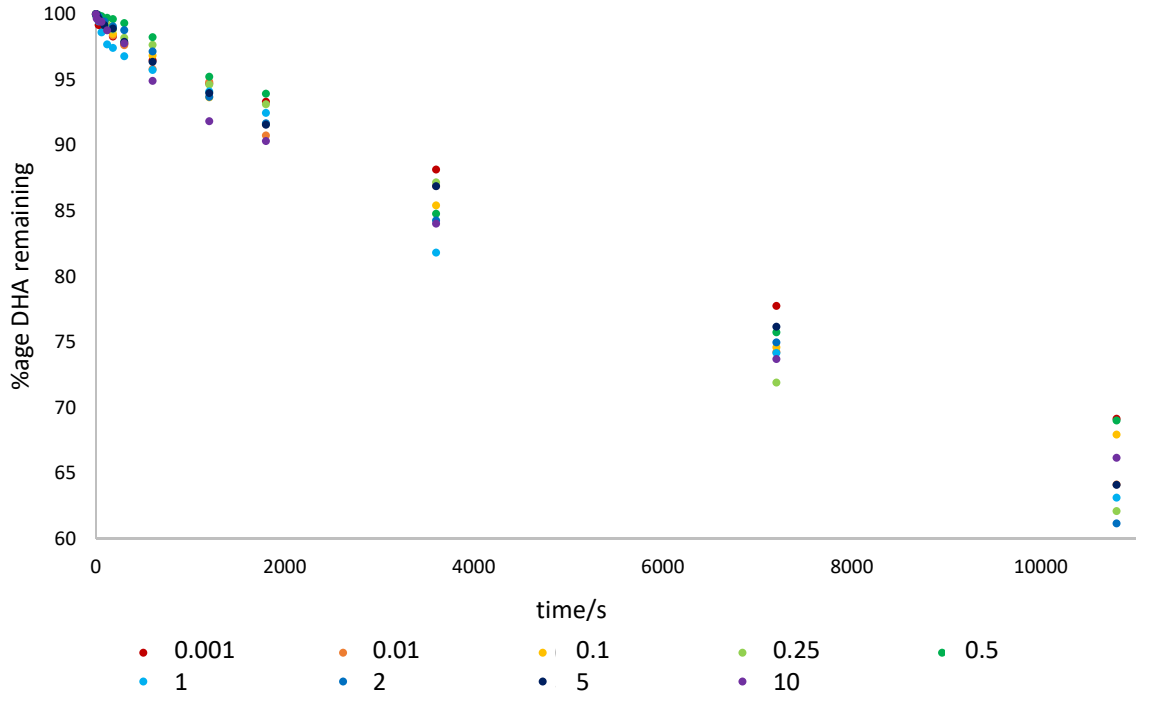

Figure 3.6 – Consumption of DHA over time with $\mathbf{U}^{\mathbf{NO3}}$ over 3 hours, 0.001–10 mol% loading.

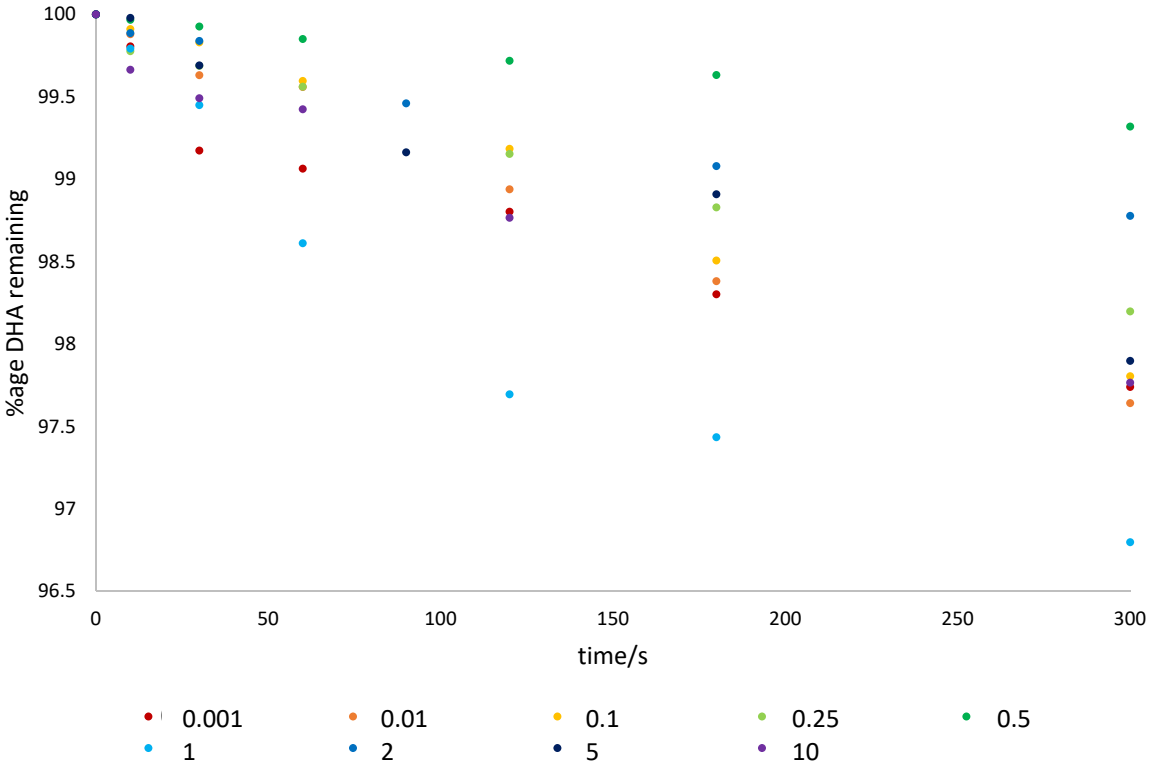

Figure 3.7 – Consumption of DHA over time with $\mathbf{U}^{\mathbf{NO3}}$ at 0.001–10 mol% loading, 0–5 minutes.

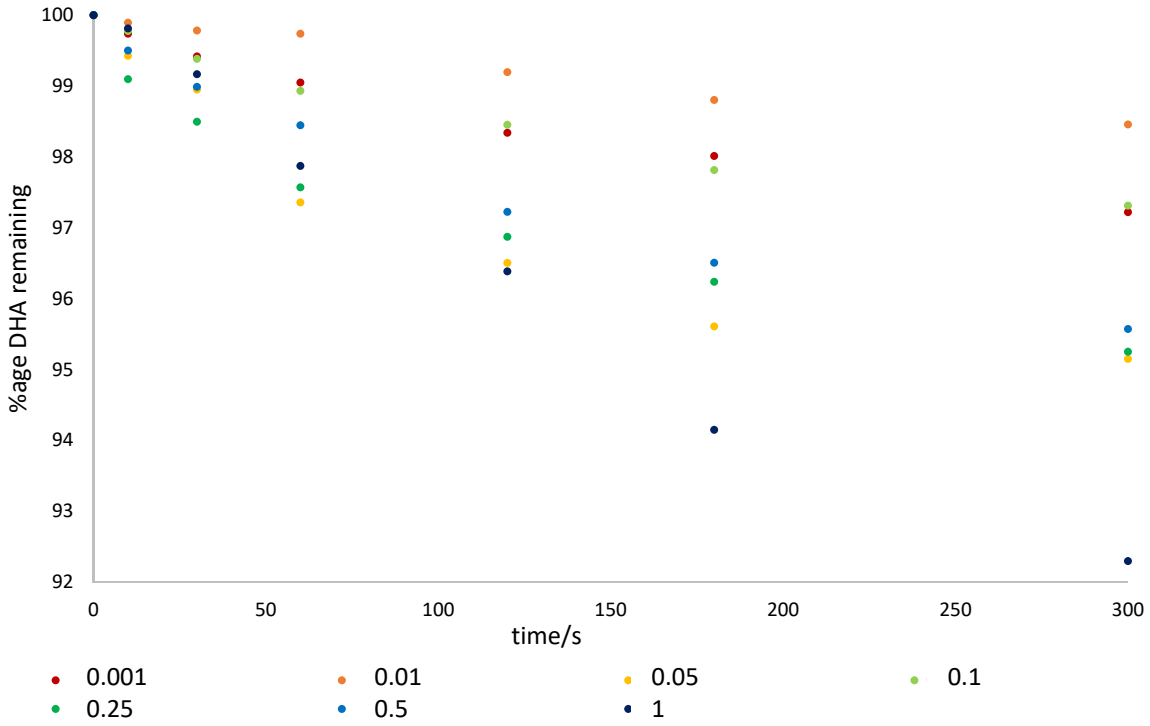

Figure 3.8 – Consumption of DHA over time with **U**^{Ph2phen} at 0.001–1 mol% in CH_3CN for the first 5 minutes of the reactions.

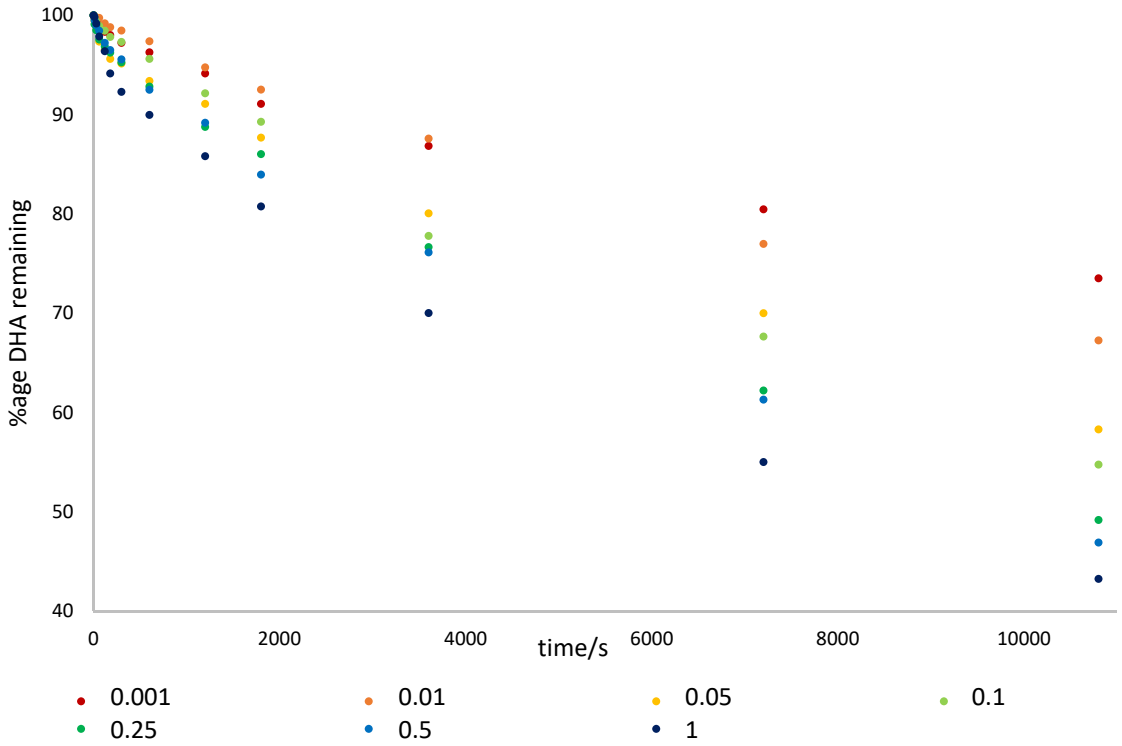

Figure 3.9 – Consumption of DHA over time with **U**^{Ph2phen} at 0.001–1 mol% in CH_3CN over 3 hours.

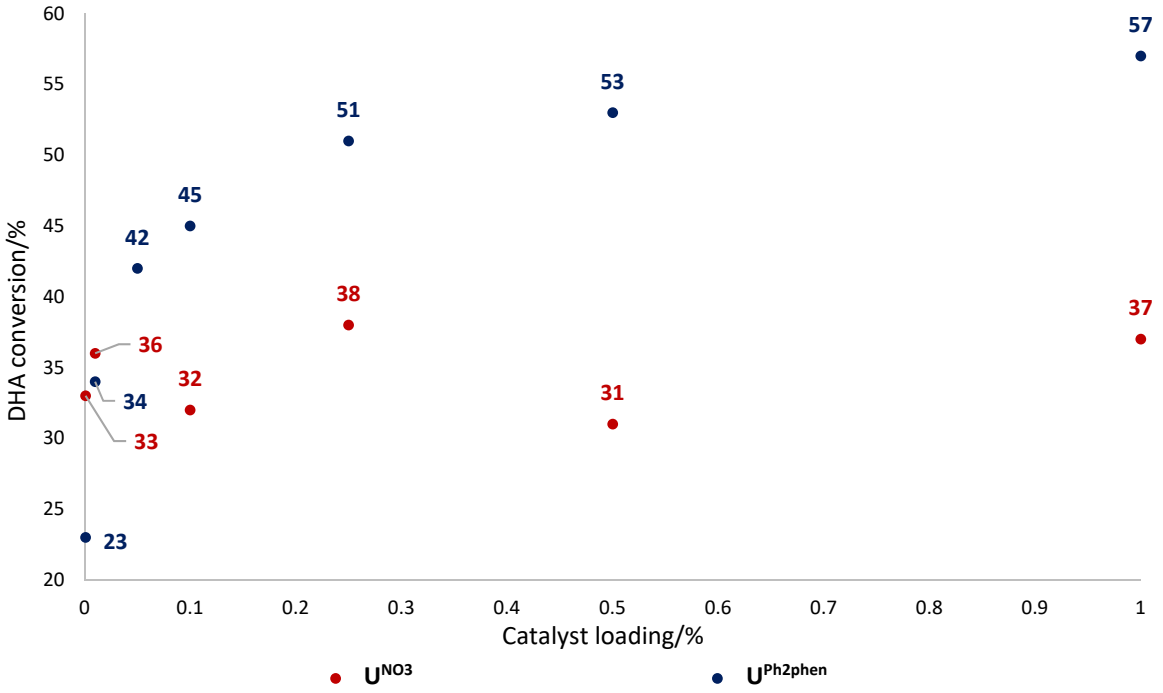

Figure 3.10 – DHA conversion against catalyst loading, 0.001–1 mol% after 3 hours for $\mathbf{U^{NO3}}$ and $\mathbf{U^{Ph2phen}}$ catalysts. Numbers are DHA conversions in percent (%), and lines of best fit are omitted for clarity.

There is no conversion for any sample of $\mathbf{U^{NO3}}$ with DHA stored in the dark for 3 hours, and photolysis of DHA in the absence of $\mathbf{U^{NO3}}$ does not show any DHA conversion by ^{1}H NMR spectroscopy, suggesting that both light and $\mathbf{U^{NO3}}$ must be present for DHA conversion to occur. The addition of several drops of mercury to a reaction containing 5 mol% $\mathbf{U^{NO3}}$ (a mercury drop test)[134] only causes a slight decrease in DHA conversion, from 36% to 32%, within the 30-40% conversion reported for all $\mathbf{U^{NO3}}$ loadings with DHA, suggesting the reaction does not occur heterogeneously (*e.g.* on the surface of solid $U^{IV}O_2$ particles, the product of $U^{VI}O_2^{2+}$ photoreduction).

Given the zeroth order nature of the $\mathbf{U^{NO3}}$ catalyst between 0.001–25 mol% loading, the catalytic mechanism under these conditions is likely complex and multistep, with the catalyst not participating in the rate-determining step of the reaction. This suggests that anthracene production is governed primarily by processes that are not catalyst controlled (*e.g.* are off-cycle). Though the photocatalytic mechanism is likely solvent dependent, and will vary in aqueous systems (compared with CH_3CN here), the very low loadings of $\mathbf{U^{NO3}}$ required to observe DHA conversion (*cf*. 0.001%, 10 ppm) suggest that environmental systems that contain very low concentrations of uranium wastes have the potential for photochemical reactivity in sunlight.

When $\mathbf{U^{NO3}}$ loading is increased above 25 mol%, DHA conversion then becomes sensitive to increasing $\mathbf{U^{NO3}}$ concentration. The conversion of DHA over 3 hours at these loadings is depicted in Figure 3.11 and entries 16-19, Table 3.5.

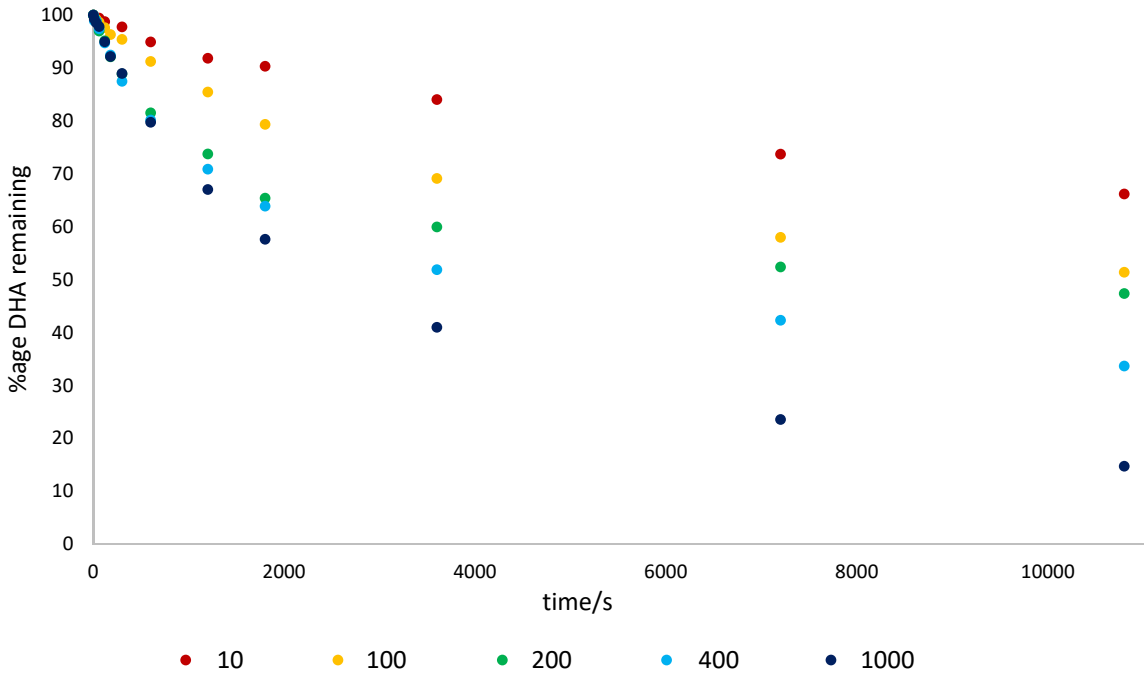

Figure 3.11 – Consumption of DHA over time with $\mathbf{U^{NO3}}$ over 3 hours, 100–1000 mol%, with 10 mol% loading for comparison.

At 100 mol% loading of $\mathbf{U^{NO3}}$, DHA conversion is 49%, increasing to 53% at 200 mol%, 66% at 400 mol%, and 85% at 1000 mol% $\mathbf{U^{NO3}}$; see entries 14 and 16–19 in Table 3.5. This is a marked increase from the *ca*. 30–40% conversion observed for < 25 mol% $\mathbf{U^{NO3}}$, suggesting that another mechanism for DHA conversion dominates under these conditions. For 400 mol% and 1000 mol% loadings of $\mathbf{U^{NO3}}$, the reactions of DHA in CH_3CN were accompanied by effervescence, heat (60°C, by digital thermometer), and generation of a dark yellow-brown solution before irradiation (and in the dark). In all cases, the only detectable product (by ^{1}H NMR spectroscopy) was anthroquinone, not anthracene, which is the favoured product at $\mathbf{U^{NO3}}$ loadings of ≤ 25 mol%.

At these concentrations of $\mathbf{U^{NO3}}$ it speculated that it is the nitrate groups, not the uranyl ions, that promote the thermal oxidation of DHA, with accompanying formation of NO_X by nitrate reduction. This has precedent in the chemical literature, where nitric acid is known to oxidise organic substrates including benzyl alcohol[135] and xanthene and isochroman (*e.g.* 95% conversion of xanthene in CH_3CN with 15 mol% HNO_3 at 140°C),[136] which occur by the thermolysis of HNO_3 to $^{\bullet}NO_2$ at elevated temperatures. The $^{\bullet}NO_2$ molecule can then quench by HAA of a benzylic C-H bond, to form nitrous acid, HNO_2, and a hydrocarbyl radical, which is further quenched by O_2 (or other oxidant(s)) to form the final ketone product, anthroquinone. Further decomposition of HNO_2 results in NO_2 (*cf*. 0.5 equiv. of N_2O_4) which is a brown gas, thus accounting for the observed dark yellow-brown colour of the

solutions here. A summary of these reactions is depicted in Scheme 3.13, below. Further details, for example on the role of oxygen in these reactions, are given elsewhere for brevity.[136]

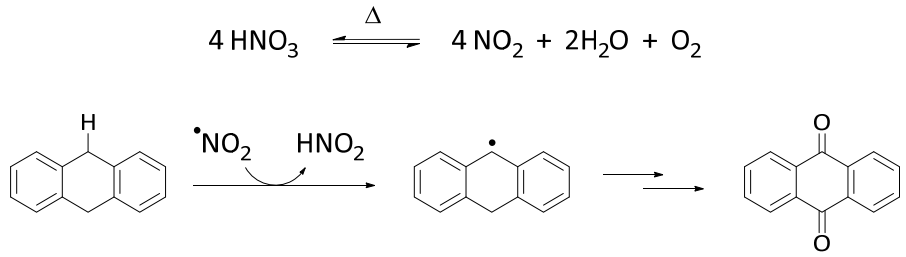

Scheme 3.13 – Proposed mechanism for the nitrate-mediated oxidation of DHA where **U^{NO3}** loading is ≥ 100 mol%. HNO_3 likely derives from the interaction of NO_3^- ions with water, which presumably comes from **U^{NO3}** (a hexahydrate).

Although the 400 and 1000 mol% **U^{NO3}**/DHA reactions were not deliberately heated, these reaction solutions were noticeably hot 30 seconds after addition of the **U^{NO3}**, reaching approximately 60°C when measured by an IR thermometer. It is speculated that this heat drives the initial thermolysis of HNO_3 or NO_3^-. In order to test the importance of these nitrate groups, a control reaction where 1000 mol% of a non-nitrate containing uranyl(VI) compound, $[UO_2Cl_2(OH_2)_2]\cdot xH_2O$, was then added to a CH_3CN solution of DHA (2.5 mmol) in the dark, and the conversion of DHA monitored by ^1H NMR spectroscopy over a three hour period. As no DHA conversion was observed, it is speculated that nitrate groups are required to drive the thermal reaction. Given the increase in observed DHA conversions, the dependence of the reaction rate on the nitrate groups is also likely non-zeroth order.

For **U^{Ph2phen}**, catalyst loading also influences DHA conversion, with catalyst loadings from 0.001–1 mol% giving sequential increases in DHA conversion from 23 to 57% after 3 hours of photolysis under these conditions. These data are summarised in Table 3.6 and Figures 3.8–3.10, and suggest a non-zero order of reaction WRT **U^{Ph2phen}**, in contrast to the zero-order dependence for **U^{NO3}**.

Entry	Catalyst loading/%	*In-situ* DHA consumption[c], $U^{Ph2phen}$/%
1	0.001	23
2	0.01	34
3	0.05	42
4	0.1	45
5	0.25	51
6	0.5	53
7	0.5[a]	27
8	0.5[b]	37
9	1	57

Table 3.6 – Conversions of DHA employing $\mathbf{U^{Ph2phen}}$, [a] with 1 equiv. anthracene added at start of reaction; [b] in benzonitrile, PhCN; [c] by ^{1}H NMR spectroscopy. Reaction conditions: 3 hours of irradiation at 420 nm in CH_3CN (unless stated).

At loadings of $\mathbf{U^{Ph2phen}}$ above 1 mol%, precipitation of yellow solid was commonly observed, typically after fewer than 5 minutes. No precipitate was observed when $\mathbf{U^{Ph2phen}}$ was photolysed in CH_3CN in the absence of DHA substrate. Negative-ion ESI-MS and Raman spectroscopic analysis on this yellow solid are consistent with formation of a peroxo-bridged uranyl(VI) complex, with ions corresponding to $[(UO_2)_2(\mu\text{-}O_2)(NO_3)_3]^-$ (758.0274 Da) and $[(UO_2)_2(\mu\text{-}O_2)(NO_3)_3(Ph_2phen)]^-$ (1090.1711 Da). Bands in the Raman spectra at 838 and 849 cm^{-1} (Figure 3.12) both compare well to previously reported uranyl(VI) peroxo complexes (*e.g.* $[(UO_2(NO_3)(py)_2)_2(\mu\text{-}O_2)]\cdot py$[137] has a symmetric $\mu\text{-}O_2$ stretch at 860 cm^{-1}, alongside other reported uranyl-peroxo oligomers, which have Raman bands between 820-870 cm^{-1}).[138] Results from elemental analysis were inconsistent and are not reported.

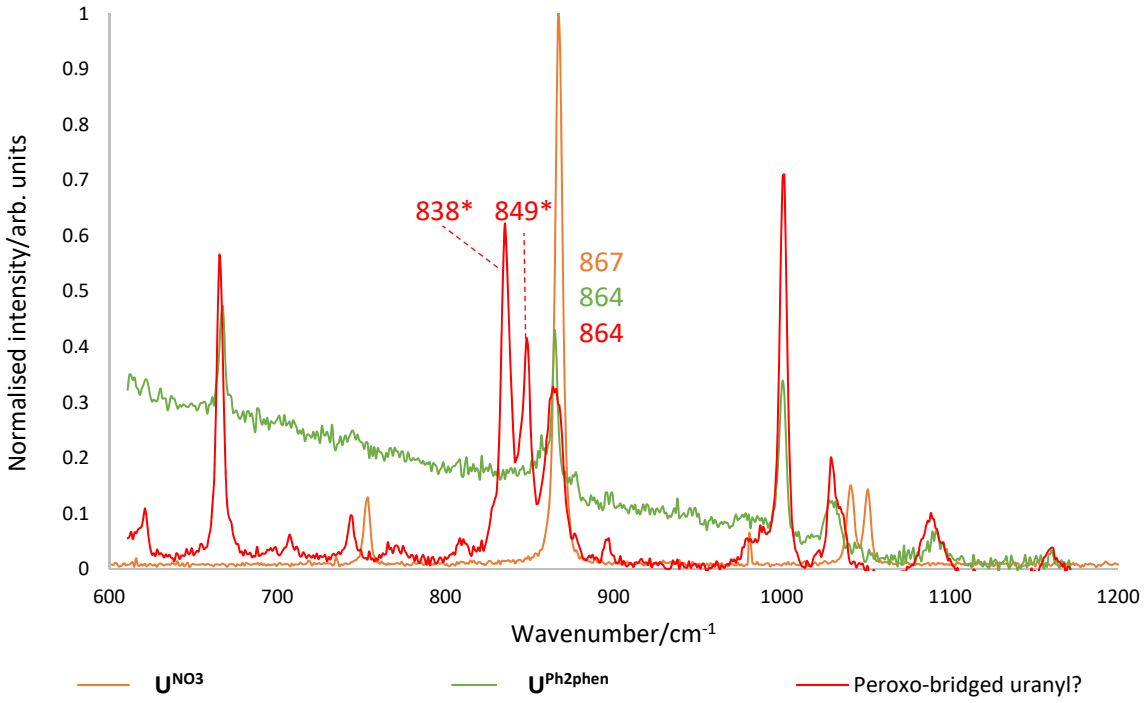

Figure 3.12 – Overlaid solid-state Raman spectra of $\mathbf{U^{NO3}}$ (ORANGE), and $\mathbf{U^{Ph2phen}}$ (GREEN) (600-1200 cm^{-1}), uranyl peroxo complex (RED), highlighting $\nu_{sym}(U{=}O)$ at 867 or 864 cm^{-1} and other peaks of interest. Peaks attributed to peroxo stretching frequencies are highlighted with an asterisk, *.

The interactions of the $*U^{VI}O_2^{2+}$ ion with dioxygen and water are not well understood for uranyl-mediated photocatalytic cycles in non-aqueous systems.[139] For example, uranium(IV) peroxide, $[U^{IV}(O_2)_2]$, is speculated to result from the aerobic chemical quenching of $[U^{VI}O_2(hfaa)_2(THF)]$ (**3.M**; hfaa = hexafluoroacetylacetonate) in heptane.[140] Although the isolation of dimeric peroxo-bridged uranyl(VI) complexes (resulting from irradiation under in aerobic conditions) has been reported, for example, $[(UO_2(NO_3)(ebpyrO))_2(\mu\text{-}O_2)]$ (**3.N**; ebpyrO = *N*,*N*'-ethylenebis(2-pyrrolidone)),[141] $[((UO_2)(Ph_3PO)_3)_2(\mu\text{-}O_2)][ReO_4]_2$ (**3.O**)[142] and $[(UO_2(2tpyr)_2)_2(\mu\text{-}O_2)]$ (**3.P**; 2tpyr = 2-thiopyrimidinate),[143] it is unclear whether water[137, 144] or oxygen[145-147] is the source of the peroxo ions in these complexes.

Here, it is suggested that oxygen or water (dissolved in CH_3CN) react with the $*U^{VI}O_2^{2+}$ group in $\mathbf{U^{Ph2phen}}$ to give O_2^{2-}, which then reacts further with two or more '$U^{VI}O_2$-Ph_2phen' motifs to give a peroxo-bridged uranyl(VI) dimer. No evidence for $\mathbf{U^{NO3}}$-peroxo complexes was observed by Raman spectroscopy from solutions containing $\mathbf{U^{NO3}}$. As the source of oxygen atoms for the speculated peroxo ligand remains unclear, further work is necessary to identify if water or oxygen is responsible, thereby identifying the necessary components for the catalytic cycle. This could be achieved by repeating the $\mathbf{U^{Ph2phen}}$ reaction with DHA in CH_3CN under anoxic or anhydrous (but oxygenated) conditions, and by analysing the resulting precipitates by ESI-MS and solid-state Raman spectroscopy. This, along with the likely effect of oxygen on the DHA/$U^{VI}O_2^{2+}$ photoreaction, is discussed in Section 3.3.5.

Returning to DHA consumption, the reaction of DHA with 0.5 mol% $\mathbf{U^{Ph2phen}}$ is mostly complete (> 95%) after 7 hours, compared with the reaction with 0.5 mol% $\mathbf{U^{NO3}}$, which plateaus at roughly 9 hours. The conversion profiles for both reactions are shown in Figure 3.13.

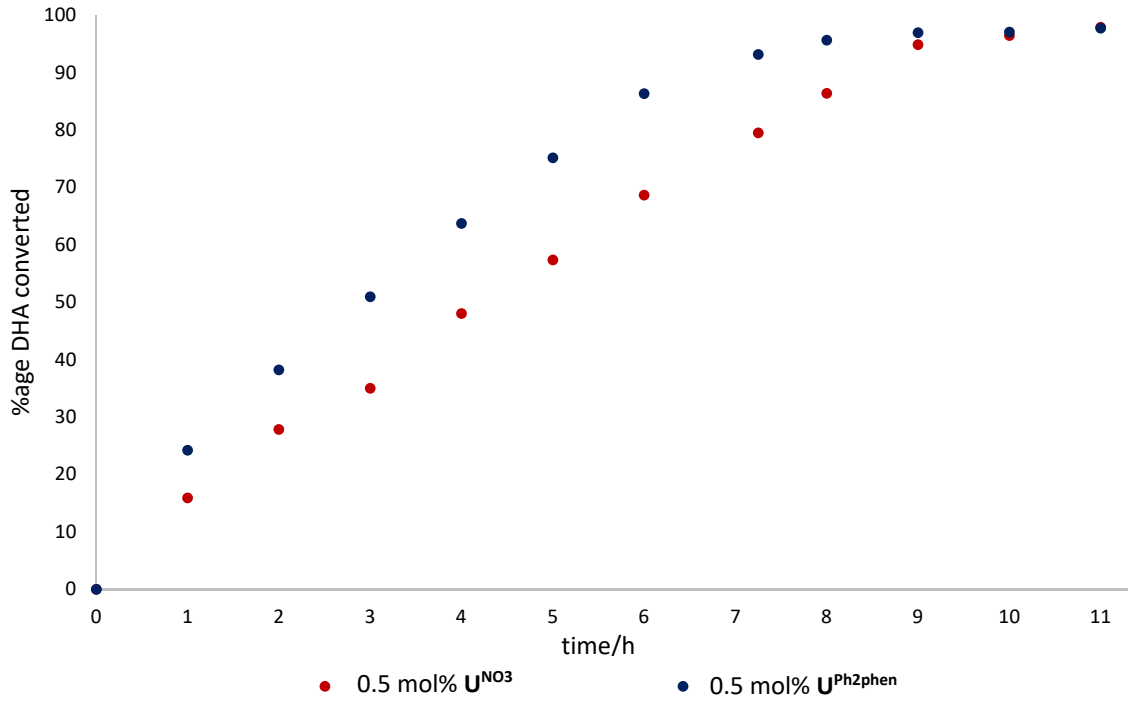

Figure 3.13 – Conversion profiles for DHA with 0.5 mol% loading of $\mathbf{U^{NO3}}$ or $\mathbf{U^{Ph2phen}}$ over 11 hours.

These data are consistent with conversions of DHA after 3 hours for $\mathbf{U^{NO3}}$ and $\mathbf{U^{Ph2phen}}$ reported earlier, (entry 5 in Table 3.5, 31%, and entry 6 in Table 3.6, 53%, respectively, compared to conversions of 35% and 51% for $\mathbf{U^{NO3}}$ and $\mathbf{U^{Ph2phen}}$ after 3 hours of irradiation in Figure 3.13). There is also a clear difference in DHA consumption between $\mathbf{U^{NO3}}$ and $\mathbf{U^{Ph2phen}}$, particularly for first 7 hours of the reactions, after which the conversion profiles plateau as DHA is mostly consumed and product photodegradation processes dominate; *e.g.* anthracene photo-oxidation.[148] ^{1}H NMR spectroscopic analysis on anthracene solutions in CH_3CN irradiated in the presence of 0.5 mol% $\mathbf{U^{NO3}}$ performed here show complete anthracene degradation after 1 hour of photolysis, with additional unidentified products becoming visible in the spectrum after *ca*. 1.5 hours of irradiation.

3.3.2 Effect of Added Anthracene

As anthracene, like other aromatic substrates, will be both an effective physical and chemical quencher of $^*U^{VI}O_2^{2+}$, investigations were undertaken so as to study the possible product inhibition of anthracene on the DHA/$U^{VI}O_2^{2+}$ photoreaction (Section 3.1.2). This was achieved by addition of a stoichiometric amount of anthracene to DHA, in CH_3CN and 0.5 mol% loadings of $\mathbf{U^{NO3}}$ and $\mathbf{U^{Ph2phen}}$.

DHA consumption after 3 hours of irradiation was then compared to the analogous reactions of 0.5 mol% $\mathbf{U^{NO3}}$ or $\mathbf{U^{Ph2phen}}$ without added anthracene, as monitored by ^{1}H NMR spectroscopy. The general reaction for DHA with $\mathbf{U^{NO3}}$ or $\mathbf{U^{Ph2phen}}$ with stoichiometric anthracene is given in Scheme 3.14, below.

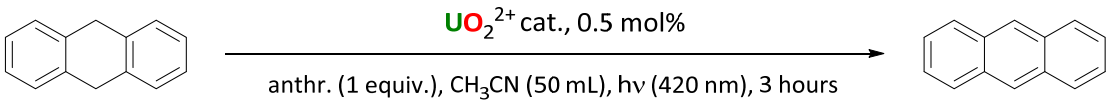

Scheme 3.14 – DHA oxidation in the presence of $\mathbf{U^{NO3}}$ or $\mathbf{U^{Ph2phen}}$ photocatalyst and added anthracene (= anthr.).

The conversion profiles for these four reactions are shown in Figure 3.14.

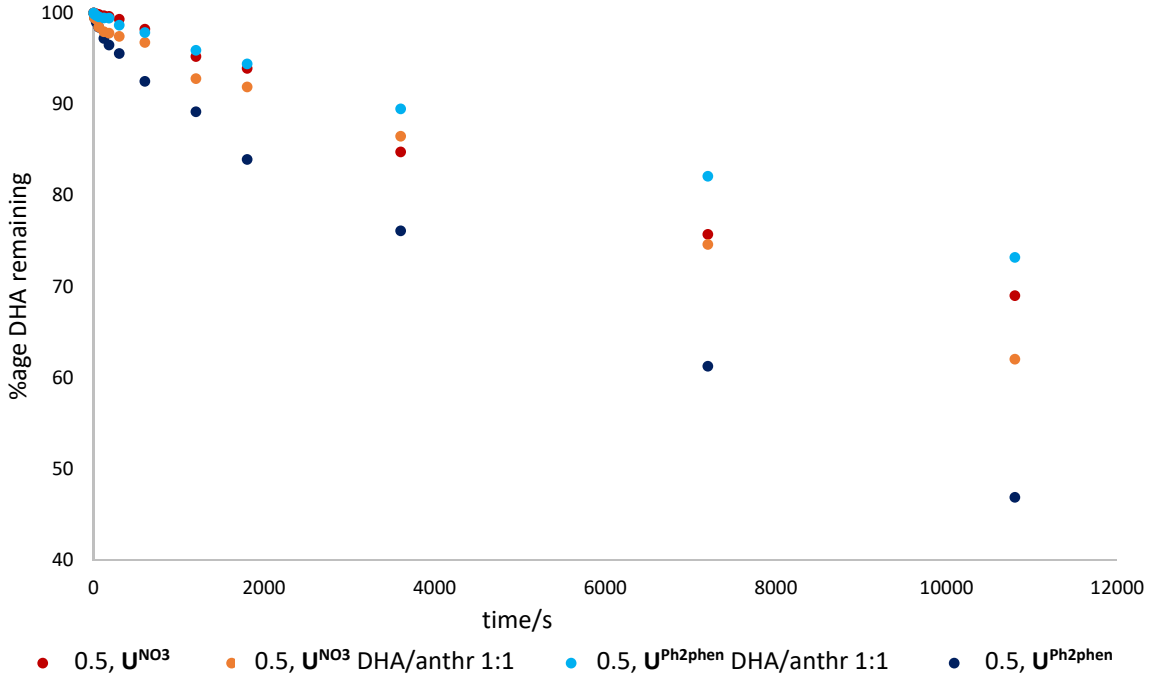

Figure 3.14 – Conversion profiles for DHA substrate with $\mathbf{U^{NO3}}$ or $\mathbf{U^{Ph2phen}}$, 0.5 mol% catalyst, with and without added stoichiometric anthracene, added at t = 0.

The addition of equimolar anthracene at the start of the reactions appears to have little influence on conversion of DHA where $\mathbf{U^{NO3}}$ is the catalyst, but upon switching to $\mathbf{U^{Ph2phen}}$, there is a clearly observable decrease in DHA conversion over time, as measured by ^{1}H NMR spectroscopy. This may be explained by competitive photon absorption between $\mathbf{U^{Ph2phen}}$ and anthracene (which both have absorption bands at *ca*. 360 nm; see Figure 2.12 for $\mathbf{U^{Ph2phen}}$ absorption spectrum) and λ_{max} for anthracene is 356 nm (this work)) at the tailing edge of the lamp spectral output (*ca.* 360–380 nm; Figure 5.1), reducing conversion when anthracene is present. This is not observed for $\mathbf{U^{NO3}}$ as there are no absorption bands at *ca*. 360 nm (Figure 2.12).

3.3.3 Effect of Solvent

To investigate the role of solvent in the reaction, two reactions using a 0.5 mol% loading of **U^{NO3}** and **U^{Ph2phen}** were undertaken using benzonitrile, PhCN, instead of CH_3CN, and DHA conversions after 3 hours compared to the analogous reactions in CH_3CN after monitoring by ^{1}H NMR spectroscopy. The general reaction for the reaction of oxidation of DHA using **U^{NO3}** or **U^{Ph2phen}** in PhCN is given in Scheme 3.15, below.

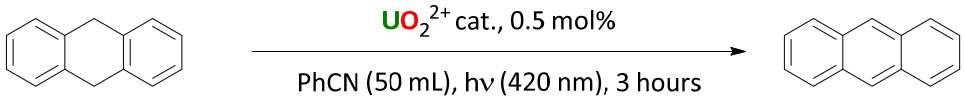

Scheme 3.15 – DHA oxidation in the presence of **U^{NO3}** or **U^{Ph2phen}** photocatalyst in benzonitrile, PhCN.

Like CH_3CN, PhCN is oxidatively inert (*cf*. non-reactivity of benzene, entry 3, Table 3.4 in Section 3.2.5) and optically transparent at 420 nm, the λ_{max} of the $U^{VI}O_2^{2+}$ ion. The conversion profiles for these reactions (DHA conversion in PhCN with **U^{NO3}** or **U^{Ph2phen}**) are given in Figure 3.15.

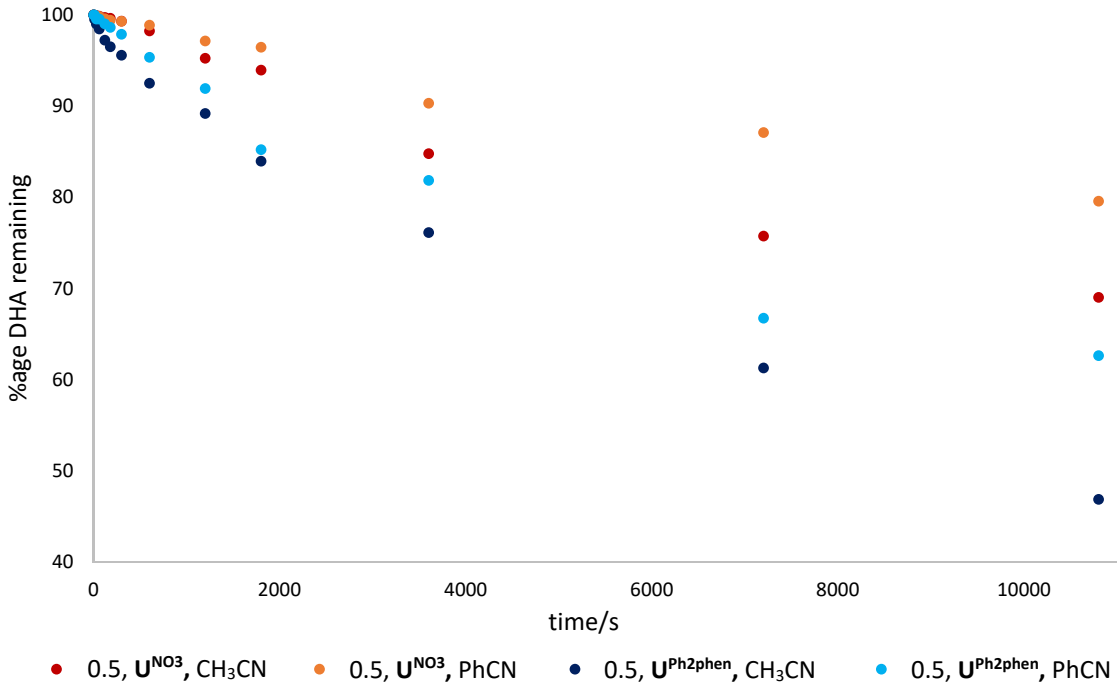

Figure 3.15 – DHA conversion profiles with **U^{NO3}**, or **U^{Ph2phen}**, 0.5 mol% loading, in CH_3CN or PhCN.

DHA conversion in PhCN solvent is roughly halved compared to the analogous reactions in CH_3CN, decreasing from 31 to 21% with **U^{NO3}** (entries 5 and 7, Table 3.5) and from 53 to 37% with **U^{Ph2phen}** (entries 6 and 8, Table 3.6). As was observed for the unsuccessful photocatalysis reactions of benzene with **U^{NO3}** or **U^{Ph2phen}** (entry 3, Table 3.4), it is speculated that switching from an aliphatic (-Me) to an aromatic (-Ph) group on the solvent nitrile increases non-radiative quenching of the $^*U^{VI}O_2^{2+}$ ion.[62]

Therefore, while benzonitrile is a possible alternative solvent if CH_3CN is unsuitable, substrate conversion will likely be inhibited by non-radiative quenching of the $*U^{VI}O_2^{2+}$ ion. Fluorescence spectroscopic (such as excited-state lifetime) measurements to investigate the effect of solvent on the $*U^{VI}O_2^{2+}$ ion are planned.

3.3.4 Effect of Water

Many of the substrate photoreactions described in Sections 3.12 and 3.13 take place in aqueous solution, and thus the role of water in the chemical quenching of the $*U^{VI}O_2^{2+}$ ion has been extensively studied in the literature; *e.g.* HAA of water generates hydroxyl radicals, which couple to form hydrogen peroxide and further secondary oxidation reactions.[15, 149] However, the role that water has on the photoreactivity of the uranyl(VI) ion in organic solutions is likely far more subtle, and is consequently generally poorly understood. It has however been reported that HAA of methanol with $\mathbf{U^{NO3}}$ gives either $^{\bullet}CH_2OH$ or $CH_3O^{\bullet}$ radicals in aqueous or anhydrous methanol, respectively.[150] Therefore to investigate the effect of water on the DHA/UO_2^{2+} photo-oxidation reaction in CH_3CN solvent, an excess (100 equiv., WRT $\mathbf{U^{NO3}}$) of water was added to a CH_3CN solution containing DHA and 5 mol% $\mathbf{U^{NO3}}$, and the solution irradiated at 420 nm for 3 hours, Scheme 3.16 and Figure 3.16.

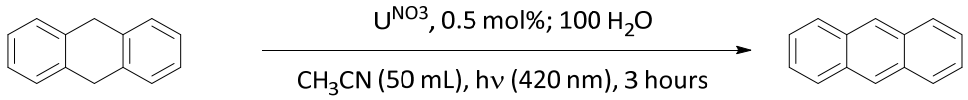

Scheme 3.16 – DHA oxidation in the presence of $\mathbf{U^{NO3}}$ and 100 equiv. (WRT $\mathbf{U^{NO3}}$) of H_2O.

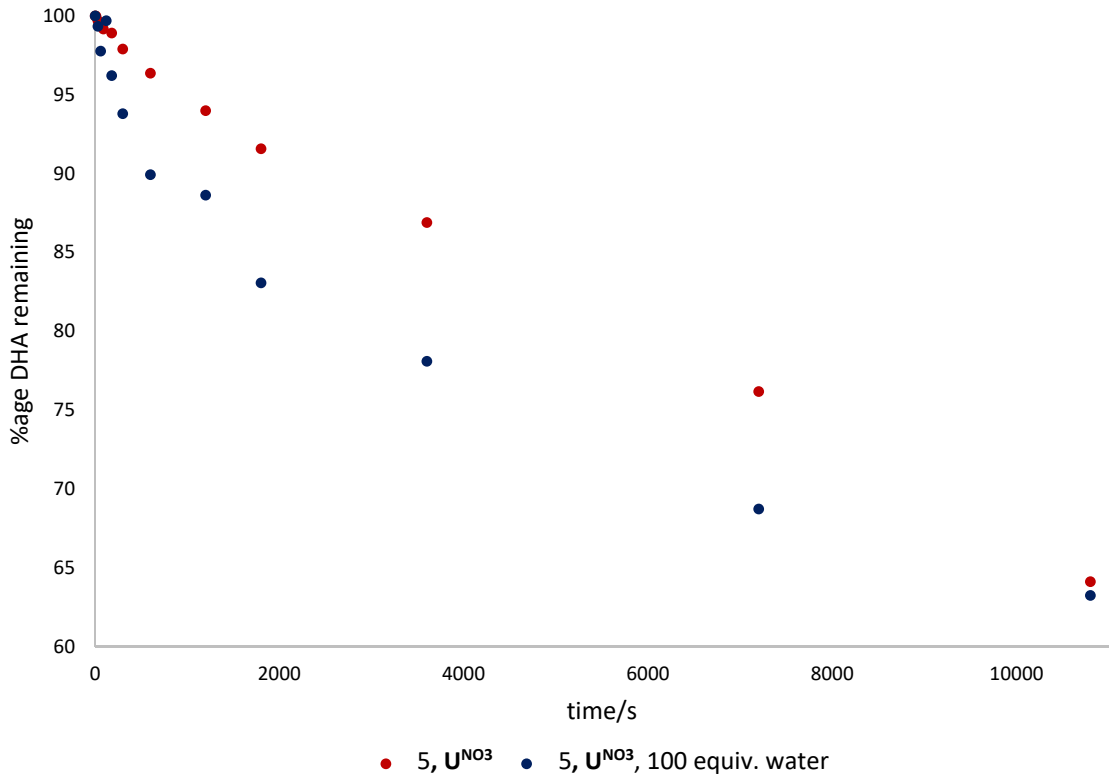

Figure 3.16 – Comparison of consumption of DHA against time using 5 mol% loading $\mathbf{U^{NO3}}$, and in the presence of 100 equiv. of water, WRT $\mathbf{U^{NO3}}$.

From this conversion profile there are two regions of interest; the first 30 minutes of the reactions, and the subsequent conversion. In this first 30 minutes, the reaction profile for the reaction containing the deliberately added water shows an increased rate of consumption of DHA compared to the reaction with no added water, with DHA conversions at 30 minutes (1800 seconds) of 17% (added water) and *ca*. 9% (no added water), respectively. The conversion of DHA is approximately equivalent at *ca*. 35% in the second portion of the reactions (after 3 hours, 10800 seconds) in both cases.

The speciation of the $U^{VI}O_2^{2+}$ ion in CH_3CN is known to be complex (*e.g.* $[U^{VI}O_2(NO_3)_2]\cdot 2CH_3CN$ by molar conductivity[151] or IR spectroscopy,[152, 153] or $[U^{VI}O_2(NO_3)_3]^-$ by EXAFS and DFT calculations)[154], raising the possibility of CH_3CN/H_2O adducts of uranyl (*e.g.* $[UO_2(NCMe)_x(OH_2)_{5-x}]$, where $x \leq 5$).[155] Water is also known to interact with simple oxyl[156] or alkyl radicals by forming complex H-bonding networks.[157] Overall, the effect of water on the uranyl/DHA reaction is not clear, and requires further investigation. A series of fluorescence quenching studies on $\mathbf{U^{NO3}}$ and $\mathbf{U^{Ph2phen}}$ in CH_3CN with increasing amounts of water are planned as part of ongoing work arising from this project, but will not be complete before submission of this thesis.

3.3.5 Effect of Oxygen

Reactions catalysed by photoactivated $U^{VI}O_2^{2+}$ ions are generally known to require oxygen[62, 68] to regenerate the intermediate $U^{V}O_2^{+}$ formed in the $U^{VI}O_2^{2+}$ catalytic cycle; several substrates (naphthalene[64] and chlorophenols[66] are specifically recorded as not reacting in its absence. A notable exception is that of alkane fluorination mediated by **U^{NO3}** under argon, where the fluorine source, NFSI (*N*-fluorobenzenesulfonimide, $(PhSO_2)_2NF$) was also the oxidant responsible for reoxidising the intermediate $U^{V}O_2^{+}$ ion back to $U^{VI}O_2^{2+}$, closing the catalytic cycle.[61] Therefore, in order to investigate the effect of oxygen on the DHA/$U^{VI}O_2^{2+}$ photoreaction, a reaction mixture containing DHA and 5 mol% **U^{NO3}** was irradiated (420 nm) in anoxic CH_3CN (50 mL, freeze-pump-thaw degassed three times) for three hours in a Teflon-tapped ampoule, Scheme 3.17, below.

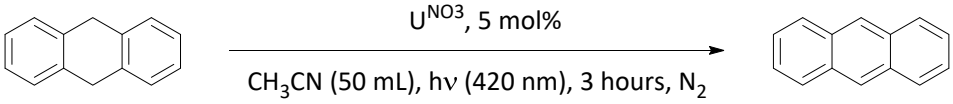

Scheme 3.17 – DHA oxidation in the presence of **U^{NO3}** photocatalyst in anoxic CH_3CN.

For the first 5 minutes of irradiation, a faint but permanent turbidity was observed, gradually turning the solution opaque after *ca.* 30 minutes. Elemental and ICP-MS analysis of this dark grey precipitate after 3 hours of irradiation (and after washing with toluene and hexanes to remove unreacted DHA) gave element percentages of 41.8% U, 46.3% C, 2.9% H and 1.3% N. These dark grey precipitates are insoluble in dry pyridine, toluene and hexanes, and upon standing in air for 48 hours, become yellow. Comparative IR spectra for this solid before and after exposure to air, along with the IR spectrum of uranium dioxide, $U^{IV}O_2$, are given in Figure 3.17. IR spectra were acquired as a Nujol mull between two KBr discs on ground powders.

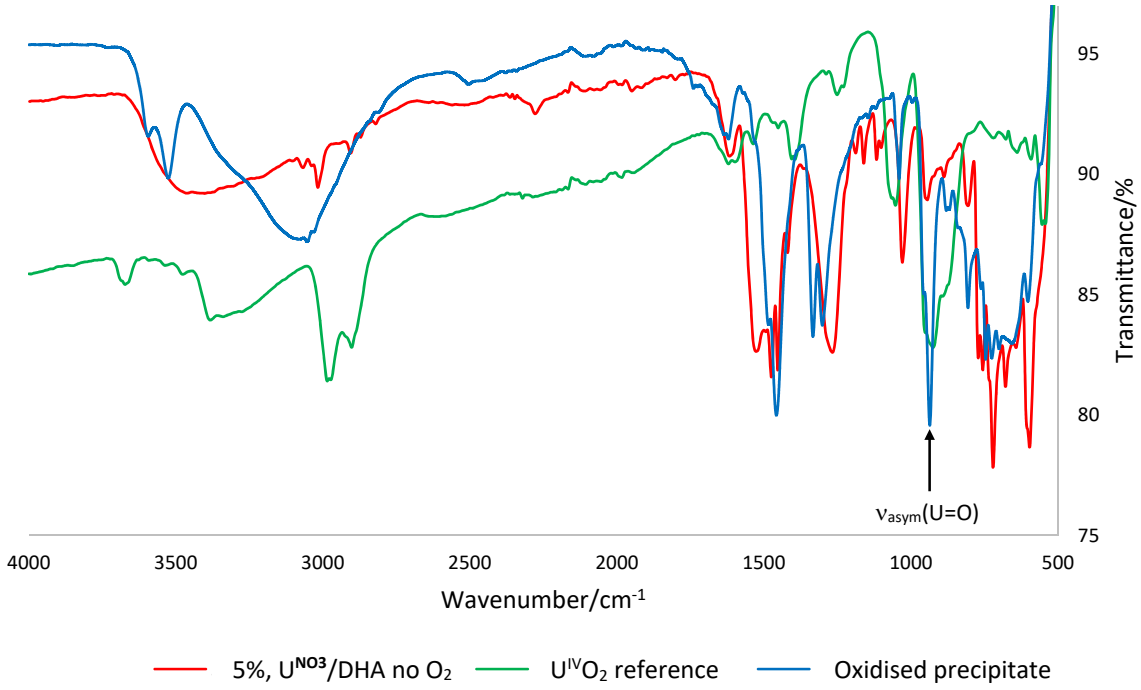

Figure 3.17 – ATR-IR spectra for reference $U^{IV}O_2$ (GREEN), precipitate from 5 mol% **U^{NO3}**/DHA photoreaction (RED), and oxidised precipitate (BLUE). The asymmetric uranyl stretching frequency, $\nu_{asym}(U{=}O)$, is highlighted.

Water and nitrate groups are present in both the anaerobic and oxidised precipitates (water; *ca*. 3100–3600 cm^{-1}, and nitrates; 1268 cm^{-1} (anaerobic precipitate) or 1300 and 1335 cm^{-1} (oxidised precipitate), respectively). There are no clear similarities between the spectra of either anaerobic or oxidised precipitates and $U^{IV}O_2$, suggesting that in agreement with ICP-MS and elemental analysis data, $U^{IV}O_2$ is not produced.

It is speculated that the anaerobic precipitate is a U^{V}- or U^{IV}-complex with an organic ligand, that is susceptible to oxidation on exposure to air, resulting in a $U^{VI}O_2^{2+}$-containing product judging from the reappearance of $\nu_{asym}(U{=}O)$ at 937 cm^{-1} in the IR spectrum of oxidised precipitate (which is not present for the anaerobic precipitate). The colour change on exposure to air from grey (U^{IV} and U^{V} compounds are usually grey-black powdery solids, *cf*. U_3O_8) to yellow also suggests the precipitate is oxidised from a lower oxidation state of uranium to $U^{VI}O_2^{2+}$, compounds of which are yellow (*cf*. **U^{NO3}**). Although the photolysis **U^{NO3}**/oxalic acid solutions produces uranium(IV) dioxide, $U^{IV}O_2$,[158] no UO_2 was observed spectroscopically here. Similar reactivity has been observed previously in the photocatalytic degradation of azulene with **U^{NO3}** in anaerobic methanol, where IR spectroscopy and elemental analysis indicated the formation of U^{IV}/U^{V}-complexes with a significant organic component (absorptions in the IR spectra of the solids at *ca*. 950 cm^{-1} (*cf.* $\nu_{asym}(U{=}O)$) and elemental analysis with high C (51–79%) and H (2–4%) but low N (< 1.4%) content, along with uranium (28.7 ± 2.0%)). The authors postulated a [U^{V}---azulene] adduct (Reaction ii), Scheme 3.3) based on these data.[65]

Further evidence for the need for oxygen in **U^{NO3}** regeneration was obtained by comparing DHA conversion for this anaerobic system with the analogous aerobic reaction. Here, an average conversion of *ca*. 11% was obtained after two runs, compared to a conversion of 37% (entries 10 and 11, Table 3.5) for the aerobic reaction, suggesting that the anaerobic reaction is stoichiometric and that consumption of $U^{VI}O_2^{2+}$ is irreversible. The only product by ^{1}H NMR spectroscopy is anthracene. The mechanism of uranium regeneration (*e.g.* of the $U^{V}O_2^{+}$ intermediate) is complex (Section 3.3.1) but is known to involve a key step outlined in Scheme 3.18, below.[39]

$$2\,[U^{V}O_2]^{+} + O_2 + 2\,H^{+} \longrightarrow 2\,[U^{VI}O_2]^{+} + H_2O_2$$

Scheme 3.18 – Oxidation of $U^{V}O_2^{+}$ under aerobic conditions, in 5 mM $HClO_4$, 0.02 mM $U^{V}O_2^{+}$.[39]

To further investigate the role of oxygen on the DHA/**U^{NO3}** reaction, uncovering identity of any solid precipitates is crucial. Due to experimental limitations at the University of Edinburgh it was unfortunately not possible to characterise these solids further, although Raman spectroscopy (to supplement detection of $U^{x}O_2^{n+}$, where x = 5, n = 1 or x = 6, n = 2) or EPR spectroscopy (for the detection of radical intermediates) could be used for further investigation. EPR spectroscopy may prove especially helpful, as it was used to detect the intermediate U^{V}-azulene complex(es) in the azulene/**U^{NO3}** photoreaction.[65] Here, it may be possible to detect intermediate radical cations, such as the anthracene radical cation.[159] Discussions are underway with the EPSRC National Service for EPR spectroscopy at the University of Manchester, UK for EPR spectroscopic characterisation on this and other (Section 2.9) reactions, but will not be complete before submission of this thesis.

3.3.6 Time-resolved UV-Vis Spectroscopy on DHA Conversion

As discussed in Section 3.3.1, DHA is speculated to have a non-photochemical decomposition pathway to anthracene in the presence of an excess of nitrate (*cf*. **U^{NO3}** loadings >100 mol%). However, the role of this decomposition pathway in competing for the uranyl-mediated photolysis pathway, particularly on the initial portion of the reaction, was not well understood, and so in order to investigate the initial portions of the DHA/$U^{VI}O_2^{2+}$ photoreactions more closely, single-wavelength monitoring of these reactions in the absence of light by UV-vis spectroscopy was undertaken. Single-wavelength monitoring by UV-vis spectroscopy can provide much more detail about the first few seconds of a reaction in comparison to monitoring a reaction by ^{1}H NMR spectroscopy.[160]

Given the spectral overlap of λ_{max} for DHA and **U^{NO3}** (both absorb strongly *ca*. < 300 nm), the production of anthracene was monitored by UV-vis spectroscopy instead. Anthracene has a diagnostic multi-band electronic absorption band *ca*. 360 nm, with ε_{356} *ca*. 7250 $M^{-1}cm^{-1}$, which is separate from

other absorption bands, measured here in CH_3CN. These values compare well with electronic absorption data of anthracene measured in cyclohexane, λ_{max} = 356 nm, ε_{356} = 9535 $M^{-1}cm^{-1}$.[161]

Figure 3.18 below shows the production of anthracene before and during irradiation, as monitored by UV-vis spectroscopy. Briefly, 10 mM of DHA and x mol% of $\mathbf{U^{NO3}}$ (x = 1, 2, 5, 10, 25 and 50, corresponding to 0.1–5 mM of $\mathbf{U^{NO3}}$) were combined in CH_3CN (3 mL), and samples measured in the dark, or after irradiation of selected durations.

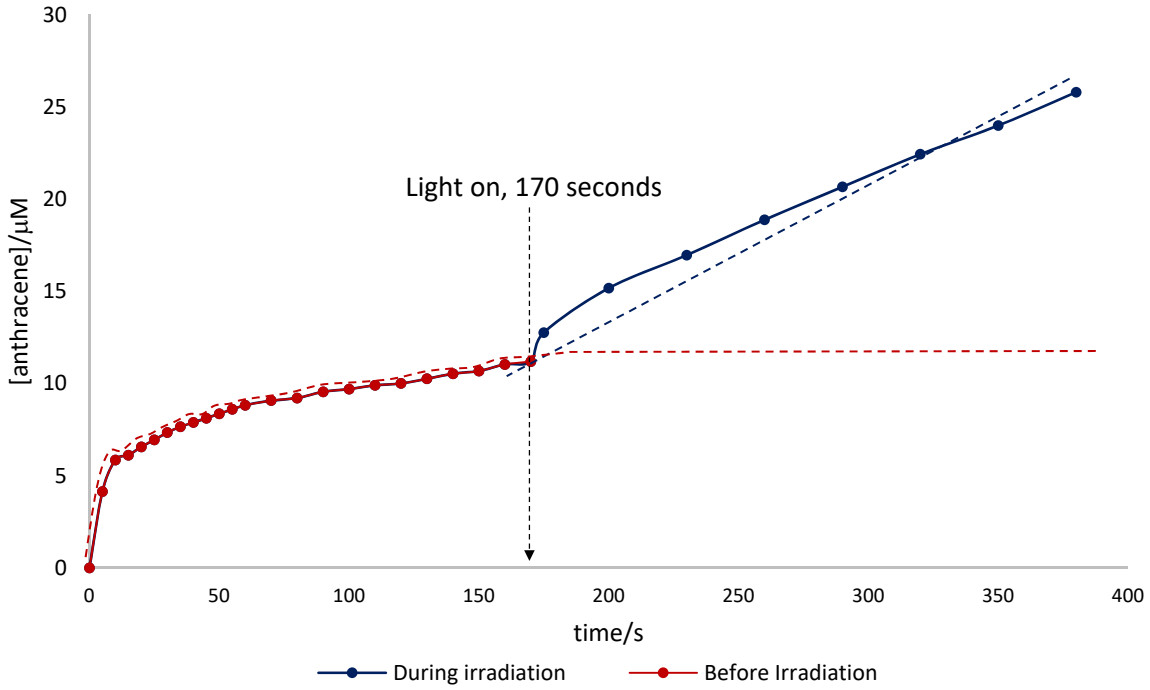

Figure 3.18 – Anthracene production over time measured by UV-vis spectroscopy ($[DHA]_0$ = 10 mM; $\mathbf{U^{NO3}}$ = 5 mol% loading, 0.5 mM). The overlaid dashed lines are extrapolations of the portions of the reaction before (----) and during (----) irradiation at 170 seconds (----).

It is clear that there is a non-photochemical pathway for the formation of anthracene, which appears to plateau after approximately three minutes in the absence of light. Subsequent irradiation of the reaction then causes the expected uranyl-mediated anthracene production pathway to occur. Unlike for the reactions employing > 100 mol% $\mathbf{U^{NO3}}$ (Section 3.31) it is speculated that this pathway is not nitrate-mediated; only 12 µM of anthracene has been produced when the non-photochemical reaction described above plateaus. Given a nitrate concentration in this reaction of 0.124 mM (5 mol% of 10 mM is 0.5 mM, and the two NO_3^- groups in $\mathbf{U^{NO3}}$ comprise 24.7% of the molecular weight of $\mathbf{U^{NO3}}$, equating to a nitrate concentration of 0.124 mM), if this thermal reaction were NO_3^- mediated, considerably more DHA should converted to anthracene before the reaction plateaus. There was no

anthracene produced in the dark in a saturated CH_3CN solution of KNO_3, or only DHA in CH_3CN solution (*e.g.* with no $\mathbf{U^{NO3}}$). This suggests this pathway requires $\mathbf{U^{NO3}}$ catalyst to be present.

The amount of anthracene converted by this non-photochemical pathway is proportional to $\mathbf{U^{NO3}}$ concentration, suggesting a non-zero order process WRT the active species. This process occurs with a rate of *ca*. 4.4 x 10^{-3} s^{-1}, obtained by plotting the initial rates of anthracene production in the dark at the various $\mathbf{U^{NO3}}$ concentrations, against these $\mathbf{U^{NO3}}$ concentrations; Figure 3.19, below.

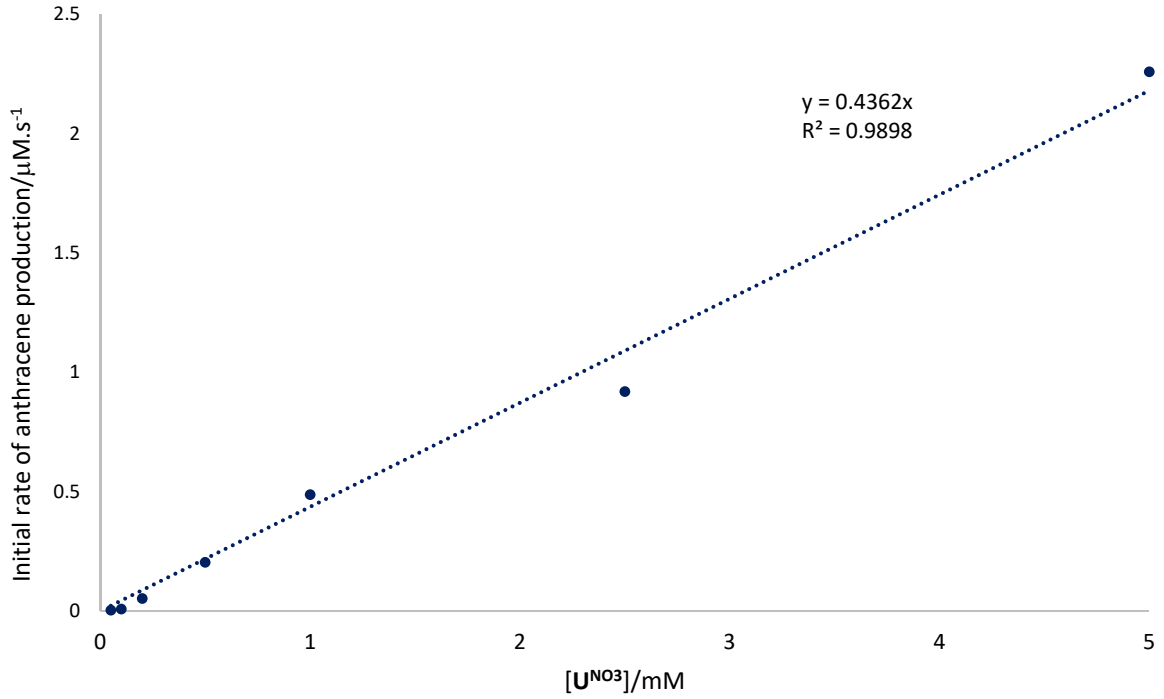

Figure 3.19 – Initial rates for anthracene production against variable concentrations of $\mathbf{U^{NO3}}$ (1, 2, 5, 10, 25 and 50 mol%, corresponding to 0.1–5 mM of $\mathbf{U^{NO3}}$) under non-photochemical conditions. Units of the gradient are ($\mu M.s^{-1}$)/mM.

The nature of the species responsible for this process is currently unclear, with nitrate, oxygen and solvent-mediated processes considered unlikely given the absence of analogous reactivity in the absence of $\mathbf{U^{NO3}}$. Neither thermal processes involving $U^{VI}O_2^{2+}$ (which is known to occur in thermal charge-transfer complexes of $U^{VI}O_2^{2+}$ with alcohols, sulfides, *etc*., producing U^{V} and substrate radicals)[3] nor the presence of trace contamination in the $\mathbf{U^{NO3}}$ catalyst or DHA substrate samples can be satisfactorily ruled out. However, the effect of this pathway *is* insignificant (< 2% DHA conversion with 50 mol% $\mathbf{U^{NO3}}$), and is therefore unlikely to affect the photocatalytic pathways for anthracene production (*cf.* DHA degradation) where $\mathbf{U^{NO3}}$ is the photocatalyst.

3.3.7 Conversion of DHA with Other Uranyl Photocatalysts

As outlined in Section 3.1.3 different uranyl species have varying photochemical properties (*e.g.* excited state lifetimes of $[UO_2(OH_2)_5]^{2+}$ (**3.A**) are 0.9 ± 0.3 μs, compared with 35 ± 5 μs for

$[UO_2(CO_3)(OH_2)_3]$ (**3.D**) in the presence of carbonate; Table 3.1). Several reports also highlight the reduced photocatalytic effectiveness of the uranyl ion in the presence of acetate ions compared to nitrate, for example, in the chemical quenching of isopropanol,[76] or fluorination of alkanes.[61] Therefore, to determine the effect of varying the counterions on the DHA/UO_2^{2+} photoreaction, the action of uranyl sulfate ($[UO_2(SO_4)]$, $\mathbf{U^{SO4}}$) and uranyl acetate ($[UO_2(OAc)_2]\cdot 2H_2O$, ($\mathbf{U^{OAc}}$) were investigated on DHA conversion analysed by ^{1}H NMR spectroscopy. The reaction was also performed with $\mathbf{U^{mal}}$ (neutral amide ligand; $[UO_2(NO_3)_2(mal)]$, Section 2.4.1). The consumption of DHA using $\mathbf{U^{SO4}}$, $\mathbf{U^{OAc}}$ or $\mathbf{U^{mal}}$ is given in Table 3.7. Comparative conversions for $\mathbf{U^{NO3}}$ and $\mathbf{U^{Ph2phen}}$ are also given.

Catalyst	DHA consumption[a]/%
$\mathbf{U^{SO4}}$	< 1%[b]
$\mathbf{U^{OAc}}$	*Ca*. 10%[b]
$\mathbf{U^{mal}}$	41%[c]
$\mathbf{U^{NO3}}$	34%[d]
$\mathbf{U^{Ph2phen}}$	57%[d]

Table 3.7 – Consumption of DHA with $\mathbf{U^{SO4}}$, $\mathbf{U^{OAc}}$ or $\mathbf{U^{mal}}$ as photocatalyst, compared to $\mathbf{U^{NO3}}$ and $\mathbf{U^{Ph2phen}}$. [a] Conversion measured by ^{1}H NMR spectroscopy; [b] 10 mol% in 2 mL CD_3CN at 420 nm for 20 hours; [c] 10 mol% in 5 mL CD_3CN at 420 nm for 16 hours; [d] 10 mol% ($\mathbf{U^{NO3}}$) or 1 mol% ($\mathbf{U^{Ph2phen}}$) in 50 mL CH_3CN at 420 nm for 3 hours.

Owing to its insolubility in CH_3CN, $\mathbf{U^{SO4}}$ was found to be ineffective for DHA photo-oxidation, giving < 1% conversion when the filtered product solution was analysed by ^{1}H NMR spectroscopy. DHA conversion with $\mathbf{U^{OAc}}$ (*ca*. 10%) was inferior to $\mathbf{U^{NO3}}$, which is consistently *ca*. 30–40% under analogous conditions. This is presumably related to the degradation of the carboxylate groups in $\mathbf{U^{OAc}}$ under irradiation, which in $[U^{VI}O_2(HCO_2)_2]$ (uranyl(VI) formate) is known to result in U^V–containing products and CO_2.[162] Conversion of DHA with $\mathbf{U^{mal}}$ is appreciable to $\mathbf{U^{NO3}}$ at 41%, suggesting that in line with the electronic spectroscopy (Figures 2.11–2.14, Section 2.2.2 for $\mathbf{U^{NO3}}$ and Figure 2.30, Section 2.4.1 for $\mathbf{U^{mal}}$), the photochemical reactivity of $\mathbf{U^{mal}}$ is unremarkable and comparable to that of $\mathbf{U^{NO3}}$.

3.4 Photoreactivity of Xanthene with the Uranyl Ion

3.4.1 Bulk-scale Reactions of Xanthene

Similarly to DHA, xanthene is a widely studied substrate for C-H bond oxidation studies given its appreciable C-H bond strength and acidity to DHA (ΔE_{diss}(C-H) ~ 316 kJmol^{-1},[163] pK_a = 30 in DMSO).[117] Unlike DHA, however, xanthene is particularly useful for studying the relative ratios of different products formed from C-H bond oxidation at its bridging CH_2 group, rather than aromatisation in the case of DHA,[164] as xanthene is capable of forming alcohols (xanthanol), ketones (xanthone), hydroperoxides (*e.g.* 9-hydroperoxy-xanthene) and peroxides (*e.g.* bis-(9-xanthenyl) peroxide) upon

oxidation. These products are depicted in Figure 3.20. All these products possess characteristic ^{1}H NMR resonances, making it convenient to probe xanthene photochemical reactions spectroscopically.

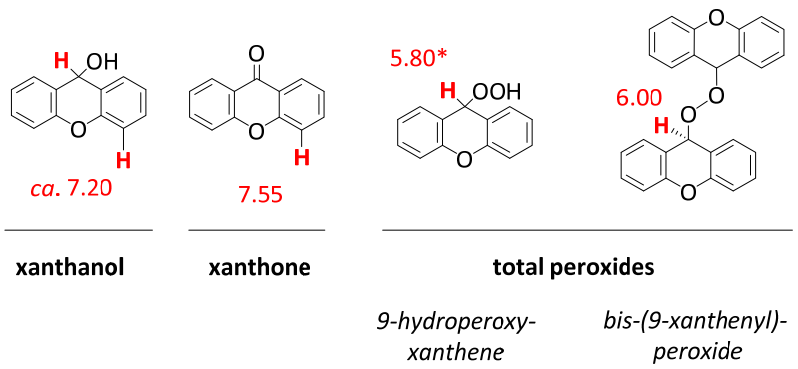

Figure 3.20 – Possible products of xanthene oxidation, grouped into alcohol (xanthanol), ketone (xanthone) and total peroxides (*e.g.* 9-hydroperoxy-xanthene and bis-(9-xanthenyl) peroxide). The numbers in red next to the highlighted hydrogen atoms are the resonances of these protons in ppm; for xanthanol and xanthone, in CD_3CN, and for the (hydro)peroxides, in $CDCl_3$; * data from the 9-xanthenyl-*tert*-butylperoxide analogue.[165]

The photocatalytic oxidation of xanthene with $\mathbf{U}^{\mathbf{Ph2phen}}$ and $\mathbf{U}^{\mathbf{NO3}}$ was investigated, using 2.5 mmol of xanthene in 50 mL of CH_3CN. Catalyst loadings of 0.5 (both $\mathbf{U}^{\mathbf{NO3}}$ and $\mathbf{U}^{\mathbf{Ph2phen}}$), or 5 ($\mathbf{U}^{\mathbf{Ph2phen}}$) and 10 ($\mathbf{U}^{\mathbf{NO3}}$) mol% were used, giving four different reactions which were irradiated at 420 nm for 9 hours. Progress was monitored by ^{1}H NMR spectroscopy. These profiles are given in Figures 3.21 and 3.22, with a general reaction scheme for photo-oxidation of xanthene with $\mathbf{U}^{\mathbf{NO3}}$ or $\mathbf{U}^{\mathbf{Ph2phen}}$ photocatalyst given in Scheme 3.19, below.

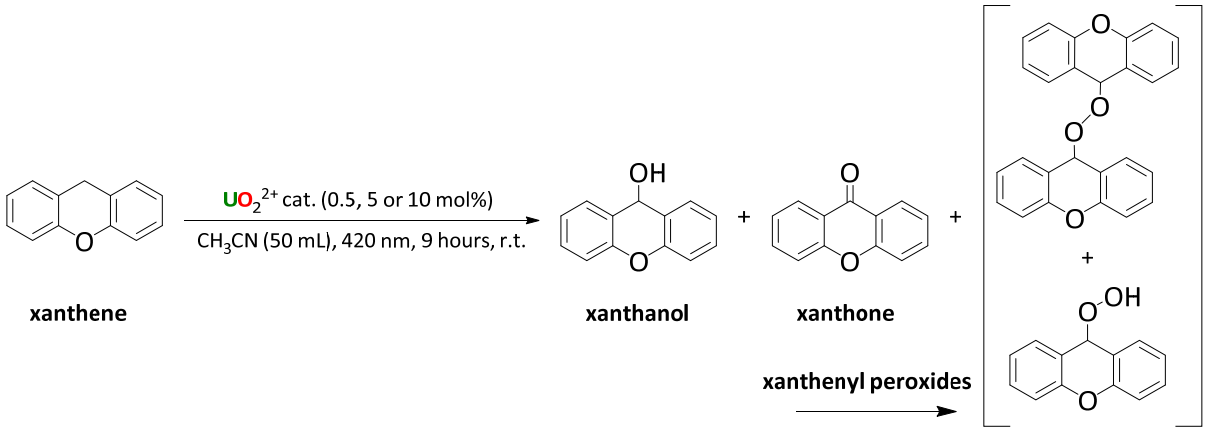

Scheme 3.19 – General reaction scheme for the photo-oxidation of xanthene using 0.5 mol % $\mathbf{U}^{\mathbf{NO3}}$ or $\mathbf{U}^{\mathbf{Ph2phen}}$, 5 mol% $\mathbf{U}^{\mathbf{Ph2phen}}$, or 10 mol% $\mathbf{U}^{\mathbf{NO3}}$.

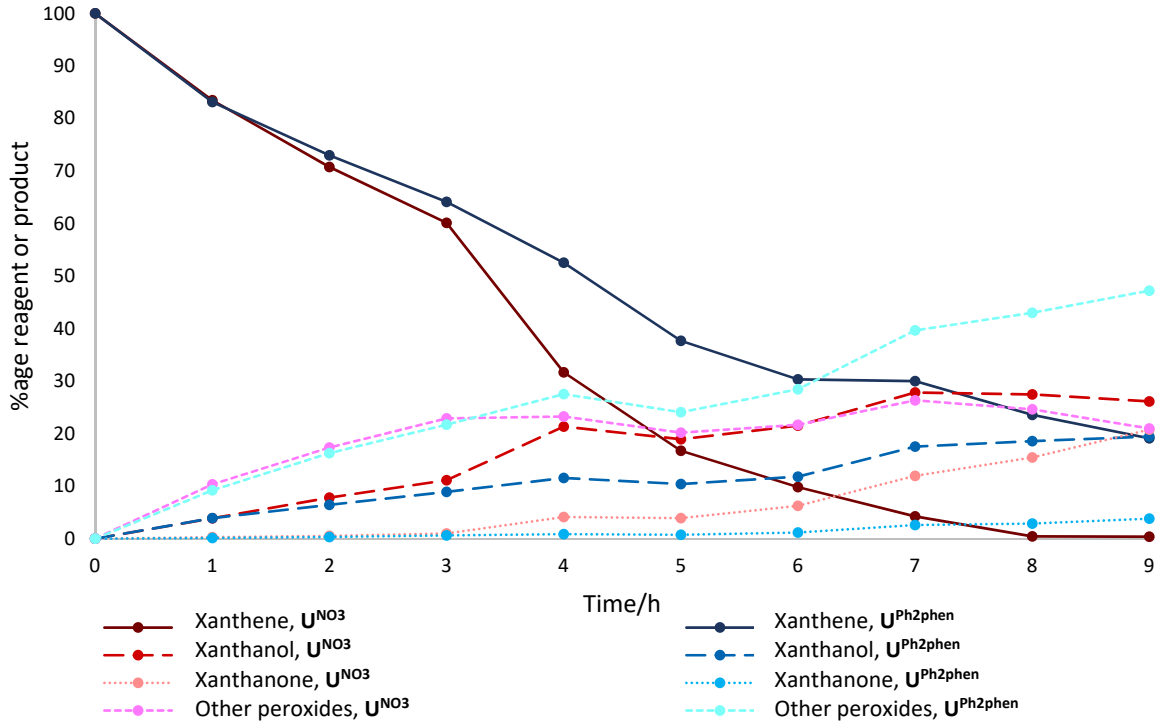

Figure 3.21 – Conversion profiles for xanthene under photocatalytic conditions over 9 hours with $\mathbf{U}^{NO3}$ (RED lines) or $\mathbf{U}^{Ph2phen}$ (BLUE lines) with 0.5 mol% loading catalyst, in CH_3CN.

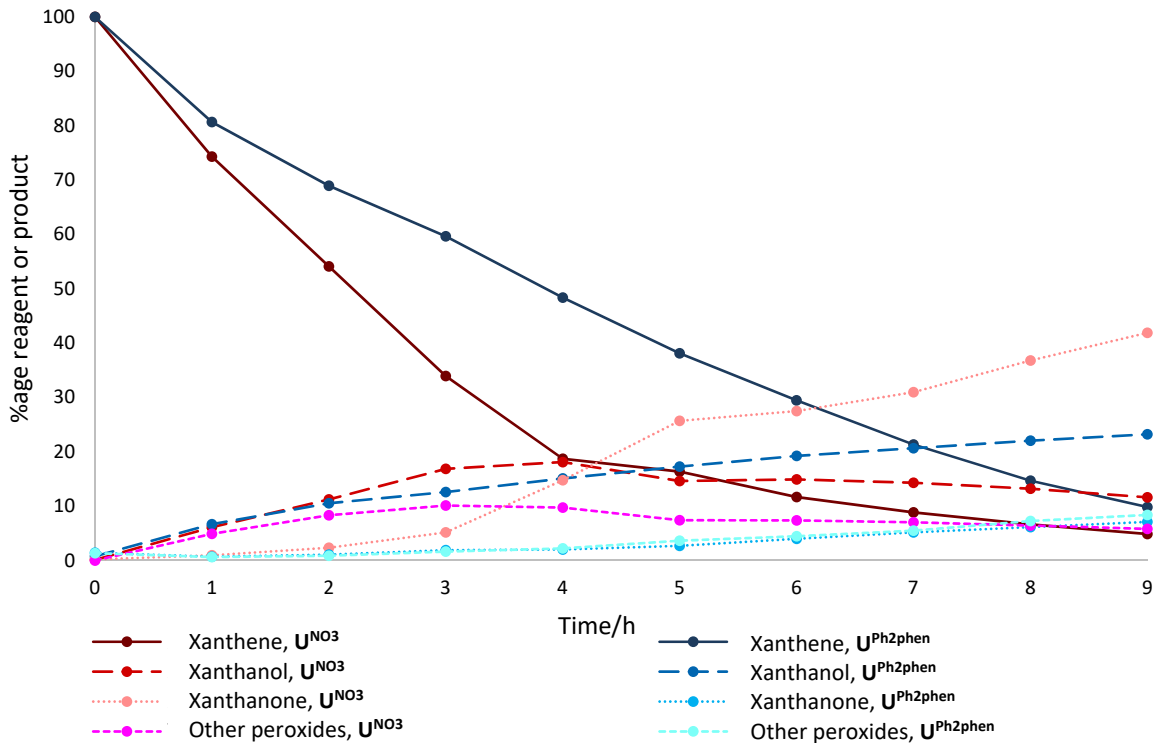

Figure 3.22 – Conversion profiles for xanthene under photocatalytic conditions over 9 hours with $\mathbf{U}^{NO3}$ (10 mol%; RED lines) or $\mathbf{U}^{Ph2phen}$ (5 mol%; BLUE lines) with 0. 5 mol% loading catalyst, in CH_3CN.

	Xanthene conversion and product distribution after 9 hours with … as catalyst (loading, mol%)			
Substrate	**U^{NO3} (0.5%)**	**U^{NO3} (10%)**	**$U^{Ph2phen}$ (0.5%)**	**$U^{Ph2phen}$ (5%)**
Xanthene	> 99%	95%	81%	90%
Xanthanol	26%	12%	19%	23%
Xanthone	20%	42%	4%	7%
Total peroxides	21%	6%	47%	8%
Unidentified products	33%	35%	11%	52%

Table 3.8 – Xanthene conversion and product distribution after 9 hours of photolysis with **U^{NO3}** (0.5 mol% or 10 mol%) or **$U^{Ph2phen}$** (0.5 mol% or 5 mol%) catalysts.

These data show that **U^{NO3}** and **$U^{Ph2phen}$** are both effective photocatalysts for the degradation of xanthene (Table 3.8), with conversions above 80% after 9 hours of photolysis in all cases. However, unlike the photoreactions involving diphenylmethane, triphenylmethane or isochroman (Sections 3.5.2 and 3.5.3), **U^{NO3}** shows better conversion than **$U^{Ph2phen}$**, particularly at lower loadings (*e.g.* > 99% for 0.5 mol% **U^{NO3}**, 81% for 0.5 mol% **$U^{Ph2phen}$**). The main difference between the two catalysts appears to be product distribution, with xanthone being favoured when **U^{NO3}** is the photocatalyst, particularly at the higher **U^{NO3}** loading (20% at 0.5 mol%, 42% at 10 mol% of **U^{NO3}**). Lower loadings of either **U^{NO3}** or **$U^{Ph2phen}$** catalyst favour peroxide formation, particularly with **$U^{Ph2phen}$** (21% with 0.5 mol% **U^{NO3}** or 47% with 0.5 mol% **$U^{Ph2phen}$**, compared to < 10% at 10 mol% **U^{NO3}** or 5 mol% **$U^{Ph2phen}$**). The lower production of peroxides at higher catalyst loadings is presumably related to their increased consumption, as higher loadings more quickly convert the peroxides to the product ketones. This also explains why xanthone production is higher at higher catalyst loadings, as higher loadings of **U^{NO3}** or **$U^{Ph2phen}$** increase the rate at which the intermediate peroxides are converted to the product xanthone.

In all cases there is one or more unidentified product(s), the ratio of which varies between **U^{NO3}** (*ca.* 34% for both 0.5 mol% and 10 mol%) and **$U^{Ph2phen}$** (11% with 0.5 mol% loading, or 52% with 5 mol% catalyst loading). The identity of this (or these) species is not clear. No precipitates were observed (except for the xanthene photoreaction with 5 mol% **$U^{Ph2phen}$**) and so these unidentified products remain in solution, meaning these products should be detectable by ^{1}H NMR spectroscopy. However, no evidence of resonances consistent with either bixanthene or acetonitrile-coupled xanthene (*e.g.* (9-xanthenyl)acetonitrile) was observed by ^{1}H NMR spectroscopy (4.37[166] and 4.31 ppm[167] respectively, both in $CDCl_3$).

3.4.2 Effect of Deuteration on Xanthene Consumption

In order to investigate the rate-determining step of the photo-oxidation of xanthene more fully (and, therefore, comparable benzylic substrates), photoreactions involving deuterated xanthene were undertaken with 0.5 mol% $\mathbf{U^{NO3}}$ in either 10 mL of either CH_3CN or CD_3CN, 420 nm. These reaction profiles are shown in Figure 3.23, alongside selected conversion data, Table 3.9.

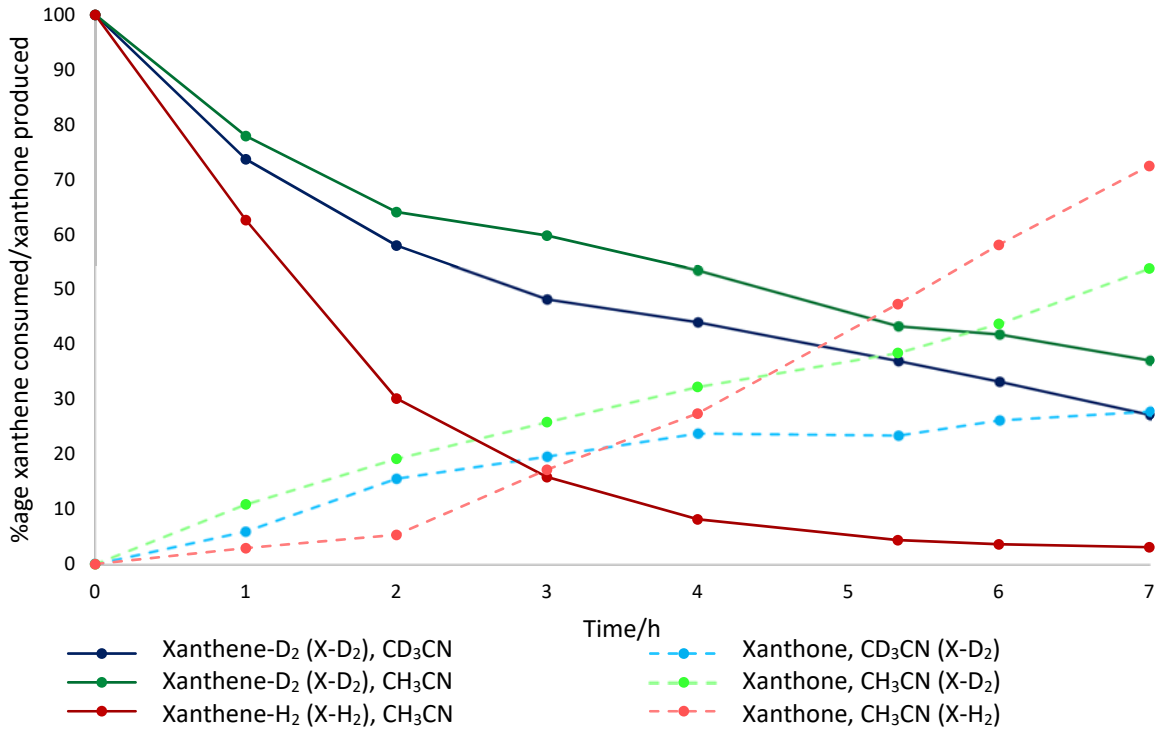

Figure 3.23 – Conversion profiles for xanthene-H_2 or xanthene-D_2 in CH_3CN or CD_3CN (10 mL) with 0.5 mol% $\mathbf{U^{NO3}}$ over 7 hours of irradiation in CH_3CN. BLUE lines correspond to xanthene-D_2 in CD_3CN, GREEN lines to xanthene-D_2 in CH_3CN, and RED lines to xanthene-H_2 in CH_3CN.

Substrate and solvent	Xanthene consumed/%	Xanthone produced/%
Xanthene-D_2, CD_3CN	73	27
Xanthene-D_2, CH_3CN	63	53
Xanthene-H_2, CH_3CN	97	72

Table 3.9 – Xanthene conversion/xanthone production after 7 hours of photolysis with 0.5 mol% $\mathbf{U^{NO3}}$ in CH_3CN or CD_3CN.

As the zero point energy for a C-H bond is higher than a C-D bond, the energy barrier required for dissociation (*e.g.* bond energy) is lower, and C-H bonds are thus easier to break than C-D bonds; that is, where reaction rates for conversion of C-D substituted substrates are slower than the C-H analogue, this is evidence that a C-H/-D bond is cleaved, and that this occurs in the rate-determining step.

Here, there is a lower conversion for xanthene-D_2 (in either CD_3CN, 73% conversion; or CH_3CN, 63% conversion) than for xanthene-H_2 (97% conversion) after 7 hours of photolysis (Table 3.9). As xanthene

conversion reflects reaction rate, it is likely that C-H bond dissociation by HAA is the key, rate-determining step in the mechanism of the photo-degradation of xanthene using **U^{NO3}** as a photocatalyst. This information allows a tentative mechanism for the uranyl-mediated photo-oxidation of xanthene to be proposed (Scheme 3.20).

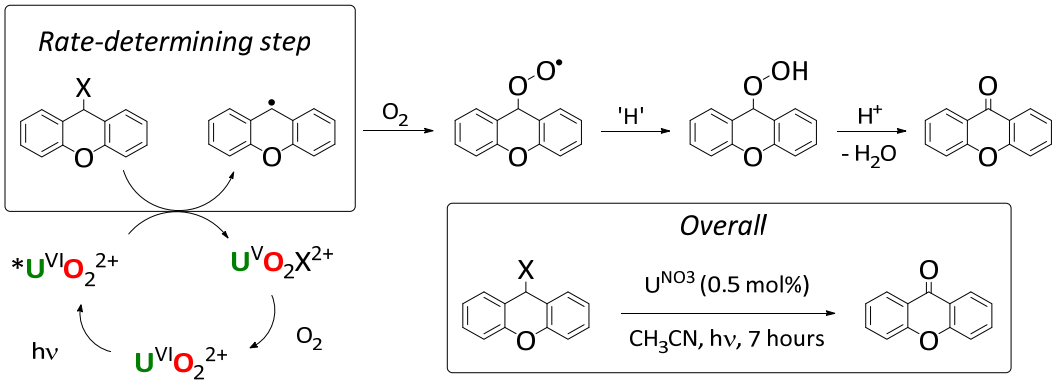

Scheme 3.20 – Tentative mechanism for the photo-oxidation of xanthene with **U^{NO3}** (0.5 mol%). X = H or D. The fate of oxygen in regeneration of the $U^{V}O_2X^{2+}$ intermediate is unspecified, as the role of oxygen in catalyst regeneration (Section 3.3.5) has not yet been fully established.

This proposed mechanism is in line with previous reports on the thermal oxidation of xanthene with TM catalysts, in which xanthene oxidation occurs *via* a HAA pathway. The effect of catalyst on product distribution is poorly understood, however, and contradictory reports of where bixanthene is present[168-170] (*e.g.* from xanthene conversion reactions involving the Mn-catalyst[169] $[(phen)_2Mn^{IV}(\mu\text{-}O)_2Mn^{III}(phen)_2]^{3+}$ (**3.Q**), and Ru-catalyst[170] $[Ru^{IV}O(bipy)_2(py)]^{2+}$ (**3.R**)) and is not present[171, 172] (*e.g.* xanthene catalysis involving $[Mn^{V}(TF_4TMAP)][OTf]_3$ (**3.S**, where TF_4TMAP = *meso*-tetrakis(2,3,5,6-tetrafluoro-*N,N,N*-trimethyl-4-aniliniumyl)porphyrinato dianion)[172]) are known in the literature. No evidence of bixanthene was observed here; bixanthene also has no commercial or industrial use outside of academic studies, where it is primarily known as a byproduct of HAA studies on xanthene.

3.5 Photoreactivity of Other Benzylic Substrates with the Uranyl Ion

Other substrates that showed effective photocatalytic reactivity with **U^{NO3}** or **U^{Ph2phen}** (*e.g.* five or fewer products in > 10% overall conversion) were then tested photocatalytically. Using the conversion data in Table 3.3, toluene, di- and triphenylmethane, and isochroman were selected, and key conclusions from the bulk scale reactions involving these substrates are discussed in Sections 3.5.1, 3.5.2 and 3.5.3. 'Bulk scale' is used to refer to the same scale as the DHA/$U^{VI}O_2^{2+}$ reactions; 2.5 mmol of substrate and an appropriate catalyst loading in 50 mL of CH_3CN, monitored by ^1H NMR spectroscopy, over time.

3.5.1 Bulk-scale Reactions of Toluene

The low conversion (2%) of toluene using **U^{NO3}** catalyst on the smaller scale reactions (entry 2, Table 3.3, and entry 1, Table 3.10) was also observed on this larger scale reaction, with very low (< 1%) conversion being observed spectrally after 16 hours; these data are omitted for clarity. Figure 3.24 therefore shows only toluene conversion using **U^{Ph2phen}** over 16 hours. The general reaction for the photo-oxidation of toluene with **U^{Ph2phen}** is given in Scheme 3.21, below.

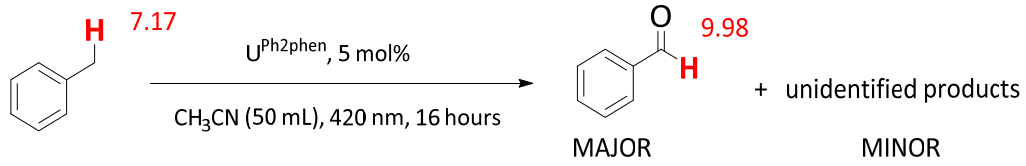

Scheme 3.21 – Photo-oxidation of toluene using **U^{Ph2phen}** in CH_3CN. Values in red are the resonances in ppm used to quantify consumption of toluene or production of benzaldehyde.

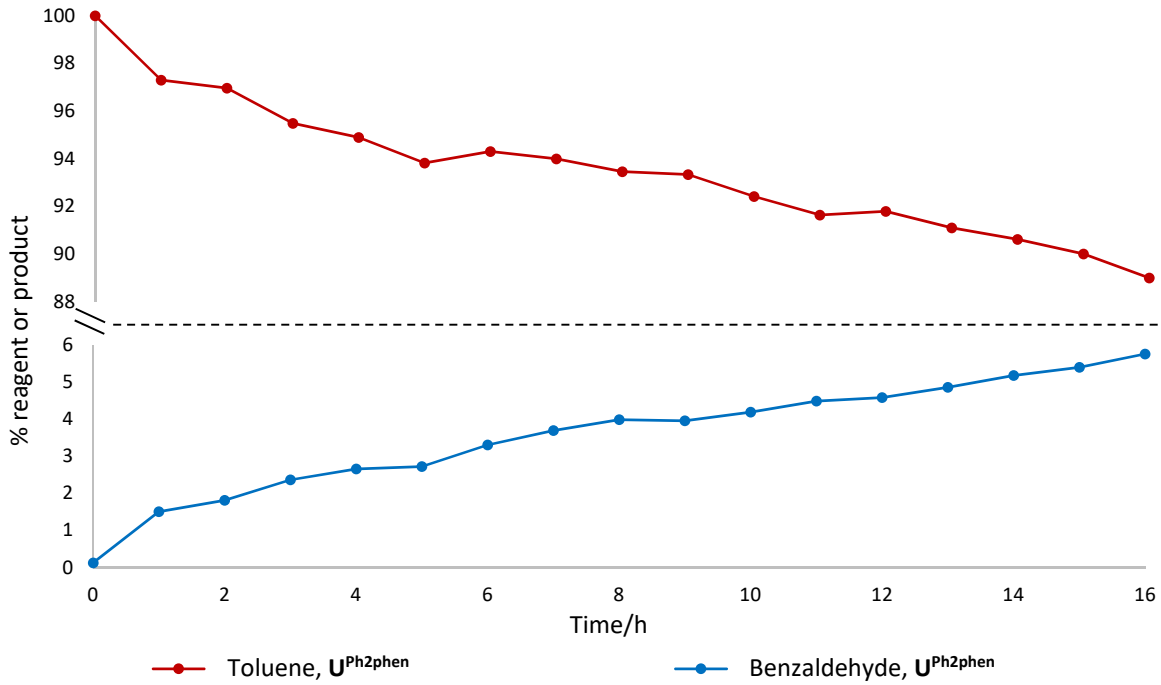

Figure 3.24 – Conversion profile for toluene under photocatalytic conditions over 16 hours with **U^{Ph2phen}** (5 mol%) catalyst loading in 50 mL CH_3CN, measured by ^{1}H NMR spectroscopy.

The only product detected by ^{1}H NMR spectroscopy was benzaldehyde, which accounts for approximately half of the 11% (entry 1, Table 3.10) of toluene that is converted; attempts to identify other product(s) by GC-MS were not successful. This conversion of 11% is also considerably smaller than that reported for the smaller scale substrate scope reaction (entry 1, Table 3.10) of 35% for **U^{Ph2phen}**, suggesting that moving from the smaller scale to larger scale reaction setup produces a change in the experimental conditions that reduces substrate conversion. This pattern of lower conversions for the larger scale reactions is repeated for all substrates tested (entries 1–4, Table 3.10).

Substrate	Entry	Substrate conversion with U^{NO3} catalyst/%		Substrate conversion with $U^{Ph2phen}$ catalyst/%	
		Small scale	Large scale	Small scale	Large scale
Toluene	1	2	< 1	35	11
Diphenylmethane	2	21	11	33	18
Triphenylmethane	3	14	11	37	32
Isochroman	4	35	34	80	69

Table 3.10 – Conversions of selected substrates for larger (50 mL CH_3CN) and smaller (5 mL CH_3CN) scale photocatalytic reactions. Data from the smaller scale reactions is taken from Table 3.3. [catalyst] = $\mathbf{U^{NO3}}$ = 10 mol%, $\mathbf{U^{Ph2phen}}$ = 5 mol%, and 16 hours of irradiation (420 nm).

While CH_3CN solvent is optically transparent to 420 nm photons, these photons are still refracted. As refraction obeys the inverse square law, the larger volume of solvent (50 mL) compared to the smaller scale reactions (5 mL) will reduce the total number of photons absorbed by these uranyl catalysts. This lower photon absorption is likely the reason why conversions are lower on these larger scales compared to the smaller scale reactions.

3.5.2 Bulk-scale Reactions of Di- and Tri-phenylmethane

Unlike toluene, it was possible to observe viable conversions for diphenylmethane and triphenylmethane by ^{1}H NMR spectroscopy with $\mathbf{U^{NO3}}$ as the photocatalyst, entries 2 and 3, Table 3.10. The reaction profiles and schemes for these two substrates with both $\mathbf{U^{NO3}}$ and $\mathbf{U^{Ph2phen}}$ catalysts are shown in Figures 3.25 and 3.26, and Schemes 3.22 and 3.23, respectively.

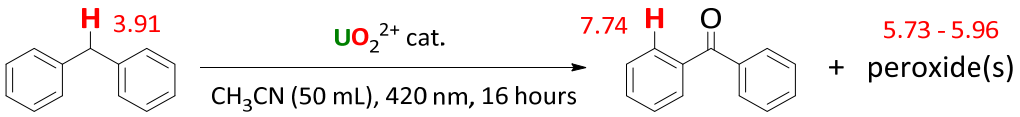

Scheme 3.22 – General reaction scheme for the photo-oxidation of diphenylmethane using $\mathbf{U^{NO3}}$ (10 mol%) or $\mathbf{U^{Ph2phen}}$ (5 mol%) catalyst. Values in red are resonances in ppm used to quantify consumption of diphenylmethane, or benzophenone or peroxide(s) production by ^{1}H NMR spectroscopy. Values for peroxide(s) are reported as a range as a positive identification could not be established on the nature of the formed peroxides, extrapolated from analogous resonances for xanthenyl peroxides (Scheme 3.19).

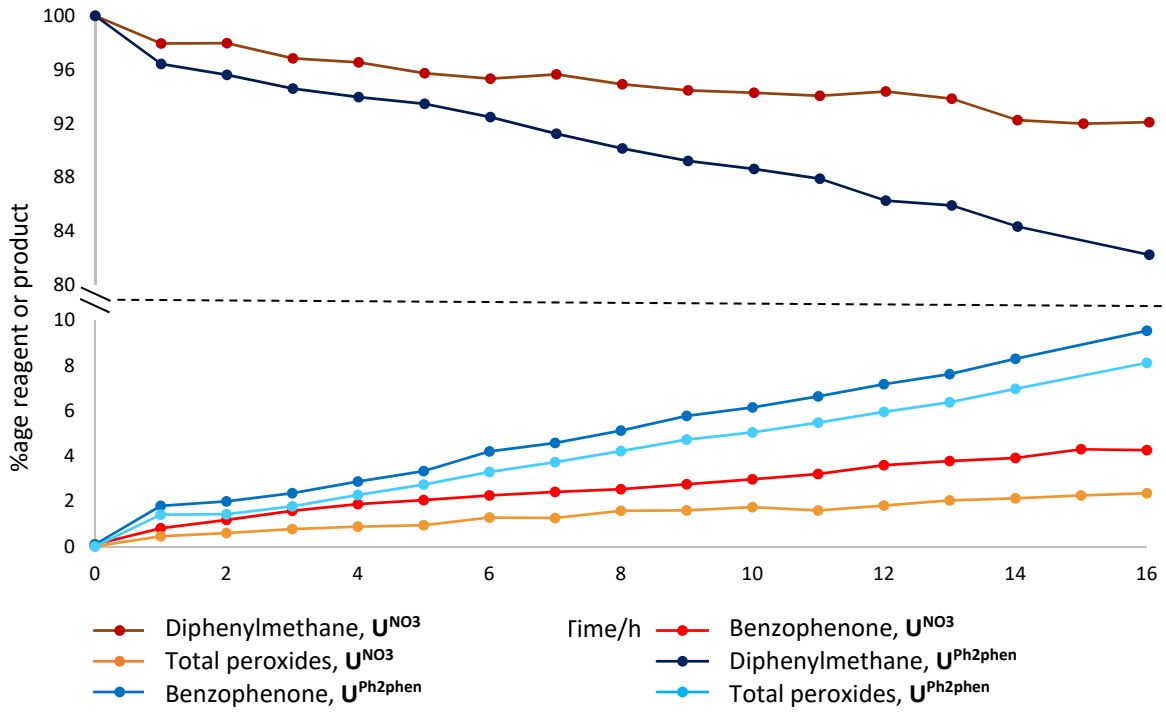

Figure 3.25 – Conversion profiles for diphenylmethane under photocatalytic conditions over 16 hours with $\mathbf{U^{NO3}}$ (10 mol%) and $\mathbf{U^{Ph2phen}}$ (5 mol%) catalyst in CH_3CN, measured by ^1H NMR spectroscopy.

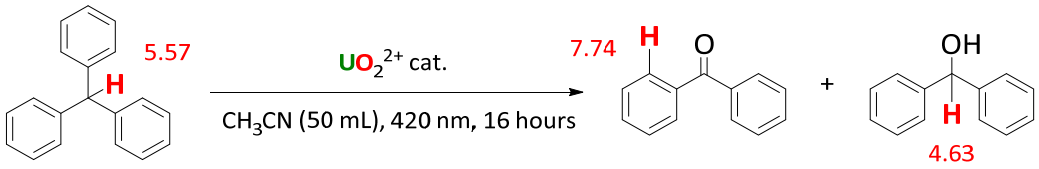

Scheme 3.23 – General reaction scheme for the photo-oxidation of triphenylmethane using $\mathbf{U^{NO3}}$ (10 mol%) or $\mathbf{U^{Ph2phen}}$ (5 mol%) catalyst. Values in red are the resonances in ppm used to quantify consumption of triphenylmethane or production of benzophenone or diphenylmethanol by ^1H NMR spectroscopy.

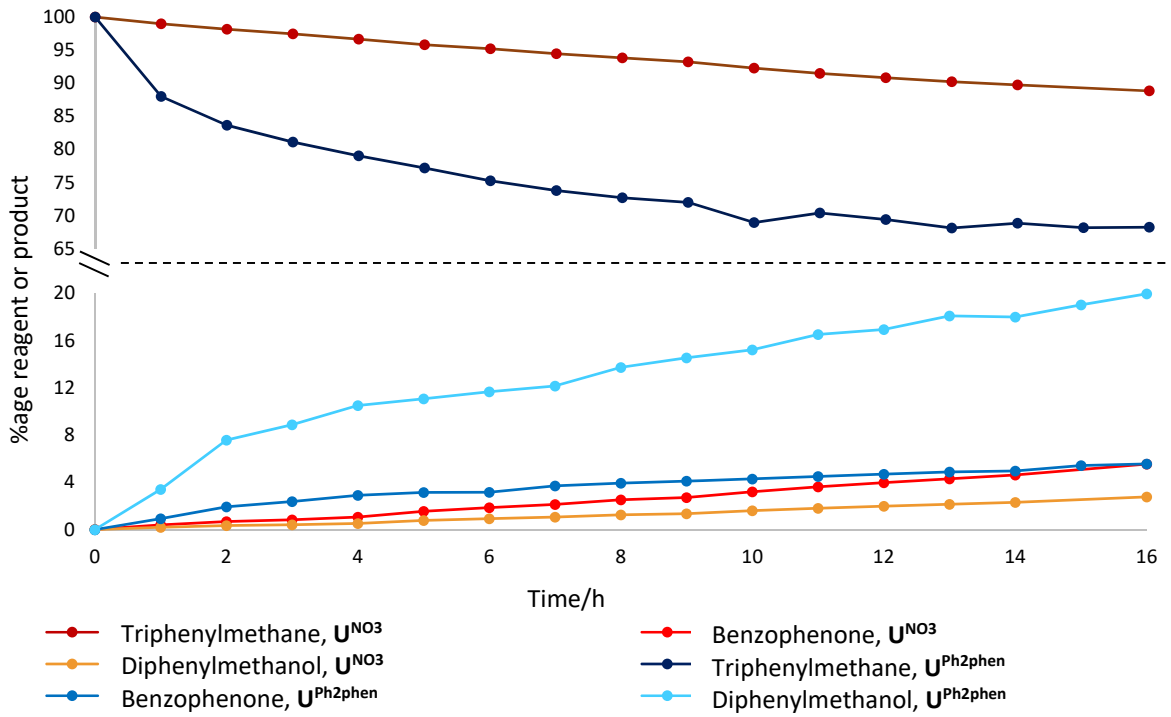

Figure 3.26 – Conversion profiles for triphenylmethane under photocatalytic conditions over 16 hours with **U^{NO3}** (10 mol%) and **U^{Ph2phen}** (5 mol%) catalyst in CH_3CN, measured by ^{1}H NMR spectroscopy.

For both di- and tri-phenylmethane, conversion is higher with **U^{Ph2phen}** than with **U^{NO3}**, in agreement with results for the smaller scale reactions (entries 2 and 3, Table 3.10). For diphenylmethane, resonances consistent with diphenylmethyl peroxides were observed at 5.94, 5.75, and 5.72 ppm in CH_3CN in the ^{1}H NMR spectra of reactions with both **U^{NO3}** and **U^{Ph2phen}**. Intermediates responsible for these shifts probably include the peroxo-dimer (bis(diphenylmethyl) peroxide, $(Ph_2\underline{H}CO)_2$) or hydroperoxide (diphenylmethyl hydroperoxide, $Ph_2\underline{H}COOH$), which have resonances for the underlined protons of 6.08 ppm in $CDCl_3$,[173] though further examination would be required to conclusively prove the identity of these likely peroxides.

For both **U^{NO3}** and **U^{Ph2phen}** reactions with triphenylmethane, a substantial amount of white precipitate was observed after *ca*. 2 hours. Analysis of these solids (^{1}H NMR and ^{13}C, and IR spectroscopies, and elemental and melting point analyses) proved consistent with the formation of the air-stable triphenylmethyl (trityl) peroxide, $(Ph_3CO)_2$, the product of quenching of the trityl radical, $Ph_3C^{\bullet}$, with oxygen. It is known that homolytic cleavage of the peroxo bond in trityl peroxide results in a triphenylmethoxyl radical,[174] resulting in products including benzophenone and diphenylmethanol.[175] These appear to be the favoured products in these larger scale reactions involving triphenylmethane, with diphenylmethanol being the clearly favoured product where **U^{Ph2phen}** is the photocatalyst under these conditions (20%, compared with *ca*. 6% for benzophenone).

3.5.3 Bulk-scale Reaction of Isochroman with $U^{Ph2phen}$

The reaction profiles of the photocatalytic decomposition of isochroman with U^{NO3} and $U^{Ph2phen}$ are given below in Figure 3.27. The general reaction scheme for the photo-oxidation of isochroman with U^{NO3} and $U^{Ph2phen}$ is also given below, in Scheme 3.24.

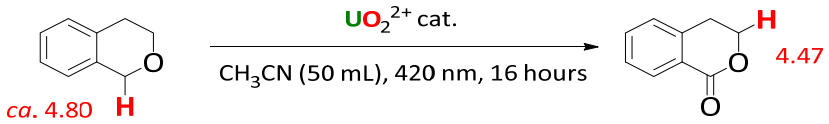

Scheme 3.24 – General reaction scheme for the photo-oxidation of isochroman using U^{NO3} (10 mol%) or $U^{Ph2phen}$ (5 mol%) catalyst. Values in red are the resonances in ppm used to quantify consumption of isochroman or production of 1-isochromanone by ^{1}H NMR spectroscopy.

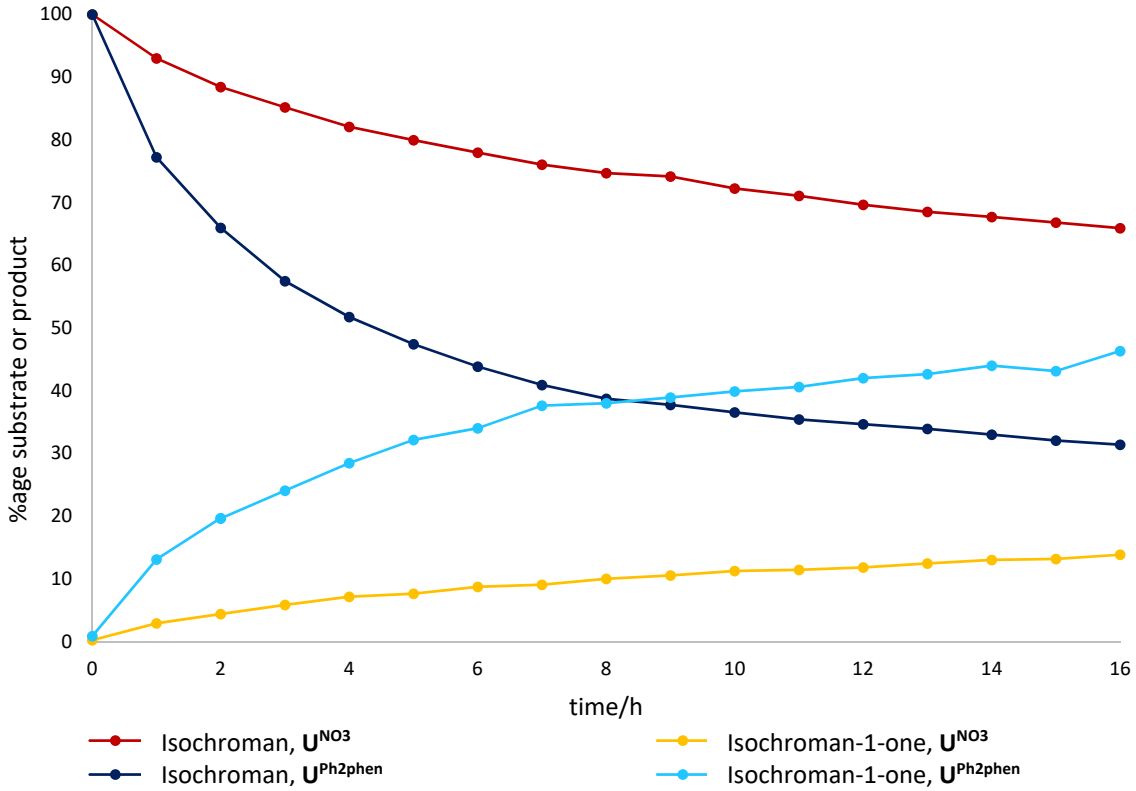

Figure 3.27 – Conversion profiles for isochroman under photocatalytic conditions over 16 hours with U^{NO3} (10 mol%) and $U^{Ph2phen}$ (5 mol%) catalyst in CH_3CN, measured by ^{1}H NMR spectroscopy.

In agreement with the smaller scale photocatalytic oxidation of isochroman (entry 7, Table 3.3), $U^{Ph2phen}$ is a superior photocatalyst compared to U^{NO3}, with conversions of approximately 69% and 34%, respectively. The major product also appears to remain the same between the larger and smaller scale reactions as isochroman-1-one, formed in 46% and 14% *in-situ* yields for the $U^{Ph2phen}$ and U^{NO3} reactions, respectively.

3.5.4 Unsuccessful Trifluoromethylation of Xanthene, and Effect of Iodine

The addition of both fluorine[176] or trifluoromethyl[177] groups to organic molecules is of interest in the synthesis of pharmaceuticals and agrochemicals. Therefore, the use of NFSI as an electrophilic fluorinating agent by Sorensen *et al*.[61] in the uranyl-mediated fluorination of alkanes prompted consideration that an alternative substrate functionalisation reaction with photoactive uranyl(VI) ions, namely trifluoromethylation, may be possible.

Several common trifluoromethylating agents including Langlois' Reagent (sodium triflinate or sodium trifluoromethylsulfinate,[178, 179] Umemoto's Reagent ((trifluoromethyl)dibenzothiophenium tetrafluoroborate) and Togni's Reagent (3,3-dimethyl-1-(trifluoromethyl)-1,2-benziodoxole)[180] were reacted with xanthene under photolysis conditions (5 hours, 420 nm, in < 2 mL CH_3CN; $\mathbf{U^{NO3}}$, 10 mol%, $\mathbf{U^{Ph2phen}}$, 5 mol%). The reaction solutions were analysed hourly by ^1H and ^{19}F NMR spectroscopy. A general procedure for these unsuccessful trifluoromethylation reactions is given in Scheme 3.25.

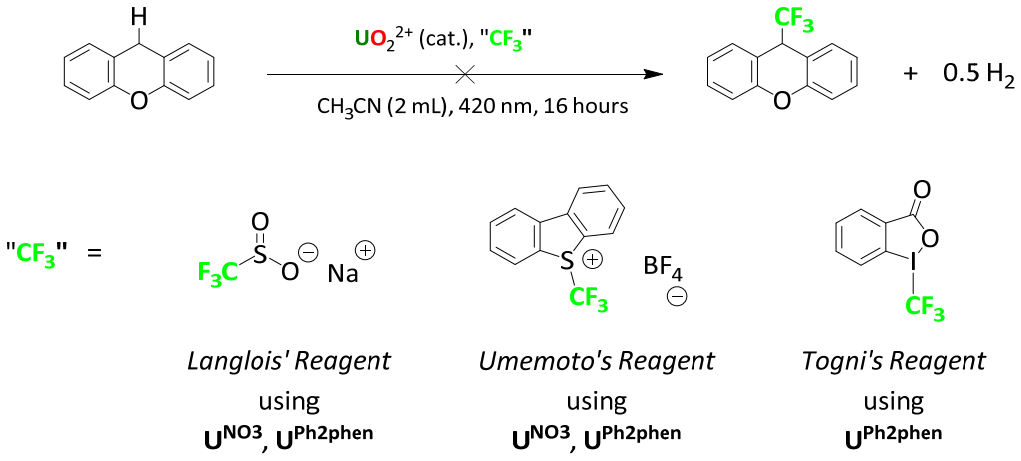

Scheme 3.25 – Unsuccessful trifluoromethylation of xanthene at the 9-position using the trifluoromethylation agents and catalysts shown ($\mathbf{U^{NO3}}$, 10 mol%; $\mathbf{U^{Ph2phen}}$, 5 mol%).

The predominant product in all cases was trifluoromethane, CHF_3, detectable by the distinct resonances at -80 ppm (s), and 7.25, 7.05, 6.85 and 6.65 ppm (q) in the ^{19}F and ^1H NMR spectra in CD_3CN, respectively. The ^{19}F NMR signals for trifluoromethane in C_6D_6[181] or THF-D_8[182] are -79 and -81 ppm, respectively, and for ^1H NMR spectroscopy, resonances appear as a quartet at *ca*. 7 ppm.[183] There was no evidence of any trifluoromethylated product of xanthene which, for 9-(trifluoromethyl)xanthene, appears at – 72.5 ppm in the ^{19}F NMR spectrum in C_6D_6.[184]

Similarly, ^1H NMR spectroscopy in all cases indicated the complete consumption of all trifluoromethylating agents after 5 hours, probably by indiscriminate oxidation of these reagents by the $\mathbf{U^{NO3}}$, or by HAA with intermediate $^{\bullet}CF_3$ radicals, producing trifluoromethane as the by-product.

Curiously, the ^{1}H NMR spectra after one hour of irradiation in the presence of Langlois' Reagent for both **U^{NO3}** and **U^{Ph2phen}** showed no xanthene peroxides or hydroperoxides (*e.g.* no resonances between 5–6 ppm). This suggests that the addition of Langlois' Reagent influences the product profile of the reaction. Xanthene is completely consumed after three hours.

To examine the role that additives may have on the consumption of the xanthenyl peroxide(s) further, the reaction of xanthene with **U^{NO3}** (10 mol%) or **U^{Ph2phen}** (5 mol%) was repeated, this time with iodine (2.5 equiv.) as an additive in CH_3CN (3 mL). This reaction is depicted in Scheme 3.26, below.

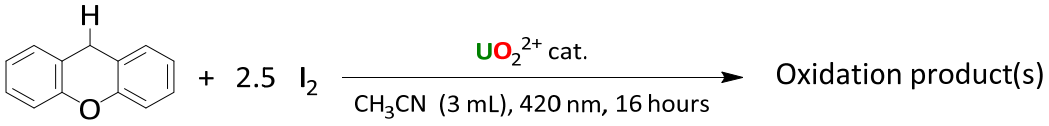

Scheme 3.26 – Xanthene photo-oxidation (420 nm) with **U^{NO3}** (10 mol%) or **U^{Ph2phen}** (5 mol%) in presence of iodine.

Iodine is known to have a complex oxidation chemistry with (hydrogen) peroxide,[185] forming numerous iodine oxides by the consumption of peroxides (*cf*. the Bray-Liebhafsky reaction)[186]. With $^*U^{VI}O_2^{2+}$ ions, I_2 is oxidised to iodate, IO_3^-, by the uranyl-mediated consumption of peroxides.[32] It was therefore expected that adding iodine to a reaction containing either **U^{NO3}** or **U^{Ph2phen}** and xanthene would result in much quicker consumption of intermediate xanthenyl (hydro)peroxides.

Analysis by ^{1}H NMR spectroscopy of these two reactions showed no detectable peroxides (*ca*. 5.9 ppm, Scheme 3.19), with complete consumption of xanthene after approximately one hour of photolysis. The main identifiable product from these reactions is xanthone (*ca*. 30% in both cases), with an unidentified product comprising the remainder of the product mixture (*ca*. 70% in both cases). This unidentified product has 4 signals in the ^{1}H NMR spectra of the product mixtures for both **U^{NO3}** and **U^{Ph2phen}** (10.34, 8.68–8.60, 8.39 and 8.11 ppm, in 1:4:2:2 ratio), with the resonance at 10.34 ppm suggesting the formation of an aldehyde.

Though the effect of the small reaction scale (3 mL CH_3CN) has not been fully compared with the larger scale reactions involving xanthene (10 mL or 50 mL CH_3CN, Section 3.4.1) it is speculated that iodine influences the mechanism by which the xanthene is converted, by consumption of the intermediate peroxides. By the careful selection and addition of reagents, other organic transformations of xanthene might therefore be possible; for example, chlorination or bromination, by addition of *N*-chloro- or *N*-bromo-succinimide, respectively. If feasible, these reactions would add to the slowly increasing number of uranyl-mediated transformations (*e.g.* C-H bond fluorination[61] or the cyanation of anilines,[82] and highlight the potential synthetic utility of uranyl photocatalytic reactions in organic transformations.

3.6 Substrate Photoreactivity of the Uranyl Ion under Anaerobic Conditions

*For the purposes of clarity, this section will only consider the reactivity of hydrocarbon substrates (and those with O atoms). The reactivity of uranyl (**U**^{tetNO3}) with B- or Si-containing substrates, which tends to be dominated towards reductive oxo-functionalisation, is discussed further in chapter 4.*

The overwhelming majority of reactions using photoactivated uranyl(VI) catalysts involve intermediate organic radicals that quench by indiscriminate oxidation (C-O bond formation) rather than radical coupling (which would lead to C-C bond formation). Although uranyl-mediated photoreactions that do not involve C-O bond formation (*e.g.* radical oxidation) have been reported (*e.g.* C-C bond formation in the uranyl-mediated polymerisation of acrylamide,[73] the dimerization of substituted phenols[67] or aniline cyanation[82]; C-F bond formation as reported by Sorensen *et al.*, *etc.*)[61] these reactions are unusual, and factors influencing product selectivity are poorly understood.

3.6.1 Reactivity of U^{tetNO3} with Xanthene and DHA

Therefore, in an effort to explore new reactivity of the photoactivated uranyl ion, the anaerobic uranyl(VI) complex **U**^{tetNO3} (Section 2.8) was reacted with two simple substrates, DHA and xanthene, under anaerobic conditions in CD_3CN (1 mL). Scheme 3.27 outlines these reactions, and the major detectable products. The thermal (not photochemical) formation of a C-C bond has also been previously reported by Arnold *et al.*, with serendipitous isolation of bixanthene in the reductive lithiation of the uranyl(VI) ion in a tetrapyrrolic Schiff-base macrocyclic framework (compound **4.O**).[187]

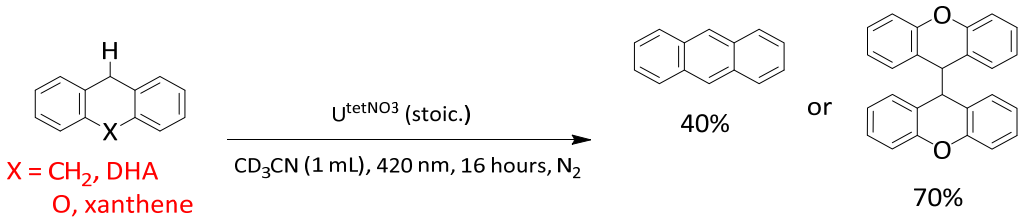

Scheme 3.27 – Anaerobic DHA or xanthene oxidation with **U**^{tetNO3}, and products of photolysis with *in-situ* yields.

For both DHA and xanthene, all substrate was consumed after 16 hours of photolysis by ^{1}H NMR spectroscopy. The main products, anthracene (for DHA) and bixanthene (for xanthene), were detected primarily by ^{1}H NMR spectroscopy (for bixanthene, 4.37 and 49.5 ppm in $CDCl_3$),[166] respectively, with X-ray crystallography and melting point analysis supplementing the detection of bixanthene (*ca*. 200°C from methanol)[188]. *In-situ* yields of approximately 40% and 70% respectively for anthracene and bixanthene were obtained against residual CH_3CN as the standard by ^{1}H NMR spectroscopy. It is likely, given the absence of oxygen to both regenerate the uranyl (**U**^{tetNO3}) catalyst and quench the

xanthenyl radical, that C-C bond formation results. The proposed formation of bixanthene from xanthene and **U^{tetNO3}** under anaerobic photolysis is given in Scheme 3.28, below.

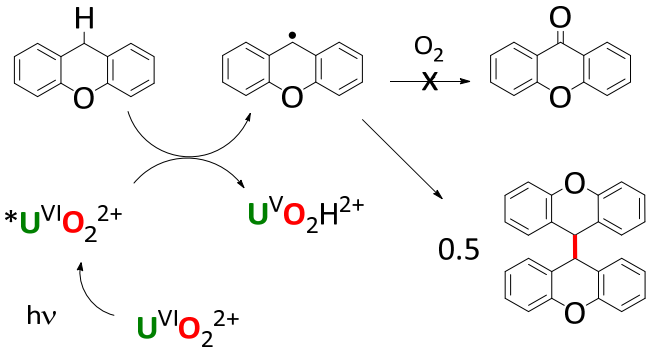

Scheme 3.28 – Proposed production of bixanthene by irradiation of xanthene in the presence of stoichiometric **U^{tetNO3}**. The highlighted bond in red is the new C-C bond formed.

Other examples for the formation of bixanthene from the oxidation of xanthene include with *tert*-butyl peroxide (10% bixanthene),[166] $[Ru^{IV}O(bipy)_2(py)]^{2+}$ (**3.R**, 3.6% bixanthene),[170] (diacetoxyiodo)benzene (28% bixanthene),[189] dioxygen and cyclopentanone (3% bixanthene),[164] ^{n}BuLi in THF (31% bixanthene),[190] and $[AlCl_3(\eta^1\text{-TEMPO})]$ (**3.T**, 51% bixanthene; TEMPO is 2,2,6,6-tetramethylpiperidine-*N*-oxyl).[191] The other product(s) could not be identified, and there was no reaction for either substrate when photolysed in the absence of **U^{tetNO3}** in CD_3CN. Attempts to use catalytic amounts of **U^{tetNO3}** (10 mol% in 5 mL CD_3CN) also resulted in the conversion of xanthene dropping to only 8% after 16 hours of irradiation (^{1}H NMR spectroscopy; *ca*. 5% bixanthene and 3% other product(s)), suggesting further work remains to make the process catalytic WRT the uranyl compound.

3.6.2 Reactivity of U^{tetNO3} with Other Hydrocarbon Substrates

In light of the detection of bixanthene, the photoreactivity of stoichiometric **U^{tetNO3}** with a variety of other substrates was investigated, to see if other reagents could form C-C bonds under similar conditions (1 mL CD_3CN, 16 hours of irradiation at 420 nm; analysis by ^{1}H NMR spectroscopy). A list of (hydrocarbon and O-containing) substrates along with conditions is given in Scheme 3.29, below.

As THF, cyclohexane, cyclohexene, hexane, toluene and 2P1PE have been shown to be effectively decomposed by **U^{NO3}** and **U^{Ph2phen}** previously, these substrates were selected in order to demonstrate a reactivity with a range of chemical functionalities. Isopropanol is known to undergo photolytic C-C bond coupling to form pinacol (1,2-dimethylbutane-1,2-diol),[192] and phenylacetylene was selected on account of the diagnostic resonance of the single alkyne proton at 3.43 ppm (*e.g.* convenient to detect by ^{1}H NMR spectroscopy).

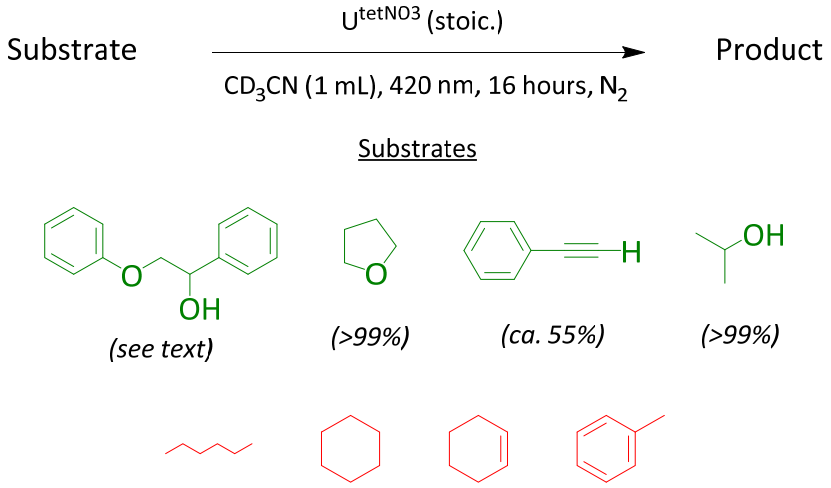

Scheme 3.29 – Additional substrates reacted photolytically with stoichiometric **U^{tetNO3}** under anaerobic conditions. The substrates in green showed at least partial conversion (in parentheses). Substrates in red showed no conversion.

For substrates showing conversion, THF and isopropanol had quantitative decomposition, whereas phenylacetylene had only partial conversion (*ca*. 55%) after 16 hours of photolysis (420 nm). Each of these three substrates had resonances consistent with numerous products in their ^{1}H NMR spectra after photolysis with stoichiometric **U^{tetNO3}**, with several products in each case showing multiplicities and resonances remarkably similar to the protons on the butyl groups of the [^{n}Bu$_4$N]$^+$ cations of **U^{tetNO3}** (*e.g.* multiplets at or near 3.11, 1.61, 1.37 and 0.97 ppm in CD_3CN). Analysis of the product mixtures by GC-MS resulted only in the detection of ^{n}Bu$_3$N, suggesting that the products after conversion of these substrates are unstable either in air or the elevated temperatures in the GC column.

For 2P1PE, decomposition is slower, reaching *ca*. 70% conversion after 64 hours (2.67 days) of photolysis. The reaction and associated conversion profile, as monitored by ^{1}H NMR spectroscopy, is shown in Scheme 3.30 and Figure 3.28, where stoichiometric amounts of 2P1PE and **U^{tetNO3}** were irradiated at 420 nm in CD_3CN (0.7 mL).

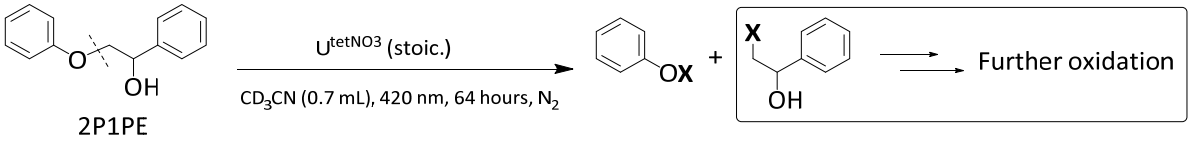

Scheme 3.30 – Anaerobic decomposition of 2P1PE with stoichiometric **U^{tetNO3}**. The dashed line over 2P1PE indicates the bond that is cleaved to yield phenol and 1-phenylethanol as products; 1-phenylethanol is further oxidised to an unidentified product under these conditions. The emboldened X atom is either H or D, and is the product of quenching the intermediate radical with either H, or D, from CD_3CN solvent.

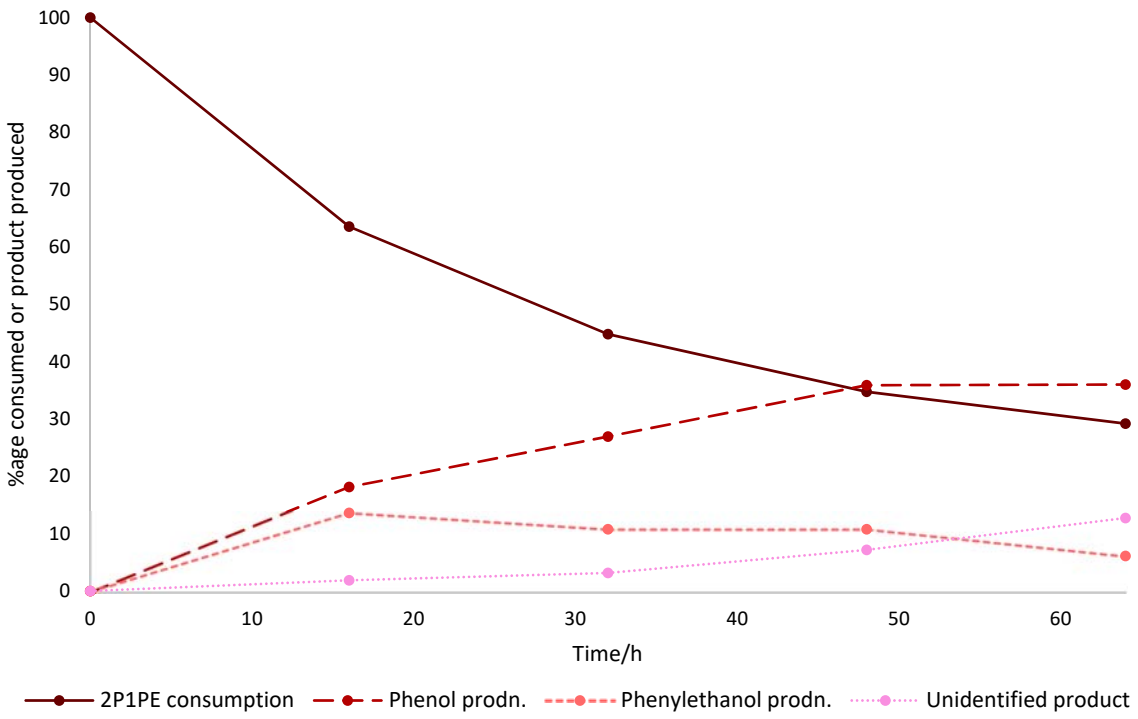

Figure 3.28 – Conversion profile for 2P1PE with stoichiometric $\mathbf{U^{tetNO3}}$ under anaerobic photolysis, in CD_3CN, over 64 hours of photolysis.

There are two major products from the decomposition of 2P1PE, phenol and 1-phenylethanol, detected by characteristic ^{1}H NMR spectroscopic shifts of *ca.* 6.87 ppm (phenol)[193] and 4.91 ppm (1-phenylethanol)[194] (both $CDCl_3$). 1-Phenylethanol appears to undergo further decomposition to another, unidentified product that has a ^{1}H NMR spectroscopic resonance at 5.44 ppm in CD_3CN. GC-MS analysis on this product mixture showed only 1-phenylethanol and phenol. There is no evidence of products consistent with C-C bond cleavage (*e.g.* benzaldehyde), unlike the aerobic reactions of 2P1PE with $\mathbf{U^{NO3}}$ or $\mathbf{U^{Ph2phen}}$ (entry 8, Table 3.3). The formation of phenol and 1-phenylethanol is consistent with C-O bond cleavage, in the position indicated by the dashed line in Scheme 3.30. This suggests that either the absence of oxygen or water or the use of $\mathbf{U^{tetNO3}}$ influences the mechanism of 2P1PE decomposition compared to aerobic conditions using $\mathbf{U^{NO3}}$ or $\mathbf{U^{Ph2phen}}$, for which products of both C-C bond cleavage (*e.g.* benzaldehyde) and C-O bond cleavage (*e.g.* phenol) were observed.

No reactivity was observed for hexane, cyclohexane, cyclohexene or toluene under anaerobic conditions, suggesting that oxygen and/or water are required for reactivity of these substrates with photoactivated uranyl.

3.7 Summary and Outlook

In the first major substrate study involving a uranyl photocatalyst, a large number of functional groups are shown to be incompatible with the $*U^{VI}O_2^{2+}$ ion, with indiscriminate oxidation (aliphatic

hydrocarbons, *etc.*) or non-chemical quenching of $*U^{VI}O_2^{2+}$ (leading to no overall substrate conversion; *e.g. N*-heterocycles, *etc.*) the two most common reaction outcomes. However, comparing the conversions of hydrocarbon substrates possessing benzylic C-H bonds is a useful tool in examining the activity of uranyl photocatalysts, with experiments suggesting that **U^{Ph2phen}** is a superior photocatalyst to **U^{NO3}** for the conversions of these substrates. Examples include toluene (2% conversion with **U^{NO3}**, 35% with **U^{Ph2phen}**), indane (47% conversion for **U^{NO3}**, 87% with **U^{Ph2phen}**), and isochroman (35% conversion with **U^{NO3}**, 80% with **U^{Ph2phen}**). There is no discernible difference between **U^{NO3}** and **U^{Ph2phen}** in the reactivity of selected substrates without benzylic C-H bonds (*e.g.* benzene, cyclohexene). The conversion efficiency of solutions where the substrates are the solvent (*e.g.* THF) are lower than the analogous conversions of THF with **U^{NO3}** or **U^{Ph2phen}** in CH_3CN solvent.

Both **U^{NO3}** and **U^{Ph2phen}** are also effective photocatalysts for the degradation (*ca*. 20% after 16 hours of photolysis) of a lignin model compound, 2P1PE, suggesting that uranyl-containing wastes that are exposed to sunlight may be capable of degrading ligninosic and cellulosic (bio-)matter in the environment. Further investigation on the effect of irradiation on uranyl-contaminated field samples (*e.g.* pond effluents) may therefore be warranted, as the interactions of uranyl wastes with organic matter remain poorly understood.

Employing a specific substrate, DHA, to study differences in **U^{NO3}** and **U^{Ph2phen}** reactivity has highlighted important variations between the two photocatalysts, where the conversion of DHA is likely zeroth order WRT **U^{NO3}** (conversions of 30–40% with 0.001–25 mol% loading) and non-zeroth order WRT **U^{Ph2phen}** (conversion of 23% at 0.001 mol% loading, increasing to 57% at 1 mol%). At loadings of **U^{NO3}** above 100 mol% the predominant DHA conversion pathway is a non-photochemical, nitrate-mediated oxidation, and at loadings of **U^{Ph2phen}** above 1 mol% a yellow solid is observed after several minutes of photolysis. Raman spectroscopy and mass spectrometry analysis on this solid are consistent with peroxo-containing analogue of **U^{Ph2phen}**, suggesting that uranyl peroxo complexes may have an important and as-yet unidentified role in uranyl photocatalytic cycles. Although the role of water in the DHA conversion reaction with **U^{NO3}** also remains unclear, oxygen appears necessary for catalyst regeneration, with the anaerobic photolysis of DHA with 5 mol% of **U^{NO3}** resulting in precipitates that are probably organic-U^{IV}/U^{V} aggregates by IR spectroscopy and elemental analysis. Further work to identify these intermediates is likely to be of further use to the research community as their elucidation would help develop a broader mechanistic understanding of photocatalytic processes involving **U^{NO3}** and **U^{Ph2phen}**. For **U^{Ph2phen}** this is particularly important, as the role that complexation of the Ph_2phen ligand plays in modifying the photochemistry of $*U^{VI}O_2^{2+}$ is still unclear and may help elucidate the effect of Ph_2phen coordination on the photoreactivity of $*U^{VI}O_2^{2+}$ in **U^{Ph2phen}**.

Other larger scale photolysis reactions involving toluene, di- and tri-phenylmethane, isochroman and xanthene with $\mathbf{U^{NO3}}$ and $\mathbf{U^{Ph2phen}}$ also highlight differences between the two catalysts. The larger scale reactions have lower conversions than the smaller scale ones, likely resulting from reduced light penetration. While conversions for toluene, di- and tri-phenylmethane and isochroman after 16 hours are higher for $\mathbf{U^{Ph2phen}}$ than for $\mathbf{U^{NO3}}$, the reverse is true for xanthene, with $\mathbf{U^{NO3}}$ giving higher conversions than $\mathbf{U^{Ph2phen}}$ after 9 hours of photolysis. Xanthene deuteration suggests HAA is a key and probably rate-limiting step in the oxidation of xanthene with $\mathbf{U^{NO3}}$, in line with other *d*-block metal-oxo catalysts. Although attempts to trifluoromethylate xanthene were unsuccessful, iodine markedly increases consumption of intermediate xanthenyl peroxides.

The adoption of anaerobic conditions with a rigorously anhydrous source of uranyl(VI) ions, $\mathbf{U^{tetNO3}}$, appears to modify the outcomes of several substrate photoreactions with the $U^{VI}O_2^{2+}$ ion, including xanthene and 2P1PE. In these cases the products (bixanthene or those of C-O, not C-C bond cleavage, respectively) are different from those observed with the analogous aerobic reactions of these substrates with $\mathbf{U^{NO3}}$. Attempts to produce C-C coupled products of other substrates were generally unsuccessful, resulting either in indiscriminate substrate decomposition (*e.g.* THF, isopropanol, phenylacetylene), or simply no reaction (hexane, cyclohexane, cyclohexene, toluene). Further work in this area may focus on attempting to make these and other reactions catalytic in uranyl (*e.g.* by the use of oxygen-free and photochemically robust oxidants) and particularly for $\mathbf{U^{tetNO3}}$, to identify the nature of the uranyl-containing product in these reactions.

3.8 References

1. A. D. McNaught and A. Wilkinson, *IUPAC Compendium of Chemical Terminology (the "Gold Book")*, 2nd edn., IUPAC and Blackwell Scientific Publications, Oxford, 1997.
2. A. B. Yusov and V. P. Shilov, *Russ. Chem. Bull., Int. Ed.*, 2000, **49**, 1925.
3. X. Sun, D. R. J. Rolling, S. Deskins and E. Adkins, *Inorg. Chim. Acta*, 2018, **483**, 12.
4. S. Sostero, O. Traverso, C. Bartocci, P. Di Bernardo, L. Magon and V. Carassiti, *Inorg. Chim. Acta*, 1976, **19**, 226.
5. G. Gordon and H. Taube, *J. Inorg. Nucl. Chem.*, 1961, **16**, 272.
6. G. Gordon and H. Taube, *J. Inorg. Nucl. Chem.*, 1961, **19**, 189.
7. H. D. Burrows and T. J. Kemp, *Chem. Soc. Rev.*, 1974, **3**, 139.
8. R. Matsushima and S. Sakuraba, *Bull. Chem. Soc. Jpn.*, 1970, **43**, 2359.
9. R. Matsushima and S. Sakuraba, *Bull. Chem. Soc. Jpn.*, 1971, **44**, 2915.
10. R. Matsushima and S. Sakuraba, *Bull. Chem. Soc. Jpn.*, 1973, **46**, 2784.
11. R. Matsushima and S. Sakuraba, *J. Am. Chem. Soc.*, 1971, **93**, 5421.
12. R. Matsushima and S. Sakuraba, *J. Am. Chem. Soc.*, 1972, **94**, 6010.
13. M. D. Mercantonatos, *Inorg. Chim. Acta*, 1978, **26**, 41.
14. M. D. Mercantonatos, *J. Chem. Soc., Faraday Trans. 1*, 1980, **76**, 1063.
15. S. J. Formosinho, M. G. M. Miguel and H. D. Burrows, *J. Chem. Soc., Faraday Trans. 1*, 1984, **80**, 1717.
16. M. G. M. Miguel, S. J. Formosinho, A. C. Cardoso and H. D. Burrows, *J. Chem. Soc., Faraday Trans. 1*, 1984, **80**, 1735.

17. M. E. D. G. Azenha, H. D. Burrows, S. J. Formosinho and M. G. M. Miguel, *J. Chem. Soc., Faraday Trans. 1*, 1989, **85**, 2625.
18. T. J. Kemp, *Rev. Port. Chim.*, 1975, **17**, 131.
19. V. Natrajan, S. V. Godbole, A. Argekar, A. G. Page, M. D. Sastry and P. R. Natrajan, *J. Radioanal. Nucl. Chem., Lett.*, 1992, **165**, 255.
20. H. D. Burrows and S. J. Formosinho, *J. Chem. Soc., Faraday Trans. 2*, 1977, **73**, 201.
21. Y. Katsumura, H. Abe, T. Yotsuyanagi and K. Ishigure, *J. Photochem. Photobiol. A: Chem.*, 1989, **50**, 183.
22. R. M. Haas and K.-H. Gayer, *Z. Anorg. Allg. Chem.*, 1967, **367**, 102.
23. V. Sladkov, *J. Photochem. Photobiol. A: Chem.*, 2014, **295**, 40.
24. C. Görller-Walrand and K. Servaes, *Helv. Chim. Acta*, 2009, **92**, 2304.
25. Y.-Y. Park and H. Tomiyasu, *J. Photochem. Photobiol. A: Chem.*, 1992, **64**, 25.
26. W. Mooner and G. Folcher, *Inorg. Chim. Acta*, 1985, **110**, 119.
27. H. B. Ambroz, K. R. Butter and T. J. Kemp, *Faraday Discuss. Chem. Soc.*, 1984, **78**, 107.
28. Y.-Y. Park and H. Tomiyasu, *J. Photochem. Photobiol. A: Chem.*, 1993, **74**, 11.
29. K. R. Butter and J. K. Kemp, *J. Chem. Soc., Dalton Trans.*, 1984, 923.
30. M. S. Sidhu, K. B. Kohli, P. V. K. Bhatia and S. S. Sandhu, *J. Radioanal. Nucl. Chem., Lett.*, 1994, **187**, 375.
31. X. Sun, D. R. J. Kolling, H. Mazagri, B. Karawan and C. Pierron, *Inorg. Chim. Acta*, 2015, **435**, 117.
32. T. Sakurai, *J. Nucl. Sci. Technol.*, 1996, **33**, 266.
33. S. S. Sandhu, K. B. Kohli and A. S. Brar, *Inorg. Chem.*, 1984, **23**, 3609.
34. T. J. Kemp and M. A. Shand, *Inorg. Chem.*, 1986, **25**, 3840.
35. S. S. Sandhu, R. J. Singh and S. K. Chawla, *J. Photochem. Photobiol. A: Chem.*, 1990, **52**, 65.
36. Z. Fazekas, H. Tomiyasu, Y.-Y. Park, T. Yamamura and M. Harada, *ACH Models Chem.*, 1998, **135**, 738.
37. D. S. Umreiko, N. P. Vileishikova, A. P. Zajogin and A. I. Komyak, *J. Appl. Spectrosc.*, 2015, **82**, 839.
38. O. Traverso, R. Rossi, L. Magon, A. Cinquantini and T. J. Kemp, *J. Chem. Soc., Dalton Trans.*, 1978, 569.
39. A. Bakac and J. H. Espenson, *Inorg. Chem.*, 1995, **34**, 1730.
40. T. Yamamura, Z. Fazekas, M. Harada and H. Tomiyasu, *Phys. Chem. Chem. Phys.*, 1999, **1**, 3491.
41. T. Rosenfeld-Grunwald, M. Brandeis and J. Rabani, *J. Phys. Chem.*, 1982, **86**, 4745.
42. Y. Yokoyama, M. Moriyasu and S. Ikeda, *J. Inorg. Nucl. Chem.*, 1974, **36**, 375.
43. S. Tsushima, C. Gotz and K. Fahmy, *Chem. Eur. J.*, 2010, **16**, 8029.
44. C. P. Baird and T. J. Kemp, *Prog. React. Kinet.*, 1997, **22**, 87.
45. S. S. Sandhu, A. S. Brar and A. S. Sarpal, *Ind. J. Chem., Sect. A*, 1978, **16**, 587.
46. S. S. Sandhu, A. S. Brar and A. S. Sarpal, *Ind. J. Chem., Sect. A*, 1979, **18**, 19.
47. S. S. Sandhu, A. S. Brar and A. S. Sarpal, *Ind. J. Chem., Sect. A*, 1980, **19**, 413.
48. S. S. Sandhu, A. S. Brar and A. S. Sarpal, *Ind. J. Chem., Sect. A*, 1980, **19**, 902.
49. M. P. Redmond, S. M. Cornet, S. D. Woodall, D. Whittaker, D. Collison, M. Helliwell and L. S. Natrajan, *Dalton Trans.*, 2011, **40**, 3914.
50. M. S. Sidhu, P. V. K. Bhatia and R. J. Singh, *J. Radioanal. Nucl. Chem., Lett.*, 1994, **188**, 355.
51. S. S. Sandhu, M. S. Sidhu and R. J. Singh, *J. Photochem. Photobiol. A: Chem.*, 1989, **46**, 213.
52. S. M. Cornet, L. J. L. Haller, M. J. Sarsfield, D. Collison, M. Helliwell, I. May and N. Kaltsoyannis, *Chem. Commun.*, 2009, 917.
53. C. K. Rofer-Depoorter and G. L. Depoorter, *J. Inorg. Nucl. Chem.*, 1977, **39**, 631.
54. C. K. Rofer-Depoorter and G. L. Depoorter, *J. Inorg. Nucl. Chem.*, 1978, **40**, 1895.
55. C. K. Rofer-Depoorter and G. L. Depoorter, *J. Inorg. Nucl. Chem.*, 1979, **41**, 215.
56. G. Cauzzo, G. Gennari, G. Giacometti, G. C. Agostini and A. Gambaro, *Inorg. Chim. Acta*, 1979, **32**, 45.

57. M. S. Sidhu and P. V. K. Bhatia, *Ind. J. Chem., Sect. A*, 1994, **33**, 253.
58. S. S. Sandhu, M. S. Sidhu and R. J. Singh, *J. Photochem.*, 1987, **39**, 229.
59. L. S. Natrajan, *Coordin. Chem. Rev.*, 2012, **256**, 1583.
60. L. Wu, X. Cao, X. Chen, W. Fang and M. Dolg, *Angew. Chem. Int. Ed.*, 2018, **57**, 11812.
61. J. G. West, T. A. Bedell and E. J. Sorensen, *Angew. Chem. Int. Ed.*, 2016, **55**, 8923.
62. Y. Mao and A. Bakac, *J. Phys. Chem.*, 1996, **100**, 4219.
63. M. S. Sindu and V. Kapila, *J. Radioanal. Nucl. Chem.*, 1995, **198**, 429.
64. Y. Mao and A. Bakac, *J. Phys. Chem. A*, 1997, **101**, 7929.
65. H. D. Burrows, A. C. Cardoso, S. J. Formosinho, A. M. P. C. Gil, M. G. M. Miguel, B. Barata and J. J. G. Moura, *J. Photochem. Photobiol. A: Chem.*, 1992, **68**, 279.
66. M. Sarakha, M. Bolte and H. D. Burrows, *J. Phys. Chem. A*, 2000, **104**, 3142-3149.
67. M. Sarakha, M. Bolte and H. D. Burrows, *J. Photochem. Photobiol. A: Chem.*, 1997, **107**, 101.
68. W.-D. Wang, A. Bakac and J. H. Espenson, *Inorg. Chem.*, 1995, **34**, 6034.
69. M. Ahmad, A. Cox, T. J. Kemp and Q. Sultana, *J. Chem. Soc., Perkin Trans. 2*, 1975, 1867.
70. E. Murayama and T. Sato, *Bull. Chem. Soc. Jpn.*, 1978, **51**, 3022.
71. E. Murayama, A. Kohda and T. Sato, *J. Chem. Soc., Perkin Trans. 1*, 1980, 947.
72. T. M. McCleskey, C. J. Burns and W. Tumas, *Inorg. Chem.*, 1999, **38**, 5924.
73. H. D. Burrows., I. M. D. Faria, S. J. Formosinho, M. G. M. Miguel, L. J. A. Martins, G. Maillhot and M. Bolte, *Bur. Bunsenges. Phys. Chem.*, 1992, **96**, 712.
74. W. L. Waltz, J. Lilie, X. Xu, P. Sedlak and H. Möckel, *Inorg. Chim. Acta*, 1999, **285**, 322.
75. T. M. Bergfeldt, W. L. Waltz, X. Xu, P. Sedlák, U. Dreyer, H. Mockel, J. Lilie and J. W. Stephenson, *Can. J. Chem.*, 2003, **81**, 219.
76. V. N. Salomone, J. M. Meichtry, G. Schinelli, A. G. Leyva and M. I. Litter, *J. Photochem. Photobiol. A: Chem.*, 2014, **277**, 19.
77. D. Greatorex, R. J. Hill, T. J. Kemp and T. J. Stone, *J. Chem. Soc., Faraday Trans. 1*, 1974, **70**, 216.
78. S. Tsushima, *Inorg. Chem.*, 2009, **48**, 4856.
79. J. Cunningham and S. Srijaranai, *J. Photochem. Photobiol. A: Chem.*, 1990, **55**, 219.
80. R. J. Hill, T. J. Kemp, D. M. Allen and A. Cox, *J. Chem. Soc., Faraday Trans. 1*, 1974, **70**, 847.
81. G. Meinrath, Y. Kato, T. Kimura and Z. Yoshida, *Radiochim. Acta*, 1998, **82**, 115.
82. M. Azam, S. I. Al-Resayes, A. Trzesowska-Kruszynska, R. Kruszynski, P. Kumar and S. L. Jain, *Polyhedron*, 2017, **124**, 177.
83. D. D. Schnaars, G. Wu and T. Hayton, *J. Am. Chem. Soc.*, 2009, **131**, 17532.
84. M. Azam, G. Velmurugan, S. M. Wabaidur, A. Trzesowska-Kruszynska, R. Kruszynski, S. I. Al-Resayes, Z. A. Al-Othman and P. Venuvanalingam, *Sci. Rep.*, 2016, **6**, 32898.
85. Q. Zhang, B. Jin, R. Peng, X. Wang, Z. Shi, Q. Liu, S. Lei and H. Liang, *Int. J. Photoenerg.*, 2017, 8041647.
86. Y. Zhen-Tao, L. Zuo-Lei, J. Yu-Sheng, L. Hua-Guang and C. Jie-Shang, *Chem. Eur. J.*, 2005, **11**, 2642.
87. J. T. Bell, *J. Inorg. Nucl. Chem.*, 1969, **31**, 703.
88. C. Talbot-Eeckelaers, S. J. A. Pope, A. J. Hynes, R. Copping, C. J. Jones, R. J. Taylor, S. Faulkner, D. Sykes, F. R. Livens and I. May, *J. Am. Chem. Soc.*, 2007, **129**, 2442.
89. M. P. Wilkerson and J. M. Berg, *J. Phys. Chem. A*, 2008, **112**, 2515.
90. S. D. Woodall, A. N. Swinburne, N. L. Banik, A. Kerridge, P. D. Pietro, C. Adam, P. Kaden and L. S. Natrajan, *Chem. Commun.*, 2015, **51**, 5402.
91. F. P. Rotzinger, *Inorg. Chem.*, 2018, **57**, 2425.
92. B. J. Barker, J. M. Berg, S. A. Kozimor, N. R. Wozniak and M. P. Wilkerson, *J. Phys. Chem. A*, **121**, 2353.
93. J. Su, W. H. E. Schwartz and J. Li, *Inorg. Chem.*, 2012, **51**, 3231.
94. L. M. Toth and H. A. Friedman, *Radiochim. Acta*, 1980, **27**, 173.
95. H. A. Friedman and L. M. Toth, *J. Inorg. Nucl. Chem.*, 1981, **43**, 1611.

96. A. J. Zielen, J. C. Sullivan and D. Cohen, *J. Inorg. Nucl. Chem.*, 1958, **7**, 378.
97. J. T. Bell and H. A. Friedman, *J. Inorg. Nucl. Chem.*, 1976, **38**, 831.
98. V. P. Shilov and A. B. Yusov, *Radiochem.*, 2001, **43**, 371.
99. Y.-R. Luo, *Comprehensive Handbook of Chemical Bond Energies*, Taylor & Francis Group, Boca Raton (Florida, USA), 2007.
100. K. A. Gardner and J. M. Mayer, *Science*, 1995, **269**, 1849.
101. W. W. Y. Lam, S.-M. Yiu, D. T. Yiu, T.-C. Lau, W.-P. Yip and C.-M. Che, *Inorg. Chem.*, 2003, **42**, 8011.
102. P. K. Jha and G. P. Halada, *Chem. Cent. J.*, 2011, **5**, 12.
103. R. Bhatt, P. S. Shrimali, S. C. Amete and H. C. Chowdhry, *Z. Phys. Chemie*, 1986, **267**, 817.
104. S. M. Fonseca, H. D. Burrows, M. G. Miguel, M. Sarakha and M. Bolte, *Photochem. Photobiol. Sci.*, 2004, **3**, 317.
105. A. Ochiai, J. Imoto, M. Suetake, T. Komiya, G. Furuki, R. Ikehara, S. Yamasaki, G. T. W. Law, T. Ohnuki, B. Grambow, R. C. Ewing and S. Utsunomiya, *Environ. Sci. Technol.*, 2018, **52**, 2586.
106. U. Schuchardt, W. A. Carvalho and E. V. Spinacé, *Synlett.*, 1993, 713.
107. N. W. Alcock, N. Herron, T. J. Kemp and C. W. Shoppee, *J. Chem. Soc., Chem. Commun.*, 1975, 785.
108. T. Kekki and A. Titta, *Evaluation of the radioactive waste characterisation at the Olkiluoto nuclear power plant*, STUK, Suomi (RNSA, Finland), Helsinki, 2000.
109. A. K. Tripathi and R. Vinu, *Lubricants*, 2015, **3**, 54.
110. M. Carrott, K. Bell, J. Brown, A. Geist, C. Gregson, X. Héres, R. Malmbeck, C. Mason, G. Modolo, U. Mullich, M. Sarsfield, A. Wilden and R. Taylor, *Solv. Extr. Ion Exch.*, 2014, **32**, 447.
111. H. Zegota, Z. N. Schuchmann and C. Von Sonntag, *J. Phys. Chem.*, 1984, **88**, 5589.
112. A. Krestou and D. Panias, *Eur. J. Miner. Process. Environ. Protect.*, 2004, **4**, 113.
113. D. J. T. Hill, J. H. O'Donnell, P. O'Sullivan, P. J. Pomery and A. K. Whittaker, *J. Macromol. Sci. A: Chem.*, 1986, **23**, 403.
114. G. Dasmohapatra and T. Wolff, *J. Photochem. Photobiol. A: Chem.*, 1992, **62**, 209.
115. T. Takata, K. Ishibashi and W. Ando, *Tet. Lett.*, 1985, **26**, 4609.
116. F. G. Bordwell, *Acc. Chem. Res.*, 1988, **21**, 456.
117. F. G. Bordwell, J. E. Bares, J. E. Bartmess, G. J. McCollum, M. van der Puy, N. R. Varnier and W. S. Matthews, *J. Org. Chem.*, 1977, **42**, 321.
118. V. W.-W. Yam, C.-M. Che and W.-T. Tang, *J. Chem. Soc., Chem. Commun.*, 1988, 100.
119. G.-L. Liang, Y.Y.-Liu, L. Chen and H. J. Zhu, *Asian J. Chem.*, 2010, **22**, 7267.
120. K. A. Gardner, L. L. Kuehnert and J. M. Mayer, *Inorg. Chem.*, 1997, **36**, 2069.
121. S. Ni, M. E. Remaily and J. Franzén, *Adv. Synth. Catal.*, 2018, **360**, 4197.
122. K. K. Laali, M. Herbert, B. Cushnyr, A. Bhatt and D. Terrano, *J. Chem. Soc., Perkin Trans. 1*, 2001, 578.
123. F. A. Luzzio and W. J. Moore, *J. Org. Chem.*, 1993, **58**, 512.
124. Y. Hitomi, K. Arakawa and M. Kodera, *Chem. Commun.*, 2014, **50**, 7485.
125. S. Lai and D. G. Lee, *Tetrahedron*, 2002, **58**, 9879.
126. K. C. Hwang and S. Arunachalam, *Science*, 2014, **346**, 1495.
127. M. Eikawa and S. Sakaguchi, *J. Org. Chem.*, 1999, **64**, 4676.
128. S. Yamakazi, *Org. Lett.*, 1999, **1**, 2129.
129. Y. Watanabe, M. Ishimaru and S. Ozaki, *Chem. Lett.*, 1994, **23**, 2163.
130. L. C. Finney, L. J. Mitchell and C. J. Moody, *Green Chem.*, 2018, **20**, 2242.
131. G. L. Bykov and B. G. Ershov, *Radiochem.*, 2009, **51**, 292.
132. S. K. Hanson, R. Wu and L. A. Silks, *Angew. Chem. Int. Ed.*, 2012, **51**, 3410.
133. R. Ma, Y. Xu and X. Zhang, *ChemSusChem.*, 2015, **8**, 24.
134. G. M. Whitesides, M. Hackett, R. L. Brainard, J.-P. P. M. Lavalleye, A. F. Sowinski, A. N. Izumi, S. S. Moore, D. W. Brown and E. M. Staudt, *Organometallics*, 1985, **4**, 1819.
135. C. Aellig, C. Girard and I. Hermans, *Angew. Chem. Int. Ed.*, 2011, **50**, 12355.

136. X. Tian, F. Ren, B. Zhao, Y.-L. Ren, S. Zhao and J. Wang, *Chem. Commun.*, 2018, **106**, 44.
137. B. T. McGrail, L. S. Pianowski and P. C. Burns, *J. Am. Chem. Soc.*, 2014, **136**, 4797.
138. B. T. McGrail, G. E. Sigmon, L. J. Jouffret, C. R. Andrews and P. C. Burns, *Inorg. Chem.*, 2014, **53**, 1562.
139. S. O. Odoh and G. Schreckenbach, *Inorg. Chem.*, 2013, **52**, 5590.
140. G. M. Kramer, M. B. Dines, A. Kaldor, R. Hall and D. McClure, *Inorg. Chem.*, 1981, **20**, 1421.
141. G. A. Doyle, D. M. L. Goodgame, A. Sniden and D. J. Williams, *J. Chem. Soc., Chem. Commun.*, 1993, 1170.
142. G. H. John, I. May, M. J. Sarsfield, H. M. Steele, D. Collinson, M. Helliwell and J. D. McKinney, *Dalton Trans.*, 2004, 734.
143. D. Rose, Y.-D. Chang, Q. Chen and J. Zubieta, *Inorg. Chem.*, 1994, **53**, 5167.
144. M. C. Kirkegaard, A. Miskowiec, M. W. Ambrogio and B. B. Anderson, *Inorg. Chem.*, 2018, **57**, 5711.
145. S. G. Thangavelu and C. L. Cahill, *Inorg. Chem.*, 2015, **54**, 4208.
146. J. A. Ridenour and C. L. Cahill, *New. J. Chem.*, 2018, **42**, 1816.
147. J. Lee, I. J. T. Brewster, B. Song, V. M. Lynch, I. Hwang, X. Lib and J. L. Sessler, *Chem. Commun.*, 2018, **54**, 9422.
148. G. W. Breton and X. Vang, *J. Chem. Ed.*, 1998, **75**, 81.
149. A. B. Yusov and V. P. Shilov, *Russ. Chem. Bull.*, 2000, **49**, 285.
150. A. Ledwith, P. J. Russell and L. H. Sutcliffe, *Proc. R. Soc. Lond.*, 1973, **332**, 151.
151. B. Jezowska-Trzebiatowska and M. Chmielowska, *J. Inorg. Nucl. Chem.*, 1961, **20**, 106.
152. L. V. Kobets, N. G. Bend, N. M. Ksenofotova and D. S. Umbreko, *Radiokhim.*, 1986, **27**, 652.
153. G. I. Kobyshev and D. N. Suglobov, *Dokl. Akad. Nauk SSSR (Proc. USSR Acad. Sci.)*, 1956, **120**, 330.
154. K. Servaes, C. Hennig, I. Billard, C. Gaillard, K. Binnemans, C. Görller-Walrand and R. V. Deun, *Eur. J. Inorg. Chem.*, 2007, 5120.
155. F. Réal, V. Vallet, U. Wahlgren and I. Grenthe, *J. Am. Chem. Soc.*, 2008, **130**, 11742.
156. S. Hammerum, *J. Am. Chem. Soc.*, 2009, **131**, 8627.
157. E. R. Johnson and G. A. Dilabio, *Interdiscip. Sci. Comput. Life Sci.*, 2009, **1**, 133.
158. T. M. McCleskey, T. M. Foreman, E. E. Hallman, C. J. Burns and N. N. Sauer, *Environ. Sci. Technol.*, 2001, **35**, 547.
159. G. K. Oster and N.-L. Yang, *J. Phys. Chem.*, 1973, **77**, 2159.
160. D. G. Blackmond, *Angew. Chem. Int. Ed.*, 2005, **44**, 4302.
161. W. R. Dawson and M. W. Windsor, *J. Phys. Chem.*, 1968, **72**, 3251.
162. C. Lucks, A. Rossberg, S. Tsushima, H. Foerstendorf, K. Kahmy and G. Bernhard, *Dalton Trans.*, 2013, **42**, 13584.
163. F. G. Bordwell, J. Cheng, G. Z. Ji, A. V. Satish and X. Zhang, *J. Am. Chem. Soc.*, 1991, **113**, 9790.
164. B. Schweitzer-Chaput, A. Sud, Á. Pintér, S. Dehn, P. Schulze and M. Klussmann, *Angew. Chem. Int. Ed.*, 2013, **52**, 13228.
165. D. H. R. Barton and V. N. L. Gloahec, *Tetrahedron*, 1998, **54**, 15457.
166. P.-C. Li, T.-S. Wang, G.-H. Lee, Y.-H. Liu, Y. Wang, C.-T. Chen and I. Chao, *J. Org. Chem.*, 2002, **67**, 8002.
167. X. Huang and T. Zhang, *J. Org. Chem.*, 2010, **75**, 506.
168. E. Larionov, M. M. Mastandrea and M. A. Pericásm, *ACS Catal.*, 2017, **7**, 7008.
169. A. S. Larsen, K. Wang, M. A. Lockwood, G. L. Rice, T.-J. Won, S. Lovell, M. Sadilek, F. Turecek and J. M. Mayer, *J. Am. Chem. Soc.*, 2002, **124**, 10112.
170. J. R. Bryant and J. M. Mayer, *J. Am. Chem. Soc.*, 2003, **125**, 10351.
171. M. Curcio, S. Sproules, G. C. Lloyd-Jones and J. B. Love, *Inorg. Chem.*, 2018, **57**, 5915.
172. C. Arunkumar, Y.-M. Lee, J. Y. Lee, S. Fukuzumi and W. Nam, *Chem. Eur. J.*, 2009, **15**, 11482.
173. D. V. Avila, K. U. Ingold, A. A. D. Nardo, F. Zerbetto, M. Z. Zgierski and J. Lusztyk, *J. Am. Chem. Soc.*, 1995, **117**, 2711.

174. H. Wieland, *Chem. Ber.*, 1911, **44**, 2550.
175. D. E. Falvey, B. S. Khambatta and G. B. Schuster, *J. Phys. Chem.*, 1990, **94**, 1056.
176. W. R. Dolbier, *J. Fluorine Chem.*, 2005, **126**, 157.
177. X. Pan, H. Xia and J. Wu, *Org. Chem. Front.*, 2016, **3**, 1163.
178. C. Zhang, *Adv. Synth. Catal.*, 2014, **356**, 2895.
179. J. Yang, J. Hu, Y. Huang, X. Xu and F. Qing, *Chin. J. Chem.*, 2017, **35**, 867.
180. S. Barata-Vallejo, B. Lantaño and A. Postigo, *Chem. Eur. J.*, 2014, **20**, 16806.
181. G. Meißner, M. Feist, T. Braun and E. Kemnitz, *J. Organomet. Chem.*, 2017, **847**, 234.
182. Y. Zhang, M. Fujiu, H. Serizawa and K. Mikami, *J. Fluorine Chem.*, 2013, **156**, 367.
183. L. Gagliardi and B. O. Roos, *Nature*, 2005, **433**, 848.
184. H.-J. Tang, L.-Z. Lin, C. Feng and T.-P. Loh, *Angew. Chem. Int. Ed.*, 2017, **56**, 9872.
185. G. Schmitz, *Phys. Chem. Chem. Phys.*, 2010, **12**, 6605.
186. W. C. Bray and H. A. Liebhafsky, *J. Am. Chem. Soc.*, 1921, **53**, 38.
187. P. L. Arnold, A.-F. Pecharman, E. Hollis, A. Yahia, L. Maron, S. Parsons and J. B. Love, *Nat. Chem.*, 2010, **2**, 1056.
188. A. Schönberg, E. Singer, W. Stephan and W. S. Sheldrick, *Tetrahedron*, 1983, **39**, 2429.
189. S. K. Sahoo, *Tet. Lett.*, 2016, **57**, 3476.
190. R. Falkenstein, T. Mall, D. Speth and H. Stamm, *J. Org. Chem.*, 1993, **58**, 7377.
191. T.-A. D. Nguyen, A. M. Wright, J. S. Page, G. Wu and T. W. Hayton, *Inorg. Chem.*, 2014, **53**, 11377.
192. H. Lu, B. Zhao, D. Zhang, Y. Lv, B. Shi, X. Shi, J. Wen, J. Yao and Z. Zao, *J. Photochem. Photobiol. A: Chem.*, 2013, **272**, 1.
193. J. Luo, B. Hu, A. Sam and T. L. Liu, *Org. Lett.*, 2018, **20**, 361.
194. L. Gao, K. Kojima and H. Nagashima, *Tetrahedron*, 2015, **71**, 6414.

Chapter 4: Reductive Oxo-Group Functionalisation of the Uranyl(VI) Ion under Anaerobic Conditions

4.1 Introduction

As discussed in Section 1.2, the environmental mobility of $U^{VI}O_2^{2+}$ ions is affected by microbial and mineralogical reduction; Scheme 1.1.[1] In addition to fundamental academic curiosity (for example, of understanding why the reactivity of the inert uranyl-oxo groups differs from analogous group 6 oxo chemistry), $U^{V}O_2^{+}$ compounds are also known to inhibit the PUREX process by formation of oligomeric actinyl compounds.[2] Understanding the conditions under which $U^{V}O_2^{+}$ complexes react is therefore crucial to understanding, and hence improving, nuclear waste remediation processes.

4.1.1 Cation-Cation Interactions of the Uranyl(V) Ion

Oligomeric actinyl complexes commonly contain Lewis adduct interactions between the 'yl' oxo-groups, and the Lewis acidic actinide metal centres.[3] These interactions (sometimes but diminishingly referred to as cation-cation interactions, CCIs, in the literature) were first investigated in 1961 by Sullivan *et al*., on the effect that the presence of $Np^{V}O_2^{+}$ in acidic media has on the reduction of $U^{VI}O_2^{2+}$, by the formation of $[Np^{V}O_2^{+}\text{---}U^{VI}O_2^{2+}]$-containing complexes.[4]

Typically, $U^{V}O_2^{+}$ is used as a model for adducts between heavier, more radioactive actinyl ions, such as $Np^{V}O_2^{+}$, $Np^{VI}O_2^{2+}$, and $Pu^{VI}O_2^{2+}$ given uranium is less toxic and less radioactive than these elements. Common motifs adopted by complexes of $U^{V}O_2^{+}$ with other actinyl ions are depicted in Figure 4.1, along with an example, $[(U^{V}O_2(dbm))_2(\mu\text{-}K(py)_2)(\mu_8\text{-}K)]_2I_2{\cdot}2(py)$ (**4.A**), which is of one of several oligomeric complexes derived from $U^{V}O_2^{+}$ by Mazzanti *et al*.[5-8]

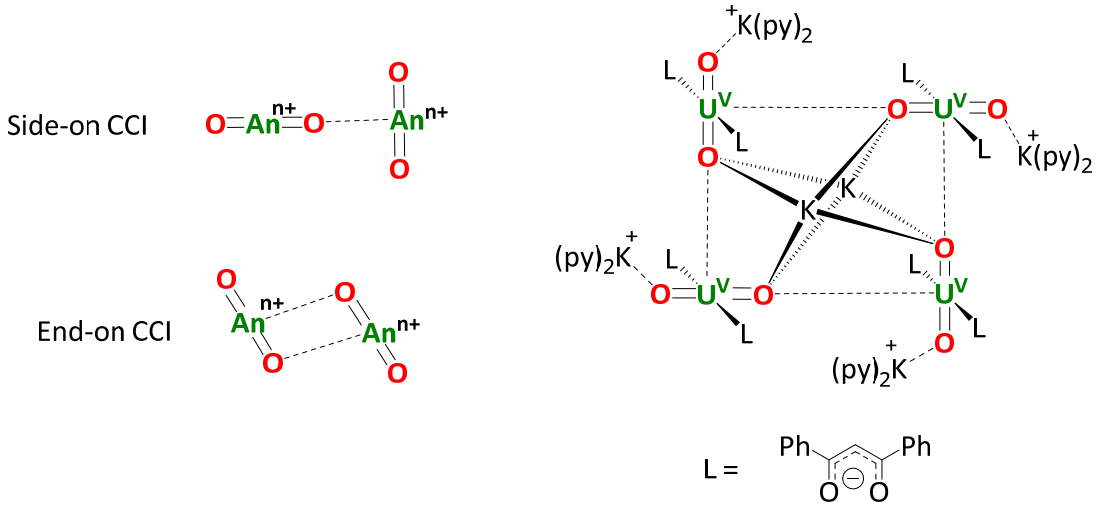

Figure 4.1 – (L) Diamond-shaped (side-on) or T-shaped (end-on) cation-cation interactions between $An^{V/VI}O_2^{n+}$ (An = U, n = 1; An = Np or Pu, n = 1 or 2), and (R) $[(U^{V}O_2(dbm))_2(\mu\text{-}K(py)_2)(\mu_8\text{-}K)]_2I_2{\cdot}2(py)$ (**4.A**) (dbm = dibenzoylmethanate).[5]

The reduction of $U^{VI}O_2^{2+}$ to $U^{V}O_2^{+}$ is concomitant with an increase in the Lewis basicity of the uranyl oxo-groups, promoting adduct formation, which is rare with $U^{VI}O_2^{2+}$. It is thought that the reaction of $U^{V}O_2^{+}$ in water may occur *via* oxo- or hydroxido-bridged uranyl dimers and incorporates numerous water, proton and electron transfer steps.[9, 10] Given their intolerance for aerobic conditions, however, complexes of $U^{V}O_2^{+}$ are poorly understood, and much work[11] has evolved in recent years to examine these complexes.

4.1.2 Uranyl(VI) to Uranyl(V) Oxo-Functionalisation

The decade to 2019 has seen the publication of several reviews examining uranyl-oxo functionalisation in some detail, including Baker,[12] Arnold *et al.*,[13] Hayton and Fortier,[14] and Kiplinger and Graves.[15] Developments since 2010 have also been reviewed and are currently in press.[16]

Oxo-group reductive functionalisation of the $U^{VI}O_2^{2+}$ ion is generally achieved in combination with the ligation (to $U^{VI}O_2^{2+}$) of strongly electron donating equatorial ligands, and oxophilic functionalising groups, factors that both weaken the otherwise chemically inert $U{=}O_{yl}$ bonds.[14] Examples of reductively oxo-functionalised complexes derived from the $U^{VI}O_2^{2+}$ ion include: oxo-borylation, with $B(C_6F_5)_3$ in $[U^{V}O(OB(C_6F_5)_3)(L^{pyrrin})]$ (**4.B**) and $[U^{V}O(OB(C_6F_5)_3)_2(L^{pyrrin})]$ (**4.C**) (L^{pyrrin} = a monoanionic dipyrrin ligand);[17] silylation with SiR_3 in $[U^{V}(OSiR_3)_2(^{Ar}acnac)_2][X]$ ($^{Ar}acnac$ = Ar*N*C(Ph)CHC(Ph)*O*, Ar = 3,5-$^{t}Bu_2$-C_6H_3; R = Ph, X = OTf[18] (**4.D.1**) or R = Et, X = $HB(C_6F_5)_3$ (**4.D.2**))[19] or $SiPh_3$ in $[U^{V}(OSiPh_3)_2(dbm)_2(OTf)]$[18] (**4.E**) and $SiMe_3$ in $[U^{V}(OSiMe_3)_2I_2(^{Ar}acnac)]$ (**4.F**);[20] combined oxo-silylation and -borylation in $[U^{V}(OB(C_6F_5)_3)(OSiR_3)(dbm)_2]$[21] (R = Et (**4.G.Et**) or Ph (**4.G.Ph**)) and $[U^{V}(OSiPh_3)(OB(C_6F_5)_3)(^{Ar}acnac)_2]$ (**4.H**);[22] and oxo-metalation, with Ti^{IV} in $[U^{V}O(OTiCp_2Cl)(L^{pyrrin})Cl]$[23]

(**4.I**), and Ln^{III} in $[(U^{V}O_2(py)_5)_2(Ln^{III}I_4)][I]$ (for Ln^{III} = Sm (**4.J.Sm**) or Dy (**4.J.Dy**)) or $[(U^{V}O_2I_4)(Sm^{III}(NCMe)_6)]_n$ (**4.K**).[24] Structures of these complexes are given below in Figure 4.2.

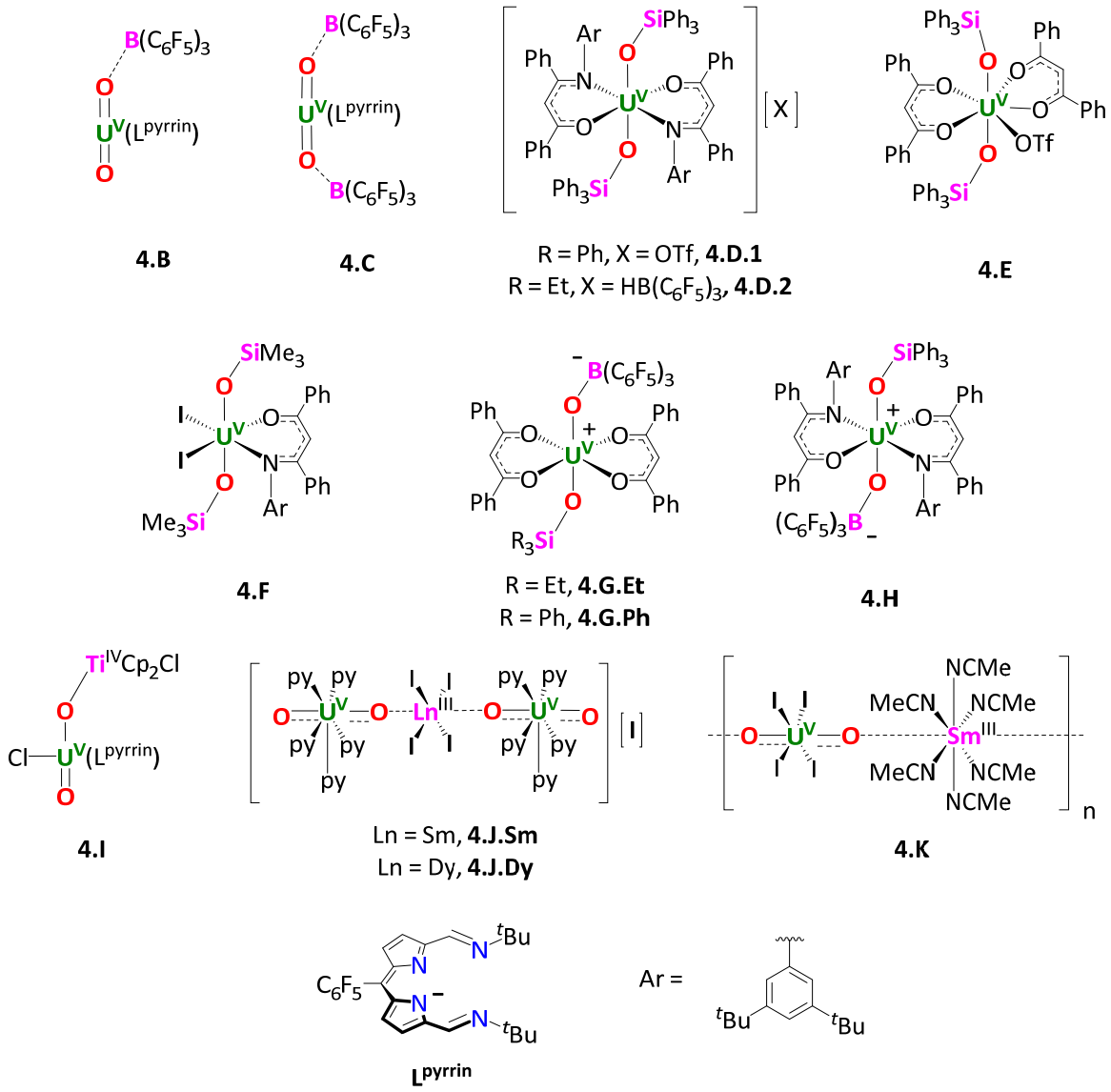

Figure 4.2 – Selected examples of reductively oxo-functionalised $U^{V}O_2^{+}$ complexes, with the functionalising atoms displayed in pink. py is pyridine, and n is an integer value.

In addition to these, the Arnold and Love groups have reported many examples of reductively oxo-functionalised complexes supported by a macrocyclic 'Pacman' ligand framework, Scheme 4.1.

4.1.3 Uranyl(VI) to Uranyl(V) Oxo-functionalisation with 'Pacman' Ligands

The 'Pacman' macrocyclic ligand framework, H_4L^{Me},[25] is a tetrapyrrolic, Schiff-base macrocycle capable of binding various metals through two separate dianionic N_4-donor pockets.[26] The resulting adduct from uranyl(VI) ion complexation ('mono-uranyl Pacman', $[(UO_2(solv))(H_2L^{Me})]$, solv = THF (**4.L.THF**) or py (**4.L.py**))[27] possesses a desymmetrised uranyl motif caused by H-bonding between the pyrrolic N-H protons of the vacant cleft and endogenous oxo-group. Together with the structural rigidity of the

macrocycle, this property has been used to promote unique reactivity at each oxo-group. Scheme 4.1, below, displays the orientation of both H_4L^{Me} and $[(UO_2(THF))(H_2L^{Me})]$ (**4.L.THF**).

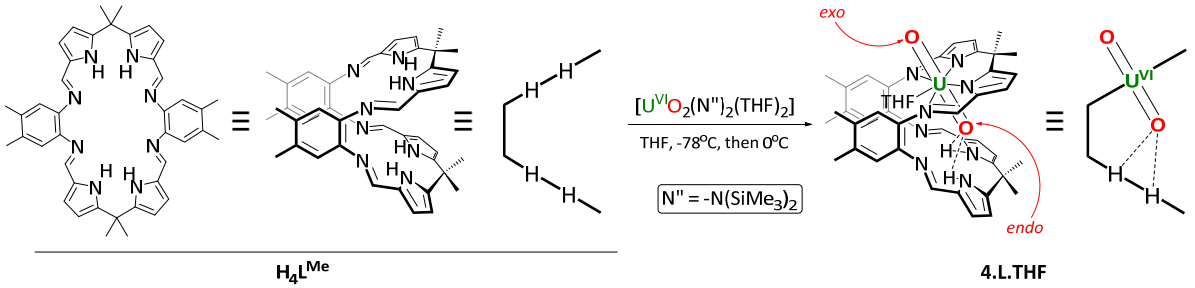

Scheme 4.1 – Structural representations of both H_4L^{Me} and $[(UO_2(THF))(H_2L^{Me})]$ (**4.L.THF**) with the positions of the *exo*- (‘*exo*-oxo’) or *endo*- (‘*endo*-oxo’) oxo atoms depicted. The desymmetrised uranyl(VI) ion is reflected in the bond lengths for these *exo*- and *endo*-oxo atoms in **4.L.THF**; $U–O_{exo}$ = 1.766(4) Å *vs*. $U–O_{endo}$ = 1.790(4) Å. Solvent molecules (py or THF) are omitted from the abbreviated form of $[(UO_2(THF))(H_2L^{Me})]$ (**4.L.THF**) on the RHS, for clarity.

Using this ‘Pacman’ ligand, Arnold and Love *et al*. have demonstrated that reductive oxo-functionalisation of $U^{VI}O_2^{2+}$ is feasible using elements from across the periodic table. Examples include $[(U^{V}O(OSiMe_2R)(THF))M^{II}_2X_2(L^{Me})]$ (M = Fe, X = I, R = Me (**4.M.Me**) or Ph (**4.M.Ph**); M = Zn, X = Cl (**4.N.Cl**) or I (**4.N.I**), R = Me);[28] $[(U^{V}O(OLi(solv)_3)(solv))(HL^{Me}Li)]$ (solv = THF (**4.O.THF**) or py (**4.O.py**));[29] $[(U^{V}O(OH)(py))(H_2L^{Me})]$ (**4.P**) and $[(U^{V}O(OSiR_3)(py))(H_2L^{Me})]$ (SiR_3 = $SiMe_3$ (**4.Q.1**); $SiMe_2{}^tBu$ (**4.Q.2**); SiH_2Ph (**4.Q.3**));[30] $[(U^{V}O_2)(L^{Me})(M(py)_2)]_2$ (**4.R.M**, where M = Y (**4.R.Y**) and Sm (**4.R.Sm**),[31] and Sc (**4.R.Sc**), Ce (**4.R.Ce**), Eu (**4.R.Eu**), Gd (**4.R.Gd**), Dy (**4.R.Dy**), Er (**4.R.Er**), Yb (**4.R.Yb**), Lu (**4.R.Lu**));[32] $[(U^{V}O(OSiR_3))_2(L^{Me})]$ (SiR_3 = $SiMe_3$ (**4.S.1**); $SiMe_2Ph$ (**4.S.2**));[33] $[(U^{V}O(OM(py)_2))_2(L^{Me})]$ (M = Li (**4.T.Li**), K (**4.T.K**));[34] $[(U^{V}O(OLi(py)_3))(L^{Me}Ln^{II}(py))(\mu\text{-}X)]$ (X = Cl, Ln = Y (**4.U.Cl-Y**), La (**4.U.Cl-La**), Sm (**4.U.Cl-Sm**), Dy (**4.U.Cl-Dy**); X = I, Ln = Y (**4.U.I-Y**), La (**4.U.I-La**), Sm (**4.U.I-Sm**), Dy (**4.U.I-Dy**));[32] $[(U^{V}O(OLi(py)_3))(U^{V}O(OSiMe)_3)(L^{Me})]$ (**4.V**), $[(U^{V}O(OSnR_3))_2(L^{Me})]$ (R = ^nBu (**4.W.^{n}Bu**), Ph (**4.W.Ph**)), $[(U^{V}O(OLi(py)_3))(U^{V}O(O^iPr))(L^{Me})]$ (**4.X**) and $[(U^{V}O(O^iPr))_2(L^{Me})]$ (**4.Y**);[35] $[(U^{V}O(py)(OAl(py)R_2))(H_2L^{Me})]$ (R = Me (**4.Z.Me**), ^{i}Bu (**4.Z.^{i}Bu**)), $[(U^{V}O(py)(OLi(py))(H_2L^{Me})]_2$ (**4.AA**), and $[(U^{V}O(py)(OM(py)_3))(H_2L^{Me})]$ (M = Li (**4.AB.Li**), Na (**4.AB.Na**), K (**4.AB.K**));[36] $[(U^{V}O(OZnX_2(py)_2))(HL^{Me}Zn(py))]$ (X = Cl (**4.AC.Cl**), I (**4.AC.I**)) and $[(U^{V}O(OMg(N'')(py)_2))(L^{Me}Mg(py))]$ (**4.AD**) (N'' = $-N(SiMe_3)_2$);[37] $[(U^{V}O(OAnCp_3))(H_2L^{Me})]$ (An = U (**4.AE.U**), Np (**4.AE.Np**));[38] and $[(U^{V}O(OMCp_2(solv)))(H_2L^{Me})]$ (M = Ti^{III}, solv = py (**4.AF.1**); M = Ti^{IV}, solv = C_6H_6 (**4.AF.2**); M = Zr^{IV}, solv = py (**4.AG**)) and $[(U^{V}O(OMX(py)_2))(H_2L^{Me})]$ (M = Mg, X = Cl (**4.AH**); M = Ca, X = I (**4.AI**); M = Zn, X = Cl (**4.AJ**)), and $[(U^{V}O(OM))(H_2L^{Me})]_6$ (M = Rb (**4.AK.Rb**), Cs (**4.AK.Cs**)).[39] These complexes are depicted in Scheme 4.2, along with the conditions for their synthesis. Performed thermally, these reactions involve reductive oxo-functionalisation of the uranyl(VI)-oxo ‘yl’ atoms with an oxophilic element, including metals from groups 1–4, aluminium, lanthanides or early actinides (U and Np), highlighting the potential interactions that uranyl-oxo groups may have with inorganic ions in nuclear wastes.[38]

For silicon, reaction of [(UO_2(THF))(H_2L^{Me})] (**4.L.THF**) with a uranyl silylamide, [$U^{VI}O_2$(N")$_2$(solv)$_2$] (N" = -N($SiMe_3$)$_2$, solv = THF (**4.AL.THF**) or py (**4.AL.py**); reaction vi in Scheme 4.2) led, unexpectedly, to the formation of a new $U^V_2O_4$ 'butterfly' structural motif, Figure 4.3.

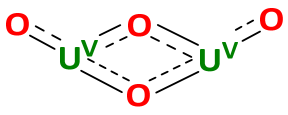

Figure 4.3 – The $U^V_2O_4$ 'butterfly' structural motif present in [($U^VO(OSiR_3)$)$_2$(L^{Me})] (**4.S.1** and **4.S.2**).

Although two proximal U^V centres normally disproportionate (to U^{VI} and U^{IV}), once silylated in [($U^VO(OSiR_3)$)$_2$(L^{Me})] (**4.S.1 and 4.S.2**) the two U^V centres do not react, even in the presence of strong oxidants such as I_2, [$Ce^{IV}(OTf)_4$] and [Fc][OTf] (Fc = ferrocenium, $FeCp_2^+$). This is despite the short $U^V\cdots U^V$ distances of 3.3557(5) and 3.3562(4) Å for compounds **4.S.1** and **4.S.2** respectively.[33] In contrast the K- and Li-functionalised analogues, **4.T.Li** and **4.T.K**, decompose immediately upon exposure to air,[34] suggesting that strongly oxophilic 'protecting' groups (*e.g.* Si) are required for redox inertness of uranium in this $U^V_2O_4$ 'butterfly' motif. The lithiated version, [($U^VO(OLi(py)_2)$)$_2$(L^{Me})] (**4.T.Li**) was however a valuable synthon from which carbon- and tin-oxo-functionalisation was possible (route x, compound **4.W**, and xii, compound **4.Y**; Scheme 4.2).[34, 35] Further exploration of the reactivity of this motif (*cf*. $U^V_2O_4$), along with attempted optimisations for its synthesis, are described in Section 4.2.

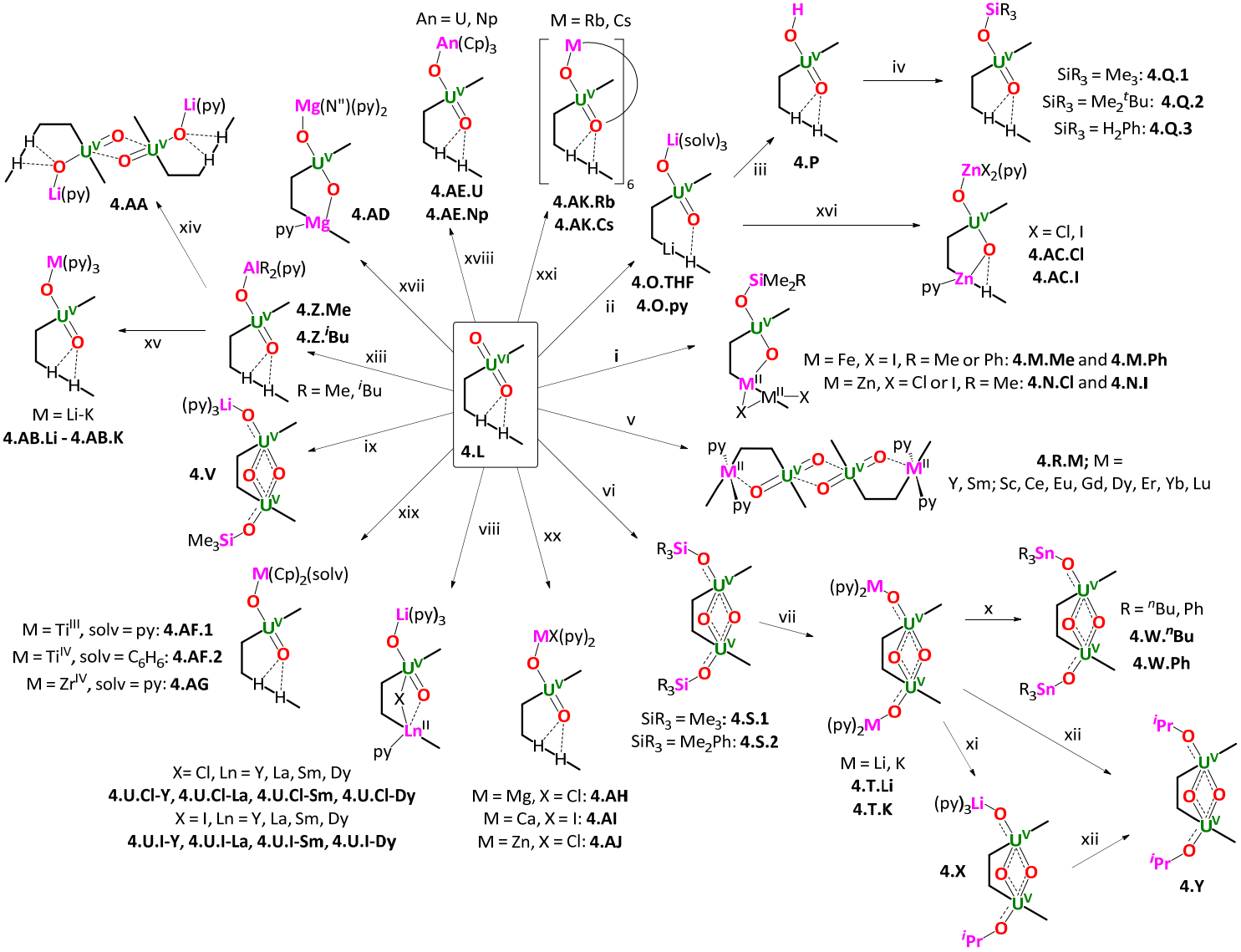

i: [K(N")], MX_2 (M = Fe, Zn; X = Cl, I) THF, -80°C
ii: 2LiR (R = H, $NiPr_2$, CPh_3, Cp), THF
iii: 2HCl, py, Et_2O
iv: $ClSiR_3$ (R = 3xMe; 2xMe, 1x^{t}Bu; 2xH, 1xPh), py
v: [$Sm^{II}(THF)_2(N")_2$] or [$Y^{III}(N")_3$], py
OR
[$Ln(N")_3$] (M = Sc, Ce, Eu, Gd, Dy, Er, Yb, Lu)
vi: 1.5[$U^{VI}O_2(N")_2(py)_2$], 120°C, py, 12 h
vii: 2K, then py-*N*-oxide, py, Δ
viii: [$Ln^{III}(N")_3$] (Ln = Y, La, Sm, Dy), then LiX (X = Cl, I), py
ix: [$Li(py)_2$][$U^{VI}O_2(N")_3$], py, 12h, Δ
x: [$ClSnR_3$] (R = ^{n}Bu, Ph), py
xi: [$TiCl(O^iPr)_3$], py, 6h
xii: excess [$TiCl(O^iPr)_3$], py, 4d
xiii: [$Cp_2TiCl(CH_2)(AlMe_2)$], C_6D_6, py, r.t.
OR
DIBAL-H, toluene, 70°C
xiv: LiMe, C_6D_6
xv: MH (M = Li-K), py
xvi: $2ZnX_2$ (X = Cl, I)
xvii: 2[$Mg(N")_2$], py, 80°C
xviii: [$AnCp_3$] (An = U, Np), THF
xix: M = Ti^{III}; [$Cp_2Ti(\eta^2\text{-}C_2(SiMe_3)_2)$], C_6H_6
M = Ti^{IV}; [$Cp_2TiCl]_2$, C_6H_6
M = Zr^{IV}; [Cp_2ZrCl_2], C_6H_6, r.t.
xx: 0.5MX_2 (M = Mg, X = Cl; M = Ca, X = I; M = Zn, X = Cl), py
xxi: M (M = Rb or Cs metal), py

Scheme 4.2 – Summary of reductive oxo-functionalisations of [(UO_2(solv))(H_2L^{Me})] (**4.L.THF and 4.L.py**) reported to date. Conditions on the RHS of the scheme are the conditions for synthesis (i-xxi) for each of the compounds, **4.L** through to **4.AK**. Functionalising atoms or groups are shown in pink, with solvent coordinated to the uranium in each case omitted for clarity. N" = -$N(SiMe_3)_2$.

4.1.4 Photochemical Reductive Functionalisation of the Uranyl(VI) Ion

To the best knowledge of the author no examples of the photochemical reductive oxo-group functionalisation of the uranyl(VI) are known in the literature. However, a small number of investigations into the photochemical production of uranium(V) and (IV) from $U^{VI}O_2^{2+}$-containing compounds are known, often occurring under anaerobic conditions.

For example, on photolysing (> 405 nm) a solution of $[U^{VI}O_2Cl_2(py)_2]$ in anhydrous ethanol, Sostero *et al*. were able to detect $[U^{V}OCl_3]$ (**4.AM**).[40] Folcher *et al*. later reported the synthesis of a U^{V}-crown ether complex, $[U^{V}O(18\text{-c-}6)][ClO_4]_3$ (**4.AN**; 18-c-6 = 18-crown-6), from the photolysis (254 nm) of $[U^{VI}O_2(18\text{-c-}6)][ClO_4]_2$ in anoxic CH_3CN.[41] While both these reports identified U^{V} as the final uranium oxidation state, the products were not well defined and the authors relied solely on IR spectroscopy and elemental analysis to provide characterisation of the products. More recent reports, for example by Duval *et al*., have postulated products of uranyl(VI) photoreduction after photolysis. These include $[U^{IV}(OR)_2(OPPh_3)_4][OTf]_2$ (R = Me (**4.AO.Me**) or Et (**4.AO.Et**)), which is reversibly obtained from the photolysis (254 nm) of $[U^{VI}O_2(OPPh_3)_4][OTf]_2$ in methanol (R = Me) or ether/CH_3CN (R = Et),[42] and $[U^{IV}F_2(dppmo)_3]$ (**4.AP**) (dppmo = diphenylphosphinomethylene oxide, $Ph_2P(O)CH2P(O)Ph_2$), which is obtained from the photolysis (254 nm) of $[U^{VI}O_2(dppmo)_2(OPPh_3)][BF_4]_2$ in methanol.[43] These results may be questionable, however, particularly in light of other reports by the Duval group[44] which have previously been challenged.[45] These complexes are depicted in Scheme 4.3, below.

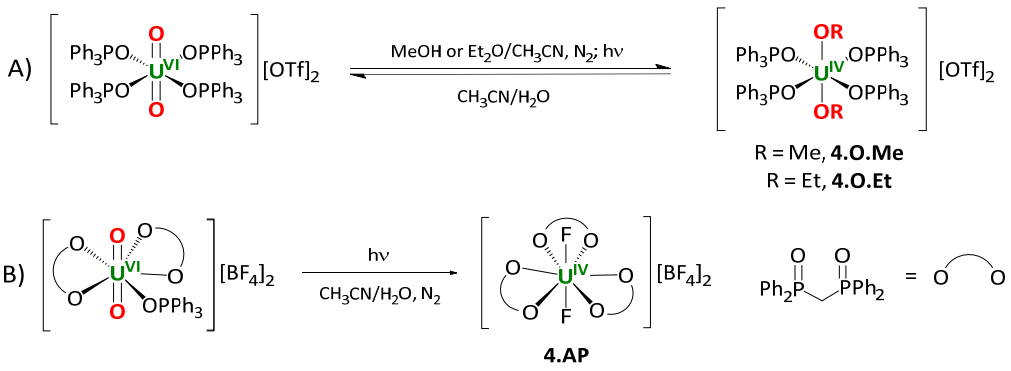

Scheme 4.3 – Examples of well-defined uranium complexes resulting from photoreduction of $U^{VI}O_2^{2+}$, reported by Duval *et al*. Top, $[U^{IV}(OR)_2(OPPh_3)_4][OTf]_2$ (**4.AO.Me** and **4.AO.Et**); bottom, $[U^{IV}F_2(dppmo)_3]$ (**4.AP**). Equation B) features ligand redistribution steps, which are omitted for clarity. The assignment of the U^{IV} oxidation state in **4.O.Me** and **4.O.Et** arises from SCXRD and charge balance.

For all four compounds ($[U^{V}OCl_3]$ (**4.AM**), $[U^{V}O(18\text{-c-}6)][ClO_4]_3$ (**4.AN**), $[U^{IV}(OR)_2(OPPh_3)_4][OTf]_2$ (**4.AO.Me** and **4.AO.Et**) and $[U^{IV}F_2(dppmo)_3]$ (**4.AP**)) one or both of the uranyl-oxo groups has been substituted, in line with reports that photo-induced oxo-atom exchange is very rapid.[46] More recently, Mazzanti *et al*. have reported the isolation of a mixed $U^{VI}O_2^{2+}/U^{V}$ cluster derived from the photolysis

(254 nm) of $[U^{VI}O_2(NO_3)_2(OH_2)_{1.5}]$ and potassium benzoate in anhydrous pyridine.[47] The structure of this cluster, $[U^{V}(U^{VI}O_2)_5(\mu_3\text{-}O)_5(C_6H_5COO)_5(py)_7]$ (**4.AQ**) is shown below in Scheme 4.4.

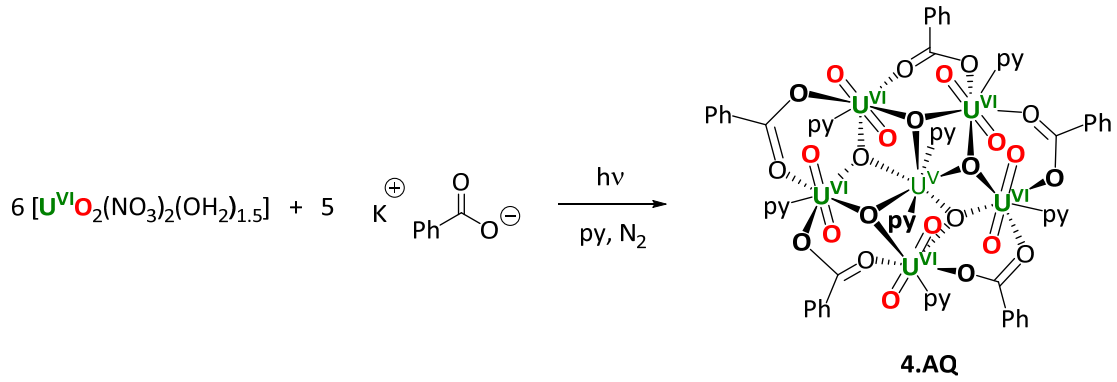

Scheme 4.4 – Synthesis of $[U^{V}(U^{VI}O_2)_5(\mu_3\text{-}O)_5(C_6H_5COO)_5(py)_7]$ (**4.AQ**), reported by Mazzanti *et al.*[47]

This complex, **4.AQ**, was the first example of the isolation of a U^{V}-containing complex from a $U^{VI}O_2^{2+}$ starting material by photolysis, studied by the authors as a potential intermediate in the photolytic reduction of $U^{VI}O_2^{2+}$ ions in anaerobic conditions. The photolytic production of $U^{V}O_2^{+}$ in the environment plays an important role in the formation of actinide-oxo clusters.[48]

4.1.5 Overview of Chapter 4

In order to investigate the anaerobic reactivity of the $U^{VI}O_2^{2+}$ ion in more detail, particularly with regards to reductive oxo-functionalisation, two avenues were pursued.

The first section of this chapter describes efforts towards a straightforward, *thermal* synthesis of $[(U^{V}O(OM(py)_2))_2(L^{Me})]$ (**4.T**), which were targeted in a series of test reactions to explore the reactivity of the asymmetry of the uranyl(VI) ion in the 'Pacman' framework and the unusual stability of the $U^{V}_2O_4$ butterfly core in more detail. The synthetic usefulness of the lithiated $U^{V}_2O_4$ species, $[(U^{V}O(OLi(py)_2))_2(L^{Me})]$ (**4.T.Li**), has been demonstrated (routes x–xii, Scheme 4.2) in accessing numerous other functionalised $U^{V}_2O_4$ analogues. The potassium-functionalised analogue, **4.T.K**, has longer metal-oxo ($U{=}O_{yl}\cdots K$) bond lengths than **4.T.Li** and may therefore have unique reactivity. Potential routes leading to the simple synthesis of $[(U^{V}O(OK(py)_2))_2(L^{Me})]$ (**4.T.K**) are discussed.

The second section of this chapter is concerned with the *photo*-reactivity of $U^{VI}O_2^{2+}$-containing molecules, under anaerobic conditions, a subject targeted to address the paucity of well-characterised U^{V} complexes in the literature, particularly those derived from photoreduction of $U^{VI}O_2^{2+}$-containing precursors. Reactions discussed include photochemical oxo-group functionalisation of $[(UO_2(THF))(H_2L^{Me})]$ (**4.L.THF**), building on the wide large number of reactions this molecule can

undertake (Scheme 4.2). Continuing the anaerobic reactivity of the uranyl(VI) ion discussed in Section 3.6, the reactivity of $\mathbf{U^{tetNO3}}$ with non-hydrocarbon containing substrates is also expanded.

4.2 Synthesis of $[(U^{V}O(OK(py)_2))_2(L^{Me})]$, **4.T.K**

4.2.1 Exploratory Test Reactions

In an effort to develop a simple synthesis of a functionalised $U^{V}_2O_4$ bis(uranyl(V)) core, the direct reaction of $[K][U^{VI}O_2(N'')_3]$ (**4.AR**) with H_4L^{Me} was undertaken to circumvent the complex and multistep synthetic route to $[(U^{V}O(OLi(py)_2))_2(L^{Me})]$ (**4.T.Li**), as outlined in routes vi and vii in Scheme 4.2. This is summarised in Figure 4.5, below. As a one-pot route to $[(U^{V}O(OLi(py)_2))_2(L^{Me})]$ (**4.T.Li**) is known,[34] this approach was optimised here by reacting two equiv. of the uranyl silylamide, $[K][U^{VI}O_2(N'')_3]$ (**4.AR**) with H_4L^{Me} in C_5D_5N (< 2 mL; Teflon-tapped NMR tube) under reflux in an inert atmosphere.

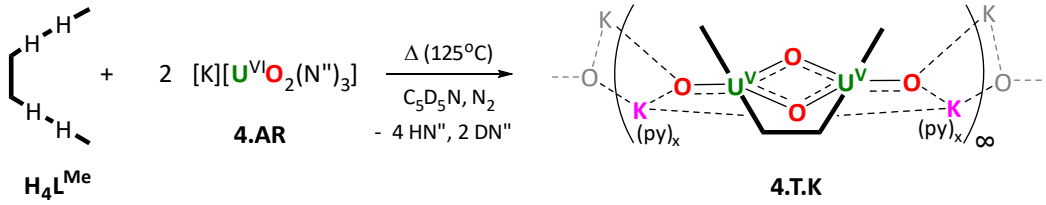

Scheme 4.5 –Procedure for the synthesis of $[(U^{V}O(OK(py)_2))_2(L^{Me})]$ (**4.T.K**). The structure is tentatively assigned based on the crystallographically-characterised structure isolated by Arnold *et al.*,[34] given in Figure 4.4. x is an integer value.

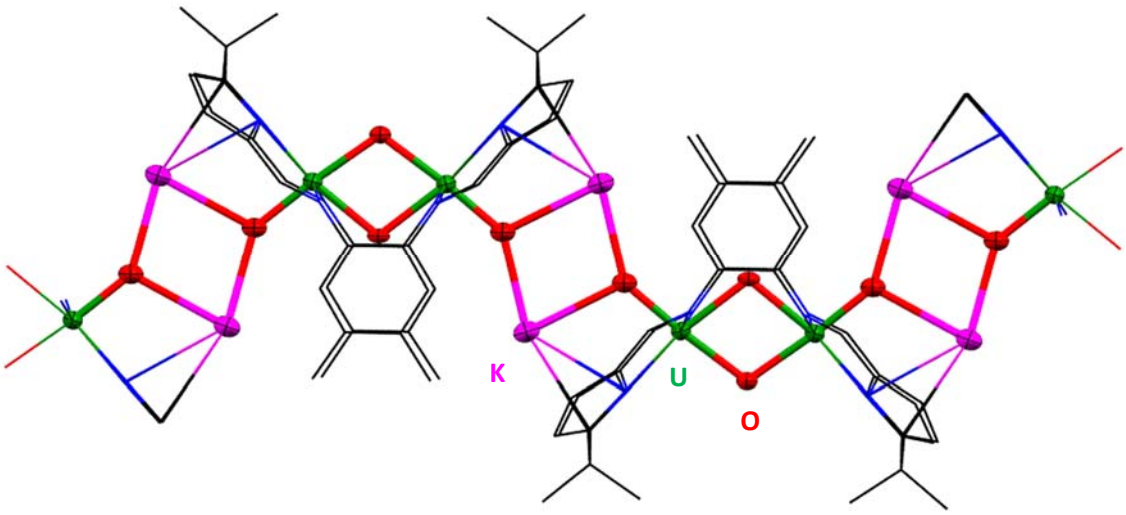

Figure 4.4 – Structure of $[(U^{V}O(OK(py)_2))_2(L^{Me})]$ (**4.T.K**) isolated by Arnold *et al.*[34] Key: uranium, oxygen, nitrogen, carbon, potassium. Coordinated pyridine molecules are omitted for clarity and ellipsoids are drawn at 50% probability.

The assignment of the structure of $[(U^{V}O(OK(py)_2))_2(L^{Me})]$ (**4.T.K**) is based on the ^{1}H NMR spectroscopic resonances observed for this reaction (Scheme 4.5), which were identical to those reported by Arnold *et al.*[34] Experiments to further confirm identity of the product by CHN microanalysis, IR spectroscopy and ESI- or APPI-MS were unsuccessful, yielding inconsistent results.

Reaction progress monitored by ^{1}H NMR spectroscopy suggested that the thermal reduction of two equiv. of $U^{VI}O_2^{2+}$ to $U^V_2O_4$ (*e.g.* **4.AR** → **4.T.K**, Scheme 4.5) requires prolonged reflux (days) of the reaction solution; only minor (< 5%) conversion was observed after 12 hours at 125°C. This is in contrast to the synthesis of $[(U^VO(OK(py)_2))_2(L^{Me})]$ (**4.T.K**) from $[(U^VO(OSiMe_3))_2(L^{Me})]$ (**4.S.1**) which required only 12 hours of refluxing with potassium metal, reported by Arnold *et al*.[34] Resonances corresponding to the starting H_4L^{Me} material only disappeared after 10 days of reflux. However, prolonged heating (15 days) led to a notable increase in the number of resonances observed in the resulting ^{1}H NMR spectrum of the reaction mixture, suggesting product decomposition. Heating is also required for $U^{VI}O_2^{2+}$ reduction; a reaction mixture stored in the dark for 40 days at r.t. showed only ^{1}H NMR spectroscopic resonances that corresponded to unreacted starting materials. Lower temperatures (50 or 100°C for 10 days) resulted in lower *in-situ* conversions (*ca*. 7% and 11%, respectively) than *in-situ* conversion (*ca*. 30%) for the reaction refluxed for 125°C for 10 days, and no evidence of silylated products, *e.g.* $[(U^VO(OSiMe_3))_2(L^{Me})]$ (**4.S.1**), was observed by ^{1}H NMR spectroscopy for any of the reactions described.

The aggressive conditions (10 days, refluxing pyridine) required here suggest there is a significant barrier to the formation of the $U^V_2O_4$ motif directly from H_4L^{Me}. This is in contrast to the formation of $[(U^VO(OSiMe_3))_2(L^{Me})]$ (**4.S.1**) prepared from the preformed complex $[U^{VI}O_2(THF)(H_2L^{Me})]$ (**4.L.THF**) reported by Arnold *et al.* (12 hours, refluxing pyridine).[34] As formation of $[(UO_2(THF))(H_2L^{Me})]$ (**4.L.THF**) occurs spontaneously at -78°C (Scheme 4.1), the key step for this reaction is either reduction of the $U^{VI}O_2^{2+}$ group in $[(UO_2(THF))(H_2L^{Me})]$ (**4.L.THF**) to U^V (unlikely, given the r.t. formation of $[(U^VO(py)(OAl(py)Me_2))(H_2L^{Me})]$ (**4.Z.Me**) from $[(UO_2(THF))(H_2L^{Me})]$ (**4.L.THF**) and $[Cp_2TiCl(CH_2)(AlMe_2)]$])[36] in route xiii, Scheme 4.2), or accommodation of two uranyl ions into the H_4L^{Me} framework. This ligand, H_4L^{Me}, is known to be too small to accommodate two linear $U^VO_2^+$ or $U^{VI}O_2^{2+}$ units,[49] meaning the uranyl 'yl' oxo-groups must rearrange to form the $U^V_2O_4$ motif and it is likely that this oxo-group rearrangement is the key step for the formation of the $U^V_2O_4$ motif directly from H_4L^{Me}.

4.2.2 Synthesis of $[(U^VO(OK(py)_2))_2(L^{Me})]$ (4.T.K) in the Presence of 18-c-6

The attempted synthesis of $[(U^VO(OK(py)_2))_2(L^{Me})]$ (**4.T.K**) outlined in Scheme 4.5 leads to a significant amount of intractable brown precipitate, previously characterised by Arnold *et al*.[33] as variously oxo-functionalised uranyl(VI) and uranyl(V)-containing 'Pacman' oligomers. Given that the formation of these oligomers consumes H_4L^{Me} starting material (that would be used to form $[(U^VO(OK(py)_2))_2(L^{Me})]$ (**4.T.K**)), strategies that focus on de-oligomerising (and thus decomplexing) these unwanted by-products should enable more H_4L^{Me} to be present in solution, in turn increasing the *in-situ* yields of $[(U^VO(OK(py)_2))_2(L^{Me})]$ (**4.T.K**), which are poor at *ca*. 30% by ^{1}H NMR spectroscopy.

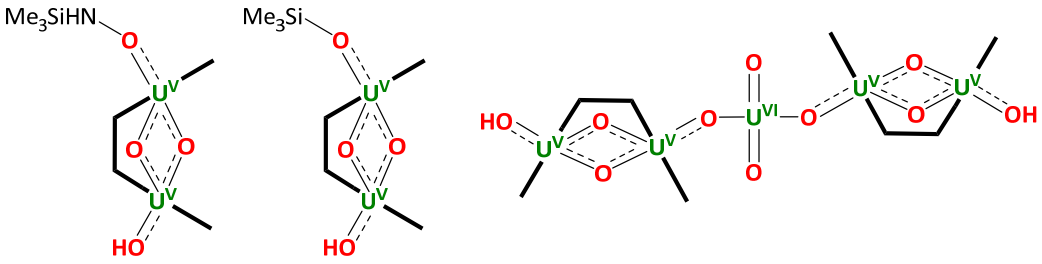

Figure 4.5 – Selected structures of solids derived from the isolation of $[(U^{V}O(OSiMe_3))_2(L^{Me})]$ (**4.S.1**), and detected by mass spectrometry by Arnold *et al.*[33]

Therefore, to favour formation of $[(U^{V}O(OK(py)_2))_2(L^{Me})]$ (**4.T.K**) over these insoluble, unwanted by-products (Figure 4.5), 18-crown-6 (18-c-6) was added alongside the reagents described in Scheme 4.5, and the reaction repeated under analogous conditions. It was envisaged that addition of 18-c-6 may aid in the fragmentation of K-templated uranyl-'Pacman' oligomeric intermediates and by-products (Figure 4.5, above), which would increase the concentration of $U^{VI}O_2^{2+}$ available for the successful formation of $[(U^{V}O(OK(py)_2))_2(L^{Me})]$ (**4.T.K**), thus increasing *in-situ* yields. Scheme 4.6, below, outlines the reaction of 2 equiv. of $[K][U^{VI}O_2(N'')_3]$ (**4.AR**) and 18-c-6 with H_4L^{Me} in refluxing C_5D_5N.

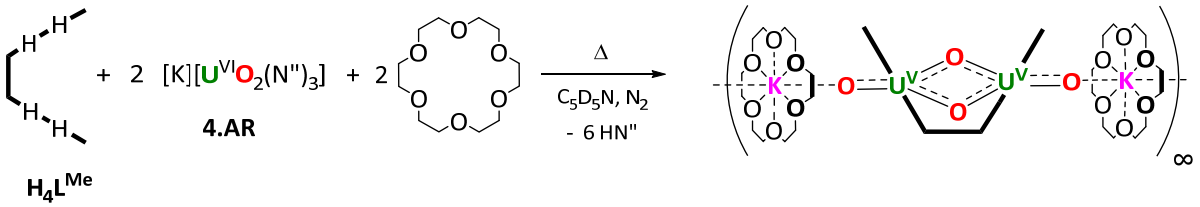

Scheme 4.6 – General procedure for the reaction between 18-c-6, $[K][U^{VI}O_2(N'')_3]$ (**4.AR**), and H_4L^{Me}, along with the hypothesised product.

On the basis of ^{1}H NMR spectroscopic resonances, the major product is structurally related to $[(U^{V}O(OK(py)_2))_2(L^{Me})]$ (**4.T.K**), described in Section 4.2.1 above. The ^{1}H NMR spectra of $[(U^{V}O(OK(py)_2))_2(L^{Me})]$ (**4.T.K**), and $[(U^{V}O(OK(py)_2))_2(L^{Me})]$ (**4.T.K**) synthesised in the presence of 2 equiv. of 18-c-6 are displayed in Figure 4.6, below.

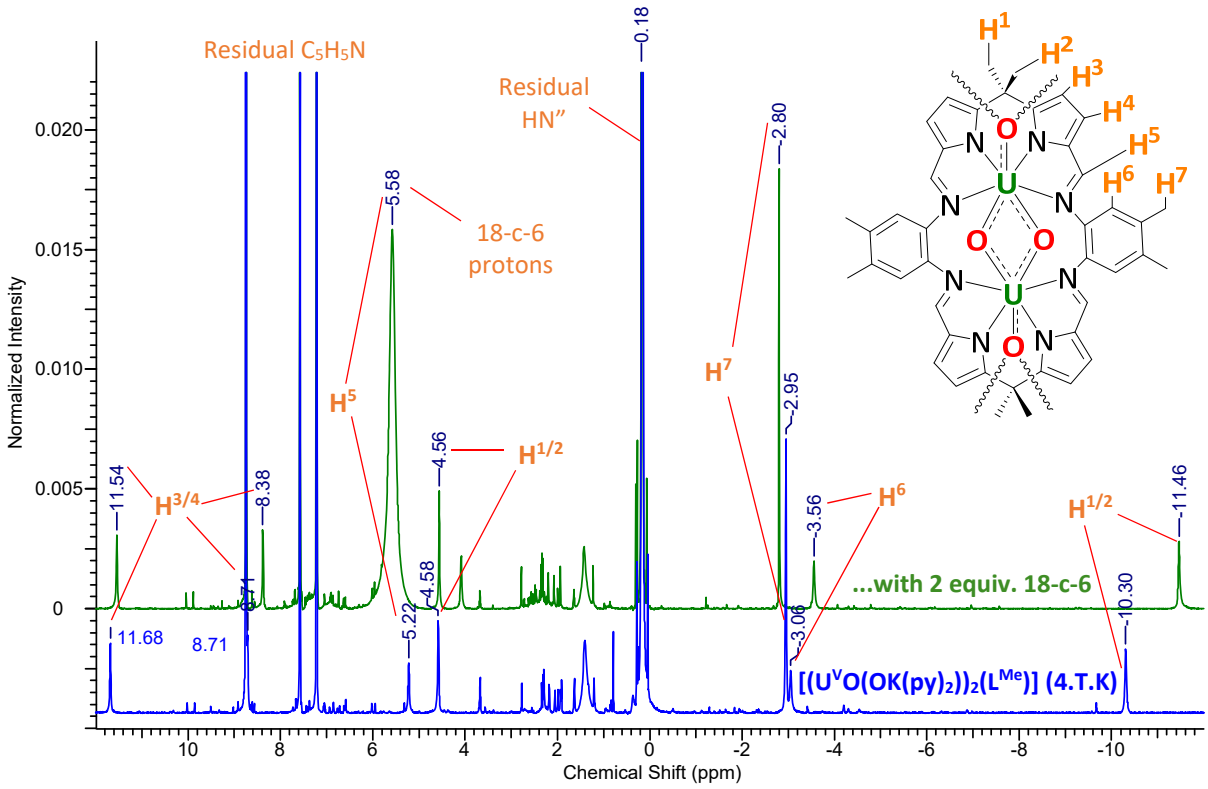

Figure 4.6 – ^{1}H NMR spectra of $[(U^{V}O(OK(py)_2))_2(L^{Me})]$ (**4.T.K**; Scheme 4.5) and the crown-chelated derivative discussed above in Scheme 4.6. A representation of the core structure in both cases is given along with highlighted protons. Solvating pyridine molecules and potassium ions are removed for clarity.

By adding 18-c-6 the *in-situ* yield of $[(U^{V}O(OK(py)_2))_2(L^{Me})]$ (**4.T.K**) increased from *ca*. 30% to 40%, measured by ^{1}H NMR spectroscopy using residual C_5H_5N as the reference. The addition of compounds, such as 18-c-6, to de-oligomerise K- (or other metal-)templated intermediate oligomers may therefore prove useful in increasing *in-situ* yields further but due to the low increase in *in-situ* yield (and overall disappointing yield, < 40%), this was not pursued further. Addition of excess Me_3SiCl resulted in dissolution of all precipitates and ^{1}H NMR spectroscopic resonances consistent with $[(U^{V}O(OSiMe_3))_2(L^{Me})]$ (**4.S.1**).[33]

4.2.3 Isolation of a U^{VI}/U^{V} Intermediate

Evidence that may highlight a potential intermediate in the formation of $[(U^{V}O(OK(py)_2))_2(L^{Me})]$ (**4.T.K**) was obtained by single crystal X-ray diffraction. The structure shown in Figure 4.7, below, is a U^{V}/U^{VI} dimer, incorporating two $[L^{Me}]^{4-}$ units, charge-balancing K^{+} ions and numerous coordinated pyridine solvent molecules. The crystal structure was obtained by SCXRD on a dark brown single crystal, isolated from the reaction solution of 2 equiv. of $[K][UO_2(N'')_3]$ (**4.AR**) and H_4L^{Me} in C_5D_5N, at 125°C after 2 days. The crystal selected was grown by vapour diffusion of hexanes into this solution under an inert atmosphere in the glove box over 2 weeks at r.t.

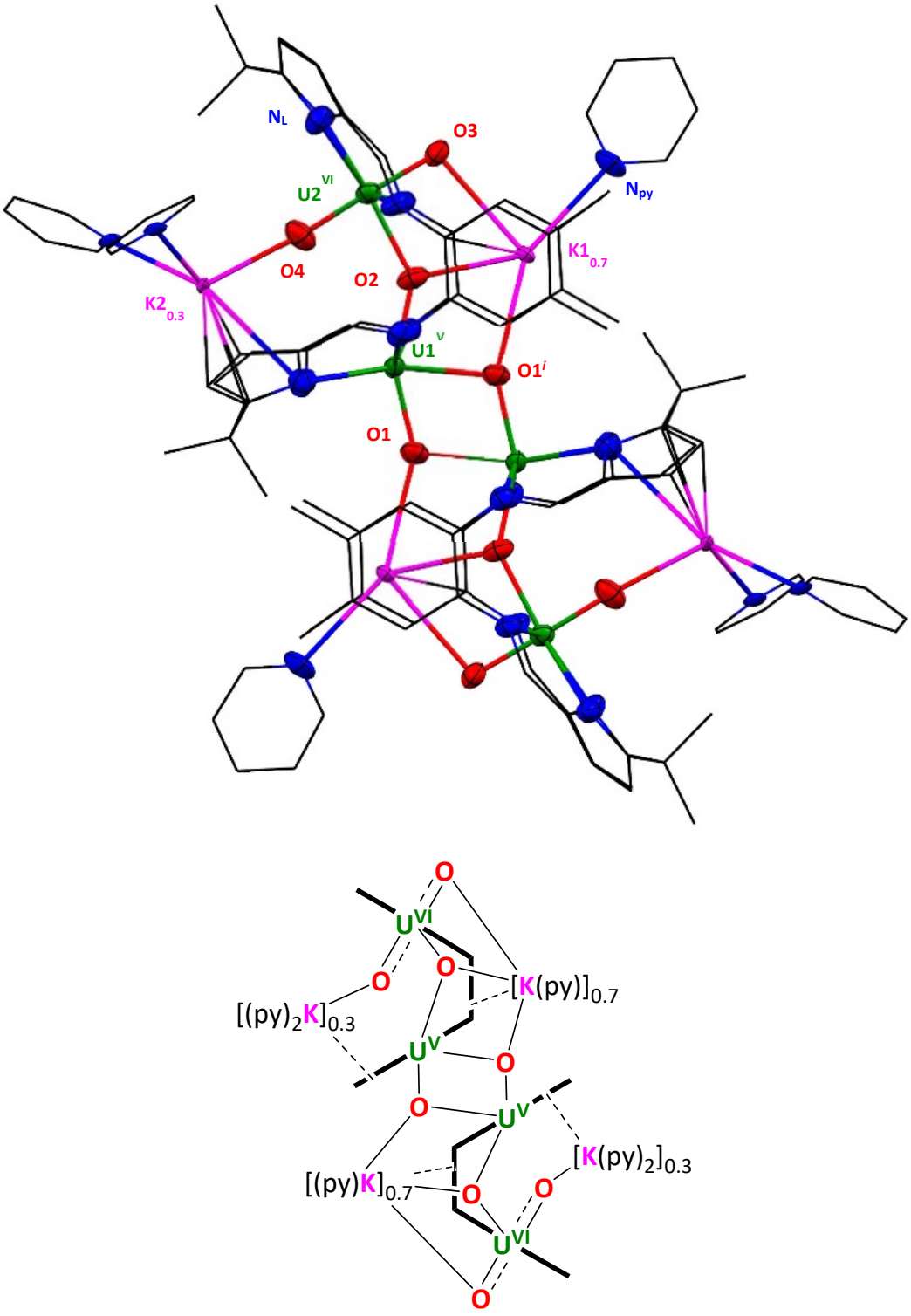

Figure 4.7 – Top, thermal ellipsoid plot (50% probability) of the tetranuclear U^{VI}/U^{V} dimer, $[(K(py))_{0.7}]_2[(K(py)_2)_{0.3}]_2[(U^{VI}O_2)(U^{V}O_2)(L^{Me})]_2$ (**4.1**), with H-atoms omitted for clarity. Bottom, simplified graphic to highlight key bonds of comples **4.1**, with dashed lines from the K^+ ions to the emboldened macrocyclic framework representing π-cation interactions. Key: uranium, oxygen, nitrogen, carbon, potassium.

Distances			Angles	
Atom 1	**Atom 2**	**Distance/Å**	**Atoms**	**Angle/°**
$U2^{VI}$	-O2	2.161(7)	O4-$U2^{VI}$-O3	178.85(7)
	-O3	1.799(8)	O1-$U1^{V}$-O2	155.83(6)
	-O4	1.797(8)	$K2_{0.3}$-O4-$U2^{VI}$	173.92(5)
	-N_L	2.446(7)-2.597(6)	$U2^{VI}$-O2-$U1^{V}$	140.83(6)
$U1^{V}$	-O1	2.003(7)	O1-$U1^{V}$-$O1^{i}$ *and* O2-$U1^{V}$-$O1^{i}$	71.98(7) *and* 83.17(5)
	-$O1^{i}$	2.314(8)	O4-$U2^{VI}$-O2 *and* O3-$U2^{VI}$-O2	86.17(5) *and* 92.68(5)
	-O2	2.039(5)		
	-N_L	2.529(7)-2.602(8)		
$K1_{0.7}$	-O1/$O1^{i}$	2.815(7)		
	-O2	2.626(9)		
	-O3	3.042(8)		
	-arene (avg.)	3.542		
	-N_{py}	2.813(6)		
$K2_{0.3}$	-O4	2.480(7)		
	-pyrrole (avg.)	3.173		
	-N_{py}	2.767(8), 2.902(7)		

Table 4.1 – Key parameters (bond lengths/Å, angles/°) for $[(K(py))_{0.7}]_2[(K(py)_2)_{0.3}]_2[(U^{VI}O_2)(U^{V}O_2)(L^{Me})]_2$ (**4.1**).

The assignment of a U^{VI}/U^{V} dimer complex arises from U-O bond lengths and angles, and charge balance. While U1 (U^{V}) has U-O bond lengths of 2.003(7) and 2.039(5) Å and ∠(OUO) = 155.83(6)°, U2 (U^{VI}) has U-O bond lengths of 1.797(8) and 1.799(8) Å and ∠(OUO) = 178.85(7)°, which are more consistent with *ca*. 1.70–1.80 Å and ∠(OUO) ≈ 180° for other $U^{VI}O_2^{2+}$-containing molecules.[16] Further, the two N_4-donor clefts of L^{Me} are dianionic upon deprotonation, making the '$(U^{V}O_2)(U^{VI}O_2)(L^{Me})$' unit monoanionic. This is counterbalanced by incorporation of one K^+ ion per macrocycle, which are ligated by K-O Lewis adducts, π-cation interactions and pyridine solvent molecules, and are distributed unequally across two sites in the crystal structure (70% and 30% occupation for K1 and K2, respectively). As this complex (**4.1**) was isolated from the H_4L^{Me}/[K][$UO_2(N'')_3$] (**4.AR**) reaction after only two and not ten days (the time required for consumption of starting materials), it is speculated that the structure shown in Figure 4.7, complex **4.1**, is a precursor to $[(U^{V}O(OK(py)_2))_2(L^{Me})]$ (**4.T.K**). The presence of U^{VI} suggests that the complex has not yet fully reduced, and that the $U^{V}_2O_4$ core has not fully formed, with one bridging oxo-group, O2, present. The parameters for this U^{VI}-O-U^{V} unit ($U2^{VI}$-O2 = 2.161(7) Å, $U1^{V}$-O2 = 2.039(5) Å, ∠($U^{VI}OU^{V}$) = 140.83(6)°) are comparable to other bridging oxo-groups in U^{VI}/U^{V} complexes, including the crystallographically-characterised [($U^{VI}O_2$)(μ-O-U^{V}O)(μ-Cl)(BIPMH)$_2$] (**4.AS**) complex (BIPMH = HC-(PPh_2NSiMe_3; U^{VI}-O = 2.315(5) Å, U^{V}-O = 1.932(3) Å, ∠($U^{VI}OU^{V}$) = 126.4(2)°),[50] or the computed structure of the U^{VI}/U^{V} complex [(THF)(OU^{VI})(μ-

O)($U^{V}O(SiMe_3)$)(THF)(L^{Me})] (**4.AT**), with the U^{VI}-O bond length in the U^{VI}-O-U^{V} unit calculated at 2.001(2) Å.[51]

Scheme 4.7, below, is a proposed mechanism for the formation of the complex **4.1**, from two equiv. of [K][$UO_2(N'')_3$] (**4.AR**) and one equiv. of H_4L^{Me}, in C_5D_5N.

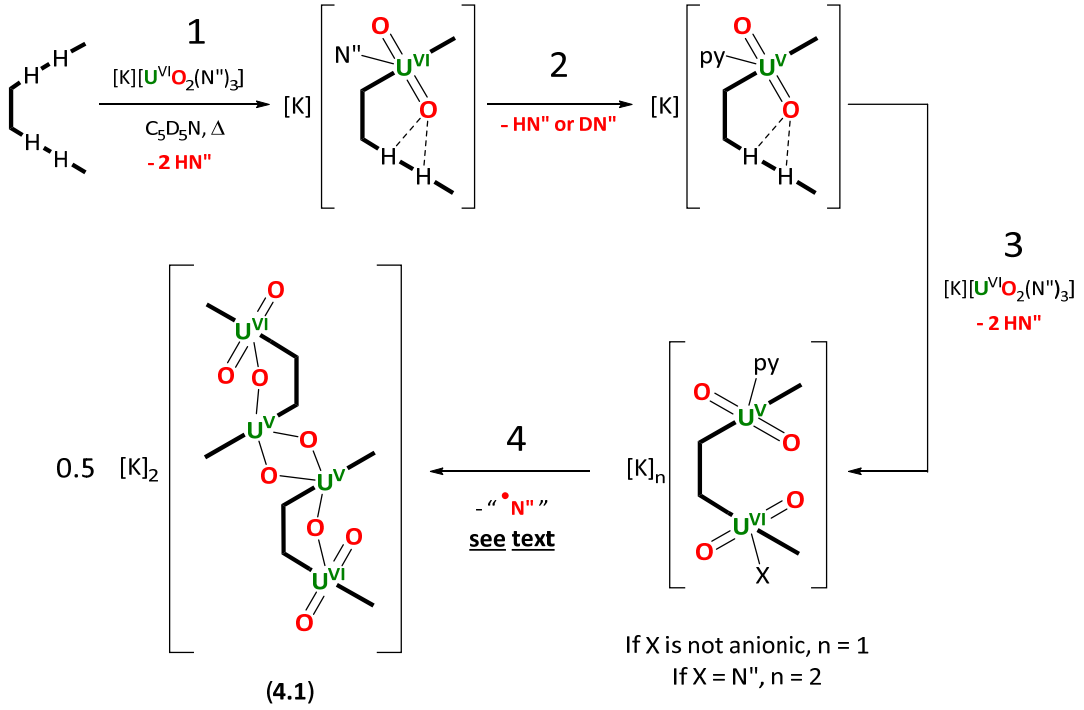

Scheme 4.7 – Hypothesised scheme for the formation of complex **4.1**. Step 1 represents complexation of $U^{VI}O_2^{2+}$ to the H_4L^{Me} 'Pacman' framework, step 2 is a reduction of the $U^{VI}O_2^{2+}$ to $U^{V}O_2^{+}$, step 3 is complexation of the second equiv. of $U^{VI}O_2^{2+}$, and step 4 is an oxo-group rearrangement, in one or multiple steps, leading to formation of the complex **4.1**. Coordinated K^+ ions and pyridine solvent molecules are omitted for clarity.

As two equiv. of [K][$UO_2(N'')_3$] (**4.AR**) were used to make complex **4.1**, and complex **4.1** contains no N" (N" = -$N(SiMe_3)_2$) groups, any mechanism accounting for the formation of complex **4.1** must also account for consumption of six equiv. of N". Four equiv. of N" are consumed by deprotonation of H_4L^{Me} in steps 1 and 3 in Scheme 4.7, leaving two equiv. of N". Given that N" is known to reduce $U^{VI}O_2^{2+}$ ions,[33] it is reasonable to consider that a fifth equiv. of N" is consumed to take $U^{VI}O_2^{2+}$ to $U^{V}O_2^{+}$, step 2 in Scheme 4.7. However, the sixth equiv. of N" is only vaguely considered in this mechanism. Assuming that X in Scheme 4.7 is the sixth equiv. of N" then the oxo-group rearrangement step(s), step 4, involves loss of N", presumably as HN" or DN" by quenching with solvent, *etc.* The stoichiometry of potassium counter-cations also depends on the identity of X after step 3 in Scheme 4.7. Further, as the 'mono-uranyl Pacman' complex (*cf.* **4.L.THF**) is known to form within seconds at -78°C, Scheme 4.1, this is postulated as the first step. As H_4L^{Me} is known to be insufficiently flexible to accommodate two $U^{VI}O_2^{2+}$ ions directly,[49] the complexation of the second equiv. of $U^{VI}O_2^{2+}$ ion is posited to require $U^{V}O_2^{+}$, which is less rigid (*e.g.* $\angle(O_{yl}U^{V}O_{yl})$ often deviate from linearity),[16] thus enabling the L^{Me}

framework to encapsulate the second $U^{VI}O_2^{2+}$ ion by distorting the $U^{V}O_2^{+}$ ion. Steps 2 and 3 are therefore in the order of reduction and coordination, and are hypothesised to be unlikely in the reverse order; *e.g.* coordination of two uranyl ions followed by reduction. Step 4 is then an oxo-rearrangement step(s) to form complex **4.1**.

Analysis of the bulk solids (from which crystals of the complex **4.1** were selected) by ^{1}H NMR spectroscopy (C_5D_5N) suggested only $U^{VI}O_2^{2+}$-containing compounds were present in solution, with no paramagnetic resonances (*e.g.* outside the 0–*ca*. 10 ppm range) being observed; that is, no U^{V} (*cf*. complex **4.1** remained in solution. It is unclear why this should be the case, but may result from contaminated C_5D_5N (used in ^{1}H NMR spectroscopy sample preparation) or serendipitous crystal selection. There was unfortunately not enough material to analyse complex **4.1** further, and attempts to repeat the procedure to obtain further material were unsuccessful.

4.2.4 Alternative Larger-scale Syntheses of $[(U^{V}O(OK(py)_2))_2(L^{Me})]$ (4.T.K)

In an attempt to isolate pure $[(U^{V}O(OK(py)_2))_2(L^{Me})]$ (**4.T.K**) to further study the reactivity of the K-functionalised $U^{V}_2O_4$ motif WRT uranyl reductive oxo-functionalisation, the scale of the synthesis discussed in Section 4.2.1 (Scheme 4.5) was increased, from 2 mL to 25 mL of C_5D_5N and an ampoule, not an NMR tube, was used as the reaction vessel.

However, analysis by ^{1}H NMR spectroscopy on three separate iterations of this procedure showed in all cases only diamagnetic resonances (*e.g.* 0–*ca*. 11 ppm), suggesting the reactions to synthesise $[(U^{V}O(OK(py)_2))_2(L^{Me})]$ (**4.T.K**) were not feasible on a larger scale. A number of alternative procedures were also attempted, consisting of varying the reaction solvent (dioxane, CH_3CN, *N,N*-dimethylaniline, or THF) or the energy source (microwave-assisted synthesis, or photoirradiation), but these methods all produced complex mixtures of products and $[(U^{V}O(OK(py)_2))_2(L^{Me})]$ (**4.T.K**) was not detected by ^{1}H NMR spectroscopy in any of these reactions. These reactions were not pursued further.

4.3 Reductive, Anaerobic Photochemical Oxo-Functionalisation of the Uranyl Ion

As the reactivity of hydrocarbon and O-containing substrates with $\boldsymbol{U^{tetNO3}}$ *is previously discussed in Section 3.6, only reactions involving the reductive oxo-functionalisation of the* $U^{VI}O_2^{2+}$ *ion with Lewis acidic substrates are discussed here.*

Given the focus on the reaction of $U^{VI}O_2^{2+}$ ions with Si- and B-containing substrates in the existing literature, Figure 4.2, it was decided that in order to fully explore the reactivity of **4.L.THF** in more detail, the photochemical reactivity of **4.L.THF** with heavier group 14 substrates would be explored here. The thermal reactivity of Ge- and Sn-containing substrates with **4.L.THF** has been previously

investigated by Arnold *et al*. (Scheme 4.8),[52] in which unidentified paramagnetic products were observed by ^{1}H NMR spectroscopy.

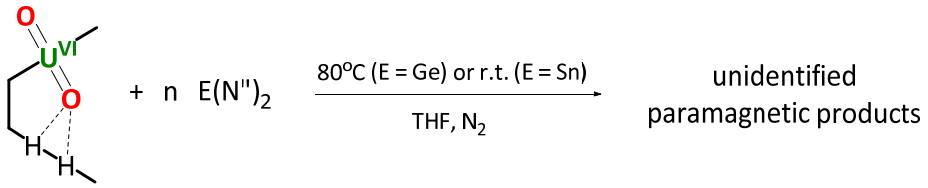

Scheme 4.8 – Formation of paramagnetic products from [(UO_2(THF))(H_2L^{Me})] (**4.L.THF**) with [E(N'')$_2$] (E = Ge, n = 1; E = Sn, n = 1.1) in THF, reported by Arnold *et al*.[52] Coordinated THF solvent molecules are omitted for clarity.

4.3.1 Photochemical Reactivity of [(UO_2(THF))(H_2L^{Me})] (4.L.THF)

Therefore, to explore the photochemical reactivity of Ge- and Sn-containing substrates with [(UO_2(THF))(H_2L^{Me})] (**4.L.THF**) further, solutions of [(UO_2(THF))(H_2L^{Me})] (**4.L.THF**) in C_6D_6 were irradiated for sixteen or more hours with one equiv. of E_2R_6 (E = Ge, R = Me; E = Sn, R = Me; E = Sn, R = Ph; E = Si, R = Me) or Ph_3SnH, according to Schemes 4.9 and 4.10. The Si-containing analogue, Si_2Me_6, was also used for comparison. Given the ubiquity of E-functionalised $U^VO_2^+$ complexes (Figure 4.2), $B_2(pin)_2$ (pin = pinacolato, $^-OC(Me)_2C(Me)_2O^-$) was also used as a source of boron. The thermal reductive oxo-functionalisation reactivity of diboranes with $U^{VI}O_2^{2+}$ has been reported previously[53] and so for comparative purposes, the photochemical reactivity was also investigated here.

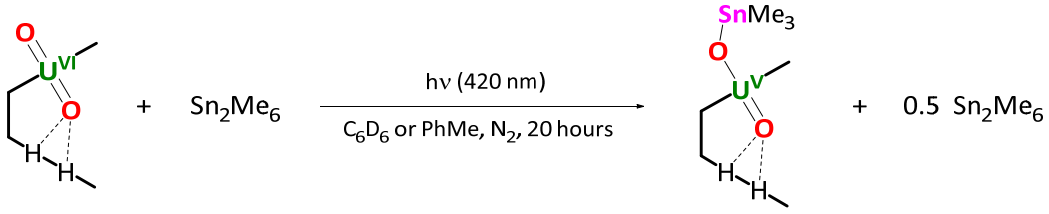

Scheme 4.9 – Synthesis of [(U^VO(OSnMe_3)(THF))(H_2L^{Me})] (**4.2**) from irradiation of [(UO_2(THF))(H_2L^{Me})] (**4.L.THF**) with Sn_2Me_6 in C_6D_6 or toluene, PhMe. Coordinated THF molecules are omitted for clarity.

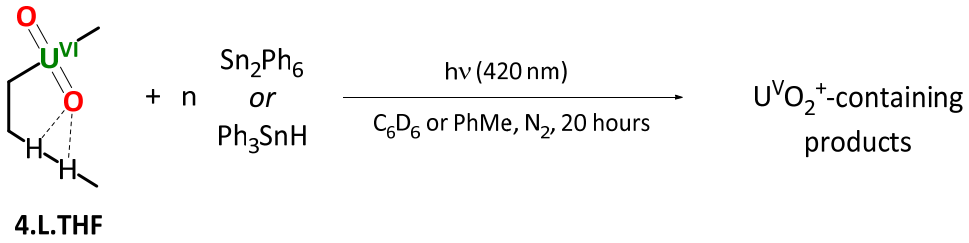

Scheme 4.10 – Reactivity of [(UO_2(THF))(H_2L^{Me})] (**4.L.THF**) with other Sn-containing substrates, Sn_2Ph_6 (n = 1) or Ph_3SnH (n = 1.2), with irradiation to produce $U^VO_2^+$-containing products from ^{1}H NMR spectroscopic proton resonances. Coordinated THF in **4.L.THF** is omitted for clarity.

In all cases where Sn-containing substrates were irradiated in the presence of **4.L.THF**, there was a colour change from opaque dark brown to transparent orange in the reaction solution, with no

precipitate formed. Analysis by ^{1}H NMR spectroscopy on reactions with Sn-containing substrates (*e.g.* [(UO_2(THF))(H_2L^{Me})] (**4.L.THF**) with one equiv. of Sn_2Me_6 in C_6D_6 or toluene, Scheme 4.9, and Sn_2Ph_6 or Ph_3SnH in C_6D_6, Scheme 4.10) indicated that paramagnetic products had been formed (*cf*. $U^VO_2^+$), as evidenced by the appearance of ^{1}H NMR resonances outside the 'diamagnetic' region (0–c*a*. 11 ppm).

With the reaction between Sn_2Me_6 and **4.L.THF** in C_6D_6 (Scheme 4.9), it was also possible to isolate and structurally characterise [($U^VO(OSnMe_3)$(THF))(H_2L^{Me})] (**4.2**), a highly air and moisture-sensitive orange solid isolated in 49% yield. The solid-state structure of this compound is given below in Figure 4.8, along with structural parameters, Table 4.2.

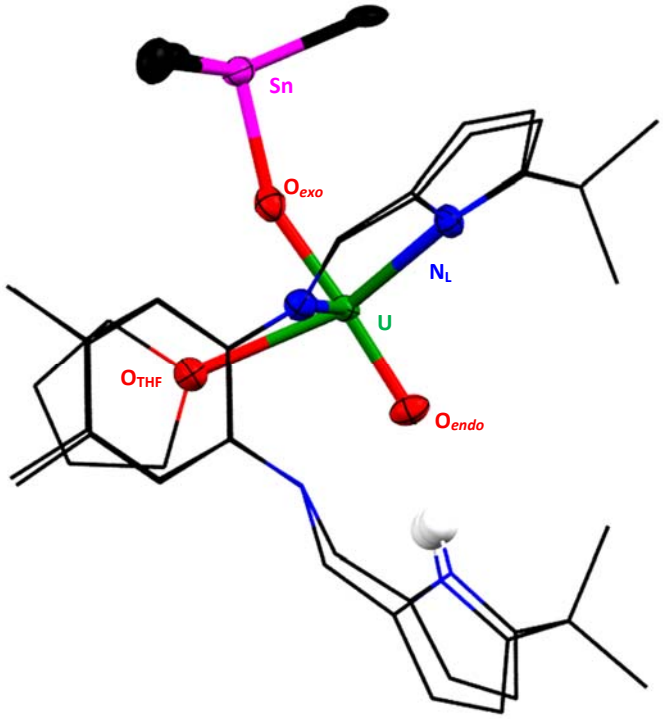

Figure 4.8 – Thermal ellipsoid plot (50% probability) of [($U^VO(OSnMe_3)$(THF))(H_2L^{Me})] (**4.2**). Non H-bonding H-atoms are removed and the H_4L^{Me} framework is drawn in wireframe projection. Key: uranium, oxygen, nitrogen, carbon, tin.

Distances			Angles	
Atom 1	**Atom 2**	**Distance/Å**	**Atoms**	**Angle/°**
U	-O_{exo}	1.943(8)	O_{endo} -U- O_{exo}	177.3(3)
	-O_{endo}	1.820(8)	U- O_{exo} -Sn	155.9(4)
	-O_{THF}	2.513(8)	O_{endo} -U-O_{THF}	98.2(3)
	-N_L	2.470(8)-2.648(8)		
O2	-Sn	2.029(8)		

Table 4.2 – Key structural parameters (bond lengths/Å, angles/°) for [($U^VO(OSnMe_3)$(THF))(H_2L^{Me})] (**4.2**).

The uranium centre in [($U^VO(OSnMe_3)$(THF))(H_2L^{Me})] (**4.2**) is seven-coordinate $U^VO_2^+$, with the N_4-donor cleft of $[H_2L^{Me}]^{2-}$ and one THF solvent molecule occupying the equatorial coordination sphere. The *exo*-oxo group (see Scheme 4.1) has been functionalised with one -$SnMe_3$ group from Sn_2Me_6,

presumably with the reaction of the intermediate U^{V}-O$^{\bullet}$ species with the Sn–Sn bond, producing the reductively oxo-functionalised '$U^{V}O(OSnMe_3)$' unit in [($U^{V}O(OSnMe_3)$(THF))(H_2L^{Me})] (**4.2**). The asymmetry in bond lengths between U-O_{endo} (1.820(8) Å) and U-O_{exo} (1.943(8) Å), and ∠(OUO) parameter (177.3(3)°), is consistent with U-O bond lengths and angles in the $U^{V}O_2^{+}$ ion[16] and, specifically, the Si-containing analogue, [($U^{V}O(OSiMe_3)$(py))(H_2L^{Me})] (**4.Q.1**) (U-O_{endo} = 1.854(4) Å, U-O_{exo} = 2.034(4) Å, ∠(OUO) = 176.00(17)°).[30] The ^{1}H NMR spectrum of [($U^{V}O(OSnMe_3)$(THF))(H_2L^{Me})] (**4.2**) in C_6D_6 shows one major product with the number of resonances (16) consistent with the number of unique proton environments. The reaction also works in toluene-D_8 ($C_6D_5CD_3$). The resonance for the –NH (pyrrole) protons in [($U^{V}O(OSnMe_3)$(THF))(H_2L^{Me})] (**4.2**), 60.84 ppm in C_6D_6, is consistent with that in [($U^{V}O(OSiMe_3)$(py))(H_2L^{Me})] (**4.Q.1**), 56.56 ppm in C_5D_5N,[30] further suggesting similarities between these two structures. The ^{119}Sn NMR spectrum in C_6D_6 of complex **4.2** shows a single resonance at 2936.32 ppm (scan width = 8000 ppm, between ±4000 ppm; normal scan range for ^{119}Sn NMR is *ca*. +1000 to -2000 ppm). APPI mass spectroscopy shows peaks with m/z values consistent with [($U^{V}O(OSnMe_3)$(THF))(H_2L^{Me})] (**4.2**) in the gas phase (Section 5.18.1), and electronic absorption spectroscopy in C_6D_6 showed only a single, broad (full-width, half maximum of *ca*. 200 nm) and intense (ε_{max} ≈ 78000 $M^{-1}cm^{-1}$) absorption centred at 339 nm. Repeated attempts to obtain consistent elemental analysis data were unsuccessful.

Given the similarities in these structural parameters and the comparative ease of the synthesis of [($U^{V}O(OSnMe_3)$(THF))(H_2L^{Me})] (**4.2**) (one step from [(UO_2(THF))(H_2L^{Me})] (**4.L.THF**)) compared to multiple steps for [($U^{V}O(OSiMe_3)$(py))(H_2L^{Me})] (**4.Q.1**); routes iii–iv in Scheme 4.2), the photochemical reduction of $U^{VI}O_2^{2+}$ to $U^{V}O_2^{+}$ by Sn_2Me_6 may provide an alternative, non-thermal avenue to access $U^{V}O_2^{+}$ in the 'Pacman' framework.

Separately, the irradiation of [(UO_2(THF))(H_2L^{Me})] (**4.L.THF**) with E_2Me_6 in C_6D_6 for 16 hours did not produce any discernible change in the ^{1}H NMR spectrum when E = Ge, and only extremely slight conversion when E = Si (≤ 1% by integration compared to starting materials, Scheme 4.11). This suggests no reaction of the *$U^{VI}O_2^{2+}$ ions in the presence of either the Ge-Ge or Si-Si bonds something which might be expected given the similarities in the Ge-Ge, Si-Si and Sn-Sn bond energies; ΔE_{diss}(Ge-Ge) = 274(21) $kJmol^{-1}$, ΔE_{diss}(Si-Si) = 327(10) $kJmol^{-1}$ and ΔE_{diss}(Sn-Sn) = 195(17) $kJmol^{-1}$, respectively, in the gas phase under standard conditions.[54] This is particularly surprising as *$U^{VI}O_2^{2+}$ is capable of cleaving C-H bonds which are considerably stronger (ΔE_{diss}(C-H) ~ 400 $kJmol^{-1}$) than any of the homo-element Ge, Si or Sn bonds. It is not clear why Sn-Sn bonds are more photochemically reactive than compounds containing Ge-Ge or Si-Si bonds under these conditions.

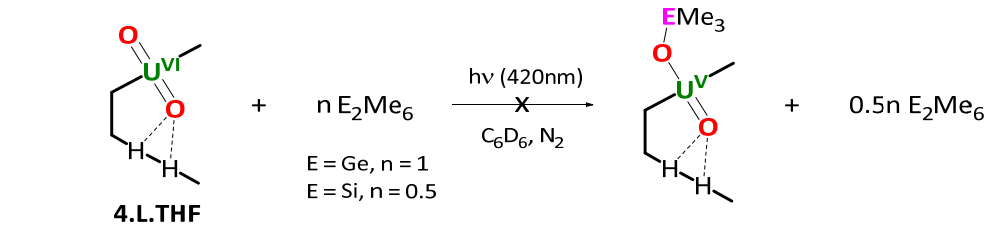

Scheme 4.11 – Unsuccessful photochemical reaction of [(UO_2(THF))(H_2L^{Me})] (**4.L.THF**) with E_2R_6 in C_6D_6. Coordinated THF in **4.L.THF** is omitted for clarity.

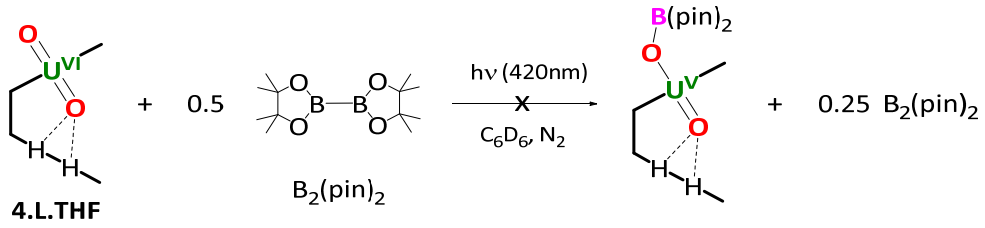

Scheme 4.12 – Unsuccessful photochemical reaction of [(UO_2(THF))(H_2L^{Me})] (**4.L.THF**) with $B_2(pin)_2$, shown in C_6D_6. Coordinated THF in **4.L.THF** is omitted for clarity.

There was also no reaction between $B_2(pin)_2$ and (**4.L.THF**), Scheme 4.12. Control reactions containing only [(UO_2(THF))(H_2L^{Me})] (**4.L.THF**) or Sn_2Me_6, Sn_2Ph_6, Ph_3SnH, Ge_2Me_6, Si_2Me_6 or $B_2(pin)_2$ in C_6D_6 did not react, by ^{1}H NMR spectroscopy after irradiation for 20 hours (420 nm) or less in C_6D_6.

4.3.2 Photochemical Reactivity of U^{tetNO3} with Non-Hydrocarbon Substrates

As discussed in Section 3.6, photoreactions under anaerobic conditions with **U^{tetNO3}** may lead to products not observed under aerobic photoirradiation, such as bixanthene from xanthene. Therefore, to explore the non-hydrocarbon substrate photoreactivity of $U^{VI}O_2^{2+}$ with a view towards reductive oxo-functionalisation, solutions of **U^{tetNO3}** in CD_3CN were irradiated at 420 nm for 16 hours in the presence of stoichiometric amounts of heteroatom-containing substrates; $B_2(cat)_2$ (cat = catecholato, 1,2-diphenolate), Sn_2Me_6, Ph_3P, HB(pin) (pin = pinacolato, 2,3-dimethylbutane-2,3-diolate) and Et_3SiH, reactions 1)–5), Schemes 4.13 and 4.14. The product solutions were then analysed by ^{1}H and multinuclear NMR spectroscopy, as appropriate.

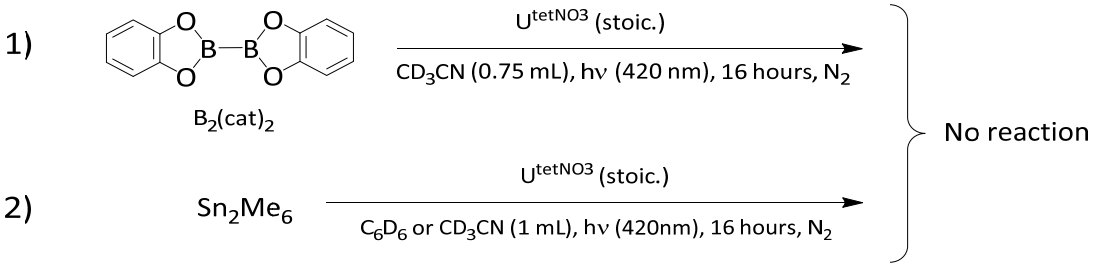

Scheme 4.13 – Heteroatomic substrates reacted photochemically with stoichiometric **U^{tetNO3}** under anaerobic conditions. cat is catecholato, 1,2-diphenolate; **U^{tetNO3}** is [^{n}Bu$_4$N]$_2$[U^{VI}O$_2$(NO$_3$)$_4$], Section 2.8.

Neither Sn_2Me_6 (tested in CD_3CN or C_6D_6) nor $B_2(cat)_2$ (tested in CD_3CN) showed any reaction with stoichiometric **U^{tetNO3}**, Scheme 4.13, with ^{1}H NMR spectra after irradiation (16 hours) being identical to those taken before irradiation.

However, for the phosphine Ph_3P ($\delta(^{31}P)$ = -5.86 ppm) and the borane HB(pin) ($\delta(^{11}B)$ = 33.36 ppm), > 99% conversion to the phosphine oxide, Ph_3PO ($\delta(^{31}P)$ = 25.69 ppm) and the boryl ether (pin)BOB(pin) ($\delta(^{11}B)$ = 22.45 ppm), respectively, was observed ^{1}H NMR spectroscopy, Scheme 4.14.

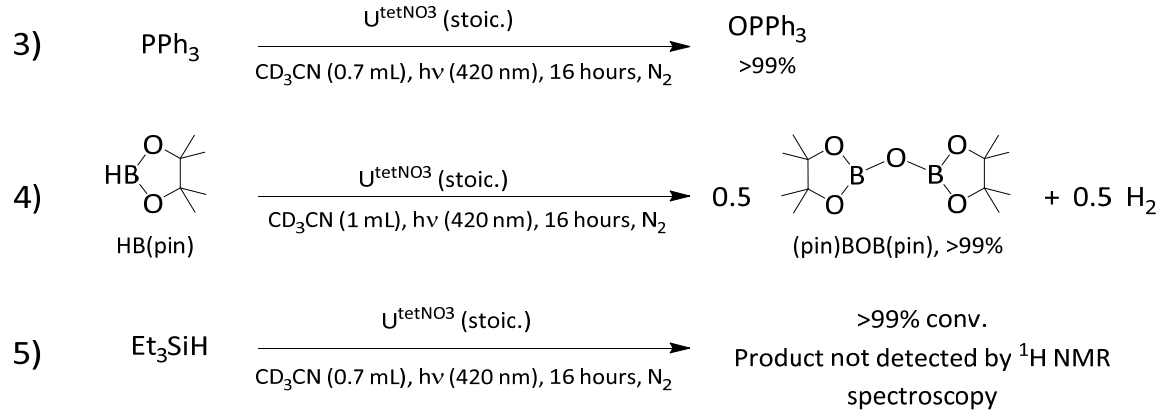

Scheme 4.14 – Heteroatomic substrates reacted photochemically with stoichiometric **U^{tetNO3}** under anaerobic conditions. pin is pinacolato, 2,3-dimethylbutane-2,3-diolate; **U^{tetNO3}** is [^{n}Bu$_4$N]$_2$[U^{VI}O$_2$(NO$_3$)$_4$], Section 2.8.

There was also evidence for the formation of dihydrogen in the reaction with HB(pin) ($\delta(^1H)$ = 4.60 ppm; reaction 4), Scheme 4.14),[55] suggesting formation of the B-O-B unit occurs *via* cleavage of the H-B bond to liberate 0.5 equiv. of H_2. Although Et_3SiH ($\delta(^{29}Si)$ = 0.42 ppm) was consumed (*e.g.* was not detected by ^{1}H or ^{29}Si NMR spectroscopy) it is not clear how the 'Et_3Si' unit reacted, as no evidence of H_2 or the silyl ether $Et_3SiOSiEt_3$ ($\delta(^{29}Si)$ = 9.00 ppm in CD_3CN)[56] was detected by either ^{1}H NMR or ^{29}Si NMR spectroscopy, respectively, and no precipitates were observed visually in the product solution.

4.4 Summary and Outlook

Continuing investigations into the oxo-group chemistry of the uranyl ion, new synthetic routes to the $U^V_2O_4$-Pacman 'butterfly' structural motif have been investigated. The K^+-functionalised $[(U^VO(OK(py)_2))_2(L^{Me})]$ (**4.T.K**) was identified by ^{1}H NMR spectroscopy by refluxing H_4L^{Me} and $[K][UO_2(N'')_3]$ (**4.AR**) in pyridine, forming with an *in-situ* yield of approximately 30%. The addition of 18-crown-6 increases the *in-situ* yield of K^+-functionalised product to *ca*. 40%.

A possible intermediate in the formation of $[(U^VO(OK(py)_2))_2(L^{Me})]$ (**4.T.K**) was obtained after 2 days of refluxing H_4L^{Me} and $[K][UO_2(N'')_3]$ (**4.AR**) in pyridine solution. This mixed U^{VI}/U^V species, $[(K(py))_{0.7}]_2[(K(py)_2)_{0.3}]_2[(U^{VI}O_2)(U^VO_2)(L^{Me})]_2$ (**4.1**) is a rare example of a mixed valence U^{VI}/U^V bimetallic

uranyl complex, with one oxo-bridge that suggests this complex is a precursor in the formation of $[(U^{V}O(OK(py)_2))_2(L^{Me})]$ (**4.T.K**). Attempts to isolate or scale-up either the $[(U^{V}O(OK(py)_2))_2(L^{Me})]$ (**4.T.K**) or $[(K(py))_{0.7}]_2[(K(py)_2)_{0.3}]_2[(U^{VI}O_2)(U^{V}O_2)(L^{Me})]_2$ (**4.1**) complexes were unsuccessful. It was also not possible to obtain supplementary spectroscopic evidence for the formation of either of these complexes. The inability to either isolate or further analyse these complexes is proposed to be related to their instability, suggesting that a K^+-functionalised $U^{V}{}_2O_4$ unit is not a suitable synthon for further investigations on the reactivity of this unit. These reactions were not investigated further.

In the first photochemical route to reductive oxo-functionalisation of the $U^{VI}O_2^{2+}$ ion, $[(U^{V}O(OSnMe_3)(THF))(H_2L^{Me})]$ (**4.2**), has been isolated and characterised, from the photoirradiation of a C_6D_6 solution of $[(UO_2(THF))(H_2L^{Me})]$ (**4.L.THF**) and Sn_2Me_6. Characterisation data (^{1}H and ^{119}Sn NMR spectroscopy, SCXRD and APPI-MS) are consistent with a Sn-functionalised $U^{V}O_2^{+}$ unit. Homobimetallic tin substrates are the most successful substrates tested towards the isolation of a $U^{V}O_2^{+}$-containing product, unlike the lighter group 14 congeners, E_2R_6 (E = Ge, R = Me; E = Si, R = Me) or $B_2(pin)_2$, for which negligible $U^{V}O_2^{+}$-containing products were detected by ^{1}H NMR spectroscopy.

Preliminary investigations into using non-macrocyclic $U^{VI}O_2^{2+}$ sources for photochemical uranyl reductive oxo-functionalisation, namely $\mathbf{U^{tetNO3}}$, suggest that oxophilic substrates such as HB(pin) or Et_3SiH are most suitable to induce 'yl' oxo-group reactivity, and that the former reacts by cleavage of the B-H bond. Further work remains to characterise the products of these reactions, and study the mechanism of possible oxo-atom cleavage under photoirradiation in more detail.

4.5 References

1. D. R. Lovley, E. J. P. Phillips, Y. A. Gorby and E. R. Landa, *Nature*, 1991, **350**, 413.
2. H. Steele and R. J. Taylor, *Inorg. Chem.*, 2007, **46**, 6311.
3. S. M. Cornet, L. J. L. Haller, M. J. Sarsfield, D. Collison, M. Helliwell, I. May and N. Kaltsoyannis, *Chem. Commun.*, 2009, 917.
4. J. C. Sullivan, J. C. Hindman and A. J. Zielen, *J. Am. Chem. Soc.*, 1961, **83**, 3373.
5. G. Nocton, P. Horeglad, J. Pécaut and M. Mazzanti, *J. Am. Chem. Soc.*, 2008, **130**, 16633.
6. F. Burdet, J. Pécaut and M. Mazzanti, *J. Am. Chem. Soc.*, 2006, **128**, 16512.
7. V. Mougel, P. Horeglad, G. Nocton, J. Pécaut and M. Mazzanti, *Chem. Eur. J.*, 2010, **16**, 14365.
8. V. Mougel, P. Horeglad, G. Nocton, J. Pécaut and M. Mazzanti, *Angew. Chem. Int. Ed.*, 2009, **48**, 8477.
9. H. P. Hratchian, J. L. Sonnenberg, P. J. Hay, R. L. Martin, B. E. Bursten and H. B. Schlegel, *J. Phys. Chem. A*, 2005, **109**, 8579.
10. M. C. F. Wander, S. Kerisit, K. M. Rosso and M. A. A. Schoonen, *J. Phys. Chem. A*, 2006, **110**, 9691.
11. S. T. Liddle, *Angew. Chem. Int. Ed.*, 2015, **54**, 8604.
12. R. J. Baker, *Chem. Eur. J.*, 2012, **18**, 16258.
13. P. L. Arnold, J. B. Love and D. Patel, *Coordin. Chem. Rev.*, 2009, **253**, 1973.
14. S. Fortier and T. W. Hayton, *Coordin. Chem. Rev.*, 2010, **254**, 197.
15. C. R. Graves and J. L. Kiplinger, *Chem. Commun.*, 2009, 3831.

16. B. E. Cowie, J. M. Purkis, P. L. Arnold, J. B. Love and J. Austin, *Chem. Rev.*, 2019, **119**, 10595.
17. N. L. Bell, B. Shaw, P. L. Arnold and J. B. Love, *J. Am. Chem. Soc.*, 2018, **140**, 3378.
18. E. A. Pedrick, G. Wu and T. W. Hayton, *Inorg. Chem.*, 2014, **53**, 12237.
19. D. D. Schnaars, G. Wu and T. W. Hayton, *Inorg. Chem.*, 2011, **50**, 9642.
20. J. L. Brown, G. Wu and T. Hayton, *J. Am. Chem. Soc.*, 2010, **132**, 7248.
21. E. A. Pedrick, G. Wu, N. Kaltsoyannis and T. W. Hayton, *Chem. Sci.*, 2014, **5**, 3204.
22. D. D. Schnaars, G. Wu and T. W. Hayton, *Inorg. Chem.*, 2011, **50**, 4695.
23. N. L. Bell, M. Zegke, L. N. Platts, C. A. Lamfsus, L. Maron, L. S. Natrajan, S. Sproules, P. L. Arnold and J. B. Love, *Chem. Sci.*, 2017, **8**, 108.
24. P. L. Arnold, B. E. Cowie, M. Zegke, N. Magnani, E. Colineau, J.-C. Griveau, R. Caciuffo and J. B. Love, *Angew. Chem. Int. Ed.*, 2017, **56**, 10775.
25. G. Givaja, A. J. Blake, C. Wilson, M. Schröder and J. B. Love, *Chem. Commun.*, 2003, 2508.
26. J. B. Love, *Chem. Commun.*, 2009, 3154.
27. P. L. Arnold, A. J. Blake, C. Wilson and J. B. Love, *Inorg. Chem.*, 2004, **43**, 8206.
28. P. L. Arnold, D. Patel, C. Wilson and J. B. Love, *Nature*, 2008, **451**, 315.
29. P. L. Arnold, A.-F. Pecharman, E. Hollis, A. Yahia, L. Maron, S. Parsons and J. B. Love, *Nat. Chem.*, 2010, **2**, 1056.
30. P. L. Arnold, A.-F. Pécharman and J. B. Love, *Angew. Chem. Int. Ed.*, 2011, **50**, 9456.
31. P. L. Arnold, E. Hollis, F. J. White, N. Magnani, R. Caciuffo and J. B. Love, *Angew. Chem. Int. Ed.*, 2011, **50**, 887.
32. P. L. Arnold, E. Hollis, G. S. Nichol, J. B. Love, J.-C. Griveau, R. Caciuffo, N. Magnani, L. Maron, L. Castro, A. Yahia, S. O. Odoh and G. Schreckenbach, *J. Am. Chem. Soc.*, 2013, **135**, 3841.
33. P. L. Arnold, G. M. Jones, S. O. Odoh, G. Schreckenbach, N. Magnani and J. Love, *Nat. Chem.*, 2012, **4**, 221.
34. G. M. Jones, P. L. Arnold and J. B. Love, *Angew. Chem. Int. Ed.*, 2012, **51**, 12584.
35. G. M. Jones, P. L. Arnold and J. B. Love, *Chem. Eur. J.*, 2013, **19**, 10287.
36. M. Zegke, G. S. Nichol, P. L. Arnold and J. B. Love, *Chem. Commun.*, 2015, **51**, 5876.
37. P. L. Arnold, A.-F. Pécharman, R. M. Lord, G. M. Jones, E. Hollis, G. S. Nichol, L. Maron, J. Fang, T. Davin and J. B. Love, *Inorg. Chem.*, 2015, **54**, 3702.
38. P. L. Arnold, M. S. Dutkiewicz, M. Zegke, O. Walter, C. Apostolidis, E. Hollis, A.-F. Pécharman, N. Magnani, J.-C. Griveau, E. Colineau, R. Caciuffo, X. Zhang, G. Schreckenbach and J. B. Love, *Angew. Chem. Int. Ed.*, 2016, **55**, 12797.
39. M. Zegke, X. Zhang, I. Pidchenko, J. A. Hilna, R. M. Lord, J. M. Purkis, G. S. Nichol, N. Magnani, G. Schreckenbach, T. Vitova, J. B. Love and P. L. Arnold, *Chem. Sci.*, 2019, **10**, 9740.
40. S. Sostero, O. Traverso, C. Bartocci, P. D. Bernardo, L. Magon and V. Carassiti, *Inorg. Chim. Acta*, 1976, **19**, 229.
41. G. Folcher, J. Lambard and G. C. de Villardi, *Inorg. Chim. Acta*, 1980, **45**, 59.
42. S. Kannan, A. E. Vaughn, E. M. Weis, C. L. Barnes and P. B. Duval, *J. Am. Chem. Soc.*, 2006, **128**, 14024.
43. S. Kannan, M. A. Moody, C. L. Barnes and P. B. Duval, *Inorg. Chem.*, 2006, **45**, 9206.
44. A. E. Vaughn, C. L. Barnes and P. B. Duval, *Angew. Chem. Int. Ed.*, 2007, **46**, 6622.
45. C. Villiers, P. Thuéry and M. Ephritikhine, *Angew. Chem. Int. Ed.*, 2008, **47**, 5892.
46. F. Réal, V. Vallet, U. Wahlgren and I. Grenthe, *J. Am. Chem. Soc.*, 2008, **130**, 11742.
47. L. Chatelain, S. White, R. Scopelliti and M. Mazzanti, *Angew. Chem. Int. Ed.*, 2016, **55**, 14325.
48. F. Blanchard, M. Ellart, M. Rivenet, N. Vigier, I. Hablot, B. Morel, S. Grandjean and F. Abraham, *Chem. Commun.*, 2016, **52**, 3947.
49. Q. J. Pan, S. O. Odoh, G. Schreckenbach, P. L. Arnold and J. B. Love, *Dalton Trans.*, 2012, **41**, 8878.
50. D. P. Mills, O. J. Cooper, F. Tuna, E. J. L. McInnes, E. S. Davies, J. McMaster, F. Moro, W. Lewis and A. J. Blake, *J. Am. Chem. Soc.*, 2012, **134**, 10047.
51. J. Yao, X.-J. Zheng, Q.-J. Pan and G. Schreckenbach, *Inorg. Chem.*, 2015, **54**, 5438.

52. N. L. Bell, P. L. Arnold and J. B. Love, *Dalton Trans.*, 2016, **45**, 15902.
53. B. E. Cowie, G. S. Nichol, J. B. Love and P. L. Arnold, *Chem. Commun.*, 2018, **54**, 3839.
54. D. R. Lide, *CRC Handbook of Chemistry and Physics*, 85th edn., CRC Press, Boca Raton, Florida, 2004.
55. G. R. Fulmer, A. J. M. Miller, N. H. Sherden, H. E. Gottlieb, A. Nudelman, B. M. Stoltz, J. E. Bercaw and K. I. Goldberg, *Organometallics*, 2010, **29**, 2176.
56. B. Pan and F. P. Gabbai, *J. Am. Chem. Soc.*, 2014, **136**, 9564.

Chapter 5: Synthetic and Characterisation Methods

5.1 Characterisation Methods

All manipulations, unless otherwise stated, were performed under ambient conditions. All chemicals were the highest commercial grade available obtained from commercial suppliers, including Sigma Aldrich, Acros Organics, Alfa Aesar, Polium Technologies or TCI Chemicals.

Air-sensitive manipulations, where used, were performed using standard Schlenk and glovebox techniques (VAC Omni-Lab and MBraun LabStar, under nitrogen), with equipment (glassware, cannulae, Fisherbrand 1.2 μm retention glass microfibre filters, *etc.*) dried at ≥ 150°C for at least 1 hour prior to use. Gases were supplied by BOC Gases, UK. Solvents treatments for air-sensitive manipulations: THF, hexane, toluene and diethyl ether were dried for 16 hours in a drying column (VAC Atmosphere, over 4Å molecular sieves) and degassed three times. Pyridine and 1,4-dioxane were refluxed for 4 days over Na, collected, distilled and degassed three times. *N,N*-dimethylaniline was magnetically stirred over CaH_2 for 5 days at r.t., filtered (cannula) and degassed three times. CD_3CN was either refluxed over CaH_2, or stored for 4Å sieves, for one week. All other deuterated NMR solvents were purchased from Cambridge Isotope Laboratories (> 99% D) and dried by refluxing over potassium for > 2 days, collected, freeze-pump-thaw degassed three times, and collected by static vacuum trap-to-trap distillation. *In vacuo* refers to vacuum of < 10^{-1} mbar unless otherwise stated. Anoxic acetonitrile was prepared by freeze-pump-thaw degassing reagent grade CH_3CN three times on a Schlenk line prior to use. Water was deionised using an Arium Comfort system, filtered through a 0.4 μm microfilter pad with a measured electrical resistance of 18.2 MΩ prior to use. Hexamethyldigermane, Me_6Ge_2, was purchased from Aldrich and freeze-pump-thaw degassed twice prior to use. The following compounds were prepared by literature methods: *N*,*N*′-dimethyl-2,6-pyridinedicarboxamide (py(CONHMe)$_2$),[1] 2,2′-Oxybis(*N*,*N*-dioctylacetamide) (*N,N,N′,N′*-TetraOctaDiGlycolAmide, TODGA),[2] *N,N*-diphenylbenzamide (benzNPh$_2$),[3] *N*,*N*-diisopropyl-2,2-dimethylpropionamide (*N*,*N*-diisopropylpivalamide, piv^{i}Pr$_2$),[4] *N*,*N*′-diphenylmalonamide (malPh$_2$),[5] *N*,*N*,*N*′,*N*′-tetraphenylmalonamide (malPh$_4$),[6] *N*,*N*,*N*′,*N*′-tetraisopropylmalonamide (mal^{i}Pr4),[7] xanthene-D_2,[8] H_4L^{Me} and precursors,[9] and [(UO_2(THF))(H_2L^{Me})], **4.L.THF**.[10]

5.1.1 Neptunium Chemistry

All chemical manipulations were performed in the specialist radiological laboratories of the National Nuclear Laboratory at Sellafield, UK, by Dr. Mark Sarsfield and the radiochemistry team. The elemental and isotopic purity of the ^{237}Np sample used for synthesis of the $Np^{VI}O_2^{2+}$ complexes was confirmed by gamma spectroscopy against a ^{237}Np standard (Section 5.3).

Raman spectra were recorded using a 514 or 785 nm laser on a Renishaw inVia spectrophotometer with Qontor attachment and optical microscope.

UV-vis-NIR spectra were recorded on a Perkin-Elmer lambda 900 instrument between 350–1300 nm with variable path lengths (1 mm – 1 cm) in quartz cuvettes, using Oceanoptics fibre-optic attachments and holders.

5.1.2 NMR Spectroscopy

Standard and J. Youngs (Teflon-tapped) NMR tubes were supplied by Norrell Ltd. All reported NMR shifts were recorded relative to ^{1}H NMR frequencies of 399.9, 500.1 or 599.9 MHz, using Bruker Avance III spectrometers, equipped with a BBFO+ broad-band probe (400 and 500MHz), a ^{1}H/^{13}C-optimised DCH cryoprobe (500MHz), and TXI cryoprobe (600MHz), respectively. NMR spectral references: ^{1}H and ^{13}C, internal solvent; ^{11}B, 15% $BF_3{\cdot}OEt_2$ in $CDCl_3$; ^{19}F, $CFCl_3$; ^{29}Si, dilute (< 0.1 M) $SiMe_4$ in $CDCl_3$; ^{31}P, 85% H_3PO_4 in D_2O; ^{119}Sn, 90% Me_4Sn in C_6D_6. ^{11}B NMR spectra were processed by spectral subtraction from Teflon-tapped NMR tubes containing only C_5D_5N. NMR spectra were analysed using the ACD Labs NMR package and software within.[11]

5.1.3 Mass Spectrometry and Gas Chromatography

Positive-mode Electron Impact Mass Spectrometry (EI^+-MS) was performed using a Waters Synapt G2 Q-TOF spectrometer. Atmospheric Pressure PhotoIonisation Mass Spectrometry (APPI-MS),[12] Fourier Transform Ion Cyclotron Resonance Mass Spectrometry (FT-ICR-MS) and ElectroSpray Ionisation Mass

Spectrometry (ESI-MS) were performed on a Bruker 12 T SolariX using the University of Edinburgh's SIRCAMS facility, with detector voltage relative to sample. Gas chromatography-mass spectrometry (GC-MS) was performed with a Shimadzu GCMS-QP2010 SE spectrometer fitted with autochanger. Samples of substrate in CH_3CN were also run to ensure no solvent or substrate decomposition in the column occurred at detectable levels. Representative procedure: split injection, injection temperature = 220°C, column oven temperature = 40°C, column flow ($Ar_{(g)}$) = 1.7 mL min^{-1}, ion source temperature = 220°C, interface temperature = 250°C, detector gain relative to sample. Temperature program: initial, 40°C (held for 3 minutes), 15°C min^{-1} to 100°C (held for 1 minute), 5°C min^{-1} to 270°C (held for 1 minute), total 43 minutes.

5.1.4 Vibrational Spectroscopy

IR spectra were recorded using a Nicolet Avatar 360 FT-IR spectrometer between 4000–400 cm^{-1} using the neat powder for solids (ATR-IR), and mounted KBr/NaCl Specac Omni cells for solutions.

Raman spectroscopy was performed on a Renishaw inVia Qontor spectrophotometer, with solution-phase spectra acquired in CH_3CN or PhCN (1M $\mathbf{U^{NO3}}$, saturated solution for $\mathbf{U^{Ph2phen}}$) in 300 μm glass capillaries affixed with adhesive tape onto a glass slide (SuperFrost, Menzel Gläser); a 10 –20 mW, 785 nm laser was used. Capillaries were sealed with Dow Corning high-vacuum grease, or by flame sealing, prior to irradiation to prevent evaporation. Solid-phase spectra were acquired on the neat powders. Spectra were also acquired on a blank glass capillary, CH_3CN and PhCN solvent for comparison. As required, Raman spectra were also collected between 600–1200 cm^{-1} using a 785 nm, 2 mW laser through a 3 mm aperture, with multiple scans collected to reduce the signal-to-noise ratio.

5.1.5 Electronic Spectroscopy

UV-vis absorption spectra were recorded on a Jasco V-670 spectrophotometer in 1 cm Hellma Suprasil-300 quartz cuvettes, fused to a Teflon screw tap for air-sensitive compounds. Kinetic analysis by UV-vis spectroscopy was run using variable parameters; representative method: scan rate and range = 1000 nm min^{-1} over 190–500 nm, data interval 0.2 nm, baseline corrected to blank solvent (CH_3CN) and collected at r.t. (295 K ± 2 K, monitored by digital thermometer affixed to the outside of the reaction container). Stock solutions were prepared at the appropriate concentration and stored in the dark at -35°C when not used.

Fluorescence (emission and excitation) spectra were recorded on a Horiba Fluoromax-P spectrophotometer with typical slit width of 5 nm and data interval of 1 nm. Excitation and emission measurements started or stopped 20 nm after or before the park wavelength (*e.g.* if emission park wavelength 420 nm, data range collection started at 440 nm).

5.1.6 Inductively Coupled Plasma-Mass Spectrometry, ICP-MS

ICP-MS analyses were performed on an Agilent 7500CE spectrometer employing a r.f. forward power of 1540 W and reflected power of 1 W, with argon gas flows of 0.81 L.min^{-1} and 0.21 L.min^{-1} for carrier and makeup flows, respectively. Sample solutions were nebulised by peristaltic pump at a rate of approximately 1.2 mL.min^{-1}. Skimmer and sample cones were made of nickel. The instrument was operated in spectrum acquisition mode and samples run in triplicate. The mass analysed was ^{238}U, analysed in fully quant mode (three points per unit mass). A series of standards were prepared using single element 1000 mg.dm^{-3} ^{238}U diluted with 3% v/v HNO_3 to give a range of standards (1, 5, 10, 50, 100 ppb). An external reference standard (Merck Multi element solution VI at 10 mg dm^{-3} ^{238}U) was used to verify the standard calibration graph for U.

5.1.7 Photochemical Measurements

Photo-irradiation was performed using one of: **(1)** a UVP 254 nm photochemical mercury-quartz lamp (effective 2200 W.cm^{-2} at 2.54 cm distance, and 18mA; maximum 6W; Pen-Ray PCQ-9G1-2.50-PO-Hg), **(2)** a UVP MineralLight XX-20S UV bench lamp (broad-spectrum with $\lambda_{max} \sim 254$ nm, 20 W high-pressure, Hg-vapour lamp), **(3)** a UVP 365 nm photochemical lamp (effective 450 W.cm^{-2} at 2.54 cm distance, 18mA; maximum 6 W; Pen-Ray Light Source 11SC-1.75), **(4)** a 420 nm/660 nm Kessil H380 dual-function horticultural lamp (90 W total, 19.3 W at 420 nm, and 17.8 W at 660 nm; total photon output at 420 nm = 4.41 x 10^{19} s^{-1}), **(5)** a 1 kW halogen-discharge lamp (colour T ~ 3000 K) and mount, purchased from RS components Ltd. (UK), or **(6)** a UVP 351 nm photochemical lamp (effective 850 W.cm^{-2} at 1.91 cm distance, 18mA; maximum 8W; P/N 90-0019-06, Pen-Ray Light Source 11SC-3.75). Lamp distance from sample, 8–10 cm unless otherwise stated. The reaction temperature was monitored by digital thermometer in order to avoid heating samples above 30°C unless stated; the probe was affixed to the external wall of the reaction vessels, where reported.

Spectral output for lamp **(4)**:

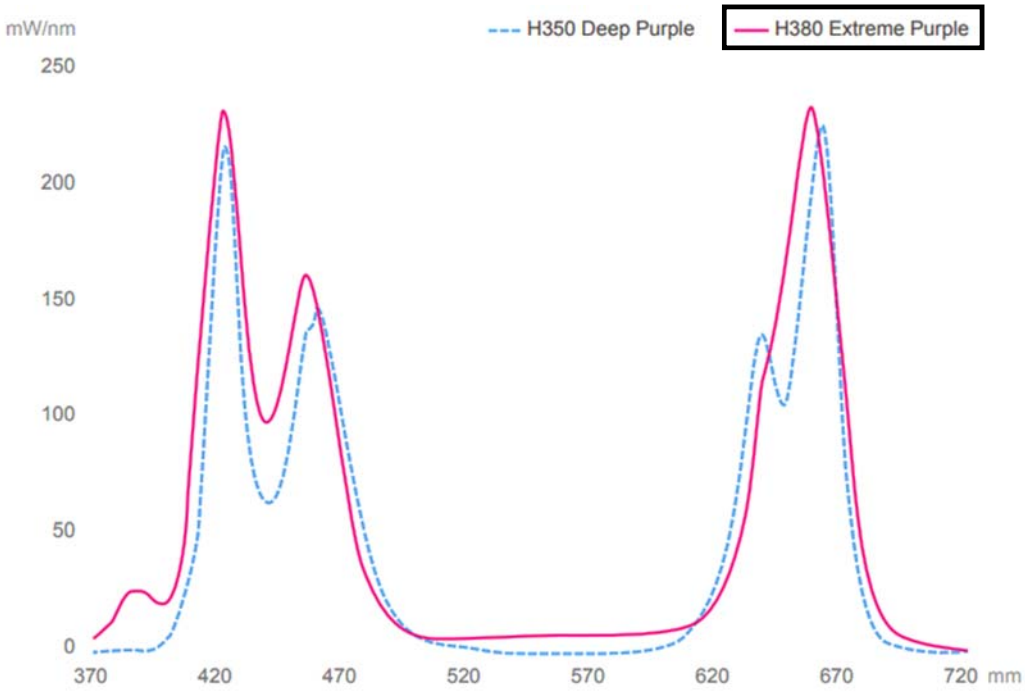

Figure 5.1 – Output spectrum from Kessil H380 horticultural lamp. Original available at http://www.kessil.com/horticulture/downloadfiles/H380vsH350.pdf

5.1.8 Elemental Analysis

Elemental analysis was performed in duplicate by Mr. Stephen Boyer, London Metropolitan University, U.K., with results averaged.

5.1.9 Karl-Fischer Titrations

Karl-Fischer titrations were carried out using a Mettler-Toledo Coulometric KF Titrator C30S with DM 143-SC probe.

5.1.10 Single-crystal X-ray Diffraction, SCXRD

Single-crystal X-ray diffraction (SCXRD) data were collected on an Oxford Diffraction Excalibur Eos diffractometer[13] with Mo Kα radiation (variable temperature), or Agilent Technologies Supernova dual source Atlas diffractometer[14] using a Cu Kα radiation source. Structure solutions and refinements were

computed using the SHELXT[15] and SHELXL[16] algorithms, respectively, supported within the Olex2 suite of programs.[17] Absorption corrections were applied using *Crysalis PRO* software.[13, 14] Analytical numeric absorption corrections used a multifaceted crystal model.[18] Numerical absorption correction was based on a Gaussian integration over a multifaceted crystal model. Empirical absorption correction using spherical harmonics was implemented in the SCALE3 ABSPACK scaling algorithm.[19] Non-hydrogen atoms were refined using anisotropic displacement ellipsoids, with H atoms constrained to the parent atom.

Experimental Details for Chapter 2

5.2 Complexes of the Uranyl Ion with *N*-heterocycles

5.2.1 Synthesis of $[UO_2(NO_3)_2(Ph_2phen)]$, $\mathbf{U^{Ph2phen}}$

To a solution of 4,7-diphenyl-1,10-phenanthroline (Ph_2phen, 1.5 g, 4.51 mmol) in CH_3CN (*ca*. 50 mL) was added a solution of uranyl nitrate, $[UO_2(NO_3)_2(OH_2)_2]\cdot 4H_2O$, $\mathbf{U^{NO3}}$ (2.27 g, 4.51 mmol), also in CH_3CN (*ca*. 50 mL), resulting in an immediate darkening of the magnetically-stirred solution from pale to dark yellow. After approx. 1 hour, volatiles were removed *in vacuo*, resulting in a yellow powder, characterised as $[UO_2(NO_3)_2(Ph_2phen)]$, $\mathbf{U^{Ph2phen}}$ (3.08 g, 94%). Analysis was by ^{1}H NMR, ATR-IR, Raman, and electronic absorption, emission and excitation spectroscopies, elemental analysis, ESI-MS, and SCXRD (grown by slow evaporation of saturated CH_3CN solution at 4°C over 4 days in the dark).

The complex $\mathbf{U^{Ph2phen}}$ is sparingly soluble in CH_3CN (*ca*. 3 mg mL^{-1}), and more soluble in PhCN (*ca*. 20 mg mL^{-1}). $\mathbf{U^{Ph2phen}}$ is also soluble in toluene and THF, but reacts with these solvents photolytically.

A sample of protonated ligand (4,7-diphenyl-1,10-phenanthrolinium trifluoroacetate, $[Ph_2phen\text{-}H][CF_3CO_2]$) was separately prepared by addition of two drops of trifluoroacetic acid, CF_3CO_2H, TFA (99% in water) to an NMR tube containing *ca*. 3 mg of Ph_2phen in 1 mL CD_3CN.

^{1}H NMR (500 MHz, CD_3CN): δ/ppm = 10.48 (br s, 2H, N–CH_{Ar}), 8.25 (m, 4H, CH_{Ar}), 7.84–7.44 (m, 10H, CH_{Ph}); *cf.* ^{1}H NMR of free ligand, Ph_2phen (500 MHz, CD_3CN): δ/ppm = 9.17 (d, 2H, N–CH_{Ar}, *J* = 4.4 Hz), 7.86 (s, 2H, CH_{Ar}), 7.65 (d, 2H, CH_{Ar}, *J* = 4.4 Hz), 7.60–7.53 (m, 10H, CH_{Ph}); ^{1}H NMR of $[Ph_2phen\text{-}H][CF_3CO_2]$ (500 MHz, CD_3CN): δ/ppm = 9.22 (d, 2H, N–CH_{Ar}, *J* = 5.2 Hz), 8.17 (s, 2H, CH_{Ar}), 8.10 (d, 2H, CH_{Ar}, *J* = 5.2 Hz), 7.66 (s, 10H, CH_{Ph}), 6.63 (s, acid). ATR-IR (cm^{-1}): 1527 (s), 1270 (m), 1254 (s), 1234 (s), 1024 (m), 937 (s, uranyl), 696 (m), 678 (m); *cf.* ATR-IR of free ligand, Ph_2phen (cm^{-1}): 1554 (m), 1487 (m), 1412 (m), 842 (m), 765 (s), 701 (s). UV-vis (CH_3CN): λ/nm (ε/$M^{-1}cm^{-1}$): 413–475 (< 65), *ca*. 360 (3500), 288 (62000), 201 (90000). Mass spec., *m/z* (Da; relative intensity, assignment): 333.131 (100%, $[(Ph_2phen)\text{-}H]^+$), 526.163 (82%), 665.268 (8%, $[UO_2(NO_3)(Ph_2phen)\text{-}H]^+$), 687.250 (6%, $[UO_2(NO_3)(Ph_2phen)\text{-}Na]^+$), 996.282 (1%, $[UO_2(NO_3)(Ph_2phen)_2]^+$). Elemental analysis: Calc. C, 39.68%, H, 2.22%, N, 7.71%; found C, 39.55%, H, 2.01%, N, 7.62%.

5.2.2 Water-, Redox- and Photo-stability of $\mathbf{U^{Ph2phen}}$

A) Water stability: To a Teflon-tapped NMR tube was added $\mathbf{U^{Ph2phen}}$ (3.2 mg, 4.41 μmol), CD_3CN (1 mL) and increasing amounts of H_2O, with aliquots analysed by ^{1}H NMR spectroscopy after each addition. The CD_3CN solvent for analysis was found by ^{1}H NMR spectroscopy to contain 11 equiv. of water without any water added, with subsequent additions of water (by microsyringe) increasing this to 16, 21, 28, 40, 80 and 400 equiv. (of water WRT the $\mathbf{U^{Ph2phen}}$ complex).

The collected ^{1}H NMR spectra showed clearly in both cases that the **U^{Ph2phen}** complex can tolerate small excesses (*ca*. 20–30 equiv.) of water but that above this, signal broadening consistent with water-induced ligand decomplexation is observed.

B) Redox stability: To a solution of **U^{Ph2phen}** (8.8 mg, 12.1 μmol, 1 equiv.) in CH_3CN/C_6D_6 (1 mL and 0.3 mL, 1.3 mL total) in a Teflon-tapped NMR tube was added KC_8 (1.9 mg, 14.1 μmol, 1.17 equiv.), and the golden yellow suspension shaken to immediately produce immediately a rose pink solution and suspension. This mixture was then allowed to stand for 16 hours at r.t. in the glovebox, filtered through glass fibre to remove excess KC_8/graphite, and analysed by ^{1}H NMR spectroscopy.

The reaction was repeated using $[Co^{II}(C_5Me_5)_2]$ (1.5 mg, 4.55 μmol, 1.2 equiv.) and **U^{Ph2phen}** (2.8 mg, 3.85 μmol, 1 equiv.) in CH_3CN (1 mL) and C_6D_6 (5 drops, *ca*. 100 μL). The yellow solution/suspension was sonicated for 20 minutes, and analysed by ^{1}H NMR spectroscopy. The solution was then allowed to stand for 5 days at r.t., and reanalysed.

In both cases the ^{1}H NMR spectra of the product mixtures showed additional resonances, matching those of free ligand, Ph_2phen, solvent, and where used, $[Co^{II}(C_5Me_5)_2]$. No evidence of **U^{Ph2phen}** was observed by ^{1}H NMR spectroscopy in either of the reactions.

C) Photolytic stability: The photolytic stability of **U^{Ph2phen}** and Ph_2phen were tested by irradiation in saturated CD_3CN (1 mL) solutions for 16 hours using lamp **(4)** at r.t. and monitored by ^{1}H NMR spectroscopy.

A small decrease of *ca*. 5% in the integrals of resonances corresponding to **U^{Ph2phen}** was observed after photolysis, along with numerous signals, *ca*. 7–8 ppm, < 5% the total integral of **U^{Ph2phen}** signals.

The photostability of **U^{Ph2phen}** was also tested by UV-vis spectroscopy, using a 4.3 μM solution in CH_3CN. The colourless solution was initially irradiated for and analysed after t = 10s, 20s, 30s, 45s, 1m, 1.5m, 2m and 3m with lamp **(4)**, after which no spectral change was observed.

5.2.3 Synthesis of $[UO_2(NO_3)_2(phen)]$, U^{phen}

To a magnetically stirred solution of 1,10-phenanthroline, phen (197.6 mg, 1 mmol, 1 equiv.) in CH_3OH (15 mL) was added a solution of **U^{NO3}** (501.4 mg, 1 mmol, 1 equiv.) also in CH_3OH (15 mL; 30 mL total). The resulting yellow precipitate which formed after 5 minutes of stirring at r.t. was filtered (frit) and dried in air, giving a powdery yellow solid, $[UO_2(NO_3)_2(phen)]$, **U^{phen}** (444 mg, 77%), which was analysed by ^{1}H NMR and ATR-IR spectroscopy, ESI-MS, and elemental analysis.

Protonated phenanthroline (phenanthrolinium trifluoroacetate, $[phen\text{-}H][CF_3CO_2]$) was prepared by addition of excess TFA (99% in water; *ca*. 10 drops) to a solution of phenanthroline in CD_3OD, and analysed by ^{1}H NMR spectroscopy.

The photolytic stability of the complex, **U^{phen}**, and free ligand, phen, were tested by irradiation in saturated CD_3CN (1 mL) solution for 16 hours using lamp **(4)** at r.t.

^{1}H NMR (500 MHz, CD_3OD): δ/ppm = 9.42 (br s, 2H, N–CH_{Ar}), 8.92 (d, 2H, CH_{Ar}, *J* = 8.0 Hz), 8.26 (s, 2H, CH_{Ar}), 8.17 (br s, 2H, CH_{Ar}); c*f.* ^{1}H NMR of free ligand, phen (500 MHz, CD_3OD): δ/ppm = 9.07 (dd, 2H, N–CH_{Ar}, *J* = 4.4, 1.7 Hz), 8.41 (dd, 2H, CH_{Ar}, *J* = 8.1, 1.7 Hz), 7.89 (s, 2H, CH_{Ar}), 7.73 (dd, 2H, CH_{Ar}, *J* = 8.1, 4.4 Hz); ^{1}H NMR of $[phen\text{-}H][CF_3CO_2]$ (500 MHz, CD_3OD): δ/ppm = 9.25 (dd, 2H, N–CH_{Ar}, *J* = 5.0, 1.5 Hz), 8.96 (dd, 2H, CH_{Ar}, *J* = 8.2, 1.5 Hz), 8.25 (s, 2H, CH_{Ar}), 8.16 (dd, 2H, CH_{Ar}, *J* = 8.2, 5.0 Hz), 5.39 (s, acid H). ATR-IR (cm^{-1}): 1520 (s), 1427 (m), 1264 (s), 1147 (m), 1028 (m), 938 (s, uranyl), 857 (s), 723 (s); c*f.* ATR-IR of free ligand, phen (cm^{-1}): 3369 (m br), 1586 (m), 1503 (m), 1421 (m), 1138 (w), 1090 (m), 851 (s), 680 (m br), 622(s). Mass spec., *m/z* (Da*;* relative intensity, assignment): 181.0780 (100%, $[(phen)–H]^+$), 203.0574 (7%), 383.1251 (6%, $[(phen)_2–Na]^+$), 692.1640 (0.7%, $[UO_2(NO_3)(phen)_2]^+$), 755.1605 (0.4%,

$[UO_2(NO_3)_2(phen)_2\text{-}H]^+$). Elemental analysis: Calc. C, 25.10%, H, 1.40%, N, 9.76%; found C, 25.71%, H, 1.10%, N, 10.18%.

5.2.4 Unsuccessful Complexation of U^{NO3} with Me_2phen, 2.1.Me_2phen

To a magnetically stirred solution of 2,9-dimethyl-1,10-phenanthroline, Me_2phen (100 mg, 0.48 mmol, 1 equiv.) in CH_3CN (3 mL) was added **U^{NO3}** (241 mg, 0.48 mmol, 1 equiv.) also in CH_3CN (3 mL; 6 mL total). The resulting yellow precipitate which formed after 1 hour of stirring at r.t. was filtered (frit) and dried (in air), giving a powdery yellow solid (205.7 mg, good yield), which was analysed by ^{1}H NMR and ATR-IR spectroscopy.

Protonated Me_2phen, [Me_2phen-H][CF_3CO_2] was prepared by addition of excess CF_3COOH, TFA (99 % in water; *ca*. 10 drops) to a solution of Me_2phen in CD_3OD, and analysed by ^{1}H NMR spectroscopy.

^{1}H NMR (500 MHz, CD_3OD): δ/ppm = 8.69 (d, 2H, N–CH_{Ar}, *J* = 8.4 Hz), 8.09 (s, 2H, CH_{Ar}), 7.92 (d, 2H, CH_{Ar}, *J* = 8.4 Hz), 3.02 (s, 6H, CH_3); *cf.* ^{1}H NMR of free ligand, Me_2phen (500 MHz, CD_3OD): δ/ppm = 8.29 (d, 2H, N–CH_{Ar}, *J* = 8.2 Hz), 7.81 (s, 2H, CH_{Ar}), 7.61 (d, 2H, CH_{Ar}, *J* = 8.2 Hz), 2.87 (s, 6H, CH_3); ^{1}H NMR of [Me_2phen-H][CF_3CO_2] (500 MHz, CD_3OD): δ/ppm = 8.74 (d, 2H, N–CH_{Ar}, *J* = 8.4 Hz), 8.11 (s, 2H, CH_{Ar}), 7.94 (d, 2H, CH_{Ar}, *J* = 8.4 Hz), 5.79 (s, acid H), 3.03 (s, 6H, CH_3). ATR-IR (cm^{-1}): 1502 (m), 1304 (s), 1279 (s), 1030 (m), 926 (s, uranyl), 862 (m), 742 (m); *cf.* ATR-IR of free ligand, Me_2Phen (cm^{-1}): 3350 (w br), 1672 (m), 1591 (m), 1494 (m), 1357 (m), 849 (s), 732 (m).

5.2.5 Unsuccessful Complexation of U^{NO3} with Me_2Ph_2phen, 2.1.Me_2Ph_2phen

To a magnetically stirred solution of 2,9-dimethyl-4,7-diphenyl-1,10-phenanthroline, Me_2Ph_2phen (100.1 mg, 0.28 mmol, 1 equiv.) in CH_3CN (3 mL) was added **U^{NO3}** (139 mg, 0.277 mmol, 1 equiv.), also in CH_3CN (3 mL; 6 mL total). The resulting yellow precipitate which formed after 1 hour of stirring at r.t. was filtered (frit) and dried in air, giving a powdery yellow solid (119 mg, moderate yield), as for Me_2phen, above (Section 5.2.4). Crystals suitable for SCXRD were grown by slow evaporation of the reaction solution at 0°C over five days. Analysis was by ^{1}H NMR and ATR-IR spectroscopy.

Protonated Me_2Ph_2phen, [Me_2Ph_2phen-H][CF_3CO_2], was prepared by addition of excess TFA (99% in water; *ca*. 10 drops) to a solution of Me_2Ph_2phen in CD_3OD, and analysed by ^{1}H NMR spectroscopy.

^{1}H NMR (500 MHz, CD_3OD): δ/ppm = 8.02 (s, 2H, N–CH_{Ar}), 7.91 (s, 2H, CH_{Ar}), 7.68–7.56 (m, 10H, CH_{Ph}), 3.08 (s, 6H, CH_3); c*f.* ^{1}H NMR of free ligand, Me_2Ph_2phen (500 MHz, CD_3OD): δ/ppm = 7.76 (s, 2H, N–CH_{Ar}), 7.63–7.42 (m, 12H, 2 x CH_{Ar}, 10 x CH_{Ph}), 2.93 (s, 6H, CH_3); ^{1}H NMR of [Me_2Ph_2phen-H][CF_3CO_2] (500 MHz, CD_3OD): δ/ppm = 8.09 (s, 2H, N–CH_{Ar}), 7.98 (s, 2H, CH_{Ar}), 7.67–7.61 (m, 10H, CH_{Ph}), 6.03 (s, acid H), 3.12 (s, 6H, CH_3). ATR-IR (cm^{-1}): 1483 (s), 1283 (s), 1031 (m), 926 (s, uranyl), 744 (m), 702 (s) cm^{-1}; *cf.* ATR-IR of free ligand, Me_2Ph_2phen (cm^{-1}): 3026 (w), 1482 (m), 1443 (m), 1028 (m), 882 (m), 830 (m), 770 (m), 705 (s).

5.2.6 Complexation of U^{NO3} with terpy (1 or 2 equiv.)

To magnetically stirred solutions of **U^{NO3}** in acetone (total 5 mL) was added (dropwise) acetone solutions of terpyridine, terpy (see masses below), creating copious amounts of a very pale yellow precipitate, after approximately 15 seconds in both cases. These solutions were stirred for one week in the dark in sealed vials, and were then filtered (frit), washed with acetone (the precipitates are insoluble in acetone; 3 x 100 mL), dissolved in methanol (3 mL) and analysed by ^{1}H NMR and ATR-IR spectroscopies, and ESI-MS.

Protonated terpy, [terpy-H][NO_3], was prepared by addition of excess HNO_3 (70% in water; *ca*. 10 drops) to a solution of terpy in CD_3OD, and analysed by ^{1}H NMR spectroscopy.

Reaction of U^{NO3} with 1 equiv. terpy: U^{NO3} (100 mg, 199.2 μmol, 1 equiv.) and terpyridine (46.5 mg, 200 μmol, 1 equiv.). 126.7 mg of a yellow solid was isolated (good yield).

^{1}H NMR (500 MHz, CD_3OD): δ/ppm = 10.53 (s, 2H, terpy), 8.92 (dq, 8H, terpy, *J* = 5.33, 0.98 Hz), 8.88 (d, 2H, terpy, *J* = 7.88 Hz), 8.83 (d, 2H, terpy, *J* = 7.85 Hz), 8.76 (dt, 8H, terpy, *J* = 8.22, 0.98 Hz), 8.59 (t, 2H, terpy, *J* = 7.78 Hz), 8.54 (q, 8H, terpy, *J* = 7.78 Hz), 8.52 (q, 1H, terpy, *J* = 7.89 Hz), 8.45 (td, 8H, terpy, *J* = 7.98, 1.56 Hz), 8.29 (t, 4H, terpy, *J* = 7.88 Hz), 8.24 (t, 2H, terpy, *J* = 6.38 Hz), 7.91–7.87 (m, 8H); *cf.* ^{1}H NMR of free ligand, terpy (400 MHz, CD_3OD): 8.83 (t, 2H, *J* = 4.23 Hz), 8.59–8.56 (m, 2H), 8.36–8.32 (m, 2H), 8.04–7.99 (m, 1H), 7.98–7.93 (m, 2H), 7.45–7.42 (m, 1H); *cf*. ^{1}H NMR of [terpy-H][NO_3] (400 MHz, CD_3OD): 8.13 (ddd, 2H, *J* = 5.86, 1.52, 0.76 Hz), 8.94 (dq, 2H, *J* = 7.88, 0.83 Hz), 8.86 (td, 2H, *J* = 7.88, 1.49 Hz), 8.70 (d, 2H, *J* = 7.89 Hz), 8.51–8.47 (m, 1H), 8.27–8.23 (m, 2H). ATR-IR (cm^{-1}): 3659 (w), 2989 (w), 2901 (w), 1600 (m), 1574 (w), 1512 (s), 1469 (s), 1439 (w), 1402 (w), 1293 (w), 1275 (s), 1239 (w), 1015 (s), 933 (vs, uranyl), 776 (s), 746 (m), 652 (m).

Reaction of U^{NO3} with 2 equiv. terpy: U^{NO3} (82.5 mg, 164.3 μmol, 1 equiv.) and terpyridine (79.3 mg, 340 μmol, 2.07 equiv.); 119.5 mg of a yellow solid was isolated (moderate yield). Yellow plate crystals suitable for SCXRD were grown by slow evaporation of a saturated CH_3OH solution at 4°C over 5 days, which was found to have the formula $[UO_2(MeOH)(MeO)(terpy)]_2[UO_2(NO_3)_4]$, **2.2**.

^{1}H NMR (500 MHz, CD_3OD): δ/ppm = 10.16 (d, 2H, terpy, *J* = 4.72 Hz), 9.02 (m, 4H, terpy, *J* = 4.75 Hz), 8.82 (d, 1H, terpy, *J* = 4.02 Hz), 8.72 (d, 1H, terpy, *J* = 7.86 Hz), 8.68 (t, 1H, terpy, *J* = 7.86 Hz), 8.58 (t, 2H, terpy, *J* = 7.56 Hz), 8.50 (d, 1H, terpy, *J* = 7.89 Hz), 8.27 (t, 1H, terpy, *J* = 7.95 Hz), 8.23 (p, 2H, terpy, *J* = 6.93 Hz), 7.72 (t, 1H, terpy, *J* = 5.67 Hz). ATR-IR (cm^{-1}): 3082 (w), 1600 (w), 1564 (w), 1513 (m), 1470 (m), 1293 (m), 1277 (m), 1238 (w), 1016 (m), 933 (s, uranyl), 776 (s), 746 (w), 652 (m). Mass spec., *m/z* (Da*;* relative intensity, assignment): 234.1023 (100%, $[(terpy)\text{-}H]^+$), 256.0837 (45%, $[(terpy)\text{-}Na]^+$), 396.0794 (8%, $[UO_2(NO_3)(MeOH)_2]^+$), 489.1777 (65%, $[(terpy)_2\text{-}Na]^+$), 521.5886 (40%, $[(terpy)_2\text{-}Na\text{-}MeOH]^+$), 534.1531 (90%, $[UO_2(terpy)(MeO)]^+$), 565.1220 (10%, $[UO_2(terpy)(NO_3)]^+$), 767.2444 (9%, $[UO_2(terpy)_2(MeO)]^+$), 883.1838 (1%, $[UO_2(terpy)(NO_3)_2\text{-}Na]^+$).

5.2.7 Unsuccessful Complexation of U^{NO3} with 2,3-bis(2-pyridyl)pyrazine, Reaction 2.3.A

To a magnetically stirred solution of 2,3-bis(2-pyridyl)pyrazine (20 mg, 85.4 μmol, 0.5 equiv.) in CH_3CN (5 mL) was added U^{NO3} (85.7 mg, 171 μmol, 1 equiv.), with a yellow solid precipitating from the reaction mixture almost instantly upon addition of the uranyl. This suspension was stirred for 1 hour, filtered, and dried on the frit to give a pale yellow powdery solid (62.4 mg, moderate yield), insoluble in CH_3CN, CH_3OH and acetone. The solid was analysed by ATR-IR spectroscopy.

ATR-IR (cm^{-1}): 3111 (m br), 1481 (m), 1285 (m), 1032 (m), 915 (vs), 745 (m), 702 (m); c*f.* ATR-IR of free ligand, 2,3–bis(2–pyridyl)pyrazine (cm^{-1}): 1585 (m), 1564 (m), 1391 (m), 1104 (m), 1087 (m), 1033 (m), 788 (s), 746 (m).

5.2.8 Unsuccessful Complexation of U^{NO3} with tetra-2-pyridinyl pyrazine, TPP, Reaction 2.3.B

To a solution of tetra-2-pyridinyl pyrazine, TPP (100 mg, 0.26 mmol, 0.5 equiv.) in CH_3CN (5 mL) was added, dropwise, U^{NO3} (259 mg, 0.515 mmol, 1 equiv.), also in CH_3CN (5 mL; total 10 mL). The yellow solution and suspension was magnetically stirred for 1 hour, filtered (frit), and volatiles removed *in vacuo* to give a yellow powdery solid (243 mg, moderate yield). Analysis was by ^{1}H NMR and ATR-IR spectroscopy, and SCXRD, with yellow crystals of [TPP-2H][$(UO_2(\mu\text{-}OH)(NO_3)_2)_2$] (**2.4**) grown by slow evaporation of the reaction solution for 16 hours at r.t.

The photostability of the product was tested by irradiation of a saturated solution in CD_3CN (*ca*. 1 mL) for 16 hours using lamp **(4)** at r.t., and analysing the resultant darker yellow solution by ^{1}H NMR spectroscopy. There was no change in the NMR spectra before and after irradiation.

Protonated pyrazine ligand was prepared by addition of two drops of TFA (99% in water) to an NMR tube containing a saturated CD_3CN solution of tetra-2-pyridinyl pyrazine. The solution was analysed by ^1H NMR spectroscopy and there was no spectral change after photolysis.

^1H NMR (500 MHz, CD_3CN): δ/ppm = 8.70–8.51 (m, 4H, N–CH_{Ar}), 8.32 (d, 4H, CH_{Ar}, *J* = 7.2 Hz), 8.16 (s, 4H, CH_{Ar}), 7.69 (s, 4H, CH_{Ar}); *cf.* ^1H NMR of free ligand, tetra–2–pyridinyl pyrazine (500 MHz, CD_3CN): δ/ppm = 8.31 (ddd, 4H, N–CH_{Ar}, *J* = 4.8, 1.8, 1.0 Hz), 8.01 (d, 4H, CH_{Ar}, *J* = 7.9 Hz), 7.88 (d, 4H, CH_{Ar}), 7.36–7.28 (m, 4H, CH_{Ar}); *cf*. ^1H NMR of protonated pyrazine (500 MHz, CD_3CN): δ/ppm = 9.03 (d, 4H, N–CH_{Ar}, *J* = 5.7 Hz), 8.55 (d, 4H, CH_{Ar}, *J* = 1.6 Hz), 8.47 (dd, 2H, CH_{Ar}, *J* = 8.3, 0.8 Hz), 8.19–8.12 (m, 4H, CH_{Ar}), 5.93 (s, acid H). ATR-IR (cm^{-1}): 3400 (br w), 1615 (w), 1525 (m), 1496 (m), 1369 (m), 1261 (s), 1081 (s), 936 and 923 (br s), 835 (w), 783 (m), 739 (s).

5.2.9 Unsuccessful Complexation of U^{NO3} with 2,2′-biquinoline, Reaction 2.3.C

To a solution of 2,2′-biquinoline (25.6 mg, 0.1 mmol, 1 equiv.) in CH_3CN (3 mL) was added a solution of $\mathbf{U^{NO3}}$ (100 mg, 0.2 mmol, 2 equiv.) in CH_3CN (3 mL, 6 mL total), and the mixture magnetically stirred for 1 hour to give a yellow precipitate. This precipitate was collected by filtration (frit) and dried *in vacuo* to yield a powdery yellow solid (95.2 mg, good yield). Analysis was by ^1H NMR and ATR-IR spectroscopy.

The photostability of the product was tested by irradiation of a saturated solution in CD_3CN (*ca*. 1 mL) for 16 hours using lamp **(4)** at r.t., and analysing the resultant darker yellow solution by ^1H NMR spectroscopy.

Protonated biquinolinium ligand was prepared by addition of two drops of TFA (99% in water) to an NMR tube containing a saturated CD_3CN solution of ligand.

^1H NMR (500 MHz, CD_3CN): δ/ppm = 8.78–8.70 (m, 4H, CH_{Ar}), 8.35 (d, 2H, CH_{Ar}, *J* = 8.5 Hz), 8.13 (d, 2H, CH_{Ar}, *J* = 8.5 Hz), 8.00–7.94 (m, 2H, CH_{Ar}), 7.82–7.76 (m, 2H, CH_{Ar}); *cf.* ^1H NMR of free ligand, 2,2′–biquinoline (500 MHz, CD_3CN): δ/ppm = 8.84 (d, 2H, CH_{Ar}, *J* = 8.6 Hz), 8.47 (d, 2H, CH_{Ar}, *J* = 8.6 Hz), 8.22–8.18 (m, 2H, CH_{Ar}), 8.03–7.92 (m, 2H, CH_{Ar}), 7.85–7.79 (m, 2H, CH_{Ar}), 7.68–7.62 (m, 2H, CH_{Ar}); *cf*. ^1H NMR of protonated 2,2′–biquinoline (400 MHz, CD_3CN): δ/ppm = 9.01 (d, 2H, CH_{Ar}, *J* = 8.7 Hz), 8.66 (d, 2H, CH_{Ar}, *J* = 8.7 Hz), 8.55–8.50 (m, 2H, CH_{Ar}), 8.28–8.23 (m, 2H, CH_{Ar}), 8.16–8.10 (m, 2H, CH_{Ar}), 7.96–7.90 (m, 2H, CH_{Ar}), 5.92 (s, acid H). ATR-IR (cm^{-1}): 3499 (w br), 3181 (w br), 1602 (m), 1505 (s), 1293 (s), 1277 (s), 1218 (m), 1030 (s), 906 (s), 863 (s), 833 (s), 742 (s); c*f.* ATR-IR of free ligand, 2,2′–biquinoline (cm^{-1}): 3047 (w), 1594 (m), 1419 (m), 1129 (m), 828 (s), 788 (m), 737 (s), 626 (m).

5.3 Complexes of the Neptunyl(VI) Ion with *N*-heterocycles

To a sample of electrochemically conditioned neptunyl nitrate (*ca*. 40 mg, $[Np^{VI}O_2(NO_3)_2(OH_2)_2]\cdot 4H_2O$) was added CH_3CN (1 mL), forming a brown solution ($^{237}Np_{(sol)}$) and white precipitate (mainly $^{233}Pa_{(s)}$, detected the characteristic emission lines at 312 and 340 keV by α-spectroscopy). The brown solution was decanted and analysed by UV-vis-NIR and Raman spectroscopy, and again after 24 hours, to ensure all components of the reaction solution were redox stable.

This brown solution was then further diluted with CH_3CN (total 5 mL; $[Np^{VI}]$ = 0.016 M), and reanalysed by UV-vis-NIR and Raman spectroscopy. Aliquots (typically 400 μL) of this stock solution were taken and aliquots of ligand (phen, terpy or Ph_2phen) added sequentially as needed. The solution resulting from addition of each aliquot of ligand in CH_3CN was then analysed by UV-vis-NIR spectroscopy, and/or Raman spectroscopy, as required. These pale brown solutions became increasingly turbid and yellow as phen and terpy were added, eventually forming crystalline dark-yellow solids that were analysed by light microscopy and Raman spectroscopy (on the solids). Ph_2phen was insufficiently soluble in CH_3CN under these conditions to detect spectroscopically.

To an aliquot of the Np^{VI} stock solution (*ca.* 400 μL) was also added increasing equivalents of water, and the resulting solutions analysed by UV-vis-NIR and Raman spectroscopy.

Separately, a sample of CH_3CN (1 mL) with added HNO_3 (70% w/v, *ca*. 200 μL) was analysed by Raman spectroscopy, to give a reference spectrum of HNO_3 in CH_3CN under analogous conditions.

5.4 Complexes of the Uranyl Ion with Multidentate Amides

5.4.1 Synthesis of $[UO_2(NO_3)_2(mal)]$, $\mathbf{U^{mal}}$

To a magnetically stirred solution of $\mathbf{U^{NO3}}$ (5 g, 9.96 mmol, 1 equiv.) in CH_3CN (50 mL) was added a suspension of malonamide, mal (1 equiv.: 1.02 g, 10 mmol; 2 equiv.: 2.03 g, 20 mmol) in CH_3CN (1.3 L total). The reactions were stirred for 16 hours and volatiles removed *in vacuo*. The yellow solid, $\mathbf{U^{mal}}$ (4.65 g, 94% based on U) isolated from reaction employing 1 equiv. of mal was subsequently analysed by ESI-MS, ^{1}H NMR, IR (ATR and solution-phase), Raman, UV-vis (absorption), emission and excitation spectroscopies, and elemental analysis. Pale yellow prismatic crystals suitable for SCXRD were grown by slow evaporation from a saturated CH_3CN solution of $\mathbf{U^{mal}}$ from the reaction employing 1 equiv. of mal at r.t.

Anhydrous $\mathbf{U^{mal}}$ was obtained after drying *in vacuo* for 48 hours (< 10^{-3} mbar). Water content was tested by Karl-Fischer titration on 10 mg of sample in anhydrous CH_3CN (1 mL).

^{1}H NMR (600 MHz, CD_3CN): δ/ppm = 8.07 (br s, 2H, NH), 7.89 (br s, 2H, NH), 3.95 (s, 2H, CH_2), 2.14 (br s, water); *cf*. ^{1}H NMR of free ligand, mal (500 MHz, CD_3CN): 6.74 (br s, 2H, NH), 5.81 (br s, 2H, NH), 3.09 (s, 2H, CH_2), 2.16 (br s, water). ATR-IR (cm^{-1}): 3438 (m), 3352 (m), 3302 (w), 1673 (s), 1651 (s), 1605 (s), 1499 (w), 1486 (s), 1401 (w), 1292 (+ 1312 and 1280 sh), 1192 (w), 1113 (m), 1032 (m), 945 (vs, uranyl; *cf*. solution-phase IR, 940), 896 (m), 868 (w), 810 (m), 750 (m), 714 and 701 (m), 640 (s), 606 (m), 592 (s); *cf*. ATR-IR of free ligand, mal (cm^{-1}): 3297 (br s), 3144 (s), 2801 (w), 1661 (s), 1599 (w), 1396 (s), 1262 (s), 1187 (s), 1180 (m), 903 (w), 700 (w), 687 (s), 602 (vs). Raman (cm^{-1}): 860 (uranyl); *cf*. $\mathbf{U^{NO3}}$ (cm^{-1}): 869 (uranyl). UV-vis (CH_3CN): λ/nm (ε/$M^{-1}cm^{-1}$): 425–469 (< 20), 289 (400). Mass spec., *m/z* (Da*;* relative intensity, assignment): 125.0347 (100%, $[(mal)\text{-}Na]^+$), 434.0757 (20%, $[UO_2(NO_3)_2(mal)]^+$), 519.0510 (27%, $[UO_2(NO_3)_2(mal)\text{-}Na]^+$), 536.1182 (31%, $[UO_2(NO_3)(mal)_2]^+$), 621.0969 (28%, $[UO_2(NO_3)_2(mal)_2\text{-}Na]^+$). Elemental analysis: Calc. C, 7.26%, H, 1.22%, N, 11.29%; found C, 7.48%, H, 1.10%, N, 11.05%.

Water stability

A sample of $\mathbf{U^{mal}}$ (*ca*. 5 mg) was dissolved in bench (*e.g.* wet; < 0.1%) CD_3CN (1 mL) in an NMR tube, allowed to stand in the dark for one week at r.t., and analysed by ^{1}H NMR spectroscopy.

The ^{1}H NMR spectrum showed a peak, a 1:1:1 triplet, centred at 6.00 ppm, consistent with production of NH_4^+, along with resonances consistent with $\mathbf{U^{mal}}$. Approximately 80% of the $\mathbf{U^{mal}}$ remained.

Thermal stability

To a Teflon-tapped NMR tube was added $\mathbf{U^{mal}}$ (5 mg) in CD_3CN (0.7 mL), the solution heated under reflux for 16 hours, and analysed by ^{1}H NMR spectroscopy.

The complex $\mathbf{U^{mal}}$ is stable (> 90%; NMR integrals) by ^{1}H NMR spectroscopy under these conditions, with a 1:1:1 triplet centred at 5.91 ppm, consistent with NH_4^+, observed (integral < 5% of $\mathbf{U^{mal}}$).

Photolytic stability

To a quartz NMR tube was added $\mathbf{U^{mal}}$ (25 mg, 50.4 μmol) in CD_3CN (1 mL) and the solution irradiated for 20 hours using lamp **(1)**. The resulting solution was analysed by ^{1}H NMR spectroscopy.

The complex **U^{mal}** is stable under photolysis conditions at 254 nm by ^{1}H NMR spectroscopy.

Addition of acetamide (1 or 2 equiv.)

To a magnetically stirred solution of **U^{mal}** (25 mg, 5.04 μmol, 1 equiv.) in CD_3CN (0.75 mL) was added acetamide (3 mg, 5.04 μmol, 1 equiv.; 6 mg, 10.1 μmol, 2 equiv.) in CD_3CN (0.75 mL; total 1.5 mL). After stirring for *ca*. 5 minutes, the solutions were analysed by ^{1}H NMR spectroscopy.

Two distinct sets of resonances were observed by ^{1}H NMR spectroscopy, those corresponding to **U^{mal}**, and those to uncomplexed acetamide.

5.4.2 Synthesis of $[UO_2(NO_3)_2(malPh_2)]$, U^{malPh2}

To a magnetically stirred suspension of *N*,*N*′-diphenylmalonamide, $malPh_2$ (1 g, 3.94 mmol, 1 equiv.) in CH_3CN (180 mL) was added **U^{NO3}** (1.98 g, 3.94 mmol, 1 equiv.), causing the dissolution of $malPh_2$ and the gradual formation of a yellow solution. The reaction was allowed to stir for 16 hours, and volatiles then removed *in vacuo* to yield 2.42 g (95%) of a powdery yellow solid, **U^{malPh2}**. Analysis was by ^{1}H NMR, IR (ATR-IR and solution-phase), electronic absorption, emission and excitation spectroscopies and elemental analysis. Pale yellow crystals (plates) suitable for SCXRD were grown by slow evaporation of a saturated solution of **U^{malPh2}** in CH_3CN at 4°C over 2 weeks.

^{1}H NMR (600 MHz, CD_3CN): δ/ppm = 10.13 (br s, 2H, NH), 8.06–7.96 (m, 4H, Ph), 7.65–7.53 (m, 4H, Ph), 7.41 (br s, 2H, Ph), 4.22 (s, 2H, CH_2), 2.30 (br s, water); *cf*. ^{1}H NMR free ligand, $malPh_2$ (500 MHz, CD_3CN): 8.91 (br s, 2H, NH), 7.57 (dt, 4H, Ph, *J* = 8.83, 0.96 Hz), 7.35 (tt, 4H, Ph, *J* = 7.18, 0.96 Hz), 7.12 (tt, 4H, Ph, *J* = 7.22, 1.25 Hz), 3.44 (s, 2H, CH_2), 2.13 (br s, water). ATR-IR (cm^{-1}): 3338 (m), 1645 (s), 1609 (w), 1586 (w), 1545 (s), 1512 (w), 1495 (m), 1455 (m), 1293 (s), 1260 (s), 1020 (m), 982 (m), 928 (vs, uranyl; *cf*. solution-phase IR, 942), 806 (w), 745 (s), 671 (w); *cf*. ATR-IR of free ligand, $malPh_2$ (cm^{-1}): 3274 (m), 1667 (m), 1646 (m), 1597 (m), 1536 (m), 1498 (m), 1443 (s), 1415 (w), 1356 (m), 1293 (w), 1250 (m), 1193 (w), 1161 (w), 981 (w), 905 (w), 857 (w), 750 (s), 689 (s). UV-vis (CH_3CN): λ/nm (ε/$M^{-1}cm^{-1}$): 418–488 (< 20), 249 (49000), 200 (107000). Elemental analysis: Calc. C, 27.79%, H, 2.18%, N, 8.64%; found C, 27.67%, H, 2.08%, N, 8.64%.

Water stability

A sample of **U^{malPh2}** (*ca*. 5 mg) was dissolved in bench (*e.g.* wet; < 0.1%) CD_3CN (1 mL) in an NMR tube, allowed to stand in the dark for one week at r.t., and analysed by ^{1}H NMR spectroscopy.

The ^{1}H NMR spectrum showed a peak, a 1:1:1 triplet, centred at 6.00 ppm, consistent with production of NH_3Ph^+. A clear decrease in the height and integrations of resonances corresponding to **U^{malPh2}** was also observed; approximately 45% of **U^{malPh2}** remained after one week, compared to initial integrals.

Thermal stability

To a Teflon-tapped NMR tube was added **U^{malPh2}** (5 mg) in CD_3CN (0.7 mL), the solution heated under reflux for 16 hours in the dark, and analysed by ^{1}H NMR spectroscopy. Colour change from pale to dark yellow.

^{1}H NMR spectroscopy of the resulting solution displayed some complex (*ca*. 50% starting amount, by integration), along with many new resonances, corresponding to numerous minor decomposition products (integrals < 5% of complex).

Photolytic stability

To a quartz NMR tube was added **U^{malPh2}** (25 mg, 38.6 μmol) and CD_3CN (1 mL), and the solution was irradiated using lamp **(3)** for 18 hours at r.t. The resulting product solution was observed to have darkened slightly, and was analysed by ^{1}H NMR spectroscopy.

No degradation of the complex **U^{malPh2}** was observed by ^{1}H NMR spectroscopy under these conditions.

5.4.3 Synthesis of $[UO_2(NO_3)_2(malPh_4)]$, U^{malPh4}

Synthesis, characterisation, and water, photolytic and thermal stability testing as for **U^{malPh2}**, Section 5.4.2. Masses: *N*,*N*,*N*′,*N*′-tetraphenylmalonamide, $malPh_4$ (1.251 g, 3.08 mmol, 1 equiv.), **U^{NO3}** (1.545 g, 3.08 mmol, 1 equiv.) and CH_3CN (200 mL). Yield of **U^{malPh4}** = 2.31 g, 94%.

^{1}H NMR (600 MHz, CD_3CN): δ/ppm = 7.70 (br s, Ph), 7.57 (t, Ph, *J* = 6.8 Hz), 7.46 (br s, Ph), 7.41–7.36 (m, Ph), 4.02 (br s, CH_2), 2.29 (br s, water); *cf*. ^{1}H NMR of free ligand, $malPh_4$ (500 MHz, CD_3CN): 7.42–7.40 (m, Ph), 7.36–7.32 (m, Ph), 7.26–7.23 (m, Ph), 7.11 (br s, Ph), 3.28 (s, CH_2), 2.13 (br s, water) [*aryl protons were overlapping and thus not integrated for both* ***U^{malPh4}*** *and* $malPh_4$]. ATR-IR (cm^{-1}): 1634 (m), 1589 (w), 1558 (w), 1488 (s), 1443 (w), 1295 (w), 1280 (m), 1032 (w), 998 (w), 944 (s, uranyl; *cf*. solution-phase IR, 941), 846 (w), 812 (w), 758 (m), 694 (s), 587 (m); *cf*. ATR-IR of free ligand, $malPh_4$ (cm^{-1}): 1662 (s), 1594 (m), 1491 (s), 1406 (w), 1359 (s), 1263 (w), 1205 (w), 1144 (m), 1075 (w), 758 (s), 695 (s), 662 (w), 588 (m). UV-vis (CH_3CN): λ/nm (ε/M^{-1}cm^{-1}): 409–488 (< 15), 239 (7600), 201 (50700). Mass spec., *m/z* (Da*;* relative intensity, assignment): 407.1570 (5%, $[(malPh_4)\text{-}H]^+$), 429.1587 (15%, $[(malPh_4)\text{-}Na]^+$), 738.1966 (12%, $[UO_2(NO_3)(malPh_4)]^+$), 823.1756 (< 1%, $[UO_2(NO_3)_2(malPh_4)\text{-}Na]^+$), 835.3256 (40%, $[(malPh_4)_2\text{-}Na]^+$), 1144.3642 (100%, $[UO_2(NO_3)(malPh_4)_2]^+$). Elemental analysis: Calc. C, 40.51%, H, 2.77%, N, 7.01%; found C, 40.65%, H, 2.88%, N, 7.08%.

The photolytic stability test was also repeated anaerobically, using **U^{malPh4}** (9 mg, 11.2 μmol) in CD_3CN (0.6 mL). The solution was freeze-pump-thaw degassed three times, irradiated for 16 hours using lamp **(4)** at r.t., and the resulting solution analysed by ^{1}H NMR spectroscopy. For both photolytic stability tests of **U^{malPh4}** (aerobic, and anaerobic), significant amounts (*ca*. 65%, by ^{1}H NMR integration) of $Ph_2NH_x^{y+}$ (x = 1, y = 0, diphenylamine; x = 2, y = 1, diphenylammonium) were observed, along with remaining (*ca*. 30%) **U^{malPh4}**, and unidentified products (*ca*. 5% of total integrals).

^{1}H NMR spectroscopic analysis of the sample tested for water stability, stored in the dark for one week, showed a peak, a 1:1:1 triplet, consistent with production of $NH_2Ph_2^+$ (at *ca*. 6.0 ppm). No resonances consistent with **U^{malPh4}** were observed.

^{1}H NMR spectroscopic analysis of the sample refluxed in CD_3CN (*e.g.* tested for thermal stability) showed no resonances consistent with **U^{malPh4}**, though a large number of resonances, including a 1:1:1 triplet consistent with $NH_2Ph_2^+$ were observed.

5.4.4 Synthesis of $[UO_2(NO_3)_2(mal^iPr_4)]$, U$^{mali Pr4}$

To two separate vials was added **U^{NO3}** (46 mg, 92 μmol, 1 equiv.), and mal^iPr_4 (25 mg, 92 μmol, 1 equiv.) in CH_3CN (4 mL), the solutions combined, and the resulting pale yellow solution magnetically stirred for 16 hours at r.t. The volatiles were subsequently removed *in vacuo*, yielding a brown powdery solid, **U$^{mali Pr4}$** (55.6 mg, 91%), which was characterised by ^{1}H NMR spectroscopy and ESI-MS. Small yellow crystals of **U$^{mali Pr4}$** suitable for SCXRD were isolated by slow evaporation of a saturated solution of **U$^{mali Pr4}$** in CH_3CN at r.t. over 5 days.

^{1}H NMR (500 MHz, CD_3CN): δ/ppm = 4.28 (br s, 2H, CH_2), 4.08 (br s, 2H, N-CH), 2.47 (br s, 2H, N-CH), 1.74 (d, 12H, N-CH-C$\underline{H}_3$, *J* = 6.6 Hz), 1.42 (d, 12H, N-CH-C$\underline{H}_3$, *J* = 6.7 Hz); *cf*. ^{1}H NMR of free ligand,[20] mal^iPr_4 (300 MHz, $CDCl_3$): 3.94 (m, 4H, N-CH), 3.10 (s, 2H, CH_2), 1.20 (d, 24H, N-CH-C$\underline{H}_3$). Mass spec., *m/z* (Da*;* relative intensity, assignment): 271.2387 (100%, $[(mal^iPr_4)\text{-}H]^+$), 602.2610 (5%,

$[UO_2(NO_3)(mal^iPr_4)]^+$), 687.2362 (6%, $[UO_2(NO_3)_2(mal^iPr_4)\text{-}Na]^+$), 872.4943 (18%, $[UO_2(NO_3)(mal^iPr_4)_2]^+$), 957.4707 (< 5%, $[UO_2(NO_3)_2(mal^iPr_4)_2\text{-}Na]^+$).

5.4.5 Complexation of U^{NO3} with $py(CONH_2)_2$, Product Mixture 2.6

To a solution of **U^{NO3}** (100.2 mg, 199 μmol, 1 equiv.) in CH_3CN (3 mL) was added a CH_3CN solution of 2,6-pyridinedicarboxamide, $py(CONH_2)_2$ (32.8 mg, 199 μmol, 1 equiv.; another 3 mL). The yellow suspension was diluted with further CH_3CN (50 mL), and the resulting yellow solution magnetically stirred for 1 hour at r.t. Removal of volatiles *in vacuo* resulted in a powdery yellow solid (64.1 mg, moderate yield), which was analysed by ^{1}H NMR and ATR-IR spectroscopies, and ESI-MS. Attempts to grow crystals suitable for SCXRD by solvent evaporation were unsuccessful.

A sample of protonated ligand was separately prepared by addition of two drops of TFA (99% in water) to an NMR tube containing a saturated solution of $py(CONH_2)_2$ in CD_3CN (1 mL).

The photostability of the product was tested by irradiation of a saturated solution in CD_3CN (*ca*. 1 mL) for 16 hours using lamp **(4)** at r.t., and analysing the resultant darker yellow solution by ^{1}H NMR spectroscopy.

^{1}H NMR (500 MHz, CD_3CN): δ/ppm = 9.03 (s, 1H), 8.82 (s, 2H), 8.59 (s, 1H), 8.36 (s, 1H), 8.14 (s, 1H), 6.43 (br s, 1H), 5.98 (1:1:1 t, NH_4^+, J = 53.2 Hz); *cf.* ^{1}H NMR of free ligand, $py(CONH_2)_2$ (500 MHz, CD_3CN): δ/ppm = 8.26 (d, 2H, CH_{Ar}, J = 7.7 Hz), 8.09 (t, 1H, CH_{Ar}, J = 7.7 Hz), 7.96 (br s, 2H, N–H_{amide}), 6.21 (br s, 2H, N–H_{amide}); *cf*. ^{1}H NMR of protonated ligand (500 MHz, CD_3CN): 10.12 (br s, acid H), 8.53 (br s, 2H, amide NH), 8.36 (d, 2H, CH_{Ar}, J = 7.6 Hz), 8.20 (t, 1H, CH_{Ar}, J = 7.6 Hz), 7.30 (br s, 2H, amide NH). ATR-IR (cm^{-1}): 3303 (m br), 3089 (m br), 1666 (m), 1478 (m), 1270 (s), 938 (s, uranyl), 748 (s), 648 (m), 557 (m br); c*f.* ATR-IR of free ligand, $py(CONH_2)_2$ (cm^{-1}): 3399 (m), 3227 (m br), 1664 (s), 1585 (m), 1381 (m), 765 (m), 586 (s), 539 (s). Mass spec., *m/z* (Da*;* relative intensity, assignment): 166.0610 (7%, $[(L)–H]^+$), 188.0428 (13%, $[(L)–Na]^+$), 497.0827 (100%, $[UO_2NO_3–(L)]^+$). Note, L = $py(CONH_2)_2$.

^{1}H NMR spectroscopy of the irradiated product solution showed no resonances consistent with the starting product mixture, Product 2.6.

5.4.6 Complexation of U^{NO3} with $py(CONHMe)_2$, Product 2.7

To a magnetically stirred solution of **U^{NO3}** (250 mg, 0.498 mmol, 1 equiv.) in CH_3CN (5 mL) was added *N*,*N*′-dimethyl-2,6-pyridinedicarboxamide, $py(CONHMe)_2$ (102 mg, 0.528 mmol, 1.06 equiv.), also in CH_3CN (total 15 mL). After 2 minutes of stirring the yellow solution became turbid, gradually producing a small amount of an off-white precipitate over the next hour of stirring. This mixture was then allowed to stir for 16 hours, and the eventual precipitate filtered off (frit) with the remaining yellow solution taken to dryness *in vacuo*, to give a viscous yellow oil. Dissolving this oil in CH_3CN (1 mL) gave more off-white precipitate which was sonicated for *ca*. 5 minutes. Addition of water (0.5 mL) to this mixture dissolved all solids, which after 5 days yielded small yellow crystals suitable for SCXRD; a solid consistent with a formula of $[UO_2(py(CONHMe)_2)_2][NO_3]_2$ (**2.7**) was obtained.

Attempts to analyse the product **2.7** by ^{1}H NMR spectroscopy (CH_3CN or CD_3OD) were unsuccessful.

5.4.7 Unsuccessful Complexation of U^{NO3} with Diglycolamide, Reaction 2.8

To a magnetically stirred suspension of diglycolamide (41.7 mg, 0.316 mmol, 1 equiv.) in CH_3CN (30 mL) was added **U^{NO3}** (159 mg, 0.317 mmol, 1 equiv.), and the yellow suspension allowed to stand in the dark for 4 days. The resulting yellow solution was filtered (frit; fine white precipitate) and taken to dryness *in vacuo* to give a pale brown oil, and solid on trituration, which was analysed by ^{1}H NMR spectroscopy. Mass of solid = 47 mg, poor yield.

The ^{1}H NMR spectrum showed a large number of resonances consistent with either decomposition, or degradation of diglycolamide in solution. The characteristic 1:1:1 triplet for NH_4^+ at *ca.* 6 ppm dominated the spectrum (*ca*. 80% of total integrals).

5.4.8 Unsuccessful Complexation of U^{NO3} with TODGA, Reaction 2.9

To a magnetically stirred solution of TODGA (50 mg, 89 μmol, 1 equiv.) in CH_3CN (2.5 mL) was added **U^{NO3}** (43.3 mg, 86.2 μmol, 1 equiv.), also in CH_3CN (2.5 mL; total, 5 mL). The yellow solution was stirred for 16 hours and volatiles removed *in vacuo*, yielding a pale yellow solid (82.1 mg, good yield) that was analysed by ^{1}H NMR and solution-phase IR spectroscopies.

^{1}H NMR (500 MHZ, CD_3CN): δ/ppm = 5.45 (s, 4H, O-CH_2), 3.85 (br s, 4H, N-CH_2), 3.41 (t, 4H, N-CH_2, *J* = 7.6 Hz), 1.46–1.26 (m, 48H, *N*-alkyl), 0.88–0.83 (m, 12 H, -CH_3); *cf*. ^{1}H NMR of free TODGA (500 MHz, CD_3CN): 4.14 (s, 4H, O-CH_2), 3.22 (t, 4H, N-CH_2, *J* = 7.5 Hz), 3.18 (t, 4H, N-CH_2, *J* = 7.6 Hz), 1.53–1.41 (m, 8H, N-CH_2-C$\underline{H}_2$), 1.31–1.21 (m, 40H, *N*-alkyl), 0.86 (t, 12H, -CH_3, *J* = 6.9 Hz). Solution-IR (cm^{-1}): 3638 (br s), 3544 (br s), 3370 (w), 1624 (vs), 1283 (s), 1276 (s), 1194 (m), 1128 (w), 1102 (w), 945 (s, uranyl); *cf*. free TODGA, solution-IR of free ligand, TODGA (cm^{-1}): 3541 (br s), 1653 (br s), 1413 (w), 1215 (s), 1190 (m), 1096 (w), 978 (w), 825 (br s).

Photolytic stability

To an NMR tube was added a portion of the reaction solution used for ^{1}H NMR analysis (*ca*. 1 mL), which was then irradiated at r.t. using lamp **(4)** for 16 hours. The resulting dark yellow solution was analysed using ^{1}H NMR spectroscopy with solvent suppression.

The ^{1}H NMR spectrum of the product mixture of photolysis showed numerous resonances between 1–3 ppm, consistent with degradation of the TODGA ligand (*e.g.* alkyl C-H proton environments).

5.4.9 Complexation of U^{NO3} with *N*,*N*'-dimethyloxamide, Reaction 2.10

To two separate vials was added solutions of **U^{NO3}** (50 mg, 0.1 mmol, 1 equiv.) and *N*,*N*'-dimethyloxamide (11.6 mg, 0.1 mmol, 1 equiv.), both in CD_3CN (0.6 mL each; total, 1.25 mL). Combination of these two solutions in a Teflon-tapped NMR tube led to a dark yellow solution which, after sonication (*ca.* 5 minutes), was allowed to stand for 16 hours at r.t. in the dark, and the resulting yellow solution analysed by ^{1}H NMR spectroscopy. No solid was isolated from the product solution.

^{1}H NMR (600 MHz, CD_3CN): δ/ppm = 8.27 (br s, 2H, NH), 3.65 (br s, water), 2.98 (d, 6H, NMe, *J* = 3.7 Hz), 2.09 (br s, water); *cf*. ^{1}H NMR of free ligand, *N,N*'-dimethyloxamide (500 MHz, CD_3CN): 7.64 (br s, 2H, NH), 2.77 (d, 6H, NMe, *J* = 5.1 Hz), 2.15 (br s, water).

Photolytic stability

To a quartz NMR tube was added a portion of the product solution described above (0.5 mL), which was irradiated at r.t. using lamp **(1)** for 16 hours. The resulting dark orange solution was analysed by ^{1}H NMR spectroscopy.

The ^{1}H NMR spectrum of the product solution after photolysis showed numerous resonances consistent with formation of multiple degradation products, including the characteristic 1:1:1 triplet of NH_4^+ at *ca*. 6 ppm.

5.4.10 Unsuccessful Complexation of U^{NO3} with Adipamide, Reaction 2.11

To a magnetically stirred solution of **U^{NO3}** (28.8 mg, 57.4 μmol, 1 equiv.) in CH_3CN (30 mL) was added adipamide (8.6 mg, 60.2 μmol, 1.08 equiv.) and the reaction stirred for 4 days at r.t. An off-white

precipitate was filtered (frit) from the pale yellow solution. Addition of this solution to CD_3CN, CD_3OD or acetone-D_6 for analysis by ^1H NMR spectroscopy resulted instead in precipitation of a white solid, found by ATR-IR spectroscopy (after filtering and drying) to be free adipamide ligand.

5.4.11 Unsuccessful Complexation of U^{NO3} with Phthalamide, Reaction 2.12

To a solution of **U^{NO3}** (100.1 mg, 199 μmol, 1 equiv.) in CH_3CN (3 mL) was added a CH_3CN solution of phthalamide (16.3 mg, 99 μmol, 0.5 equiv.; another 3 mL), and the resulting yellow solution magnetically stirred for 1 hour at r.t. Removal of volatiles *in vacuo* produced a powdery yellow solid (57.3 mg, moderate yield), which was analysed by ^1H NMR spectroscopy.

Curiously, this powder was found to be insoluble in both CD_3CN and CD_3OD (despite being isolated from CD_3CN). As such, attempts to analyse this product by ^1H NMR spectroscopy (*e.g.* to study the solution-phase behaviour) were unsuccessful. ATR-IR spectroscopy analysis was not attempted, given the primary objective of determining solution-phase behaviour in CH_3CN (in which the product(s) of this reaction was insoluble).

5.4.12 Unsuccessful Complexation of U^{NO3} with Isophthalamide, Reaction 2.13

To two separate vials was added **U^{NO3}** (76 mg, 0.15 mmol, 1 equiv.) and isophthalamide (25 mg, 0.16 mmol, 1.06 equiv.) in a CH_3OH:CH_3CN co-solvent mixture (1:1 b/v, 30 mL total), and the combined solution magnetically stirred for 16 hours at r.t. The resulting dark yellow solution and precipitate were filtered (frit), with both the white precipitate (21 mg) and solid (58 mg, moderate yield; resulting from removal of volatiles from the filtrate *in vacuo*) being insoluble in CD_3CN or CD_3OD. No further attempts were made to analyse the product(s) from this reaction by ^1H NMR spectroscopy. ATR-IR spectroscopy analysis was not attempted on these solids, given the primary objective of determining solution-phase behaviour in CH_3CN.

5.4.13 Unsuccessful Complexation of U^{NO3} with *N*,*N*'-diphenylterephthalamide, Reaction 2.14

To a magnetically stirred solution of **U^{NO3}** (24.8 mg, 49.4 μmol, 1 equiv.) was added a suspension of *N*,*N*'-diphenylterephthalamide (1 equiv.: 16.2 mg, 51.2 μmol, 1.04 equiv.; 2 equiv.: or 32.5 mg, 102.6 μmol) in CH_3CN (total 30 mL), and the reaction allowed to stir for 7 days at r.t. The resulting suspension was filtered (frit), the filtrate taken to dryness *in vacuo*, and the resulting off-white solid weighed (39.6 mg, good yield).

Given the analogous behaviour of **U^{NO3}** with phthalamide and isophthalamide (being insoluble in CD_3CN or CD_3OD) it was decided that no further effort would be undertaken to characterise the products of this reaction further.

5.5 Complexes of the Uranyl Ion with Monodentate Amides

5.5.1 Synthesis of $[UO_2(NO_3)_2(benzNH_2)_2]$, $U^{benzNH2}$

To two separate vials was added solutions of **U^{NO3}** (50 mg, 0.1 mmol, 1 equiv.) and benzamide, $benzNH_2$ (24.1 mg, 0.2 mmol, 2 equiv.) in CD_3CN (each 1.25 mL; total, 2.5 mL), leading to a dark yellow solution and suspension when these two reaction components were combined in a Teflon-tapped NMR tube. Brief sonication (*ca*. 5 minutes) of this mixture dissolved all solids, and the resulting dark yellow solution was allowed to stand for 16 hours at r.t. and analysed by ^1H NMR and solution-IR spectroscopies, and ESI-MS.

This synthesis was subsequently scaled-up using 4.02 g of **U^{NO3}** and 1.94 g of $benzNH_2$. 5.01 g of a yellow solid was obtained, and analysed by ^1H NMR and IR spectroscopy, and ESI-MS. 4.99 g of **$U^{benzNH2}$** was isolated, 98%.

^{1}H NMR (500 MHZ, CD_3CN): δ/ppm = 8.11 (d, 2H, Ph, *J* = 7.0 Hz), 7.90 (br s, 1H, NH), 7.65 (t, 1H, Ph, *J* = 7.6 Hz), 7.11 (br s, 1H, NH), 2.80 (br s, water); *cf*. ^{1}H NMR of free ligand, benzNH_2 (500 MHz, CD_3CN): 7.84–7.82 (m, 2H, Ph), 7.56–7.52 (m, 1H, Ph), 7.48–7.44 (m, 2H, Ph), 6.77 (br s, 1H, NH), 6.06 (br s, 1H, NH), 2.16 (br s, water). ATR-IR (cm^{-1}): 3491 (m), 3455 (w), 3369 (s), 2158 (m), 2031 (w), 1973 (w), 1631 (s), 1598 (w), 1526 (s), 1449 (m), 1274 (s), 1027 (m), 933 (s, uranyl), 911 (s), 803 (m), 745 (s), 711 (s); *cf*. ATR-IR of free ligand, benzNH_2 (cm^{-1}): 3363 (br m), 3163 (br m), 2159 (w), 1653 (s), 1623 (s), 1578 (s), 1449 (m), 1396 (s), 1123 (w), 1026 (m). Solution-IR (cm^{-1}): 3369 (br s), 1683 (s), 1658 (s), 1281 (s), 945 (s), 939 (sh), 932 (sh), 928 (sh); *cf*. solution-IR of free ligand, benzNH_2 (cm^{-1}): 3485 (br s), 3377 (br s), 1686 (vs), 1610 (s). Mass spec., *m/z* (Da*;* relative intensity, assignment): 122.0642 (20%, [(benzNH_2)-H]$^+$), 574.1386 (20%, $[UO_2(NO_3)(benzNH_2)_2]^+$), 696.1932 (100%, $[UO_2(NO_3)(benzNH_2)_3]^+$).

Photolytic stability

To a quartz NMR tube was added a portion of **U^{benzNH2}** solid (< 20 mg) in CD_3CN (1 mL), and the yellow solution irradiated at r.t. using lamp **(1)** for 16 hours. There was no colour change after irradiation for 16 hours, and the resulting solution was analysed by ^{1}H NMR spectroscopy.

The ^{1}H NMR spectrum of the product solution showed resonances corresponding only to **U^{benzNH2}**, suggesting no degradation of **U^{benzNH2}** occurred during or after irradiation.

5.5.2 Synthesis of $[UO_2(NO_3)_2(benzNHPh)_2]$, U^{benzNHPh}

To a magnetically stirred solution of **U^{NO3}** (501.3 mg, 1 mmol, 1 equiv.) in CH_3CN (5 mL) was added a suspension of benzanilide, benzNHPh (*N*-phenylbenzamide; 401.1 mg, 2.03 mmol, 2.03 equiv.) in CH_3CN (15 mL; total, 20 mL). Any suspended solids (*cf*. benzNHPh) rapidly dissolved and the resulting solution gradually darkened on stirring over 15 minutes, becoming dark yellow. The volatiles were then removed *in vacuo* and the resulting yellow solid analysed by ^{1}H NMR, IR (ATR-IR and solution-phase) and electronic absorption spectroscopies, ESI-MS and elemental analysis.

The synthesis was subsequently scaled-up, using 2.5 g of **U^{NO3}**, 2.02 g of amide and 200 mL of CH_3CN. 3.82 g (97%) of a yellow solid, **U^{benzNHPh}**, was obtained, which was further analysed by UV-vis spectroscopy (1.1 mg in 50 mL CH_3CN). Colourless crystals of free benzNHPh ligand were isolated by slow evaporation of a saturated CH_3CN solution of **U^{benzNHPh}**, stored in the dark at 4°C over five days.

^{1}H NMR (500 MHZ, CD_3CN): δ/ppm = 9.16 (br s, 1H, NH), 8.00 (br s, 2H, Ph), 7.75 (d, 2H, Ph, *J* = 6.9 Hz), 7.62 (tt, 1H, Ph, *J* = 7.3, 1.3 Hz), 7.52 (t, 2H, Ph, *J* = 7.6 Hz), 7.35 (br t, 2H, Ph, *J* = 6.9 Hz), 7.17 (t, 1H, Ph, *J* = 7.3 Hz), 3.76 (br s, water); *cf*. ^{1}H NMR of free ligand, benzNHPh (400 MHz, CD_3CN): 8.73 (br s, 1H, NH), 7.93 (d, 2H, Ph, *J* = 7.1 Hz), 7.72 (d, 2H, Ph, *J* = 7.6 Hz), 7.61–7.57 (m, 1H, Ph), 7.52 (t, 2H, Ph, *J* = 7.6 Hz), 7.38 (t, 2H, Ph, *J* = 8.3 Hz), 7.15 (t, 1H, Ph, *J* = 7.3 Hz), 2.14 (br s, water). ATR-IR (cm^{-1}): 3354 (br m), 1607 (s), 1594 (m), 1548 (s), 1476 (s), 1279 (vs), 1029 (m), 942 (vs, uranyl), 902 (m), 755 (s), 690 (s); *cf*. ATR-IR of free ligand, benzNHPh (cm^{-1}): 3343 (m), 3053 (w), 1653 (s), 1599 (s), 1525 (s), 1490 (m), 1436 (s), 1320 (m), 1253 (m), 1027 (m), 747 (s), 714 (m), 689 (s), 645 (s). Solution-IR (cm^{-1}): 3356 (br m), 1675 (s), 1600 (m), 1271 (s), 954 (br m), 948 (sh), 936 (sh), 932 (sh). UV-vis (CH_3CN): λ/nm (ε/$M^{-1}cm^{-1}$): 466–401 (< 20), 264 (11300), 227 (10900), 200 (40600). Mass spec., *m/z* (Da*;* relative intensity, assignment): 198.0911 (85%, [(benzNHPh)-H]$^+$), 220.0715 (80%, [(benzNHPh)-Na]$^+$), 417.1582 (100%, $[UO_2(NO_3)_2\text{-Na}]^+$), 726.1972 (10%, $[UO_2(NO_3)(benzNHPh)_2]^+$), 811.1773 (5%, $[UO_2(NO_3)_2(benzNHPh)_2\text{-Na}]^+$), 923.2826 (35%, $[UO_2(NO_3)(benzNHPh)_3]^+$). Elemental analysis: Calc. C, 39.16%, H, 2.91%, N, 7.05%; found C, 39.25%, H, 2.85%, N, 7.09%.

Photolytic stability

To a quartz NMR tube was added **U^{benzNHPh}** (25 mg) in CD_3CN (1 mL), and the resulting yellow solution irradiated at r.t. using lamp **(1)**. After 2 hours of irradiation the solution had darkened to pale orange, eventually becoming pale brown after 22 hours. This solution was analysed by ^{1}H NMR spectroscopy.

The ^{1}H NMR spectrum of the product solution showed resonances corresponding only to **U^{benzNHPh}**, suggesting no degradation of the complex had occurred during or after irradiation.

Effect of added water on benzNHPh ^{1}H NMR signal

To an NMR tube was added free benzanilide, benzNHPh (26.6 mg, 0.135 mmol) and CD_3CN (0.6 mL), and the solution analysed by ^{1}H NMR spectroscopy. Water was added in two aliquots (1st aliquot, 2.4 mg, 0.133 mmol, 1 equiv.; 2nd aliquot, 21.6 mg, 1.33 mmol, 10 equiv. total), and shaken briefly. The solution was analysed by ^{1}H NMR spectroscopy after each aliquot was added.

The ^{1}H NMR spectrum of the product solution showed a steadily increasing shift to higher frequencies in the position of the resonance caused by water protons (*e.g.* 2.13 ppm → *ca*. 2.5 ppm), consistent with interactions of the ligand (benzNHPh) N-H amide proton with water.

*Addition of extra equivalents of benzNHPh to **U^{benzNHPh}***

To a solution of **U^{benzNHPh}** (20.2 mg, 25.6 μmol, 1 equiv.) was added free benzanilide, benzNHPh (10.4 mg, 52.8 μmol, 2.06 equiv.) in CD_3CN (1 mL total). The solution was shaken briefly, sonicated for 5 minutes, and analysed by ^{1}H NMR spectroscopy at both 293 K and 233 K, and by solution-phase IR spectroscopy.

^{1}H NMR spectroscopic analysis showed resonances attributed to **U^{benzNHPh}** that were broadened on addition of excess free ligand, benzNHPh, consistent with dynamic exchange in solution. Four new resonances attributed to the N-H protons of **U^{benzNHPh}** (9.16 ppm at 293 K) appeared in the ^{1}H NMR spectrum of **U^{benzNHPh}** at 233 K. Solution-phase IR spectroscopy (CH_3CN) of **U^{benzNHPh}** indicated multiple uranyl-containing species (five very sharp bands, 960–920 cm^{-1}).

5.5.3 Synthesis of $[UO_2(NO_3)_2(benzNPh_2)_2]$, U^{benzNPh2}

To a magnetically stirred solution of **U^{NO3}** (100 mg, 0.2 mmol, 1 equiv.) in CH_3CN (3 mL) was added *N,N*-diphenylbenzamide, $benzNPh_2$ (109.8 mg, 0.402 mmol, 2.01 equiv.) also in CH_3CN (< 15 mL), and the resultant pale yellow solution stirred for 16 hours at r.t. The volatiles were then removed *in vacuo*, and the resulting yellow solid, **U^{benzNPh2}** (178 mg, 95%), was analysed by ^{1}H NMR spectroscopy.

^{1}H NMR (500 MHZ, CD_3CN): δ/ppm = 7.47 (d, 2H, Ph, *J* = 7.3 Hz), 7.33–7.30 (m, 6H, Ph), 7.25–7.20(m, 8H, Ph), 2.85 (br s, water); *cf*. ^{1}H NMR of free ligand, $benzNPh_2$ (400 MHz, $CDCl_3$):[21] 7.49–7.46 (m, 3H), 7.33–7.29 (m, 4H), 7.25–7.16 (m, 8H).

5.5.4 Synthesis of $[UO_2(NO_3)_2(piv^iPr_2)_2]$, U$^{piv^iPr2}$

To two separate vials was added **U^{NO3}** (63 mg, 0.125 mmol, 1 equiv.) and *N,N*-diisopropylpivalamide, piv^iPr_2 (50 mg, 0.25 mmol, 2.01 equiv.), in CH_3CN (5 mL each), and the reaction magnetically stirred for 16 hours at r.t. The volatiles were removed *in vacuo*, and the yellow solid, **U$^{piv^iPr2}$** (103 mg, 94%), analysed by ^{1}H NMR and ATR-IR spectroscopy. Yellow crystals suitable for SCXRD were obtained by slow evaporation of a saturated CH_3CN solution of **U$^{piv^iPr2}$** at 4°C over five days in the dark.

^{1}H NMR (500 MHZ, CD_3CN): δ/ppm = 4.37 (br s, 1H, N-CH), 3.38 (br s, 1H, N-CH), 1.40–1.20 (m, 21H, ^{i}Pr and ^{t}Bu-CH_3); *cf*. ^{1}H NMR of free ligand, piv^iPr_2 (300 MHz, $CDCl_3$): 4.27 (m, 1H, N-CH), 3.23 (m, 1H, N-CH), 1.34 (d, 6H, ^{i}Pr-CH_3), 1.20 (s, 9H, ^{t}Bu-CH_3), 1.14 (d, 6H, ^{i}Pr-CH_3).[22] ATR-IR (cm^{-1}): 2983 (w), 2937 (w), 2161 (br w), 2034 (w) (+ 1979 (sh)), 1540 (s), 1515 (s), 1481 (s), 1450 (m), 1360 (m), 1335 (w), 1279 (vs), 1030 (s), 943 (s, uranyl) (+ 946 (sh)), 747 (m); *cf*. ATR-IR of free ligand, piv^iPr_2 (cm^{-1}): 2968 (m), 2956 (w), 1811 (w), 1734 (w), 1617 (s), 1479 (w), 1429 (m), 1354 (s), 1313 (s), 1214 (m), 1155 (m), 1122 (m), 1038 (s), 755 (w).

Photolytic stability

To an NMR tube was added **U$^{piv/Pr2}$** (25 mg) in CD_3CN (1 mL) and the yellow solution irradiated at r.t. using lamp **(4)** for 16 hours. The resulting dark yellow solution was then analysed by ^1H NMR spectroscopy, which showed no resonances corresponding to **U$^{piv/Pr2}$**, indicating decomposition.

5.6 Complexes of the Uranyl Ion with Oximes

5.6.1 Unsuccessful Complexation of U^{NO3} with Ph_2-oxime, Reaction 2.15

To a magnetically stirred solution of **U^{NO3}** (202 mg, 0.402 mmol, 1 equiv.) in CH_3CN (5 mL) was added benzophenone oxime, Ph_2-oxime (for 1 equiv. oxime = 79 mg, 0.4 mmol; for 2 equiv. = 158.2 mg, 0.802 mmol; for 5 equiv. = 393.3 mg, 1.99 mmol) dropwise in CH_3CN (30 mL; total, 35 mL). The resulting solutions (no colour change with 1 equiv. oxime, pale orange for 2 and 5 equiv. of oxime) were stirred for 16 hours at r.t., and the reaction solutions (of 1, 2 or 5 equiv. of Ph_2-oxime with **U^{NO3}**) were analysed by ^1H NMR spectroscopy. Solids isolated in good or quantitative yields.

^1H NMR spectra acquired on all product solutions contained multiple, very broad resonances (*ca*. 6–8 ppm), consistent with multiple species, in rapid exchange on the NMR timescale.

5.6.2 Unsuccessful Complexation of U^{NO3} with fl-oxime, Reaction 2.16

To a magnetically stirred solution of **U^{NO3}** (201 mg, 0.4 mmol, 1 equiv.) in CH_3CN was added 9-fluorenone oxime, fl-oxime (391 mg, 2 mmol, 5 equiv.), as a solution in CH_3CN (total 50 mL). The initially pale yellow solution turned orange after stirring for 16 hours at r.t. This solution yielded dark brown microcrystalline powder on drying *in vacuo* (169 mg, poor yield), which was analysed by ^1H NMR spectroscopy. A portion of retained solids were redissolved in CH_3CN (minimum volume), giving a saturated orange solution separated from remaining solids by filtration through microfibre glass filters. Attempts to obtain crystals suitable for SCXRD (vapour- and solvent-diffusion at r.t. with CH_3CN and hexane as antisolvent, and slow evaporation) yielded powders (total 517 mg) which were analysed by ^1H NMR and ATR-IR spectroscopies.

This synthesis was subsequently scaled-up using 2.06 g of **U^{NO3}** and 4 g of oxime in 400 mL of CH_3CN. The ^1H NMR spectrum on dark orange-red product (5.6 g, good yield) after 5 days of magnetic stirring at r.t. was identical to the smaller scale reaction. From this reaction orange-red crystals suitable for SCXRD were grown by solvent diffusion of hexane antisolvent into a saturated product solution (**2.16**) at r.t. for one week; $[UO_2(NO_3)_2(OH_2)_2]\cdot(\text{fl-one})_4$ (**2.20**).

^1H NMR spectra acquired on product solutions in CD_3CN contained multiple resonances consistent with multiple species, in dynamic exchange, on the NMR timescale for these reactions.

ATR-IR (cm^{-1}): 3185 (br w), 3069 (w), 1684 (s + 1690 sh), 1658 (m), 1591 (s), 1559 (s), 1522 (s), 1451 (s), 1352 (m), 1302 (m), 1275 (m), 1193 (m), 1154 (w), 1098 (w), 1025 (w), 945 (s + 953 sh, 938 sh, 925 sh, 920 sh), 835 (m), 804 (m + 756 sh), 743 (w), 735 (s), 724 (br s); *cf*. ATR-IR of free ligand, fl-oxime (cm^{-1}): 3154 (br m), 3023 (w), 2799 (br m), 1642 (w), 1601 (m), 1443 (s), 1433 (w), 1319 (w), 1159 (s), 1107 (w), 1089 (m), 995 (s), 934 (m), 778 (s), 726 (vs), 675 (w), 640 (m).

Photolytic stability

To a quartz NMR tube was added a small portion of solid isolated from the larger scale reaction (20 mg; "as-is", without purification), dissolved in CD_3CN (1 mL), and the solution irradiated using lamp **(1)** for 16 hours at r.t. The resulting orange solution and copious orange-yellow precipitate were analysed by ^1H NMR spectroscopy.

The ^{1}H NMR spectrum of this mixture displayed multiple sharp aromatic resonances additionally to multiple broad singlets, consistent with photolytic degradation of the product(s).

5.6.3 Unsuccessful Complexation of U^{NO3} with cy-oxime, Reaction 2.17

To a magnetically stirred solution of **U^{NO3}** (200 mg, 0.398 mmol, 1 equiv.) in CH_3CN (25 mL) was added cyclohexanone oxime, cy-oxime (226 mg, 2 mmol, 5.03 equiv.), and the resulting yellow solution refluxed for 16 hours at 70°C. Cooling the reaction mixture to r.t. and removal of volatiles *in vacuo* yielded an orange-yellow powdery solid (406 mg, good yield), which was analysed by ^{1}H NMR spectroscopy. Colourless crystals of uncomplexed ligand (cy-oxime) were isolated by slow evaporation of the reaction solution (2 mL) at r.t. for 2 days.

A ^{1}H NMR spectrum acquired on the product contained multiple and broad resonances consistent with multiple species, in dynamic exchange, on the NMR timescale for these reactions. It was not possible to satisfactorily deconvolute and therefore assign individual resonances.

5.6.4 Unsuccessful Complexation of U^{NO3} with ind-oxime, Reaction 2.18

To a magnetically stirred solution of **U^{NO3}** (200 mg, 0.4 mmol, 1 equiv.) in CH_3CN (5 mL) was added 1-indanone oxime, ind-oxime (for 1 equiv. oxime = 120 mg, 0.4 mmol; for 2 equiv. = 240 mg, 0.816 mmol; for 3 equiv. = 360.4 mg, 1.22 mmol; for 4 equiv. = 481.6 mg, 1.64 mmol; for 5 equiv. = 299.5 mg 2.04 mmol; 5 equiv. with pyridine = 302 mg, 2.06 mmol of ind-oxime and pyridine, 32.8 mg, 0.414 mmol) in CH_3CN (30 mL, total < 35 mL). In all cases addition of the oxime caused the solutions to immediately become dark orange. These were stirred for 16 hours at r.t., with the volatiles removed *in vacuo* and analysis of the resulting solids by ^{1}H NMR spectroscopy. Where 2 equiv. of oxime was used, vapour diffusion of a saturated CH_3CN solution with hexane antisolvent produced large dark orange crystals suitable for SCXRD after 6 months in the dark at r.t., found to be $[UO_2(NO_3)_3$(ind-oxime-H)] (**2.19**). With 4 equiv. of oxime, large colourless crystals were obtained similarly, but found to be starting material ind-oxime. Solids isolated in good or quantitative yields.

^{1}H NMR spectra acquired on all product solutions (*e.g.* 1–5 equiv. of ind-oxime, and 5 equiv. of ind-oxime with 2 equiv. of pyridine) contained multiple, very broad resonances consistent with multiple species, in fast exchange. Typical range of broad peaks *ca*. 7–10 ppm, oxime protons.

5.7 Complexes of the Uranyl Ion with Other *O*-donors

5.7.1 Synthesis of $[UO_2(NO_3)_2(^tBu_2\text{-urea})_2]$, $U^{tBu2urea}$

To a magnetically stirred solution of **U^{NO3}** (100 mg, 0.2 mmol, 1 equiv.) in CH_3CN (5 mL) was added 1,3-di-*tert*-butylurea, $^tBu_2$-urea (98.8 mg, 0.57 mmol, 2.85 equiv.), causing an immediate darkening of the initially pale yellow solution to dark yellow. Slow evaporation of this solution resulted in yellow plate crystals suitable for SCXRD, a portion of which were retained and analysed by SCXRD, $[UO_2(NO_3)_2(^tBu_2\text{-urea})_2]]\cdot 2(CH_3CN)$, **$U^{tBu2urea}$**$\cdot 2(CH_3CN)$. The resulting dark yellow solids (165 mg, 92%; **$U^{tBu2urea}$**) were washed with hexane(s) (2 x 10 mL), dried by rotary evaporation, and analysed by ^{1}H NMR and ATR-IR spectroscopy, ESI-MS and elemental analysis.

^{1}H NMR (500 MHZ, CD_3CN): δ/ppm = 5.28 (br s, 2H, NH), 2.39 (br s, water), 1.36 (s, 18H, ^{t}Bu); *cf*. ^{1}H NMR of free ligand, $^tBu_2$-urea (500 MHz, CD_3CN): 4.55 (br s, 2H, NH), 2.15 (s, water), 1.23 (s, 18H, ^{t}Bu). ATR-IR (cm^{-1}): 3452 (w), 3401 (w), 2976 (m), 1596 (s), 1566 (s), 1508 (s + 1474 (sh)), 1424 (m), 1368 (s), 1276 (s), 1232 (w), 1204 (s), 1116 (w), 1028 (m), 910 (vs), 804 (w), 750 (m); *cf*. ATR-IR of free ligand, $^tBu_2$-urea (KBr): 3355 (m), 2964 (m), 1637 (s), 1560 (s).[23] Mass spec., *m/z* (Da*;* relative intensity, assignment): 173.1618 (60%, $[(^tBu_2\text{-urea})\text{-H}]^+$), 195.1461 (100%, $[(^tBu_2\text{-urea})\text{-Na}]^+$), 367.3022 (40%, $[(^tBu_2\text{-urea})_2\text{-Na}]^+$), 676.3409 (7%, $[UO_2(NO_3)(^tBu_2\text{-urea})_2]^+$), 848.4953 (30%, $[UO_2(NO_3)_2(^tBu_2\text{-urea})_3]^+$). Elemental analysis: Calc. C, 29.27%, H, 5.46%, N, 11.38%; found C, 29.17%, H, 5.78%, N, 10.95%.

5.7.2 Unsuccessful Complexation of U^{NO3} with Phthalic (Hpht) and Isophthalic (Hipht) Acids, Reactions 2.21 and 2.22

To a solution of **U^{NO3}** (100 mg, 200 μmol, 1 equiv.) in CH_3OH (3 mL) was added a suspension of either phthalic acid, Hpht or isophthalic acid, Hipht (both 33.0 mg, 200 μmol, 1 equiv.) with $NaHCO_3$ (33.3 mg, 392 μmol, *ca*. 2 equiv.), forming a yellow precipitate immediately in both cases. These were briefly magnetically stirred (5 minutes) and filtered (frit) to isolate yellow solids (85.6 mg and 79.4 mg, respectively, good yields). Attempts to analyse the stabilities of either product in solution were unsuccessful as the solids were insoluble in CH_3CN, CH_3OH or acetone. The solids were analysed by ATR-IR spectroscopy.

For reaction of **U^{NO3}** with phthalic acid, Hpht: ATR-IR (cm^{-1}): 3359 (w br), 1508 (s), 1495 (s), 1416 (s), 1394 (s), 928 (s), 753 (m), 696 (m); *cf.* ATR-IR of free ligand, Hpht (cm^{-1}): 2870 (m br), 2648 (m br), 1665 (s), 1585 (m), 1400 (m), 1266 (m), 897 (s), 795 (s), 734 (s), 672 (s).

For reaction of **U^{NO3}** with isophthalic acid, Hipht: ATR-IR (cm^{-1}): 3104 (w br), 1560 (m), 1574 (m), 1400 (s), 934 (s), 739 (m), 712 (s); *cf.* ATR-IR of free ligand, Hipht (cm^{-1}): 2819 (m br), 2544 (m br), 1682 (s), 1610 (m), 1417 (m), 1268 (s), 920 (m), 724 (s), 689 (s), 670 (s).

5.8 Preparation of Anaerobic Uranyl Photocatalysts

5.8.1 Synthesis of $[^nBu_4N]_2[UO_2(NO_3)_4]$, U^{tetNO3}

To a magnetically stirred solution of **U^{NO3}** (1.13 g, 2.25 mmol, 1 equiv.) in acetone (30 mL) was added $[^nBu_4][NO_3]$ (1.37 g, 4.51 mmol, 2 equiv.) and excess $MgSO_4$ (*ca*. 2 g), forming a dark yellow solution (alongside solid magnesium sulfate). This mixture was magnetically stirred for 16 hours at r.t., filtered (frit), and taken to dryness *in vacuo* to leave a bright yellow solid. This was re-dissolved in the minimum amount of acetone (*ca*. 1 mL), precipitated with hexane(s), filtered (frit), washed again with hexane(s) (3 x 150 mL) and dried for two days (10^{-2} mbar, r.t.). The product, **U^{tetNO3}** (1.96 g, 87%), a dark yellow solid, was analysed by ^1H NMR, electronic absorption, emission and excitation, and Raman spectroscopies, elemental analysis, ESI-MS, and Karl-Fischer titration, to determine water content. Yellow plates suitable for SCXRD were grown by solvent diffusion of hexane(s) into a saturated acetone solution of **U^{tetNO3}** at 4°C over 4 weeks.

^1H NMR (600 MHz, CD_3CN): δ/ppm = 3.09–3.06 (m, 2H, N-C$\underline{H}_2$), 1.62–1.57 (m, 2H, N-CH_2-C$\underline{H}_2$), 1.35 (sext), 2H, (N-$(CH_2)_2$-C$\underline{H}_2$), *J* = 7.6 Hz), 0.96 (t, 3H, -Me, *J* = 7.2 Hz). Solution-phase Raman (cm^{-1}; saturated solution in CH_3CN): 1043 and 1027 (nitrate), 866 (uranyl). UV-vis (CH_3CN): λ/nm (ε/$M^{-1}cm^{-1}$): 394–467 (< 20). Mass spec., *m/z* (Da*;* relative intensity, assignment): 456.0059 (100%, $[UO_2(NO_3)_3]^-$). Elemental analysis: Calc. C, 38.3%, H, 7.24%, N, 8.38%; found C, 37.59%, H, 8.86%, N, 8.05%.

Photolytic stability

A solution of **U^{tetNO3}** (10 mg, 10 μmol) in dry CD_3CN (2 mL) in a Teflon-tapped NMR tube was irradiated for 16 hours using lamp **(4)** at r.t. The dark yellow solution become brown over the course of irradiation, and was analysed by ^1H NMR spectroscopy.

Slight degradation of the $[^nBu_4N]$ cations was observed by ^1H NMR spectroscopy, with small signals (*e.g.* < 1% integration of remaining cation) observed at *ca*. 5–6 ppm.

Experimental Details for Chapter 3

5.9 Substrate-only Photoreactions

All the substrates reacted photochemically with $\mathbf{U^{NO3}}$, $\mathbf{U^{Ph2phen}}$ or $\mathbf{U^{tetNO3}}$ were also tested photochemically without the uranyl catalysts present, in control reactions to ensure that the substrates themselves were not sensitive to photolytic degradation. Substrates that were found to be photolytically sensitive in the absence of uranyl catalysts were not tested further.

General procedure: To a borosilicate glass vial (1.5 mL) was added a substrate (*ca*. 10 mg) in CD_3CN (1 mL) and the solution analysed by ^1H NMR spectroscopy, irradiated for 16 hours using lamp **(4)** at r.t, and reanalysed by ^1H NMR spectroscopy and GC-MS. Only substrates that had no discernible spectral changes (*e.g.* decomposition products, no reaction *etc*.) were then further reacted with the appropriate uranyl photocatalyst.

5.10 Substrate Photoreactivity of the Uranyl(VI) Ion

Section 5.10.1 General Catalyst Screening Reactions

General procedure: To a borosilicate glass vial (7 mL) was added $\mathbf{U^{NO3}}$ (10 mol%), CH_3CN (5 mL) and a corresponding amount of substrate (Table 5.1). These solutions were then shaken, and where appropriate, an aliquot was removed for ^1H NMR spectroscopy before irradiation. With magnetic stirring and lid on the vials (with a 2 mm perforation to maximise air ingress but minimise evaporation), solutions were irradiated for 16 hours using lamp **(4)** at r.t. The resulting product solutions were then analysed by GC-MS, and ^1H NMR spectroscopy, as appropriate. Resonances were detected and quantified without solvent lock, relative to CH_3CN as the largest peak at 1.94 ppm.[24] The maximum temperature of the solutions from the heat of the lamp was 30 ± 2°C (digital thermometer).

Entry	Substrate	Structure	Mass, substrate/mg	Moles, substrate/µmol	Mass, U^{NO3}/mg	Moles, U^{NO3}/µmol
1	Ethylbenzene	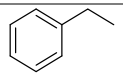	38.3	360.5	18.1	36.0
2	Toluene		31.0	336.6	16.9	33.7
3	Triphenylmethane	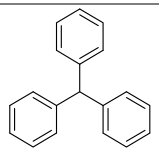	95.4	390.3	19.6	39.0
4	Diphenylmethane	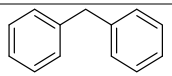	66.3	394.3	19.8	39.4
5	Cumene	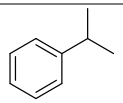	39.3	326.6	16.4	32.7
6	Tetramethylcyclopropane	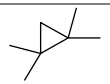	36.0	366.4	18.4	36.6
7	1-Hexene	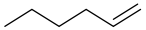	34.0	404.3	20.3	40.4
8	Indane	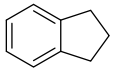	40.0	338.6	17.0	33.9
9	Cyclohexane		15.3	182.2	9.2	18.2
10	Cyclohexene		13	158.1	7.8	15.5
11	1,5-Hexadiene	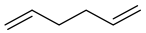	24.0	292.8	14.7	29.3
12	Styrene	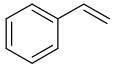	40.5	389	19.5	38.9
13	Tetralin	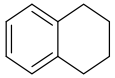	48.2	364.4	18.3	36.4
14	Lignin (Alkali)		113	Not soluble	70.9	141.2
15	Xanthene	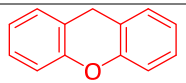	67.5	370.4	18.6	37.0
16	Tetrahydropyran		31.0	360.5	18.1	36.0

17	Benzyl alcohol	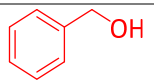	35.5	328.6	16.5	32.9
18	Benzyl methyl ether	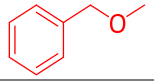	49.9	408.3	20.5	40.8
19	Benzyl phenyl ether	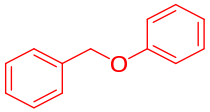	73.0	396.3	19.9	39.6
20	THF		24.3	336.6	16.9	33.7
21	Furan		21.3	312.7	15.7	31.3
22	1,4-Dioxane		32.1	364.4	18.3	36.4
23	Oxazole		25.2	364.4	18.3	36.4
24	*p*-Nitrotoluene	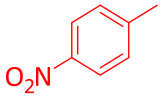	48.1	350.5	17.6	35.1
25	2P1PE	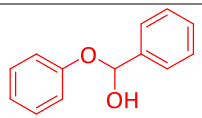	75.5	352.5	17.7	35.2
26	Isochroman	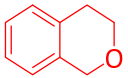	44.9	334.6	16.8	33.5
27	Menthofuran	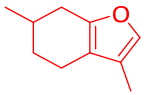	59.2	394.3	19.8	39.4
28	Phthalan	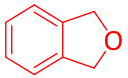	51.0	424.2	21.3	42.4
29	5-*Tert*-butyl-2-hydroxybenzaldehyde	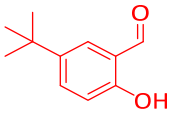	59.3	332.6	16.7	33.3

30	2-Cyclohexenone	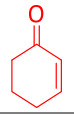	34.1	354.5	17.8	35.4
31	2-Hydroxy-5-methoxy-benzaldehyde	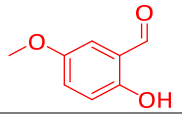	53.0	348.5	17.5	34.9
32	α-Tetralone	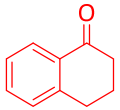	53.0	362.5	18.2	36.2
33	4-Benzylpyridine	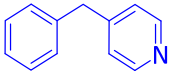	60.3	356.5	17.9	35.6
34	Benzylamine	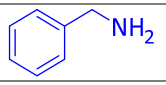	36.1	336.6	16.9	33.7
35	2-Benzylpyridine	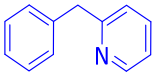	53.6	316.7	15.9	31.7
36	Indoline	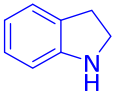	37.5	314.7	15.8	31.5
37	Tetrahydroisoquinoline	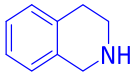	48.3	362.5	18.2	36.2
38	Pyrrolidine		23.7	332.6	16.7	33.3
39	Pyrrole		23.6	352.5	17.7	35.2
40	Imidazole		25.6	376.4	18.9	37.6
41	Pyrazole		24.4	358.5	18.0	35.8
42	1,2,3-Triazole		24.5	354.5	17.8	35.4
43	Piperidine		27.6	324.6	16.3	32.5

44	Pyrazine		29.3	366.4	18.4	36.6
45	Pyridazine		28.2	352.5	17.7	35.2
46	Tetrahydrocarbazole	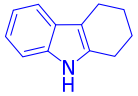	56.7	330.6	16.6	33.1
47	Neopentylamine	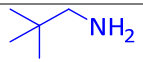	32.6	374.4	18.8	37.4
48	Valeronitrile		14.9	180	9.0	17.9
49	Perfluorononane	C_9F_{20}	198.3	406.3	20.4	40.6
50	Fluorobenzene		30.8	320.6	16.1	32.1
51	Thiazole		28.1	330.6	16.6	33.1
52	Thianapthalene	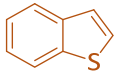	50.0	372.4	18.7	37.2
53	Dibenzothiophene	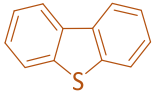	67.2	364.4	18.3	36.4
54	Tetrahydrothiophene		32.3	366.4	18.4	36.6
55	1,3-Dithiolane		37.9	356.5	17.9	35.6
56	Thiophene		31.2	370.4	18.6	37.0
57	3-Methylbenzothiophene	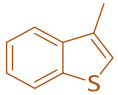	55.5	374.4	18.8	37.4
58	Benzyl mercaptan	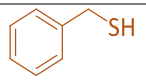	47.5	382.4	19.2	38.2
59	Dibutyl disulfide	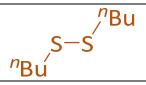	61.2	342.5	17.2	34.3
60	Dibenzyl sulfoxide	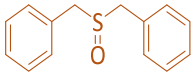	75.2	326.6	16.4	32.7

61	Tetrahydrothiopyran		33.4	326.6	16.4	32.7
62	Selenophene		41.2	314.7	15.8	31.5
63	Triphenylsilane	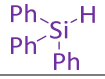	89.7	344.5	17.3	34.5
64	Triphenylphosphine		100.3	382.4	19.2	38.2
65	Tri(methyl)silylacetylene		34.2	348.5	17.5	34.9

Table 5.1 – Complete list of substrates reacted with $\mathbf{U^{NO3}}$ in substrate screening. **Carbon**-, **oxygen**-, **nitrogen**-, **fluorine**-, and **sulfur**-containing, and **miscellaneous** substrates, are colour-coded.

5.10.2 Screening Reactions for Substrates with Substrates of Interest

Note: 'substrates of interest' refers to hydrocarbon substrates outlined in Tables 3.3 and 3.4. Benzylic hydrocarbon substrates, alongside cyclohexane, cyclohexane and benzene are discussed here. The author also wishes to highlight that the masses of substrates (etc.) given in Table 5.2, below, are different from those reported in Table 5.1, above (which describes substrates used in the substrate screening, performed in order to establish substrates that were compatible with only $\boldsymbol{U^{NO3}}$*). Substrates found compatible with* $\boldsymbol{U^{NO3}}$ *for further reactivity were then reacted with* $\boldsymbol{U^{NO3}}$ *and* $\boldsymbol{U^{Ph2phen}}$*, in order to investigate differences between these two catalysts. Table 5.2, below, describes the masses of these compatible substrates used in these comparative reactions. While some substrates appear in both Tables 5.1 and 5.2, the masses reported for the same substrate in different tables are unrelated.*

Substrates that were effectively and cleanly converted with $\mathbf{U^{NO3}}$ (here, taken to mean substrates with conversion of >10% with four or fewer products, containing only C, H and O) were then reacted again with $\mathbf{U^{NO3}}$ under analogous conditions (section 5.10.1), to confirm the repeatability of the procedure and product mixtures. These substrates, which are reported in Tables 3.3 and 3.4, were then irradiated in the presence of $\mathbf{U^{Ph2phen}}$ to compare the photocatalytic efficiencies of the two photocatalysts, $\mathbf{U^{NO3}}$ and $\mathbf{U^{Ph2phen}}$. The procedure used here was identical to that reported in section 5.10.1 above, with 10 mol% $\mathbf{U^{NO3}}$ and 5 mol% $\mathbf{U^{Ph2phen}}$, using the masses reported in Table 5.2, below.

			U^{NO3}		$U^{Ph2phen}$	
Entry	**Substrate**	**Structure**	**Mass of Substrate/mg**	**Mass of Catalyst/mg**	**Mass of Substrate/mg**	**Mass of Catalyst/mg**
			µmol	***µmol***	***µmol***	***µmol***
1	Toluene	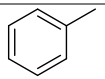	36.2 *392.3*	19.7 *39.2*	37.3 *404.7*	14.7 *20.2*
2	Diphenyl-methane	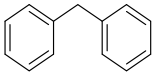	61.0 *362.5*	18.2 *36.2*	62.5 *371.7*	13.5 *18.6*
3	Triphenylmethane	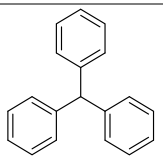	99.8 *408.4*	20.5 *40.8*	98.2 *402.0*	14.6 *20.1*
4	Indane	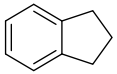	51.3 *434.2*	21.8 *43.4*	49.5 *418.5*	15.2 *20.9*
5	Phthalan	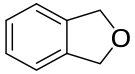	47.4 *394.3*	19.8 *39.4*	46.0 *382.7*	13.9 *19.1*
6	Isochroman	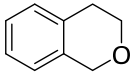	54.8 *408.3*	20.5 *40.8*	55.8 *415.7*	15.1 *20.8*
7	2-Phenyl-1-phenoxy-ethanol (2P1PE)	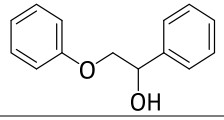	96.4 *450.1*	22.6 *45.0*	87.3 *407.5*	14.8 *20.4*
8	Cyclohexane		38.9 *462.0*	23.2 *46.2*	37.3 *443.3*	16.1 *22.2*
9	Cyclohexene		32.6 *396.3*	19.9 *39.6*	33.7 *410.2*	14.9 *20.5*
10	1,5-Hexadiene	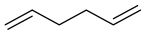	32.1 *390.3*	19.6 *39.0*	31.9 *388.2*	14.1 *19.4*
11	Benzene		36.2 *464.0*	23.3 *46.4*	34.8 *446.0*	16.2 *22.3*

Table 5.2 – Masses and moles of substrate and catalyst used for the comparative substrate reactions of U^{NO3} and $U^{Ph2phen}$.

5.11 Other Substrate Reactivity with $\mathbf{U^{NO3}}$ and $\mathbf{U^{Ph2phen}}$

5.11.1 Photoreaction with Solvent as Substrate

With THF/$\mathbf{U^{NO3}}$: To a small vial was added $\mathbf{U^{NO3}}$ (39.1 mg, 77.8 μmol, 1 equiv., 0.125 mol% catalyst loading) in THF (5 mL, 4.45 g, 61.6 mmol, 800 equiv.), and the yellow solution magnetically stirred under irradiation for 16 hours using lamp **(4)** at r.t. (with 2 mm perforation in vial lid to ensure sufficient air ingress). The transparent grey-brown solution (no precipitate) was analysed by ^{1}H NMR spectroscopy and GC-MS.

With THF/$\mathbf{U^{Ph2phen}}$: To a small vial was added $\mathbf{U^{Ph2phen}}$ (56.6 mg, 77.9 μmol, 1 equiv., 0.125 mol% catalyst loading) in THF (5 mL, 4.45 g, 61.6 mmol, 800 equiv.), and the dark yellow solution magnetically stirred under irradiation for 16 hours using lamp **(4)** at r.t. (with 2 mm perforation in vial lid to ensure sufficient air ingress). The resultant product mixture, a dark yellow solution with pale brown precipitate, was filtered (frit) and analysed by ^{1}H NMR spectroscopy and GC-MS.

5.12 Photoreactivity of 9,10-Dihydroanthracene (DHA) with $\mathbf{U^{NO3}}$ or $\mathbf{U^{Ph2phen}}$

For selected examples the reactions of substrates with benzylic C-H bonds were then scaled up, to monitor how scale affects the photocatalytic reactivity with $\mathbf{U^{NO3}}$ and $\mathbf{U^{Ph2phen}}$. These larger scale reactions were monitored by ^{1}H NMR spectroscopy, with ^{1}H NMR spectra collected without a solvent lock or sweep width optimisation and manual spectral referencing of the $C\underline{H}_3CN$ ^{1}H NMR resonance set against that of CH_3CN in CD_3CN (1.97 ppm). Conversions were calculated by first grouping all spectra for a particular run in recorded chronological order, then collectively phasing and smoothing the baselines of the spectra and, finally, taking a common integral using a diagnostic resonance for that particular substrate (*e.g.* for DHA, using the singlet at 3.94 ppm (*meso*-CH_2), which is adequately encompassed by integrating in a range from 3.80–4.00 ppm). Percentage conversions were calculated by representing the integrals of each data point relative to the integral of the t = 0 data point as 100%.

For example, in order to calculate the DHA conversion for a DHA/$\mathbf{U^{NO3}}$ photoreaction, the ^{1}H NMR spectra recorded over the course of the reaction (usually three hours) would be collated in chronological order (t = 0, 10s, 30s, …), the spectra baselined and phased together as one entity using a common algorithm, and the integrals for each spectrum with the range of 3.80–4.00 ppm compared. Final percentage conversion would then be calculated by taking the integral value between 3.80–4.00 ppm in the ^{1}H NMR spectrum recorded for the end of the reaction (usually t = 3 hours), and dividing this value by the integral of the same range in the t = 0 ^{1}H NMR spectrum, expressed as a percentage.

Consider the reaction of DHA with 10 mol% $\mathbf{U^{NO3}}$. In the t = 0 ^{1}H NMR spectrum, the peak at *ca*. 3.80–4.00 ppm has an absolute integration of, for example, $3.22\text{x}10^{-2}$ arbitrary units. This value is then set as the relative integral of 1. Then, the corresponding peak in the t = 3 hours (for example) ^{1}H NMR spectrum would be integrated. Take, as an example, the absolute integral of this peak to be $2.12\text{x}10^{-2}$ arbitrary units. The conversion after t = 3 hours would then be reported as ($2.12\text{x}10^{-2}$/$3.22\text{x}10^{-2}$) = 65.8%, or 34% expressed as percentage conversion with appropriate rounding, which is the value reported in entry 14, Table 3.5.

5.12.1 Representative Procedure for DHA, 0.001–25 mol% Catalyst

To a Schott jar (100 mL) was added DHA (450 mg, 2.49 mmol) and CH_3CN or PhCN (50 mL), along with an appropriate amount of catalyst (Table 5.3). The reaction solution was allowed to stand for 3 minutes in the dark (blackout screen), and an aliquot (0.6 mL) extracted for ^{1}H NMR spectroscopy at t = 0. The magnetically stirred sample was then irradiated using lamp **(4)** (3 hours, unless stated), at 11 cm from the lamp and 22 ± 2°C in all cases (measured with digital thermometer), with aliquots (0.6 mL) extracted from the solutions at the appropriate time points.

Catalyst loading WRT DHA/%	Entry (→)	Mass of U^{NO3}/mg	Entry (→)	Mass of $U^{Ph2phen}$ /mg
0.001	1a	0.0125[a]	1b	0.0181[a]
0.01	2a	0.125[a]	2b	0.18[a]
0.05	--	--	3b	0.91[a]
0.1	3a	1.25[a]	4b	1.81[a]
0.25	4a	3.125[a]	5b	4.5[a]
0.5	5a	6.25[a]	6b	9.1[a]
1	6a	12.5	7b	18.1
2	7a	25		
5	8a	62.5		
10	9a	125		
25	10a	312.5		
100	11a	1250		
200	12a	2500		
400	13a	5000		
1000	14a	12500		

Table 5.3 – Masses of catalyst used for photocatalytic reactions with DHA in 50 mL of CH_3CN. [a] Serial dilution.

For entry 7b, Table 5.3 (1 mol% $\mathbf{U^{Ph2phen}}$), the yellow precipitate formed (which was not formed at loadings < 1 mol% $\mathbf{U^{Ph2phen}}$) was removed by Hirsch filtration, washed twice with CH_3CN (2 x 12.5 mL), and dried *in vacuo* for 16 hours. This yellow solid was analysed by (negative mode ESI-) mass spectrometry and Raman spectroscopy.

5.12.2 Representative Procedure for DHA Photocatalysis, Mercury Drop Test

The reaction of DHA with 5 mol% $\mathbf{U^{NO3}}$ catalyst and DHA was additionally repeated over Hg (3 drops, *ca*. 60 μL) to test for catalyst heterogeneity, entry 13, Table 3.5.

5.12.3 Representative Procedure for DHA Photocatalysis with 100–1000 mol% U^{NO3} "Catalyst"

As for Section 5.12.1, except using > 100 mol% of $\mathbf{U^{NO3}}$, entries 11a–14a, Table 5.3.

Observations varied depending on the $\mathbf{U^{NO3}}$ loading employed: for 100 and 200 mol%, the reactions became hot (60°C, by digital thermometer) and turned from yellow to dark yellow, on addition of the $\mathbf{U^{NO3}}$ after *ca*. 5 minutes in the light or dark; for 400 and 1000 mol% of $\mathbf{U^{NO3}}$, the reactions also became hot (*ca.* 60°C), but turned intensely dark yellow (or dark brown), along with vigorous effervescence after *ca*. 15–30 seconds after $\mathbf{U^{NO3}}$ was added in both cases. All these reactions were analysed by ^{1}H NMR spectroscopy at selected time intervals. Attempts to analyse the gas by ^{1}H NMR spectroscopy (*e.g.* dissolved hydrogen gas, 4.60 ppm in CD_3CN)[24] by repeating the 1000 mol% $\mathbf{U^{NO3}}$ reaction in a Teflon-tapped NMR tube were unsuccessful.

5.12.4 Representative Procedure for DHA Photocatalysis with Added Anthracene

The reaction of 0.5 mol% $\mathbf{U^{NO3}}$ and $\mathbf{U^{Ph2phen}}$ with stoichiometric DHA and anthracene was achieved by addition of DHA (225 mg, 1.25 mmol) and anthracene (222.5 mg, 1.25 mmol) to the appropriate amounts of either $\mathbf{U^{NO3}}$ (entry 6, Table 3.5) or $\mathbf{U^{Ph2phen}}$ (entry 7, Table 36) in CH_3CN (50 mL). The reactions were then performed as previously, Section 5.12.1.

5.12.5 Representative Procedure for DHA Photocatalysis in Benzonitrile

DHA (450 mg, 2.49 mmol) was added to a solution of benzonitrile, PhCN (50 mL) and catalyst (**U^{NO3}**, 6.25 mg, or **$U^{Ph2phen}$**, 9.07 mg; 12.5 μmol, 0.5 mol%), and irradiated as previously, Section 5.12.1. The solutions stayed yellow throughout with no precipitate observed.

5.12.6 Representative Procedure for DHA Photocatalysis with Added Water

DHA (450 mg, 2.49 mmol) was added to a solution of CH_3CN (50 mL), catalyst (**U^{NO3}**, 62.5 mg, 125 μmol, 5 mol%) and water (225 mg, 12.5 mmol, 100 equiv. WRT **U^{NO3}**), and the solution irradiated as previously (Section 5.12.1). There was no colour change over the course of the reaction, which remained pale yellow throughout.

5.12.7 Representative Procedure for DHA Photocatalysis in Anoxic CH_3CN, 5 mol% Catalyst

To an oven-dried ampoule was added the DHA, **U^{NO3}** and CH_3CN, as for Section 5.12.1, and the sample solution was freeze-pump-thaw degassed three times prior to use. The reaction solution was irradiated for 3 hours using lamp **(4)** at r.t., with magnetic stirring. After *ca*. 5 minutes, a faint but permanent turbidity was observed, becoming darker over time, until after approx. 30 minutes copious amounts of a dark grey precipitate were formed. After 3 hours of irradiation this precipitate was filtered (cannula, under N_2) dried *in vacuo*, washed sequentially with anhydrous CH_3CN (2 x 30 mL) and toluene (2 x 30 mL), and dried for 16 hours *in vacuo*. The resulting dark grey powder (302 mg) was analysed by ATR-IR spectroscopy, elemental analysis and ICP-MS, *vs*. a commercial sample of $U^{IV}O_2$.

5.12.8 Time-resolved DHA Conversion Measured by UV-vis Spectroscopy

The initial portions of the reactivity of DHA with **U^{NO3}** in CH_3CN were probed using UV-vis spectroscopy. The loadings of **U^{NO3}** used were 1, 2, 5, 10, 25 and 50 mol%, corresponding to 0.1–5 mM of **U^{NO3}**.

Separately, two solutions of DHA (361.1 mg in 100 mL CH_3CN, 20 mM) and catalyst (**U^{NO3}**, 100.5 mg in 100 mL) were prepared and stored at -35°C in the dark when not in use. Solutions of DHA/$U^{VI}O_2^{2+}$ for analysis were prepared by addition of 1.5 mL of each of these (DHA, and $U^{VI}O_2^{2+}$) solutions to a quartz cuvette (total solution volume 3 mL), using the appropriately diluted catalyst stock solution. For example, if 5 mol% loading, 2x dilution with CH_3CN from 10 mol% loaded stock, if 1 mol% loading, 10x dilution with CH_3CN from 10 mol% loaded stock, *etc*., giving a solution with 10 mM DHA and appropriate catalyst concentration. The quartz cuvette was then irradiated for the specified duration using lamp **(4)** at 22 ± 2°C with a lid on the cuvette to limit evaporation of solvent in the heat of the lamp. UV-vis spectra were then recorded, typically between 200–500 nm, after each duration of irradiation, where t typically = 0, 10s, 30s, 1m, 2m, 3m, 5m, 10m, 20m, 30m, 1h, 2h, 3h. The λ_{max} of anthracene is 356–357 nm, and changes in ε_{356} against time were correlated for each catalyst loading to determine Δ[anthracene]/t.

Molar extinction coefficients for anthracene were determined by using the gradient of a line of best fit of varying concentrations of anthracene (1.25 μM to 270 μM, in CH_3CN).

Temperature-only effects were examined by the preparation of solutions as above, without irradiation; that is, solutions were added to the cuvette in the dark and monitored by continuous single wavelength monitoring at 356 nm every 0.05 seconds over 600 seconds (10 minutes), in the spectrophotometer. A saturated solution of KNO_3 in CH_3CN was also prepared and anthracene production in the presence of KNO_3 tested by the analogous method.

5.13 Conversion of DHA with Other Uranyl Photocatalysts

5.13.1 DHA Conversion with U^{SO4}

To a magnetically stirred suspension of uranyl sulfate, $\mathbf{U^{SO4}}$ (6 mg, 14.0 μmol, 1 equiv./10 mol%) in CD_3CN (1 mL) was added DHA (25.1 mg, 139.3 μmol, 9.96 equiv.), also in CD_3CN (1 mL; total, 2 mL). The yellow solution/suspension (uranyl sulfate is poorly soluble in CH_3CN) was then stirred under irradiation with lamp **(4**) for 20 hours at r.t., the product mixture (no colour changes) filtered (frit), and the solution analysed by ^{1}H NMR spectroscopy and GC-MS.

No conversion of DHA was observed by ^{1}H NMR spectroscopy.

5.13.2 DHA Conversion with U^{OAC}

To a magnetically stirred solution of uranyl acetate, $\mathbf{U^{OAc}}$ (5 mg, 11.8 μmol, 1 equiv./10 mol%) in CD_3CN (1 mL) was added DHA (21.7 mg, 102 μmol, 10.2 equiv.), also in CD_3CN (1 mL; total, 2 mL). The yellow solution was stirred under irradiation for 20 hours with lamp **(4)** at r.t., and the resulting pale brown solution/precipitate filtered (frit), and the solution analysed by ^{1}H NMR spectroscopy and GC-MS.

Approximately 10% of DHA was consumed (^{1}H NMR spectroscopy), with anthracene the only product.

5.13.3 DHA Conversion with U^{mal}

To a quartz NMR tube was added the $\mathbf{U^{mal}}$ (5 mg, 10.1 μmol, 1 equiv./10 mol%) and DHA (17.8 mg, 98.7 μmol, 9.8 equiv.) in CD_3CN (5 mL), and the reaction irradiated using lamp **(4)** for 16 hours at r.t. The resulting brown solution was analysed by ^{1}H NMR spectroscopy and GC-MS.

^{1}H NMR spectroscopy and GC-MS indicated that conversion of DHA using $\mathbf{U^{mal}}$ is comparable to $\mathbf{U^{NO3}}$ (41% and 34%, respectively), under these conditions.

5.14 Photoreactivity of Xanthene with the Uranyl Ion

Note: the general method for xanthene photoreactivity with the uranyl ion is given in Section 5.15.

5.14.1 Unsuccessful Trifluoromethylation of Xanthene

General procedure: To a solution of xanthene in CH_3CN in an NMR tube was added trifluoromethylating reagent, and either $\mathbf{U^{NO3}}$ or $\mathbf{U^{Ph2phen}}$. The reaction was then irradiated using lamp **(4)** and analysed by ^{1}H and ^{19}F NMR spectroscopy after 5 hours, after filtration (frit) as necessary.

For Langlois' reagent: xanthene (27.3 mg, 150 μmol, 10 equiv.), Langlois' reagent (53 mg, 339.6 μmol, 22.7 equiv.) and $\mathbf{U^{NO3}}$ (7.5 mg, 14.9 μmol, 1 equiv./10 mol% *vs*. xanthene) in CH_3CN (2 mL). No colour change during or after irradiation (5 hours).

The reaction was also repeated using $\mathbf{U^{Ph2phen}}$: xanthene (9.2 mg, 50.1 μmol, 20 equiv.), Langlois' reagent (12.0 mg, 81.4 μmol, 32.8 equiv.) and $\mathbf{U^{Ph2phen}}$ (3.6 mg, 4.96 μmol, 1 equiv./5 mol% *vs*. xanthene) in CH_3CN (1.5 mL). The initially pale yellow solution became pale pink on irradiation, along with a white precipitate.

For Umemoto's reagent: xanthene (4.5 mg, 24.7 μmol, 10 equiv.), Umemoto's reagent (12.7 mg, 12.7 μmol, 5 equiv.) and $\mathbf{U^{NO3}}$ (1.25 mg, 2.49 μmol, 1 equiv./10 mol% *vs*. xanthene) in CH_3CN (1 mL). Yellow solution becoming orange, then dark orange, during irradiation, with precipitation of orange solids.

The reaction was also repeated using $\mathbf{U^{Ph2phen}}$: xanthene (9.1 mg, 49.9 μmol, 20 equiv.), Umemoto's reagent (25.5 mg, 63.4 μmol, 29.6 equiv.) and $\mathbf{U^{Ph2phen}}$ (3.6 mg, 4.96 μmol, 1 equiv./5 mol% *vs*. xanthene) in CH_3CN (1.5 mL).

For Togni's reagent: xanthene (9.1 mg, 49.9 μmol, 20 equiv.), Togni's reagent (24.7 mg, 74.8 μmol, 30.2 equiv.) and $\mathbf{U^{Ph2phen}}$ (3.6 mg, 4.96 μmol, 1 equiv./5 mol% *vs*. xanthene) in CH_3CN (1.5 mL). The initially very pale yellow solution became dark yellow on irradiation, with no precipitate observed.

In all cases ^1H and ^{19}F NMR spectroscopic data showed the major product, > 90% by integrations, was trifluoromethane, CHF_3 (for $\delta(^1H)$, *ca*. 7 ppm in CD_3CN, for $\delta(^{19}F)$, -79 or -81 ppm in C_6D_6 or THF-D_8). No resonances consistent with any of the trifluoromethylating agents was ever observed after irradiation by ^1H NMR spectroscopy, also suggesting these compounds are unstable under these conditions.

5.14.2 Effect of Iodine on Xanthene Photoreactivity

General procedure: To a solution of xanthene in CH_3CN in a small vial was added iodine and either $\mathbf{U^{NO3}}$ or $\mathbf{U^{Ph2phen}}$. The reaction was then irradiated using lamp **(4)** for 5 hours, with analysis by ^1H NMR spectroscopy at selected intervals over this time period.

For $\mathbf{U^{NO3}}$: xanthene (27.3 mg, 149.8 μmol, 10 equiv.), iodine (95 mg, 374.3 μmol, 25.1 equiv.) and $\mathbf{U^{NO3}}$ (7.5 mg, 14.9 μmol, 10 mol% *vs*. xanthene) in CH_3CN (3 mL). The colour of the initial, dark brown/gold solution remained unchanged during irradiation.

For $\mathbf{U^{Ph2phen}}$: xanthene (9.1 mg, 49.9 μmol, 10 equiv.), iodine (20 mg, 78.8 μmol, 15.9 equiv.) and $\mathbf{U^{Ph2phen}}$ (3.6 mg, 4.96 μmol, 5 mol% loading *vs*. xanthene) in CH_3CN (3 mL).

5.15 Photoreactivity of Other Benzylic Substrates with the Uranyl Ion

The method of determining conversions here was analogous to the method used for quantifying DHA conversions, Section 5.12. The ranges of integrations for diagnostic resonances used for calculating conversions of substrates or generation of products (numbers are ppm):

- **Xanthene**, singlet, integrating between 3.98–4.17; xanthanol, multiplet, integrating between 7.14–7.25; xanthanone, multiplet, integrating between 7.45–7.61; 'peroxides', integrating between range of 5.70–6.08;
- **Toluene**, multiplet, integrating between 7.07–7.27; benzaldehyde, singlet, integrating between 9.95–10.03,
- **Diphenylmethane**, singlet, at 3.84–3.99; benzophenone, multiplet, integrating between 7.72–7.77; 'peroxide(s)', integrating between range of 5.73–5.96;
- **Triphenylmethane**, singlet, integrating between 5.52–5.62; benzophenone, multiplet, integrating between 7.72–7.77; diphenylmethanol, singlet, integrating between 4.62–4.68;
- **Isochroman**, multiplet, integrating between 4.71–4.85; isochroman-1-one, integrating between 4.43–4.56;
- Quantification of **anthracene** was not necessary as complete conversion was observed (by disappearance of diagnostic resonance (singlet) at 8.51 ppm after one hour of irradiation).

The general synthetic procedure was the same as for the DHA reactions (Section 5.12; *cf*. 50 mL solvent, irradiation using lamp **(4)** over time with magnetic stirring at r.t., *etc*.), using the following masses of substrate and catalyst:

For xanthene: 456 mg, 2.5 mmol, with 0.5 mol% ($\mathbf{U^{NO3}}$, 6.25 mg, or $\mathbf{U^{Ph2phen}}$, 9.07 mg; 12.5 μmol), 5 mol% $\mathbf{U^{Ph2phen}}$ (90.8 mg) or 10 mol% $\mathbf{U^{NO3}}$ (125 mg) catalyst loading over either 9 or 10 hours. The reactions generally started as pale yellow, becoming sequentially dark yellow, orange, brown and

finally dark brown, over time. No precipitates were observed except for the 5 mol% **U^{Ph2phen}** reaction, in which a yellow precipitate was observed after *ca*. 5 minutes.

The reaction was also repeated on a smaller scale, using a 30 mL vial, in which xanthene-H_2 (91 mg, 500 μmol) and **U^{NO3}** (25 mg, 50 μmol, 10 mol%) were dissolved in CH_3CN (10 mL), and the reaction irradiated for 8 hours, using lamp **(4)** (with 2 mm aperture perforated into the vial lid). Analysis was by ^{1}H NMR spectroscopy, over time.

For xanthene-D_2 (and effect of solvent): To separate vials was added solutions of xanthene-D_2 (92.1 mg, 500 μmol) and **U^{NO3}** (25 mg, 50 μmol, 10 mol%), in either CH_3CN, or CD_3CN (both 10 mL), to give two separate reaction solutions; xanthene-D_2/CH_3CN, or xanthene-D_2/CD_3CN, in addition to the third xanthene-H_2/CH_3CN reaction described above. With magnetic stirring, these two reactions were irradiated for 7 hours, using lamp **(4)** at r.t and a screw top lid perforated with a 2 mm aperture. Analysis of both solutions was by ^{1}H NMR spectroscopy, over time. The initially pale yellow solutions both became very dark yellow/brown after 7 hours of irradiation.

For the xanthene-D_2/CD_3CN reaction, the initially pale yellow solution became brightly fluorescent green after *ca*. 5 seconds of irradiation, a colouration that disappeared over the subsequent 30 seconds. This initial green colour was not observed for the xanthene-D_2/CH_3CN reaction. Both reactions involving xanthene-D_2 were also noticeably paler yellow in colour than the xanthene-H_2/CH_3CN reaction.

For anthracene: 445 mg, 2.5 mmol, with 0.5 mol% catalyst (**U^{NO3}**, 6.25 mg, or **U^{Ph2phen}**, 9.07 mg; 12.5 μmol).

The photostability of anthracene itself was also tested, by dissolving anthracene (445 mg) in CH_3CN (50 mL) and photolysing the solution using lamp **(4)** for 5 hours. A small amount of white precipitate was observed after 5 hours.

^{1}H NMR spectroscopy of the product solutions (for both **U^{NO3}** and **U^{Ph2phen}** as photocatalyst) showed no resonances consistent with anthracene after 1 hour of irradiation.

For toluene: 230.4 mg, 2.5 mmol, with 5 mol% **U^{Ph2phen}** (90.8 mg), with irradiation over 16 hours.

For diphenylmethane: 420.6 mg, 2.5 mmol, with 0.5 mol% **U^{Ph2phen}** (9.07 mg), 5 mol% **U^{Ph2phen}** (90.8 mg), or 10 mol% **U^{NO3}** (125 mg) over 16 hours of irradiation. The initially yellow solution darkened slightly during the reaction.

For triphenylmethane: 611 mg, 2.5 mmol, with 5 mol% **U^{Ph2phen}** (90.8 mg) or 10 mol% **U^{NO3}** (125 mg) over 16 hours of irradiation. A white precipitate appeared after two hours in both cases, increasing over time. A portion of this precipitate was removed from the 10 mol% **U^{NO3}** reaction by filtration (frit), washed with CH_3CN (50 mL) and analysed by ^{1}H and ^{13}C{^{1}H} NMR, and ATR-IR spectroscopies, and elemental and melting point analyses.

For isochroman: 335.4 mg, 2.5 mmol, with 5 mol% **U^{Ph2phen}** (90.8 mg) or 10 mol% **U^{NO3}** (125 mg) over 16 hours of irradiation. There was in both cases very slight darkening of the yellow colour of the reaction solution, along with small amounts of yellow precipitate after 16 hours.

Only data for the photo-oxidation reaction with **U^{Ph2phen}** are discussed; conversion with **U^{NO3}** was too low to adequately analyse the reaction products.

5.16 Anaerobic Photochemical Reactivity of **U^{tetNO3}** with Hydrocarbon Substrates

General procedure: To a Teflon-tapped NMR tube in the glovebox was added **U^{tetNO3}** and substrate, in CD_3CN. The solutions were shaken briefly, analysed by ^{1}H NMR spectroscopy, irradiated for 16 hours using lamp **(4)** at r.t., and analysed again by ^{1}H NMR spectroscopy.

With xanthene: **U^{tetNO3}** (50.8 mg, 50.6 μmol, 1 equiv.) and xanthene (9.2 mg, 50.5 μmol, 1 equiv.) in CD_3CN (0.7 mL). Yellow solution to brown solution, but unidentified ^1H NMR resonances after 16 hours. The solution was subsequently irradiated for a further 16 hours at r.t. and reanalysed by ^1H NMR spectroscopy, additionally to $^{13}C\{^1H\}$ NMR spectroscopy, melting point analysis and SCXRD on colourless crystals deposited on the inner wall of the NMR tube (a = 10.752 Å, b = 6.874 Å, c = 12.481 Å, $\alpha = \beta = \gamma = 90°$, v = 922 Å^3; bixanthene).[25]

This was repeated with a saturated xanthene solution; **U^{tetNO3}** (49.6 mg, 49.5 μmol, 1 equiv.) and xanthene (90 mg, 493.9 μmol, 10 equiv.) in CD_3CN (5 mL). Yellow solution became clear brown solution with off-white precipitate after irradiation.

With DHA: U^{tetNO3} (7.9 mg, 44 μmol, 1 equiv.) and DHA (46.1 mg, 46 μmol, 1.05 equiv.) in CD_3CN (1 mL). Yellow solution to pale brown solution with no precipitate.

With cyclohexane: cyclohexane (60 mg, 713 μmol, 27.5 equiv.) and **U^{tetNO3}** (26 mg, 25.9 μmol, 1 equiv.) in CD_3CN (1.5 mL). Yellow solution to dark orange solution.

^1H NMR spectroscopy showed only resonances consistent with starting materials.

With cyclohexene: cyclohexene (40 mg, 487 μmol, 27.5 equiv.) and **U^{tetNO3}** (26 mg, 25.9 μmol, 18.8 equiv.) in CD_3CN (1.5 mL). Yellow solution to dark brown solution with brown microcrystalline precipitate. Also repeated with substoichiometric amounts of cyclohexene: cyclohexene (8.6 mg, 104 mmol, 0.8 equiv.) and **U^{tetNO3}** (129.7 mg, 130 μmol, 1 equiv.), in CD_3CN (0.7 mL).

^1H NMR spectroscopy showed only resonances consistent with starting materials.

With 2P1PE: 2-phenoxy-1-phenylethanol, 2P1PE (10.8 mg, 50 μmol, 1 equiv.) and **U^{tetNO3}** (50.4 mg, 50.2 μmol, 1 equiv.) in CD_3CN (0.7 mL). Yellow solution to orange solution.

^1H NMR spectroscopy showed a sustained decrease in the integrals of the diagnostic resonance corresponding to 2P1PE (multiplet at 4.11–4.02 ppm) over time on photolysis, along with increases in the integrations of resonances corresponding to phenol (6.87 ppm), 1-phenylethanol (4.91 ppm) and an unidentified component (5.44 ppm).

With THF: U^{tetNO3} (50 mg, 49 μmol, 1 equiv.) and THF (3.6 mg, 49 μmol, 1 equiv.) in CD_3CN (0.7 mL). Yellow solution to brown solution.

^1H NMR spectroscopy did not show any resonances characteristic of THF (3.64 and 1.80 ppm in CD_3CN)[24] after 16 hours of irradiation, suggesting complete consumption of THF.

With hexane: U^{tetNO3} (50 mg, 49 μmol, 1 equiv.) and hexane (4.3 mg, 49.4 μmol, 1 equiv.) in CD_3CN (0.7 mL). Yellow solution to black solution.

^1H NMR spectroscopy showed only resonances consistent with starting materials.

With toluene: U^{tetNO3} (49.5 mg, 49.3 μmol, 1.14 equiv.) and toluene (4.0 mg, 43.4 μmol, 1.05 equiv.) in CD_3CN (0.7 mL). Yellow solution to clear brown solution.

^1H NMR spectroscopy showed only resonances consistent with starting materials.

With phenylacetylene: U^{tetNO3} (50.3 mg, 50.2 μmol, 1 equiv.) and phenylacetylene (5.1 mg, 50 μmol, 1 equiv.) in CD_3CN (0.7 mL). Yellow solution to clear brown solution with no precipitate.

^1H NMR spectroscopy showed a decrease of approximately 55% in the integration of the resonance at 3.43 ppm (alkyne proton) of phenylacetylene.

With isopropanol: U^{tetNO3} (55 mg, 54.8 μmol, 1 equiv.) and isopropanol (3.4 mg, 56.6 μmol, 1.03 equiv.) in CD_3CN (0.75 mL). Pale yellow solution to dark brown, translucent solution.

^{1}H NMR spectroscopy showed no evidence of any isopropanol remaining after irradiation.

The reaction was repeated using an excess of isopropanol; **U^{tetNO3}** (34.8 mg, 34.7 μmol, 1 equiv.) and isopropanol (5.7 mg, 94.8 μmol, 2.7 equiv.) in CD_3CN (1 mL). Pale yellow solution to dark brown solution with no precipitate.

Experimental details for Chapter 4

5.17 Synthesis of $[(U^VO(OK(py)_2))_2(L^{Me})]$, **4.T.K**

To two separate vials in the glovebox was added $[K][UO_2(N'')_3]$ (**4.AR**) and H_4L^{Me} in C_5D_5N or 4:1 C_6D_6:THF (2 mL) which, when combined and agitated briefly in a Teflon-tapped NMR tube, typically gave a dark yellow-brown solution. These solutions were refluxed (125°C) over time, with analysis by ^{1}H NMR spectroscopy at selected time intervals. In each case a dark brown solution and dark brown precipitate was produced, which could be solubilised upon sequential addition of 18-c-6 (2 equiv.) and Me_3SiCl (3–5 drops), as needed.

The following were tested:

1. H_4L^{Me} (9 mg, 13.6 μmol, 1 equiv.), $[K][UO_2(N'')_3]$ (**4.AR**) (21.5 mg, 27.2 μmol, 2 equiv.) in C_5D_5N (1 mL) at 50, 100 and 125°C.

^{1}H NMR (500 MHZ, C_5D_5N): δ/ppm = 11.68 (s, 4H, pyrrole), 8.71 (masked by C_5D_5N at 8.74 ppm), 5.22 (s, 4H, imine), 4.58 (s, 6H, *meso*-Me), -2.95 (s, 12 H, aryl-Me), -3.06 (s, 4H, aryl-H), -10.30 (s, 6H, *meso*-Me).

A small number of brown crystals suitable for XRD were obtained from a portion of the reaction solution at 125°C after 2 days, after vapour diffusion of hexane(s) into the solution at r.t. over two weeks. This material was found to have the formula $[(K(py))_{0.7}]_2[(K(py)_2)_{0.3}]_2[(U^{VI}O_2)(U^VO_2)(L^{Me})]_2$, **4.1**, with the remainder of the material being microcrystalline powder. Attempts to analyse the material consistent with complex **4.1** by ^{1}H NMR and IR spectroscopy, elemental analysis and ESI-MS yielded inconsistent results.

2. H_4L^{Me} (9.1 mg, 13.7 μmol, 1 equiv.), $[K][UO_2(N'')_3]$ (**4.AR**) (21.3 mg, 27.0 μmol, 1.97 equiv.), 18-c-6 (7.1 mg, 27.0 μmol, 1.97 equiv.) in C_5D_5N (1 mL) at 125°C.

^{1}H NMR (500 MHZ, C_5D_5N): δ/ppm = 11.54 (s, 4H, pyrrole), 8.38 (s, 4H, pyrrole), 5.58 (br s, 18-c-6; also masking imine protons), 4.56 (s, 6H, *meso*-Me), -2.80 (s, 12 H, aryl-Me), -3.56 (s, 4H, aryl-H), -11.46 (s, 6H, *meso*-Me).

3. H_4L^{Me} (9.0 mg, 13.5 μmol, 1 equiv.), $[K][UO_2(N'')_3]$ (**4.AR**) (21.1 mg, 26.8 μmol, 1.98 equiv.) in C_5D_5N (1 mL) at r.t.

Only resonances consistent with starting materials were observed by ^{1}H NMR spectroscopy.

4. H_4L^{Me} (9 mg, 13.6 μmol, 1 equiv.), $[K][UO_2(N'')_3]$ (**4.AR**) (21.5 mg, 27.3 μmol, 2.01 equiv.) in 4:1 C_6D_6:THF-H_8 (1 mL total) at 125°C.

No paramagnetic signals (*e.g.* outside 0–11 ppm range) were observed by ^{1}H NMR spectroscopy.

Unsuccessful use of microwave synthesis to target $[(U^VO(OK(py)_2))_2(L^{Me})]$ ***4.T.K***

To three separate vials in the glovebox was added $[K][UO_2(N'')_3]$, **4.AR** (100 mg, 127 μmol, 1.96 equiv.), H_4L^{Me} (42.8 mg, 64.8 μmol, 1 equiv.) and 18-c-6 (33.3 mg, 126 μmol, 1.94 equiv.), with the three components dissolved together in C_5D_5N (< 5 mL) and transferred to a Teflon-tapped ampoule. The brown solution was then irradiated using the microwave synthesiser for 19 hours (115°C, 20 W upper

limit, open-vessel mode, ramp/cool rate (ΔT) 18°C min^{-1}). The resulting dark brown solution was filtered (glass wool) from dark brown precipitate, and analysed by ^{1}H NMR spectroscopy.

Analysis of the product solution by ^{1}H NMR spectroscopy showed numerous resonances between 0 and *ca*. 11 ppm, consistent with multiple, diamagnetic species (*e.g.* no paramagnetic proton resonances), which did not correspond to starting materials. Also, no resonances corresponding to $[(U^{V}O(OK(py)_2))_2(L^{Me})]$ **4.T.K** were observed. This is interpreted as heat-induced decomposition of starting material(s), intermediates, or both, resulting in numerous by-products which were not characterised further.

*Unsuccessful use of UV irradiation to target $[(U^{V}O(OK(py)_2))_2(L^{Me})]$ **4.T.K***

To three separate vials in the glovebox was added solutions of $[K][UO_2(N'')_3]$ **4.AR** (62.7 mg, 79.4 μmol, 1.92 equiv.), H_4L^{Me} (27.3 mg, 41.3 μmol, 1 equiv.) and 18-c-6 (21.5 mg, 81.3 μmol, 1.97 equiv.) in C_5D_5N (total 1.5 mL). After thorough mixing, these solutions were transferred to a Teflon-tapped NMR tube, resulting in a yellow-brown solution that was allowed to stand for 16 hours, and irradiated for 22 hours using lamp **(1)** at r.t. The resulting solution was analysed by ^{1}H NMR spectroscopy after 6, 14 and 22 hours of irradiation.

^{1}H NMR spectroscopy showed numerous resonances between 0 and *ca*. 11 ppm in the product solution, consistent with multiple, diamagnetic species, in all spectra. No resonances corresponding to $[(U^{V}O(OK(py)_2))_2(L^{Me})]$ **4.T.K** or protons in paramagnetic environments were observed.

Unsuccessful synthesis using different solvents

In 1,4-dioxane: To three separate vials in the glovebox was added $[K][UO_2(N'')_3]$ **4.AR** (62.5 mg, 79.1 μmol, 1.91 equiv.), H_4L^{Me} (27.4 mg, 41.5 μmol, 1 equiv.) and 18-c-6 (21.5 mg, 81.3 μmol, 1.96 equiv.) and the solids dissolved together in 1,4-dioxane (< 3 mL; $[K][UO_2(N'')_3]$ **4.AR** is poorly soluble in 1,4-dioxane) and C_5D_5N (3–5 drops). The reaction was then heated to reflux (125°C) for 5 days, producing a dark brown solution and precipitate. This mixture was filtered (glass wool), and the filtrate analysed by ^{1}H NMR spectroscopy (solvent suppression, limiting size of dioxane peaks).

No evidence of resonances in paramagnetic environments (*e.g.* consistent with $[(U^{V}O(OK(py)_2))_2(L^{Me})]$ **4.T.K** were observed. All resonances observed were between *ca*. 0–11 ppm.

In *N,N*-dimethylaniline*:* To three separate vials in the glovebox was added $[K][UO_2(N'')_3]$ **4.AR** (62.5 mg, 79.1 μmol, 1.91 equiv.), H_4L^{Me} (27.3 mg, 41.5 μmol, 1 equiv.) and 18-c-6 (21.5 mg, 81.3 μmol, 1.96 equiv.) and dissolved in *N,N*-dimethylaniline (< 2.5 mL) and C_5D_5N (3–5 drops). After brief shaking, the dark yellow-brown solution was heated at 125°C for one week. The resulting dark brown solution and precipitate were filtered (cannula), the filtrate dried *in vacuo* for 16 hours, and analysed by ^{1}H NMR spectroscopy.

No evidence of resonances in paramagnetic environments (*e.g.* consistent with $[(U^{V}O(OK(py)_2))_2(L^{Me})]$ **4.T.K** were observed. All resonances observed were between *ca*. 0–11 ppm.

Unsuccessful scale-up

*Note, this procedure was repeated exactly, three times, in an attempt to isolate larger quantities of $[(U^{V}O(OK(py)_2))_2(L^{Me})]$ **4.T.K**.*

To a Teflon-tapped ampoule in the glovebox was added $[K][UO_2(N'')_3]$ **4.AR** (998.7 mg, 1.26 mmol, 2 equiv.), H_4L^{Me} (418.1 mg, 0.63 mmol, 1 equiv.) and 18-c-6 (333.5 mg, 1.26 mmol, 2 equiv.), in pyridine (25 mL), causing an immediate colour change from pale to dark brown upon addition of H_4L^{Me}. The resulting solutions were then refluxed for 7 days with periodic analysis by ^{1}H NMR spectroscopy (solvent suppression). The resulting dark brown precipitates and solutions (all cases) were centrifuged (2000 rpm, 30 minutes), filtered (cannula), and volatiles (*e.g.* HN'') removed *in vacuo* for 16 hours.

Small amounts of resulting dark brown solids were retained for analyses by ^{1}H NMR spectroscopy, with any remaining solids dissolved in the minimum amount of pyridine and placed in a freezer (-35°C) for five days. All attempts to purify by crystallisation were unsuccessful, yielding dark brown powders in call cases.

^{1}H NMR spectroscopy revealed diamagnetic-only resonances (*e.g.* 0–11 ppm) in all cases. No evidence of resonances consistent with $[(U^{V}O(OK(py)_2))_2(L^{Me})]$ **4.T.K** was observed.

5.18 Reductive, Photochemical Oxo-Functionalisation of the Uranyl Ion under Anaerobic Conditions

5.18.1 Stannylation with Sn_2Me_6; Synthesis of $[(U^{V}O(OSnMe_3)(THF))(H_2L^{Me})]$, 4.2

To a Teflon-tapped NMR tube was added $[(UO_2(THF))(H_2L^{Me})]$ **4.L.THF** (90.1 mg, 90 μmol, 1 equiv.) and Sn_2Me_6 (30.8 mg, 94 μmol, 1.04 equiv.), and C_6D_6 (< 1.5 mL) added to give a brown solution which was analysed by ^{1}H NMR spectroscopy. Photolysis using lamp **(4)** for 2–3 days at r.t. then gave a transparent orange solution, which was analysed by ^{1}H and ^{119}Sn NMR spectroscopy. Vapour diffusion on the crude mixture (C_6D_6 solvent, hexane(s) anti-solvent) deposited orange plates (51.8 mg, 49%) which were suitable for SCXRD after 3 months at r.t. in the glovebox. This pure (by ^{1}H NMR spectroscopy) material was further analysed by UV-vis spectroscopy and APPI-MS. Conflicting results were obtained by elemental analysis.

The analogous reaction was repeated using toluene, instead of C_6D_6 as the reaction solvent; $[(UO_2(THF))(H_2L^{Me})]$ **4.L.THF** (25.5 mg, 25.5 μmol, 1 equiv.) and Sn_2Me_6 (8.4 mg, 25.6 μmol, 1 equiv.), and toluene:C_6D_6 (50:1, 2 mL b.v.). After volatiles were removed *in vacuo*, analysis of the resulting solids was performed by ^{1}H NMR spectroscopy. Resonances (measured in C_6D_6) for this reaction were identical to the reaction performed in C6D6 as the reaction solvent, suggesting toluene is also a suitable solvent for this reaction.

^{1}H NMR (500 MHz, C_6D_6): δ/ppm = 60.84 (s, 2H, pyrrole –NH), 16.68 (s), 11.31 (d, *J* = 3.1 Hz), 9.84 (d, *J* = 3.1 Hz), 7.91 (s), 3.00 (s), 2.71 (d, *J* = 3.8 Hz), 2.61 (d, *J* = 3.8 Hz), 2.29 (s), 2.16 (s, 9H, -$SnCH_3$), -0.78 (br s), -3.54 (s), -5.87 (s), -6.74 (s), -7.55 (s), -11.02 (s). ^{119}Sn NMR (186.362 MHz, C_6D_6): δ/ppm = 2936.32 (s); c*f.* ^{119}Sn NMR of Sn_2Me_6 (186.362 MHz, C_6D_6): δ/ppm = -110.3 (s). UV-vis (CH_3CN): λ/nm (ε/$M^{-1}cm^{-1}$): 278–*ca*. 500 (broad; λ_{max} = 339 nm, $\varepsilon_{339} \approx 78000$), 276 (sh, 32000). Mass spec., *m/z* (Da*;* relative intensity, assignment): 1093.380 (20%, $[(U^{V}O(OSnMe_3))(H_2L^{Me})\text{-}H]^+$), 1256.344 (100%, $[(U^{V}O(O(SnMe_3)_2))(H_2L^{Me})]^+$), 2185.789 (19%, $[(U^{V}O(OSnMe_3))(H_2L^{Me})_2\text{-}H]^+$).

Stannylation with Sn_2Ph_6

To a Teflon-tapped NMR tube in the glovebox was added $[(UO_2(THF))(H_2L^{Me})]$ **4.L.THF** (30.1 mg, 30.1 μmol, 1 equiv.) and Sn_2Ph_6 (21.6 mg, 31.0 μmol, 1.03 equiv.) in C_6H_6/C_6D_6 (2:1 b.v., 1.5 mL) yielding a brown solution that was irradiated using lamp **(1)** for 16 hours at r.t. Analysis by ^{1}H NMR spectroscopy showed limited conversion, so the reaction was again irradiated with lamp **(1)** for 16 hours at r.t., yielding a translucent orange solution, which was analysed further by ^{1}H NMR spectroscopy.

The ^{1}H NMR spectrum of the product solution showed a large number of new resonances consistent with multiple products. A small number of signals were observed between 0 – -12 ppm, suggesting that paramagnetic proton environments (*e.g.* U^{V}-containing products) were also present, but these could not be adequately identified and so are not discussed further.

Stannylation with Ph_3SnH

To two separate vials in the glovebox was added $[(UO_2(THF))(H_2L^{Me})]$ **4.L.THF** (25.1 mg, 25.1 μmol, 1 equiv.) and Ph_3SnH (10.5 mg, 30 μmol, 1.2 equiv.) in C_6D_6 (< 1.5 mL total), and the solutions combined and briefly shaken in a Teflon-tapped NMR tube. The dark brown solution was irradiated for 16 hours

using lamp **(1)** at r.t., resulting in the formation of a dark orange/pale brown solution, which was analysed by ^{1}H NMR spectroscopy.

The ^{1}H NMR spectrum of the product solution showed a large number of new resonances consistent with multiple products. A small number of signals were observed between 0 – -12 ppm, suggesting that paramagnetic proton environments (*e.g.* U^{V}-containing products) were also present, however, these could not be adequately identified.

5.18.2 Unsuccessful Germanylation with Ge_2Me_6

To two separate vials in the glovebox was added hexamethyldigermane, Ge_2Me_6 (5.7 mg, 23 μmol, 1 equiv.) and [$(UO_2(THF))(H_2L^{Me})$] **4.L.THF** (23.2 mg, 23.2 μmol, 1 equiv.), dissolved in C_6D_6 (total < 3 mL), and the vial contents combined, shaken briefly, and analysed by ^{1}H NMR spectroscopy. The resulting brown solution was then irradiated using lamp **(1)** for 32 hours, and analysed by ^{1}H NMR spectroscopy.

There was no colour change in the reaction before, during or after irradiation, with ^{1}H NMR spectroscopy after 32 hours of irradiation showing only resonances consistent with starting materials.

5.18.3 Unsuccessful Silylation with Si_2Me_6

To two separate vials in the glovebox was added [$(UO_2(THF))(H_2L^{Me})$] **4.L.THF** (54 mg, 53.9 μmol, 1 equiv.) and Si_2Me_6 (4.1 mg, 28 μmol, 0.52 equiv.), in C_6D_6 (< 3 mL). These were combined in a Teflon-tapped NMR tube, the resulting dark brown solution agitated briefly, and irradiated for 16 hours using lamp **(1)** at r.t. Dark brown plate-like crystals suitable for SCXRD were also deposited along the inner walls of the NMR tube after 3 days, though were later found to be [$(UO_2(THF))(H_2L^{Me})$] **4.L.THF** starting material.

^{1}H and ^{29}Si NMR spectroscopy after irradiation on the product solution showed some resonances consistent with paramagnetic material in solution (*e.g.* 0–11 ppm shift range), but the integrals of these resonances were < 1% of those for starting materials, which dominated the spectrum.

5.18.4 Unsuccessful Borylation with $B_2(pin)_2$

To two separate vials in the glovebox was added [$(UO_2(THF)](H_2L^{Me})$] **4.L.THF** (25.0 mg, 25.0 μmol, 2 equiv.) and $B_2(pin)_2$ (pin = pinacolato; 3.2 mg, 12.5 μmol, 1 equiv.) in C_6D_6 (total < 1.5 mL), and the solutions combined, added to a Teflon-tapped NMR tube, and shaken briefly. The resulting solution was analysed by ^{1}H NMR spectroscopy, irradiated using lamp **(4)** for 16 hours at r.t., and reanalysed by ^{1}H NMR spectroscopy. There was no colour change of the reaction solution before and after irradiation (dark yellow).

The ^{1}H NMR spectra before and after irradiation were identical, suggesting no reaction occurred.

5.19 Anaerobic Photochemical Reactivity of $\mathbf{U^{tetNO3}}$ with Non-Hydrocarbon Substrates

General procedure: To a Teflon-tapped NMR tube in the glovebox was added $\mathbf{U^{tetNO3}}$ and substrate, in CD_3CN. The solutions were shaken briefly, analysed by ^{1}H NMR spectroscopy, irradiated for 16 hours using lamp **(4)** at r.t., and analysed again by ^{1}H and multinuclear (^{31}P, ^{29}Si, ^{11}B or ^{119}Sn) NMR spectroscopy, as appropriate.

With triphenylphosphine: $\mathbf{U^{tetNO3}}$ (50.6 mg, 50.4 μmol, 1.02 equiv.) and triphenylphosphine, PPh_3 (13 mg, 49.6 μmol, 1 equiv.) in CD_3CN (0.7 mL). Yellow solution to clear, very dark brown solution.

Analysis by ^{31}P NMR spectroscopy showed only resonances consistent with $Ph_3P{=}O$ (25.69 ppm (this work), CD_3CN, 161.976 MHz; 26.71 ppm in C_6D_6, 161.976 MHz).[26] No evidence of Ph_3P starting material was observed by ^{31}P NMR spectroscopy (*e.g.* -5.86 ppm (this work), C_6D_6, 161.976 MHz).

With triethylsilane: **U^{tetNO3}** (55.7 mg, 55.5 μmol, 1.04 equiv.) and triethylsilane, Et_3SiH (6.2 mg, 53.3 μmol, 1 equiv.) in CD_3CN (0.7 mL). Yellow solution to pale brown solution.

Analysis by ^{1}H and ^{29}Si NMR spectroscopy showed no evidence of Et_3SiH starting material (0.42 ppm, CD_3CN, 99.362 MHz), and no additional signals were observed by ^{29}Si NMR spectroscopic analysis on the product mixture; the fate of the Et_3SiH starting material in this reaction therefore remains unclear.

With HB(pin): U^{tetNO3} (60.2 mg, 60.1 μmol, 1 equiv.) and HB(pin) (7.6 mg, 59.4 μmol, 1 equiv.) in CD_3CN (1 mL). Yellow solution to pale brown solution. Vapour diffusion of hexane(s) into a saturated product solution at r.t. over two months yielded pale brown powdery solids, unsuitable for SCXRD analysis.

Analysis by ^{1}H and ^{11}B NMR spectroscopy showed no evidence of resonances consistent with starting materials (*e.g.* HB(pin), 33.36 ppm, CD_3CN, 160.462 MHz). Dissolved hydrogen gas (4.60 ppm, CD_3CN, 500 MHz)[24] and (pin)BOB(pin) (22.45 ppm (this work), CD_3CN, 160.462 MHz; 21.7 ppm, THF-D_8 128.4 MHz)[27] were the only observed resonances in the ^{1}H NMR and ^{11}B NMR spectra (aside from unreacted **U^{tetNO3}** in the ^{1}H NMR spectra) respectively, suggesting complete consumption of the starting materials during irradiation.

With $B_2(cat)_2$: U^{tetNO3} (50 mg, 49.9 μmol, 1.07 equiv.) and $B_2(cat)_2$ (cat = catecholato; 11.8 mg, 46.5 μmol, 1 equiv.) in CD_3CN (0.75 mL). Yellow solution, turning green on addition of $B_2(cat)_2$, with precipitation of a green solid after 5 minutes. Black solution after irradiation (16 hours, lamp **(4)**, r.t.).

Analysis by ^{1}H and ^{11}B NMR spectroscopy showed only resonances consistent with starting materials.

With Sn_2Me_6: U^{tetNO3} (28.3 mg, 28.3 μmol, 1 equiv.) and Sn_2Me_6 (92.2 mg, 28.2 μmol, 1 equiv.) in CD_3CN (1 mL). The reaction was also repeated in C_6D_6 (0.85 mL).

Analysis by ^{1}H and ^{119}Sn NMR spectroscopy in either CD_3CN or C_6D_6 in both cases showed only resonances consistent with starting materials.

5.20 Crystallographic Tables

Full crystallographic information (diffractometer, software, *etc*.) is outlined in Section 5.1.10.

Compound	$U^{Ph2phen}$	$[UO_2(MeOH)(MeO)(terpy)]_2[UO_2(NO_3)_4]$ Compound 2.2
Local code	p17136	p17110
Chemical formula	$C_{24}H_{16}N_4O_8U$	$N_4O_{14}U{\cdot}2(C_{17}H_{18}N_3O_4U)$
Space group	*P*-1	*P*-1
Density (g/cm^3)	2.117	2.484
Colour	dark yellow	yellow
***M*$_r$**	726.43	1650.79
Temperature (K)	298	120
***a*, *b*, *c* (Å)**	10.8042 (3), 11.8206 (3), 18.9026 (4)	10.56815 (16), 10.93966 (16), 11.2575 (2)
α, β, γ (°)	80.168 (2), 83.420 (2), 73.870 (2)	90.9733 (13), 110.7700 (15), 112.8209 (14)
***V* (Å^3)**	2279.23 (11)	1103.48 (3)
Z	2	2
μ (mm^{-1})	7.18	11.08
Crystal size (mm)	0.17 × 0.14 × 0.03	0.11 × 0.07 × 0.06
Diffractometer (Radiation type)	Xcalibur, Eos (MoKα)	Xcalibur, Eos (MoKα)
Absorption correction	Analytical	Multi-scan
***T*$_{min}$, *T*$_{max}$**	0.903, 0.976	0.849, 1.000
No. of measured, independent and observed [*I* > 2s(*I*)] reflections	52686, 10439, 8248	54191, 5601, 4776
***R*$_{int}$**	0.054	0.058
(sin θ/λ)$_{max}$ (Å^{-1})	0.649	0.691
R*[*F*^{2} > 2s(*F*^{2})], *wR*(*F*^{2}), *S	0.032, 0.054, 1.03	0.027, 0.055, 0.91
No. of reflections	10439	5601
No. of parameters	667	319
No. of restraints	0	0
Δ⟩$_{max}$, Δ⟩$_{min}$ (e Å^{-3})	0.85, −0.72	1.19, −1.18
GooF	1.028	0.905
I/σ	21.6	26.3
Max/min holes	0.9/-0.7	1.2/-1.2

Compound	**[TPP-2H][(UO_2(μ-OH)(NO_3)$_2$)$_2$]** *TPP: tetra-2-pyridinylpyrazine* **Compound 2.4**	**U^{mal}**
Local code	p17140	p17018
Chemical formula	$N_4O_{18}U_2 \cdot C_{24}H_{18}N_6$	$C_3H_6N_4O_{10}U \cdot C_3H_6N_2O_2$
Space group	$P2_1/c$	*Pnma*
Density (g/cm^3)	2.381	2.499
Colour	pale yellow	yellow
M_r	1210.54	598.22
Temperature (K)	298	293
***a*, *b*, *c* (Å)**	7.1674 (2), 16.7808 (4), 14.3441 (3)	9.17092 (11), 12.8093 (2), 13.5131 (2)
α, β, γ (°)	90, 101.801 (2), 90	90, 90, 90
***V* (Å^3)**	1688.77 (7)	1587.42 (4)
Z	2	4
μ (mm^{-1})	9.67	10.31
Crystal size (mm)	0.33 × 0.26 × 0.15	0.58 × 0.17 × 0.11
Diffractometer (Radiation type)	Xcalibur, Eos (MoKα)	Xcalibur, Eos (MoKα)
Absorption correction	Analytical	Analytical
T_{min}, T_{max}	0.845, 0.902	0.390, 0.749
No. of measured, independent and observed [$I > 2s(I)$] reflections	38261, 3875, 3506	32818, 1895, 1735
R_{int}	0.047	0.036
(sin θ/λ)$_{max}$ (Å^{-1})	0.649	0.649
$R[F^2 > 2s(F^2)]$, $wR(F^2)$, S	0.027, 0.052, 1.16	0.022, 0.044, 1.09
No. of reflections	3875	1895
No. of parameters	248	129
No. of restraints	0	0
Δ⟩$_{max}$, Δ⟩$_{min}$ (e Å^{-3})	0.84, −0.52	1.47, −0.86
GooF	1.158	1.091
I/σ	44.8	68.9
Max/min holes	0.8/-0.5	1.5/-0.9

Compound	**U^{malPh2}**	**U^{malPh4}**
Local code	p17071	p17033
Chemical formula	$C_{15}H_{14}N_4O_{10}U$	$C_{27}H_{22}N_4O_{10}U{\cdot}C_2H_3N$
Space group	$P2_1/c$	P-1
Density (g/cm^3)	2.211	1.645
Colour	yellow	dark yellow
M_r	648.33	841.57
Temperature (K)	298	298
a, b, c (Å)	7.00936 (17), 25.5713 (8), 10.8668 (3)	9.1913 (5), 10.5110 (3), 18.2945 (7)
α, β, γ (°)	90, 90.988 (2), 90	86.941 (3), 80.822 (4), 76.813 (4)
V (Å^3)	1947.46 (9)	1698.53 (13)
Z	4	2
μ (mm^{-1})	8.40	4.84
Crystal size (mm)	0.45 × 0.36 × 0.04	0.34 × 0.29 × 0.24
Diffractometer (Radiation type)	Xcalibur, Eos (Mo$K\alpha$)	Xcalibur, Eos (Mo$K\alpha$)
Absorption correction	Multi-scan	Multi-scan
T_{min}, T_{max}	0.159, 1.000	0.744, 1.000
No. of measured, independent and observed [$I > 2s(I)$] reflections	47340, 5429, 4429	28907, 7663, 6260
R_{int}	0.068	0.059
$(\sin\theta/\lambda)_{max}$ (Å^{-1})	0.708	0.649
$R[F^2 > 2s(F^2)]$, $wR(F^2)$, S	0.041, 0.071, 1.10	0.049, 0.116, 1.07
No. of reflections	5429	7663
No. of parameters	259	407
No. of restraints	0	0
$\Delta\rangle_{max}$, $\Delta\rangle_{min}$ (e Å^{-3})	1.62, −1.15	3.27, −1.25
GooF	1.102	1.069
I/σ	22.6	16.0
Max/min holes	1.6/-1.2	3.3/-1.2

Compound	$U^{mal\textit{i}Pr4}$	$[UO_2(py(CONHMe)_2)_2][NO_3]_2$ Compound 2.7
Local code	p17029	p17003_080tri
Chemical formula	$C_{15}H_{30}N_4O_{10}U$	$C_{18}H_{22}N_6O_6U{\cdot}2(NO_3)$
Space group	*Pnma*	*P*-1
Density (g/cm^3)	1.900	1.915
Colour	dark yellow	yellow
M_r	664.45	780.46
Temperature (K)	298	170
***a*, *b*, *c* (Å)**	16.3436 (2), 20.3522 (2), 6.9846 (1)	7.2379 (5), 7.6267 (6), 14.0862 (6)
α, β, γ (°)	90, 90, 90	99.160 (5), 91.043 (5), 117.590 (7)
***V* (Å^3)**	2323.28 (5)	676.60 (9)
Z	1	1
μ (mm^{-1})	7.04	6.07
Crystal size (mm)	0.36 × 0.22 × 0.05	0.22 × 0.12 × 0.03
Diffractometer (Radiation type)	Xcalibur, Eos (MoKα)	Xcalibur, Eos (MoKα)
Absorption correction	Multi-scan	Analytical
T_{min}, T_{max}	0.215, 1.000	0.350, 0.821
No. of measured, independent and observed [$I > 2s(I)$] reflections	47784, 3163, 2615	14062, 2766, 2765
R_{int}	0.057	0.049
$(\sin\theta/\lambda)_{max}$ (Å^{-1})	0.689	0.625
$R[F^2 > 2s(F^2)]$, $wR(F^2)$, S	0.032, 0.066, 1.05	0.037, 0.094, 1.18
No. of reflections	3163	2766
No. of parameters	145	199
No. of restraints	0	36
$\Delta\rangle_{max}$, $\Delta\rangle_{min}$ (e Å^{-3})	2.63, −1.80	2.01, −1.38
Restraint details	-	Nitrate disorder treated with FVAR and RIGU restraints. With FVAR restraint, occupancy freely set for two nitrate ions to 0.45 and 0.55.
GooF	1.047	1.184
I/σ	34.2	24.3
Max/min holes	2.6/-1.8	2.0/-1.4

Compound	$U^{piv/Pr2}$	$[UO_2(NO_3)_3(ind\text{-}oxime\text{-}H)]$ Compound 2.19
Local code	p17017	p17089_tri087
Chemical formula	$C_{22}H_{46}N_4O_{10}U$	$C_9H_6N_4O_{12}U$
Space group	$P2_1/n$	$P1$
Density (g/cm³)	1.927	2.273
Colour	very dark yellow	yellow
M_r	764.65	600.19
Temperature (K)	293	298
a, b, c (Å)	8.5543 (4), 17.4248 (7), 10.5899 (5)	8.4892 (2), 13.3884 (3), 13.8095 (4)
α, β, γ (°)	90, 103.058 (5), 90	97.460 (2), 106.511 (2), 108.319 (2)
V (Å³)	1537.68 (12)	1386.53 (6)
Z	4	2
μ (mm⁻¹)	5.33	8.84
Crystal size (mm)	0.23 × 0.14 × 0.11	0.50 × 0.22 × 0.13
Diffractometer (Radiation type)	Xcalibur, Eos (MoKα)	Xcalibur, Eos (MoKα)
Absorption correction	Multi-scan	Analytical
T_{min}, T_{max}	0.551, 1.000	0.951, 0.982
No. of measured, independent and observed [$I > 2s(I)$] reflections	18472, 2216, 2063	24505, 8796, 8608
R_{int}	0.118	0.028
$(\sin\theta/\lambda)_{max}$ (Å⁻¹)	0.705	0.575
$R[F^2 > 2s(F^2)]$, $wR(F^2)$, S	0.050, 0.071, 1.01	0.028, 0.068, 1.03
No. of reflections	2216	8796
No. of parameters	176	703
No. of restraints	0	0
$\Delta\rangle_{max}$, $\Delta\rangle_{min}$ (e Å⁻³)	4.76, −1.41	0.73, −0.57
GooF	1.011	1.030
I/σ	12.2	28.7
Max/min holes	4.8/-1.4	0.7/-0.6

Compound	$[UO_2(NO_3)_2(OH_2)_2]\cdot(fl\text{-}one)_4$ Compound 2.20	$[UO_2(NO_3)_2(^tBu_2\text{-}urea)_2]\cdot2(CH_3CN)$ $U^{tBu2urea}\cdot2(CH_3CN)$
Local code	edap15	p18059
Chemical formula	$H_4N_2O_{10}U\cdot4(C_{13}H_8O)$	$C_{18}H_{40}N_6O_{10}U\cdot2(C_2H_3N)$
Space group	*Ccce*	*P*-1
Density (g/cm^3)	1.469	1.611
Colour	pale yellow	yellow
M_r	1150.86	820.70
Temperature (K)	100	170
***a*, *b*, *c* (Å)**	14.024 (4), 20.039 (6), 15.819 (5)	8.7682 (3), 10.0889 (3), 10.5159 (3)
α, β, γ (°)	90, 90, 90	94.416 (2), 113.817 (3), 92.316 (2)
***V* (Å^3)**	4446 (2)	845.90 (5)
Z	4	1
μ (mm^{-1})	3.73	4.85
Crystal size (mm)	0.2 × 0.05 × 0.06	0.26 × 0.18 × 0.07
Diffractometer (Radiation type)	Xcalibur, Eos (MoKα)	Xcalibur, Eos (MoKα)
Absorption correction	Analytical	Multiscan
T_{min}, T_{max}	0.286, 0.847	0.850, 1.000
No. of measured, independent and observed [$I > 2s(I)$] reflections	25834, 2054, 1509	19608, 3862, 3862
R_{int}	0.094	0.041
0.649	0.604	0.649
$R[F^2 > 2s(F^2)]$, $wR(F^2)$, S	0.041, 0.106, 1.01	0.021, 0.050, 1.08
No. of reflections	2054	3862
No. of parameters	160	194
No. of restraints	0	0
$\Delta\rangle_{max}$, $\Delta\rangle_{min}$ (e Å^{-3})	1.44, −0.89	1.32, −0.89
GooF	1.013	1.084
I/σ	19.5	31.0
Max/min holes	1.4/-0.9	1.3/-0.9

Compound	**$[(K(py))_{0.7}]_2[(K(py)_2)_{0.3}]_2[(U^{VI}O_2)(U^{V}O_2)(L^{Me})]_2$ Compound 4.1**	**$[(U^{V}O(OSnMe_3)(THF))(H_2L^{Me})]$ Compound 4.2**
Local code	p15179	PO17037_mono
Chemical formula	$C_{97}H_{93}K_2N_{18.6}O_8U_4$ *Note, 18.6N from partial py occupancies*	$C_{49}H_{61}N_8O_3SnU$
Space group	$P2_1/n$	$P2_1/n$
Density (g/cm^3)	1.379	1.514
Colour	dark red	orange
M_r	2677.61	1166.80
Temperature (K)	170	120
***a*, *b*, *c* (Å)**	17.9545 (2), 18.00685 (19), 20.5176 (3)	15.4204 (1), 19.3986 (2), 31.9589 (4)
α, β, γ (°)	103.5353 (14)	96.766 (1)
***V* (Å^3)**	6449.19 (15)	9493.42 (17)
Z	2	4
μ (mm^{-1})	5.12	14.10
Crystal size (mm)	0.37 × 0.20 × 0.17	0.22 × 0.11 × 0.03
Diffractometer (Radiation type)	Xcalibur, Eos (MoKα)	SuperNova, Dual, Cu at zero, Atlas
Absorption correction	Analytical	Multi-scan
T_{min}, T_{max}	0.827, 0.900	0.142, 1.000
No. of measured, independent and observed [$I > 2s(I)$] reflections	109452, 14700, 12109	150179, 19407, 16980
R_{int}	0.044	0.095
(sin θ/λ)$_{max}$ (Å^{-1})	0.649	0.625
$R[F^2 > 2s(F^2)]$, $wR(F^2)$, S	0.066, 0.185, 1.18	0.069, 0.180, 1.12
No. of reflections	14700	19407
No. of parameters	681	1139
No. of restraints	287	0
Δ⟩$_{max}$, Δ⟩$_{min}$ (e Å^{-3})	3.04, −1.70	5.31, −2.94
Restraint details	K^+ ions modelled with PART command (0.7 and 0.3). Pyridine disorder treated with DFIX, FLAT and EADP restraints.	-
GooF	1.183	1.124
I/σ	32.8	24.8
Max/min holes	3.0/-1.7	5.3/-2.9

5.21 References

1. O. Golubev, T. Lönnberg and H. Lönnberg, *J. Inorg. Biochem.*, 2014, **139**, 21.
2. A. Leoncini, J. Huskens and W. Verboom, *Synlett.*, 2016, **27**, 2463.
3. G. Barbe and A. B. Charette, *J. Am. Chem. Soc.*, 2008, **130**, 18.
4. G. Wieland and G. Simchen, *Liebigs Ann. Chem*, 1985, 2178.
5. M. D. Ferretti, A. T. Neto, A. F. Morel, T. S. Kaufman and E. L. Larghi, *Eur. J. Med. Chem.*, 2014, **81**, 253.
6. E. Pretsch, D. Ammann, H. F. Osswald, M. Güggi and W. Simon, *Helv. Chim. Acta*, 1980, **63**, 191.
7. S. Guoxin, L. Min, C. Yu, Y. Meilong and Y. Shaohong, *Solv. Extr. Ion Exch.*, 2010, **28**, 482.
8. S. C. Sawant, X. Wu, J. Cho, K.-B. Cho, S. H. Kim, M. S. Seo, Y.-M. Lee, M. Kubo, T. Ogura, S. Shaik and W. Nam, *Angew. Chem. Int. Ed.*, 2010, **49**, 8190.
9. G. Givaja, A. J. Blake, C. Wilson, M. Schröder and J. B. Love, *Chem. Commun.*, 2003, 2508.
10. P. L. Arnold, A. J. Blake, C. Wilson and J. B. Love, *Inorg. Chem.*, 2004, **43**, 8206.
11. ACD Labs, NMR Processor Academic Edition (12.01, Build 39104), 2010.
12. D. B. Robb, T. R. Covey and A. P. Bruins, *Anal. Chem.*, 2000, **72**, 3653.
13. Agilent Technologies, CrysAlis PRO (version 1.171.37.34, 2014).
14. Rigaku OD, CrysAlis PRO (version 1.171.38.46, 2015).
15. G. M. Sheldrick, *Acta Cryst. Sect. A*, 2015, **71**, 3.
16. G. M. Sheldrick, *Acta Cryst. Sect. C*, 2015, **71**, 3.
17. O. V. Dolomanov, L. J. Bourhis, R. J. Gildea, J. A. K. Howard and H. Puschmann, *J. Appl. Crystallogr.*, 2009, **42**, 339.
18. R. C. Clark and J. S. Reid, *Acta Cryst. Sect. A*, 1995, **51**, 887.
19. Oxford Diffraction Ltd., SCALE 3 ABSPACK (version 1.0.4, 2005).
20. A. B. Patil, S. Ghosh, S. D. Phadatare, P. Pathak, G. K. Sharma, B. A. Chopade and V. S. Shinde, *New. J. Chem.*, 2015, **39**, 1267.
21. G. Pandey, S. Koley, R. Talukdar and P. K. Sahani, *Org. Lett.*, 2018, **20**, 5861.
22. S. Kannan, M. Kumar, B. Sadhu, M. Jaccob and M. Sundararajan, *Dalton Trans.*, 2017, **46**, 16939.
23. B. Gabriele, G. Salerno, R. Mancuso and M. Costa, *J. Org. Chem.*, 2004, **69**, 4741.
24. G. R. Fulmer, A. J. M. Miller, N. H. Sherden, H. E. Gottlieb, A. Nudelman, B. M. Stoltz, J. E. Bercaw and K. I. Goldberg, *Organometallics*, 2010, **29**, 2176.
25. P.-C. Li, T.-S. Wang, G.-H. Lee, Y.-H. Liu, Y. Wang, C.-T. Chen and I. Chao, *J. Org. Chem.*, 2002, **67**, 8002.
26. H. Rao, Y. Jin, H. Fu, Y. Jiang and Y. Zhao, *Chem. Eur. J.*, 2006, **12**, 3636.
27. S. R. Tamang and M. Findlater, *Dalton Trans.*, 2018, **47**, 8199.